plants

Special Issue Reprint

Abiotic Stress of Crops

Molecular Genetics and Genomics—2nd Edition

Edited by
Zhaoshi Xu

mdpi.com/journal/plants

MDPI

Abiotic Stress of Crops: Molecular Genetics and Genomics—2nd Edition

Abiotic Stress of Crops: Molecular Genetics and Genomics—2nd Edition

Guest Editor

Zhaoshi Xu

MDPI

Basel • Beijing • Wuhan • Barcelona • Belgrade • Novi Sad • Cluj • Manchester

Guest Editor
Zhaoshi Xu
Institute of Crop Sciences
Chinese Academy of
Agricultural Sciences (CAAS)
Beijing
China

Editorial Office
MDPI AG
Grosspeteranlage 5
4052 Basel, Switzerland

This is a reprint of the Special Issue, published open access by the journal *Plants* (ISSN 2223-7747), freely accessible at: https://www.mdpi.com/journal/plants/special_issues/OZTFWK5V1H.

For citation purposes, cite each article independently as indicated on the article page online and as indicated below:

Lastname, A.A.; Lastname, B.B. Article Title. *Journal Name* **Year**, *Volume Number*, Page Range.

ISBN 978-3-7258-6868-1 (Hbk)
ISBN 978-3-7258-6869-8 (PDF)
https://doi.org/10.3390/books978-3-7258-6869-8

Contents

About the Editor

Zhaoshi Xu

Zhaoshi Xu, Professor, Head of the Research Group of Wheat Molecular Breeding, Institute of Crop Sciences, Chinese Academy of Agricultural Sciences. He was awarded the titles of Changbai Mountain's leading talents and Tianshan Talent. He mainly engages in analysis of molecular regulatory networks of drought-tolerant genes, and synergistic regulation mechanism between Fusarium crown rot resistance and drought tolerance in wheat. He presided more than 10 national projects, obtained more than 50 national invention patents, and published more than 100 papers. He was selected for the "Top 2% of Global Scientists" list in 2025.

plants

MDPI

Article

Genome-Wide Identification and Salinity Response Analysis of the Germin-like Protein (*GLP*) Gene Family in *Puccinellia tenuiflora*

Yueyue Li [1,2,†], Zhe Zhao [2,†], Bo Li [1,†], Hongxia Zheng [1,2], Zhen Wu [2], Ying Li [1,*], Meihong Sun [2,*] and Shaojun Dai [2,*]

[1] Key Laboratory of Saline-Alkali Vegetation Ecology Restoration, College of Life Sciences, Northeast Forestry University, Ministry of Education, Harbin 150040, China; 2021031283@nefu.edu.cn (Y.L.); lb19941016@163.com (B.L.); zhenghongxia2020@foxmail.com (H.Z.)

[2] Development Center of Plant Germplasm Resources, College of Life Sciences, Shanghai Normal University, Shanghai 200234, China; lmy2121@126.com (Z.Z.); zhen_wu@shnu.edu.cn (Z.W.)

* Correspondence: ly7966@nefu.edu.cn (Y.L.); sunmeihong@shnu.edu.cn (M.S.); daishaojun@shnu.edu.cn (S.D.)

† These authors contributed equally to this work.

Abstract: The germin-like protein (GLP) family plays vital roles for plant growth, stress adaptation, and defense; however, its evolutionary dynamics and functional diversity in halophytes remain poorly characterized. Here, we present the genome-wide analysis of the GLP family in the halophytic forage alkaligrass (*Puccinellia tenuiflora*), which identified 54 *PutGLPs* with a significant expansion compared to other plant species. Phylogenetic analysis revealed monocot-specific clustering, with 41.5% of *PutGLPs* densely localized to chromosome 7, suggesting tandem duplication as a key driver of family expansion. Collinearity analysis confirmed evolutionary conservation with monocot *GLPs*. Integrated gene structure and motif analysis revealed conserved cupin domains (BoxB and BoxC). Promoter *cis*-acting elements analysis revealed stress-responsive architectures dominated by ABRE, STRE, and G-box motifs. Tissue-/organ-specific expression profiling identified root- and flower-enriched *PutGLPs*, implying specialized roles in stress adaptation. Dynamic expression patterns under salt-dominated stresses revealed distinct regulatory pathways governing ionic and alkaline stress responses. Functional characterization of PutGLP37 demonstrated its cell wall localization, dual superoxide dismutase (SOD) and oxalate oxidase (OXO) enzymatic activities, and salt stress tolerance in *Escherichia coli*, yeast (*Saccharomyces cerevisiae INVSc*1), and transgenic *Arabidopsis*. This study provides critical insights into the evolutionary innovation and stress adaptive roles of GLPs in halophytes.

Keywords: *Puccinellia tenuiflora*; germin-like protein (*GLP*) gene family; expression pattern; salt tolerance

1. Introduction

Germin-like proteins (GLPs) were first identified during wheat seed germination and have since been characterized across diverse plant lineages including gymnosperms, dicots, monocots, and mosses [1–4]. As members of the versatile cupin superfamily, all GLPs possess conserved cupin domains characterized by a β-barrel structure that facilitates metal ion binding [5]. These proteins exhibit exceptional stability as oligomeric complexes, demonstrating remarkable resistance to thermal denaturation and proteolytic degradation [6]. In plants, GLPs contribute to multiple biological processes such as developmental regulation, osmoregulation, and pathogen defense through cell wall fortification mechanisms [5,7–9].

The majority of GLPs exhibit enzymatic activities, including oxalate oxidase (OXO), superoxide dismutase (SOD), and cysteine peptidase functions [10–12]. For example, rice (*Oryza sativa*) OsGLP3-7 demonstrates SOD activity and regulates H_2O_2 accumulation in transgenic plants [12]. Enzymatic assays of *Calotropis procera* latex fluids identified OXO activity in the latex-derived CpGLP1 and CpGLP2 proteins [13]. Similarly, the azalea *(Rhododendron mucronatum*) GLP (RmGLP2) exhibited OXO activity in both in vitro and in vivo assays, while negative staining further revealed its concurrent SOD activity [14]. Notably, a GLP purified from *Thevetia peruviana* demonstrated proteolytic activity characteristic of cysteine peptidase [15].

GLPs participate in plant developmental processes and mediate responses to biotic and abiotic stresses, potentially through enhanced enzymatic activity [4,16]. In rice, suppression of *OsGLP2-1* expression accelerated dormancy release in immature seeds, while its overexpression enhanced seed dormancy [8]. Notably, the rice GLP (OsGER4) acts as a negative regulator of gibberellin (GA)-mediated crown root development [17]. Furthermore, in *Arabidopsis*, plasmodesmata GLP (PDGLP1/2) regulate root architecture by controlling phloem-mediated resource allocation between primary and lateral root meristems [18]. Critically, GLPs also mediate biotic and abiotic stress responses. The *Craterostigma plantagineum* CpGLP1, which defines a novel GLP subfamily, demonstrates SOD activity and pectin-binding capacity, coordinating ROS homeostasis and cell wall remodeling during desiccation tolerance [19]. Likewise, transgenic expression of the sunflower *(Helianthus annuus*) HaGLP1 in *Arabidopsis* conferred significant tolerance to *Sclerotinia sclerotiorum* and protects against *Rhizoctonia solani* infection, likely through elevated ROS levels [20]. Recently, OsGLP8-7 in rice was shown to alleviate copper toxicity through lignin biosynthesis-mediated cell wall remodeling, which enhances Cu^{2+} retention, suppresses oxidative stress, and preserves cellular ultrastructure under excess Cu conditions [21].

Alkaligrass (*Puccinellia tenuiflora*), a halophytic forage species exhibiting exceptional saline-alkaline stress tolerance [22], serves as a model organism for studying stress resistance mechanisms with applications in saline soil remediation and functional genomics [23,24]. Although GLP gene family has been functionally characterized in soybean (*Glycine max*), longan (*Dimocarpus longan*), Citrus (*Citrus sinensis*), peanut (*Arachis hypogaea*), melon (*Cucumis melo*), rapeseed (*Brassica napus*), cotton (*Gossypium hirsutum*), maize (*Zea mays*), rice (*O. sativa*), barley (*Hordeum vulgare*), *Arabidopsis* (*Arabidopsis thaliana*), and moss (*Physcomitrella patens*) [3,4,16,25–32], research on the GLP family in *P. tenuiflora* remains limited.

In this study, we aim to comprehensively identify and annotate *PutGLP* members through genome-wide analysis. We will elucidate their evolutionary relationships, structural features, expression levels across tissues and organs, and salinity-responsive dynamics. On these bases, we further functionally validate the key *PutGLP37* via subcellular localization, enzymatic assays, and phenotypic analysis in transgenic plants. These objectives will establish a foundation for deciphering the molecular mechanisms by which *PutGLPs* mediate development and environmental resilience in halophytes.

2. Results

2.1. Identification of PutGLPs in P. tenuiflora

Using a Hidden Markov Model (HMM) scan and BLASTP searches, 53 *PutGLPs* were identified in the *P. tenuiflora* genome, designated as *PutGLP1-PutGLP36* and *PutGLP38-PutGLP54* (Table S1). PutGLP37 was subsequently isolated from the *P. tenuiflora* cDNA library but lacked a corresponding genomic position in the published genome assembly [22]. Therefore, a total of 54 family members encoding the cupin_1 domain (PF00190) were analyzed. The amino acid sequences varied in length from 171 residues (PutGLP33) to

280 residues (PutGLP4), with predicted theoretical isoelectric points (pI) ranging from 4.51 (PutGLP46) to 9.51 (PutGLP11) (Table S1). The predicted molecular weights (MW) of these proteins ranged from 18.33 kDa (PutGLP33) to 30.91 kDa (PutGLP4). Subcellular localization predictions indicated that most PutGLP proteins localize to the cell wall.

2.2. Phylogenetic and Evolutionary Analysis of the PutGLPs

To investigate the functional and evolutionary relationships within the GLP gene family, an unrooted phylogenetic tree was constructed using sequences from six plant species: alkaligrass (*P. tenuiflora*), soybean *(G. max*), barley (*H. vulgare*), *Arabidopsis* (*A. thaliana*), rice (*O. sativa*), and maize (*Z. mays*) (Figure 1 and Table S2). The 218 *GLPs* analyzed were classified into seven major clades (I–VII). *PutGLPs* were distributed across clades III, V, VI, and VII, comprising 24, nine, one, and 20 members, respectively. Among all clades, clade III represented the largest group, encompassing 80 *GLP* members (36.7% of the total). This clade was further subdivided into four subgroups: IIIa (ten *PutGLPs*), IIIb (one *PutGLP*), IIIc (three *PutGLPs*), and IIId (ten *PutGLPs*). Similarly, clade VII was partitioned into subclades VIIa (eight *PutGLPs*), VIIb (five *PutGLPs*), VIIc (seven *PutGLPs*), and VIId (no *P. tenuiflora* representatives). Maize ZmGLPs in subclade VIId only contain cupin_1 domain and cupin_2 domain, while PutGLPs within subclade VIIc have cupin_1 domain, cupin_2 domain, and cupin_3 domain, suggesting potential functional divergence.

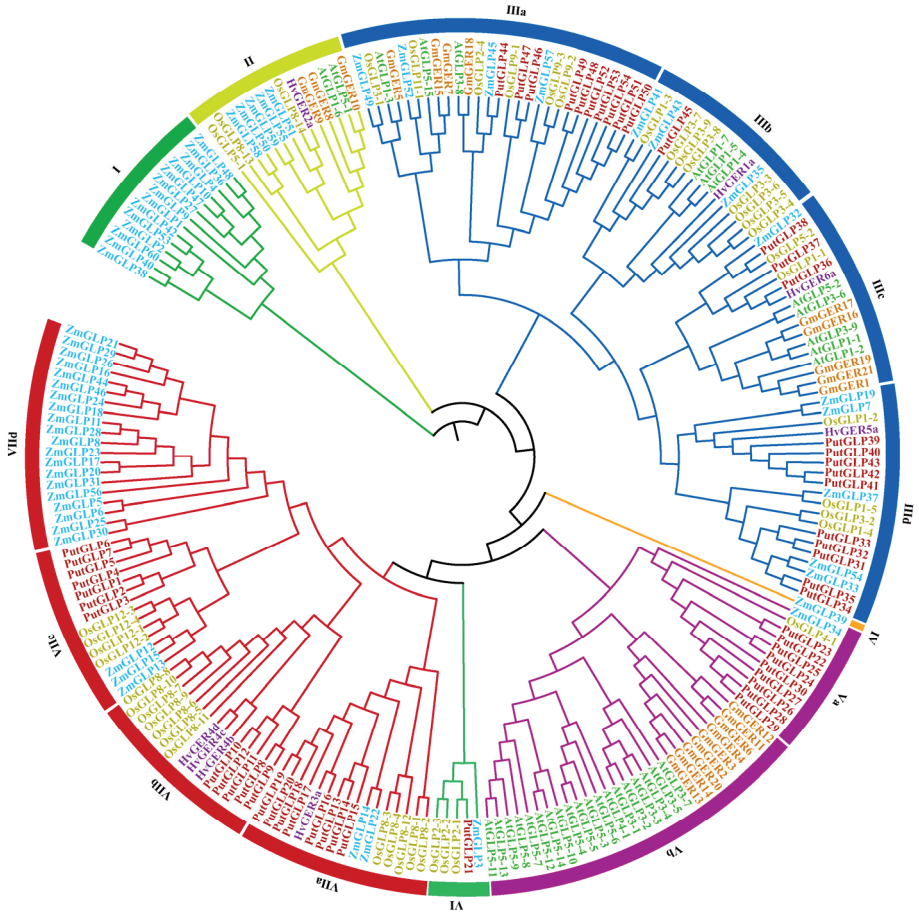

Figure 1. Phylogenetic tree constructed from GLP protein sequences of alkaligrass (*Puccinellia tenuiflora*), soybean (*Glycine max*), barley (*Hordeum vulgare*), *Arabidopsis* (*Arabidopsis thaliana*), rice (*Oryza sativa*), and maize (*Zea mays*). Different-colored circles represent distinct phylogenetic groups, whereas gene names are color-coded according to their respective species.

2.3. Chromosomal Distribution and Collinearity Analysis of the PutGLPs

Chromosomal distribution analysis revealed that 53 *PutGLP*s were unevenly distributed across all seven chromosomes of *P. tenuiflora* (Figure 2A). Chromosomes 1 and 3 each harbored four *PutGLPs*, while chromosomes 2, 4, and 6 contained seven, eight, and six *PutGLPs*, respectively, while chromosome 5 carried only two *PutGLPs*. Notably, chromosome 7 exhibited the highest density with 22 *PutGLP*s, accounting for 41.5% of the total.

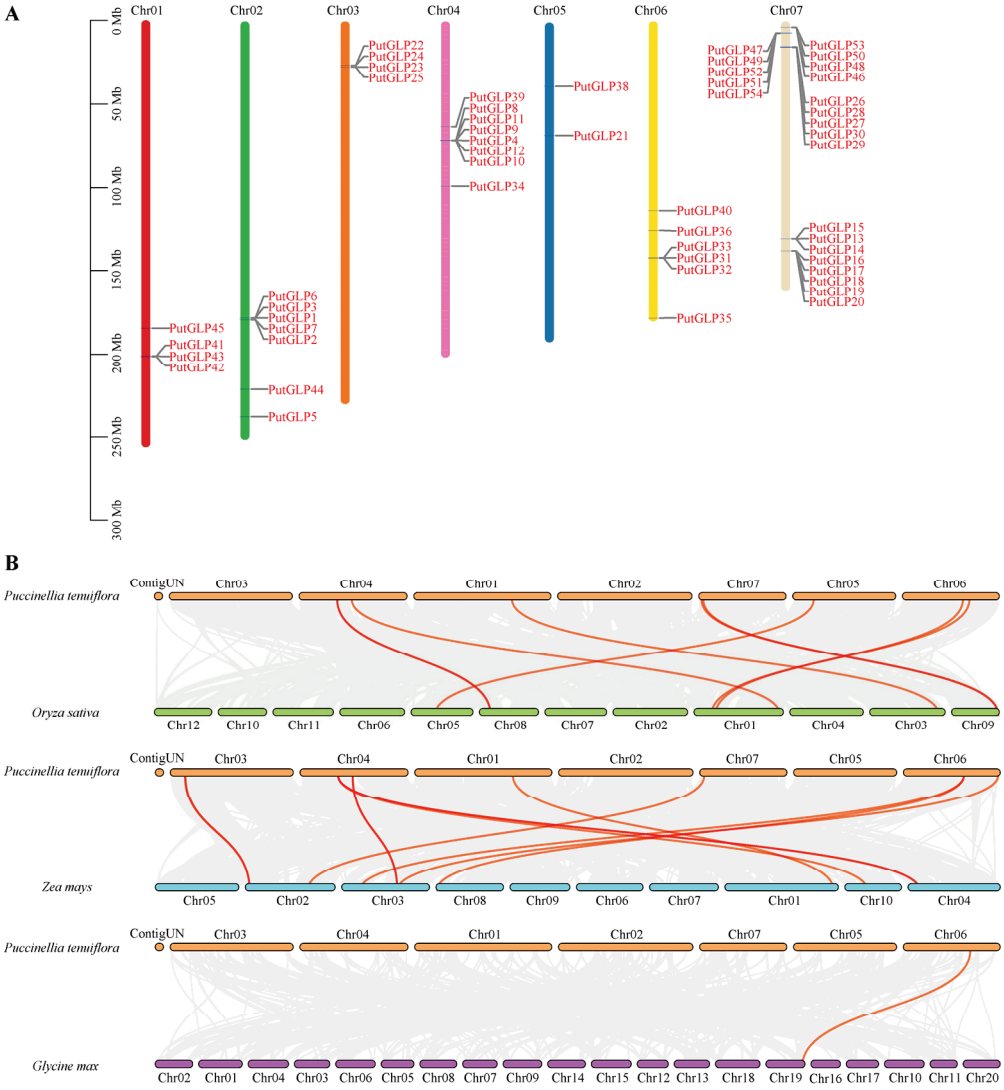

Figure 2. Chromosomal distribution and collinearity analysis of *PutGLP*s in *Puccinellia tenuiflora*. (**A**) Chromosomal localization of *PutGLPs* across the *P. tenuiflora* genome. (**B**) Comparative collinearity analysis of *GLPs* between alkaligrass (*P. tenuiflora*) and three angiosperm species, rice (*Oryza sativa*), maize (*Zea mays*), and soybean (*Glycine max*). Gray lines depict collinear genomic regions between *P. tenuiflora* and the reference species, while red lines specifically denote syntenic *GLP* gene pairs.

To elucidate evolutionary relationships, we performed collinearity analysis between *P. tenuiflora* and three related species (rice, maize, and soybean) (Figure 2B). The results identified nine orthologous *GLP* pairs between *P. tenuiflora* and rice, 11 pairs with maize, and one pair with soybean. Notably, *PutGLP54* showed homologous relationships with both *OsGLP9-1* and *ZmGLP57*, while *PutGLP36* exhibited homology with *OsGLP1-1* and *GmGER1*. The more homologous gene pairs from *PutGLPs* with rice and maize than

with soybean indicate closer phylogenetic affinity of *PutGLPs* to monocotyledons than to dicotyledons.

2.4. Gene Structure, Conserved Domain, and Motif Analysis of PutGLPs

To elucidate the structural and functional characteristics of the GLP gene family in *P. tenuiflora*, the gene structure, conserved domain, and conserved motif of *PutGLPs* were analyzed (Figure 3). A phylogenetic tree constructed from the *PutGLPs* divided them into five distinct clades (Figure 3A). Gene structure analysis revealed that *PutGLPs* contain one to four exons (Figure 3B). Motif prediction analysis identified three conserved domains: motif 1, motif 2, and motif 4, which encode the BoxB, BoxA, and BoxC domains, respectively (Figures 3C and S1). These motifs (motif 1, motif 2, and motif 4) were observed in all PutGLPs except PutGLP18 and PutGLP33. Multiple sequence alignment further confirmed that the GLP proteins contain BoxA, BoxB, and BoxC domains, with the cupin domain comprising BoxB and BoxC (Figures S2 and S3). Additionally, two conserved cysteine residues were identified in the aligned sequences (Figure S2).

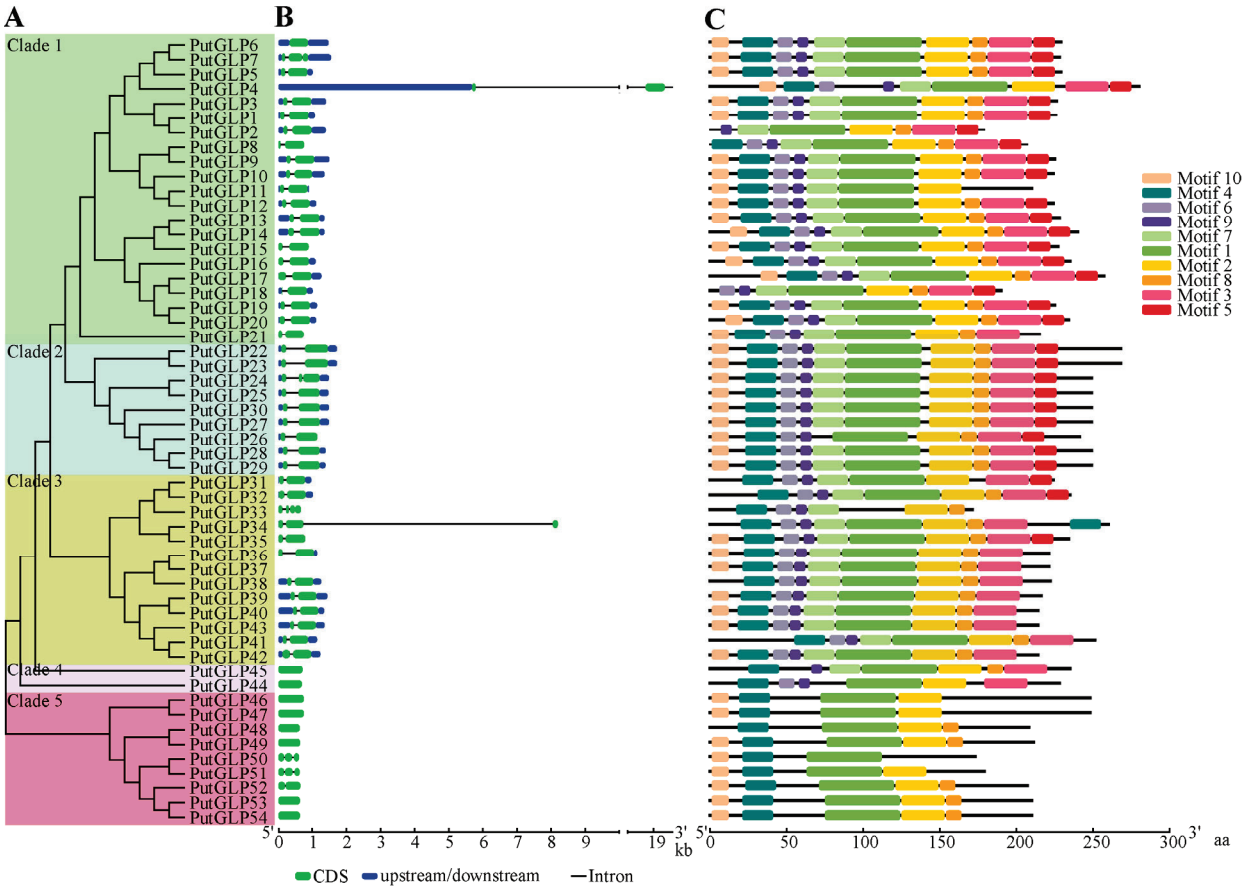

Figure 3. Phylogenetic, structural, and motif analysis of PutGLPs. (**A**) Neighbor-Joining phylogenetic tree of PutGLP proteins. Bootstrap values (1000 replicates) are labeled at branch nodes. (**B**) Genomic organization of *PutGLPs*. Structural components are annotated as follows: untranslated regions (UTRs, blue boxes), exons (green boxes), and introns (black lines). Scale bar indicates sequence length. (**C**) Distribution of conserved protein motifs. Ten motifs (Motif 1–10) are identified and color-coded with numerical identifiers. Motif positions are mapped to the corresponding protein sequences.

2.5. Analysis of Cis-Acting Elements of PutGLP Promoters

To better understand potential regulation and function of *PutGLPs*, we analyzed *cis*-acting elements within the 3000-bp upstream promoter regions of *PutGLP* members (Figure 4A,B). A total of 2619 *cis*-acting elements were identified and categorized into

three functional groups based on previous research [33]: plant growth and development, phytohormone regulation, and stress response. Stress-responsive elements constituted nearly half of all elements (1282/2619, 48.9%), with the G-box (10.84%) and STRE (8.29%) being the two most prevalent. Among phytohormone regulatory elements, abscisic acid (ABA)-responsive element (ABRE), TGACG-motif, and CGTCA-motif collectively accounted for the highest proportion (25.47%). Notably, ABRE was detected in all *PutGLP*s except *PutGLP52*. Within the plant growth and development category, nine elements were identified, of which AS-1 exhibited the highest proportion (7.75%).

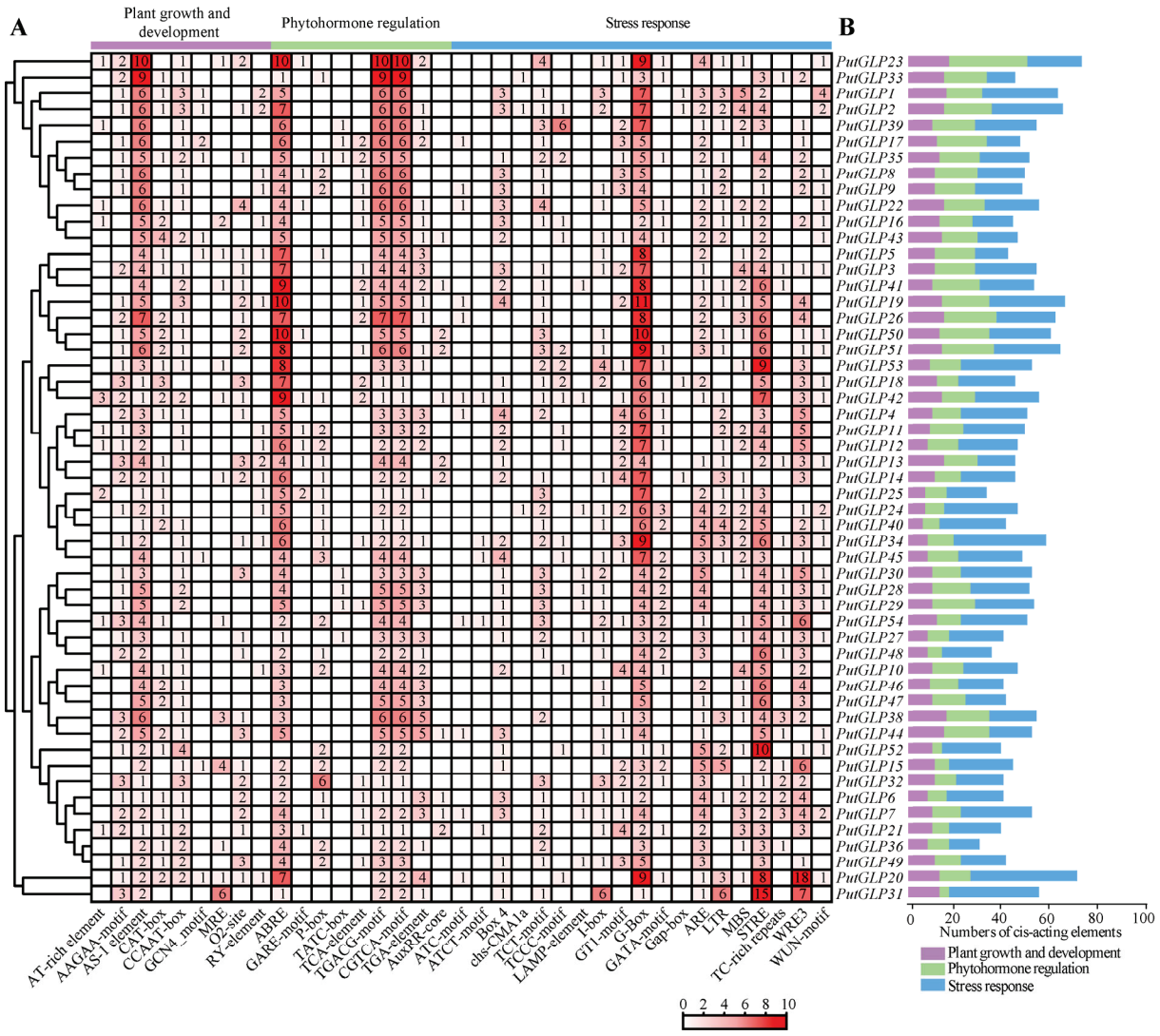

Figure 4. Quantitative and functional profiling of *cis*-acting elements in *PutGLP*s. (**A**) Heatmap visualization of *cis*-acting element abundance across *PutGLPs*. Element counts are color-coded (red intensity gradient) and numerically annotated in grid cells. (**B**) Functional classification of *cis*-acting elements. Grouped bar plots quantify elements associated with three biological processes, plant growth and development (purple), phytohormone regulation (green), and stress response (blue).

2.6. Subcellular Localization of PutGLP37 and Expression Profiles of PutGLPs in Various Organs

To determine the subcellular localization of PutGLP37, we performed transient expression assays in tobacco (*Nicotiana benthamiana*) leaves (Figure 5A). The coding sequence of *PutGLP37* was fused in-frame to the C-terminus of GFP under the control of the CaMV 35S promoter. Both the *35S::PutGLP37-GFP* fusion construct and *35S::GFP* control were transiently expressed in tobacco epidermal cells, respectively. Results revealed that the GFP-only control localized diffusely in the cytosol, nucleus, and plasma membrane

(PM). In contrast, PutGLP37-GFP was predominantly localized to the cell wall and PM (Figures 5A and S4).

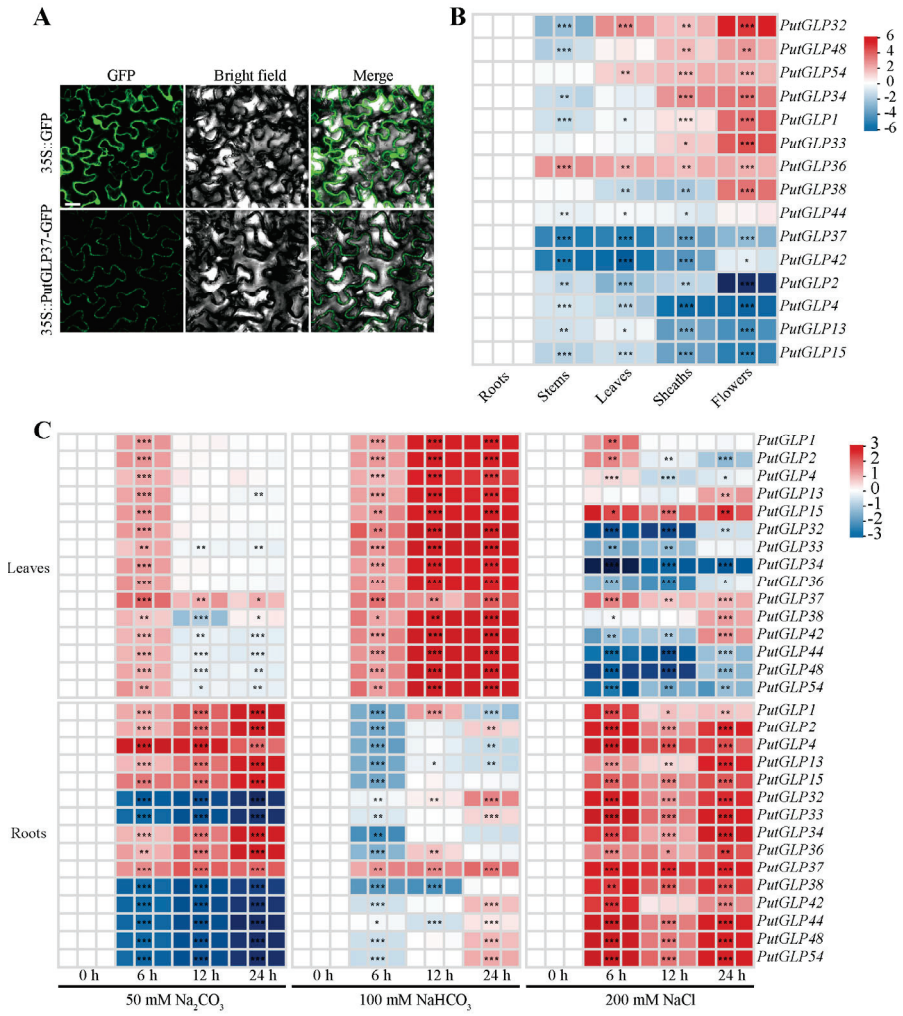

Figure 5. Subcellular localization and expression dynamics of *PutGLPs*. (**A**) Transient subcellular localization of PutGLP37 in *Nicotiana benthamiana* epidermal cells. Confocal micrographs show GFP fluorescence (green channel) from leaves co-infiltrated with *Agrobacterium tumefaciens* strains carrying either *35S::GFP* (vector control) or *35S::PutGLP37-GFP* constructs. Images were captured at 48 h post-infiltration. Scale bar = 25 µm. (**B**) Tissue-/Organ-specific expression profiles of 15 *PutGLPs*. Real-time quantitative PCR (RT-qPCR) analysis quantifies transcript abundance in five organs: roots, stems, leaves, sheaths, and flowers. Expression values were normalized to *PutActin* using the $2^{-\Delta\Delta Ct}$ method. (**C**) Salt stress-responsive regulation of *PutGLPs* in leaves and roots. Heatmaps display log_2-transformed fold-changes in expression levels under three sodium treatments: 50 mM Na_2CO_3, 200 mM NaCl, and 100 mM $NaHCO_3$, sampled at 0, 6, 12, and 24 h post-treatment. Color gradients (red: upregulation; blue: downregulation) reflect standardized expression relative to untreated controls (0 h). Significant differences compared to the control group were determined by Student's *t*-test, *** $p < 0.001$, ** $p < 0.01$, and * $p < 0.05$.

To investigate potential functional roles, we analyzed the expression patterns of *PutGLPs* across five tissues (roots, stems, leaves, sheaths, and flowers) using RT-qPCR (Figure 5B). Based on relative expression levels, *PutGLPs* were classified into three distinct groups. *PutGLP2*, *PutGLP4*, *PutGLP13*, *PutGLP15*, *PutGLP37*, and *PutGLP42* exhibited the highest expression in roots. *PutGLP1*, *PutGLP32*, *PutGLP33*, *PutGLP34*, *PutGLP38*, *PutGLP48*, and *PutGLP54* were predominantly expressed in flowers, while *PutGLP36* was exclusively expressed in stems.

2.7. Expression Patterns of PutGLPs in Roots and Leaves Under Various Abiotic Stresses

To validate the potential involvement of *PutGLPs* in stress responses suggested by *cis*-acting element analysis, we investigated the expression level of 15 *PutGLPs* in roots and leaves under various salt treatments including Na_2CO_3, NaCl, and $NaHCO_3$ (Figure 5C). In roots, Na_2CO_3 treatment led to upregulation in half of the 15 tested genes (8/15) and downregulation in the remaining half (7/15). Strikingly, all 15 genes exhibited varying degrees of upregulation under NaCl treatment. Under $NaHCO_3$ stress, 14 *PutGLPs* showed suppressed expression at 6 h, except *PutGLP37*. Notably, *PutGLP1* and *PutGLP36* reached peak expression levels at 12 h, while *PutGLP2*, *PutGLP32*, *PutGLP33*, *PutGLP37*, *PutGLP42*, *PutGLP44*, *PutGLP48*, and *PutGLP54* peaked at 24 h. In leaves, all 15 genes displayed maximal expression at 6 h under Na_2CO_3 treatment. Remarkably, *PutGLP15* and *PutGLP37* showed sustained upregulation throughout NaCl treatment, whereas all 15 genes were significantly upregulated at 12 h and 24 h under $NaHCO_3$ stress compared to the control.

2.8. Tolerance Analysis by Overexpressing PutGLP37 in Yeast and E. coli

To investigate the biological role of PutGLP37, we expressed this gene in yeast *(S. cerevisiae INVSc*1) and *E. coli*. Under non-stress conditions in YPD medium, the growth of *pYES2-PutGLP37* yeast strains was comparable to the *pYES2* empty vector control (Figure S5A). However, when exposed to osmotic stressors including 1.3 M NaCl, 26 mM $NaHCO_3$, or 12 mM Na_2CO_3, the *pYES2-PutGLP37* strains exhibited significantly enhanced growth relative to the control, indicating that PutGLP37 conferred tolerance to ionic and alkaline stresses. To further validate this stress-adaptive function, we overexpressed PutGLP37 in *E. coli* as well (Figure S5B). On Luria-Bertani (LB) agar plates supplemented with 100 mM or 250 mM NaCl, *E. coli* cells expressing *PutGLP37* showed markedly improved growth compared to the control strain. This phenotype was corroborated in liquid culture assays in liquid LB medium containing 250 mM NaCl; the *PutGLP37*-expressing strain displayed a significantly higher growth rate than the control (Figure S5C). These results demonstrate that PutGLP37 enhances NaCl stress tolerance in prokaryotic systems.

2.9. SOD and OXO Activity Assays of Recombinant PutGLP37 Protein

Previous studies have demonstrated that barley GLP proteins exhibit both OXO and SOD activities, which are critical for their defensive roles [34–36]. To assess whether PutGLP37 shares these enzymatic functions, we purified the recombinant protein and measured its SOD and OXO activities (Figure 6A,B). A semi-native PAGE gel assay confirmed that recombinant PutGLP37 was properly folded and enzymatically active, indicating potential SOD activity (Figure 6A). OXO activity was further evaluated using in-gel activity staining (Figure 6B). Incubation with oxalate revealed strong OXO activity in purified PutGLP37, whereas supplementation with the inhibitor glycolic acid significantly suppressed this activity, confirming reaction specificity.

2.10. Salt-Responsive Phenotype of PutGLP37-Overexpressing Arabidopsis Plants

To investigate the function of PutGLP37 in salt tolerance, we generated *PutGLP37*-overexpressing *Arabidopsis* plants under the control of the strong constitutive CaMV 35S promoter and compared survival rates between Col-0 and *PutGLP37*-overexpressing seedlings under NaCl treatment (Figure 6C,D). Under normal conditions, survival rates did not differ significantly between *PutGLP37*-overexpressing plants and Col-0 controls. In contrast, NaCl stress significantly increased green seedling survival in *PutGLP37*-overexpressing plants compared to Col-0, with the most pronounced difference observed under 150 mM NaCl. These results suggest that PutGLP37 may play a role in salt stress response mechanisms.

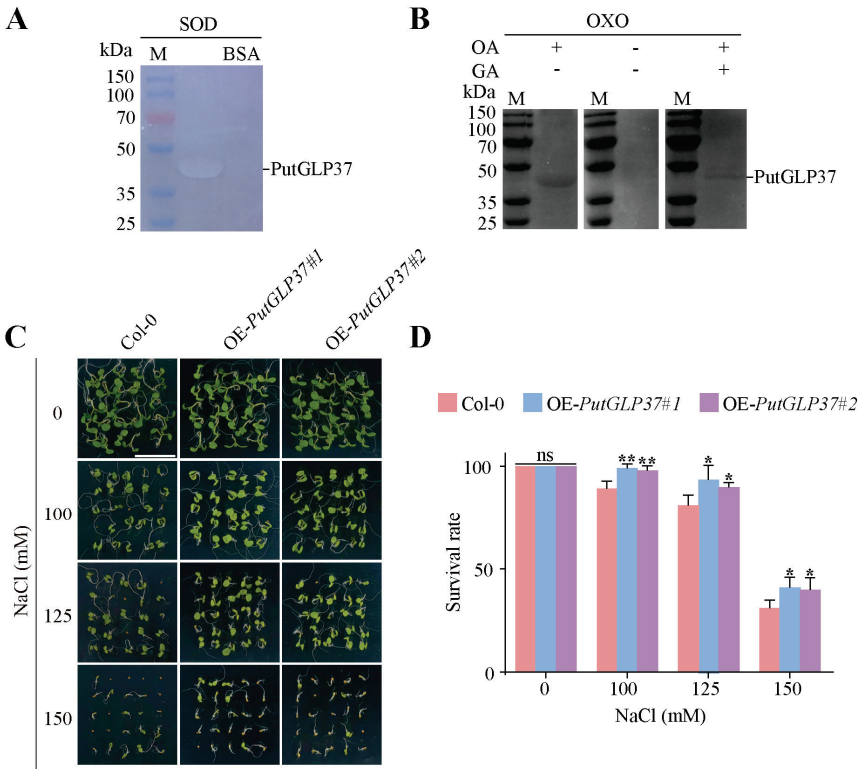

Figure 6. Functional characterization of PutGLP37 in enzymatic activities and salt stress phenotypes in transgenic *Arabidopsis*. (**A**) Superoxide dismutase (SOD) activity analysis. The semi-native PAGE showing SOD activity bands in PutGLP37 samples. Bovine serum albumin (BSA) served as negative control. (**B**) Oxalate oxidase (OXO) activity assay of PutGLP37 through in-gel activity staining. Reaction mixtures containing 2 mM oxalic acid (OA) or glycolic acid (GA) were incubated with purified protein. (**C**) Salt stress tolerance phenotypes of wild-type (Col-0) and *PutGLP37*-overexpression *Arabidopsis* lines. The seedlings grown under 22 °C were treated with 0–150 mM NaCl for 7 days under 16 h light/8 h dark conditions at 22 °C. (**D**) Survival rate quantification post-NaCl treatment. Each bar indicated the mean ± standard deviation (SD) (n = 4, significant differences compared to the control group were determined by Student's *t*-test, ** $p < 0.01$ and * $p < 0.05$; "ns" represents no significance).

3. Discussion

3.1. Evolutionary Expansion and Stress-Adaptive Innovation of the PutGLP Family in P. tenuiflora

Research on the GLP gene family in plants reveals evolutionary expansion of *GLPs*. Currently, this gene family has been characterized in 12 species, comprising dicotyledons such as soybean (*G. max*) (21 *GLPs*), longan (*D. longan*) (35 *GLPs*), Citrus (*C. sinensis*) (57 *GLPs*), peanut (*A. hypogaea*) (84 *GLPs*), melon (*C. melo*) (22 *GLPs*), rapeseed (*B. napus*) (77 *GLPs*), and cotton (*G. hirsutum*) (106 *GLPs*), monocotyledons such as maize (*Z. mays*) (60 *GLPs*), rice (*O. sativa*) (43 *GLPs*), barley (*H. vulgare*) (80 *GLPs*), and *Arabidopsis* (*A. thaliana*) (32 *GLPs*), and bryophytes moss (*P. patens*) (77 *GLPs*) [3,4,16,25–32]. In this study, 54 *PutGLPs* were systematically identified in the halophytic model species *P. tenuiflora* (Figure 1). Compared to species exhibiting *GLP* gene expansion (such as *B. napus*, moss, cotton, and barley), members of PutGLP gene family also show significant expansion, potentially reflecting genomic adaptations to extreme saline-alkaline habitats of *P. tenuiflora*.

Previous evolutionary analyses of rice GLP family showed that 23 rice *GLPs* and 13 *Arabidopsis GLPs* clustered together, whereas maize GLP family analysis revealed that distinct clustering of 32 rice and 41 maize *GLPs* [29,30]. Here, *PutGLPs* primarily clustered in Clade III (24 *GLPs*) and Clade VII (20 *GLPs*), with 47 and 25 monocot GLPs, respectively (Figure 1),

indicating monocot-specific orthology. Chromosomal distribution analyses further suggested that tandem duplication drives GLP family expansion across species. For instance, chromosome 2 contained 15 of 35 *GLPs* in *D. longan* [25], while 38 of 84 *GLPs* formed duplicated gene pairs in peanut [26]. Moreover, rice chromosome 8 harbored 14 of 43 *GLPs* in rice [30], *Arabidopsis* chromosome 5 carried 12 of 32 *GLPs* [30], while melon chromosome 8 contained 8 of 22 *GLPs* [27]. Here, we found the high density of *PutGLPs* on chromosome 7 (22 of 53) (Figure 2A). This suggests that gene family expansion of PutGLP gene family was highly likely to be driven by tandem duplication or chromosomal rearrangements.

Conserved cupin domains are essential for GLP function, enabling enzymatic activities such as OXO and SOD, as well as roles in plant development and defense [5]. These domains occur universally across GLPs in diverse species [3,4,16,25–32]. Our study confirms the conserved cupin domain is also ubiquitous within PutGLPs (Figure 3C), demonstrating its extensive conservation across the GLP family. This further underscores the conserved functional importance of cupin domains in fundamental enzymatic activities like OXO and SOD [37].

Promoter *cis*-acting elements critically govern gene expression patterns, stress responses, and biological functions, such as hormone-responsive elements (AREB) and stress-responsive elements (STRE) [38–40]. ABRE-binding transcription factors were reported to mediate ABA-triggered chlorophyll degradation and leaf senescence in *Arabidopsis* [39], while STREs were known to bind osmotic stress-responsive transcription factors [40]. Although prior analyses of the GLP gene family did not explicitly quantify ABREs and STREs, functional categories encompassing these elements were significantly enriched [25,26]. For instance, *DlGLP* promoters in longan exhibited enrichment for methyl jasmonate (MeJA)-response (70 elements), ABA-response (44 ABREs), and drought-inducible elements (35 elements) [25]. Furthermore, hormone-responsive elements and stress-responsive elements were also enriched in peanut [26]. Here, we identified 259 ABREs and 217 STREs in *PutGLP* promoters (Figure 4), indicating potent ABA-mediated regulation and osmotic stress responses. This conservation supports the role of *PutGLPs* in halophytic adaptation in *P. tenuiflora* [23].

3.2. Organ-Specific and Stress-Inducible Expression Patterns of PutGLPs

The members of GLP gene family exhibit tissue-/organ-specific expression patterns across diverse plant tissues, indicating their functional specialization for stress adaptation [25]. Approximately half of its 35 *GLPs* are highly expressed in roots in longan, whereas only four *GLPs* show root-specific expression in rapeseed [4,25]. The rice root germin-like protein (*OsRGLP1*) was induced by salinity stress, supporting its potential utility for developing transgenic crops with enhanced stress tolerance [41]. In our study, six *PutGLPs* exhibit root-predominant expression (Figure 5B), implying their involvement in root architecture and ion homeostasis essential for salt exclusion and osmoregulation in halophytes [22,42]. Moreover, five *GLPs* in melon exhibit peak expression in flowers, suggesting their functional significance in key developmental phases such as floral transition and fruit maturation [27]. Moreover, flower-enriched genes may also regulate salt stress responses. In alfalfa (*Medicago sativa*), the flavonol synthase gene *MsFLS13* exhibits flower-enriched expression and enhances saline-alkali stress tolerance [43]. Consequently, seven *PutGLPs* exhibiting both flower-enriched and NaCl-induced expression likely regulate floral reproductive traits and participate in the salt stress response during seed formation.

GLPs play a critical role in salt stress resistance across diverse species. Salt stress prolongs the expression of two *HvGLPs* in barley [44], and drives 11 *OsGLP* expression in rice [30]. Furthermore, salt stress induces peanut *AhGLP* expression, and overexpressing *AhGLP2* or *AhGLP3* in *Arabidopsis* enhances its salt tolerance [45]. Our study identified up-

regulated expression of 15 *PutGLPs* in roots exposed to NaCl stress and in leaves subjected to $NaHCO_3$ stress (Figure 5C). Notably, the sustained induction of *PutGLP15* in leaves under both NaCl and $NaHCO_3$ stress implies its role in long-term ionic stress adaptation. This functional conservation aligns with the phylogenetically related rice *OsGLP8-12* (Clade VIIa), where stress-responsive differential methylation occurs within promoter *cis*-acting elements, linking epigenetic modification to *OsGLP* regulation under drought and salinity conditions [46]. These results suggest *PutGLPs* play critical roles in plant salt stress response and tolerance.

3.3. Functional Significance of PutGLP37 in Salt Stress Adaptation

Notably, *PutGLP37*, identified through salt-tolerant yeast lines [47], was absent from the alkaligrass reference genome assembly, highlighting the challenges of resolving complex genomic regions in halophytes [48,49]. However, this absence sparked our interest in its functional verification. We found that PutGLP37 was localized to the cell wall (Figures 5A and S4), a pattern similar to that observed in peanut AhGLP2/5 and rice OsGLP2-1 [45,50], where it may participate in cell wall remodeling or ROS scavenging [51].

GLPs from various plant species have been reported to exhibit SOD or OXO activities, including rice OsGLP3-7 [12], *Capsicum chinense* CchGLP [52], *C. procera* CpGLP1/CpGLP2 [13], and *R. mucronatum* RmGLP2 [14]. The SOD activity neutralizes superoxide radicals (O_2^-) [53], while OXO activity generates H_2O_2 [54]. The dual SOD and OXO activities of recombinant PutGLP37 (Figure 6A,B) suggest functional conservation of its enzymatic activity. These imply that the dual SOD and OXO activities of PutGLP37 potentially maintain ROS homeostasis in response to stress conditions [6,12,19,25].

GLP family members exhibit multifunctional roles in coordinating plant growth and mediating defense against abiotic stress [31,55]. CRISPR/Cas9-mediated knockout of *OsGLP1* in rice resulted in UV-B-dependent lesion formation [56]. Under heat stress, rice *osger4* mutant lines exhibit significantly reduced crown root production compared to wild-type rice [57]. Overexpression of potato (*Solanum tuberosum*) *StGLP* boosts heat stress tolerance by elevating $H_2O_2^-$ triggered ROS scavenging and upregulating antioxidant enzymes in transgenic plants [6]. However, the involvement of *GLPs* in salt stress adaptation is lacking. In this study, overexpression of *PutGLP37* conferred NaCl tolerance in *Arabidopsis*, indicating its role in salt stress regulation (Figure 6C,D). In addition, enhanced survival of *PutGLP37*-overexpressing yeasts and *E. coli* under ionic and alkaline stresses demonstrates its conserved function across kingdoms (Figure S5) [31,56]. Furthermore, the universal presence of ABRE elements in *PutGLP* promoters (Figure 4) suggests that PutGLP37 likely enhances salt tolerance by integrating ABA signaling, potentially through modulating ion homeostasis and ROS scavenging [12,58]. Future studies should investigate PutGLP37's interactions with salt tolerance pathways (e.g., SOS or ABA) and cell wall components (e.g., pectin or lignin) [59–64].

4. Materials and Methods

4.1. Sequence Search and Identification of PutGLPs

The whole-genome sequence of *P. tenuiflora* was obtained from the Alkaligrass Genome Database V1.0 (http://xhhuanglab.cn/data/alkaligrass.html; accessed on 10 March 2025) [22]. Candidate *GLPs* were initially identified by performing a local BLASTp v2.14 search against the *Arabidopsis* GLP protein database (TAIR, https://www.arabidopsis.org/; accessed on 10 March 2025) by setting a cutoff value of 1×10^{-100} for the expected value (e-value). To refine the selection, domain-specific screening was conducted using HMMER 3.0 (http://hmmer.org/; accessed on 10 March 2025), employing the Cupin_1 domain (PF00190) from the Pfam database (http://pfam.xfam.org/; accessed on 10 March 2025) as a query.

Candidate proteins containing the Cupin_1 domain were further validated using NCBI-CDD (https://www.ncbi.nlm.nih.gov/cdd/; accessed on 10 March 2025) by setting the e-value to 0.01. Coding sequences (CDS), amino acid sequences, and genomic sequences of the identified *PutGLPs* were extracted for downstream analyses. Notably, *PutGLP37* was isolated from full-length cDNA libraries derived from salt-tolerant yeast strains. MW and theoretical pI of PutGLP proteins were predicted using the ExPASy ProtParam tool (https://web.expasy.org/compute_pi/; accessed on 12 March 2025). Subcellular localization was predicted using the Plant-mPLoc server (http://www.csbio.sjtu.edu.cn/bioinf/plant-multi/; accessed on 12 March 2025).

4.2. Phylogenetic and Classification Analysis of PutGLPs

The multiple sequence alignments of GLP proteins among six species, alkaligrass (*P. tenuiflora*), soybean (*G. max*), barley (*H. vulgare*), *Arabidopsis* (*A. thaliana*), rice (*O. sativa*), and maize (*Z. mays*), were initially analyzed using the MAFFT alignment program [65]. The databases include Alkaligrass Genome Database V1.0 (http://xhhuanglab.cn/data/alkaligrass.html; accessed on 10 March 2025), GenBank database (http://www.ncbi.nlm.nih.gov/Entrez/; accessed on 10 March 2025), Phytozome (https://phytozome-next.jgi.doe.gov/info/HvulgareMorex_V3; accessed on 10 March 2025), TAIR 10 (http://arabidopsis.org; accessed on 10 March 2025), RGAP 7 (http://rice.plantbiology.msu.edu/; accessed on 10 March 2025), and Phytozome (https://phytozome-next.jgi.doe.gov/info/Zmays_Zm_B73_REFERENCE_NAM_5_0_55; accessed on 10 March 2025). Subsequently, an unrooted phylogenetic tree was constructed through the Maximum Likelihood (ML) method implemented in FastTree version 2.1.11 by Jones-Taylor-Thornton (JTT) model [66], based on the alignment results. The phylogenetic tree was further refined and visualized using the Interactive Tree Of Life (iTOL) online platform [67].

4.3. Gene Structure and Conserved Motif Analysis of PutGLP Proteins

The exon/intron structures of *PutGLPs* were analyzed using the Gene Structure Display Server (GSDS 2.0, http://gsds.gao-lab.org/index.php; accessed on 13 March 2025) [68]. Conserved motifs in PutGLP proteins were identified using the Multiple Expectation Maximization for Motif Elicitation (MEME, https://meme-suite.org/meme/tools/meme; accessed on 13 March 2025), configured to detect a maximum of ten motifs [69].

4.4. Analysis of Cis-Acting Elements in PutGLP Promoters

Genomic DNA sequences spanning 3000 bp upstream of the transcription start site for each PutGLP gene family member were retrieved and analyzed for *cis*-acting elements using the PlantCARE online tool (http://bioinformatics.psb.ugent.be/webtools/plantcare/html/; accessed on 14 March 2025) [70]. Promoter *cis*-acting elements associated with plant growth and development, phytohormone regulation, and stress response were selected for detailed analysis.

4.5. Chromosomal Distribution and Collinearity Analysis of PutGLPs

Based on the *P. tenuiflora* genome annotation, chromosomal locations of *PutGLPs* (excluding *PutGLP37*) were determined. Their physical positions were mapped to chromosomes using TBtools (v2.322) software [71]. Interspecific collinearity analysis between *P. tenuiflora* and three related species (rice, maize, or soybean) was performed and visualized using TBtools to infer evolutionary relationships.

4.6. Plant Material and Abiotic Stress Treatment

Seeds of alkaligrass (*P. tenuiflora*) were germinated hydroponically on gauze-lined baskets under controlled conditions: fluorescent light (200 $\mu mol \cdot m^{-2} \cdot s^{-1}$ intensity, 12 h

light/12 h dark cycle), 25 °C daytime and 20 °C nighttime temperatures, and 75% relative humidity for 21 days. Seedlings were subsequently subjected to abiotic stress treatments by exposure to 50 mM Na_2CO_3, 200 mM NaCl, or 100 mM $NaHCO_3$ for durations of 0 h, 6 h, 12 h, and 24 h. Following treatment, leaf and root tissues were harvested, immediately flash-frozen in liquid nitrogen, and stored at −80 °C. For tissue-specific expression profiling, roots, stems, leaves, sheaths, and flowers were collected from mature plants at the reproductive stage.

4.7. RNA Extraction and Real-Time Quantitative PCR (RT-qPCR) Analysis

Total RNA was extracted from alkaligrass (*P. tenuiflora*) tissue samples using TRIzol™ reagent (Invitrogen). Complementary DNA (cDNA) was synthesized from the PrimeScript™ RT Reagent Kit with gDNA Eraser (TaKaRa, Tokyo, Japan). Gene-specific primers were designed using the Primer3 online tool (https://bioinfo.ut.ee/primer3-0.4.0/; accessed on 20 March 2025) and were listed in Table S4. RT-qPCR was performed on an ABI 7500 Real-Time PCR System (Thermo Fisher Scientific, Waltham, MA, USA) using SYBR® Green Master Mix (Vazyme), with the following cycling parameters: initial denaturation at 95 °C for 5 min, followed by 40 cycles of 95 °C for 15 s, 60 °C for 30 s, and 72 °C for 30 s. Relative transcript levels were quantified via the $2^{-\Delta\Delta Ct}$ method [72], normalized to the reference gene *PutActin*. Three biological replicates were analyzed per sample. Heatmaps of relative expression values were generated using TBtools.

4.8. Subcellular Localization Analysis

To determine subcellular localization, the CDS of PutGLP37 was amplified using gene-specific primers (Table S4) and subsequently cloned into the *pCAMBIA1300-GFP* expression vector under the control of the CaMV 35S promoter. The recombinant plasmid (*pCAMBIA1300-PutGLP37-GFP*) and the empty vector control (*pCAMBIA1300-GFP*) were separately expressed in *N. benthamiana* leaves via *Agrobacterium tumefaciens*-mediated transient transformation. After 48–72 h incubation, transformed leaf sections were plasmolyzed by immersion in 1 M mannitol solution for 30 min. GFP fluorescence was visualized using confocal microscopy. Three independent biological replicates were performed to confirm localization patterns.

4.9. Stress Tolerance Assay of Yeast Transformants Expressing PutGLP37

The CDS of *PutGLP37*, flanked by KpnI/XhoI restriction sites, was amplified and ligated into the *pYES2* expression vector, generating the recombinant plasmid pYES2-PutGLP37. Recombinant plasmids (*pYES2-PutGLP37* and empty *pYES2* control) were transformed into yeast (*S. cerevisiae INVSc*1). Transformed yeast strains were grown in YPD medium. Cultures were then serially diluted to 10^{-1}, 10^{-2}, 10^{-3}, and 10^{-4} times, and spotted onto YPD agar plates supplemented with 1.3 M NaCl, 26 mM $NaHCO_3$, and 12 mM Na_2CO_3. Untreated YPD plates served as controls. Stress tolerance was assessed by comparing growth between recombinant and control strains. Experiments included three independent biological replicates.

4.10. Production and Purification of Recombinant PutGLP37 Protein

The recombinant plasmid *pET32a-PutGLP37* was constructed by amplifying the *PutGLP37* coding sequence and inserting it into the linearized *pET32a* vector using BamHI and SalI restriction sites. The recombinant plasmid was transformed into chemically competent *E. coli* BL21 (DE3) cells. Recombinant strains were cultured overnight in LB medium supplemented with 100 μg/mL ampicillin at 37 °C with shaking (220 rpm). Bacterial cultures were diluted 6-fold in fresh LB medium and incubated at 37 °C until reaching OD_{600} = 0.6–0.8. Protein expression was induced by adding 1 mM isopropyl β-D-1-thiogalactopyranoside

(IPTG) under three temperature conditions: 16 °C for 20 h, 28 °C for 10 h, and 37 °C for 4 h. Based on comparative yield analysis, the optimal induction condition (1 mM IPTG at 37 °C for 4 h) was selected for large-scale protein production. His-tagged recombinant proteins were purified using a nickel-nitrilotriacetic acid (Ni-NTA) affinity column, following established protocols.

4.11. Salt Stress Tolerance Assay of E. coli Transformants Expressing PutGLP37

To assess salt tolerance, *E. coli* BL21 (DE3) cells harboring *pET32a-PutGLP37* were induced with 1 mM IPTG at 37 °C for 4 h. Cultures were serially diluted to 10^{-1}, 10^{-2}, and 10^{-3} and spotted onto LB agar plates supplemented with 0, 100, or 250 mM NaCl. *E. coli* BL21 (DE3) carrying the empty *pET32a* vector served as the control. For liquid culture assays, IPTG-induced *E. coli* transformants were inoculated in LB medium containing NaCl at 28 °C for 8 h. Bacterial growth was monitored by measuring OD_{600} at 2-h intervals over an 8-h period. All experiments included four independent biological replicates.

4.12. SOD and OXO Activity Assays of PutGLP37

SOD activity was assessed as described previously [73]. Briefly, proteins were separated by semi-native PAGE, and gels were immersed in 0.1 M potassium phosphate buffer (pH 7.8) containing 0.1 mg/mL riboflavin and 20 mg/mL nitroblue tetrazolium (NBT) under dark conditions. After negative staining, gels were rinsed twice with distilled water and exposed to light for 40 min to visualize activity bands. Bovine serum albumin (BSA) served as the negative control. OXO activity of PutGLP37 was analyzed through in-gel activity staining to detect oxalate-dependent H_2O_2 production. Horseradish peroxidase (HRP) was used to catalyze the oxidation of 4-chloro-1-naphthol (4CN) dye substrates in an ethanolic system [74]. Recombinant PutGLP37 protein was resolved via non-reducing 10% SDS-PAGE, after which gels were incubated at 25 °C for 1–3 h in a combined solution of substrate (2 mM oxalic acid, 100 mM succinate buffer pH 3.5, and 60% v/v ethanol) and developing solution (5 U/mL HRP and 0.5 mg/mL 4CN in sodium phosphate buffer pH 5.5). Oxalic acid served as the substrate and glycolic acid as the inhibitor. Experiments were performed in triplicate.

4.13. Salinity Tolerance Analysis of PutGLP37-Overexpressing Transgenic Arabidopsis

A. tumefaciens strain EHA105 harboring the *pCAMBIA1300-PutGLP37-GFP* plasmid was introduced into *Arabidopsis* Col-0 plants via the floral dip method to generate *PutGLP37*-overexpressing transgenic lines. Transgenic seedlings were selected over three successive generations on half-strength Murashige and Skoog (1/2 MS) agar medium containing 30 μg mL^{-1} hygromycin. Homozygous T_3 lines were validated for *PutGLP37* expression levels using RT-qPCR with gene-specific primers (Table S4), and the lines exhibiting the highest expression were chosen for salinity tolerance assays. For salt stress analysis, Col-0 and *PutGLP37*-overexpressing seedlings were germinated and grown on 1/2 MS medium either control (0 mM NaCl) or 100 mM, 125 mM, or 150 mM NaCl under controlled conditions (22 °C/16 h light, 20 °C/8 h dark, 75% relative humidity) for seven days. Post-treatment survival rates were quantified to assess salt tolerance. The experiment was performed with three independent biological replicates.

4.14. Statistical Analysis

Statistical analyses were performed using GraphPad Prism 6. Data are shown as the means ± SD. Significant differences compared to the control group were determined by Student's *t*-test, *** $p < 0.001$, ** $p < 0.01$, and * $p < 0.05$.

5. Conclusions

This study elucidates the evolutionary expansion and functional diversification of the PutGLP gene family in the halophyte *P. tenuiflora*. The *PutGLPs* exhibit significant expansion driven by tandem duplication on chromosome 7, implying the genomic plasticity underlying stress adaptation in alkaligrass. Collinearity, gene structure, and motif analyses reveal monocot-specific conservation among *PutGLPs*. Stress-responsive *cis*-acting elements and tissue-/organ-specific expression patterns highlight roles of *PutGLPs* in stress adaptation, particularly in root ion homeostasis and floral resilience. Dynamic responses to salt stresses revealed that *PutGLPs* could be involved in distinct signaling pathways for ionic and alkaline stress. Functional characterization demonstrates that cell wall-localized PutGLP37 possesses dual enzymatic activity and is critical for salt adaptation as evidenced by heterologous expression in yeast (*S. cerevisiae INVSc*1), *E. coli*, and transgenic *Arabidopsis*. These findings advance our understanding of GLP multifunctionality in *P. tenuiflora* stress tolerance and provide a foundation for molecular engineering of salt-tolerant crops.

Supplementary Materials: The following supporting information can be downloaded at: https://www.mdpi.com/article/10.3390/plants14152259/s1, Figure S1: Sequence logos depicting conserved amino acid residues across the ten identified protein motifs; Figure S2: Multiple sequence alignment of PutGLPs. The atypical Cupin domain was marked; Figure S3: Multiple sequence alignment of PutGLP37 with orthologous germin-like proteins: OsGLP1-1 (*Oryza sativa*), OsGLP5-2 (*O. sativa*), ZmGLP32 (*Zea mays*), and HvGER6v (*Hordeum vulgare*). The atypical Cupin domain and conserved cysteine residues were marked; Figure S4: Plasmolysis of *Nicotiana benthamiana* cells expressing PutGLP37-GFP. Scale bar = 25 μm; Figure S5: Heterologous expression of PutGLP37 enhances salt stress tolerance in yeast (*Saccharomyces cerevisiae INVSc*1) and *Escherichia coli*. (A) Yeast complementation assay under sodium stress. Recombinant strains harboring *pYES2-PutGLP37* or empty vector (EV, *pYES2*) were serially diluted (10^{-1} to 10^{-4}) and spotted on YPD agar plates containing 1.3 M NaCl, 26 mM $NaHCO_3$, and 12 mM Na_2CO_3. Plates were incubated at 30 °C for 48–72 h. Scale bar = 1 cm. (B) *E. coli* BL21 (DE3) survival assay on Luria-Bertani (LB) solid medium. Transformants expressing *pET32a-PutGLP37* or EV (*pET32a*) were plated with 10-fold serial dilutions (10^{-1} to 10^{-3}) under NaCl gradients (0, 100, 250 mM). Scale bar = 1 cm. (C) Growth kinetics of *E. coli* BL21 (DE3) strains in liquid LB medium supplemented with 250 mM NaCl. Growth was monitored at 28 °C for 8 h. Optical density (OD600) was recorded hourly. EV transformants served as negative controls. Data represents mean ± standard deviation (SD) (n = 4, significant differences compared to the control group were determined by Student's *t*-test, *** $p < 0.001$, ** $p < 0.01$, and * $p < 0.05$); Table S1: Basic characteristics of *GLP* gene family in *Puccinellia tenuiflora*; Table S2: Protein sequences of GLP in soybean (*Glycine max*), barley (*Hordeum vulgare*), *Arabidopsis* (*Arabidopsis thaliana*), rice (*Oryza sativa*), alkaligrass (*Puccinellia tenuiflora*), and maize (*Zea mays*); Table S3: List of *GLP* orthologous gene pairs identified between alkaligrass (*Puccinellia tenuiflora*) and three angiosperm species, rice (*Oryza sativa*), maize (*Zea mays*), and soybean (*Glycine max*); Table S4: Primer sequences were designed for both RT-qPCR analysis of *GLP* gene expression and vector construction of *PutGLP37* in *Puccinellia tenuiflora*.

Author Contributions: Conceptualization, S.D., M.S. and Y.L. (Ying Li); data curation, Y.L. (Yueyue Li), Z.Z. and B.L.; formal analysis, Y.L. (Yueyue Li) and Z.Z.; funding acquisition, S.D.; investigation, S.D., Y.L. (Ying Li), Y.L. (Yueyue Li), Z.Z. and B.L.; methodology, S.D., Y.L. (Ying Li), Y.L. (Yueyue Li) and Z.Z.; project administration, S.D., M.S. and Y.L. (Ying Li); resources, Y.L. (Yueyue Li), Z.Z. and B.L.; software, Y.L. (Yueyue Li), Z.Z., H.Z. and Z.W.; supervision, S.D., M.S. and Y.L. (Ying Li); writing—original draft, S.D., Y.L. (Yueyue Li) and Z.Z.; writing—review and editing, S.D., Y.L. (Yueyue Li) and Z.Z. All authors have read and agreed to the published version of the manuscript.

Funding: This work was funded by the National Natural Science Foundation of China (No. 32441006 and 32070300); and the Fund of Shanghai Engineering Research Center of Plant Germplasm Resources, China (No. 17DZ2252700) to Shaojun Dai.

Data Availability Statement: Data are contained within the article and Supplementary Materials.

Conflicts of Interest: The authors declare no conflicts of interest.

References

1. Breen, J.; Bellgard, M. Germin-like proteins (GLPs) in cereal genomes: Gene clustering and dynamic roles in plant defence. *Funct. Integr. Genom.* **2010**, *10*, 463–476. [CrossRef]
2. Ilyas, M.; Rasheed, A.; Mahmood, T. Functional characterization of germin and germin-like protein genes in various plant species using transgenic approaches. *Biotechnol. Lett.* **2016**, *38*, 1405–1421. [CrossRef] [PubMed]
3. Tahir Ul Qamar, M.; Fatima, K.; Rao, M.J.; Tang, Q.; Sadaqat, M.; Ding, B.; Chen, L.L.; Zhu, X.T. Comparative genomics profiling of *Citrus* species reveals the diversity and disease responsiveness of the GLP pangenes family. *BMC Plant Biol.* **2025**, *25*, 388. [CrossRef] [PubMed]
4. Zhang, Q.; Wang, L.; Wang, X.; Qiao, J.; Wang, H. Roles of germin-like protein family in response to seed germination and shoot branching in *Brassica napus*. *Int. J. Mol. Sci.* **2024**, *25*, 11518. [CrossRef] [PubMed]
5. Patnaik, D.; Khurana, P. Germins and germin like proteins: An overview. *Indian J. Exp. Biol.* **2001**, *39*, 191–200.
6. Gangadhar, B.H.; Mishra, R.K.; Kappachery, S.; Baskar, V.; Venkatesh, J.; Nookaraju, A.; Thiruvengadam, M. Enhanced thermotolerance in transgenic potato (*Solanum tuberosum* L.) overexpressing hydrogen peroxide-producing germin-like protein (GLP). *Genomics* **2021**, *113*, 3224–3234. [CrossRef]
7. To, H.T.M.; Pham, D.T.; Le Thi, V.A.; Nguyen, T.T.; Tran, T.A.; Ta, A.S.; Chu, H.H.; Do, P.T. The germin-like protein *OsGER4* is involved in promoting crown root development under exogenous jasmonic acid treatment in rice. *Plant J.* **2022**, *112*, 860–874. [CrossRef]
8. Wang, H.; Zhang, Y.; Xiao, N.; Zhang, G.; Wang, F.; Chen, X.; Fang, R. Rice *GERMIN-LIKE PROTEIN 2-1* functions in seed dormancy under the control of abscisic acid and gibberellic acid signaling pathways. *Plant Physiol.* **2020**, *183*, 1157–1170. [CrossRef]
9. Pei, Y.; Li, X.; Zhu, Y.; Ge, X.; Sun, Y.; Liu, N.; Jia, Y.; Li, F.; Hou, Y. *GhABP19*, a novel germin-like protein from *Gossypium hirsutum*, plays an important role in the regulation of resistance to *Verticillium* and *Fusarium wilt* pathogens. *Front. Plant Sci.* **2019**, *10*, 583. [CrossRef]
10. Lane, B.G.; Dunwell, J.M.; Ray, J.A.; Schmitt, M.R.; Cuming, A.C. Germin, a protein marker of early plant development, is an oxalate oxidase. *J. Biol. Chem.* **1993**, *268*, 12239–12242. [CrossRef]
11. Yamahara, T.; Shiono, T.; Suzuki, T.; Tanaka, K.; Takio, S.; Sato, K.; Yamazaki, S.; Satoh, T. Isolation of a germin-like protein with manganese superoxide dismutase activity from cells of a moss, *Barbula unguiculata*. *J. Biol. Chem.* **1999**, *274*, 33274–33278. [CrossRef]
12. Sun, B.; Li, W.; Ma, Y.; Yu, T.; Huang, W.; Ding, J.; Yu, H.; Jiang, L.; Zhang, J.; Lv, S.; et al. *OsGLP3-7* positively regulates rice immune response by activating hydrogen peroxide, jasmonic acid, and phytoalexin metabolic pathways. *Mol. Plant Pathol.* **2023**, *24*, 248–261. [CrossRef] [PubMed]
13. Freitas, C.D.T.; Freitas, D.C.; Cruz, W.T.; Porfírio, C.; Silva, M.Z.R.; Oliveira, J.S.; Carvalho, C.P.S.; Ramos, M.V. Identification and characterization of two germin-like proteins with oxalate oxidase activity from *Calotropis procera* latex. *Int. J. Biol. Macromol.* **2017**, *105*, 1051–1061. [CrossRef]
14. Sakamoto, A.; Nishimura, T.; Miyaki, Y.I.; Watanabe, S.; Takagi, H.; Izumi, S.; Shimada, H. In vitro and in vivo evidence for oxalate oxidase activity of a germin-like protein from azalea. *Biochem. Bioph. Res.* **2015**, *458*, 536–542. [CrossRef] [PubMed]
15. da Cruz, W.T.; Bezerra, E.H.S.; Grangeiro, T.B.; Lopes, J.L.S.; Silva, M.Z.R.; Ramos, M.V.; Rocha, B.A.M.; Oliveira, J.S.; Freitas, D.C.; Freitas, C.D.T. Structural and enzymatic characterization of Peruvianin-I, the first germin-like protein with proteolytic activity. *Int. J. Biol. Macromol.* **2019**, *126*, 1167–1176. [CrossRef] [PubMed]
16. Lu, M.; Han, Y.P.; Gao, J.G.; Wang, X.J.; Li, W.B. Identification and analysis of the germin-like gene family in soybean. *BMC Genom.* **2010**, *11*, 620. [CrossRef]
17. Nguyen, T.T.; Nguyen, T.C.; Do, P.T.; To, H.T.M. Effect of gibberellin on crown root development in the mutant of the rice plasmodesmal germin-like protein *OsGER4*. *Funct. Integr. Genom.* **2024**, *24*, 59. [CrossRef]
18. Ham, B.K.; Li, G.; Kang, B.H.; Zeng, F.; Lucas, W.J. Overexpression of *Arabidopsis* plasmodesmata germin-like proteins disrupts root growth and development. *Plant Cell* **2012**, *24*, 3630–3648. [CrossRef]
19. Giarola, V.; Chen, P.; Dulitz, S.J.; König, M.; Manduzio, S.; Bartels, D. The dehydration- and ABA-inducible germin-like protein *CpGLP1* from *Craterostigma plantagineum* has SOD activity and may contribute to cell wall integrity during desiccation. *Planta* **2020**, *252*, 84. [CrossRef]
20. Beracochea, V.C.; Almasia, N.I.; Peluffo, L.; Nahirñak, V.; Hopp, E.H.; Paniego, N.; Heinz, R.A.; Vazquez-Rovere, C.; Lia, V.V. Sunflower germin-like protein *HaGLP1* promotes ROS accumulation and enhances protection against fungal pathogens in transgenic *Arabidopsis thaliana*. *Plant Cell Rep.* **2015**, *34*, 1717–1733. [CrossRef]

21. Xiao, T.; ShangGuan, X.; Wang, Y.; Tian, Z.; Peng, K.; Shen, Z.; Hu, Z.; Xia, Y. The germin-like protein *OsGLP8-7* is involved in lignin synthesis for acclimation to copper toxicity in rice. *J. Plant Physiol.* **2024**, *303*, 154335. [CrossRef]
22. Zhang, W.; Liu, J.; Zhang, Y.; Qiu, J.; Li, Y.; Zheng, B.; Hu, F.; Dai, S.; Huang, X. A high-quality genome sequence of alkaligrass provides insights into halophyte stress tolerance. *Sci. China Life Sci.* **2020**, *63*, 1269–1282. [CrossRef]
23. Zhang, X.; Wei, L.; Wang, Z.; Wang, T. Physiological and molecular features of *Puccinellia tenuiflora* tolerating salt and alkaline-salt stress. *J. Integr. Plant Biol.* **2013**, *55*, 262–276. [CrossRef] [PubMed]
24. Zhang, W.D.; Wang, P.; Bao, Z.; Ma, Q.; Duan, L.J.; Bao, A.K.; Zhang, J.L.; Wang, S.M. SOS1, HKT1;5, and NHX1 synergistically modulate Na^+ homeostasis in the halophytic grass *Puccinellia tenuiflora*. *Front. Plant Sci.* **2017**, *8*, 576. [CrossRef] [PubMed]
25. Li, Z.; Fu, Z.; Zhang, S.; Zhang, X.; Xue, X.; Chen, Y.; Zhang, Z.; Lai, Z.; Lin, Y. Genome-wide analysis of the GLP gene family and overexpression of *GLP1-5-1* to promote lignin accumulation during early somatic embryo development in *Dimocarpus longan*. *BMC Genom.* **2023**, *24*, 138. [CrossRef]
26. Yang, Q.; Sharif, Y.; Zhuang, Y.; Chen, H.; Zhang, C.; Fu, H.; Wang, S.; Cai, T.; Chen, K.; Raza, A.; et al. Genome-wide identification of germin-like proteins in peanut (*Arachis hypogea* L.) and expression analysis under different abiotic stresses. *Front. Plant Sci.* **2022**, *13*, 1044144. [CrossRef] [PubMed]
27. Zhang, Z.; Wen, Y.; Yuan, L.; Zhang, Y.; Liu, J.; Zhou, F.; Wang, Q.; Hu, X. Genome-wide identification, characterization, and expression analysis related to low-temperature stress of the CmGLP gene family in *Cucumis melo* L. *Int. J. Mol. Sci.* **2022**, *23*, 8190. [CrossRef]
28. Jin, Y.; Fan, L.; Zhang, Y.; Hu, W.; Han, X.; Yan, Q.; Yang, J.; Li, F.; Yang, Z. Functional divergence of GLP genes between *G. barbadense* and *G. hirsutum* in response to *Verticillium dahliae* infection. *Genomics* **2022**, *114*, 110470. [CrossRef]
29. Mao, L.; Ge, L.; Ye, X.; Xu, L.; Si, W.; Ding, T. *ZmGLP1*, a Germin-like protein from maize, plays an important role in the regulation of pathogen resistance. *Int. J. Mol. Sci.* **2022**, *23*, 14316. [CrossRef]
30. Li, L.; Xu, X.; Chen, C.; Shen, Z. Genome-wide characterization and expression analysis of the germin-like protein family in rice and *Arabidopsis*. *Int. J. Mol. Sci.* **2016**, *17*, 1622. [CrossRef]
31. Karlik, E. Potential stress tolerance roles of barley germins and GLPs. *Dev. Genes Evol.* **2021**, *231*, 109–118. [CrossRef]
32. Nakata, M.; Watanabe, Y.; Sakurai, Y.; Hashimoto, Y.; Matsuzaki, M.; Takahashi, Y.; Satoh, T. Germin-like protein gene family of a moss, *Physcomitrella patens*, phylogenetically falls into two characteristic new clades. *Plant Mol. Biol.* **2004**, *56*, 381–395. [CrossRef]
33. Abdullah, M.; Cheng, X.; Cao, Y.; Su, X.; Manzoor, M.A.; Gao, J.; Cai, Y.; Lin, Y. Zinc finger-homeodomain transcriptional factors (ZHDs) in upland cotton (*Gossypium hirsutum*): Genome-wide identification and expression analysis in fiber development. *Front. Genet.* **2018**, *9*, 357. [CrossRef] [PubMed]
34. Park, C.J.; An, J.M.; Shin, Y.C.; Kim, K.J.; Lee, B.J.; Paek, K.H. Molecular characterization of pepper germin-like protein as the novel PR-16 family of pathogenesis-related proteins isolated during the resistance response to viral and bacterial infection. *Planta* **2004**, *219*, 797–806. [CrossRef]
35. Woo, E.J.; Dunwell, J.M.; Goodenough, P.W.; Marvier, A.C.; Pickersgill, R.W. Germin is a manganese containing homohexamer with oxalate oxidase and superoxide dismutase activities. *Nat. Struct. Biol.* **2000**, *7*, 1036–1040. [CrossRef]
36. Manosalva, P.M.; Davidson, R.M.; Liu, B.; Zhu, X.; Hulbert, S.H.; Leung, H.; Leach, J.E. A germin-like protein gene family functions as a complex quantitative trait locus conferring broad-spectrum disease resistance in rice. *Plant Physiol.* **2009**, *149*, 286–296. [CrossRef]
37. Barman, A.R.; Banerjee, J. Versatility of germin-like proteins in their sequences, expressions, and functions. *Funct. Integr. Genom.* **2015**, *15*, 533–548. [CrossRef]
38. Osakabe, Y.; Yamaguchi-Shinozaki, K.; Shinozaki, K.; Tran, L.P. ABA control of plant macroelement membrane transport systems in response to water deficit and high salinity. *New Phytol.* **2014**, *202*, 35–49. [CrossRef]
39. Gao, S.; Gao, J.; Zhu, X.; Song, Y.; Li, Z.; Ren, G.; Zhou, X.; Kuai, B. ABF2, ABF3, and ABF4 promote ABA-mediated chlorophyll degradation and leaf senescence by transcriptional activation of chlorophyll catabolic genes and senescence-associated genes in *Arabidopsis*. *Mol. Plant* **2016**, *9*, 1272–1285. [CrossRef]
40. Hong, S.Y.; Roze, L.V.; Wee, J.; Linz, J.E. Evidence that a transcription factor regulatory network coordinates oxidative stress response and secondary metabolism in aspergilli. *Microbiol. Open* **2013**, *2*, 144–160. [CrossRef]
41. Ilyas, M.; Akhtar, W.; Rehman, S.; Naqvi, S.M.S.; Mahmood, T. Functional characterization of the rice root germin-like protein gene-1 (*OsRGLP1*) promoter in *Nicotiana tabacum*. *3 Biotech* **2019**, *9*, 130. [CrossRef]
42. Suo, J.; Zhang, H.; Zhao, Q.; Zhang, N.; Zhang, Y.; Li, Y.; Song, B.; Yu, J.; Cao, J.; Wang, T.; et al. Na_2CO_3-responsive photosynthetic and ROS scavenging mechanisms in chloroplasts of alkaligrass revealed by phosphoproteomics. *Genom. Proteom. Bioinf* **2020**, *18*, 271–288. [CrossRef]
43. Zhang, L.; Sun, Y.; Ji, J.; Zhao, W.; Guo, W.; Li, J.; Bai, Y.; Wang, D.; Yan, Z.; Guo, C. Flavonol synthase gene *MsFLS13* regulates saline-alkali stress tolerance in alfalfa. *Crop J.* **2023**, *11*, 1218–1229. [CrossRef]
44. Hurkman, W.J.; Tao, H.P.; Tanaka, C.K. Germin-like polypeptides increase in barley roots during salt stress. *Plant Physiol.* **1991**, *97*, 366–374. [CrossRef]

45. Wang, T.; Chen, X.; Zhu, F.; Li, H.; Li, L.; Yang, Q.; Chi, X.; Yu, S.; Liang, X. Characterization of peanut germin-like proteins, *AhGLPs* in plant development and defense. *PLoS ONE* **2013**, *8*, e61722. [CrossRef]
46. Anum, J.; O'Shea, C.; Skriver, K.; Saeed, M.; Hyder, M.; Farrakh, S.; Yasmin, T. The promoters of *OsGLP* genes exhibited differentially methylated sites under drought and salt stress in rice cultivars. *Euphytica* **2023**, *219*, 42. [CrossRef]
47. Li, Y.; Takano, T.; Liu, S. Discovery and characterization of two novel salt-tolerance genes in *Puccinellia tenuiflora*. *Int. J. Mol. Sci.* **2014**, *15*, 16469–16483. [CrossRef]
48. Du, H.; Liang, C. Assembly of chromosome-scale contigs by efficiently resolving repetitive sequences with long reads. *Nat. Commun.* **2019**, *10*, 5360. [CrossRef]
49. Zerpa-Catanho, D.; Zhang, X.; Song, J.; Hernandez, A.G.; Ming, R. Ultra-long DNA molecule isolation from plant nuclei for ultra-long read genome sequencing. *STAR Protoc.* **2021**, *2*, 100343. [CrossRef]
50. Liu, Q.; Yang, J.; Yan, S.; Zhang, S.; Zhao, J.; Wang, W.; Yang, T.; Wang, X.; Mao, X.; Dong, J.; et al. The germin-like protein *OsGLP2-1* enhances resistance to fungal blast and bacterial blight in rice. *Plant Mol. Biol.* **2016**, *92*, 411–423. [CrossRef]
51. Zhao, C.; Jiang, W.; Zayed, O.; Liu, X.; Tang, K.; Nie, W.; Li, Y.; Xie, S.; Li, Y.; Long, T.; et al. The LRXs-RALFs-FER module controls plant growth and salt stress responses by modulating multiple plant hormones. *Natl. Sci. Rev.* **2021**, *8*, nwaa149. [CrossRef]
52. León-Galván, F.; de Jesús Joaquín-Ramos, A.; Torres-Pacheco, I.; Barba de la Rosa, A.P.; Guevara-Olvera, L.; González-Chavira, M.M.; Ocampo-Velazquez, R.V.; Rico-García, E.; Guevara-González, R.G. A germin-like protein gene (*CchGLP*) of *Capsicum chinense* Jacq. is induced during incompatible interactions and displays Mn-superoxide dismutase activity. *Int. J. Mol. Sci.* **2011**, *12*, 7301–7313. [CrossRef]
53. Rietz, S.; Bernsdorff, F.E.; Cai, D. Members of the germin-like protein family in *Brassica napus* are candidates for the initiation of an oxidative burst that impedes pathogenesis of *Sclerotinia sclerotiorum*. *J. Exp. Bot.* **2012**, *63*, 5507–5519. [CrossRef] [PubMed]
54. Hu, X.; Bidney, D.L.; Yalpani, N.; Duvick, J.P.; Crasta, O.; Folkerts, O.; Lu, G. Overexpression of a gene encoding hydrogen peroxide-generating oxalate oxidase evokes defense responses in sunflower. *Plant Physiol.* **2003**, *133*, 170–181. [CrossRef] [PubMed]
55. Banerjee, J.; Maiti, M.K. Functional role of rice germin-like protein1 in regulation of plant height and disease resistance. *Biochem. Bioph. Res. Co.* **2010**, *394*, 178–183. [CrossRef]
56. He, Z.D.; Tao, M.L.; Leung, D.W.M.; Yan, X.Y.; Chen, L.; Peng, X.X.; Liu, E.E. The rice germin-like protein *OsGLP1* participates in acclimation to UV-B radiation. *Plant Physiol.* **2021**, *186*, 1254–1268. [CrossRef]
57. Nguyen, T.T.; Pham, D.T.; Nguyen, N.H.; Do, P.T.; To, H.T.M. The Germin-like protein gene *OsGER4* is involved in heat stress response in rice root development. *Funct. Integr. Genom.* **2023**, *23*, 271. [CrossRef]
58. Vidović, M.; Battisti, I.; Pantelić, A.; Morina, F.; Arrigoni, G.; Masi, A.; Jovanović, S.V. Desiccation tolerance in *Ramonda serbica* Panc.: An integrative transcriptomic, proteomic, metabolite and photosynthetic study. *Plants* **2022**, *11*, 1199. [CrossRef]
59. Ma, L.; Qin, D.B.; Sun, L.; Zhang, K.; Yu, X.; Dang, A.K.; Hou, S.; Zhao, X.; Yang, Y.; Wang, Y.; et al. SALT OVERLY SENSITIVE2 and AMMONIUM TRANSPORTER1;1 contribute to plant salt tolerance by maintaining ammonium uptake. *Plant Cell* **2025**, *37*, koaf034. [CrossRef]
60. Gámez-Arjona, F.; Park, H.J.; García, E.; Aman, R.; Villalta, I.; Raddatz, N.; Carranco, R.; Ali, A.; Ali, Z.; Zareen, S.; et al. Inverse regulation of SOS1 and HKT1 protein localization and stability by SOS3/CBL4 in *Arabidopsis thaliana*. *Proc. Natl. Acad. Sci. USA* **2024**, *121*, e2320657121. [CrossRef]
61. Zhang, F.; Gao, Y.; Ma, M.; Li, L.; Wei, Y.; Fan, L.; Xie, Z.; Qi, K.; Wu, J.; Tao, S.; et al. PbNAC3 coordinates AsA generation and ABA biosynthesis to improve salt tolerance in pear. *Plant J.* **2025**, *122*, e70171. [CrossRef]
62. Zha, D.; He, Y.; Song, J. Regulatory role of ABA-responsive element binding factors in plant abiotic stress response. *Physiol. Plant.* **2025**, *177*, e70233. [CrossRef]
63. Dabravolski, S.A.; Isayenkov, S.V. Expansins in salt and drought stress adaptation: From genome-wide identification to functional characterisation in crops. *Plants* **2025**, *14*, 1327. [CrossRef] [PubMed]
64. Zou, Y.; Gigli-Bisceglia, N.; van Zelm, E.; Kokkinopoulou, P.; Julkowska, M.M.; Besten, M.; Nguyen, T.P.; Li, H.; Lamers, J.; de Zeeuw, T.; et al. Arabinosylation of cell wall extensin is required for the directional response to salinity in roots. *Plant Cell* **2024**, *36*, 3328–3343. [CrossRef] [PubMed]
65. Katoh, K.; Standley, D.M. MAFFT multiple sequence alignment software version 7: Improvements in performance and usability. *Mol. Biol. Evol.* **2013**, *30*, 772–780. [CrossRef]
66. Price, M.N.; Dehal, P.S.; Arkin, A.P. FastTree 2--approximately maximum-likelihood trees for large alignments. *PLoS ONE* **2010**, *5*, e9490. [CrossRef]
67. Letunic, I.; Bork, P. Interactive Tree Of Life (iTOL) v5: An online tool for phylogenetic tree display and annotation. *Nucleic Acids Res.* **2021**, *49*, W293–w296. [CrossRef]
68. Hu, B.; Jin, J.; Guo, A.Y.; Zhang, H.; Luo, J.; Gao, G. GSDS 2.0: An upgraded gene feature visualization server. *Bioinformatics* **2015**, *31*, 1296–1297. [CrossRef]
69. Bailey, T.L.; Johnson, J.; Grant, C.E.; Noble, W.S. The MEME Suite. *Nucleic Acids Res.* **2015**, *43*, W39–W49. [CrossRef]

70. Lescot, M.; Déhais, P.; Thijs, G.; Marchal, K.; Moreau, Y.; Van de Peer, Y.; Rouzé, P.; Rombauts, S. PlantCARE, a database of plant *cis*-acting regulatory elements and a portal to tools for in silico analysis of promoter sequences. *Nucleic Acids Res.* **2002**, *30*, 325–327. [CrossRef]
71. Chen, C.; Wu, Y.; Li, J.; Wang, X.; Zeng, Z.; Xu, J.; Liu, Y.; Feng, J.; Chen, H.; He, Y.; et al. TBtools-II: A "one for all, all for one" bioinformatics platform for biological big-data mining. *Mol. Plant* **2023**, *16*, 1733–1742. [CrossRef] [PubMed]
72. Suo, J.; Zhao, Q.; Zhang, Z.; Chen, S.; Cao, J.; Liu, G.; Wei, X.; Wang, T.; Yang, C.; Dai, S. Cytological and proteomic analyses of *Osmunda cinnamomea* germinating spores reveal characteristics of fern spore germination and rhizoid tip growth. *Mol. Cell. Proteom.* **2015**, *14*, 2510–2534. [CrossRef]
73. Beauchamp, C.; Fridovich, I. Superoxide dismutase: Improved assays and an assay applicable to acrylamide gels. *Anal. Biochem.* **1971**, *44*, 276–287. [CrossRef] [PubMed]
74. Zhang, Z.; Yang, J.; Collinge, D.B.; Thordal-Christensen, H. Ethanol increases sensitivity of oxalate oxidase assays and facilitates direct activity staining in SDS gels. *Plant Mol. Biol. Rep.* **1996**, *14*, 266–272. [CrossRef]

plants

MDPI

Article

Comprehensive Genome-Wide Characterization of L-Type Lectin Receptor-like Kinase (L-LecRLK) Genes in Wheat (*Triticum aestivum* L.) and Their Response to Abiotic Stress

Wan Zhao [1,2,†], Fuyan Zhang [2,†], Jiahuan Wang [2], Shuai Fang [3], Zhongjie Cheng [2], Xuhui Ma [2], Jialin Fan [2], Zhaoshi Xu [3,*] and Xiaojie Chen [2,*]

[1] Institute of Chemistry, Henan Academy of Sciences, Zhengzhou 450002, China
[2] Isotope Institute Co., Ltd., Henan Academy of Sciences/Henan Key Laboratory of Nuclear Agricultural Sciences, Zhengzhou 450015, China
[3] State Key Laboratory of Crop Gene Resources and Breeding, Institute of Crop Sciences, Chinese Academy of Agricultural Sciences (CAAS), Beijing 100081, China
* Correspondence: xuzhaoshi@caas.cn (Z.X.); cxj2638@163.com (X.C.)
† These authors have contributed equally to this work.

Abstract: L-type lectin receptor-like kinases (L-LecRLKs) play key roles in plant responses to environmental stresses and the regulation of growth and development. However, comprehensive studies of the L-LecRLK gene family in wheat (*Triticum aestivum* L.) are still limited. In this study, 248 L-LecRLK candidate genes were identified in wheat, which is the largest number reported in any species to date. Phylogenetic analysis grouped these genes into four clades (I–IV), with Group IV exhibiting significant monocot-specific expansion. Gene duplication analysis revealed that both whole-genome/segmental and tandem duplications contributed to family expansion, while Ka/Ks ratio analysis suggested that the genes have undergone strong purifying selection. The *TaL-LecRLK* genes displayed diverse exon-intron structures and conserved motif compositions. Promoter analysis revealed a *cis*-element associated with hormone signaling and abiotic stress responses. Transcriptome profiling showed that *TaL-LecRLKs* exhibit tissue- and stage-specific expression patterns. RNA-Seq data revealed that, under drought and heat stress conditions, *TaL-LecRLK35-3D* and *TaL-LecRLK67-6B* exhibited synergistic expression patterns, whereas *TaL-LecRLK67-6A* demonstrated antagonistic expression. A qRT-PCR further demonstrated that six *TaL-LecRLKs* may function through ABA-independent regulatory mechanisms. These findings provide valuable gene candidates for stress-resistant wheat breeding and shed light on the evolution and functional diversity of L-LecRLKs in plants.

Keywords: *Triticum aestivum* L.; L-type lectin receptor-like kinase; phylogeny; gene expression; abiotic stress

1. Introduction

Wheat (*Triticum aestivum* L.) is the most widely cultivated cereal crop globally, serving not only as a primary food source for humans but also as a crucial feedstock for livestock and an important raw material for various industries, occupying a central position in food security and the global economy [1,2]. Common wheat has undergone two rounds of polyploidization during its evolution, resulting in an allohexaploid genome of approximately 15 Gb [3,4]. This large and complex genome presents significant challenges for genomic research and breeding efforts. The release of a high-quality reference genome for the hexaploid cultivar 'Chinese Spring' by the International Wheat Genome Sequencing

Consortium (IWGSC) in 2018 [5] laid the groundwork for advanced molecular breeding. Subsequent multi-omics analyses based on this reference revealed dynamic expression of homologous genes across developmental stages and stress conditions [6], facilitating gene cloning and functional characterization for key agronomic traits.

Lectin receptor-like kinases (LecRLKs) form a distinct subgroup of receptor-like protein kinases (RLKs) unique to higher plants, characterized by extracellular lectin motifs' domains [7,8]. A typical LecRLK protein comprises three domains: an extracellular lectin domain for ligand recognition, a transmembrane region for membrane anchoring, and an intracellular kinase domain responsible for signal transduction [9]. Based on extracellular lectin domain structures and phylogenetic relationships, LecRLKs are categorized into three subtypes: C-type, G-type, and L-type [7,10]. C-type LecRLKs are primarily found in mammals and contain a calcium-dependent carbohydrate-binding lectin domain [11]. Currently, only a single member has been identified in various plant species, such as *Arabidopsis*, rice, barley, foxtail millet, and soybean [12–15]. G-type LecRLKs, which were previously known as S-domain RLKs or B-type LecRLKs, have a lectin domain characterized by a β-barrel structure and are predicted to bind α-D-mannose specificity [8,16]. Many G-type LecRLKs also contain an Epidermal Growth Factor (EGF) and/or PAN motifs, both of which are absent in L-type and C-type LecRLKs [17]. The EGF motif is rich in cysteine residues and is potentially involved in the formation of disulfide bonds, while the PAN motif mediates protein–protein and protein–carbohydrate interactions [16,18]. L-type LecRLKs (L-LecRLKs), the extracellular domains, resemble legume lectins and adopt a β-sandwich fold structure [19]. These domains contain hydrophobic cavities that bind various hydrophobic ligands such as polysaccharides, phytohormones, and PAMPs [7,20], and their carbohydrate-binding activity is stabilized by Ca^{2+}/Mn^{2+} coordination [10]. The transmembrane regions (TMRs) of LecRLKs typically consist of 18–25 amino acids and exhibit low conservatism [19]. Notably, not all LecRLKs contain a TMR, nor do all members possess only one single transmembrane region [21,22]. Although the TMR is non-essential for the structural integrity of L-LecRLK proteins and shows low conservatism, it is crucial for their kinase activity. Studies demonstrated that a single amino acid mutation in the TMR can lead to a loss of kinase function [23]. The kinase domains of LecRLKs are highly conserved, typically comprising 200–300 amino acids and containing phosphorylation binding sites. These domains are located in the cytoplasm and are primarily responsible for transmitting external signals [24]. The N-terminus of the kinase domain contains a short GxGxxG (x represents any amino acid) amino acid sequence motif, which can influence nucleotide binding, while the C-terminus, consisting of 43 to 66 amino acids, is essential for the kinase's catalytic activity [24].

The sequence and structural diversity of LecRLKs underlie the molecular basis for their functional diversity. Research demonstrated that LecRLKs function as important signaling receptors that recognize extracellular carbohydrate ligands and play central roles in plant immunity and development [7]. In immune defense, LecRLKs function as pattern recognition receptors (PRRs) that detect pathogen-associated molecular patterns (PAMPs). For example, following infection with *Ralstonia solanacearum*, the *Arabidopsis* lectin receptor-like kinase LORE is activated by phosphorylation at residue S761, initiating a phosphorelay that activates reactive oxygen species' (ROS) production and cell wall lignification, thereby contributing to basal resistance in the xylem [25]. In the developmental process, OsDAF1 in rice interacts with OsINP1 to regulate pollen aperture formation [26], while Arabidopsis LecRK-VIII.2, acting as an upstream component of the MAPK signaling pathway, modulates silique number, seed size, and seed number to determine seed yield, demonstrating considerable promise for crop improvement [27]. Recent studies increasingly indicate that LecRLKs, particularly L-LecRLKs, play significant roles in various abiotic

stress responses. For example, overexpression of the rice *OsLec-RLK* gene in pigeon pea significantly enhanced plant salt stress tolerance [28]. The transgenic plants exhibited superior physiological and biochemical traits (such as higher K^+/Na^+ ratio, enhanced antioxidant enzyme activity) and yield performance under salt stress [28]. Furthermore, studies revealed that PaLectinL7 can enhance salt tolerance in sweet cherry via interaction with the lignin-metabolizing enzyme PaCAD1 to regulate lignin deposition [29]. Moreover, expression profiles and qRT-PCR experiments across multiple species further confirmed the involvement of L-LecRLKs in responses to drought, salt, and temperature stress [30–33]. Despite wheat's global importance, few studies have systematically examined the L-LecRLK gene family, and many annotations remain incomplete or imprecise [34].

Given the increasing impact of climate change and the plateauing of genetic gains in wheat, the identification of novel stress-responsive genes is essential for advancing molecular breeding. L-LecRLKs, as central regulators of stress adaptation and development, offer promising targets. In this study, we systematically analyzed the wheat *L-LecRLK* gene family, integrating phylogenetic reconstruction, evolutionary analysis, and spatiotemporal expression profiling. Our aim was to refine the classification framework of wheat L-LecRLKs, uncover evolutionary patterns, and link gene expression dynamics with potential biological functions. These findings will provide a theoretical foundation for future functional genomics research and facilitate the development of stress-resilient wheat cultivars through molecular breeding.

2. Results

2.1. Identification and Characterization of TaL-LecRLK Genes in Wheat

A total of 248 candidate genes encoding L-type lectin receptor-like kinases (L-LecRLKs) were identified in the wheat genome. These genes were designated *TaL-LecRLK1* to *TaL-LecRLK88* based on chromosomal location and homology (Tables S1 and S2). In-paralogous genes originating from the same genome were differentiated through sequential numbering. For instance, *TaL-LecRLK72-6A1*, *TaL-LecRLK72-6A2*, and *TaL-LecRLK72-6A3* were separately identified. Although all 248 candidate genes encoded the same class of protein kinase, their physicochemical properties varied widely. The encoded proteins ranged from 274 (TaL-LecRLK12-2B) to 1054 (TaL-LecRLK24-2A) amino acids in length, with an average of 663 amino acids. Corresponding molecular weights spanned from 31.2 (TaL-LecRLK12-2B) to 115.7 (TaL-LecRLK24-2A) kDa, and theoretical isoelectric points (*p*I) ranged from 5.27 (TaL-LecRLK46-4D) to 10.22 (TaL-LecRLK78-7D) (Table S1). Approximately 67.7% (168/248) of these proteins were classified as acidic. Instability indices ranged from 25.35 (TaL-LecRLK35-3A2) to 61.68 (TaL-LecRLK78-7D), with 74.2% (148/248) categorized as stable and 25.8% (64/248) as unstable at the sequence level. The aliphatic index spanned from 68.0 (TaL-LecRLK78-7D) to 104.16 (TaL-LecRLK12-2B), while the Grand Average of Hydropathicity (GRAVY) values ranged from −0.379 (TaL-LecRLK39-3B) to 0.092 (TaL-LecRLK5-1A) (Table S1).

Subcellular localization predictions indicated that 85 proteins localized to the cell membrane, while 43 were distributed across the cytoplasm, cell membrane, and various organelles. Thirty-five proteins were present in both the cytoplasm and cell membrane, another 35 were localized to the cytoplasm and organelles, and 30 were associated with the cell membrane and membrane-bound organelles such as the endoplasmic reticulum, mitochondria, lysosomes, and vacuoles. Additionally, 18 proteins localized exclusively to the cytoplasm, one to the endoplasmic reticulum and one to both the endoplasmic reticulum and lysosomes/vacuoles (Table S1). Among the proteins, 67.3% (167/248) were predicted to be soluble. Furthermore, 35 proteins contained mitochondrial targeting peptide (MTP) signals, and another 35 were identified as lipid-anchored proteins (Table S1). These findings

suggest the involvement of TaL-LecRLK proteins in diverse physiological processes such as signal transduction and cell metabolism.

2.2. Phylogenetic Relationships and Classification of TaL-LecRLK Proteins

To investigate the evolutionary relationships of L-LecRLKs across different species, a phylogenetic tree was constructed using 367 homologous sequences, including 248 from wheat (*Triticum aestivum*), 76 from rice (*Oryza sativa*), and 43 from *Arabidopsis thaliana* (Tables S1 and S3; Figure 1). An additional tree was generated exclusively for the 248 wheat TaL-LecRLK proteins (Figure S1).

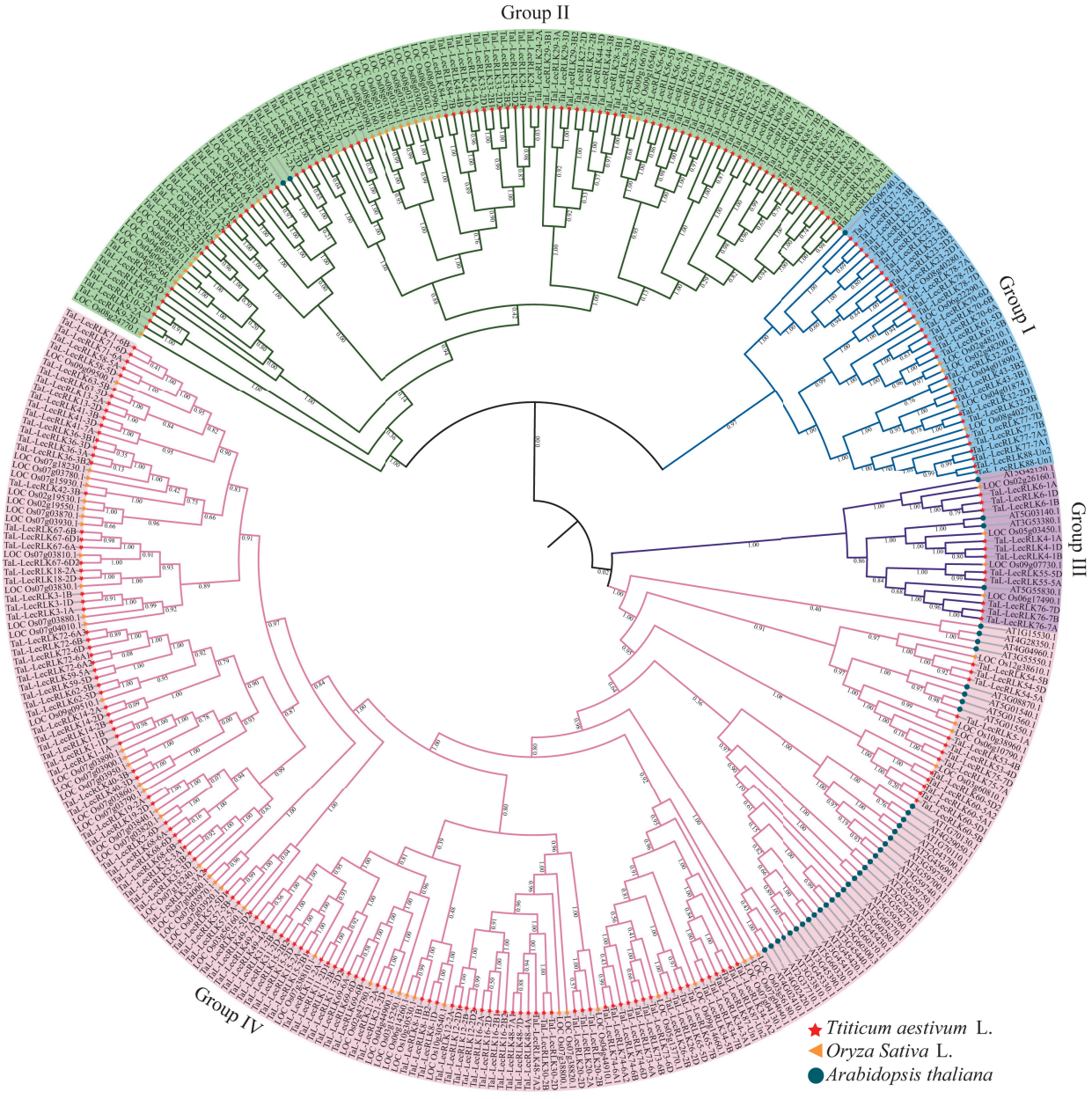

Figure 1. Phylogenetic analysis of L-LecRLK proteins in wheat (*Triticum aestivum* L.), rice (*Oryza sativa* L.), and *Arabidopsis thaliana*. Full-length amino acid sequences were aligned using MUSCLE, and the phylogenetic tree was constructed using the maximum likelihood method in FastTree. Clades are shown in different colors: Group I (green), Group II (blue), Group III (purple), and Group IV (pink). Species are marked by colored shapes: wheat (red star), rice (yellow triangle), and Arabidopsis (green circle).

Based on sequence homology and following the classification used in Arabidopsis and rice [31], the wheat proteins were categorized into four distinct groups: Group I (n = 29), Group II (n = 83), Group III (n = 11), and Group IV (n = 125). Groups II and IV were the largest subfamilies, accounting for 84.3% of all *TaL-LecRLK* genes (Figures 1 and S1). The phylogenetic analysis revealed significant expansion in Groups I, II, and IV in wheat compared to Arabidopsis and rice. Several subclades were observed to be species-specific, forming distinct monocot or dicot lineages. This pattern suggests that functional diversification of LecRLK genes may have occurred during evolution to meet species-specific physiological needs.

2.3. Gene Structure and Conserved Motif Analysis of TaL-LecRLKs

To explore structural diversity and potential functional divergence, exon-intron structures and conserved motifs were analyzed for all 248 *TaL-LecRLK* genes (Figure 2). Intron counts ranged from 0 to 6 (Table 1), with a significant inverse relationship between intron number and gene abundance. Intronless genes were the most common (148/248; 59.68%), followed by those with one intron (28.2%; 70/248). Only 12.1% of the genes had three or more introns. Within Group IV, 84% (104/125) of the genes were intronless, indicating high evolutionary conservation. In contrast, Group II displayed the greatest intron variability (0–6), suggesting extensive intron gain or loss events (Figure 2a,b; Table 1). Only one gene, *TaL-LecRLK39-3B*, contained six introns, potentially reflecting domain or exon duplication during evolution (Figure 2b; Table 1).

Table 1. The distribution of intron numbers across *TaL-LecRLK* gene subfamilies.

Subfamily	0 Intron	1 Intron	2 Introns	3 Introns	4 Introns	5 Introns	6 Introns	Total
Group I	10	18	1	0	0	0	0	29
Group II	28	31	15	3	2	3	1	83
Group III	6	5	0	0	0	0	0	11
Group IV	104	16	3	1	1	0	0	125
Total	148	70	19	4	3	3	1	248

A total of 20 conserved motifs were identified among the TaL-LecRLK proteins, with individual proteins containing between 8 and 24 motifs (Tables 2 and S1). As illustrated in Figure 2c, proteins sharing similar motif compositions clustered together, indicating potential functional similarities. Highly conserved motifs included motifs 10, 11, 3, 2, 6, 13, 7, 9, and 8 (Figure 2c). Motifs 14 and 16 were specific to Group IV and rarely appeared in other groups, suggesting evolutionary adaptation (Figure 2a,c). Motif 18 was almost entirely absent in Group II but was frequently found in Groups I, III, and IV (Figure 2a,c), further supporting functional divergence among groups.

Figure 2. Phylogenetic analysis, conserved motifs, and gene structure of wheat L-LecRLKs. (**a**) Phylogenetic tree of 248 L-LecRLK proteins in wheat constructed based on sequence alignment results; (**b**) gene structures: exons (yellow rectangles), UTRs (blue rectangles), and introns (lines connecting exons). Box and line lengths are proportional to gene length. Intron distribution is summarized in Table 1. (**c**) Motif compositions of 20 conserved motifs identified using MEME. Each motif is represented by a distinct colored box. Detailed motif data are in Table 2.

Table 2. List of the identified motifs in TaL-LecRLK proteins.

MOTIF	ID	WIDTH
1	YLHEEWEQVVIHRDIKASNVLLDSSMNGRLGDFGLARLYDH	41
2	KRVSHDSRQGMKEFVAEVVSIGRLRHRNLVQLL	33
3	WEVEFGPHRFSYKDLFRATKGFSEKNLLGRGGFGSVYK	38
4	HVVGTMGYJAPELVRTGKATPETDVFAFGVFLLE	34
5	YDADEAELVLKLGLLCSHPDPSARPSMRQ	29
6	GYCRRKGELLLVYEYMPNGSL	21
7	WPQRYKIIKGVASAL	15
8	INDNHVGIDVNSLVS	15
9	NGNGSNRIVAVEFDT	15
10	HYVLGWSFSSDGPAP	15
11	VLPETVYVGFSAATG	15
12	GAFQNLSLISGKAMQVWVDYD	21
13	TGEVASFSTSFVFAI	15
14	JDISKLPKLPRLGPKPRSKVLEIVLPIAT	29
15	LVDWVWELYGRGAJL	15
16	GLLELTNGTSQLKGHAFHPTP	21
17	GDGMAFFLAPS	11
18	ATQINVTLAPLGVAKPARPLLSA	23
19	VACGRRPIEQNAEDN	15
20	VMQYLDGDAPLPELP	15

2.4. Chromosomal Localization and Homoeolog Identification of the TaL-LecRLKs

The chromosomal positions of the *Ta-LecRLK* genes are listed in Table S1. As illustrated in Figure 3, a heterogeneous distribution pattern was observed for the 248 *TaL-LecRLK* genes across the 21 chromosomes. Chromosome 2D possessed the highest number of *TaL-LecRLK* genes (28), followed by chromosomes 2B (20), 3B (17), and 2A (16). In contrast, chromosomes 4D and 4B contained the fewest, with only 3 and 4 *TaL-LecRLK* genes, respectively. Chromosome group 2 (comprising 2A, 2B, and 2D) possessed the largest total number of *TaL-LecRLK* genes (64), while chromosome group 4 (4A, 4B, and 4D) exhibited the smallest total (16) (Figure 3a,b). The distribution of *TaL-LecRLK* genes among other chromosome groups varied, demonstrating differences among the wheat subgenomes.

To further understand the evolutionary history of the *TaL-LecRLK* genes, homoeologous group analysis was performed (Tables 3 and S2). It was found that 29% (72/248) of *TaL-LecRLK* genes were organized into complete triads, maintaining strict 1:1:1 orthologous relationships across the A, B, and D homoeologous chromosome groups. This proportion was lower than the 35.8% whole-genome triad frequency [5]. Additionally, higher proportions of homoeolog-specific duplications (n:1:1/1:n:1/1:1:n; 21.8% vs. 5.7%) and single homoeolog losses (1:1:0/1:0:1/0:1:1; 24.6% vs. 13.2%) were identified, as compared to the whole-genome averages (Table 3). However, the frequency of orphan or singleton genes within the *TaL-LecRLK* family (1.6%) was significantly lower than that of the entire wheat genome (37.1%; Table 3).

Table 3. Homoeologous genes of *TaL-LecRLKs* identified in the wheat genome.

Homoeologous Groups (A:B:D)	All Wheat Genes [1]	All wheat *TaL-LecRLK* Genes		
		Number of Groups	Number of Genes	% of Genes [2]
1:1:1	35.80%	24	72	29.00%
n:1:1/1:n:1/1:1:n [3]	5.70%	27	54	21.80%
1:1:0/1:0:1/0:1:1	13.20%	15	61	24.60%
Other ratios	8.00%	18	57	23.00%

Table 3. *Cont.*

Homoeologous Groups (A:B:D)	All Wheat Genes [1]	All wheat *TaL-LecRLK* Genes		
		Number of Groups	Number of Genes	% of Genes [2]
Orphans/Singletons	37.10%	-	4	1.60%
Total	99.80%	-	248	100%

[1] According to IWGSC (2018) [5]. [2] Percentage calculated with 248 *TaL-LecRLK* genes, see Supplementary Table S3 for detailed information. [3] n > 1.

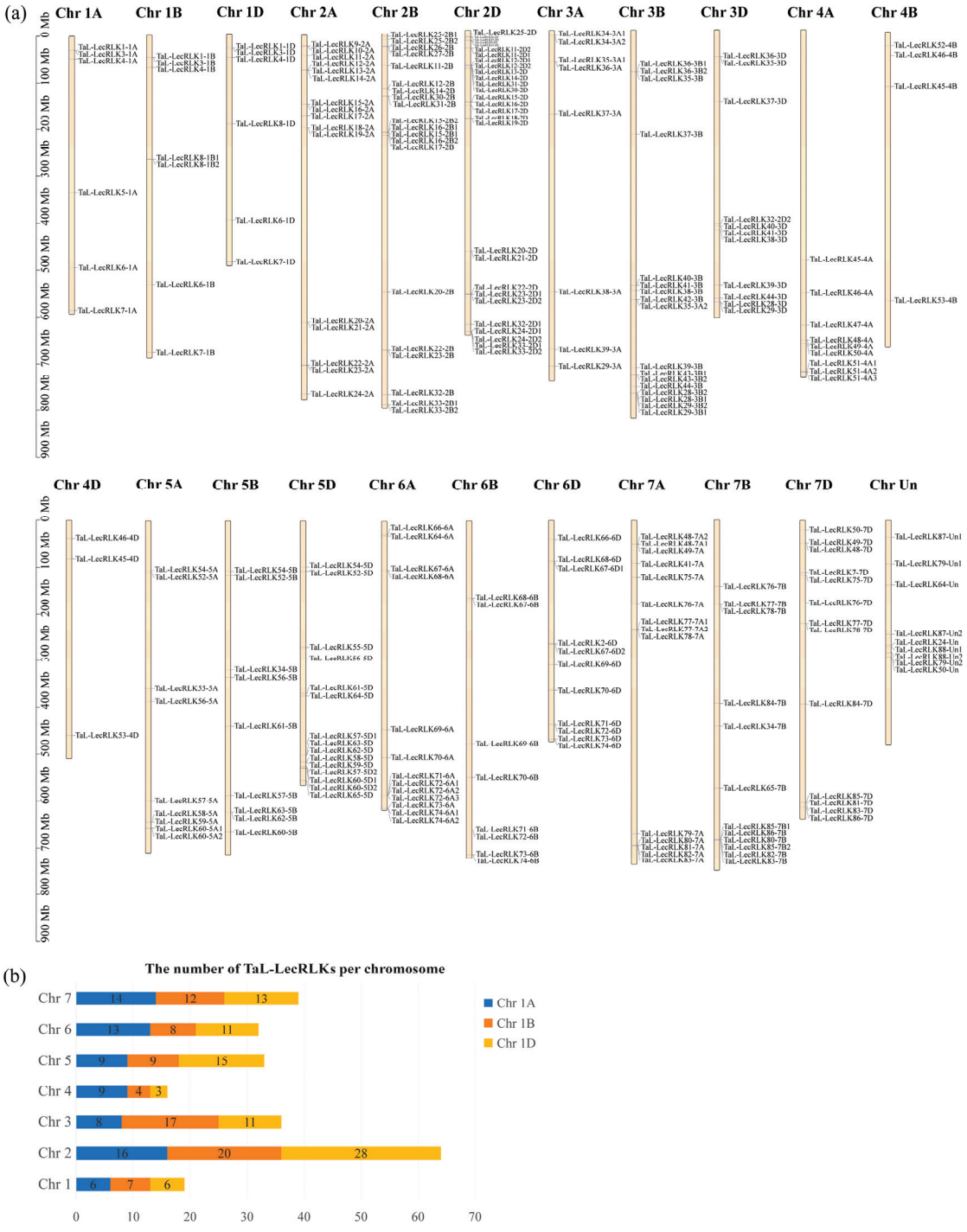

Figure 3. Chromosomal distribution of *TaL-LecRLK* genes. (**a**) Distribution map of 248 genes on wheat chromosomes. Gene names are listed on the right side, scale is in megabases (Mb); (**b**) numbers of *TaL-LecRLK* genes per chromosome (Chr1–Chr7).

2.5. Duplication and Syntenic Analyses of the L-Type LecRLK Genes

To explore the mechanisms driving the expansion of *TaL-LecRLK* genes, synteny analysis was conducted within the wheat genome. A total of 183 genes were located within syntenic blocks, forming 156 pairs of duplicated genes (Figure 4; Table S4). Of the 248 *TaL-LecRLK* genes, approximately 19% (47 genes) were identified as tandem duplicates, these included 5 sets of three tandemly duplicated genes and 22 sets of two tandemly duplicated genes. Additionally, 60% (156/248) of the genes were associated with whole-genome duplication (WGD) or segmental duplication events (Table S4). Notably, chromosome group 2 (2A, 2B, and 2D) exhibited the highest frequency of WGD/segmental duplications. These findings suggest that the polyploidization history of wheat, particularly its hexaploid genome formation, likely contributed to the extensive expansion of the L-type LecRLK gene family through WGD/segmental duplication.

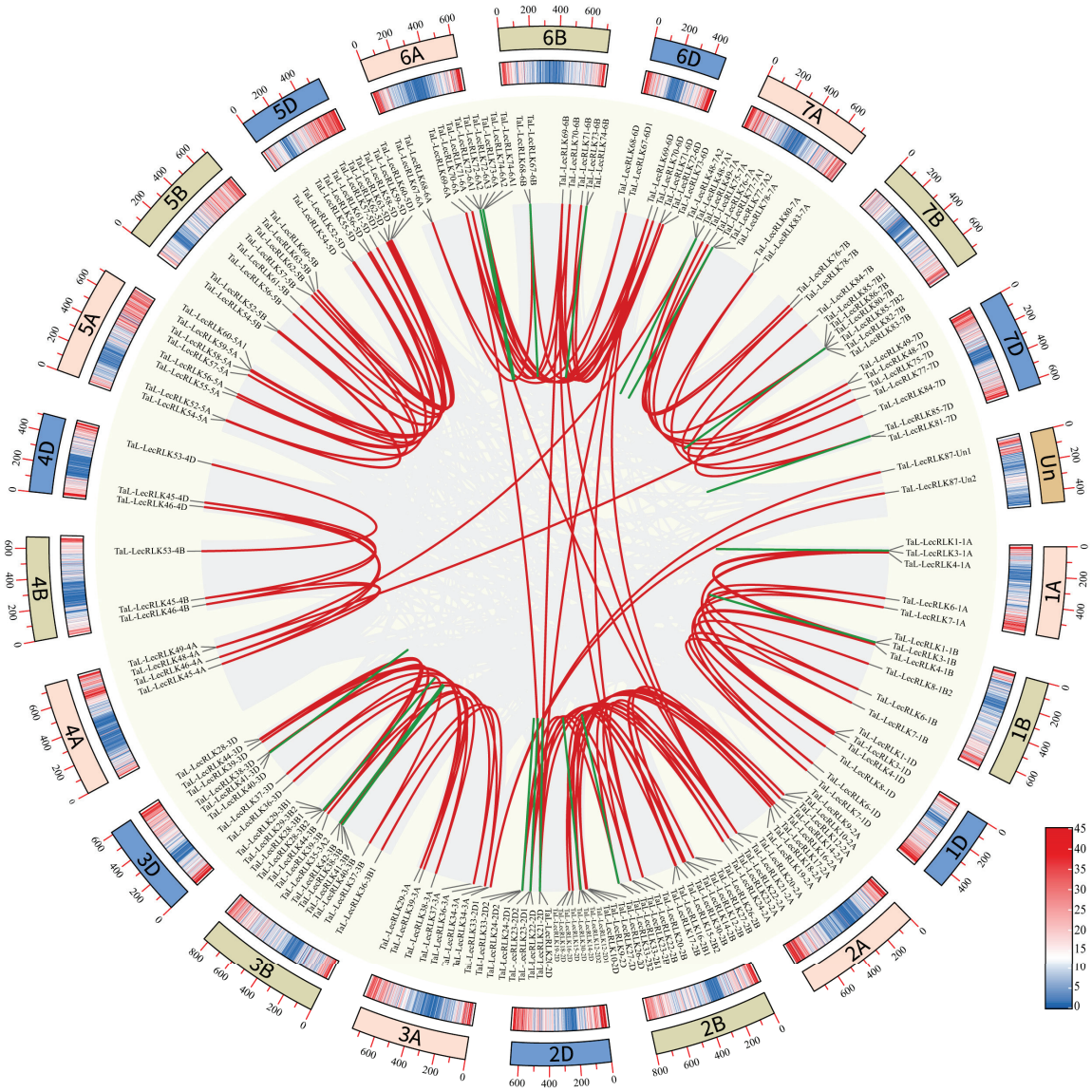

Figure 4. Duplication events of *TaL-LecRLK* genes in wheat. Chromosome numbers are labeled around the circle, with a scale bar in Mb. Segmental duplications are shown as red lines, while tandem duplications are shown as green lines. Gray areas represent syntenic blocks.

To assess the evolutionary pressures acting on duplicated *TaL-LecRLK* genes, the ratio of nonsynonymous to synonymous substitutions (Ka/Ks) was calculated for each gene

pair. The Ka/Ks ratios ranged from 0.07 to 0.90 (all ratios < 1), with an average of 0.29 (Table S4). As shown in Figure 5, more than 78% of the duplicated gene pairs exhibited Ka/Ks ratios within the 0.1 to 0.3 range. This distribution suggests that these genes underwent strong purifying selection, which acted to conserve their functional stability throughout evolutionary history.

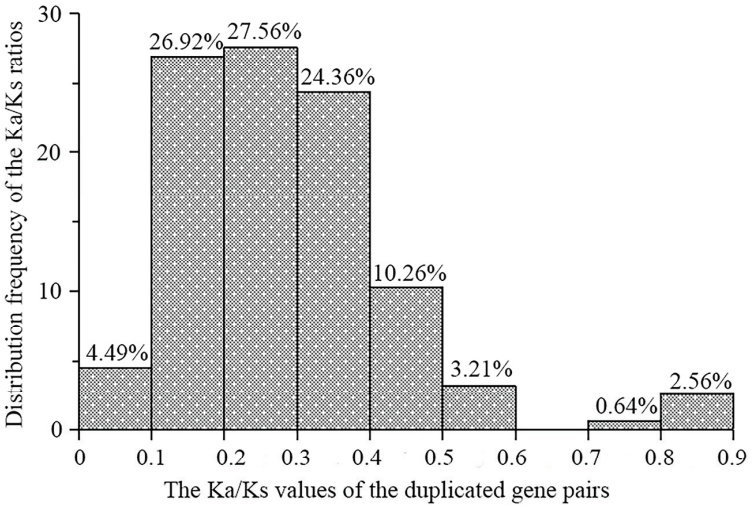

Figure 5. Histogram of pairwise *Ka*/*Ks* ratios for duplicated *TaL-LecRLK* gene pairs.

To clarify the evolutionary trajectory of *L-LecRLK* genes across plant species, a genome collinearity analysis was conducted among wheat (*Triticum aestivum* L.), rice (*Oryza sativa*), and *Arabidopsis thaliana*. As shown in Figure S2, only two L-LecRLK loci in *Arabidopsis* exhibited collinearity with two non-TaL-LecRLK loci in the wheat genome, indicating lineage-specific functional divergence of L-LecRLK genes following monocot–dicot divergence. In contrast, a stronger syntenic relationship was observed between the monocot species (rice-wheat), with 16 rice *L-LecRLK* genes corresponding to 45 wheat homologs. In most cases, one rice gene was collinear with 3–5 wheat genes (Figure S2). These results highlight the impact of polyploidization in expanding the *TaL-LecRLK* gene family and help explain the substantially higher number of *L-LecRLK* genes in hexaploid wheat relative to diploid plant species.

2.6. Analysis of Cis-Acting Elements in the Promoters of the TaL-LecRLK Genes

To further investigate the potential regulatory functions of *TaL-LecRLK* genes and their involvement in signal transduction pathways, a comprehensive analysis of cis-acting elements in their promoter regions was conducted. A total of 5804 *cis*-acting elements were identified (Table S5). As illustrated in Figure S3, these elements exhibited an uneven distribution pattern across the promoters of the 248 *TaL-LecRLK* genes.

Based on their biological roles, these elements were categorized into three major categories: hormone-responsive elements, environmental adaptation elements, and growth- and development-related elements (Table 4). Hormone-responsive elements represented the largest proportion, accounting for 49.1% of the total. These included elements responsive to five phytohormones: MeJA (methyl jasmonate), ABA (abscisic acid), GA (gibberellin), IAA (auxin), and SA (salicylic acid). Among these, ABREs (ABA-responsive elements) were the most prevalent (28.40%), followed by MeJA-responsive elements—CGTCA-motif (25.9%) and TGACG-motif (25.8%) (Table 4) —suggesting that *TaL-LecRLK* genes may play pivotal roles in ABA and MeJA signaling pathways. Environmental adaptation elements accounted for approximately 41% of the total. These included light-responsive elements (e.g., G-Box, Sp1, GT1-motif), anaerobic induction elements (ARE), drought-inducibility elements (MBS),

and low-temperature responsive elements (LTR), indicating that *TaL-LecRLK* genes are potentially involved in diverse environmental stress responses (Table 4). Notably, some *cis*-acting elements exhibited gene-specific distributions. For instance, the light-responsive 4cl-CMA2b element was found exclusively in the *TaL-LecRLK68-6A* promoter, while DRE elements (associated with dehydration, low-temperature, and salt stresses) were only detected in the *TaL-LecRLK10-2D* and *TaL-LecRLK41-7A* promoters (Table 4). These patterns imply specialized regulatory adaptations in response to environmental stimuli. Growth- and development-related elements comprised 9.1% of the total. This category included the meristem-associated CAT-box, the zein metabolism-regulating O_2-site, the seed-specific RY-element, and the endosperm expression-controlling GCN4_motif (Table 4), suggesting the involvement of *TaL-LecRLK* genes in developmental regulation throughout various growth stages. Additionally, several elements, such as ABRE, CGTCA-motif, TGACG-motif, and G-Box, were widely distributed across the promoters of various *TaL-LecRLK* homologs (Table S5; Figure S3). These conserved regulatory elements likely constitute central regulating hubs coordinating inter-pathway crosstalk during stress responses.

Table 4. Functional categorization and statistical profiling of *cis*-regulatory elements in *TaL-LecRLK* gene promoter regions.

Category	Function	Site Name	Number	Percentage for Each Category (%)	Percentage of the Total Number (%)
Hormonal responsiveness (2812, 49.1%)	abscisic acid responsiveness	ABRE	810	28.81	13.96
	MeJA-responsiveness	CGTCA-motif	739	26.28	12.73
		TGACG-motif	735	26.14	12.66
	gibberellin-responsiveness	P-box	103	3.66	1.77
		TATC-box	44	1.56	0.76
		GARE-motif	28	1.00	0.48
	auxin-responsive element	TGA-element	166	5.90	2.86
		AuxRR-core	40	1.42	0.69
	salicylic acid responsiveness	TCA-element	146	5.19	2.52
		SARE	1	0.04	0.02
Environmental adaptation (2418, 41.7%)	light responsive element	G-Box	868	35.90	14.96
		Sp1	212	8.77	3.65
		GT1-motif	152	6.29	2.62
		ACE	48	1.99	0.83
		MRE	48	1.99	0.83
		3-AF1 binding site	13	0.54	0.22
		AAAC-motif	5	0.21	0.09
		C-box	3	0.12	0.05
		4cl-CMA2b	1	0.04	0.02
	anaerobic induction	ARE	413	17.08	7.12
	drought-inducibility	MBS	261	10.79	4.50
	low-temperature responsiveness	LTR	171	7.07	2.95
	anoxic specific inducibility	GC-motif	127	5.25	2.19
	defense and stress responsiveness	TC-rich repeats	86	3.56	1.48
	wound-responsive element	WUN-motif	8	0.33	0.14
	dehydration, low-temperature, salt stresses	DRE	2	0.08	0.03

Table 4. *Cont.*

Category	Function	Site Name	Number	Percentage for Each Category (%)	Percentage of the Total Number (%)
Plant growth, development, and metabolism (534, 9.1%)	meristem expression	CAT-box	235	44.01	4.05
	zein metabolism regulation	O2-site	143	26.78	2.46
	endosperm expression	GCN4_motif	52	9.74	0.90
	seed-specific regulation	RY-element	36	6.74	0.62
	circadian control	circadian	34	6.37	0.59
	cell cycle regulation	MSA-like	27	5.06	0.47
	differentiation of the palisade mesophyll cells	HD-Zip 1	7	1.31	0.12
Total			5804		100.00

2.7. GO Analysis of the TaL-LecRLK Genes

A comprehensive Gene Ontology (GO) analysis was performed on the 248 *TaL-LecRLK* genes (Figure 6). Among them, 239 members (96.4%) were successfully annotated to 87 GO terms, of which 43 terms were statistically enriched ($p < 0.01$). These were distributed across three major categories: biological processes (26 terms), cellular components (10 terms), and molecular functions (7 terms) (Figure 6; Table S6). Within the biological process category, enriched GO terms included post-translational protein modification (GO: 0006464, GO: 0043412) and metabolic regulation (GO: 0044237, GO: 0008152), indicating potential regulatory functions in protein homeostasis and metabolic balance. Significant enrichment was also observed in cell signaling (GO: 0007165), developmental regulation (GO: 0032502), and environmental stress responses (GO: 0050896), suggesting the critical roles of *TaL-LecRLK* genes in growth and adaptation. At the molecular function level, enriched terms included kinase activity (GO: 0016301), phosphoryltransferase activity (GO: 0016772), and nucleotide binding (GO: 0000166), consistent with their roles in phosphorylation-mediated signal transduction. The enrichment of binding activity (GO: 0005488) and catalytic activity (GO: 0003824) further suggests multifunctionality in molecular interaction networks and enzymatic reactions. For cellular components, most gene products were predicted to localize to the plasma membrane (GO: 0005886) and general membrane systems (GO: 0016020). This subcellular localization aligns with their proposed functions as membrane-associated receptors in transmembrane signaling.

2.8. Spatiotemporal Expression Patterns of the TaL-LecRLK Genes

To systematically analyze the spatiotemporal expression characteristics of *TaL-LecRLK* genes, RNA-seq datasets for roots, leaves/shoots, grains, and spikes of Chinese Spring wheat during both vegetative and reproductive stages were obtained from the Wheat Expression Browser (https://www.wheat-expression.com/, accessed on 10 March 2025; Table S7). A tissue-specific expression heatmap of the *TaL-LecRLK* gene family was subsequently generated based on $\log_2$-transformed normalized expression values (TPM+1) (Figure 7; Table S8). The expression profiling revealed that, although *TaL-LecRLK* genes were broadly expressed across various tissues, including roots, leaves/shoots, grains, and spikes, their expression patterns displayed significant developmental stage specificity. During grain development (10–30 days after flowering), the majority of genes (>99%) exhibited negligible expression (TPM < 1), although limited expression was still detectable in early grain samples collected at 2 days post-anthesis (DPA). Moreover, several genes, such as *TaL-LecRLK73-6B*, *TaL-LecRLK30-2D*, and *TaL-LecRLK11-2B*, were either lowly expressed or unexpressed in vegetative-stage leaves/shoots but became upregulated during the reproductive stage in the same tissues (Figure 7; Table S8). Notably, more than half of

the *TaL-LecRLK* family members (55.6%, 138/248) showed no expression or consistently low expression levels across all sampled stages (maximum $\log_2(TPM+1) < 1$), implying possible functional redundancy or subfunctionalization (Table S8). Conversely, three homologous gene sets, *TaL-LecRLK20* (2A/2B/2D), *TaLecRLK38* (3A/3B/3D), and *TaL-LecRLK68* (6A/6B/6D), maintained relatively high expression levels in all sampled tissues and stages, suggesting that these genes may serve as core regulators in wheat growth and development (Table S7).

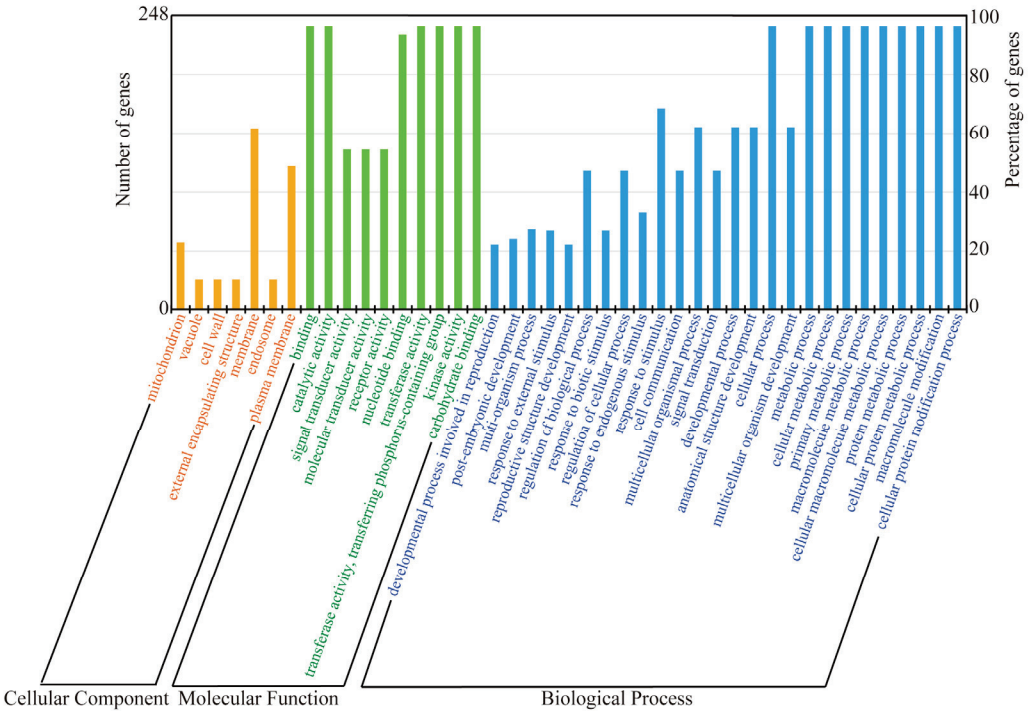

Figure 6. GO annotation of *TaL-LecRLK* genes, classified into biological process, molecular function, and cellular component. Supplementary Table S6 provides details.

2.9. Abiotic Stress-Responsive Profiling of the TaL-LecRLK Genes

To investigate the involvement of *TaL-LecRLK* genes in abiotic stress responses, one-week-old seedlings were exposed to rapid drought (filter paper dehydration) and high-temperature (42 °C) conditions. Leaf samples were collected at 0 h (CK) and 1, 3, and 6 h after stress exposure for transcriptome sequencing (three biological replicates per condition). The transcriptomic profiles of all 248 *TaL-LecRLK* genes under drought and heat stress are presented in Table S9. Expression heatmaps were generated based on the average FPKM values across replicates (Figure 8). Differential expression analysis ($|\log_2\text{FoldChange}| \geq 1$, FDR < 0.01) identified 44 and 35 *TaL-LecRLK* genes that were significantly upregulated or downregulated under drought and heat stress, respectively (Figure 8; Table S10). A Venn analysis of differentially expressed genes (DEGs) across various stress durations revealed that 4 genes were persistently regulated under drought group conditions at all three time points, while 11 genes exhibited sustained responsiveness to heat stress (Figure S4). Under drought stress, the number of DEGs increased over time. Initially, gene expression was characterized by unidirectional upregulation (1 h), which transitioned into a bidirectional pattern involving both up- and downregulation by 3 h and 6 h (Table S11). These findings suggest that *TaL-LecRLK* genes may function within temporally dynamic regulatory networks during drought stress responses. A comparative analysis further revealed coordinated expression patterns among certain genes under both stress conditions. For instance, *TaL-LecRLK34-7B* and *TaL-LecRLK78-7B* showed consistent expression trends

(either upregulated or downregulated) under both drought and heat treatments. In contrast, *TaL-LecRLK67-6A*, *TaL-LecRLK68-6A*, and *TaL-LecRLK16-2D* displayed opposing regulatory patterns, being upregulated under drought stress but downregulated under heat stress. These contrasting responses reflect a potential 'synergistic and antagonistic' dual regulatory mechanism that may enable stress-specific functional modulation through layered signal transduction pathways.

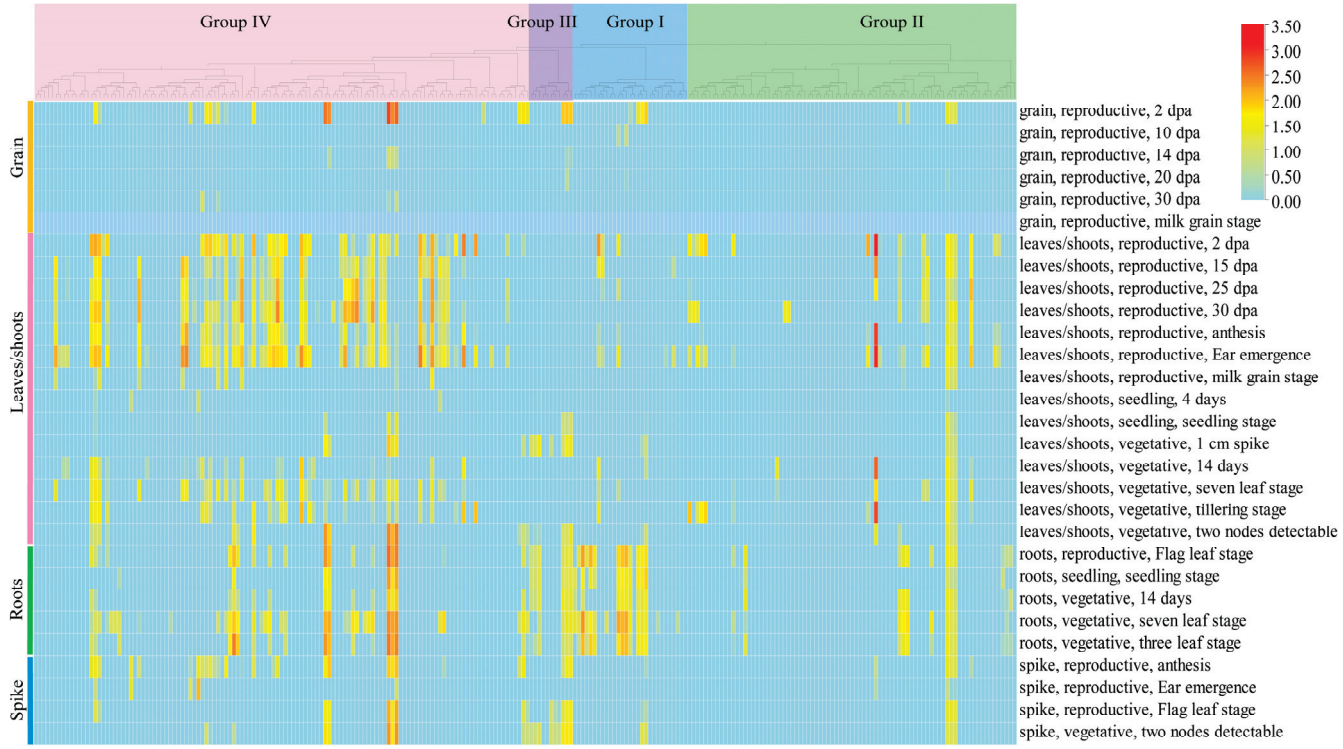

Figure 7. Heatmap of 248 *TaL-LecRLK* gene expression profiles at different wheat developmental stages, based on $\log_2$(TPM + 1) values from the wheat expression database.

To validate the RNA-seq results, the expression patterns of six stress-responsive *TaL-LecRLK* genes were examined by qRT-PCR. Under drought stress, the upregulated genes *TaLecRLK35-3D*, *TaLecRLK67-6D*, and *TaLecRLK78-7B* reached peak expression at 6 h, 6 h, and 24 h, respectively. Meanwhile, the downregulated genes *TaLecRLK39-3D*, *TaLecRLK68-6B*, and *TaLecRLK67-6B* showed maximal suppression at 6 h (Figure 9). Under heat stress, all upregulated genes reached peak expression at 6 h, while downregulated genes displayed minimal expression at 3 h, 6 h, and 6 h, respectively. These qRT-PCR results demonstrated high consistency with the transcriptome data. Additionally, a qRT-PCR analysis under exogenous ABA treatment revealed that five of the six genes (excluding *TaLecRLK68-6B*) were significantly downregulated in a time-dependent manner (Figure 9). This finding suggests that the stress-responsive regulation of these *TaL-LecRLK* genes may proceed via ABA-independent pathways.

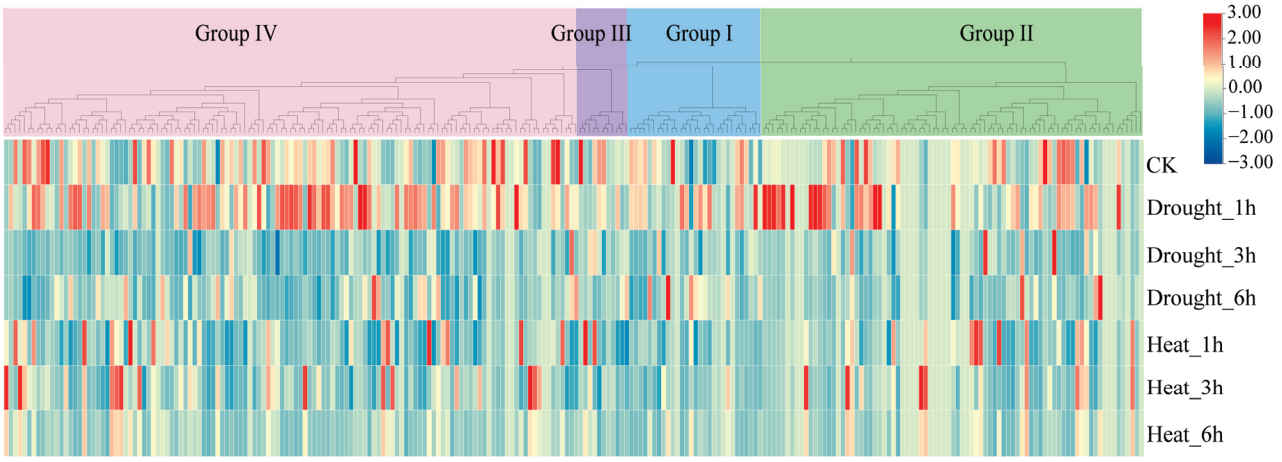

Figure 8. Heatmap of 248 *TaL-LecRLK* gene expression profiles in seedlings under drought and heat treatments. Expression values are the mean FPKM from three biological replicates.

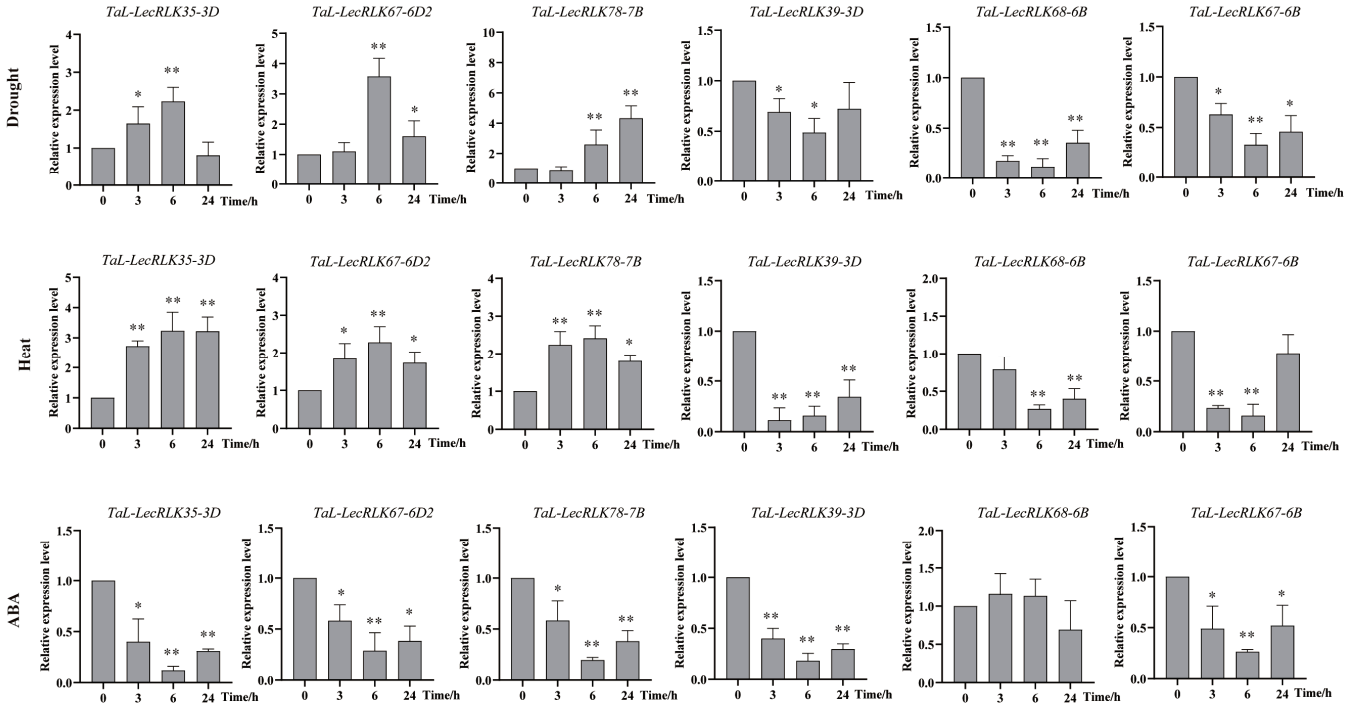

Figure 9. A qRT-PCR analysis of six *TaL-LecRLK* genes under drought, heat, and ABA treatments. *β-ACTIN* was used as an internal control. Mean and standard deviation (SD) values were calculated from three biological replicates. The y-axis shows relative expression; the x-axis indicates time points (0, 3, 6, and 24 h). Significant differences are indicated as follows: * $p < 0.05$; ** $p < 0.01$.

3. Discussion

L-type lectin receptor-like kinase (*L-LecRLK*) genes are known to play pivotal roles in regulating plant growth and development, responding to biotic and abiotic stresses and mediating transmembrane signal transduction processes [7]. Due to these diverse functions, *L-LecRLK* genes are promising targets for crop molecular breeding and improvement [28].

In the present study, a total of 248 wheat *L-LecRLK* genes were identified (Table S1). The prediction and analysis of sequence length, physicochemical properties, and subcellular localization revealed that the proteins encoded by the *TaL-LecRLK* gene family displayed significant heterogeneity in both structural characteristics and subcellular distribution. This diversity in sequence and location provides a molecular foundation for

their broad and specialized biological functions in wheat. Additionally, we found that the number of *TaL-LecRLK* genes in wheat (248) was significantly greater than those reported in *Arabidopsis* (43) and rice (76) (Table S3), representing 5.8-fold and 3.3-fold expansions, respectively. This makes wheat the flowering plant with the largest known *L-LecRLK* gene family to date [35,36]. A further analysis revealed that *TaL-LecRLKs* are relatively evenly distributed across the A, B, and D subgenomes, with 87, 77, and 75 members, respectively (Figure 3), suggesting balanced evolutionary pressures and potential functional redundancy across subgenomes [34]. Notably, compared with the whole-genome average [5], *TaL-LecRLK* homoeologs showed a significantly higher rate of lineage-specific duplication (n:1:1/1:n:1/1:1:n; 21.8% vs. 5.7%) and a markedly lower proportion of orphan or singleton genes (1.6% vs. 37.1%) (Table 3). These findings suggest that, throughout wheat evolution, paralogous genes were retained through subfunctionalization or neofunctionalization rather than eliminated as redundant copies [37,38].

To investigate the evolutionary relationships within the *L-LecRLK* gene family, a phylogenetic analysis was conducted, classifying the *TaL-LecRLKs* into four major groups (Figures 1 and S1). The classification was highly consistent with groupings observed in model species such as Arabidopsis and rice, indicating a conserved evolutionary framework across species [13,39]. Among these groups, Groups I, II, and IV exhibited notable expansions, with several subclades demonstrating monocot-specific distributions. A synteny analysis further revealed strong collinearity between monocot species (rice-wheat) (Figure S2), implying that lineage-specific functional divergence likely occurred following the monocot–dicot split. Notably, the number of Group II genes in wheat was significantly higher (83 genes, 33.5% of the wheat family) than in *Arabidopsis* (1 gene) or rice (7 genes). This pronounced expansion, likely driven by wheat's polyploidy and intense adaptive selection under complex environmental conditions, suggests a core role for Group II L-LecRLKs in wheat's evolution and adaptation to diverse stresses. Although Group IV contained the highest number of *L-LecRLK* genes (125 members), its relative proportion within the wheat family (50.4%) was notably lower than in Arabidopsis (83.7%) and rice (56.6%). This pattern—large absolute number but reduced relative proportion—suggests a distinct evolutionary trajectory for Group IV. Despite the lower proportional representation in wheat, the substantial number of Group IV genes implies their continued functional significance in wheat, potentially involving conserved core functions or roles adapted to monocot-specific or wheat-specific biology. Overall, these contrasting expansion patterns in Group II and Group IV likely reflect adaptations to wheat-specific selective pressures, contributing significantly to its ecological success.

Intron deletion and insertion are known important mechanisms driving gene evolution and functional diversification [40]. In this study, a high proportion of *TaL-LecRLK* genes (59.68%) were found to be intronless (Table 1; Figure 2a). Previous studies showed that intronless genes often function as rapid responders to environmental stimuli [41,42]. In Group IV, 84% of *TaL-LecRLK* genes lacked introns, suggesting a strong evolutionary conservation and possibly fundamental biological functions [43]. In contrast, Group II showed the greatest variation in intron number, indicating frequent intron gain/loss events that may have contributed to functional expansion and environmental adaptability. Conserved motif analysis also highlighted potential mechanisms of functional divergence. Core functional motifs such as Motifs 10 and 11 were widely distributed across all clades (Figure 2a,c), whereas Motifs 14 and 16 were predominantly found in Group IV, possibly due to selective loss in other clades under environmental pressures. The absence of Motif 18 in Group II, despite its high prevalence in other groups, suggested further differentiation in function. These findings align with previous studies on the wheat SnRK family [44], in which protein motif differences were closely associated with functional differentia-

tion. Together, these results indicate that the wheat *L-LecRLK* gene family has evolved a complex genetic architecture shaped by lineage-specific expansions, intron structural variation, and selective motif retention, which may underlie its adaptation to a wide range of ecological niches.

Chromosomal distribution, gene duplication mechanisms, and evolutionary dynamics of *TaL-LecRLKs* were further analyzed. The 248 identified genes were unevenly distributed across the 21 chromosomes, with homoeologous group 2 (2A/2B/2D) exhibiting the highest enrichment (64 genes) and group 4 (4A/4B/4D) containing the fewest (16 genes) (Figure 3). These differences are hypothesized to result from genome remodeling events during hexaploid wheat evolution [45]. Gene duplication analysis indicated that whole-genome/segmental duplication (60%) and tandem duplication (19%) served as the main drivers of gene family expansion (Figure 4; Table S4). Whole-genome duplication may facilitate adaptive evolution by retaining functional gene clusters, while tandem duplication might contribute to rapid functional innovation in response to environmental challenges [46,47]. An analysis of evolutionary rates showed that all duplicated gene pairs exhibited Ka/Ks ratios < 1 (mean = 0.29), with 78% of the ratios clustered between 0.1 and 0.3 (Figure 5), indicating that purifying selection played a dominant role in preserving gene function and restricting deleterious mutations [48].

Orthology analysis, a widely used method for inferring gene function across species, was also conducted [49]. A total of 45 *L-LecRLK* orthologous gene pairs were identified between wheat and rice (Figure S2). Given that orthologous genes often retain conserved functions while acquiring species-specific traits [50], these results suggest that a subset of wheat *L-LecRLKs* may perform evolutionarily conserved roles similar to their rice counterparts.

The precise regulation of plant gene expression is mediated by specific interactions between promoter *cis*-regulatory elements and transcription factors [51]. In this study, a systematic analysis of *cis*-acting elements within the *TaL-LecRLK* gene family was conducted (Table S5; Figure S2). The results revealed the presence of three major categories of *cis*-regulatory elements in wheat *TaL-LecRLK* genes: hormone-responsive elements (49.1%), elements related to environmental adaptation (41.7%), and elements associated with growth and metabolism regulation (9.1%) (Table 4). Among these, ABA-responsive elements (ABRE) and MeJA-responsive elements (CGTCA/TGACG motifs) were particularly enriched, suggesting the potential involvement of *TaL-LecRLK* genes in response to drought and salt stress, as well as in biotic defense mechanisms through ABA and JA signaling pathways [52–54]. Prior studies showed that MBS elements, which serve as binding sites for MYB transcription factors, regulate drought stress responses [55]. Therefore, *TaL-LecRLK* genes containing MBS elements in their promoter regions are likely regulated by related MYB transcription factors during stress responses.

Furthermore, promoter regions of *TaL-LecRLK* genes were found to contain numerous *cis*-regulatory elements associated with growth and development (e.g., CAT-box, O2-site) and protein metabolism (e.g., GCN4_motif), implying potential roles in tissue-specific development and metabolic regulation. Spatiotemporal expression analysis indicated that *TaL-LecRLK* genes were expressed across a range of organs at different developmental stages, with particularly high expression levels during early grain development, notably at 2 DPA (Figure 7). This suggests potential involvement in young embryo formation and endosperm cell differentiation. GO enrichment analysis (Figure 6) further supported their roles in signal transduction, environmental stress responses, and the regulation of growth and metabolism. Collectively, these findings provide important clues for understanding the functional diversity and regulatory potential of the *TaL-LecRLK* gene family.

L-LecRLKs were shown to play crucial roles in mediating plant stress responses to abiotic stresses such as salinity, drought, and temperature extremes [14–16]. To identify

stress-responsive gene candidates within the wheat L-LecRLK family, RNA-seq data were analyzed to assess expression patterns under drought and heat stress conditions. Multiple *TaL-LecRLK* genes were found to be differentially expressed in response to these stresses (Figure 8; Table S10). Under drought stress, the number of differentially expressed *TaL-LecRLK* genes increased over time, with distinct temporal expression peaks observed. Similar temporal expression trends were reported in other plant species [32,35], indicating that *TaLecRLK* genes may function in a stage-specific manner during stress response. Early-responsive genes are likely involved in rapid signal transmission, while late-responsive genes may contribute to metabolic reprogramming or the restoration of cellular homeostasis. Moreover, gene expression under drought and heat stress was not entirely consistent. For example, *TaL-LecRLK35-3D* and *TaL-LecRLK67-6B* exhibited synergistic expression patterns under drought and heat stress conditions (Table S11), suggesting that these genes may act in the same or interconnected pathways to confer stress tolerance. One possible hypothesis is that they form heterodimeric receptor complexes. In this scenario, each gene product could contribute distinct functional domains, with one subunit recognizing specific stress-associated ligands and the other initiating downstream signaling cascades. This cooperative action might enhance the sensitivity and specificity of the stress response, allowing the plant to more effectively combat multiple stressors simultaneously. Conversely, *TaL-LecRLK67-6A* demonstrated antagonistic expression under drought and heat stress conditions (Table S11), suggesting that *TaL-LecRLK67-6A* might be involved in two separate signaling branches that compete for limited cellular resources. Under heat stress, it could promote pathways that enhance thermotolerance but are detrimental to drought resistance, such as increased metabolic activity that consumes water. During drought, it may suppress these heat-related pathways to prioritize water-saving mechanisms [56]. The qRT-PCR validation confirmed the transcriptomic data and demonstrated that several differentially expressed *TaL-LecRLK* genes were generally downregulated in response to ABA treatment (Figure 9). This downregulation pattern suggests that these genes might be involved in non-canonical pathways such as JA or SA signaling and may not necessarily involve ABA-dependent mechanisms [57,58]. Previous studies demonstrated that drought stress can induce genes such as the soybean *GsSRK*, which enhances drought tolerance independently of ABA signaling [59]. Given the complexity of the regulatory networks involving the L-LecRLK family genes, future research should employ gene knockout and overexpression approaches, in conjunction with protein interaction assays, to further dissect the molecular mechanisms of *TaL-LecRLKs* and identify novel targets for improving crop stress resistance through molecular breeding.

4. Materials and Methods

4.1. Sequences' Acquisition and Identification of the L-Type Lectin Receptor-like Kinase (L-LecRLK) Genes in Wheat

The identification of wheat *L-LecRLK* genes was performed based on the methods described previously [15,60], with some minor modifications. The complete genome and protein sequence files of wheat were downloaded from the Ensembl Plant database (https://plants.ensembl.org/index.html/, accessed on 23 November 2024) [61]. Annotated and identified L-LecRLK protein sequences from the rice genome were obtained from the Rice Genome Annotation Project website (https://rice.uga.edu/, accessed on 23 November 2024) [62].

The Hidden Markov Model (HMM) profile of the L-type LecRLK conserved domain (PF00139, Lectin_legB) and Pfam-A models were downloaded from the Pfam database (https://pfam.xfam.org/, accessed on 28 November 2024) [63]. BLASTP (E-value < $1 \times e^{-10}$) and HMM searches were conducted using Tbtools-II software (ver-

sion 2.210) [64], using rice L-LecRLK protein sequences and the PF00139 HMM profile, respectively. The results from both searches were integrated, and only the first variant was retained for downstream analysis (with three exceptions).

Domain validation was conducted using two bioinformatics tools: the batch CD-Search tool (https://www.ncbi.nlm.nih.gov/Structure/bwrpsb/bwrpsb.cgi/, accessed on 10 December 2024) [65,66] and the SMART database (https://smart.embl-heidelberg.de/, accessed on 10 December 2024) [67]. Proteins were confirmed to contain both a complete N-terminal functional domain (PF00139) and at least one conserved kinase domain (PF00069 or PF07114). Qualified genes were uniformly designated as '*TaL-LecRLK*' followed by their chromosomal locations.

4.2. Physicochemical Properties and Subcellular Localization Prediction of TaL-LecRLKs

The basic physical and chemical properties of TaL-LecRLKs—including molecular weight, isoelectric points (*p*I), instability index, and other parameters—were analyzed using the ProtParam tool on the ExPASy Server (https://web.expasy.org/protparam/, accessed on 3 January 2025) [68]. Subcellular localization, signal peptides, and membrane classification were predicted using the Cell-PLoc 2.0 web-server (http://www.csbio.sjtu.edu.cn/bioinf/Cell-PLoc-2/, accessed on 3 January 2025) [69]. Information regarding cDNA length and amino acid number was obtained from the Ensembl Plants database [61].

4.3. Phylogenetic Analysis and Classification of TaL-LecRLK Proteins

Protein sequences encoded by *L-LecRLK* genes in wheat (*Triticum aestivum* L.), rice (*Oryza sativa* L.), and *Arabidopsis thaliana* were used for phylogenetic and evolutionary analyses. Genome and proteome data for rice and *Arabidopsis* were downloaded from Phytozome V13 (https://phytozome-next.jgi.doe.gov/, accessed on 23 November 2024) [70]. All *L-LecRLK* genes were retrieved using gene IDs from the three species, and their protein sequences were extracted using Tbtools-II.

Multiple sequence alignments were conducted using MUSCLE (Multiple Sequence Comparison by Log-Expectation) [71]. Phylogenetic trees were constructed using FastTree (version 2.1.11), with the maximum likelihood method [72]. The resulting tree was visualized and annotated using the iTOL v6 webtool (https://itol.embl.de/, accessed on 18 February 2025) [73]. Finally, a phylogenetic tree using 248 TaL-LecRLK protein sequences was reconstructed and used to categorize family members into distinct clades.

4.4. Gene Structure and Conserved Motifs' Analysis of TaL-LecRLKs

Gene structures and conserved motifs were analyzed using two tools: GSDS2.0 (v2.0; https://gsds.gao-lab.org/, accessed on 21 January 2025) [74] for gene structure visualization and the MEME Suite (v5.5.7; https://meme-suite.org/meme/, accessed on 29 January 2025) [75] for motif detection. The MEME search was configured to identify up to 20 motifs, allowing 0 or 1 occurrence per sequence, with motif widths set between 6 and 50 amino acids.

4.5. Chromosomal Distribution and Homoeolog Identification of TaL-LecRLK Genes

Chromosomal locations for *TaL-LecRLK* genes were retrieved from the Ensembl Plants database [61] and visualized using Tbtools-II software [64]. Homoeologous genes were identified through phylogenetic analysis and validated using cross-referencing from the Ensembl Plants database [76,77].

4.6. Duplication and Syntenic Analysis of L-Type LecRLK Genes

Tandem gene clusters of *TaL-LecRLK*s were identified based on definitions and methods from previous studies [12,39]. Segmental and tandem duplication events were categorized

by examining the chromosomal positions of *TaL-LecRLK* genes. Syntenic relationships within wheat and among wheat, Arabidopsis, and rice were analyzed using TBtools-II [64]. Advanced circos visualization features within TBtools-II were used to display synteny [64]. To evaluate selective pressure, Ka/Ks ratios were calculated using aKaKs_calculator [78].

4.7. Cis-Regulatory Element and Gene Ontology (GO) Analysis of TaL-LecRLKs

To identify potential regulatory elements, 2000 bp genomic sequences upstream of each *TaL-LecRLK* translation start codon were extracted and analyzed as promoter regions [79]. These sequences were submitted to the PlantCARE platform (https://bioinformatics.psb.ugent.be/webtools/plantcare/html/, accessed on 22 February 2025) for *cis*-regulatory element prediction [80]. The predicted *cis*-elements were systematically categorized, quantified, and visualized using TBtools-II [64].

GO annotations for *TaL-LecRLK* genes were retrieved from the agriGO v2 database (http://systemsbiology.cau.edu.cn/agriGOv2/, accessed on 6 March 2025) [81,82] and visualized using GraphPad Prism software (version 9.5).

4.8. Tissue Expression Profiling of TaL-LecRLK Genes

To investigate the expression patterns of *TaL-LecRLK* genes across different wheat organs, RNA-seq data representing various developmental stages were retrieved from the Wheat Expression Browser (https://www.wheat-expression.com/, accessed on 10 March 2025) [6]. Transcripts per kilobase million (TPM) values from multiple tissues and time points were extracted as measures of gene expression for *TaL-LecRLK* genes or their homologs. Expression profiles were visualized in a heatmap based on $\log_2$ (TPM+1) values [77], generated using TBtools-II [64].

4.9. Plant Cultivation, Growth Conditions, and Stress Treatments

Seeds of the wheat cultivar 'Chinese Spring' (*Triticum aestivum* L.) were germinated in plastic pots filled with a peat-based growth medium. Plants were maintained in growth chambers under controlled conditions: 22 °C/20 °C day/night temperatures, 60% relative humidity, and a 16-h light/8-h dark photoperiod. One week after sowing, seedlings were subjected to the following treatments: (1) Drought stress: seedlings were transferred to culture dishes lined with dry filter paper to rapidly induce water deficiency. (2) Heat stress: seedlings were placed in an illuminated growth chamber set to 42 °C. (3) Exogenous ABA application: a 100 μM abscisic acid (ABA) solution was uniformly sprayed onto the seedling leaves. Leaf tissues were harvested at 0, 3, 6, and 24 h after treatment, with three biological replicates per time point. All samples were immediately flash-frozen in liquid nitrogen and stored at −80 °C for further analyses.

4.10. RNA Isolation, RNA-Seq Library Preparation, and Illumina HiSeq 2000 Sequencing

Total RNA was extracted using the RNAiso Plus reagent (TaKaRa, Otsu, Japan), and first-strand cDNA synthesis was performed using an EX RT kit with gDNA remover (Zoman Biotech, Beijing, China). Three biological replicates were prepared for RNA-seq libraries. RNA quality and concentration were assessed using a NanoDrop 2000 spectrophotometer (Thermo Fisher Scientific, Wilmington, DE, USA), and RNA integrity was verified with an Agilent 2100 Bioanalyzer (Agilent Technologies, Palo Alto, CA, USA) [83].

Qualified RNA samples were submitted to Beijing Biomarker Technologies (BMKGENE, Beijing, China) for sequencing on the Illumina HiSeq 2000 platform (Illumina, San Diego, CA, USA) in PE150 mode. Raw reads were subjected to quality filtering to remove adapter sequences and low-quality reads [84]. Clean reads were aligned to the wheat reference genome (*Triticum_aestivum*.v2.1.genome.fa), and downstream analyses, including expression quantification, differential expression analysis, and functional annotation, were

performed using BMKCloud tools (https://www.biocloud.net/, accessed on 21 March 2025). DEGs were identified based on fold change ≥ 2 and FDR < 0.01.

4.11. Quantitative Real-Time PCR (qRT-PCR) Analysis and Statistical Methods

A qRT-PCR was performed on an ABI QuantStudio 7 Flex real-time PCR system (Life Technologies, Carlsbad, CA, USA) using 2× HQ SYBR qPCR Mix (Zoman Biotech, Beijing, China) according to the manufacturer's guidelines. Wheat β-actin was used as the internal control. All qRT-PCR reactions included three biological replicates. Relative gene expression level was calculated using the $2^{-\Delta\Delta Ct}$ method [85], and results were visualized using GraphPad Prism (v9.5). Data are presented as mean ± standard deviation (SD). Statistical analysis was conducted using one-way ANOVA, with significance levels set at * ($p < 0.05$) and ** ($p < 0.01$). Primer sequences are listed in Table S12.

5. Conclusions

In this study, 248 *TaL-LecRLK* genes were identified in the wheat genome, and a comprehensive analysis was conducted encompassing their phylogenetic relationships, chromosomal localization, gene structure, conserved motifs, *cis*-acting elements, and expression patterns. The *TaL-LecRLK* genes were primarily classified into four subfamilies. Segmental and tandem duplication events jointly contributed to the expansion of this gene family, with purifying selection playing a critical role in its evolutionary formation. The exon-intron structures and conserved motifs of the encoded proteins exhibited considerable diversity. *Cis*-element analysis indicated potential involvement of *TaL-LecRLKs* genes in hormonal regulation and responses to abiotic stress. Tissue-specific transcriptome data demonstrated distinct, stage-specific expression patterns. RNA-Seq analyses under drought and heat stress conditions showed that differentially expressed *TaL-LecRLK* genes displayed coordinated or antagonistic regulatory responses to different stress treatments. Furthermore, qRT-PCR validation suggested that six *TaL-LecRLKs* genes may operate through ABA-independent regulatory mechanisms. These findings lay the groundwork for future functional studies on *L-LecRLK* genes in wheat and offer new research perspectives into their evolutionary dynamics and potential biological roles.

Supplementary Materials: The following supporting information can be downloaded at https://www.mdpi.com/article/10.3390/plants14121884/s1: Figure S1. Phylogenetic analysis of the 248 L-type Lectin Receptor-like Kinases (L-LecRLKs) in wheat (*Triticum aestivem* L.). Figure S2. Syntenic relationships of wheat *L-LecRLK* genes with *Arabidopsis thaliana* and *Oryza sativa*. Genomic collinearity regions between wheat and other species are indicated by gray lines. Blue and red lines highlight syntenic L-LecRLK gene pairs between wheat-Arabidopsis and wheat-rice, respectively. Figure S3. Analysis of *TaL-LecRLK* gene promoters and their *cis*-acting elements. (a) Distribution of predicted *cis*-acting elements in the promoter regions; (b) Quantification of different *cis*-acting elements in each promoter. Figure S4. Venn diagram of differentially expressed genes (DEGs) ($|\log_2\text{FoldChange}| \geq 1$, FDR < 0.01) under drought and heat stress at different time points. Detailed data are provided in Supplementary Table S11. Table S1. List of 248 *TaL-LecRLK* genes identified in the wheat (*Triticum aestivem* L.) genome. Table S2. Detailed information on homoeologous gene groups of the *TaL-LecRLK* genes in wheat. Table S3. List of L-type LecRLKs in *Arabidopsis thaliana* and *Oryza sativa* genome. Table S4. Ka/Ks ratios of duplicated *TaL-LecRLK* gene pairs. Table S5. Identification and classification of *cis*-acting elements in the promoters of 248 *TaL-LecRLK* genes. Table S6. Gene ontology analysis of *TaL-LecRLK* genes. Table S7. TPM values of the 248 *TaL-LecRLK* genes in different wheat tissues and developmental stages. Table S8. Expression profiles of 248 *TaL-LecRLK* genes across diverse tissues and developmental stages (presented as $\log_2$(TPM+1) values). Table S9. Transcriptome sequencing data of the 248 *TaL-LecRLK* genes in wheat before and after drought and heat stress treatments. Table S10. Expression profiles of 248 *TaL-LecRLK*

genes under normal and stress conditions. Mean FPKM (Fragments Per Kilobase of transcript per Million mapped reads) values calculated from three biological replicates. Table S11. Significantly differentially expressed *TaL-LecRLK* genes in stress-treated vs control groups. Table S12. Primers used for qRT-PCR in this study.

Author Contributions: X.C. and Z.X. conceived and designed the experiments. W.Z. performed the experiments and drafted the manuscript. F.Z. collected data from previous studies and revised the manuscript. J.W., J.F. and X.M. conducted the bioinformatics analyses. Z.C. managed plant cultivation, performed RNA extraction, and maintained the experimental materials. S.F. designed the primers and performed the qRT-PCR experiments. All authors have read and agreed to the published version of the manuscript.

Funding: This work was financially supported by the High-Level Talent Research Start-up Project of the Henan Academy of Sciences (231816038), the Fundamental Research Fund of the Henan Academy of Sciences (240618032), the Joint Fund of Henan Provincial Science and Technology Research and Development Plan (235200810010), and the Agriculture Research System of Henan Province (HARS-22-01-Z1).

Data Availability Statement: All data generated or analyzed during this study are included in the article and its Supplementary Materials.

Conflicts of Interest: Authors W.Z., F.Z., J.W., Z.C., X.M., J.F. and X.C. were employed by Isotope Institute Co., Ltd., Henan Academy of Sciences. The remaining authors declare that the research was conducted in the absence of any commercial or financial relationships that could be construed as a potential conflict of interest.

References

1. Ammar, M.K.; Hanafi, R.S.; Choucry, M.A.; Handoussa, J. Structural, functional, nutritional composition and analytical profiling of *Triticum aestivum* L. *Appl. Biol. Chem.* **2023**, *66*, 48. [CrossRef]
2. Li, J.; Yang, J.; Li, Y.; Ma, L. Current strategies and advances in wheat biology. *Crop J.* **2020**, *8*, 879–891. [CrossRef]
3. Wang, J.; Luo, M.C.; Chen, Z.; You, F.M.; Wei, Y.; Zheng, Y.; Dvorak, J. *Aegilops tauschii* single nucleotide polymorphisms shed light on the origins of wheat D-genome genetic diversity and pinpoint the geographic origin of hexaploid wheat. *New Phytol.* **2013**, *19*, 925–937. [CrossRef] [PubMed]
4. Zhao, X.; Guo, Y.; Kang, L.; Yin, C.; Bi, A.; Xu, D.; Zhang, Z.; Zhang, J.; Yang, X.; Xu, J.; et al. Population genomics unravels the Holocene history of bread wheat and its relatives. *Nat. Plants* **2023**, *9*, 403–419. [CrossRef]
5. IWGSC. Shifting the limits in wheat research and breeding using a fully annotated reference genome. *Science* **2018**, *361*, eaar7191. [CrossRef]
6. Ramírez-González, R.; Borrill, P.; Lang, D.; Harrington, S.; Brinton, J.; Venturini, L.; Davey, D.; Jacobs, J.; van Ex, F.; Pashaet, A.; et al. The transcriptional landscape of polyploid wheat. *Science* **2018**, *361*, eaar6089. [CrossRef]
7. Sun, Y.; Qiao, Z.; Muchero, W.; Chen, J.G. Lectin receptor-like kinases: The sensor and mediator at the plant cell surface. *Front. Plant Sci.* **2020**, *11*, 596301. [CrossRef]
8. Vaid, N.; Macovei, A.; Tuteja, N. Knights in action: Lectin receptor-like kinases in plant development and stress responses. *Mol. Plant* **2013**, *6*, 1405–1418. [CrossRef]
9. De Coninck, T.; Van Damme, E.J.M. Plant lectins: Handymen at the cell surface. *Cell Surf.* **2022**, *8*, 100091. [CrossRef]
10. Bellande, K.; Bono, J.J.; Savelli, B.; Jamet, E.; Canut, H. Plant lectins and lectin receptor-like kinases: How do they sense the outside? *Int. J. Mol. Sci.* **2017**, *18*, 1164. [CrossRef]
11. Reidling, J.C.; Miller, M.A.; Steele, R.E. Sweet Tooth, a novel receptor protein-tyrosine kinase with C-type lectin-like extracellular domains. *J. Biol. Chem.* **2000**, *275*, 10323–10330. [CrossRef] [PubMed]
12. Liu, P.L.; Huang, Y.; Shi, P.H.; Yu, M.; Xie, J.B.; Xie, L. Duplication and diversification of lectin receptor-like kinases (LecRLK) genes in soybean. *Sci. Rep.* **2018**, *8*, 5861. [CrossRef] [PubMed]
13. Vaid, N.; Pandey, P.K.; Tuteja, N. Genome-wide analysis of lectin receptor-like kinase family from Arabidopsis and rice. *Plant Mol. Biol.* **2012**, *80*, 365–388. [CrossRef] [PubMed]
14. Zhao, W.; Liu, Y.W.; Zhou, J.M.; Zhao, S.P.; Zhang, X.H.; Min, D.H. Genome-wide analysis of the lectin receptor-like kinase family in foxtail millet (*Setaria italica* L.). *Plant Cell Tiss. Organ Cult.* **2016**, *127*, 335–346. [CrossRef]

15. Ahmed, F.F.; Dola, F.S.; Islam, M.S.U.; Zohra, F.T.; Akter, N.; Rahman, S.M.; Sarkar, M.A.R. Genome-wide comprehensive identification and in silico characterization of lectin receptor-like kinase gene family in barley (*Hordeum vulgare* L.). *Genet. Res.* **2024**, *2024*, 2924953. [CrossRef]
16. Shiu, S.H.; Bleecker, A.B. Receptor-like kinases from *Arabidopsis* form a monophyletic gene family related to animal receptor kinases. *Proc. Natl. Acad. Sci. USA* **2001**, *98*, 10763–10768. [CrossRef]
17. Tang, D.; Wang, G.; Zhou, J.M. Receptor kinases in plant-pathogen interactions: More than pattern recognition. *Plant Cell* **2007**, *29*, 618–637. [CrossRef]
18. Naithani, S.; Chookajorn, T.; Ripoll, D.R.; Nasrallah, J.B. Structural modules for receptor dimerization in the S-locus receptor kinase extracellular domain. *Proc. Natl. Acad. Sci. USA* **2007**, *104*, 12211–12216. [CrossRef]
19. Wang, Y.; Bouwmeester, K. L-type lectin receptor kinases: New forces in plant immunity. *PLoS Pathog.* **2017**, *13*, e1006433. [CrossRef]
20. Osterne, V.J.S.; Sloover, G.D.; Van Damme, E.J.M. Revisiting legume lectins: Structural organization and carbohydrate-binding properties. *Carbohydr. Res.* **2024**, *544*, 109241. [CrossRef]
21. Morillo, S.A.; Tax, F.E. Functional analysis of receptor-like kinases in monocots and dicots. *Curr. Opin. Plant Biol.* **2006**, *9*, 460–469. [CrossRef] [PubMed]
22. Wang, Y.; Weide, R.; Govers, F.; Bouwmeester, K. L-type lectin receptor kinases in *Nicotiana benthamiana* and tomato and their role in *Phytophthora* resistance. *J. Exp. Bot.* **2015**, *66*, 6731–6743. [CrossRef] [PubMed]
23. Chen, X.; Shang, J.; Chen, D.; Lei, C.; Zou, Y.; Zhai, W.; Liu, G.; Xu, J.; Ling, Z.; Cao, G.; et al. A B-lectin receptor kinase gene conferring rice blast resistance. *Plant J.* **2006**, *46*, 794–804. [CrossRef] [PubMed]
24. Barre, A.; Hervé, C.; Lescure, B.; Rougé, P. Lectin receptor kinases in plants. *Crit. Rev. Plant Sci.* **2002**, *21*, 379–399. [CrossRef]
25. Wang, R.; Li, C.; Jia, Z.; Su, Y.; Ai, Y.; Li, Q.; Guo, X.; Tao, Z.; Lin, F.; Liang, Y. Reversible phosphorylation of a lectin-receptor-like kinase controls xylem immunity. *Cell Host Microbe* **2023**, *31*, 2051–2066.e7. [CrossRef]
26. Chen, K.; Wang, Q.; Yu, X.; Wang, C.; Gao, J.; Zhang, S.; Cheng, S.; You, S.; Zheng, H.; Lu, J.; et al. OsSRF8 interacts with OsINP1 and OsDAF1 to regulate pollen aperture formation in rice. *Nat. Commun.* **2024**, *15*, 4512. [CrossRef]
27. Xiao, W.; Hu, S.; Zou, X.; Cai, R.; Liao, R.; Lin, X.; Yao, R.; Guo, X. Lectin receptor-like kinase LecRK-VIII.2 is a missing link in MAPK signaling-mediated yield control. *Plant Physiol.* **2021**, *186*, 445–458. [CrossRef]
28. Mehla, S.; Singh, Y.; Kumar, U.; Balyan, P.; Singh, K.P.; Dhankher, O.P. Overexpression of rice lectin receptor-like kinase, OsLecRLK, confers salinity stress tolerance and increases seed yield in pigeon pea (*Cajanus cajan* (L.) Millsp.). *Plant Cell Rep.* **2024**, *43*, 230. [CrossRef]
29. Wu, F.; Qu, D.; Zhang, X.; Sun, Y.; Wang, J.; Zhu, D.; Yang, L.; Liu, X.; Tian, W.; Wang, L.; et al. PaLectinL7 enhances salt tolerance of sweet cherry by regulating lignin deposition in connection with PaCAD1. *Tree Physiol.* **2023**, *43*, 1986–2000. [CrossRef]
30. Ma, N.; Liu, C.; Li, H.; Wang, J.; Zhang, B.; Lin, J.; Chang, Y. Genome-wide identification of lectin receptor kinases in pear: Functional characterization of the L-type LecRLK gene *PbLRK138*. *Gene* **2018**, *661*, 11–21. [CrossRef]
31. Yang, X.; Chen, Z.; Lu, J.; Wei, X.; Yao, Y.; Lv, W.; Han, J.; Fei, J. Identification and characterization of the LecRLKs gene family in maize, and its role under biotic and abiotic stress. *Biology* **2024**, *14*, 20. [CrossRef] [PubMed]
32. Xiong, G.; Cui, D.; Tian, Y.; Schwarzacher, T.; Heslop-Harrison, J.S.; Liu, Q. Genome-wide identification of the lectin receptor-like kinase gene family in *Avena sativa* and its role in salt stress tolerance. *Int. J. Mol. Sci.* **2024**, *25*, 12754. [CrossRef] [PubMed]
33. Biswas, S.; Mondal, R.; Srivastava, A.; Trivedi, M.; Singh, S.K.; Mishra, Y. In silico characterization, molecular phylogeny, and expression profiling of genes encoding legume lectin-like proteins under various abiotic stresses in *Arabidopsis thaliana*. *BMC Genom.* **2022**, *23*, 480. [CrossRef] [PubMed]
34. Shumayla; Sharma, S.; Pandey, A.K.; Singh, K.; Upadhyay, S.K. Molecular characterization and global expression analysis of lectin receptor kinases in bread wheat (*Triticum aestivum*). *PLoS ONE* **2016**, *11*, e0153925. [CrossRef]
35. Lv, D.; Wang, G.; Xiong, L.R.; Sun, J.X.; Chen, Y.; Guo, C.L.; Yu, Y.; He, H.L.; Cai, R.; Pan, J.S. Genome-wide identification and characterization of lectin receptor-like kinase gene family in cucumber and expression profiling analysis under different treatments. *Genes* **2020**, *11*, 1032. [CrossRef]
36. Haider, M.S.; De Britto, S.; Nagaraj, G.; Gurulingaiah, B.; Shekhar, R.; Ito, S.I.; Jogaiah, S. Genome-wide identification, diversification, and expression analysis of lectin receptor-like kinase (LecRLK) gene family in cucumber under biotic stress. *Int. J. Mol. Sci.* **2021**, *22*, 6585. [CrossRef]
37. Birchler, J.A.; Yang, H. The multiple fates of gene duplications: Deletion, hypofunctionalization, subfunctionalization, neofunctionalization, dosage balance constraints, and neutral variation. *Plant Cell* **2022**, *34*, 2466–2474. [CrossRef]
38. Cui, L.; Cheng, H.; Yang, Z.; Xia, C.; Zhang, L.; Kong, X. Comparative analysis reveals different evolutionary fates and biological functions in wheat duplicated genes (*Triticum aestivum* L.). *Plants* **2023**, *12*, 3021. [CrossRef]
39. Li, Y.; Xiang, R.; Liu, K.; Ahmad, B.; Zhang, X.; Yang, L.; Tian, Y.; Shi, X.; Du, G.; Wang, L. Genomic-organization and expression profiling of lectin receptor kinases genes suggest their involvement in multiple biological processes. *Sci. Hortic.* **2024**, *329*, 113042. [CrossRef]

40. Wang, T.; Duan, S.; Xu, C.; Wang, Y.; Zhang, X.; Xu, X.; Chen, L.; Han, Z.; Wu, T. Pan-genome analysis of 13 *Malus* accessions reveals structural and sequence variations associated with fruit traits. *Nat. Commun.* **2023**, *14*, 7377. [CrossRef]
41. Jeffares, D.C.; Penkett, C.J.; Bähler, J. Rapidly regulated genes are intron poor. *Trends Genet.* **2008**, *24*, 375–378. [CrossRef] [PubMed]
42. Chung, B.Y.; Simons, C.; Firth, A.E.; Brown, C.M.; Hellens, R.P. Effect of 5'UTR introns on gene expression in *Arabidopsis thaliana*. *BMC Genom.* **2006**, *7*, 120. [CrossRef] [PubMed]
43. Aviña-Padilla, K.; Ramírez-Rafael, J.A.; Herrera-Oropeza, G.E.; Muley, V.Y.; Valdivia, D.I.; Díaz-Valenzuela, E.; García-García, A.; Varela-Echavarría, A.; Hernández-Rosales, M. Evolutionary perspective and expression analysis of intronless genes highlight the conservation of their regulatory role. *Front. Genet.* **2021**, *12*, 654256. [CrossRef] [PubMed]
44. Chen, Z.; Zhou, L.; Jiang, P.; Lu, R.; Halford, N.G.; Liu, C. Genome-wide identification of sucrose nonfermenting-1-related protein kinase (SnRK) genes in barley and RNA-seq analyses of their expression in response to abscisic acid treatment. *BMC Genom.* **2021**, *22*, 300. [CrossRef]
45. Marcussen, T.; Sandve, S.R.; Heier, L.; Spannagl, M.; Pfeifer, M.; International Wheat Genome Sequencing Consortium; Jakobsen, K.S.; Wulff, B.B.; Steuernagel, B.; Mayer, K.F.; et al. Ancient hybridizations among the ancestral genomes of bread wheat. *Science* **2014**, *345*, 1250092. [CrossRef]
46. Feng, X.; Chen, Q.; Wu, W.; Wang, J.; Li, G.; Xu, S.; Shao, S.; Liu, M.; Zhong, C.; Wu, C.I.; et al. Genomic evidence for rediploidization and adaptive evolution following the whole-genome triplication. *Nat. Commun.* **2024**, *15*, 1635. [CrossRef]
47. Ren, R.; Wang, H.; Guo, C.; Zhang, N.; Zeng, L.; Chen, Y.; Ma, H. Widespread whole genome duplications contribute to genome complexity and species diversity in angiosperms. *Mol. Plant* **2018**, *11*, 414–428. [CrossRef]
48. Li, J.; Cui, C.; Han, F.; Liu, J. Genome-wide identification and analysis of the UBA2 gene family in wheat (*Triticum aestivum* L.). *BMC Genom.* **2025**, *26*, 180. [CrossRef]
49. Das, M.; Haberer, G.; Panda, A.; Das Laha, S.; Ghosh, T.C.; Schäffner, A.R. Expression pattern similarities support the prediction of orthologs retaining common functions after gene duplication events. *Plant Physiol.* **2016**, *171*, 2343–2357. [CrossRef]
50. Yang, Q.; Han, X.M.; Gu, J.K.; Liu, Y.J.; Yang, M.J.; Zeng, Q.Y. Functional and structural profiles of GST gene family from three *Populus* species reveal the sequence-function decoupling of orthologous genes. *New Phytol.* **2019**, *221*, 1060–1073. [CrossRef]
51. Schmitz, R.J.; Grotewold, E.; Stam, M. *Cis*-regulatory sequences in plants: Their importance, discovery, and future challenges. *Plant Cell* **2022**, *34*, 718–741. [CrossRef] [PubMed]
52. Huang, S.; Wang, C.; Ding, Z.; Zhao, Y.; Dai, J.; Li, J.; Huang, H.; Wang, T.; Zhu, M.; Feng, M.; et al. A plant NLR receptor employs ABA central regulator PP2C-SnRK2 to activate antiviral immunity. *Nat. Commun.* **2024**, *15*, 3205. [CrossRef] [PubMed]
53. Zhang, B.; Wang, Z.; Dai, X.; Gao, J.; Zhao, J.; Ma, R.; Chen, Y.; Sun, Y.; Ma, H.; Li, S.; et al. A COMPASS histone H3K4 trimethyltransferase pentamer transactivates drought tolerance and growth/biomass production in *Populus trichocarpa*. *New Phytol.* **2024**, *241*, 1950–1972. [CrossRef] [PubMed]
54. Guo, S.; Zhang, F.; Du, X.; Zhang, X.; Huang, X.; Li, Z.; Zhang, Y.; Gan, P.; Li, H.; Li, M.; et al. TaANK-TPR1 enhances wheat resistance against stripe rust via controlling gene expression and protein activity of NLR protein TaRPP13L1. *Dev. Cell* **2025**, *60*, 1–17. [CrossRef]
55. Li, Z.; Zhang, J.; Li, J.; Li, H.; Zhang, G. The functional and regulatory mechanisms of the *Thellungiella salsuginea* Ascorbate Peroxidase 6 (TsAPX6) in response to salinity and water deficit stresses. *PLoS ONE* **2016**, *11*, e0154042. [CrossRef]
56. Sato, H.; Mizoi, J.; Shinozaki, K.; Yamaguchi-Shinozaki, K. Complex plant responses to drought and heat stress under climate change. *Plant J.* **2024**, *117*, 1873–1892. [CrossRef]
57. Yekondi, S.; Liang, F.C.; Okuma, E.; Radziejwoski, A.; Mai, H.W.; Swain, S.; Singh, P.; Gauthier, M.; Chien, H.C.; Murata, Y.; et al. Nonredundant functions of Arabidopsis LecRKV.2 and LecRK-Vll.1 in controlling stomatal immunity andjasmonate-mediated stomatal closurey. *New Phytol.* **2018**, *218*, 253–268. [CrossRef]
58. Balagué, C.; Gouget, A.; Bouchez, O.; Souriac, C.; Haget, N.; Boutet-Mercey, S.; Govers, F.; Roby, D.; Canut, H. The *Arabidopsis thaliana* lectin receptor kinase LecRK-I.9 is required for full resistance to *Pseudomonas syringae* and affects jasmonate signalling. *Mol. Plant Pathol.* **2017**, *18*, 937–948. [CrossRef]
59. Sun, M.; Qian, X.; Chen, C.; Cheng, S.; Jia, B.; Zhu, Y.; Sun, X. Ectopic expression of *GsSRK* in *Medicago sativa* reveals its involvement in plant architecture and salt stress responses. *Front. Plant Sci.* **2018**, *9*, 226. [CrossRef]
60. Osman, M.E.M.; Osman, R.S.H.; Elmubarak, S.A.; Ibrahim, M.A.; Abakar, H.B.M.; Dirar, A.I.; Konozy, E.H.E. In silico analysis of L- and G-type lectin receptor kinases in tomato: Evolution, diversity, and abiotic responses. *BMC Genom.* **2024**, *25*, 1143. [CrossRef]
61. Bolser, D.M.; Staines, D.M.; Perry, E.; Kersey, P.J. Ensembl plants: Integrating tools for visualizing, mining, and analyzing plant genomic data. *Methods Mol. Biol.* **2017**, *1533*, 1–31. [CrossRef] [PubMed]
62. Kawahara, Y.; de la Bastide, M.; Hamilton, J.P.; Kanamori, H.; McCombie, W.R.; Ouyang, S.; Schwartz, D.C.; Tanaka, T.; Wu, J.; Zhou, S.; et al. Improvement of the *Oryza sativa* Nipponbare reference genome using next generation sequence and optical map data. *Rice* **2013**, *6*, 4. [CrossRef] [PubMed]

63. Mistry, J.; Chuguransky, S.; Williams, L.; Qureshi, M.; Salazar, G.A.; Sonnhammer, E.L.L.; Tosatto, S.C.E.; Paladin, L.; Raj, S.; Richardson, L.J.; et al. Pfam: The protein families database in 2021. *Nucleic Acids Res.* **2021**, *49*, D412–D419. [CrossRef] [PubMed]
64. Chen, C.; Wu, Y.; Li, J.; Wang, X.; Zeng, Z.; Xu, J.; Liu, Y.; Feng, J.; Chen, H.; He, Y.; et al. TBtools-II: A "one for all, all for one" bioinformatics platform for biological big-data mining. *Mol. Plant* **2023**, *16*, 1733–1742. [CrossRef]
65. Lu, S.; Wang, J.; Chitsaz, F.; Derbyshire, M.K.; Geer, R.C.; Gonzales, N.R.; Gwadz, M.; Hurwitz, D.I.; Marchler, G.H.; Song, J.S.; et al. CDD/SPARCLE: The conserved domain database in 2020. *Nucleic Acids Res.* **2020**, *48*, D265–D268. [CrossRef]
66. Wang, J.; Chitsaz, F.; Derbyshire, M.K.; Gonzales, N.R.; Gwadz, M.; Lu, S.; Marchler, G.H.; Song, J.S.; Thanki, N.; Yamashita, R.A.; et al. The conserved domain database in 2023. *Nucleic Acids Res.* **2023**, *51*, D384–D388. [CrossRef]
67. Letunic, I.; Khedkar, S.; Bork, P. SMART: Recent updates, new developments and status in 2020. *Nucleic Acids Res.* **2021**, *49*, D458–D460. [CrossRef]
68. Artimo, P.; Jonnalagedda, M.; Arnold, K.; Baratin, D.; Csardi, G.; de Castro, E.; Duvaud, S.; Flegel, V.; Fortier, A.; Gasteiger, E.; et al. ExPASy: SIB bioinformatics resource portal. *Nucleic Acids Res.* **2012**, *40*, W597–W603. [CrossRef]
69. Chou, K.C.; Shen, H.B. Plant-mPLoc: A top-down strategy to augment the power for predicting plant protein subcellular localization. *PLoS ONE* **2010**, *5*, e11335. [CrossRef]
70. Goodstein, D.M.; Shu, S.; Howson, R.; Neupane, R.; Hayes, R.D.; Fazo, J.; Mitros, T.; Dirks, W.; Hellsten, U.; Putnam, N.; et al. Phytozome: A comparative platform for green plant genomics. *Nucleic Acids Res.* **2012**, *40*, D1178–D1186. [CrossRef]
71. Edgar, R.C. Muscle5: High-accuracy alignment ensembles enable unbiased assessments of sequence homology and phylogeny. *Nat. Commun.* **2022**, *13*, 6968. [CrossRef] [PubMed]
72. Price, M.N.; Dehal, P.S.; Arkin, A.P. FastTree 2--approximately maximum-likelihood trees for large alignments. *PLoS ONE* **2010**, *5*, e9490. [CrossRef] [PubMed]
73. Letunic, I.; Bork, P. Interactive Tree of Life (iTOL) v6: Recent updates to the phylogenetic tree display and annotation tool. *Nucleic Acids Res.* **2024**, *52*, W78–W82. [CrossRef] [PubMed]
74. Hu, B.; Jin, J.; Guo, A.Y.; Zhang, H.; Luo, J.; Gao, G. GSDS 2.0: An upgraded gene feature visualization server. *Bioinformatics* **2015**, *31*, 1296–1297. [CrossRef]
75. Bailey, T.L.; Johnson, J.; Grant, C.E.; Noble, W.S. The MEME Suite. *Nucleic Acids Res.* **2015**, *43*, W39–W49. [CrossRef]
76. Schilling, S.; Kennedy, A.; Pan, S.; Jermiin, L.S.; Melzer, R. Genome-wide analysis of MIKC-type MADS-box genes in wheat: Pervasive duplications, functional conservation and putative neofunctionalization. *New Phytol.* **2020**, *225*, 511–529. [CrossRef]
77. Xu, X.; Zhang, L.; Zhao, W.; Fu, L.; Han, Y.; Wang, K.; Yan, L.; Li, Y.; Zhang, X.H.; Min, D.H. Genome-wide analysis of the serine carboxypeptidase-like protein family in *Triticum aestivum* reveals *TaSCPL184-6D* is involved in abiotic stress response. *BMC Genom.* **2021**, *22*, 350. [CrossRef]
78. Zhang, Z. KaKs_calculator 3.0: Calculating selective pressure on coding and non-coding sequences. *Genom. Proteom. Bioinf.* **2022**, *20*, 536–540. [CrossRef]
79. Han, Y.; Zhang, L.; Yan, L.; Xiong, X.; Wang, W.; Zhang, X.H.; Min, D.H. Genome-wide analysis of TALE superfamily in *Triticum aestivum* reveals *TaKNOX11-A* is involved in abiotic stress response. *BMC Genom.* **2022**, *23*, 89. [CrossRef]
80. Lescot, M.; Déhais, P.; Thijs, G.; Marchal, K.; Moreau, Y.; Van de Peer, Y.; Rouzé, P.; Rombauts, S. PlantCARE, a database of plant *cis*-acting regulatory elements and a portal to tools for in silico analysis of promoter sequences. *Nucleic Acids Res.* **2002**, *30*, 325–327. [CrossRef]
81. Tian, T.; Liu, Y.; Yan, H.; You, Q.; Yi, X.; Du, Z.; Xu, W.; Su, Z. agriGO v2.0: A GO analysis toolkit for the agricultural community, 2017 update. *Nucleic Acids Res.* **2017**, *45*, W122–W129. [CrossRef] [PubMed]
82. Kan, W.; Gao, Y.; Zhu, Y.; Wang, Z.; Yang, Z.; Cheng, Y.; Guo, J.; Wang, D.; Tang, C.; Wu, L. Genome-wide identification and expression analysis of TaFDL gene family responded to vernalization in wheat (*Triticum aestivum* L.). *BMC Genom.* **2025**, *26*, 255. [CrossRef] [PubMed]
83. Zhou, T.; Xing, Q.; Bu, J.; Han, W.; Shen, Z. Integrated metabolomic and transcriptomic analysis reveals the regulatory mechanisms of flavonoid and alkaloid biosynthesis in the new and old leaves of *Murraya tetramera* Huang. *BMC Plant Biol.* **2024**, *24*, 499. [CrossRef] [PubMed]
84. Burchardt, S.; Czernicka, M.; Kućko, A.; Pokora, W.; Kapusta, M.; Domagalski, K.; Jasieniecka-Gazarkiewicz, K.; Karwaszewski, J.; Wilmowicz, E. Exploring the response of yellow lupine (*Lupinus luteus* L.) root to drought mediated by pathways related to phytohormones, lipid, and redox homeostasis. *BMC Plant Biol.* **2024**, *24*, 1049. [CrossRef]
85. Udvardi, M.K.; Czechowski, T.; Scheible, W.R. Eleven golden rules of quantitative RT-PCR. *Plant Cell* **2008**, *20*, 1736–1737. [CrossRef]

plants

MDPI

Article

Genome-Wide Identification of *ATL* Gene Family in Wheat and Their Expression Analysis in Response to Salt Stress

Xuqing Li, Shuotong Liu and Pei Yu *

SDU-ANU Joint Science College, Shandong University, Weihai 264209, China;
202200700253@mail.sdu.edu.cn (X.L.); liushuotong@mail.sdu.edu.cn (S.L.)
* Correspondence: yupei@sdu.edu.cn

Abstract: Wheat (*Triticum aestivum*) is one of the most important cereal crops globally, with significant economic value. The Arabidopsis Tóxicos en Levadura (*ATL*) gene family, which comprises members of ubiquitin ligase enzymes (E3s), functions in substrate protein tagging during ubiquitin-mediated protein modification. Recent studies have demonstrated its involvement in stress responses. However, the *ATL* gene family in wheat remains poorly characterized. This study aimed to identify the members of the *ATL* gene family in wheat and investigate their roles under salt stress. We identified 334 *TaATL* genes in the wheat genome, all of which contain either RING-H2, RING U-box, or RAD18 superfamily domains, exhibiting a remarkably low proportion of intron-containing genes. The Ka/Ks (non-synonymous to synonymous substitution rate) analysis and *cis*-acting element analysis of the *TaATL* gene family indicate that its sequences are highly conserved and functionally constrained, suggesting that it may participate in abiotic stress responses through the ABA, MeJA, and MYB signaling pathways. Both RNA-seq analysis and RT-qPCR data demonstrated that the expression levels of the *TaATL* gene family were significantly upregulated under stress conditions, indicating their crucial roles in stress responses. This study demonstrates that the targeted regulation of stress-responsive signaling pathways mediated by superior *TaATL* gene family members can effectively enhance wheat salt tolerance, thereby providing a viable strategy for the development of high-yielding cultivars adapted to saline agricultural ecosystems.

Keywords: Arabidopsis Tóxicos en Levadura; E3 ligases in wheat; whole-genome characterization; abiotic stress

1. Introduction

Wheat (*Triticum aestivum*), a pivotal cereal crop in global agriculture, serves as a primary source of dietary calories and protein for a substantial proportion of the world's population. Nevertheless, wheat productivity is persistently challenged by diverse abiotic stresses, including drought, salinity, extreme thermal fluctuations, and others [1]. These environmental stresses significantly constrain wheat growth and development, ultimately affecting grain yields, thereby posing substantial threats to global food security [2]. Among these, salt stress adversely impacts plant growth and yields by inducing the accumulation of reactive oxygen species (ROS), which subsequently cause oxidative damage to DNA and proteins, disrupting cellular homeostasis and metabolic processes [3]. In the context of the escalating global population and intensifying climate change impacts, which exacerbate the frequency and magnitude of these stresses, elucidating the molecular mechanisms underlying wheat's response to abiotic stresses has become increasingly imperative [4].

The ubiquitin–proteasome system (UPS) represents a fundamental molecular mechanism in plant stress adaptation, orchestrating the degradation of misfolded or damaged proteins and modulating the turnover of regulatory proteins involved in stress signaling pathways [5]. Central to this system are E3 ubiquitin ligases, which are key determinants of target specificity for degradation by the 26S proteasome system [2,6]. Among these, the Arabidopsis Tóxicos en Levadura (*ATL*) family of RING-type E3 ubiquitin ligases, characterized by the presence of a conserved RING-H2 domain that is essential for their catalytic activity, has emerged as crucial regulators of plant stress responses [7].

The functional significance of *ATL* genes in stress adaptation has been extensively documented across diverse plant species, revealing the evolutionary conservation of their regulatory roles. In the model plant *Arabidopsis thaliana*, multiple *ATL* members have been implicated in mediating responses to various abiotic stresses, including drought, salinity, and cold stress [8]. Notably, in *Oryza sativa*, the *ATL*43 knockout line displays ABA hyposensitivity, suggesting its involvement in stress signaling through the ABA-dependent pathway [8]. Similarly, in maize (*Zea mays*), the expression of *ZmATL10* is significantly upregulated under high-temperature conditions, and the overexpression of this gene enhances thermotolerance, further underscoring the potential regulatory role of *ATL* genes in stress adaptation [9]. These collective findings position *ATL* genes as integral components of the plant stress signaling network, modulating critical physiological and biochemical processes to enhance stress tolerance.

Despite substantial progress in characterizing the functions of *ATL* genes in model plants and some crop species, the *ATL* gene family in hexaploid wheat remains largely unexplored. The inherent complexity of the wheat genome, characterized by its allohexaploid nature and substantial size, presents unique challenges for genetic investigations. However, given wheat's global agricultural significance and its particular vulnerability to abiotic stresses, it represents a crucial target for stress tolerance research. Recent breakthroughs in wheat genomics, particularly the completion of high-quality genome sequencing projects, have provided unprecedented opportunities for the comprehensive identification and functional characterization of stress-responsive genes, including those encoding E3 ubiquitin ligases.

This study systematically identifies and characterizes the wheat *ATL* (*TaATL*) gene family, with a specific focus on investigating its potential functions in salt stress responses. This research aims to elucidate the mechanisms underlying the role of this gene family in stress adaptation in wheat. Through integrative bioinformatics approaches coupled with experimental validation, we delineate the involvement of *TaATL*s in stress response pathways and identify key regulatory nodes within this gene family. The elucidation of *ATL* gene functions in wheat will not only advance our fundamental understanding of the stress response mechanisms in this crucial crop but also provide valuable genetic markers and candidate genes for molecular breeding programs aimed at developing stress-resilient wheat cultivars. This study provides the first comprehensive genome-wide analysis of the *ATL* gene family in hexaploid wheat, revealing novel insights into their evolutionary patterns and stress-responsive expression profiles and offering valuable genetic resources for wheat improvement. In light of the escalating challenges posed by climate change and the pressing need for sustainable agricultural practices, this research is anticipated to make significant contributions to global food security initiatives.

2. Results

2.1. Genome-Wide Identification of TaATL Family Genes

In this study, a combination of a HMMER search and BLASTp was used to identify 1198 genes of *TaATL*s. Next, domain screening was performed using the InterPro (version

104.0) platform, which resulted in the identification of 334 *ATL* family members containing either the RING-H2 finger domain or the E3 ubiquitin protein ligase domain, named *TaATL1* to *TaATL334* based on their chromosome localization (Figure 1). The *TaATL* family genes are uniformly distributed across all chromosomes except chromosome 3A, which lacks *TaATL* family genes. The RING-H2 finger and E3 ubiquitin protein ligase domains are characteristic structures of the *ATL* family E3 ubiquitin ligases, playing a crucial role in their enzymatic activity. To investigate the evolutionary relationships of the *TaATL* genes, a phylogenetic tree was constructed using the 334 genes from wheat in IQ-TREE. Based on the evolutionary tree branches and conserved structures and features of the genes, the *TaATL* family was classified into three phylogenetic clusters. Cluster I comprised 148 genes, Cluster II contained 83 genes, and Cluster III included 103 genes (Figure 2).

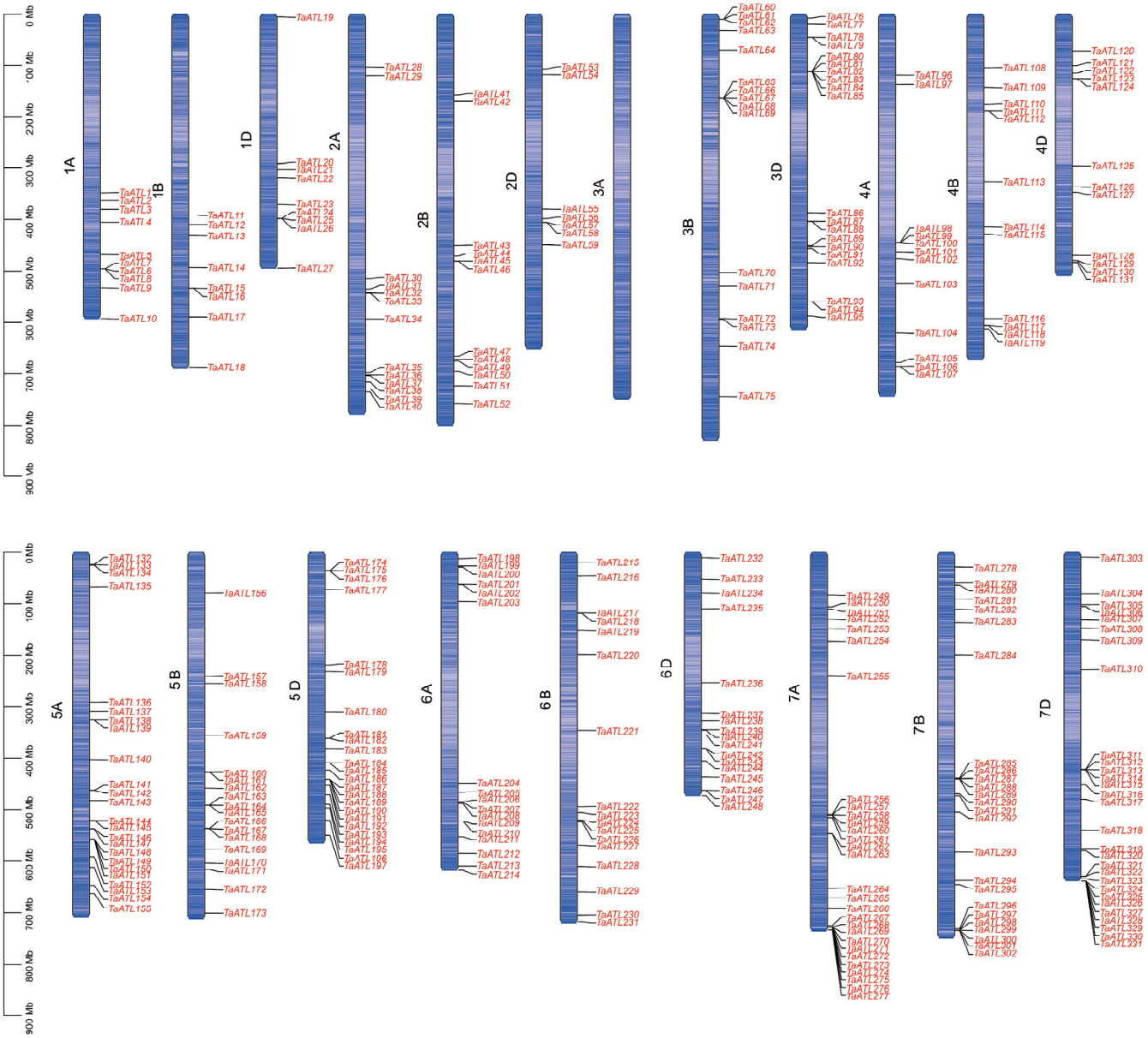

Figure 1. Chromosomal distribution of the Arabidopsis Tóxicos en Levadura gene family in wheat (*TaATL*). The gradient of the blue color on the chromosomes represents the gene density. The scale on the left indicates the base pair lengths (Mb) of the chromosomes.

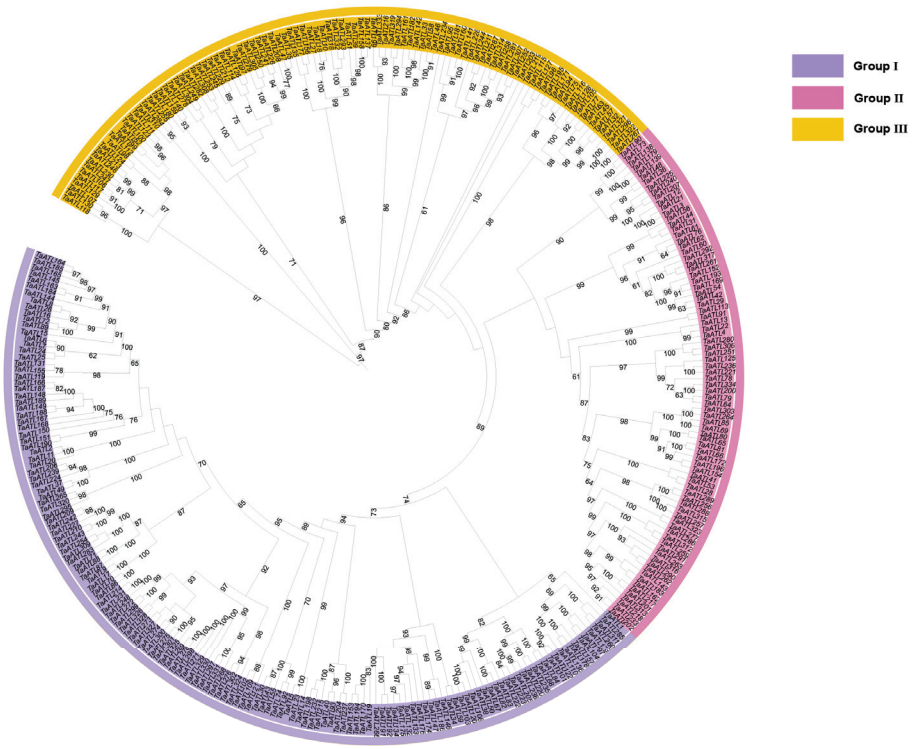

Figure 2. Phylogenetic analysis of *TaATL* family genes. Roman numerals I to III denote the three phylogenetic clusters. The numbers adjacent to the branches represent bootstrap values, with all values exceeding 60.

In addition, 105 *ATL* family genes were successfully extracted from *Aegilops tauschii*, 50 from *Triticum urartu*, 75 from *A. thaliana*, 68 from *Vitis vinifera*, and 121 from *Z. mays* (Figure S1). An ML phylogenetic tree was constructed using genes from six species, revealing six distinct evolutionary clusters, each comprising genes from all species. Among these, the *ATL* family genes of wheat exhibited the closest phylogenetic relationships with those of *A. tauschii*.

The physicochemical properties of the *TaATL* gene family were predicted, including the molecular weight, theoretical isoelectric point (pI), instability index, aliphatic index, and grand average of hydropathicity. The molecular weight varied from 13.09 kDa (*TaATL174*) to 47.85 kDa (*TaATL212*), and the theoretical isoelectric point (pI) ranged from 4.28 (*TaATL222*) to 11.1 (*TaATL220*), indicating the presence of both acidic and basic proteins in the *ATL* family. Among the proteins, 153 were acidic, 11 were neutral, and 168 were basic. The instability index spanned from 26.97 (*TaATL283*) to 95.76 (*TaATL135*), with most of the proteins exhibiting intrinsic instability. The aliphatic index ranged between 57.47 (*TaATL208*) and 121.6 (*TaATL73*). The grand average of hydropathicity varied from −0.521 (*TaATL47*) to 0.624 (*TaATL68*), with a balance between hydrophilic and hydrophobic proteins. Among them, 11 proteins were highly hydrophobic, while one protein (*TaATL242*) was highly hydrophilic. These results suggest that the *TaATL* family contains a large number of proteins with diverse characteristics. Cellular component analysis further elucidated the subcellular localization patterns, with the majority of the *TaATL* proteins predicted to be integral membrane components, while a subset was localized to intracellular organelles and nuclei (Table S1).

2.2. Gene Structure of TaATL Family Genes

Based on the wheat genome's annotation, the gene structure diagram of the *TaATL* family members was constructed using TBtools (version 2.210) (Figure 3). Upon analyzing

334 family members, only 35 genes contained introns, indicating a very low proportion of intron-containing genes within this family. Furthermore, in the *TaATL* gene family, the majority of the genes contain both 5′-UTRs and 3′-UTRs. However, 146 genes are missing untranslated regions (UTRs) on one end, and 10 genes lack untranslated regions altogether (Figure 3). The vast majority of the genes are composed of only a single exon of approximately 500–2000 bp, with only 35 genes having two to three exons. These findings indicate that the *TaATL* gene family exhibits a highly conserved and uniform gene structure, and this is consistent with the conclusions of previous studies on *Z. mays*, *A. thaliana*, and *O. sativa*, indicating that the *TaATL* family genes are likely to function as structural genes within functional modules.

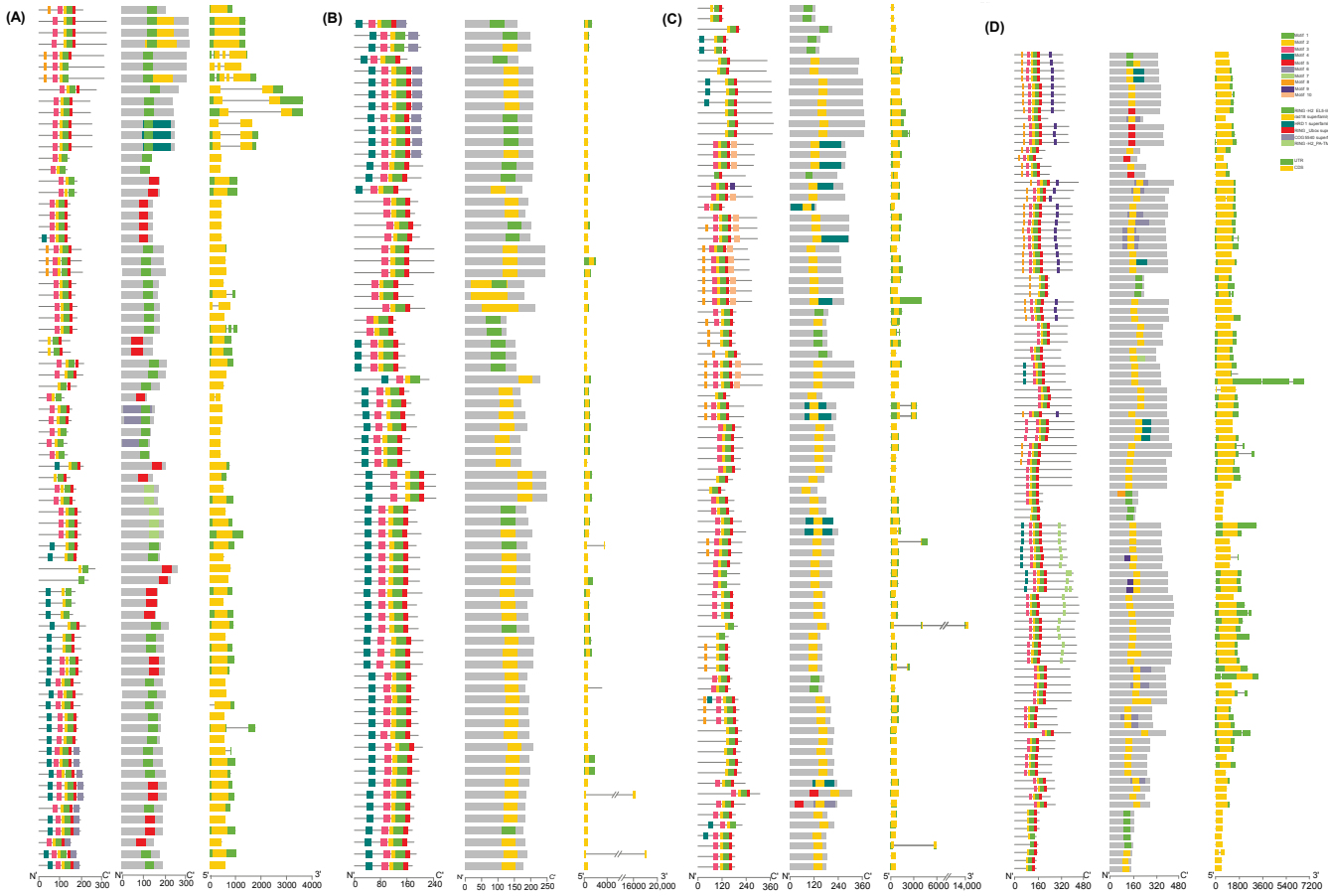

Figure 3. The motif distribution, conserved domains, and gene structures of *TaATL* genes. Panels (**A**,**B**) show genes from Cluster I, (**C**) from Cluster II, and (**D**) from Cluster III. In each subfigure, the first column represents the motif distribution, the second column displays the conserved domain information, and the third column illustrates the gene structure information.

2.3. Conserved Domains and Motif Distribution of TaATL Family Genes

The InterPro data and phylogenetic relationship analysis demonstrated that all members of the *TaATLs* possessed one of the following domains: RING-H2, RING U-box, or the RAD18 superfamily (Figure 3). The RING finger and U-box domains represent signature structural features of E3 enzymes, and RAD18 domains have also been identified in the *ATL* gene family of *Z. mays*. Notably, the distribution of the motifs exhibited distinct clustering patterns across different phylogenetic clusters. Furthermore, substantial variations in the domain composition were observed among members of distinct evolutionary clusters. Specifically, motif4 was predominantly concentrated in phylogenetic cluster I (Figure 3A) and was scarcely present in other branches (Figure 3B). Conversely, motif9 was exclusively concentrated in phylogenetic cluster III (Figure 3C). In addition, clusters 1

and 2 predominantly lacked the RAD18 superfamily domain (Figure 3A,B), whereas the majority of cluster 3 members harbored this domain (Figure 3C). To further characterize the *TaATL* gene family, a motif analysis was performed using the MEME online tool (Figure 3D). Out of the 334 family genes analyzed, 331 contained motif1, 332 contained motif2, and 321 contained motif5. These findings highlight the intricate domain architecture and motif distribution within the *TaATL* family, suggesting potential functional diversification among its members.

2.4. Gene Duplication Events and Orthology Analysis of TaATL Family Genes

To elucidate the evolutionary history and selective pressures acting on the *TaATL* gene family, we performed a selective pressure analysis and inferred gene duplication and loss events using the Notung software (version 2.9). The calculation of Ka and Ks for the *TaATL* family revealed that, with the exception of *TaATL69* and *TaATL85*, which exhibited Ka/Ks ratios greater than 1, all gene pairs displayed Ka/Ks ratios significantly smaller than 1, indicating that the majority of the *TaATL* genes are subject to strong purifying selection (Figure S2). By conducting an interspecies collinearity analysis of *TaATL* genes with two ancestral species (*T. urartu* and *A. tauschii*) and three phylogenetically related species (*A. thaliana*, *V. vinifera*, and *Z. mays*), it was found that wheat shares 91 orthologous gene pairs with *T. urartu*, 229 with *A. tauschii*, 24 with *A. thaliana*, 77 with *V. vinifera*, and 287 with *Z. mays* (Figure 4). The interspecies collinearity analysis revealed extensive collinear relationships within each chromosome set of the *TaATL* gene family. Additionally, collinear relationships were observed between chromosomes 1 and 3 and chromosomes 1 and 4, as well as between chromosomes 2 and 6 (Figure 5).

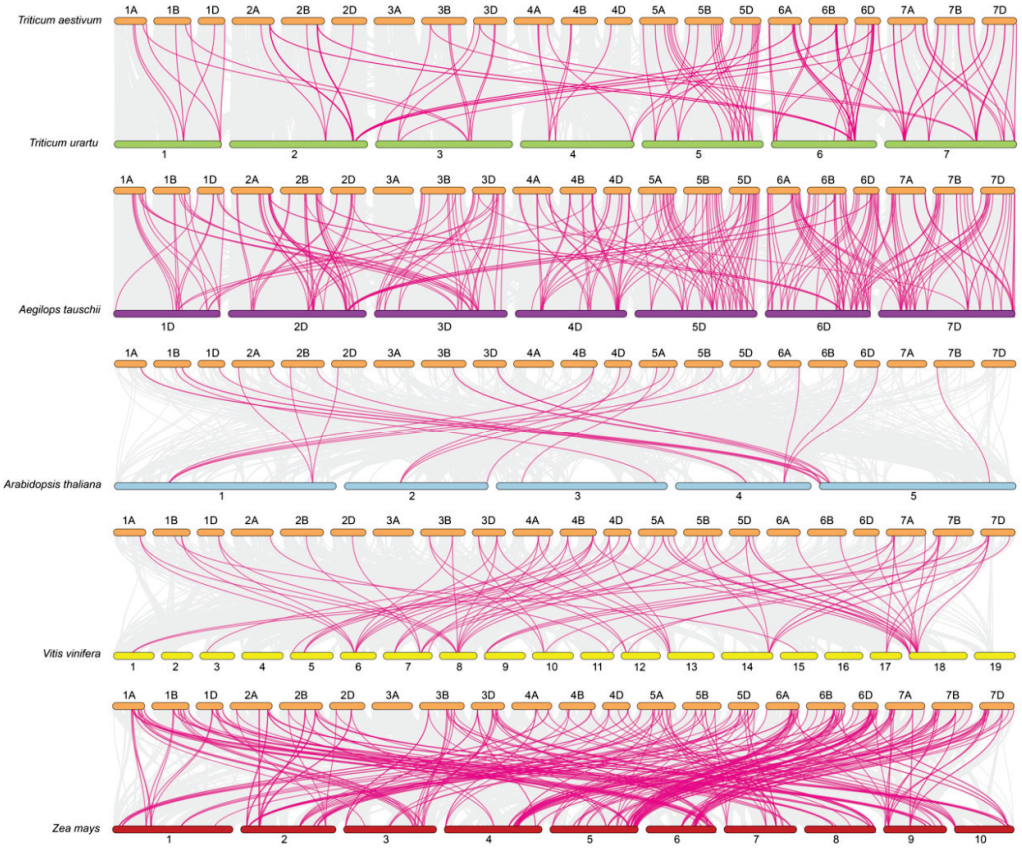

Figure 4. Interspecies collinearity analysis of the *TaATL* family genes and *ATL* genes in other plant species. The gray lines represent collinear blocks between the wheat genome and the other species, while the colored lines indicate collinearity among *ATL* genes.

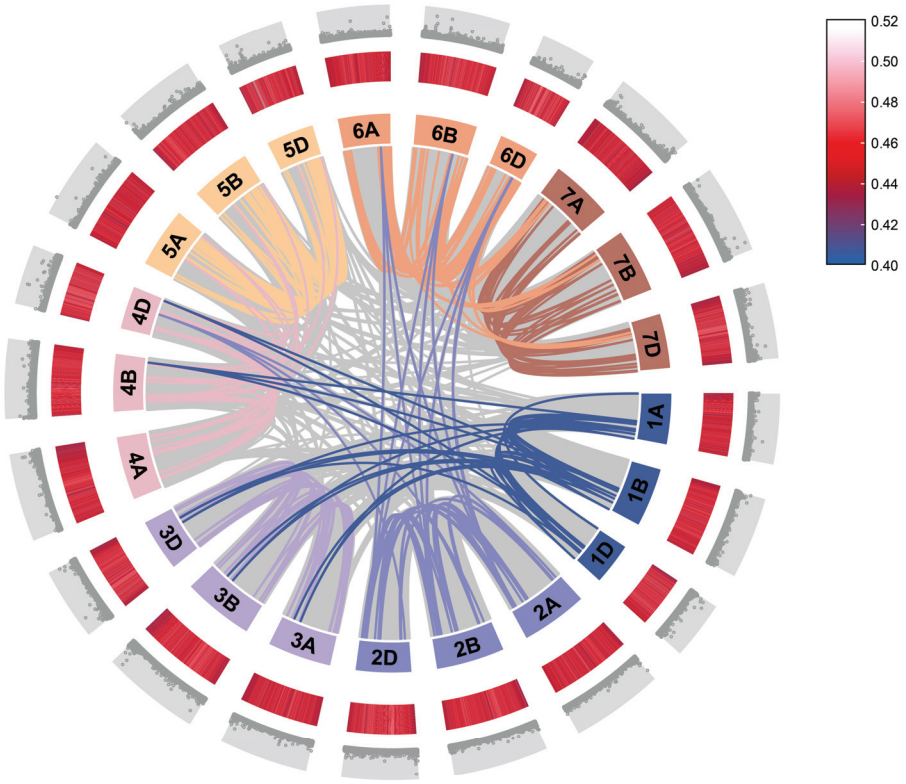

Figure 5. Intraspecies collinearity analysis of the *TaATL* family genes. From the outermost to the innermost layers, the figure shows the gene density on chromosomes and the GC content of the genome. The gray lines indicate collinear blocks from whole-genome hybridization in wheat, while the colored lines represents the segmental duplication of *TaATL* family genes.

Furthermore, the evolutionary event analysis using Notung (version 2.9) demonstrated that the *TaATL* gene family underwent 50 gene loss events and 55 gene duplication events (Table S2). Across the six species analyzed, a total of 543 gene duplication events and 705 gene loss events were identified.

2.5. GO Analysis, Protein–Protein Interactions, and Transmembrane Domain Analysis of TaATL Family Genes

The comprehensive functional characterization of the *TaATL* gene family was conducted through systematic GO enrichment analysis. The results of the GO analysis demonstrated the significant enrichment of the *TaATL* family genes in core biological processes, including protein metabolic, modification, and ubiquitination pathways (Figure 6A), consistent with the canonical functions of E3 ubiquitin ligases. Notably, we observed substantial enrichment in stress-responsive pathways, particularly those associated with salt stress responses (Figure 6A). The protein–protein interaction (PPI) analysis indicated that the *TaATL* family proteins interact closely with several HECT domain-containing proteins (e.g., A0A3B6QB19, A0A3B5ZYP8) and ubiquitin-like domain-containing proteins (e.g., W5ADS2_WHEAT, W5A9E1_WHEAT). Some family proteins also showed interactions with numerous RING-type domain-containing proteins. In addition, certain family proteins (e.g., *TaATL21*, *TaATL104*, *TaATL3*, *TaATL197*) formed a tight interaction network with glycosyltransferase 47 and conserved oligomeric Golgi complex subunit 8 (belonging to the COG8 family) (Figure 6B). The transmembrane domain analysis was conducted on four family proteins, namely *TaATL328*, *TaATL272*, *TaATL88*, and *TaATL46*. The results indicated that all four proteins were single-pass transmembrane proteins, with the predicted number of amino acids in their transmembrane helices exceeding 21. Furthermore, except for

Ta*ATL*46, the number of amino acids in the transmembrane helices within the first 60 amino acids of these proteins was greater than 15, suggesting the potential presence of signal peptides (Figure 6C).

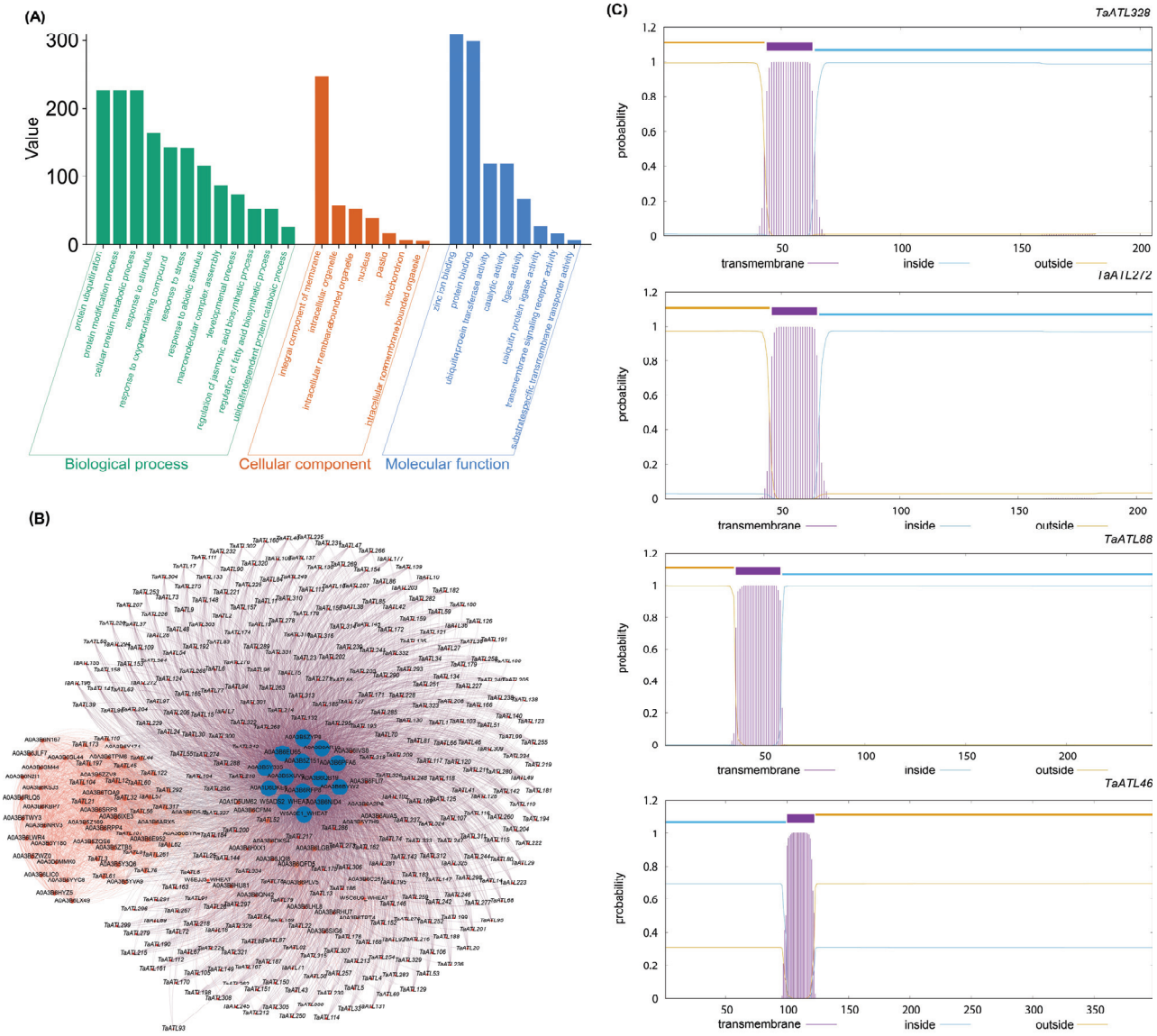

Figure 6. Functional enrichment, interaction analysis, and transmembrane domain analysis of *TaATL* gene family. (**A**) GO enrichment analysis of the *TaATLs*. The bar plot illustrates the functional enrichment of the *ATL* gene family in three Gene Ontology (GO) categories: biological process (BP, green bars), cellular component (CC, orange bars), and molecular function (MF, blue bars). (**B**) Protein–protein interaction (PPI) network analysis of the *TaATLs*. (**C**) Transmembrane domain analysis of *TaATL* family genes. The *y*-axis represents the probability values of amino acids in the regions corresponding to the colors.

2.6. Cis-Regulatory Element Analysis of TaATL Genes

To investigate the biological functions and associated signaling pathways of the *TaATL* family genes, the 2000 bp upstream sequences of the *TaATL* genes were obtained and the regulatory roles of the upstream sequence elements were analyzed. The results revealed that the promoters of the *TaATL* gene family contained a total of 70 types of elements involved in the regulation of 26 biological pathways (Figure 7A). These 70 elements are categorized into five types: common stage, transcription factors (TF), tissue, phytohormone, and environment. Among these elements, numerous *cis*-regulatory elements, such as ABA-

responsive elements (ABRE), MYB-binding sites (MBS), and TCA elements, are closely related to environmental stress, regulating important stress response pathways. Notably, the promoters of the *TaATL* family members are enriched in response elements for abscisic acid (ABRE elements) and jasmonic acid (CGTCA and TGACG motifs), as well as light-responsive elements like G-box and antioxidant response elements (ARE elements).

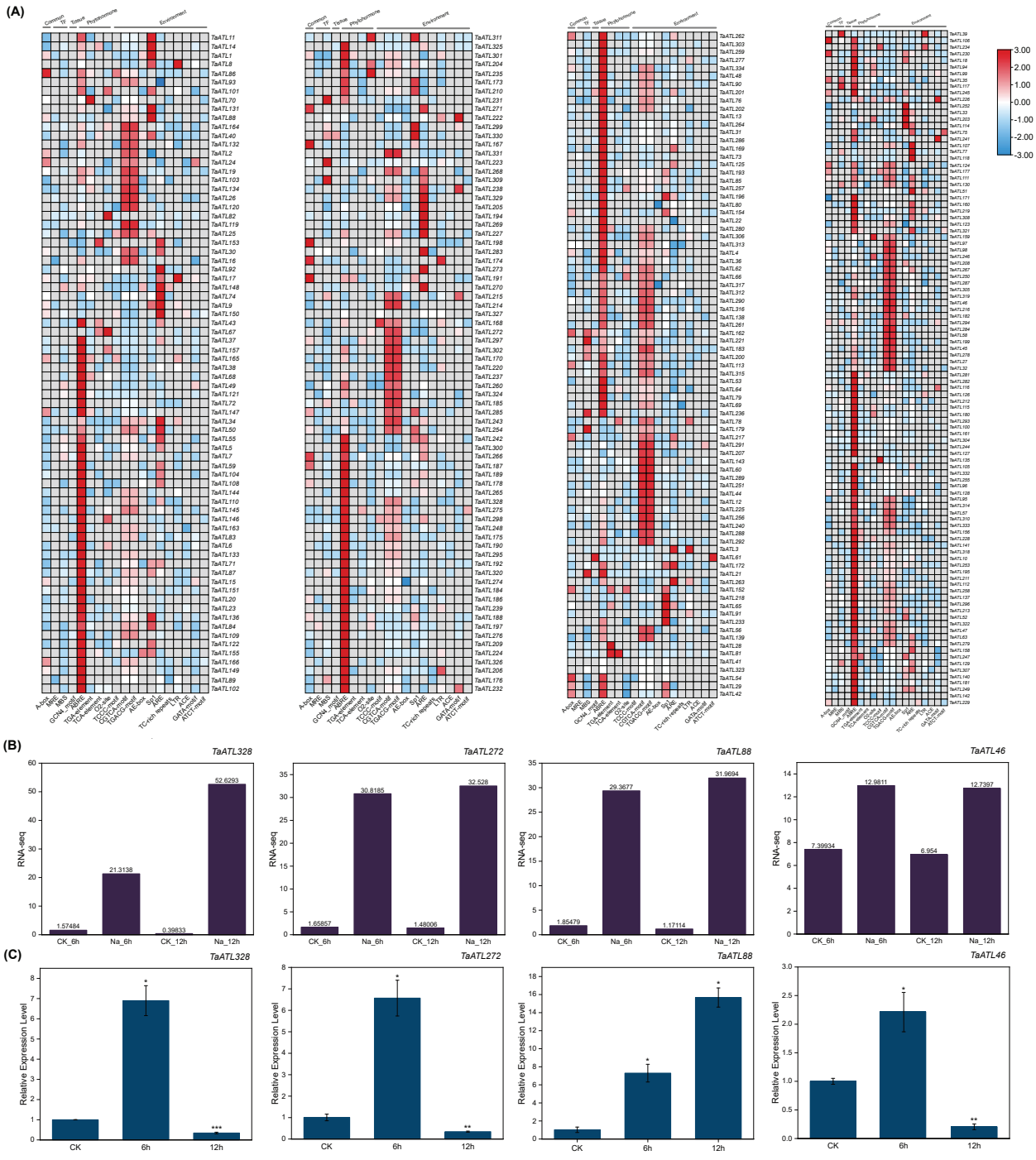

Figure 7. Heatmap of *cis*-regulatory elements and expression analysis of *TaATL* family genes. (**A**) Heatmap of *cis*-regulatory elements of *TaATLs*. The number of *cis*-acting elements for each gene is normalized by row. Genes in the first two figures are from Cluster 1, the third from Cluster 2, and the fourth from Cluster 3. (**B**) The RNA-seq expression levels of *TaATL328*, *TaATL272*, *TaATL88*, and *TaATL46* on Wheatomics. (**C**) The expression levels of *TaATL* family genes under salt stress. A T-test was used to determine statistically significant differences in the expression levels under different stress conditions (* $p < 0.05$, ** $p < 0.01$, *** $p < 0.001$).

2.7. Analysis of Expression Levels of TaATL Family Genes Under Salt Stress

To investigate the expression patterns of the *TaATL* family genes under salt stress, the RNA-seq data of the *TaATLs* were collected from the Wheatomics database (Figure S3). The results showed that genes in evolutionary clusters 1 and 3 exhibited significant upregulation within 48 h of salt stress treatment (e.g., *TaATL328*, *TaATL88*) (Figure 7B), while genes in evolutionary cluster 2 displayed overall low expression levels. In contrast, the majority of the genes in evolutionary cluster 3 maintained high expression levels even under non-stress conditions (e.g., *TaATL46*, *TaATL287*). This suggests that genes within this evolutionary cluster may be involved in regulating fundamental biological processes associated with ubiquitination, such as growth and development.

To further elucidate the expression patterns of the *TaATL* gene family under salt stress and validate the expression profiles of key genes under such conditions, wheat was subjected to NaCl-induced salt stress. The expression levels of *TaATL328*, *TaATL272*, *TaATL88*, and *TaATL46* were measured at 6 and 12 h of salinity stress (Figure 7C). The expression patterns of *TaATL328*, *TaATL272*, *TaATL88*, and *TaATL46* showed consistent trends between the RNA-seq and RT-qPCR analyses in both the control and 6 h stress treatment groups. However, in the RT-qPCR analysis, the expression levels of *TaATL328*, *TaATL272*, and *TaATL46* under 12 h stress treatment were significantly lower than those detected by RNA-seq.

The results revealed that the expression levels of *TaATL328* and *TaATL272* were significantly upregulated after 6 h of salt stress; however, their expression was markedly downregulated when the stress duration was extended to 12 h. Similarly, *TaATL46* exhibited significant downregulation in expression following 12 h of salt stress. In contrast, *TaATL88* showed substantial upregulation after 12 h of stress, with its relative expression level reaching 15-fold compared to the non-stressed control group.

3. Discussion

The *ATL* gene family is a subgroup of E3 ubiquitin ligases, regulating the specificity and efficiency of protein ubiquitination [7,10]. The functions and roles of the *ATL* family have been studied in other species; for example, in *A. thaliana*, *O. sativa*, and *Z. mays*, *ATL* family genes have been shown to respond to abiotic stresses [8,9]. However, the functional role of the *ATL* gene family in wheat under salt stress conditions has not been extensively studied.

Genomic characterization revealed that all identified *TaATL* family members contained either RING-H2, RING U-box, or RAD18 domains. This finding aligns with the established classification system for E3 ubiquitin ligases, which are categorized based on their characteristic domains (HECT, RING finger, or U-box), wherein the *ATL* family is specifically defined by the presence of RING finger domains [8,9,11].

The 334 *TaATL* genes exhibit a uniform distribution across wheat's chromosomes, except for chromosome 3A, which lacks *TaATL* family genes (Figure 1). The majority of the genes are distributed at the ends of chromosomes, facilitating their transcription under stress conditions. The absence of *TaATL* genes on chromosome 3A may reflect functional specialization, where homologs on 3B and 3D have undergone subfunctionalization or neofunctionalization to compensate for the loss. This could be driven by selective pressure, particularly if these genes play roles in stress adaptation, rendering the 3A copies redundant in hexaploid wheat. Subcellular localization predictions suggest predominant membrane association, with most proteins localized to the plasma membrane and membrane-bound organelles, consistent with their classification as transmembrane integral proteins (Figure S1). This observation aligns with previous findings in *V. vinifera* and *Z. mays*, indicating that the broad distribution and transmembrane domains of the *ATL* gene family are likely essential

for its membrane-associated functions [7,9]. The phylogenetic reconstruction of the *TaATL* family genes revealed three phylogenetic clusters (Figure 2). The intraspecies collinearity analysis revealed that, although previous studies have documented extensive segmental exchanges between chromosome 4 and chromosome 7 in wheat, the *TaATL* family genes remained unaffected and showed no evidence of collinearity [12] (Figure 5). The phylogenetic analysis of six species (*T. aestivum*, *T. urartu*, *V. vinifera*, *A. tauschii*, *Z. mays*, and *A. thaliana*) revealed that each phylogenetic cluster of the *ATL* gene family was composed of genes from all six species (Figure S1). This suggests that the evolution of the *ATL* gene family is relatively conserved in plants and that this family likely shares close relationships and similar functions in wheat and the other five species. The orthology analysis indicates that approximately half of the *TaATL*s show direct orthologous relationships with *T. urartu* and *A. tauschii ATL* genes, while specific *TaATL* subgroups (e.g., *TaATL262*, *TaATL291*, *TaATL290*, *TaATL316*, *TaATL263*) exhibit species-specific clustering, potentially reflecting functional specialization or adaptive evolution. Notably, the majority of these orthologous relationships were not one-to-one, indicating potential gene duplication or divergence events during evolution (Figure 4). However, the RNA-seq expression levels between gene pairs (e.g., *TaATL272* and *TaATL299*) were inconsistent, and the abundance of *cis*-regulatory elements between these gene pairs also varied (Figure 7A and Figure S3). This suggests that widespread whole-genome duplication events do not necessarily lead to gene redundancy but may instead contribute to the functional diversification of existing genes, resulting in new genes with distinct regulatory mechanisms. Of particular interest is the high degree of synteny observed between wheat and maize (*Z. mays*), which suggests a relatively close evolutionary relationship between these two species within the *ATL* gene family. Notably, despite the distant phylogenetic relationship between *A. thaliana* (dicot) and *T. aestivum* (monocot), collinear relationships were identified in the *ATL* gene family between these species, suggesting that the *ATL* genes may have been subject to strong functional constraints during evolution, leading to their high conservation. Further investigation into the evolutionary dynamics and functional implications of these orthologous relationships is warranted to elucidate the mechanisms underlying the conservation and divergence of the *ATL* gene family across these species.

The structural analysis of the *TaATL* genes reveals that 90.2% of the family members lack introns (Figure 3). This is consistent with previous findings regarding the *ATL* family in *Z. mays*, *A. thaliana*, and *O. sativa*, indicating that the *TaATL* gene family shares similarities with these species, providing evidence for *ATL* as a structural gene with functional modules, suggesting that these genes may operate with enhanced efficiency during transcription, enabling wheat to initiate stress resistance pathways more rapidly [8,9]. Furthermore, the Ka/Ks ratios of nearly all *TaATL* family genes were significantly less than 1, indicating that these genes have experienced strong negative selection pressure (Figure S2). The aforementioned results collectively demonstrate that the gene structure and arrangement within the *TaATL* family exhibit a high degree of similarity and conservation. These findings are consistent with previous studies on the *ATL* family in *A. thaliana*, *Z. mays*, and *V. vinifera*, indicating that the functional conservation of the *TaATL* family genes is highly preserved [7–9]. This suggests that these genes may operate with enhanced efficiency during transcription and translation, enabling them to respond rapidly to environmental stresses.

The GO enrichment analysis demonstrates the significant overrepresentation of terms related to environmental stress responses and stimulus perception, with notable enrichment on the integral components of membranes. The PPI analysis also indicated that the *TaATL* family proteins exhibit extensive interaction networks with ubiquitin ligase-related proteins, such as HECT domain-containing proteins and RING-type domain-containing proteins (Figure 6B). Furthermore, the interaction with COG8 family proteins suggests that

the *TaATL* family proteins may also enhance the response to abiotic stress by modulating the Golgi apparatus' structural reorganization through ubiquitination modifications [13]. The transmembrane domain analysis further indicated that the transmembrane regions of *TaATL* family proteins likely enable their localization to the endoplasmic reticulum (ER) (Figure 6C) [14]. As members of the E3 ubiquitin ligase family, these proteins may participate in the ER-associated degradation (ERAD) pathway by facilitating protein degradation through ubiquitination [14,15]. ERAD plays a critical role in maintaining cellular homeostasis under external stress by degrading misfolded proteins, thereby enhancing plants' salt tolerance (Figure 6A) [16]. These functional annotations were further corroborated through a *cis*-element analysis. *Cis*-acting elements are crucial molecular switches that participate in the transcriptional regulation of dynamic gene activity networks, controlling various biological processes and enabling organisms to respond to and adapt to environmental stresses [17]. The *cis*-regulatory element analysis of *TaATL* promoters identified multiple stress-responsive motifs, including ABRE, MBS, TCA, and jasmonic acid-responsive elements (CGTCA and TGACG motifs) (Figure 7A). The prominence of ABA-responsive elements correlates with ABA's established role as a key phytohormone in abiotic stress responses, particularly in stomatal regulation during drought and salt stress [18,19]. Osmotic stress induces ABA biosynthesis, and the ABA-responsive elements (ABREs) located upstream of the *TaATL* genes recognize ABA, thereby activating *TaATL* family gene expression and enhancing salt stress tolerance. The MBS element is the binding site for MYB transcription factors, which enhance plants' tolerance to abiotic stimuli, such as drought stress [20–23]. Exogenous MeJA and TCA elements can also enhance plants' tolerance to abiotic stress [24–26]. These findings collectively implicate *TaATL* genes in stress response regulation, potentially through the ABA and MeJA signaling pathways. Within the gene family, the core gene *TaATL52* in the protein–protein interaction network contains a larger number of ABRE elements (Figure 7A). Therefore, *TaATL*52 is strongly implicated as a regulatory gene within the *TaATL* family, playing a central role in mediating environmental stress responses. Furthermore, the significant enrichment of *TaATL* genes in the response to stimuli suggests additional involvement in biotic stress responses (Figure 7A).

The integrative analysis of the RNA-seq expression profiles reveals that four genes (*TaATL328*, *TaATL272*, *TaATL88*, and *TaATL46*) within cluster I demonstrate particularly robust stress-responsive expression profiles, strongly suggesting their regulatory roles in wheat's salt stress adaptation mechanisms (Figure 7B). Notably, *TaATL328* exhibits pronounced upregulation as early as 6 h following salt stress induction, with sustained elevated expression levels persisting through the 24 h time point. This temporal expression pattern strongly suggests that *TaATL328* functions as a crucial early-response regulator in salt stress adaptation, likely mediating the primary stress signaling cascade through facilitating the degradation of stress-responsive repressors such as PP2C phosphatases or modulating PYR/PYL receptor–PP2C interactions to initiate downstream stress responses [27,28]. The RT-qPCR analysis further corroborated the significant upregulation of *TaATL328*, *TaATL272*, and *TaATL46* during the early phase of salt stress (Figure 7B). However, its expression level drastically declined after 12 h of salt stress, dropping below that of the non-stressed control group, inconsistent with the RNA-seq data. In contrast, *TaATL88* exhibited sustained upregulation at 12 h of salt stress, consistent with the RNA-seq findings. This distinct expression pattern suggests that *TaATL88* may participate in long-term ion homeostasis maintenance through regulating ubiquitination modifications of SOS1 or NHX-type transporters; alternatively, it may be associated with the phosphorylation of cell wall reinforcement-related enzymes such as CESA. This gene likely contributes to the activation of long-term stress adaptation mechanisms, thereby enhancing regulatory pathways during the later stages of salt stress [29,30]. Collectively, these results identify 334 highly conserved *TaATL* genes

in wheat that are significantly upregulated under salt stress. Their low intron frequency and strong functional constraints further highlight their evolutionary importance in stress response mechanisms. Notably, these genes are likely involved in stress adaptation through key signaling pathways, including ABA, MeJA, and MYB.

The findings regarding the *TaATL* gene family provide crucial insights for improvements in wheat salt tolerance. Key genes such as *TaATL328*, *TaATL88*, and *TaATL46* show strong salt-responsive expression and represent promising targets for breeding. However, this study has certain limitations regarding experimental validation. The functional predictions, including the synteny analysis, subcellular localization, *cis*-regulatory elements, and protein–protein interaction networks, were primarily derived from in silico analyses. While these computational approaches provide valuable preliminary insights, they require further experimental validation to fully establish their biological relevance in plants. Future studies employing *TaATL* knockout/overexpression transgenic lines and yeast two-hybrid assays would provide direct evidence to substantiate the proposed roles of *TaATL* genes in the salt stress response.

4. Materials and Methods

4.1. Identification of TaATL Family Genes

To identify the *TaATL* genes, the genome and annotation data (*Triticum_aestivum*.IWGSC.60), along with protein sequences, were retrieved from the EnsemblPlants database (http://plants.ensembl.org/Triticum_aestivum/Info/Index (accessed on 23 November 2024)) [31]. The genome information, annotation data, and protein sequences of *T. urartu*, *A. tauschii*, *A. thaliana*, *V. vinifera*, and *Z. mays* were also obtained from the EnsemblPlants database (https://plants.ensembl.org/index.html (accessed on 21 December 2024)). The Hidden Markov Model (HMM) profiles were downloaded from the Pfam database (https://pfam.xfam.org (accessed on 23 November 2024)) [32]. The HMM profile of the *ATL* domain (PTHR45768) was acquired using the TBtools software (version 2.210) (https://github.com/CJ-Chen/TBtools-II (accessed on 16 November 2024)) [33]. The wheat genome was used as an inquiry for a BLASTp search (E-value < 1 e^{-5}), followed by the screening of the protein domains using InterPro (https://www.ebi.ac.uk/interpro/ (accessed on 23 November 2024)) [34]. Proteins containing RING-H2 finger and E3 ubiquitin protein ligase domains were all retained. The analysis of gene localization on chromosomes was performed using MCScanX-Super Fast within TBtools (version 2.210) [35].

4.2. Phylogenetic Analysis and Collinearity Analysis of TaATL Family Genes

The protein sequences were aligned using MAFFT (version 7), followed by the removal of low-quality regions with TrimAl [36,37]. A maximum likelihood (ML) phylogenetic tree was constructed using IQ-TREE2 with 1000 bootstrap replicates for ultrafast bootstrapping [38,39]. The phylogenetic tree was visualized with iTOL (version 7.0) (https://itol.embl.de (accessed on 7 January 2025)) [40].

The collinearity analysis of the *TaATLs* with *T. urartu*, *A. tauschii*, *A. thaliana*, *V. vinifera*, and *Z. mays* was conducted using MCScanX-Super Fast within TBtools (version 2.210), with sequence alignments performed by Diamond for BLAST. The phylogenetic tree of the *ATLs* from the aforementioned six species was analyzed using the TimeTree (version 5) website (https://timetree.org (accessed on 13 February 2025)) [41]. It was then visualized using the iTOL online platform (version 7.0) (https://itol.embl.de (accessed on 15 February 2025)), followed by an evolutionary event analysis performed using the Notung software (version 2.9) [42]. Additionally, a Ka/Ks (non-synonymous rate to synonymous substitution rate) selection pressure analysis and visualization were conducted using Rstudio (version 2024.12.1+563) scripts [43].

4.3. Analysis of cis-Acting Elements, Gene Structure, and Chromosome Location

The motifs of *TaATL* family members containing RING-H2 finger domains or E3 ubiquitin protein ligase domains were identified using MEME (version 5.5.7) (https://meme-suite.org/meme/tools/meme (accessed on 3 January 2025)) [44], with the parameter width range set to 6–50. The gene structures were obtained from the genome annotation file, while the conserved domains were acquired from the NCBI database. Additionally, the amino acid composition and hits of each motif were analyzed using the MEME online tool. The 2000 bp upstream sequences of the *TaATL* genes were extracted with TBtools (version 2.210). These sequences were subsequently submitted to the PlantCARE database (http://bioinformatics.psb.ugent.be/webtools/plantcare/html/ (accessed on 18 January 2025)) for the prediction of *cis*-acting elements [45]. The identified elements were classified and a heatmap analysis was performed using TBtools (version 2.210). The chromosome locations of the *TaATL* gene family were visualized using TBtools (version 2.210).

4.4. Protein–Protein Interaction, GO, and Physicochemical Property Analyses

The protein–protein interaction (PPI) analysis was performed using the STRING database (https://cn.string-db.org (accessed on 17 January 2025)) with a medium confidence score of 0.400 [46]. The Gene Ontology (GO) enrichment information for the *TaATL* gene family was obtained using the DAVID database [47]. A complete GO analysis was conducted using singular enrichment analysis (SEA) with the Yekutieli method (FDR under dependency) for multiple testing correction (significance level = 0.05). The physicochemical properties of all proteins were predicted using ExPASy online tools (https://web.expasy.org/protparam/ (accessed on 25 January 2025)) [48]. Additionally, to predict the subcellular localization of the *TaATL* gene family, the CELLO online tool (version 2.5) (https://cello.life.nctu.edu.tw (accessed on 26 January 2025)) was used [49]. Subsequently, transmembrane signals were examined using the PROTTER online tool (version 1.0) (https://wlab.ethz.ch/protter/start/ (accessed on 27 January 2025)) [50].

4.5. Plant Materials and Salt Stress Treatment

Plump and healthy wheat seeds were planted and germinated in a growth chamber. The chamber was maintained at a CO_2 concentration of 400 ppm, a temperature regime of 20–22 °C, and relative humidity of 60%, with a 12 h light/12 h dark photoperiod [51]. Salt stress was induced by supplementing the hydroponic solution with 150 mM NaCl. Leaf tissue samples were collected at 6 and 12 h following stress induction.

4.6. Gene Expression Analysis, RNA Extraction, and Real-Time Quantitative PCR (RT-qPCR) Analysis

Protein function annotations of the *TaATL* gene family were performed using the eggNOG online tool (version 2) (http://eggnog-mapper.embl.de accessed on 12 January 2025)) [52]. The RNA-seq of the *TaATL* family genes was conducted using the Wheatomics platform (http://wheatomics.sdau.edu.cn/expression/index.html (accessed on 27 November 2024)) [53]. The transcriptome database "Transcriptome response of two wheat cultivars to salt stress" was utilized for the bioinformatics analysis. Subsequently, all genes with total expression levels (sum across all groups) exceeding 1 TPM in the RNA-seq data were selected using TBtools (version 2.210) for heatmap generation [33].

Total RNA was isolated from the leaves of *Triticum aestivum* L. using the FastPure Plant Total RNA Isolation Kit (Nanjing Vazyme Biotech Co., Ltd., Nanjing, China). cDNA synthesis was performed using the HiScript IV All-in-One Ultra RT SuperMix for qPCR (Nanjing Vazyme Biotech Co., Ltd., Nanjing, China), and gene-specific primers were designed for the four target genes using the NCBI Primer-BLAST online platform (https://www.ncbi.nlm.nih.gov/tools/primer-blast/ (accessed on 21 February 2025))

(Table S3) [54]. The RT-qPCR analysis was conducted employing the TB Green® Premix Ex Taq™ II kit (Takara Bio, Kusatsu, Japan) on an ABI QuantStudio® Real-Time PCR System (Applied Biosystems, Waltham, MA, USA). For the quantification of RT-qPCR, we used the Ta*Actin* gene (Table S3) as the reference gene, while each analysis included three biological replicates [55–58]. Fold changes after salt treatment were calculated as $2^{-\Delta\Delta Ct_{salt}}/2^{-\Delta\Delta Ct_{control}}$, with all procedures following the manufacturer's protocols [59]. The qRT-PCR analysis was conducted with initial denaturation at 95 °C for 30 s, followed by 45 cycles of denaturation at 95 °C for 5 s and annealing at 60 °C for 1 min, and finalized with a series of terminal steps at 95 °C for 15 s, 60 °C for 1 min, and 95 °C for 15 s. The expression profiles of *TaATL328* and *TaATL272* were analyzed at 0 h, 6 h, and 12 h after NaCl stress treatment, while *TaATL88* and *TaATL176* were evaluated at 0 h and 12 h [59]. Each treatment group consisted of three independent biological replicates. The control group consisted of wheat plants without NaCl treatment (0 h), while the experimental groups (6 h and 12 h NaCl treatments) were both compared against this control group.

Supplementary Materials: The following supporting information can be downloaded at: https://www.mdpi.com/article/10.3390/plants14091306/s1, Figure S1: Gene evolutionary tree of *ATL* family genes among wheat and other species; Figure S2: Ka/Ks ratios of *TaATL* family genes; Figure S3: Heatmap of RNA-seq of *TaATL* family genes; Table S1: Physicochemical properties and subcellular localization of *TaATL* family proteins; Table S2: Gene duplication and gene loss events of the ATL family in wheat and other species; Table S3: Primer sequences of the *ATL* family. Table S4: Detailed phylogenetic analysis of the ATL gene family.

Author Contributions: Conceptualization, X.L. and P.Y.; methodology, X.L. and S.L.; software, X.L.; validation, X.L., S.L. and P.Y.; formal analysis, X.L.; investigation, X.L., S.L. and P.Y.; resources, P.Y.; writing—original draft preparation, X.L.; writing—review and editing, X.L., S.L. and P.Y.; visualization, X.L.; supervision, P.Y.; funding acquisition, P.Y. All authors have read and agreed to the published version of the manuscript.

Funding: This study was supported by the Shandong Provincial Natural Science Foundation (No. ZR2023QC278) and the Scientific Research Starting Funding of Shandong University (No. 1180509300002).

Data Availability Statement: The original contributions presented in this study are included in the article and Supplementary Materials.

Conflicts of Interest: The authors declare no conflicts of interest.

Abbreviations

The following abbreviations are used in this manuscript:

ATL	*Arabidopsis Tóxicos en Levadura*
RING	Really Interesting New Gene
RAD	RING-associated domain
ABA	Abscisic acid
MYB	Myeloblastosis
ABRE	ABA-responsive element
MeJA	Methyl jasmonate
MBS	MYB-binding site
UPS	Ubiquitin–proteasome system
UTR	Untranslated region
GO	Gene Ontology
Ka	Nonsynonymous substitution rate
Ks	Synonymous substitution rate
PPI	Protein–protein interaction

References

1. Bailey-Serres, J.; Parker, J.E.; Ainsworth, E.A.; Oldroyd, G.E.D.; Schroeder, J.I. Genetic Strategies for Improving Crop Yields. *Nature* **2019**, *575*, 109–118. [CrossRef] [PubMed]
2. Al-Saharin, R.; Hellmann, H.; Mooney, S. Plant E3 Ligases and Their Role in Abiotic Stress Response. *Cells* **2022**, *11*, 890. [CrossRef] [PubMed]
3. Kim, M.S.; Kim, J.H.; Amoah, J.N.; Seo, Y.W. Wheat (*Triticum aestivum* L.) Plant U-box E3 Ligases TaPUB2 and TaPUB3 Enhance ABA Response and Salt Stress Resistance in *Arabidopsis*. *FEBS Lett.* **2022**, *596*, 3037–3050. [CrossRef]
4. Jing, Z.; Liu, N.; Zhang, Z.; Hou, X. Research Progress on Plant Responses to Stress Combinations in the Context of Climate Change. *Plants* **2024**, *13*, 469. [CrossRef]
5. Stone, S.L. Role of the Ubiquitin Proteasome System in Plant Response to Abiotic Stress. *Int. Rev. Cell Mol. Biol.* **2019**, *343*, 1. [CrossRef]
6. Parveen, A.; Rahim, M.S.; Sharma, A.; Mishra, A.; Kumar, P.; Fandade, V.; Kumar, P.; Bhandawat, A.; Verma, S.K.; Roy, J. Genome-Wide Analysis of RING-Type E3 Ligase Family Identifies Potential Candidates Regulating High Amylose Starch Biosynthesis in Wheat (*Triticum aestivum* L.). *Sci. Rep.* **2021**, *11*, 11461. [CrossRef]
7. Ariani, P.; Regaiolo, A.; Lovato, A.; Giorgetti, A.; Porceddu, A.; Camiolo, S.; Wong, D.; Castellarin, S.; Vandelle, E.; Polverari, A. Genome-Wide Characterisation and Expression Profile of the Grapevine ATL Ubiquitin Ligase Family Reveal Biotic and Abiotic Stress-Responsive and Development-Related Members. *Sci. Rep.* **2016**, *6*, 38260. [CrossRef]
8. Serrano, M.; Parra, S.; Alcaraz, L.D.; Guzmán, P. The *ATL* Gene Family from *Arabidopsis Thaliana* and *Oryza Sativa* Comprises a Large Number of Putative Ubiquitin Ligases of the RING-H2 Type. *J. Mol. Evol.* **2006**, *62*, 434–445. [CrossRef]
9. Ding, H.; Li, X.; Zhuge, S.; Du, J.; Wu, M.; Li, W.; Li, Y.; Ma, H.; Zhang, P.; Wang, X.; et al. Genome-Wide Identification and Functional Analysis of the Genes of the ATL Family in Maize during High-Temperature Stress in Maize. *Genes* **2024**, *15*, 1106. [CrossRef]
10. Wang, S.; Lv, X.; Zhang, J.; Chen, D.; Chen, S.; Fan, G.; Ma, C.; Wang, Y. Roles of E3 Ubiquitin Ligases in Plant Responses to Abiotic Stresses. *Int. Rev. Cell Mol. Biol.* **2022**, *23*, 2308. [CrossRef]
11. Moon, J.; Parry, G.; Estelle, M. The Ubiquitin-Proteasome Pathway and Plant Development. *Plant Cell* **2004**, *16*, 3181–3195. [CrossRef] [PubMed]
12. Homology-Mediated Inter-Chromosomal Interactions in Hexaploid Wheat Lead to Specific Subgenome Territories Following Polyploidization and Introgression | Genome Biology | Full Text. Available online: https://genomebiology.biomedcentral.com/articles/10.1186/s13059-020-02225-7 (accessed on 24 February 2025).
13. Buzuk, L.; Hellerschmied, D. Ubiquitin-Mediated Degradation at the Golgi Apparatus. *Front. Mol. Biosci.* **2023**, *10*, 1197921. [CrossRef] [PubMed]
14. Guzmán, P. The Prolific ATL Family of RING-H2 Ubiquitin Ligases. *Plant Signal. Behav.* **2012**, *7*, 1014–1021. [CrossRef]
15. Vembar, S.S.; Brodsky, J.L. One Step at a Time: Endoplasmic Reticulum-Associated Degradation. *Nat. Rev. Mol. Cell Biol.* **2008**, *9*, 944–957. [CrossRef]
16. Reyes-Impellizzeri, S.; Moreno, A.A. The Endoplasmic Reticulum Role in the Plant Response to Abiotic Stress. *Front. Plant Sci.* **2021**, *12*, 755447. [CrossRef]
17. Yamaguchi-Shinozaki, K.; Shinozaki, K. Organization of Cis-Acting Regulatory Elements in Osmotic- and Cold-Stress-Responsive Promoters. *Trends Plant Sci.* **2005**, *10*, 88–94. [CrossRef]
18. Nakashima, K.; Yamaguchi-Shinozaki, K. ABA Signaling in Stress-Response and Seed Development. *Plant Cell Rep.* **2013**, *32*, 959–970. [CrossRef]
19. Waadt, R.; Seller, C.A.; Hsu, P.-K.; Takahashi, Y.; Munemasa, S.; Schroeder, J.I. Plant Hormone Regulation of Abiotic Stress Responses. *Nat. Rev. Mol. Cell Biol.* **2022**, *23*, 680–694. [CrossRef]
20. Wang, N.; Qu, C.; Wang, Y.; Xu, H.; Jiang, S.; Fang, H.; Liu, J.; Zhang, Z.; Chen, X. MdMYB4 Enhances Apple Callus Salt Tolerance by Increasing MdNHX1 Expression Levels. *Plant Cell Tissue Organ Cult. PCTOC* **2017**, *131*, 283–293. [CrossRef]
21. Dubos, C.; Stracke, R.; Grotewold, E.; Weisshaar, B.; Martin, C.; Lepiniec, L. MYB Transcription Factors in Arabidopsis. *Trends Plant Sci.* **2010**, *15*, 573–581. [CrossRef]
22. Wang, X.; Wei, H.; Wang, K.; Tang, X.; Li, S.; Zhang, N.; Si, H. MYB Transcription Factors: Acting as Molecular Switches to Regulate Different Signaling Pathways to Modulate Plant Responses to Drought Stress. *Ind. Crops Prod.* **2025**, *226*, 120676. [CrossRef]
23. Xu, W.; Dubos, C.; Lepiniec, L. Transcriptional Control of Flavonoid Biosynthesis by MYB–bHLH–WDR Complexes. *Trends Plant Sci.* **2015**, *20*, 176–185. [CrossRef] [PubMed]
24. Raskin, I. Role of Salicylic Acid in Plants. *Annu. Rev. Plant Physiol. Plant Mol. Biol.* **1992**, *43*, 439–463. [CrossRef]
25. Ramírez, V.; Coego, A.; López, A.; Agorio, A.; Flors, V.; Vera, P. Drought Tolerance in Arabidopsis Is Controlled by the OCP3 Disease Resistance Regulator. *Plant J.* **2009**, *58*, 578–591. [CrossRef]

26. Miura, K.; Tada, Y. Regulation of Water, Salinity, and Cold Stress Responses by Salicylic Acid. *Front. Plant Sci.* **2014**, *5*, 4. [CrossRef]
27. Ma, Y.; Szostkiewicz, I.; Korte, A.; Moes, D.; Yang, Y.; Christmann, A.; Grill, E. Regulators of PP2C Phosphatase Activity Function as Abscisic Acid Sensors. *Science* **2009**, *324*, 1064–1068. [CrossRef]
28. Santiago, J.; Dupeux, F.; Betz, K.; Antoni, R.; Gonzalez-Guzman, M.; Rodriguez, L.; Márquez, J.A.; Rodriguez, P.L. Structural Insights into PYR/PYL/RCAR ABA Receptors and PP2Cs. *Plant Sci.* **2012**, *182*, 3–11. [CrossRef]
29. Fahmideh, L.; Fooladvand, Z. Isolation and Semi Quantitative PCR of Na+/H+ Antiporter (SOS1 and NHX) Genes under Salinity Stress in Kochia Scoparia. *Biol. Proced. Online* **2018**, *20*, 11. [CrossRef]
30. Li, W.; Wei, J.; Lei, Y.; Yang, Z.; Zhang, S.; Feng, J.; Li, Y.; Liu, Y.; Sheng, H. Phosphorylation of Cellulose Synthases in Plant Responses to Environmental Changes. *Int. J. Biol. Macromol.* **2025**, *292*, 139313. [CrossRef]
31. Bolser, D.M.; Staines, D.M.; Perry, E.; Kersey, P.J. Ensembl Plants: Integrating Tools for Visualizing, Mining, and Analyzing Plant Genomic Data. *Methods Mol. Biol.* **2017**, *1533*, 1–31. [CrossRef]
32. Mistry, J.; Chuguransky, S.; Williams, L.; Qureshi, M.; Salazar, G.A.; Sonnhammer, E.L.L.; Tosatto, S.C.E.; Paladin, L.; Raj, S.; Richardson, L.J.; et al. Pfam: The Protein Families Database in 2021. *Nucleic Acids Res.* **2021**, *49*, D412–D419. [CrossRef] [PubMed]
33. Chen, C.; Wu, Y.; Li, J.; Wang, X.; Zeng, Z.; Xu, J.; Liu, Y.; Feng, J.; Chen, H.; He, Y.; et al. TBtools-II: A "One for All, All for One" Bioinformatics Platform for Biological Big-Data Mining. *Mol. Plant* **2023**, *16*, 1733–1742. [CrossRef] [PubMed]
34. Blum, M.; Andreeva, A.; Florentino, L.C.; Chuguransky, S.R.; Grego, T.; Hobbs, E.; Pinto, B.L.; Orr, A.; Paysan-Lafosse, T.; Ponamareva, I.; et al. InterPro: The Protein Sequence Classification Resource in 2025. *Nucleic Acids Res.* **2025**, *53*, D444–D456. [CrossRef] [PubMed]
35. Wang, Y.; Tang, H.; DeBarry, J.D.; Tan, X.; Li, J.; Wang, X.; Lee, T.; Jin, H.; Marler, B.; Guo, H.; et al. MCScanX: A Toolkit for Detection and Evolutionary Analysis of Gene Synteny and Collinearity. *Nucleic Acids Res.* **2012**, *40*, e49. [CrossRef]
36. Katoh, K.; Misawa, K.; Kuma, K.; Miyata, T. MAFFT: A Novel Method for Rapid Multiple Sequence Alignment Based on Fast Fourier Transform. *Nucleic Acids Res.* **2002**, *30*, 3059–3066. [CrossRef]
37. Capella-Gutiérrez, S.; Silla-Martínez, J.M.; Gabaldón, T. trimAl: A Tool for Automated Alignment Trimming in Large-Scale Phylogenetic Analyses. *Bioinformatics* **2009**, *25*, 1972–1973. [CrossRef]
38. IQ-TREE 2: New Models and Efficient Methods for Phylogenetic Inference in the Genomic Era | Molecular Biology and Evolution | Oxford Academic. Available online: https://academic.oup.com/mbe/article/37/5/1530/5721363 (accessed on 1 March 2025).
39. Balister, P.; Bollobás, B.; Przykucki, M.; Smith, P. Subcritical $\mathcal{U}$-Bootstrap Percolation Models Have Non-Trivial Phase Transitions. *Trans. Am. Math. Soc.* **2016**, *368*, 7385–7411. [CrossRef]
40. Letunic, I.; Bork, P. Interactive Tree of Life (iTOL) v6: Recent Updates to the Phylogenetic Tree Display and Annotation Tool. *Nucleic Acids Res.* **2024**, *52*, W78–W82. [CrossRef]
41. Kumar, S.; Suleski, M.; Craig, J.M.; Kasprowicz, A.E.; Sanderford, M.; Li, M.; Stecher, G.; Hedges, S.B. TimeTree 5: An Expanded Resource for Species Divergence Times. *Mol. Biol. Evol.* **2022**, *39*, msac174. [CrossRef]
42. Chen, K.; Durand, D.; Farach-Colton, M. NOTUNG: A Program for Dating Gene Duplications and Optimizing Gene Family Trees. *J. Comput. Biol.* **2000**, *7*, 429–447. [CrossRef]
43. RStudio: Integrated Development for R. Available online: http://www.rstudio.com/ (accessed on 12 December 2024).
44. Bailey, T.L.; Johnson, J.; Grant, C.E.; Noble, W.S. The MEME Suite. *Nucleic Acids Res.* **2015**, *43*, W39–W49. [CrossRef] [PubMed]
45. Rombauts, S.; Déhais, P.; Van Montagu, M.; Rouzé, P. PlantCARE, a Plant Cis-Acting Regulatory Element Database. *Nucleic Acids Res.* **1999**, *27*, 295–296. [CrossRef] [PubMed]
46. Szklarczyk, D.; Gable, A.L.; Lyon, D.; Junge, A.; Wyder, S.; Huerta-Cepas, J.; Simonovic, M.; Doncheva, N.T.; Morris, J.H.; Bork, P.; et al. STRING V11: Protein–Protein Association Networks with Increased Coverage, Supporting Functional Discovery in Genome-Wide Experimental Datasets. *Nucleic Acids Res.* **2019**, *47*, D607–D613. [CrossRef] [PubMed]
47. Sherman, B.T.; Panzade, G.; Imamichi, T.; Chang, W. DAVID Ortholog: An Integrative Tool to Enhance Functional Analysis through Orthologs. *Bioinformatics* **2024**, *40*, btae615. [CrossRef]
48. Gasteiger, E.; Hoogland, C.; Gattiker, A.; Duvaud, S.; Wilkins, M.R.; Appel, R.D.; Bairoch, A. Protein Identification and Analysis Tools on the ExPASy Server. In *The Proteomics Protocols Handbook*; Walker, J.M., Ed.; Humana Press: Totowa, NJ, USA, 2005; pp. 571–607. ISBN 978-1-58829-343-5.
49. Yu, C.-S.; Lin, C.-J.; Hwang, J.-K. Predicting Subcellular Localization of Proteins for Gram-Negative Bacteria by Support Vector Machines Based on n-Peptide Compositions. *Protein Sci.* **2004**, *13*, 1402–1406. [CrossRef]
50. Omasits, U.; Ahrens, C.H.; Müller, S.; Wollscheid, B. Protter: Interactive Protein Feature Visualization and Integration with Experimental Proteomic Data. *Bioinformatics* **2014**, *30*, 884–886. [CrossRef]
51. Ying, S. Genome-Wide Identification and Transcriptional Analysis of Arabidopsis DUF506 Gene Family. *Int. J. Mol. Sci.* **2021**, *22*, 11442. [CrossRef]

52. Huerta-Cepas, J.; Szklarczyk, D.; Heller, D.; Hernández-Plaza, A.; Forslund, S.K.; Cook, H.; Mende, D.R.; Letunic, I.; Rattei, T.; Jensen, L.J.; et al. eggNOG 5.0: A Hierarchical, Functionally and Phylogenetically Annotated Orthology Resource Based on 5090 Organisms and 2502 Viruses. *Nucleic Acids Res.* **2019**, *47*, D309–D314. [CrossRef]
53. Ma, S.; Wang, M.; Wu, J.; Guo, W.; Chen, Y.; Li, G.; Wang, Y.; Shi, W.; Xia, G.; Fu, D.; et al. WheatOmics: A Platform Combining Multiple Omics Data to Accelerate Functional Genomics Studies in Wheat. *Mol. Plant* **2021**, *14*, 1965–1968. [CrossRef]
54. Ye, J.; Coulouris, G.; Zaretskaya, I.; Cutcutache, I.; Rozen, S.; Madden, T.L. Primer-BLAST: A Tool to Design Target-Specific Primers for Polymerase Chain Reaction. *BMC Bioinform.* **2012**, *13*, 134. [CrossRef]
55. Son, S.; Chitnis, V.R.; Liu, A.; Gao, F.; Nguyen, T.-N.; Ayele, B.T. Abscisic Acid Metabolic Genes of Wheat (*Triticum aestivum* L.): Identification and Insights into Their Functionality in Seed Dormancy and Dehydration Tolerance. *Planta* **2016**, *244*, 429–447. [CrossRef] [PubMed]
56. Xu, X.; Zhang, L.; Zhao, W.; Fu, L.; Han, Y.; Wang, K.; Yan, L.; Li, Y.; Zhang, X.-H.; Min, D.-H. Genome-Wide Analysis of the Serine Carboxypeptidase-like Protein Family in *Triticum aestivum* Reveals TaSCPL184-6D Is Involved in Abiotic Stress Response. *BMC Genom.* **2021**, *22*, 350. [CrossRef] [PubMed]
57. Wu, Z.; Shen, S.; Wang, Y.; Tao, W.; Zhao, Z.; Hu, X.; Yu, P. Genome-Wide Identification and Expression Analysis of the Zinc Finger Protein Gene Subfamilies under Drought Stress in *Triticum aestivum*. *Plants* **2022**, *11*, 2511. [CrossRef] [PubMed]
58. Wang, Y.; Shen, S.; Wu, Z.; Tao, W.; Zhang, W.; Yu, P. Genome-Wide Analysis of *Triticum aestivum* Bromodomain Gene Family and Expression Analysis under Salt Stress. *Planta* **2024**, *260*, 117. [CrossRef]
59. Livak, K.J.; Schmittgen, T.D. Analysis of Relative Gene Expression Data Using Real-Time Quantitative PCR and the $2-\Delta\Delta CT$ Method. *Methods* **2001**, *25*, 402–408. [CrossRef]

plants

MDPI

Article

Winter Wheat Vernalization Alleles and Freezing Tolerance at the Seedling and Jointing Stages

Fangfang Liu [1,2], Wenxin Cao [1,2], Qiqi Zhang [1,2], Yao Li [1,2], Heng Zhou [1,2] and Yingxiu Wan [1,2,*]

[1] Crop Research Institute, Anhui Academy of Agricultural Sciences, Hefei 230001, China; liuff0510@163.com (F.L.); cwxchina@aliyun.com (W.C.); zhqq1982@126.com (Q.Z.); liyaohefei0551@163.com (Y.L.); 19016101618@163.com (H.Z.)
[2] Anhui Key Laboratory of Crop Quality Improvement, Hefei 230031, China
* Correspondence: wanyingxiu@163.com

Abstract: This study explores the relationship between allelic variation of the vernalization genes (*VRN*) and the freezing tolerance at the seedling and jointing stages of winter wheat growth. It provides a basis for molecular marker development for freezing tolerance breeding of winter wheat. A total of 435 wheat accessions were used to identify and evaluate the freezing tolerance at the seedling stage using field tests, while 192 wheat accessions were used to evaluate the freezing tolerance at the jointing stage in climate chamber tests. The *VRN* genes of the wheat accessions were detected using allele-specific markers of the *VRN-A1*, *VRN-B1*, *VRN-D1* and *VRN-B3* loci, and the relationship between *VRN* genotype and freezing tolerance at the two developmental stages was tested. There were significant differences in freezing tolerance between the wheat accessions. Assessing the freezing tolerance of 52 wheat accessions at both the seedling and jointing stages revealed no significant correlation between tolerance at these two stages. The genotypic analysis found that *Vrn-D1* was the most frequent dominant allele in winter wheat, while no accession contained the dominant alleles *Vrn-A1* and *Vrn-B3*. Notably, freezing tolerance showed stage-specific genetic regulation; seedling-stage freezing tolerance strongly correlated with vernalization gene allelic combinations ($p < 0.05$), whereas jointing-stage freezing tolerance exhibited no such association. The presence of all recessive alleles *vrn-A1*, *vrn-B1*, *vrn-D1* and *vrn-B3* was required for strong seedling-stage freezing tolerance. The *VRN-D1* marker was effective for screening freezing tolerance materials under the premise that *vrn-A1* and *vrn-B1* alleles are recessive at winter wheat seedling stage.

Keywords: winter wheat; vernalization gene; freezing tolerance; seedling stage; jointing stage

1. Introduction

Wheat is one of the most important food crops, providing approximately 20% of the calories and protein for human nutrition. China is one of the two largest wheat producers and consumers in the world, accounting for 17% of global production and 16% of consumption. A high and stable wheat production is important in ensuring national food security [1]. Wheat is mainly grown in temperate climates. Under the intensification of climatic instability, low-temperature freezing damage occurs frequently, and has become a major meteorological factor that affects wheat's safe production.

Freezing stress can inhibit various physiological and biochemical activities in wheat, including water use, cell membrane stability, photosynthesis, secondary metabolite synthesis, and plant hormone content [2]. In wheat production, freezing stresses are generally

classified into two categories that are distinct in terms of phenology: winter freezing damage, which occurs at the seedling stage and impairs seedling establishment and vegetative growth, and spring freezing damage, which takes place from the jointing stage to the heading stage and disrupts reproductive processes. Both types of freezing damage can lead to reduced yield and lower grain quality [3–5]. The jointing stage (the anther connective tissue formation phase, ACFP) is widely recognized as the most suitable period for identifying the spring freezing tolerance of wheat. During this stage, the wheat stems are tender. When exposed to temperatures below 0 °C, it is extremely likely to cause the death of the main stem and large tillers. The Yellow and Huai Valley Wheat Region is the largest wheat-producing area in China. Frequent occurrence of jointing-stage freezing damage in this region causes a substantial reduction in final grain yield by 30–50% in severe cases, affecting nearly 42% of wheat sown areas. Therefore, it is important to study the jointing-stage freezing tolerance.

The freezing tolerance in wheat is a complex quantitative trait, and has been extensively studied. There are two evolutionary adaptive mechanisms: cold acclimation and low temperature vernalization enable wheat to resist cold at the seedling stage. Cold acclimation involves a series of accumulative physiological and biochemical processes that enhance tissue cold tolerance, mediated by various cold-responsive genes including *COR* (cold-regulated), *LTI78* (low-temperature induced 78), and *LEA* (Late embryogenesis abundant) genes [6]. Low temperature vernalization is the physiological requirement for the transition of winter wheat from vegetative to reproductive growth [7,8], and is also an adaptation for wheat to avoid freezing damage to reproductive organs. Vernalization response is determined by vernalization genes. Allelic variation at four *VRN* loci (*VRN1*, *VRN2*, *VRN3*, and *VRN4*) is well characterized. Winter habit is a recessive trait and the dominant *Vrn* alleles function in circumventing or reducing vernalization requirement. *VRN1*, which plays the most important role in vernalization, encodes a MADS-box family protein homologous to Arabidopsis *APETALA1* that acts as a floral activator and is expressed in leaves and shoot apical meristem [9]. *VRN2* inhibits flowering by regulating the expression of *VRN1* and *VRN3* [10]. *VRN3* is an orthologue of *Arabidopsis* flowering factor *FLOWER LOCUS T* (*FT*), and its presence leads to early flowering [11]. *VRN4* regulates the vernalization process of wheat by interacting with *VRN1* and *VRN3* [12]. *VRN1* and *VRN3* promote flowering and circumvent or reduce the requirement for long-term low temperatures to induce vernalization. There are three *VRN1* loci in wheat: *VRN-A1*, *VRN-B1*, and *VRN-D1* located in chromosome arms 5AL, 5BL, and 5DL, respectively [13]. *VRN-A1* is the most sensitive to temperature and has epistatic effects on *VRN-B1* and *VRN-D1* [14]. The *VRN-B3* loci are located on group seven chromosomes [11].

Numerous studies conducted to dissect the genetic architecture of freezing tolerance have highlighted the importance of *VRN* loci in freezing tolerance. The presence of a dominant *Vrn1* allele significantly reduces freezing tolerance. Accessions with dominant alleles at two or three *VRN1* loci generally have weak freezing tolerance, whereas genotypes with recessive alleles at all three loci have strong freezing tolerance [15–17]. The *VRN1* gene may enhance the freezing tolerance of wheat by interacting with cold-regulated genes [18]. Genes *Fr-A1*, *Fr-B1* and *Fr-D1* for frost tolerance are located at or near the *VRN1* loci in homeologous group five chromosomes [19,20]. *FR1* and *VRN1* synergistically regulate the expression of *Cor* regulated by *CBF* transcription factors that can enhance the freezing tolerance of wheat [21]. Transcript analysis showed that *VRN1* alleles directly regulate *CBF* genes and repress their expression, thereby reducing freezing tolerance during reproductive growth [22–24]. The recessive allele *vrn-A1* increases freezing tolerance 2.1-and 2.4-fold in both winter and spring wheat compared to the dominant allele *Vrn-A1* [25]. Futhermore, the copy number of *vrn-A1* also influences the freezing tolerance of hexaploid wheat [26].

Spring freezing tolerance also shows complex associations with *VRN1*, where *Vrn-A1* and *Vrn-D1* increase spring freezing susceptibility, while *Vrn-B1* enhances freezing tolerance [27]. Although primarily involved in flowering regulation, *Vrn-B3* also participates in freezing tolerance-related signaling pathways. These studies have revealed complex relationships between *VRN* loci and freezing tolerance in wheat. However, there is still a knowledge gap in understanding the relationship between the combination of vernalization gene alleles rather than single loci and the multi-stage freezing tolerance of wheat.

VRN1 and *VRN-B3* genes have been cloned, and molecular markers developed from them [28,29] are widely used in breeding [30–32]. In this study, we used 575 wheat accessions to identify the allelic status of genes *Vrn-A1*, *Vrn-B1*, *Vrn-D1,* and *Vrn-B3*, investigate the freezing tolerance at the seedling stage using field tests, and at the jointing stage in climate chamber tests, and analyze the effects of various alleles on freezing tolerance across different growth stages. The results were expected to identify freezing-tolerant germplasm and molecular markers for breeding.

2. Results

2.1. Analysis of Freezing Tolerance Traits at the Seedling Stage and at the Jointing Stage

The accession panel (Table S1) showed considerable variation in freezing tolerance across environments (Table 1). The freezing tolerance grades ranged from one to five, with standard deviations between 0.89 and 0.99, and coefficients of variation (CV) ranging from 34.78% to 46.04% (Table 1). These findings indicated that the three experimental environments effectively differentiated freezing tolerance among genotypes. Histograms showed that the phenotypic distributions for the three environments were normally distributed (Figure 1). The majority of accessions exhibited freezing tolerance grades of one to three across all three environments, indicating a higher proportion of accessions with strong to moderate freezing tolerance. Highly significant correlations were observed among freezing tolerance phenotypes across three environments, with correlation coefficients ranging from 0.699 to 0.773 (Table 2), which demonstrated that the phenotypes were stable across environments.

Table 1. Phenotypic variation of freezing tolerance of 435 wheat accessions.

Years	Minimum Temperature (°C)	Grade Range	Mean	SD	CV (%)
2017	−8	1–5	2.15	0.99	46.04
2018	−12	1–5	2.41	0.98	40.76
2021	−12	1–5	12.56	0.89	34.78

SD: Standard deviation, CV: Coefficient of variation, Freezing tolerance was rated on a one to five scale: one = the strongest tolerance, five = the weakest tolerance.

A total of 435 wheat accessions were collected from four ecological wheat production zones in China: the Northern Winter Wheat Region (NWWR), the Yellow and Huai Valley Winter Wheat Region (YHVWWR), the Middle and Lower Reaches of the Yangtze River Winter Wheat Region (MLRYRWWR), and the Southwest Winter Wheat Region (SWWR). Significant regional variations in freezing tolerance were observed among these accessions. The NWWR accessions (n = 13) exhibited the highest freezing tolerance with an average damage level of 1.7, followed by YHVWWR accessions (n = 268) at 2.0. In contrast, MLRYRWWR (n = 128) and SWWR (n = 26) accessions showed comparatively lower freezing tolerance, with average damage levels of 3.0 and 3.3, respectively. Statistical analysis revealed that the freezing damage grades of NWWR and YHVWWR accessions were significantly lower than those of MLRYRWWR and SWWR accessions ($p < 0.05$; Table S2), clearly demonstrating superior freezing tolerance in wheat varieties from the northern

regions (NWWR and YHVWWR) compared to their southern counterparts (MLRYRWWR and SWWR).

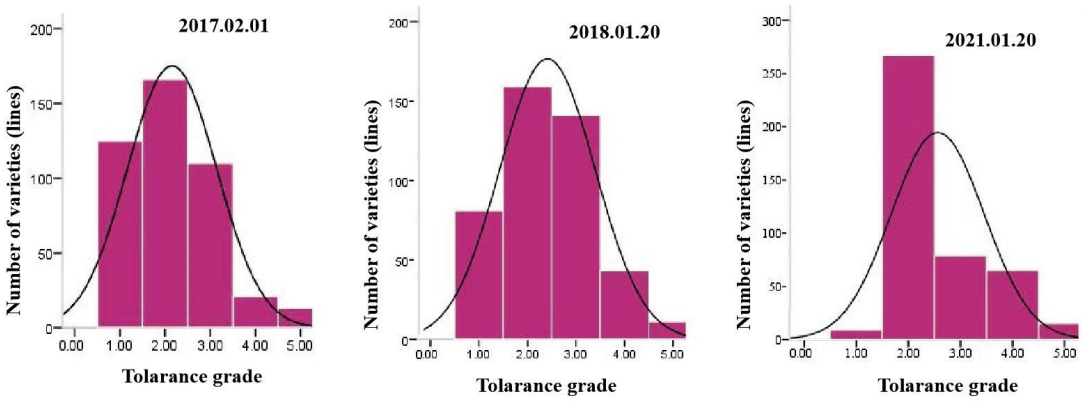

Figure 1. Distributions of freezing tolerance of 435 wheat accessions in three environments.

Table 2. Correlations of phenotypic data and genotypes of 435 wheat accessions in different environments.

	Freezing Tolerance			Gene Type	
	2017	**2018**	**2021**	***Vrn-D1***	***Vrn-B1***
2017	1				
2018	0.773 **	1			
2021	0.699 **	0.702 **	1		
Vrn-D1	0.288 **	0.280 **	0.503 **	1	—
Vrn-B1	0.050	0.078	0.141 **	—	1

** $p < 0.01$; — Not determined.

The dead stem rates of 192 accessions showed significant variation, ranging from 0.01 to 1.00 (Table S3) with a mean of 0.16 and a coefficient of variation of 52.24%. The −6 °C/6 h treatment at the jointing stage effectively distinguished differences in freezing tolerance among accessions at this growth stage. Following the dead stem grading standards from Liu et al. [33], freezing tolerance was divided into five tolerance levels (Figure 2A) with the majority in level five (Figure 2B). There were 17 accessions with grade one, and the average dead stem rate was 0.08. There were 26 accessions with grade two, and the average dead stem rate was 0.22. There were 23 accessions with grade three, and the average dead stem rate was 0.37. There were 35 accessions with grade four, and the average dead stem rate was 0.54. There were 91 accessions with grade five, and the average dead stem rate was 0.90 (Table S3). In summary, the freezing tolerance of 192 wheat accessions is obviously different, and the proportion of extremely weak accessions is the largest.

The relationship between seedling-stage and jointing-stage freezing tolerance of 52 accessions grown in the Yellow and Huai Valley Wheat Region is shown in Table 3. Some accessions such as Handan 6172, Huaimai 22, Jimai 22, Yannong 21 and Huaimai 29 had strong freezing tolerance at both growth stages. Accessions such as Annong 1124, Chuanmai 42 and Nemai 8 had strong freezing tolerance at jointing, but weak seedling freezing tolerance in winter; accessions Liangxing 99, Jinan 17 and Guomai 8 had strong seedling freezing tolerance, but weak tolerance in spring. Correlation analysis indicated that freezing tolerance at the two growth stages was not significant.

2.2. Association of Seedling Freezing and Vernalization Genotype

At *VRN-A1* locus, screening of the genotyping of the panel with PCR primer set Vrn1-AF/Int1R indicated that all 435 accessions had the 734-bp fragment for the *vrn-A1* or *Vrn-A1c* alleles. Amplification with primer set Intr1-AF2/AR3 produced no PCR product

whereas primer Intr1-CF/ABR produced a fragment of 1068-bp (Figure 3A). Results from the three independent PCRs indicated that all 435 wheat accessions carried the recessive *vrn-A1* allele (Table S1).

Table 3. The freezing grade of 52 winter wheat accessions.

Accession	Seedling-Freezing Grade (In the Field)			Jointing-Freezing Grade (In the Climate Chamber)
	2017	2018	2021	
Fengdecunmai 5	3	2	2	1
Henong 825	2	2	2	1
Handan 6172	1	1	1	1
Huaimai 22	1	1	2	1
Xiaoyan 6	2	1	2	1
Annong1124	3	3	4	2
Bainon g3217	2	2	2	2
Chuanmai 42	3	4	4	2
Jimai 22	1	1	2	2
Huaimai 30	2	3	3	2
Huaimai 29	1	1	2	2
Huiyan 22	1	2	3	2
Neimai 8	5	4	4	2
Yannong 21	1	1	2	2
An1243	1	2	2	2
Bainong 207	3	3	2	2
Huaimai 18	1	1	2	3
Huaimai 20	1	1	2	3
Luyuan 502	2	3	3	3
Yannong 19	1	1	2	3
Huaimai 25	1	1	3	3
Shijiazhuang 8	1	1	1	3
Yangnuomai 1	5	5	5	3
Zhengmai 366	2	2	2	3
Su 553	1	2	2	4
Aikang 58	1	2	2	4
Fanmai 5	2	2	3	4
Yanzhan 4110	2	2	3	4
Jimai 73	1	1	2	4
Zhengmai 9023	1	2	2	4
Wanmai 38	1	1	2	4
Zhoumai 18	2	3	2	4
Yannong 999	2	2	2	4
Jinan 17	1	1	2	4
Zhongmai 895	3	2	2	4
Luanxuan 988	3	2	2	5
Xinong 889	2	2	2	5
Qianmai 18	3	3	2	5
Guomai 8	1	1	2	5
Huiyan 77	1	2	3	5
Xinmai 18	2	3	2	5
Jimai 20	2	2	2	5
Kaimai 18	3	3	2	5
Yangmai 20	3	4	3	5
Liangxing 99	1	1	2	5
Mianmai 39	3	2	3	5
Guoshengmai 1	3	4	4	5
Yangmai 158	4	3	4	5
Wanmai 52	1	2	2	5
Ligao 6	1	2	2	5
Guinong 775	2	2	1	5
Neimai 836	5	4	4	5

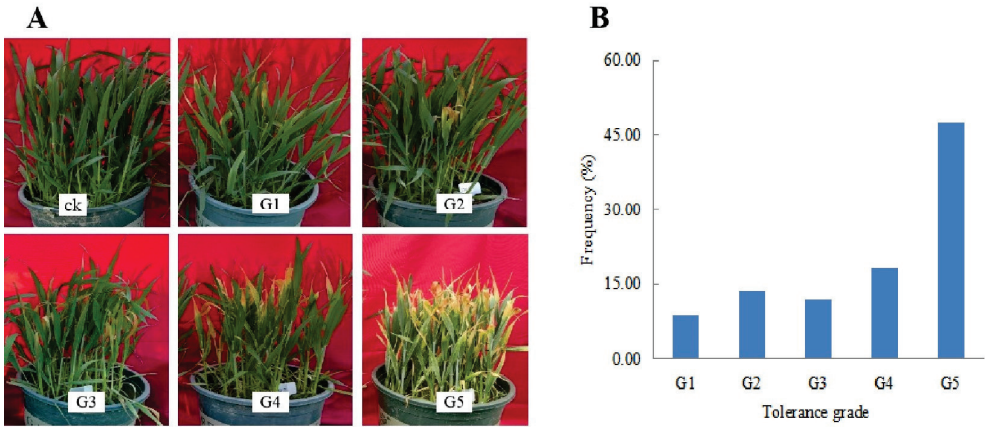

Figure 2. The freezing tolerance of wheat accessions at the jointing stage. (**A**) Growth performance of different tolerance grades of wheat accessions. (**B**) Frequency of freezing tolerance of 192 wheat accessions. Freezing tolerance was rated on a one to five grade: G1 = the strongest tolerance, G5 = the weakest tolerance.

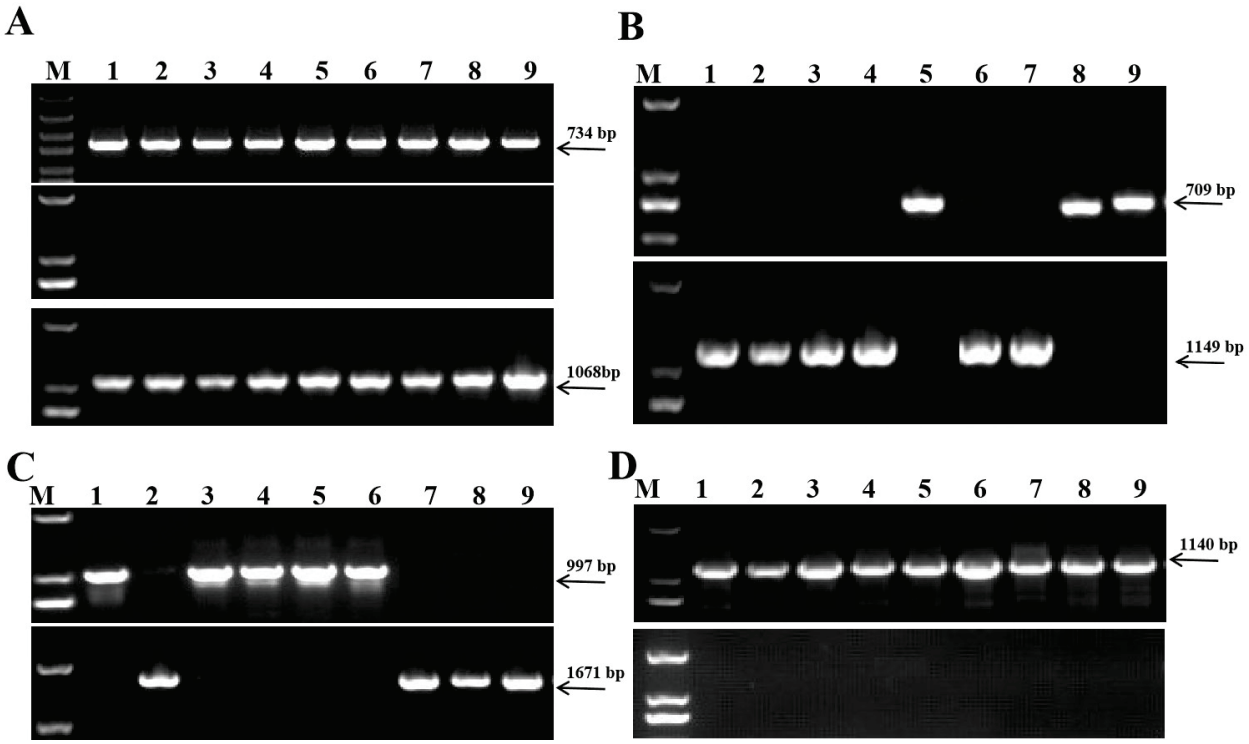

Figure 3. Allelic variation detected in the *VRN-A1*, *VRN-B1*, *VRN-D1* and *VRN-B3* loci among nine wheat accessions. Amplification with (**A**): primers Vrn1-AF/Int1R (uppermost), Intr1-AF2/AR3 (middle) and Intr1-CF/ABR (lowermost); (**B**): primers of Intr-BF/BR3 and Intr-BF/BR4; (**C**): primers Intr1-DF/DR3 and Intr1-DF/DR4; (**D**): primers of VRN4-B-INS-F/R and VRN4-B-NOINS-F/R. M, DL2000; 1, Yannong 19; 2, Yangmai 158; 3, Huaimai 20; 4, Su 553; 5, Huaimai30; 6, Bainong207; 7, Annong 1124; 8, Luo 1106; 9, Qian 110209.

Genotyping of the *VRN-B1* locus by PCR primer sets Intr-BF/BR3 and Intr-BF/BR4 (Figure 3B) indicated that 18 accessions had a 709-bp fragment, indicative of the *Vrn-B1* allele, While *vrn-B1* was detected in all other accessions (Table S1).

Genotyping of the *VRN-D1* locus with PCR primer sets VRN4-B-INS-F/R and VRN4-B-NOINS-F/R (Figure 3C) indicated that 178 accessions had the 1671-bp fragment, indicative of *Vrn-D1*, while *vrn-D1* was detected in all other accessions (Table S1).

At *VRN-B3* locus, amplification with primer set VRN4-B-INS-F/R detected no PCR product that identifies *Vrn-B3*; however, all accessions produced a 1140-bp fragment when amplified with primer set VRN4-B-NOINS-F/R (Figure 3D), indicative of *vrn-B3*.

Molecular marker detection results indicated that the highest frequency is the dominant *Vrn-D1* allele, accounting for 40.92% of the tested accessions, and a higher frequency is the dominant *Vrn-B1* allele, accounting for 4.14% of the tested accessions among 435 wheat accessions. We did not find the dominant *Vrn-A1* allele and dominant *Vrn-B3* allele (Figure 4). Characterization of the allelic combination of vernalization genes at *Vrn-A1*, *Vrn-B1*, *Vrn-D1* and *Vrn-B3* loci revealed that there was a total of four types of allelic variation compositions. Among them, there were 242 accessions that possessed the recessive *vrn-A1/vrn-B1/vrn-D1/vrn-B3* allelic variant combinations (accounting for 55.63%). There were 190 accessions carrying one dominant allelic variation; 175 out of 190 accessions had *vrn-A1/vrn-B1/Vrn-D1/vrn-B3* allelic variant combinations (accounting for 40.23%), while 15 accessions possessed *vrn-A1/Vrn-B1/vrn-D1/vrn-B3* allelic variant combinations (accounting for 3.45%; Table 4). Only 3 accessions possessed two dominant allelic variations, which were *vrn-A1/Vrn-B1/Vrn-D1/vrn-B3* allelic variant combinations (accounting for 0.69%). These suggested that the recessive allelic combination of *vrn-A1/vrn-B1/vrn-D1/vrn-B3* was predominant, but the combination of *vrn-A1/vrn-B1/Vrn-D1/vrn-B3* was prevalent in winter wheat.

A significant association was observed between the *Vrn-D1* allele and reduced freezing tolerance in three environments. The *Vrn-D1* allele was positively correlated with freezing tolerance grade with correlation coefficients of 0.288, 0.280, and 0.503, respectively ($p < 0.01$; Table 3). A Mann–Whitney U test also showed that the average freezing tolerance grade of *Vrn-D1* and *vrn-D1* genotypes was significantly different ($p < 0.01$; Figure 5). The *Vrn-B1* allele had no significant correlation with the freezing tolerance grade surveyed in 2017 and 2018, but showed a significant positive correlation with freezing tolerance grade in 2021 although the 0.141 correlation coefficient was very low (Table 3).

The average freezing tolerance level of lines carrying alleles *Vrn-B1* and *Vrn-D1* was 3.00, which was higher than accessions carrying only *Vrn-B1* (2.87) or *Vrn-D1* (2.78). The average freezing damage grade of lines with all four recessive alleles was 2.05 and significantly different from lines with one or two dominant alleles ($p < 0.05$; Table 4). Co-presence of recessive genes at all four loci was prerequisite for strong freezing tolerance in seedling.

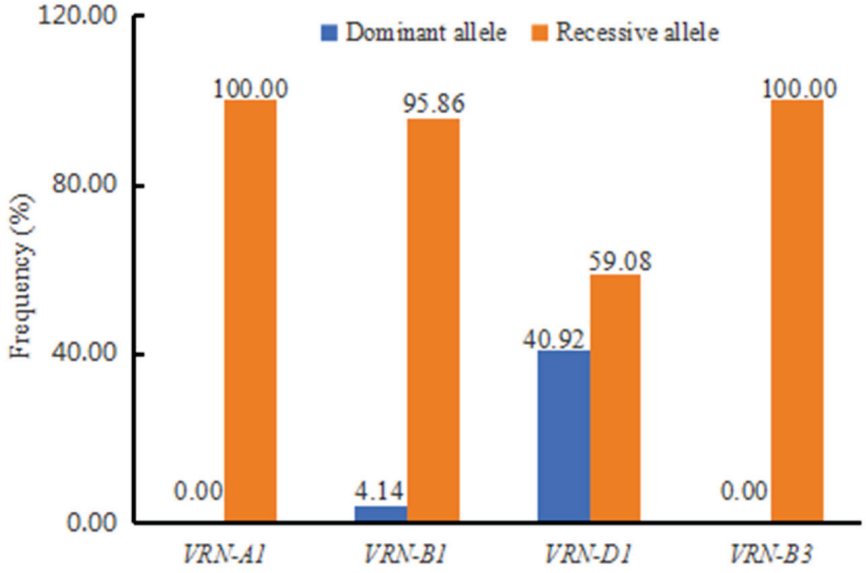

Figure 4. Frequency of alleles of vernalization genes in 435 wheat accessions.

Table 4. Effects of vernalization genotype on freezing grade.

Gene Type	Freezing Grade (Mean ± SD)	Number of Accessions	Frequency (%)
vrn-A1 + *vrn-B1* + *vrn-D1* + *vrn-B3*	2.05 ± 0.69 a [1]	242	55.63
vrn-A1 + *vrn-B1* + *Vrn-D1* + *vrn-B3*	2.78 ± 0.90 b	175	40.23
vrn-A1 + *Vrn-B1* + *vrn-D1* + *vrn-B3*	2.87 ± 0.77 b	15	3.45
vrn-A1 + *Vrn-B1* + *Vrn-D1* + *vrn-B3*	3.00 ± 0.33 b	3	0.69

[1] Different lowercase letters indicate significant differences at $p < 0.05$.

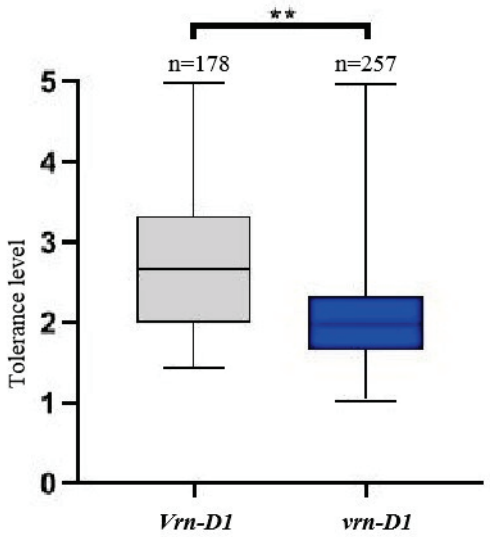

Figure 5. Comparison of freezing tolerance between the *Vrn-D1* and *vrn-D1* genotypes. ** $p < 0.01$.

2.3. Association of Jointing Freezing and Vernalization Genotype

PCR screening of the 192 wheat accessions from the Yellow and Huai Valley Wheat Region using primer set Vrn1-AF/Int1R indicated that all produced the 734-bp fragment, whereas there was no PCR product with primer set Intr1-AF2/AR3and 1068-bp fragment with primer set Intr1-CF/ABR. The combined PCR results indicated that all these accessions had *vrn-A1*. Screening with PCR primer sets Intr-BF/BR3 and Intr-BF/BR4 indicated that three wheat accessions (Bainong 3217, Huaimai 30, and Shan7859) had *Vrn-B1* allele characterized by a 709-bp fragment with primer Intr-BF/BR3; the remaining 189 accessions had *vrn-B1*. Seventy one accessions (59%) harbored *Vrn-D1* allele, and 121 carried *vrn-D1*. PCR results showed that all 192 accessions carried *vrn-B3*. The average dead-stem score of accessions carrying *Vrn-D1* was 0.62; the average score for *vrn-D1* accessions was 0.61, indicating that the *VRN-D1* locus had no obvious relationship with freezing tolerance at the jointing stage.

3. Discussion

Freezing stress on seedlings at the beginning of winter and at jointing in spring can injure wheat plants and negatively impact growth, development, and yield. Although the occurrence of frost damage is influenced by various factors, genetic variation among accessions plays a crucial role. In this study, we systematically evaluated the freezing tolerance of wheat at the seedling stage and the jointing stage. Currently, the evaluation of seeding-freezing tolerance of wheat in China follows the industry standard of the People's Republic (NY/T 1301–2007) [34] which divides freezing symptoms into five grades. Using this assessment method, we phenotyped 435 wheat accessions in three different environments. The highly significant correlations (ranging from 0.699 to 0.773) among the freezing tolerance phenotypes across these environments (Table 2) indicate that

the genetic basis for seedling-freezing tolerance is stable and heritable. This stability allows for reliable selection of freezing-tolerant germplasm during breeding.

Yellow and Huai Valley Wheat Region is in the transitional zone between north and south where frequent non-anticipated temperature fluctuations in spring can affect the wheat crop. Hence accessions with strong freezing tolerance especially at the jointing stage would be beneficial to production. The jointing-stage freezing tolerance of wheat is influenced by multiple factors, such as the occurrence-period, intensity and duration of low temperature. Because the occurrence period and intensity of low temperature in field are not consistent among years, it is difficult to get reliable and repeatable results. Artificial simulation identification is characterized by a remarkably short cycle and high repeatability, which enables researchers to efficiently obtain consistent and reliable results [35]. In this study, we applied this pot-planting and artificial simulation approach to evaluate the jointing-freezing tolerance of 192 wheat accessions from the region. Using the dead stem rate as an evaluation index, we found significant differences among different wheat accessions. The -6 °C/6 h treatment at the jointing stage effectively distinguished the genetic differences in freezing tolerance, which is consistent with previous studies [33]. However, compared with the seedling stage, a higher proportion (65.63%) of accessions showed weak freezing tolerance at the jointing stage, indicating that breeding for jointing-stage freezing tolerance is more challenging.

Assessing the freezing tolerance of 52 wheat accessions at both the seeding and jointing stages revealed no significant correlation between tolerance at these two stages, a finding consistent with previous reports by Zhong et al. [36]. This suggests that there may be different genetic mechanisms for the regulation of freezing tolerance at these two stages in wheat. In this study, only 12.19% of accessions showed a lack of seedling freezing tolerance, whereas 65.63% lacked tolerance at jointing. These findings demonstrate that freezing tolerance at the seedling stage is more amenable to selection during breeding compared to that at the jointing stage. Breeding for jointing-freezing tolerance is more challenging and future breeding programs should prioritize enhancing spring freezing tolerance, particularly during critical developmental phases such as the jointing stage.

The distribution frequencies of vernalization gene dominant alleles vary among different regions. In our study, among 435 winter wheat samples, the dominant allele frequencies were *Vrn-D1* (40.92%) > *Vrn-B1* (4.14%), with no detection of *Vrn-A1* or *Vrn-B3*. In the 192 accessions from the Yellow and Huai Valley Wheat Region, *Vrn-D1* was even more predominant at 58.68%, followed by *Vrn-B1* at 1.56%. Comparative analysis with previous studies showed notable differences: Zhang et al. [37] reported higher detection rates for *Vrn-B1* (18.2%) and *Vrn-A1* (13.8%) in broader geographical samples, though *Vrn-D1* (45.3%) remained predominant. Jiang et al. [38] documented a *Vrn-D1* frequency (56.12%) closely aligned with our Yellow and Huai Valley data. These discrepancies primarily stem from sample heterogeneity—prior studies included accessions from northern spring wheat regions, whereas our investigation strictly focused on winter wheat germplasm. By integrating geographical distribution patterns [39], we discerned that the high-frequency occurrence of *Vrn-A1/B1* in spring wheat regions directly explains their absence in our winter wheat samples. This robustly confirms that winter wheat accessions are predominantly characterized by the *Vrn-D1* dominant allele, with *Vrn-B1* as a secondary component-a distribution pattern consistent with China's wheat ecoregionalization mechanisms.

We also analyzed the relationship between vernalization gene alleles and freezing tolerance. At the seedling stage, we found that the dominant gene *Vrn-D1* was positively correlated with the freezing damage grade (Table 3), negatively regulating the freezing tolerance of wheat. The result is strongly associated with Zhang et al. [40], who found the recessive *vrn-D1* allele was more effective than dominant *Vrn-D1* allele in improving winter

tolerance of wheat. The average freezing tolerance level of accessions carrying *Vrn-B1* and *Vrn-D1* was higher than that of accessions carrying only one of these dominant alleles. Moreover, the average freezing damage grade of accessions with all four recessive alleles (*vrn-A1/vrn-B1/vrn-D1/vrn-B3*) was significantly lower (2.05) compared to accessions with one or two dominant alleles (Table 4). This indicates that the recessive *VRN1* allelic combination is closely related to strong seedling-freezing tolerance, which is correlated with You et al. [41]. Therefore, under the premise that *VRN-A1* site is recessive, *VRN-D1* gene markers can be effectively used for screening strong seedling-freezing tolerance wheat materials.

However, at the jointing stage, there was no obvious relationship between the vernalization gene and spring freezing tolerance. Although previous studies have shown that some *VRN1* alleles can affect spring freezing tolerance [27], in our study, due to the limited sample size and type, no dominant alleles *Vrn-A1* and *Vrn-B3* were detected in 192 accessions from the Yellow and Huai Valley Wheat Region, and only two samples contained the dominant *Vrn-B1* gene. Despite the high proportion (58.68%) of dominant *Vrn-D1*, there was no difference in the dead stem rate between the recessive *vrn-D1* and dominant *Vrn-D1* accessions. This suggests that other genetic or environmental factors may play more important roles in regulating jointing-freezing tolerance.

In this study, freezing tolerance of 435 wheat germplasm at the seedling stage and 192 wheat germplasm at the jointing stage were systematically evaluated, and allelic variation analysis of *VRN* gene was combined to screen out germplasm resources with significant frost resistance potential. Among the 435 accessions evaluated at the seedling stage, 47 exhibited consistently high freezing tolerance (grade one) in at least two independent environments. Notably, seven accessions—Handan 6172, ENESCO, Shijiazhuang 8, Shijiazhuang 15, Tai 10604, Niavt14, and Gushenmai 9—maintained grade one tolerance across all three testing environments. These accessions carried the recessive allelic combination of *vrn-A1/vrn-B1/vrn-D1/vrn-B3*. Such accessions can serve as valuable genetic resources for breeding wheat varieties with enhanced seedling freezing tolerance. For the 192 wheat accessions from the Yellow and Huai Valley Wheat Region evaluated at the jointing stage, although most of the accessions (65.63%) showed very weak tolerance (Figure 2B), some accessions such as Anke 20, Fengde Cunmai 5, Gu Shen 6, Huacheng 2019, Anke 237, Fengde Cunmai 1, An 1302, Anke 238, Henong 825, Hengjinmai 8, Anke 2101, Bifeng 1, Handan 6172, Huacheng 3366, Anke 239, Huaimai 22, and Xiaoyan 6 showed relatively strong freezing tolerances at the jointing stage. Although the relationship between vernalization genes and jointing-freezing tolerance was not clear in this study, these accessions can still be considered as potential germplasm for improving spring freezing tolerance in wheat breeding programs. Further research on their genetic mechanisms of freezing tolerance may provide new insights into enhancing wheat's resistance to spring cold stress.

4. Materials and Methods

4.1. Plant Materials

A total of 435 wheat accessions from different ecological wheat production zones were used for the evaluation of freezing tolerance in seedlings (Table S1). Among them, 268 accessions are from the Yellow and Huai Valley Winter Wheat Region (YHVWWR), 128 are from the Middle and Lower Reaches of the Yangtze River Winter Wheat Region (MLRYRWWR), 26 are from the Southwestern Winter Wheat Region (SWWWR), 13 are from the Northern Winter Wheat Region (NWWR). Since wheat in the Yellow and Huai Valley Wheat Region is frequently affected by freezing injury in spring, we also assessed 192 accessions (52 from the above accessions) from the Yellow and Huai Valley Wheat Region for freezing tolerance at jointing (Table S3).

4.2. Assessing of Freezing Tolerance Traits in Seedlings

A total of 435 wheat accessions were grown in field trial at the Huaibei Experiment Station (116°45′ N, 33°54′ E) of Anhui Academy of Agricultural Sciences (Hefei in Anhui province). They were planted in the conventional autumn season on 26 October 2016, 2017 and 2020, which is during the recommended seeding period for winter wheat in this region. The experimental design was a randomized complete block with two replicates. Plot size was 2-m-long rows with row spacing of 25 cm. All trials were seeded by manual dibbling at a seedling rate of 80 seeds row^{-1}. The total amount of urea applied during the whole growth period of wheat is 390 kg/hm. The application ratio of the base fertilizer to the top dressing is 7:3. Nitrogen fertilizer should be top-dressed during the jointing stage of wheat, and this should be carried out in combination with irrigation.

Meteorological information was provided by the Weather Bureau of Suixi County, Huaibei City. Frost damaging events occurred during 22~25 January 2017 (environment E1), 19~21 January 2018 (environment E2), and 6~9 January 2021 (environment E3). The lowest temperatures were −8 °C, −12 °C, and −12 °C, respectively. Before freezing stress, the diurnal temperature variation was relatively stable, which is generally suitable for the initial growth and development of wheat. Adequate sunlight ensured normal photosynthesis and promoted the growth of seedlings. The soil moisture content was maintained at a relatively optimal level, which provided sufficient water for the plants. Freezing tolerance phenotypes were recorded two weeks after freezing. According to the agricultural industry standard of China (NY/T1301–2007) [31], freezing tolerance was recorded on a five-grade, as follows:

Grade 1 (G1): no freezing damage;
Grade 2 (G2): leaf yellowing;
Grade 3 (G3): 50% leaf death;
Grade 4 (G4): All leaves dead or withered;
Grade 5 (G5): entire plants or most tillers dead.

4.3. Assessing Freezing Tolerance Traits in Spring

This experiment was conducted in 2020–2021 at the experimental station of Anhui Academy of Agricultural Sciences (31.83° N, 117.24° E), Hefei, China. The 192 wheat accessions were used in the experimentation. Wheat accessions were sown in pots of 28 cm diameter × 35 cm height, on 4 November 2021. There were 13 pots for each accession. Each pot was filled with 8 kg soil and 5.00 g compound fertilizer (N:P:K = 15:15:15) incorporated in it. The soil was taken from the field of 0∼20 cm upper plowing layer. Twenty seeds were planted in each pot and seedlings were thinned to ten at the three-leaf stage. All the pots were placed in the field conditions. The field environment for wheat growth is suitable, with stable day-night temperatures, ample sunlight, and appropriate soil moisture, creating favorable conditions for the growth of wheat.

When the plants reached the jointing stage (ACFP), eight pots of uniformly grown wheat plants from each accession were moved to a climate chamber for exposure to −6 °C for 6 h (humidity: 60%; light intensity: 0 μmol m^{-2} s^{-1}). The pots were moved back to the field after the treatment. The numbers of dead main stem and first and second tillers were assessed after 10 days of low temperature treatment. The dead-stem rate per pot was calculated as: Dead-stem rate = number of dead stems/total number of stems. The mean dead-stem rate was calculated for each accession using 8 replicated pots, and the tolerance grade of wheat accessions were classified based on these mean values. According to the criteria of jointing-freezing tolerance [30], the jointing-freezing tolerance of wheat was divided into 5 grades (Table 5).

Table 5. Evaluation criteria of jointing-freezing tolerance.

Tolerance Grade	Dead Stem Rate	Tolerance Type
1	0.00~0.13	Extremely strong
2	0.14~0.28	Strong
3	0.29~0.42	Moderate
4	0.43~0.65	Weak
5	0.66~1.00	Extremely weak

4.4. Molecular Marker Detection

Genomic DNA (gDNA) was extracted from young leaves of ten-day-old seedlings using the phenol chloroform method [42]. DNA concentration and quality were checked with NanoDrop2000 (Thermo Scientific, Waltham, MA, USA). DNA samples with a 260 nm/280 nm ratio equal to or higher than 1.8 were considered suitable for further PCR analysis. Nine functional markers (Table S4) specific for *Vrn-A1*, *Vrn-B1*, *Vrn-D1* and *Vrn-B3* alleles [10,26,27] were used to genotype all accessions. Primers were synthesized by Sangon Biological Engineering Technology and Service Co., Ltd. (Shanghai, China). DNA amplification was carried out in 20-μL reaction volumes, each consisting of 1 μL of 50–100 ng/μL DNA, 1 μL of 10 μmol/L of each primer, 10 μL of 2 × Taq PCR Master Mix (Tsingke Biotechnology Co., Ltd., Beijing, China), and 7 μL of sterilized ddH_2O. The annealing temperature and extension time used for the PCR are provided in Supplementary Materials Table S4. PCR products were separated in 1–3% agarose gels depending on the PCR product size (Table S4) and visualized under UV light after staining with ethidium bromide.

4.5. Statistical Analysis

Phenotypic differences in freezing tolerance among accessions were tested using analysis of variance (ANOVA) in the SPSS software 20.0, and multiple comparisons were made using the least significant difference (LSD) test at $p < 0.05$.

5. Conclusions

Vernalization genes play an important role in seedling-stage freezing tolerance of wheat. The *VRN-D1* molecular marker can be used as an effective tool for screening freezing-tolerant accessions at the seedling stage. However, jointing-stage freezing tolerance did not show a significant association with *VRN* genotypes, which may involve other low-temperature responsive genes or interactions with environmental factors. Han 6172, Huai Mai 29, and other germplasms with strong freezing tolerance at both the seedling and jointing stages were selected, which provided the core parents for multi-stage resistance breeding. Future studies should further analyze the molecular basis of freezing tolerance at the jointing stage, develop efficient molecular markers, and integrate phenomics with gene-editing technologies to accelerate the cultivation of new wheat varieties exhibiting broad adaptability to climate change.

Supplementary Materials: The following supporting information can be downloaded at: https://www.mdpi.com/article/10.3390/plants14091350/s1. Table S1. The Seedling-freezing grade and vernalizing genotypes of 435 wheat accessions. Table S2. The differences in freezing tolerance across different ecological regions. Table S3. The jointing-freezing tolerance and vernalizing genotypes of 192 wheat varieties. Table S4. Primer sequences used to identify *VRN-1* and *VRN-B3* alleles.

Author Contributions: Conceptualization, Y.W.; methodology, F.L. and W.C.; formal analysis, F.L. and Q.Z.; resources, H.Z. and Y.L.; data curation, F.L. and Y.L.; writing—original draft preparation, F.L.; writing—review and editing, F.L. and W.C.; supervision, W.C. and Q.Z. All authors have read and agreed to the published version of the manuscript.

Funding: This work was funded by National Key R and D Program of China (2024YFD1201100), the First Level Youth Talent Program of Anhui Academy of Agricultural Sciences (2022), the joint research of improved wheat variety of Anhui (2021-), the China Agriculture Research System of MOF and MARA (CARS-03-76).

Data Availability Statement: Data are contained within the article and Supplementary Materials.

Acknowledgments: We are grateful to Zhaoshi Xu and Maoyun She for their excellent technical assistance.

Conflicts of Interest: The authors declare no conflicts of interest.

References

1. He, Z.H.; Zhuang, Q.S.; Cheng, S.H.; Yu, Z.W.; Zhao, Z.D.; Liu, X. Wheat production and technology improvement in China. *J. Agric.* **2018**, *8*, 99–106.
2. Gang, J.; Hassan, M.A.; Muhammad, N.; Arshad, M.; Chen, X.; Xu, Y.H.; Li, J.C. Comparative Physiology and Transcriptome Analysis of Young Spikes in Response to Late Spring Coldness in Wheat (*Triticum aestivum* L.). *Front. Plant Sci.* **2022**, *13*, 811884.
3. Wu, Y.F.; Liu, B.H.; Gong, Z.H.; Hu, X.; Ma, J.C.; Ren, D.C.; Liu, H.J.; Ni, Y.J. Predicting yield loss in winter wheat due to frost damage during stem elongation in the central area of the Huang-huai plain in China. *Field Crop Res.* **2022**, *276*, 108399. [CrossRef]
4. Zheng, D.X.; Yang, X.G.; Mínguez, M.I.; Mu, C.Y.; He, Q.; Wu, X. Effect of freezing temperature and duration on winter survival and grain yield of winter wheat. *Agric. Forest Meteorol.* **2018**, *260*, 1–8. [CrossRef]
5. Zheng, B.; Chapman, S.C.; Christopher, J.T.; Frederiks, T.M.; Chenu, K. Frost trends and their estimated impact on yield in the Australian wheat belt. *J. Exp. Bot.* **2015**, *66*, 3611–3623. [CrossRef]
6. Monroy, A.F.; Dryanova, A.; Malette, B.; Oren, D.H.; Ridha, F.M.; Liu, W.C.; Danyluk, J.; Ubayasena, L.W.C.; Kane, K.; Scoles, G.J.; et al. Regulatory gene candidates and gene expression analysis of cold acclimation in winter and spring wheat. *Plant Mol. Biol.* **2007**, *64*, 409–423. [CrossRef]
7. Niu, D.; Gao, Z.; Cui, B.W.; Zhang, Y.X.; He, Y.H. A molecular mechanism for embryonic resetting of winter memory and restoration of winter annual growth habit in wheat. *Nat. Plants* **2024**, *10*, 37–52. [CrossRef]
8. Chepurnov, G.Y.; Ovchinnikova, E.S.; Blinov, A.G.; Chikida, N.N.; Belousova, M.K.; Goncharov, N.P. Analysis of the Structural Organization and Expression of the *Vrn-D1* Gene Controlling Growth Habit (Spring vs. Winter) in *Aegilops tauschii* Coss. *Plants* **2023**, *12*, 3596. [CrossRef]
9. Trevaskis, B. The central role of the *VERNALIZA TION1* gene in the vernalization response of cereals. *Funct. Plant Biol.* **2010**, *37*, 479–487. [CrossRef]
10. Yan, L.; Loukoianov, A.; Blechl, A.; Tranquilli, G.; Ramakrishna, W.; Sanmiguel, P.; Bennetzen, J.; Echenique, V.; Dubcovsky, J. The wheat *VRN2* gene is a flowering repressor down-regulated by vernalization. *Science* **2004**, *303*, 1640–1644. [CrossRef]
11. Yan, L.; Fu, D.; Li, C.; Blechl, A.; Tranquilli, G.; Bonafede, M.; Sanchez, A.; Valarik, M.; Yasuda, S.; Dubcovsky, J. The wheat and barley vernalization gene *VRN3* is an orthologue of *FT*. *Proc. Natl. Acad. Sci. USA* **2006**, *103*, 9581–19586. [CrossRef] [PubMed]
12. Kippes, N.; Debernardi, J.M.; Vasquez-Gross, H.A.; Akpinar, B.A.; Budak, H.; Kato, K.; Chao, S.; Akhunov, E.; Dubcovsky, J. Identiifcation of the *VERNALIZATION4* gene reveals the origin of spring growth habit in ancient wheats from South Asia. *Proc. Natl. Acad. Sci. USA* **2004**, *112*, 5401–5410.
13. Yan, L.; Helguera, M.; Kato, K.; Fukuyama, S.; Sherman, J.; Dubcovsky, J. Allelic variation at the *VRN-1* promoter region in polyploid wheat. *Theor. Appl. Genet.* **2004**, *109*, 1677–1686. [CrossRef]
14. Sun, Q.M.; Zhou, R.H.; Gao, L.F.; Zhao, G.Y.; Jia, J.Z. The characterization and geographical distribution of the genes responsible for vernalization requirement in Chinese bread wheat. *J. Integr. Plant. Biol.* **2009**, *51*, 423–432. [CrossRef]
15. Dhillon, T.; Pearce, S.P.; Stockinger, E.J. Regulation of freezing tolerance and flowering in temperate cereals: The *VRN-1* connection. *Plant Physiol.* **2010**, *153*, 1846–1858. [CrossRef]
16. Koemel, J.E.; Guenzi, A.C.; Anderson, J.A.; Smith, L. Cold hardiness of wheat near-isogenic lines differing in vernalization alleles. *Theor. Appl. Genet.* **2004**, *109*, 839–846. [CrossRef]
17. Reddy, L.; Allan, R.E.; Garland-Campbell, K.A. Evaluation of cold hardiness in two sets of near-isogenic lines of wheat (*Triticum aestivum* L.) with polymorphic vernalization alleles. *Plant Breed.* **2006**, *125*, 448–456. [CrossRef]
18. Galiba, G.; Vagujfalvi, A.; Li, C.; Soltesz, A.; Dubcovsky, J. Regulatory genes involved in the determination of frost tolerance in temperate cereals. *Plant Sci.* **2009**, *176*, 12–19. [CrossRef]
19. Efremova, T.T.; Chumanova, E.V.; Zhukova, I.M. Winter hardiness analysis of wheat-rye 5R(5A)-substituted lines in Western Siberia. *Cereal. Res. Commun.* **2021**, *50*, 25–35. [CrossRef]
20. Sutka, J.; Galiba, G.; Vagujfalvi, A.; Gill, B.S.; Snape, J.W. Physical mapping of the *Vrn-A1* and *Fr1* genes on chromosome 5A of wheat using deletion lines. *Theor. Appl. Genet.* **1999**, *99*, 199–202. [CrossRef]

21. Kobayashi, F.; Takumi, S.; Kume, S. Regulation by *Vrn-1/Fr-1* chromosomal intervals of *CBF*-mediated *Cor/Lea* gene expression and freezing tolerance in common wheat. *J. Exp. Bot.* **2005**, *56*, 887–895. [CrossRef] [PubMed]
22. Winfield, M.O.; Lu, C.; Wilson, I.D. Plant responses to cold: Transcriptome analysis of wheat. *Plant Biotechnol. J.* **2010**, *8*, 749–971. [CrossRef] [PubMed]
23. Laudencia-Chingcuanco, D.; Ganeshan, S.; You, F.; Fowler, B.; Chibbar, R.; Anderson, O. Genome-wide gene expression analysis supports a developmental model of low temperature tolerance gene regulation in wheat (*Triticum aestivum* L.). *BMC Genom.* **2011**, *12*, 299. [CrossRef] [PubMed]
24. Alonso-Peral, M.M.; Oliver, S.N.; Casao, M.C.; Greenup, A.A.; Trevaskis, B. The promoter of the cereal *VERNALIZATION1* gene is sufficient for transcriptional induction by prolonged cold. *PLoS ONE* **2011**, *6*, e29456. [CrossRef]
25. Linmin, A.E.; Fowler, D.B. Low-temperature tolerance and genetic potential in wheat (*Triticum aestivum* L.): Response to photoperiod vernalization, and plant development. *Planta* **2006**, *224*, 360–366. [CrossRef]
26. Zhu, J.; Pearce, S.; Burke, A.; See, D.R.; Skinner, Z.D.; Dubcovsky, J.; Garland-Campbell, K. Copy number and haplotype variation at the *VRN-A1* and central *FR-A2* loci are associated with frost tolerance in hexaploid wheat. *Theor. Appl. Genet.* **2014**, *127*, 1183–1197. [CrossRef]
27. Zhang, J.J.; Shahidul, I.M.D.; Zhao, Y.; Anwar, M.; Alhabbar, Z.; She, M.Y.; Ben, B.; Lu, M.Q.; Mayer, J.E.; Ma, W.J. Non-escaping frost tolerant QTL linked genetic loci at reproductive stage in six wheat DH populations. *Crop J.* **2022**, *10*, 147–165. [CrossRef]
28. Fu, D.P.; Szücs, L.; Yan, M.; Helguera, J.S.; Skinner, J.V.; Zitzewitz, P.M.; Hayes, D.J. Large deletions within the first intron in *VRN-1* are associated with spring growth habit in barley and wheat. *Mol. Genet. Genom.* **2005**, *273*, 54–65. [CrossRef]
29. Milec, Z.; Tomková, L.; Sumíková, T.; Pánková, K. A new multiplex PCR test for the determination of *Vrn-B1* alleles in bread wheat (*Triticum aestivum* L.). *Mol. Breeding* **2012**, *30*, 317–323. [CrossRef]
30. Yang, F.P.; Guo, Y.; Lv, Y.C.; Dong, Y.C.; Li, Y.; Hua, Q.C.; Hu, M.X.; Liu, J.D. Distribution frequency of vernalization and photoperiod genes in Gansu wheat landraces and winter hardness analysis. *J. Plant Genet. Resour.* **2023**, *24*, 1558–1567.
31. Kirill, O.P.; Alexandra, I.K.; Ekaterina, S.O.; Sergey, A.L.; Nikolay, P.G. Analysis of the Effects of the *Vrn-1* and *Ppd-1* Alleles on Adaptive and Agronomic Traits in Common Wheat (*Triticum aestivum* L.). *Plants* **2024**, *13*, 1453. [CrossRef] [PubMed]
32. Palomino, C.; Cabrera, A. Evaluation of the Allelic Variations in Vernalisation (*VRN1*) and Photoperiod (*PPD1*) Genes and Genetic Diversity in a Spanish Spelt Wheat Collection. *Int. J. Mol. Sci.* **2023**, *24*, 16041. [CrossRef] [PubMed]
33. Liu, F.F.; Wan, Y.X.; Cao, W.X.; Li, Y.; Zhang, Q.Q.; Li, Y.; Zhang, P.Z. Evaluation method of late spring coldness tolerance in wheat. *Acta Agron. Sin.* **2023**, *49*, 438–446.
34. *NY/T 1301-2007*; Technical Procedures for Wheat Variety Regional Trials. Ministry of Agriculture and Rural Affairs of the People's Republic of China: Beijing, China, 2007; pp. 1–17.
35. Liu, F.F.; Wan, Y.X.; Cao, W.X.; Zhang, Q.Q.; Li, Y.; Li, Y.; Zhang, P.Z. Advances on identification of wheat freezing tolerance in spring. *J. Plant Genet. Resour.* **2021**, *22*, 1193–1199.
36. Zhong, X.L.; Wang, D.L.; Ji, T.J.; Hu, X.; Zhao, P.; Han, L.S.; Wang, X.G.; Huang, S.H.; Huang, J.Y.; Sun, Z.F. Analysis on the factors affecting frost tolerance for winter wheat. *Acta Agron. Sin.* **2007**, *33*, 1810–1814.
37. Zhang, X.K.; Xiao, Y.G.; Zhang, Y.; Xia, X.C.; Dubcovsky, J.; He, Z.H. Allelic variation at the vernalization genes *Vrn-A1*, *Vrn-B1*, *Vrn-D1* and *Vrn-B3* in Chinese wheat cultivars and their association with growth habit. *Crop Sci.* **2008**, *48*, 458–470. [CrossRef]
38. Jiang, Y.; Huang, L.Z.; Hu, Y.G. Distribution of vernalization genes in Chinese wheat landraces and their relationship with winter hardness. *Sci. Agric. Sin.* **2010**, *43*, 2619–2632.
39. Li, Z.; Yang, J.; Li, R.B.; Wang, X.L.; Zhang, X.K.; Zhang, L.L. Composition and distribution of major vernalization genes in wheat cultivars from main production areas in China. *J. Northwest Agric. For. Univ.* **2018**, *46*, 35–40.
40. Zhang, H.J.; Xue, X.H.; Guo, J.; Huang, Y.W.; Dai, X.R.; Li, T.; Hu, J.H.; Qu, Y.F.; Yu, L.Q.; Mai, C.Y.; et al. Association of the recessive allele *vrn-D1* with winter frost tolerance in bread wheat. *Front. Plant Sci.* **2022**, *13*, 879768–879780. [CrossRef]
41. You, G.X.; Sun, G.Z.; Zhang, X.Y.; Xiao, S.H. Cold hardiness and its relationship with the *VRN1* genotypes in wheat accessions in the Yellow-Huai-Hai river valley region of China. *Acta Agron. Sin.* **2015**, *41*, 557–564. [CrossRef]
42. Zhang, X.; Wang, L.; Shou, L.L. A rapid modified CTAB method of extracting genomic DNA from wheat leaf. *Chin. Agric. Sci. Bull.* **2012**, *28*, 46–49.

plants

MDPI

Article

Identification and Characterization of SQUAMOSA Promoter Binding Protein-like Transcription Factor Family Members in *Zanthoxylum bungeanum* and Their Expression Profiles in Response to Abiotic Stresses

Shengshu Wang [1,2,†], Weiming Hu [2,†], Xueli Zhang [1], Yulin Liu [1,*] and Fen Liu [2,*]

[1] College of Forestry, Northwest A&F University, Yangling 712100, China; wss24616@163.com (S.W.); zxl980505@nwafu.edu.cn (X.Z.)
[2] Lushan Botanical Garden, Jiangxi Province and Chinese Academy of Sciences, Jiujiang 332900, China; huwm@lsbg.cn
* Correspondence: liuyulin@nwafu.edu.cn (Y.L.); liuf@lsbg.cn (F.L.)
† These authors contributed equally to this work.

Abstract: Plant-specific transcription factors known as SQUAMOSA promoter binding protein-like (*SPL*) genes are essential for development, growth, and abiotic stress responses. While the *SPL* gene family has been extensively studied in various plant species, a systematic characterization in *Zanthoxylum bungeanum* (*Zb*) is lacking. This study used transcriptomic and bioinformatics data to conduct a thorough genomic identification and expression investigation of the *ZbSPL* gene family. Eight subfamilies including 73 *ZbSPL* members were identified, most of which are predicted to be localized in the nucleus. Ka/Ks ratio analysis indicates that most *ZbSPL* genes have undergone purifying selection. According to evolutionary research, segmental duplication is a major factor in the amplification of the *ZbSPL* gene family. Gene structures, conserved motifs, and domains were found to be highly conserved among paralogs. *Cis*-element research revealed that *ZbSPLs* may be implicated in hormone and abiotic stress responses. Codon usage pattern analysis showed that the *ZbSPL* gene family was more inclined to A/T base endings; the higher the A/T content, the stronger the preference of the codons; and the use pattern was mainly affected by natural selection. Additionally, 36 *ZbSPLs* were found to be potential targets of miR156. RNA-seq demonstrated that *SPL* genes in *Zb* are differentially expressed in response to distinct abiotic stressors. Two *ZbSPL* genes (*ZbSPL10* and *ZbSPL17*) were implicated in the response to salt stress, while four *ZbSPL* genes (*ZbSPL06*, *ZbSPL43*, *ZbSPL60*, and *ZbSPL61*) showed response to drought stress, based on a qRT-PCR investigation of the *ZbSPL* genes under various abiotic stress conditions. This study will help us gain a deeper understanding of the functions of *ZbSPLs* and lay a genetic foundation for future breeding of high-quality, highly abiotic resistant varieties of *Z. bungeanum*.

Keywords: *SQUAMOSA promoter binding protein-like* (*SPL*); *Zanthoxylum bungeanum*; transcription factors; abiotic stress; gene expression

1. Introduction

Transcription factors (TFs) play a crucial role in regulating gene expression by either activating or repressing target genes [1,2]. These DNA-binding proteins are essential for controlling a wide range of plant biological processes, including growth, development, and stress responses [3,4]. The SQUAMOSA Promoter Binding Protein (SPL) family is a group

of plant-specific transcription factors. First discovered in *Antirrhinum majus*, *SBP1* and *SBP2* were found to have a significant impact on the early stages of flower development [5]. They used the method of screening the cDNA expression library to demonstrate that the expression levels of *SBP1* and *SBP2* were closely associated with the initiation and progression of floral organogenesis. Subsequent research [6] has further explored the molecular mechanisms underlying the function of *SPLs* in flower development and other plant physiological processes. The highly conserved 76-amino acid SBP domain of the SPL proteins contains a C-terminal nuclear localization signal (NLS) and two zinc fingers (found at the Zn-1 and Zn-2 zinc binding sites) that are crucial for DNA binding and nuclear localization [7–10]. In *Arabidopsis thaliana* (*At*), 16 *SPL* family members have been identified and classified into eight subgroups [11]. As more plant genomes have been sequenced, additional *SPL* family members have been identified and studied across various species, including rice (*Oryza sativa*) [12], tobacco (*Nicotiana tabacum*) [13], citrus (*Citrus clementina*) [14], poplar (*Populus euphratica*) [15], barley (*Hordeum vulgare*) [16], and wheat (*Triticum aestivum*) [17]. These investigations have revealed that *SPL* genes are involved in a wide range of plant growth processes, including vegetative growth [18,19], flowering and fruit development [20,21], and hormone regulation [22,23]. More recent investigations have also highlighted the crucial role that *SPL* genes play in regulating abiotic stress tolerance in a range of plant species. *SPL1* and *SPL12* in *At*, for example, are known to provide heat tolerance throughout the reproductive stage, and their overexpression boosts seed yield and heat resistance of the inflorescence [24]. In rice, *OsSPL10* controls drought tolerance through the regulating the expression of *OsNAC2*, which impacts stomatal movement and reactive oxygen species (ROS) production [25]. It also influences soil metabolites to promote salt stress resistance [26].

Additionally, miR156 negatively regulates many *SPL* family members through mRNA cleavage or post-transcriptional repression [27], which can either improve or impair a plant's response to abiotic stress. *TcmiR156*, for example, may play an important role in salt stress response by negatively controlling *TcSPLs* [28]. *MdWRKY100* is upregulated by the miR156/*SPL* module, which also improves salt resistance in apples [29]. Growing evidence suggests that the miR156/*SPL* module is a crucial mediator in balancing plant responses to abiotic stress and developmental processes.

Zanthoxylum bungeanum (*Zb*) is widely distributed and possesses significant economic and medicinal value. Nevertheless, no prior research has been conducted on the *SPL* gene family in *Zb*. In this investigation, *ZbSPL* genes in the *Zb* genome were identified and characterized. Comprehensive examinations of their gene structures, chromosomal locations, phylogenetic relationships, synteny, codon preference, miR156 binding sites, and *cis*-regulatory elements were also conducted. Additionally, we investigated the expression patterns of *ZbSPL* genes under various abiotic stress conditions, providing insights into their biological functions. The results from this thorough examination of the *ZbSPL* gene family establish a foundation for further studies into the functional differentiation and possible uses of these genes.

2. Results

2.1. Identification of ZbSPL Gene Family and Analysis of Its Physicochemical Properties

Our results demonstrated that the *Zb* genome harbored a total of 73 *SPL* genes. These genes were categorized as *ZbSPL01* through *ZbSPL73* based on their chromosomal locations (Table S1). In terms of their amino acid sequence, the ZbSPL proteins range in length from 126 aa (ZbSPL47/48) to 2084 aa (ZbSPL59), and their molecular weights range from 14.46 kDa (ZbSPL48) to 230.75 kDa (ZbSPL59). The ZbSPL proteins are hydrophilic, as evidenced by their negative average hydrophilicity values. Only ZbSPL01, ZbSPL02, and

ZbSPL25 are anticipated to be found in the plasma membrane, according to subcellular localization predictions, which showed that the bulk of the ZbSPL proteins are located in the nucleus (Table S2).

2.2. Chromosome Localization and Gene Replication

According to the genomic data, there are 72 *ZbSPLs* in *Z. bungeanum* (Figure 1), with one not dispersed among the chromosomes. Chromosome 41 contains the greatest number of *ZbSPL* genes (6), as shown in Figure 1. On the other hand, only one *ZbSPL* gene was found on each chromosome for chromosomes 12, 21, 22, 36, and 43. To gain insights into the mechanisms of gene amplification in the *ZbSPL* gene family, we analyzed repetitive events in the *Zb* genome. Only 107 pairs of segmental duplications and 2 pairs of tandem duplications were found among these 73 *ZbSPL* genes, as shown in Figure 2 and Table S3, indicating that segmental duplications are the primary mechanism for expansion of the *ZbSPL* gene family. Only the 12th and 36th chromosomes did exhibit any duplications, whereas the *ZbSPL* genes on 27 other chromosomes were implicated in these duplication events. Therefore, the *ZbSPL* gene family has experienced purifying selection throughout its evolutionary history, as evidenced by the fact that all gene pairs implicated in duplications have a Ka/Ks (non-synonymous/synonymous) ratio < 1 (range: 0.08–0.89).

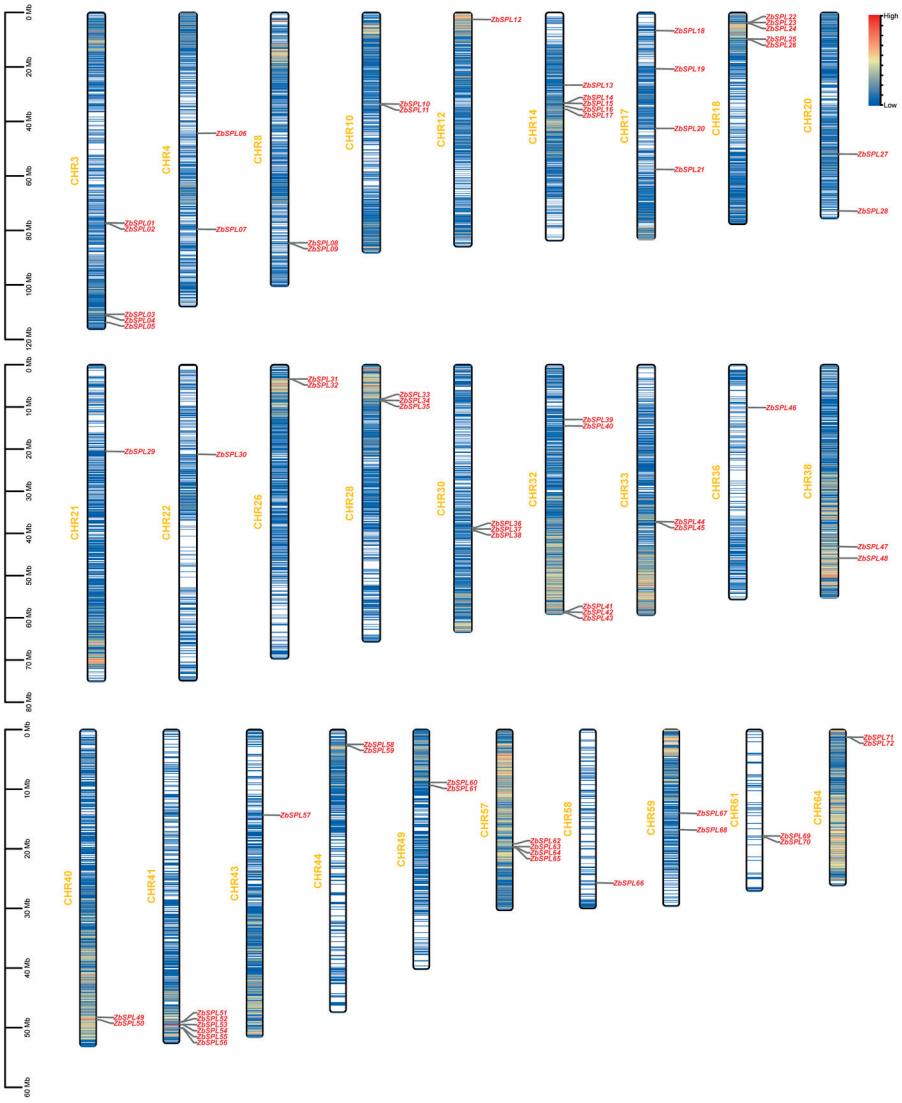

Figure 1. The distribution of the *ZbSPL* genes on the chromosomes of *Zb*. The scale indicates chromosome length. The variation in the shade of the center color indicates gene density.

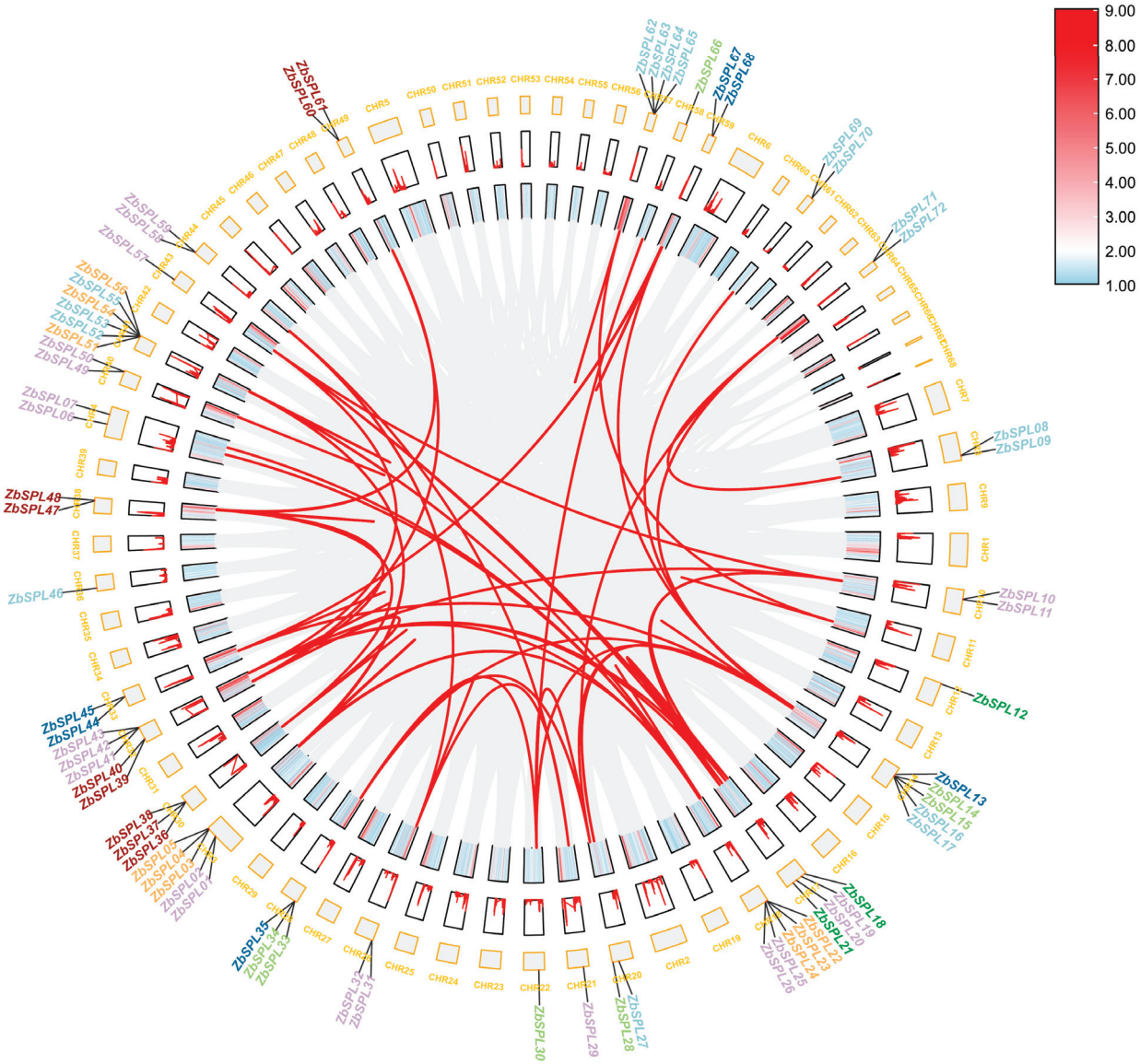

Figure 2. Synteny analysis of *ZbSPLs* within *Zb* genome. Red lines represent collinearity of *ZbSPL* gene; gray lines represent collinearity of entire *Zb* genome.

To better understand the origin and evolutionary relationships of *ZbSPL* genes, we analyzed the synteny relationships between *SPL* genes in *Zb* and those in *At*, *Zanthoxylum armatum* (*Za*), *O. sativa* (*Os*), *C. sinensis* (*Csi*), *Cucumis sativus* (*Csa*), and *Z. mays* (*Zm*). As shown in Figure 3, we identified 46, 271, 20, 64, 46, and 7 syntenic *SPL* gene pairs in *At*, *Zb*, *Os*, *Csi*, *Csa*, and *Zm*, respectively. There is not a one-to-one correspondence between all *SPL* genes in *Zb* and *Za*, but rather a many-to-many relationship, indicating that genome rearrangement and reshuffling of *SPL* orthologs occurred after the divergence of *Zb* and *Za*. The *SPL* genes of *Csi* and *Zb* are more evolutionarily conserved and share a closer phylogenetic link between species. This high similarity suggests they may have developed from a common ancestor shared by several plants.

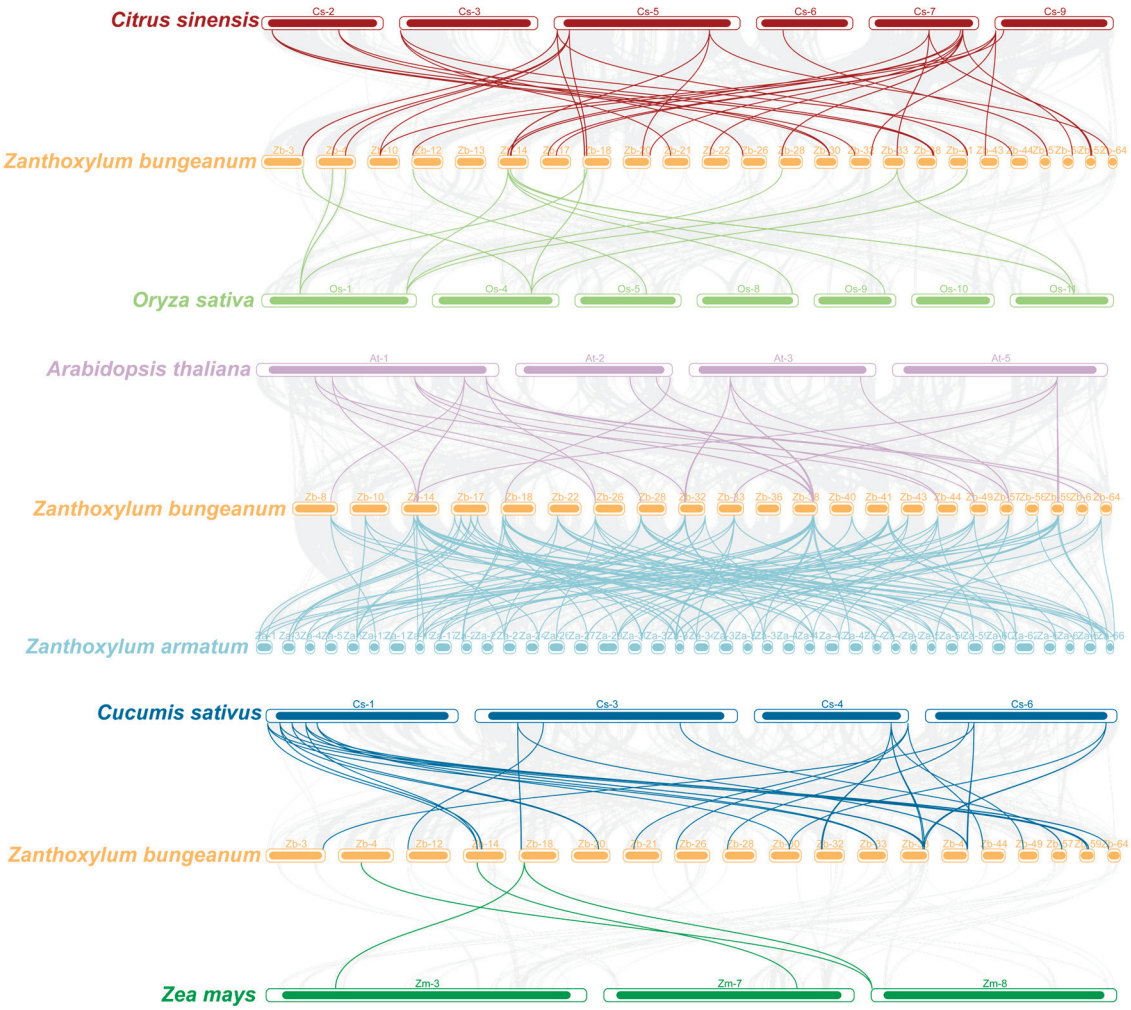

Figure 3. An analysis of syntenic relationships between *ZbSPL* genes in *Zb*, *Csi*, *Os*, *At*, *Za*, *Csa*, and *Zm*. Syntenic *SPL* gene pairs are highlighted by lines with colors corresponding to the color of the genome *Zb* is being compared to. The gray lines represent collinearity across the entire genome between different species and *Zb*.

2.3. Analysis of Conserved Motifs, Conserved Binding Domains, and Gene Structure

The presence of shared motifs among different proteins was determined based on the 20 conserved motifs identified within the ZbSPL family. As shown in Figure S1b, the number of conserved motifs per protein ranges from three to sixteen. Subfamily II contains the highest number of conserved motifs (16), whereas subfamilies VI and VII have the fewest (3). Within each subfamily (Figure S1a), most ZbSPL members share a common motif composition. For instance, all members of subfamily II, which have the most conserved motifs, share 15 common motifs. Subfamily I members have nine common motifs, while subfamilies V and VIII each have four common motifs, and the remaining three subfamilies have three common motifs each. Motif numbers and arrangements vary between subfamilies. Conserved motifs 1, 3, and 4 are present in all ZbSPL proteins, arranged in the specific order of motif 3, followed by motif 1, and then by motif 4.

Analysis of the conserved domains revealed that all identified ZbSPL proteins possess an SBP domain (Figures S1c and S2), with most subfamily II members containing an additional Ankyrin repeat domain-containing protein domain (ANKYR). Further sequence alignment showed that the SBP domain of the ZbSPL proteins is approximately 76 amino acids in length and includes two conserved zinc-binding sites (Zn1 and Zn2) and an NLS. In subfamily IV, the His residue at the Zn1 site is replaced by a Cys residue, resulting in a

characteristic Cys-Cys-Cys-Cys sequence for family members such as ZbSPL12, ZbSPL18, and ZbSPL21, in contrast to the Cys-Cys-Cys-His sequence found in the other subfamilies. Regarding the Zn2 site, the remaining proteins exhibit the Cys-Cys-His-Cys motif, with the exception of ZbSPL03, ZbSPL04, and ZbSPL05, where the His residue is substituted by Gln. Additionally, ZbSPL49 and ZbSPL50 lack an NLS. Further development of the protein phylogenetic tree and mapping of the intron/exon structure of the ZbSPL gene family will allow for a more thorough assessment of the structural traits of related genes. The number of introns in the 73 *ZbSPL* genes ranges from one to eleven (Figure S1d). Subgroup II contains the highest average number of introns, while subgroup VI contains the lowest. The majority of *ZbSPL* genes in the same subgroup have comparable gene architectures, especially regarding exon length and intron count.

2.4. Phylogenetic Analysis

To investigate the evolutionary relationships of the ZbSPLs, an additional 78 SPL proteins were selected for phylogenetic analysis, comprising 17 AtSPLs, 18 OsSPLs, 15 CsSPLs, and 28 PtSPLs from *At*, *Os*, *Citrus reticulata* (*Cr*), and *Populus tomentosa* (*Pt*), respectively. Following the classification method used for AtSPLs, the SPL proteins were categorized into eight groups, with each group containing at least one AtSPL. Subfamily II is the largest, comprising 20 ZbSPLs, followed by subfamilies IV and VI, which contain 9 and 10 members, respectively. Subfamily I is the smallest, with only three members. Proteins that group together in a single branch of the evolutionary tree are likely to share comparable structural traits and potentially have similar biological roles (Figure 4).

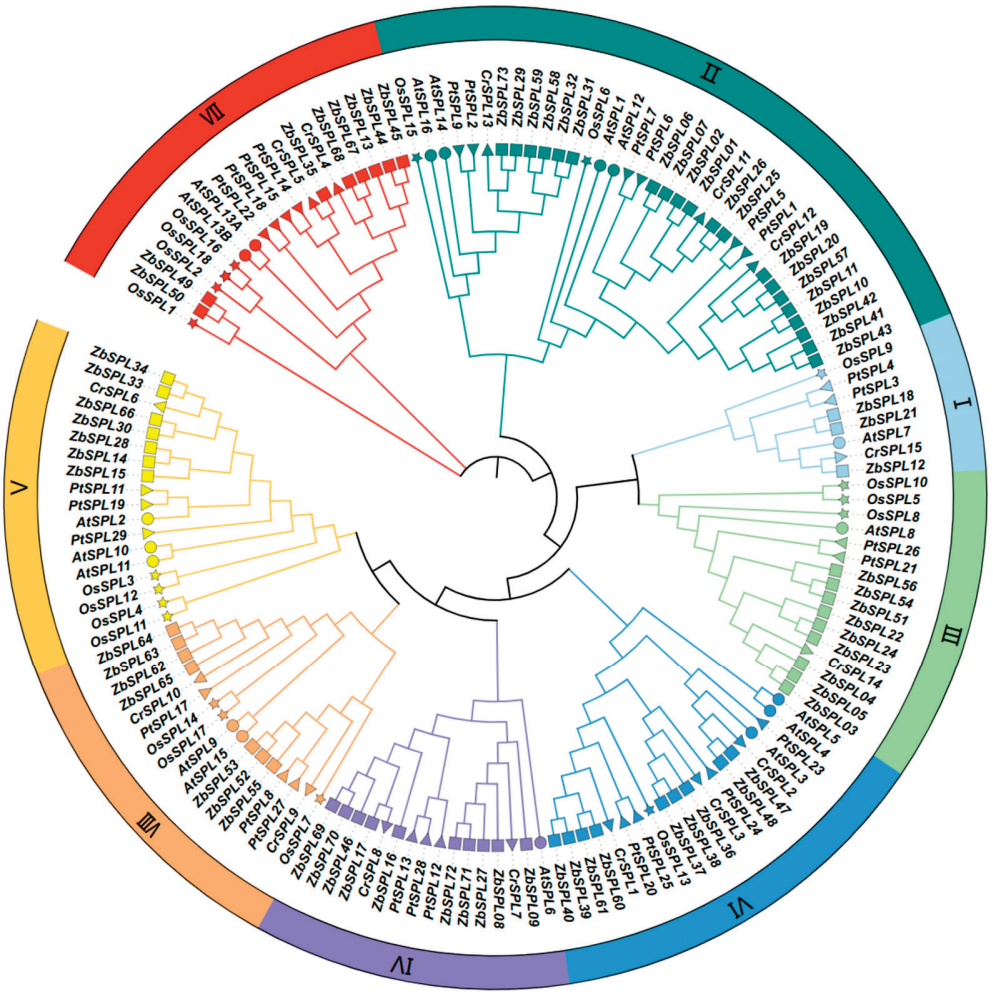

Figure 4. Phylogenetic tree of *SPL* family genes from *Zb*, *At*, *Os*, *Cr*, and *Pt*.

2.5. Cis-Acting Elements

Using the 2000 bp upstream of the start codon, we examined the promoter *cis*-regulatory element sequences in the *ZbSPL* genes, to elucidate their potential transcriptional regulatory roles. The functions of *ZbSPL* genes can be categorized into three main groups: responses to abiotic and biotic stresses, phytohormone responsiveness, and plant growth and development. The number of elements in all of the genes' promoters spans from 23 (*ZbSPL69*) to 52 (*ZbSPL20*) (Figure 5b). Of these categories, elements related to plant growth and development are the most prevalent, with 18 distinct types identified (Figure 5a). Almost all of the *ZbSPL* gene promoters contain light-responsive elements. Phytohormone-related response elements, including those responsive to abscisic acid (ABA), methyl jasmonate (MeJA), salicylic acid (SA), auxin, and gibberellin (GA), are also prominent, suggesting that these hormones may regulate *ZbSPL* genes during growth and development in *Zb*. Additionally, nine types of stress-related elements were identified, with antioxidant response elements (ARE) being widely distributed among these *ZbSPL* genes. Thus, each *ZbSPL* gene exhibits a unique composition of regulatory elements. For example, *ZbSPL52*, *ZbSPL53*, and *ZbSPL55* are enriched with abscisic acid response elements (ABREs), while *ZbSPL01* and *ZbSPL02* have a higher number of Box 4 light-responsive elements.

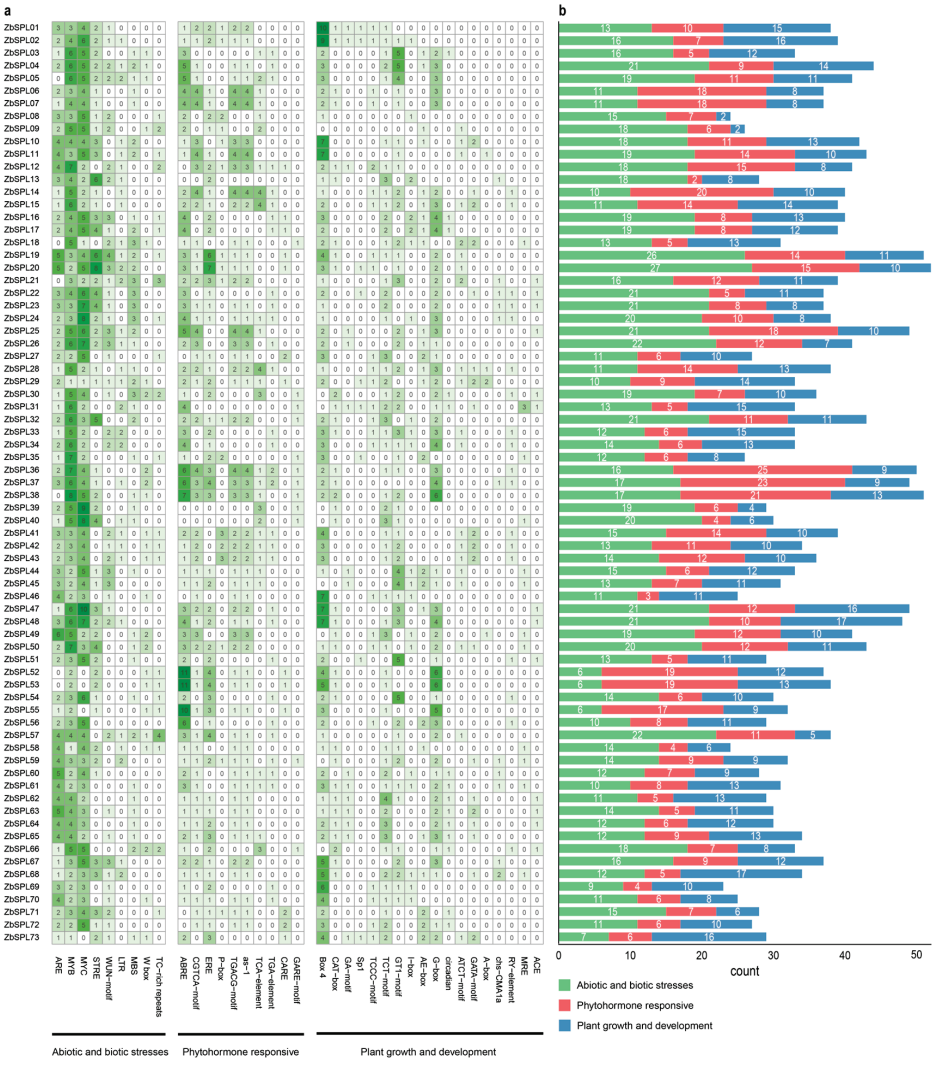

Figure 5. The quantity and arrangement of *cis*-elements in the promoter regions of the *ZbSPL* genes. (**a**) Heat maps showing *cis*-acting components; the number indicates how many *cis*-regulatory elements are present in the promoter region of that *ZbSPL* gene. (**b**) The number of *cis*-reactive element types within each response category for each gene is displayed in the bar chart (according to color).

2.6. Patterns of Codon Use in the ZbSPL Genes

Utilizing CodonW and EMBOSS, the codon use patterns of the *ZbSPLs* were examined to understand the significant influence of gene evolution and mutations on gene expression levels and functional differentiation. In the *ZbSPLs*, the percentages for each of the four bases in the third position of synonymous codons are 44.10% for T3s, 31.88% for A3s, 22.89% for C3s, and 27.58% for G3s (Figure 6a). The proportion of T3s and A3s is much greater than that of C3s and G3s, indicating that codons in the ZbSPL gene family are more likely to end in an A/T base than a G/C base. Pearson correlation analysis revealed that ENC has a strong positive correlation with GC, GC3s, CAI, CBI, Fop, and C3s, but a significant negative correlation with T3s and A3s (Figure 6b). This implied that the higher the content of A and T in bases of a *ZbSPL*, the stronger its codon preference. Neutral analysis showed that the regression coefficient after data fitting was 0.15, with a low coefficient of determination (R^2) (0.084), indicating that there is a large difference in the composition preference of the first, second, and third bases of each codon, and that the codon preference has been greatly affected by natural selection (Figure 7a). In Figure 7b, gene loci were primarily found in the lower half of the region, with the regions A3/(A3 + T3) < 0.5 and G3/(G3 + C3) > 0.5 having the largest distributions. According to the findings, the third base use follows the order T > A, G > C, reflecting the preference in selection for this position in the ZbSPL genes. Codon preference is mostly influenced by natural selection. As shown in Figure 7c, gene loci are mainly distributed in the lower side of the standard curve, with some distributed near or on the upper side of the standard curve, indicating that the codon use preference of *ZbSPL* gene is mainly affected by natural selection.

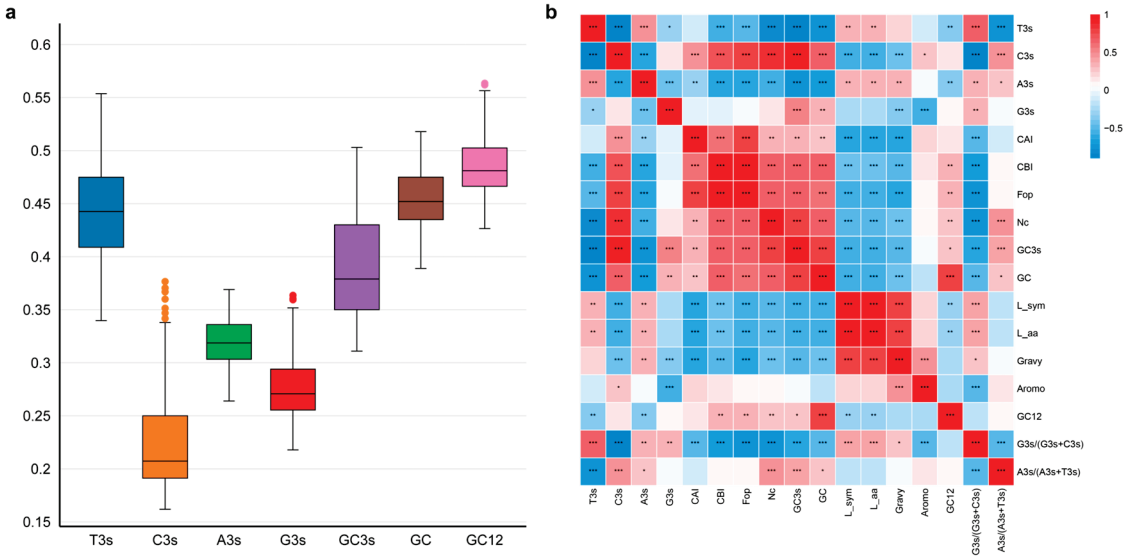

Figure 6. The *ZbSPL* gene family's codon composition (**a**) and parameter correlation analysis (**b**). In the figure on the left, box shapes of different colors correspond to different parameters below. In the figure on the right, the more stars there are, the higher the correlation. Red represents a highly significant positive correlation, while blue represents a highly significant negative correlation.

An essential statistic for determining codon preference is RSCU. The most preferred codons are those with RSCU values > 1 and a ΔRSCU ≥ 0.08. The range of optimum codons was found to be between six and 20 for the eight subfamilies. Seven of these codons (TGG, TAG, TTT, GAC, AAT, TTG, and CAG) were found in only a single subfamily. Based on their presence in six subfamilies, the four codons CAA, GAT, TTC, and TGC exhibited the most widespread distribution (Figure S3).

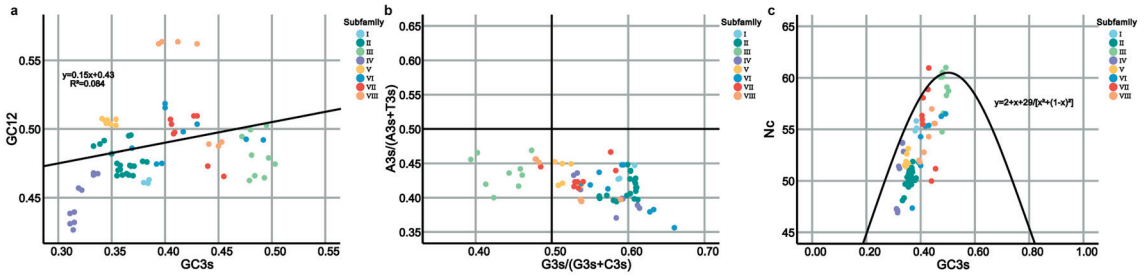

Figure 7. Neutrality plot (**a**), PR2-plot (**b**), and ENC-plot (**c**). The various colors in the upper-right corner indicate the distinct subfamilies to which the *ZbSPL* genes belong.

2.7. miR156/SPL Module Prediction

The miR156/*SPL* module is essential for tolerance to abiotic stress, which highlights the importance of identifying *ZbSPL* genes potentially regulated by miR156. A total of 36 *ZbSPL* genes containing target sites for miR156 were identified, representing nearly half of the *ZbSPL* gene family (Figure 8, Table S5). Of these 36 genes, 29 (81%) possess target sites within the coding region, while seven (19%) have target sites within the 3′ UTR. Notably, *ZbSPL63* is the only gene with target sites in both the coding region and the 3′ UTR, whereas *ZbSPL61* is unique in having two target sites within the 3′ UTR.

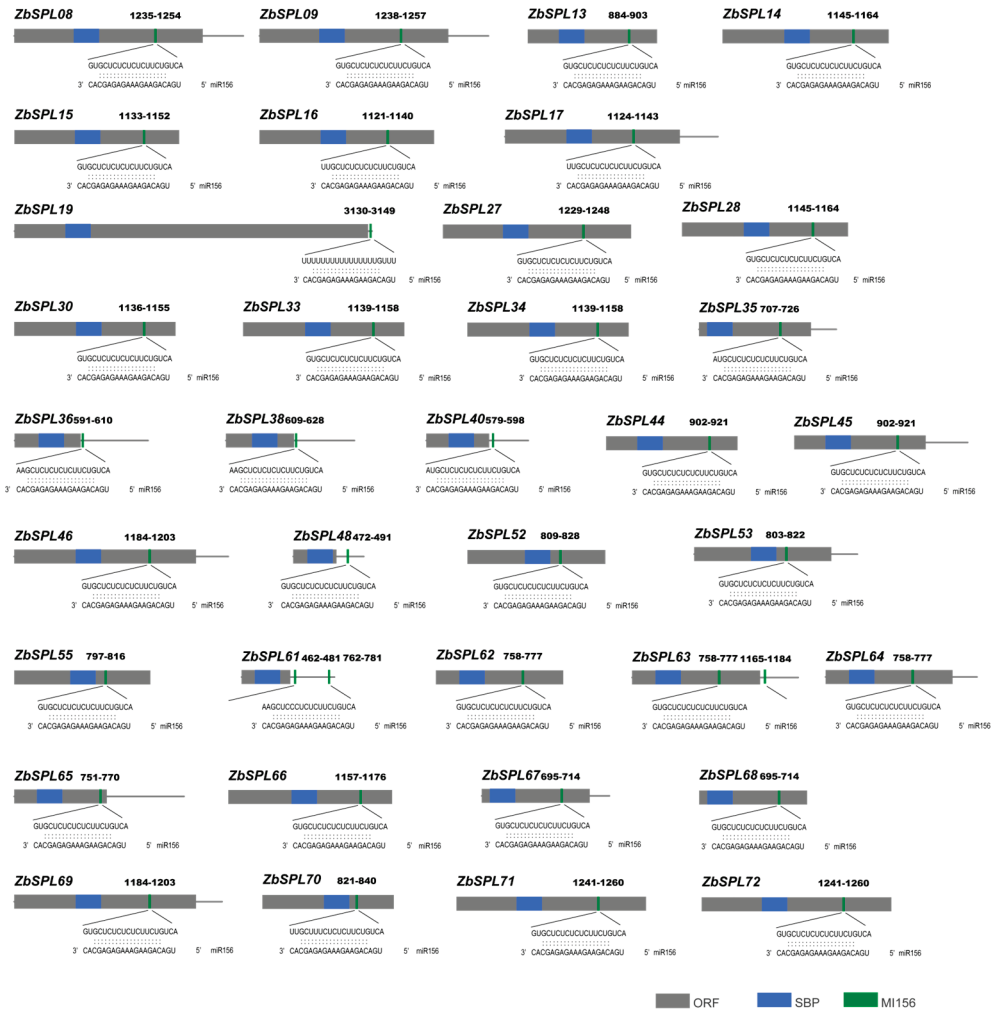

Figure 8. MiR156 predicted target sites on the *ZbSPL* genes. The open reading frame is represented by the gray area, the SBP domain by the blue area, and the complementary sites predicted by miR156 and represented by the green area, with the specific sequences at the bottom and the position information at the top. The gray line segment on the far right is the 3′UTR.

2.8. The Expression Profile of the ZbSPL Genes in Response to Abiotic Stress

To further investigate the functions of the *ZbSPL* gene family under adverse stresses, we analyzed the transcriptional expression patterns of the *ZbSPL* genes using transcriptomic data from *Zb* plants subjected to salt, drought, and cold stress (Figure 9). *ZbSPL06* and *ZbSPL07* exhibited relatively high expression levels under all three abiotic stress conditions, but showed no significant change trends. Under salt stress, *ZbSPL60* and *ZbSPL61* displayed higher expression levels in the control group, which initially increased with treatment and then decreased over time (Figure 9a). When experiencing drought stress, both genes are clearly upregulated (Figure 9b), while no significant changes are observed under cold stress (Figure 9c). *ZbSPL10*, *ZbSPL11*, *ZbSPL12*, *ZbSPL17*, *ZbSPL32*, *ZbSPL42*, and *ZbSPL59* all exhibit a decrease in expression levels during the early stages of salt treatment, followed by a gradual increase over time. During drought stress, their expression remains relatively stable, with only *ZbSPL32* showing significant upregulation under cold stress. *ZbSPL41*, *ZbSPL42*, and *ZbSPL43* are significantly upregulated only under drought stress, with no noticeable changes under salt or cold stress. Finally, *ZbSPL31* shows a distinct upregulation only under cold stress. Overall, the different *ZbSPL* genes exhibit diverse expression responses to salt, drought, and cold stresses, with some genes showing specific regulation under particular stress conditions, while others display a more general response to abiotic stress or stable expression patterns.

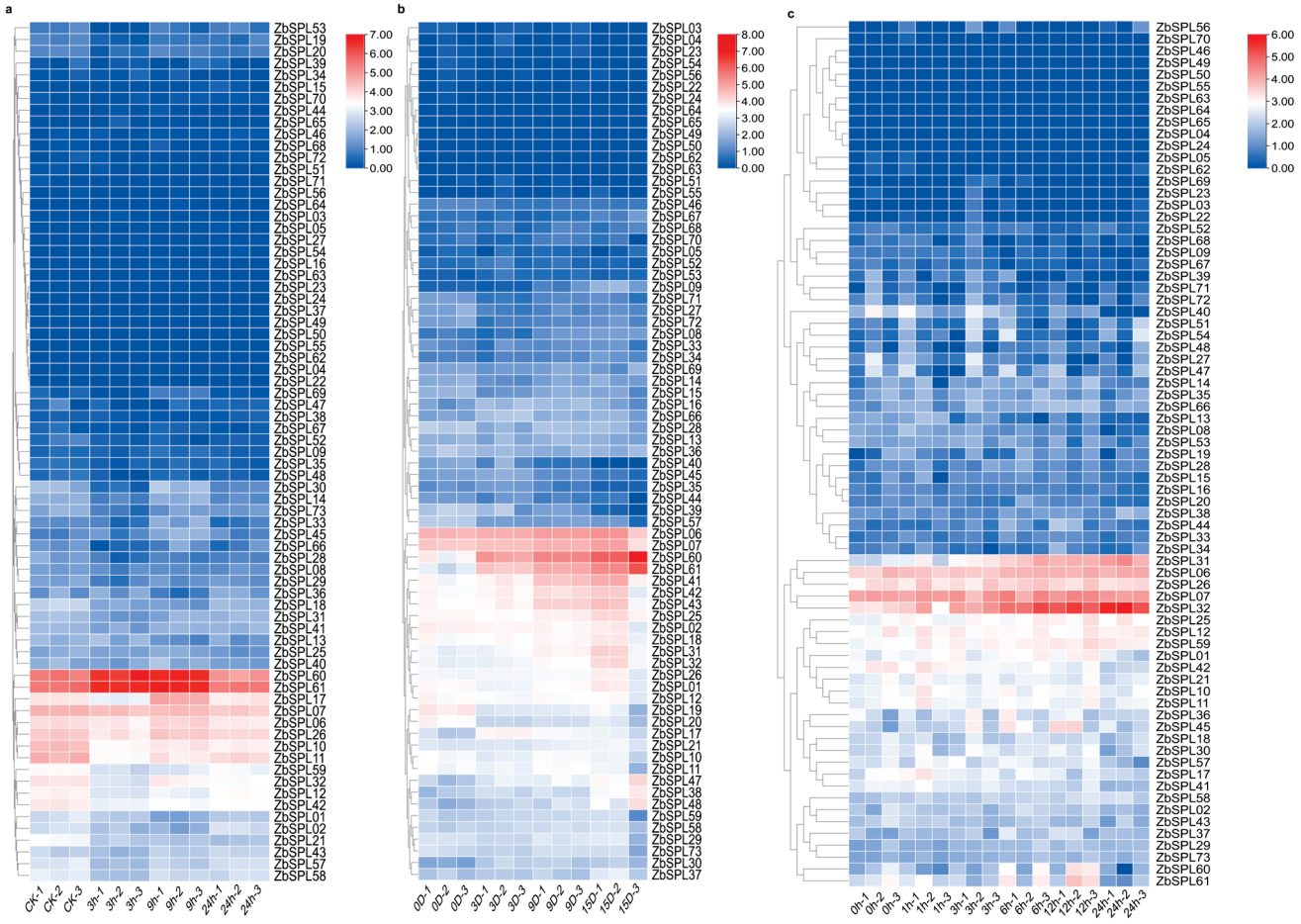

Figure 9. Based on fragments per kilobase of transcript per million mapped reads (FPKM) values, heatmaps of *ZbSPL* expression patterns for salt stress (**a**), drought stress (**b**), and cold stress (**c**) are presented. TBtools was used to visualize the log2 (FPKM) values. The degree of gene expression is shown on the upper-right scale.

Building on these findings, we further performed combined transcriptomeand *cis*-regulatory element analysis to identify a subset of *ZbSPL* genes and investigate their expression patterns under abiotic stresses, including salt, drought, and cold. Under salt stress, *ZbSPL10* and *ZbSPL17* exhibited similar expression profiles, with *ZbSPL10* showing strong upregulation at 24 h of salt treatment (nearly a 10-fold increase). *ZbSPL11*, *ZbSPL12*, *ZbSPL32*, *ZbSPL42*, and *ZbSPL59* exhibited similar expression patterns, showing significant upregulation at 9 h, followed by downregulation. *ZbSPL60* and *ZbSPL61* were significantly increased at 24 h following salt treatment; however, they were suppressed earlier at 9 h and 3 h, respectively (Figure 10a). *ZbSPL06*, *ZbSPL43*, *ZbSPL60*, and *ZbSPL61* all exhibited notable upregulation following 9 h of drought stress. *ZbSPL07* and *ZbSPL41* displayed a pattern of initial upregulation followed by downregulation; however, these changes were not as pronounced. *ZbSPL42* was significantly upregulated at 3 h, followed by a notable downregulation (Figure 10b). Under cold stress, *ZbSPL07*, *ZbSPL19*, and *ZbSPL32* were strongly and rapidly suppressed early on, but subsequently exhibited gradual induction (Figure 10c).

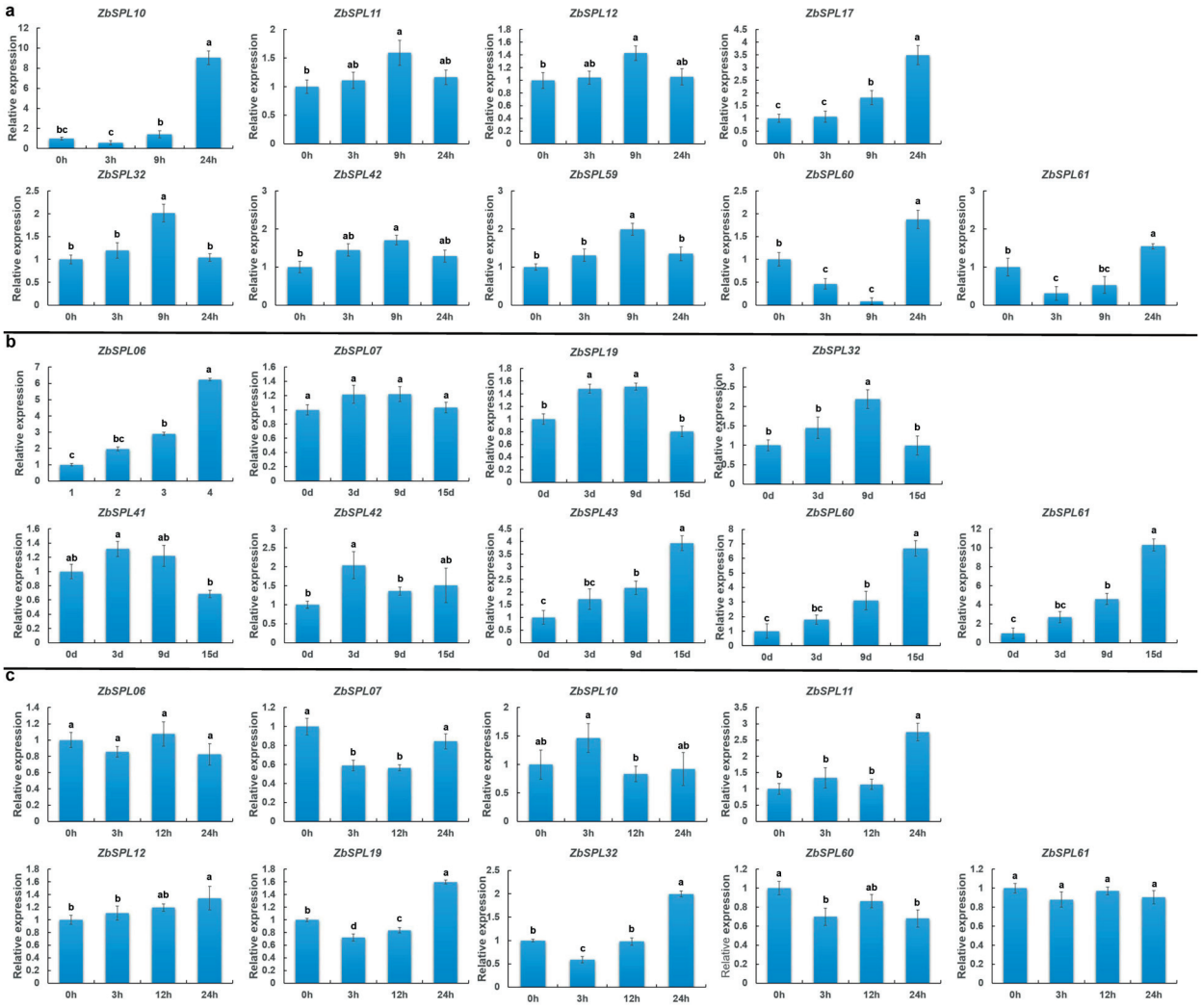

Figure 10. Relative expression levels of 9 *ZbSPL* genes under salt (**a**), drought (**b**), and cold (**c**) stress. Significant variations between various time periods are indicated by distinct letters. LSD tests were used to examine significant differences between groups ($p < 0.05$). The mean ± SD is represented by the data points.

3. Discussion

A set of plant-specific transcription factors known as *SPL* genes, characterized by highly conserved SBP domains, are critical for plant growth, development, and responses to both abiotic and biotic stresses. The acquisition of the whole-genome sequence of *Zb* provides strong support for the comprehensive genome-wide identification of *ZbSPL* genes [30]. In our study, we identified a total of 73 *ZbSPL* family members, surpassing the 8 identified in sugar beet [31], 36 in *Fraxinus mandshurica* [32], 56 in *Vaccinium corymbosum* [33], 22 in *Pisum sativum* [34], and 23 in *Ms* [35], but fewer than the 177 found in cotton (*Gossypium* spp.) [36]. The variation in the number of *SPL* family members across different plant species suggests differential contraction and expansion of the *SPL* gene family during long-term evolutionary processes [37].

In the *Zb* genome, 107 pairs of segmental repeats and 2 pairs of tandem repeats of the *ZbSPL* genes were identified, indicating that segmental repeats are the primary contributors to the expansion of the *ZbSPL* gene family. These findings are consistent with the results observed in the *SPL* gene families of the *Cicer arietinum* and *Carya illinoinensis* genomes, where segmental repeats are the main driving force in the evolutionary process [38,39]. The Ka/Ks ratios for all homologous genes are below 1, suggesting that purifying selection significantly influences the evolution of SPL transcription factors in *Zb*, reflecting a high degree of conservation [40]. Additionally, we compared the repeat patterns in *Zb* with those of six other species. Specifically, we identified 46, 271, 20, 64, 46, and 7 repeat events in comparisons between *Zb* and *At*, *Za*, *Os*, *Cs*, *Csa*, and *Zm*, respectively. The highest collinearity was observed between *Zb* and *Cs*, suggesting their closer evolutionary relationship, which is consistent with the proposal of a recent common ancestor between these two species by Feng et al. [30]. Additionally, the collinearity between *Zb* and dicotyledonous plants exceeds that of with monocotyledonous plants, indicating extensive evolution and duplication of SPL transcription factors following the divergence of monocots and dicots. Phylogenetic analysis of SPL proteins across species reveals that *Zb* is most closely related to *Cs*, which is consistent with the fact that *Zb*, *Cs*, *Pt*, and *At* are all dicotyledonous plants.

Gene structure analysis indicated that members of the *ZbSPL* gene family in subgroup II have the highest number of introns, ranging from nine to eleven, followed by subgroup I with nine introns. In contrast, other subgroups typically have only one or two introns. Early intron theories suggest that eukaryotic ancestors were highly intron-rich, and that intron loss has generally exceeded intron gain throughout evolution [41–44]. This pattern implies that genes in subgroups V and IV may be more ancient. A previous study indicated that intron loss can contribute to the formation of new genes [45], suggesting that the independent gain and loss of introns may have influenced the expansion of the *ZbSPL* gene family. Different subgroups exhibit distinct motifs and domain characteristics, yet all share highly conserved sequences, particularly motifs 1, 3, and 4. Genes within the same subgroup tend to be more similar; for example, subgroup II consistently has the most motifs. Additionally, some members of subgroup II contain ANKYR domains, which may be involved in protein–protein interactions [46].

Changes in the expression levels of individual genes under particular abiotic stress conditions were validated using qRT-PCR following the RNA-seq study. There were differences in the *Zb* varieties selected, but the healthy annual plants were all selected and treated with the same method. However, comparison of the results with the transcriptome data revealed differences. There are several plausible reasons for these discrepancies, such as the use of different platforms for qRT-PCR and RNA-seq [47], variations in the reference genes chosen for normalization [48], cultivar-specific variability in *Zb* (a different cultivar was used for the RNASeq and qRT-PCR analysis) [49], and the intrinsic complexity of transcriptomic data [50].

Plant growth and development are mostly controlled by *cis*-regulatory elements linked to auxin (IAA), gibberellin (GA), salicylic acid (SA), abscisic acid (ABA), methyl jasmonate (MeJA), and abiotic stress [51,52]. According to our findings, the promoter region of the *ZbSPL* genes were predicted to have a significant number of *cis*-regulatory elements associated with IAA, GA, SA, ABA, MeJA, and abiotic stress. In contrast to *ZbSPL16*, *ZbSPL43*, *ZbSPL60*, and *ZbSPL61*, which were significantly elevated under drought stress, *ZbSPL10* and *ZbSPL17* were highly upregulated under salt stress, according to qRT-PCR data. These results imply that *ZbSPLs* might be crucial in controlling stress responses and hormone-dependent pathways. Conserved in plants, the miR156/*SPL* module is essential for controlling plant development and abiotic stress responses [53,54]. This relationship has been observed by investigating the role of miR156 in regulating *AtSPLs* during cold stress: miR156 was upregulated in the cold, which resulted in downregulation of *AtSPL3* and *AtSPL13*, while *AtSPL9*, another target of miR156, increased in expression and was shown to increase freezing tolerance by upregulating *CBF2* expression [55]. In *Ms* leaves, it has been demonstrated that overexpression or knock-down of *MsSPL13* (which can be achieved by miR156) are more drought-resistant [56]. Additionally, Ms's salt tolerance is substantially enhanced by the miR156/*SPL4* module, with *MsSPL4OE* lines showing greater salt tolerance [57]. *ZbSPL07*, *ZbSPL19*, and *ZbSPL32* displayed comparable expression patterns under cold stress, being markedly downregulated at 3 h and then markedly increased at 24 h, based on the qRT-PCR results. *ZbSPL60* and *ZbSPL61* also showed a similar pattern of expression when treated with salt. *ZbSPL19* and *ZbSPL61*, targets of miR156, exhibit a suppression-response mode under stress, which may be the result of regulation by miR156.

4. Conclusions

The results of this investigation demonstrated there are 73 *ZbSPL* genes in total, which could mostly be categorized into eight subfamilies. Purifying selection has been essential to the formation of the SPL transcription factor family in Zb, with segmental duplication being the primary mechanism for gene family expansion. Synteny analysis revealed the close evolutionary relationship between *Zb* and *Cs*. Numerous regulatory elements linked to plant hormone signaling, light responses, and stress signaling pathways were found in the promoter regions of *ZbSPL* genes. According to the examination of usage patterns, codons of *ZbSPL* gene family members are more likely to end in having A/T bases. The preference for such codons is enhanced with increasing A/T content, suggesting that the use pattern is mostly influenced by natural selection. Moreover, 36 *ZbSPL* genes are anticipated to be possible targets of miR156, suggesting they are likely regulated by this miRNA. Expression profile data show variations in the expression levels of the *ZbSPL* genes under abiotic stress. The qRT-PCR results for the *ZbSPL* genes under different abiotic stress settings suggests that some may be involved in responses to drought and salt stresses. These findings establish a foundation for thoroughly investigating the biological role of *bSPL* genes in *Zb* and offer a fresh viewpoint on their evolution and biological relevance.

5. Materials and Methods

5.1. Identification and Physicochemical Analysis of ZbSPL Gene Family Members

The genomic data and annotation information for *Zb* were obtained from BioProject ID PRJNA524242 [30]. The amino acid sequences of 16 known SPL proteins from *At* were obtained from the TAIR database (http://www.arabidopsis.org, accessed on 12 July 2024). These *AtSPL* sequences were used as queries in BLAST searches against the *Zb* genome to identify all candidate *ZbSPL* genes. To exclude non-SPL domain sequences and eliminate redundancy, annotations were cross-referenced using the CDD database (http://www.ncbi.

nlm.nih.gov/Structure/cdd/wrpsb.cgi, accessed on 12 July 2024) and the Pfam database (http://pfam.xfam.org/, accessed on 12 July 2024). The physicochemical properties of the *ZbSPL* gene family members were predicted using the ExPasy online tool (https://web.expasy.org/, accessed on 12 July 2024). Subcellular localization predictions were performed using the WoLF PSORT tool (https://wolfpsort.hgc.jp/, accessed on 12 July 2024).

5.2. Chromosome Positioning and Gene Replication

The physical position information of *ZbSPL* genes in *Zb* was extracted using the TBtools v2.149 software [58], mapped onto the chromosomes, and then visualized. Gene duplication events were analyzed using the MCScanX toolkit with default parameters to conduct a synteny analysis of the *ZbSPL* genes, and the results were also processed using TBtools. The Ka/Ks ratio was computed to evaluate the selection pressure on the duplicated genes.

5.3. Gene Structure, Conserved Motifs, and Conserved Binding Domains

Multiple sequence alignment of the ZbSPL proteins was conducted using MEGA7 [59]. The full-length protein sequences of the ZbSPL family' members were examined to determine the top 20 conserved motifs using the MEME web tool (https://meme-suite.org/meme/tools/MEME, accessed on 12 July 2024).

Conserved domains in the ZbSPL proteins were investigated using the NCBI Batch CD-Search tool. The visualization of conserved domains, motifs, and intron/exon structures of the ZbSPL proteins was performed using TBtools.

5.4. Phylogenetic Analysis of ZbSPLs

At, *Os*, *Cr*, and *Pt* SPL protein sequences are provided in Table S4. The protein sequences were aligned using MEGA 7.0 's Muscle function. The optimal amino acid substitution model was selected using the maximum likelihood (ML) approach, and tree reliability was assessed through 1000 bootstrap replicates. The iTOL online tool (https://itol.embl.de/, accessed on 18 July 2024) was used to process and illustrate the final phylogenetic relationships.

5.5. Examination of Codon Usage Bias

Codon composition (GC3s, T3s, C3s, A3s, G3s, GC, and GC12), relative synonymous codon use (RSCU), optimal codon (Fop), effective codon number (ENC), codon adaptation index (CAI), and codon bias index (CBI) were all calculated using the CodonW software. The RSCUs and ΔRSCUs of the eight subgroups were calculated using the EMBOSS website (https://www.bioinformatics.nl/cgi-bin/emboss/cusp, accessed on 24 July 2024). The most preferred codons are those with a high frequency (RSCU > 1) and high expression ($\Delta RSCU \geq 0.08$). SPSS (Version 26) was utilized for the scatter plot and correlation analysis. ChiPlot (https://www.chiplot.online/, accessed on 24 July 2024) was used to generate box plots and upset plots.

5.6. Cis-Acting Elements and miR156 Prediction

Potential *cis*-acting elements within the 2000 bp upstream promoter regions of the *ZbSPL* genes were predicted using the PlantCare website (https://bioinformatics.psb.ugent.be/webtools/plantcare/html/, accessed on 18 July 2024). Data extraction and organization were performed using the TBtools v2.149 software, utilizing genomic data and annotation information. Based on the previous classification, the results from using R's ggplot function are shown [60]. The psRNATarget tool (https://www.zhaolab.org/psRNATarget/, accessed on 18 July 2024) was employed to search for complementary sequences of miR156 in the coding and 3' UTR regions of the *ZbSPL* genes.

5.7. Transcriptome Analysis

RNA-seq data for *Zb* under drought (PRJNA784034), cold stress (PRJNA597398), and salt stress (PRJNA1107841) conditions were retrieved from the NCBI SRA database. Initially, SRA files were converted to FASTQ format using the fastdump tool of the SRA Toolkit [61]. The quality of the raw sequencing data was assessed using FastQC [62]. Adapter sequences and low-quality reads were subsequently removed using Trimmomatic [63] to produced clean data. The clean data were then aligned to the *Zb* genome using Hisat2 [64]. The unified FPKM value was expressed after the gene expression value was calculated using String-Tie [65]. Heatmaps and clustering of log2 (FPKM) values for the *ZbSPL* genes were generated using ChiPlot.

5.8. Plant Materials and qRT-PCR

One-year-old *Zb* plants, "Fengxiandahongpao", were raised in a greenhouse at 25 °C, 60–70% humidity, and a 16/8 h light/dark cycle. After treating plants to salt stress with a 250 mmol/L NaCl solution, leaf samples were collected at 0 h, 3 h, 9 h, and 24 h. To obtain leaf samples for drought stress, irrigation was stopped, and tissue was collected at 0 days (0 d), 6 days (6 d), 9 days (9 d), and 15 days (15 d). Cold stress was implemented using a growth chamber set at 4 °C, and leaf samples were taken at 0 h, 3 h, 12 h, and 24 h. In almost all cases, these methods are based on those used in other RNA-seq studies I quantified. Three biological replicates were cultivated for each time point, with each replicate consisting of three independent seedlings. Samples were immediately frozen in liquid nitrogen and stored at −80 °C until further use in experiments.

RNA was extracted using the FastPure Plant Total RNA Isolation Kit (Vazyme Biotech Co., Ltd., Nanjing, China), and RNA concentration and purity were assessed. cDNA was synthesized using the HiScript II Q RT SuperMix (Vazyme Biotech Co., Ltd., Nanjing, China) for qRT-PCR. Primers were designed using Primer 5.0 software (Table S6) and validated for specificity using the TBtools v2.149 software. The *Zb* actin gene, *ZbActin*, was used as a reference gene [66]. qRT-PCR analysis of the *ZbSPL* genes was performed using the 2×ChamQ Universal SYBR qPCR Master Mix (Vazyme Biotech Co., Ltd., Nanjing, China), with at least three biological replicates and three technical replicates. The 10 μL reaction mixture consisted of 0.5 μL of cDNA template, 0.2 μL of each primer (upstream and downstream), 5 μL of SYBR MIX, and 4.1 μL of RNase-free water. The PCR conditions were as follows: 95 °C for 30 s; followed by 40 cycles of 95 °C for 10 s, 60 °C for 30 s; 65 °C for 5 s; and a final incubation 95 °C for 5 s to obtain a melt curve. Relative quantification was conducted using the $2^{(-\Delta\Delta Ct)}$ method [67]. Statistical analysis was performed with SPSS software (Version 26), with one-way ANOVA followed by the least significant difference (LSD) test. Gene expression levels were visualized using histograms generated in Excel 2021.

Supplementary Materials: The following supporting information can be downloaded at https://www.mdpi.com/article/10.3390/plants14040520/s1, Figure S1. Phylogenetic tree, motif patterns, gene structures, and conserved domain of ZbSPL proteins. (**a**) The phylogenetic tree was constructed using the full-length sequences of the ZbSPL proteins with 1000 replicates on each node. (**b**) The amino acid motifs (numbered 1–20) in the ZbSPL proteins are displayed in 20 colored boxes, and the black lines indicate amino acid length. (**c**) Conserved domains for the ZbSPL members: SBP domains, indicated by green boxes; and ANKYR domains, represented by yellow boxes. (**d**) Gene structure of *ZbSPL* members: untranslated region (UTR), represented by green boxes and coding sequence (CDS), represented by yellow boxes. Figure S2. Alignment of the SBP domain in ZbSPL proteins. Sequence logo for the SBP-box in the ZbSPLs. The overall height of each stack indicates the degree of conservation of the corresponding residue site, while the height of the characters in each stack represents the relative frequency. Shown at the bottom are two conserved zinc-binding sites (Zn1

and Zn2) and a nuclear localization signal (NLS). Figure S3. Clustering of the relative synonymous codon usage in the gene of the eight subfamilies. Table S1. Gene names and locus information for the SPL proteins in *Zb*. Table S2. Analysis of the physical and chemical properties and prediction of the ZbSPLs of their cell localization in *Zb*. Table S3. Ka/Ks ratio of *ZbSPL* genes in clades I–VIII. Table S4. Sequence features of *AtSPLs* in *A. thaliana*, *O. sativa*, *C. reticulata*, and *Populus tomentosa*. Table S5. *ZbSPLs* targeted by miR156. Table S6. Primers for real-time quantitative PCR.

Author Contributions: The authors confirm their contributions to this work: W.H., X.Z. and Y.L. in its conceptualization; S.W. in the original draft preparation, data analysis, and writing; S.W. and F.L. in the sample preparation; and W.H., Y.L. and F.L. in revising and reviewing. All authors have read and agreed to the published version of the manuscript.

Funding: This work was supported by grants from the Double Thousand Plan of Jiangxi Province (jxsq2023201126 to Fen Liu), the International Science and Technology Cooperation Project of Jiangxi Province (20232BBH80003 to Fen Liu), the Xuncheng Talent Program (JJXC2023053 to Fen Liu), a key project at the central government level—the ability establishment of sustainable use for valuable Chinese medicine resources (2060302 to Weiming Hu)—the National Natural Science Foundation of China (32160099 to Weiming Hu), and the Young Breeding Expert Support Program of the Yangling Agricultural Hi-tech Industries Demonstration Zone to Yulin Liu.

Data Availability Statement: Data sharing is available upon request.

Acknowledgments: We apologize to the authors whose works are not cited because of space limitations.

Conflicts of Interest: The authors declare no conflicts of interest.

References

1. Liu, T.; Chen, T.; Kan, J.; Yao, Y.; Guo, D.; Yang, Y.; Ling, X.; Wang, J.; Zhang, B. The GhMYB36 transcription factor confers resistance to biotic and abiotic stress by enhancing PR1 gene expression in plants. *Plant Biotechnol. J.* **2021**, *20*, 722–735. [CrossRef]
2. Koyama, T. Regulatory Mechanisms of Transcription Factors in Plant Morphology and Function 2.0. *Int. J. Mol. Sci.* **2024**, *25*, 2010. [CrossRef] [PubMed]
3. Mao, T.; Wang, X.; Gao, H.; Gong, Z.; Liu, R.; Jiang, N.; Zhang, Y.; Zhang, H.; Guo, X.; Yu, C. Ectopic Expression of MADS-Box Transcription Factor VvAGL12 from Grape Promotes Early Flowering, Plant Growth, and Production by Regulating Cell-Wall Architecture in Arabidopsis. *Genes* **2023**, *14*, 2078. [CrossRef]
4. Ma, Z.; Hu, L. WRKY Transcription Factor Responses and Tolerance to Abiotic Stresses in Plants. *Int. J. Mol. Sci.* **2024**, *25*, 6845. [CrossRef] [PubMed]
5. Klein, J.; Saedler, H.; Huijser, P. A new family of DNA binding proteins includes putative transcriptional regulators of the *Antirrhinum majus* floral meristem identity geneSQUAMOSA. *Mol. Genet. Genom.* **1996**, *250*, 7–16. [CrossRef]
6. Preston, J.C.; Hileman, L.C. SQUAMOSA-PROMOTER BINDING PROTEIN 1 initiates flowering in *Antirrhinum majus* through the activation of meristem identity genes. *Plant J.* **2010**, *62*, 704–712. [CrossRef] [PubMed]
7. Yu, N.; Cai, W.J.; Wang, S.; Shan, C.M.; Wang, L.J.; Chen, X.Y. Temporal control of trichome distribution by microRNA156-targeted SPL genes in *Arabidopsis thaliana*. *Plant Cell* **2010**, *22*, 2322–2335. [CrossRef] [PubMed]
8. Yamasaki, K.; Kigawa, T.; Inoue, M.; Tateno, M.; Yamasaki, T.; Yabuki, T.; Aoki, M.; Seki, E.; Matsuda, T.; Nunokawa, E.; et al. A novel zinc-binding motif revealed by solution structures of DNA-binding domains of Arabidopsis SBP-family transcription factors. *J. Mol. Biol.* **2004**, *337*, 49–63. [CrossRef] [PubMed]
9. Yamasaki, K.; Kigawa, T.; Inoue, M.; Yamasaki, T.; Yabuki, T.; Aoki, M.; Seki, E.; Matsuda, T.; Tomo, Y.; Terada, T.; et al. An Arabidopsis SBP-domain fragment with a disrupted C-terminal zinc-binding site retains its tertiary structure. *FEBS Lett.* **2006**, *580*, 2109–2116. [CrossRef]
10. Birkenbihl, R.P.; Jach, G.; Saedler, H.; Huijser, P. Functional dissection of the plant-specific SBP-domain: Overlap of the DNA-binding and nuclear localization domains. *J. Mol. Biol.* **2005**, *352*, 585–596. [CrossRef]
11. Cardon, G.; Höhmann, S.; Klein, J.; Nettesheim, K.; Saedler, H.; Huijser, P. Molecular characterisation of the Arabidopsis SBP-box genes. *Gene* **1999**, *237*, 91–104. [CrossRef]
12. Li, L.; Shi, F.; Wang, G.; Guan, Y.; Zhang, Y.; Chen, M.; Chang, J.; Yang, G.; He, G.; Wang, Y.; et al. Conservation and Divergence of *SQUAMOSA-PROMOTER BINDING PROTEIN-LIKE (SPL)* Gene Family between Wheat and Rice. *Int. J. Mol. Sci.* **2022**, *23*, 2099. [CrossRef]

13. De Paola, C.; Garcia-Carpintero, V.; Vazquez-Vilar, M.; Kaminski, K.; Fernandez-Del-Carmen, A.; Sierro, N.; Ivanov, N.V.; Giuliano, G.; Waterhouse, P.; Orzaez, D. Comparative analysis of the Squamosa Promoter Binding-Like (SPL) gene family in *Nicotiana benthamiana* and *Nicotiana tabacum*. *Plant Sci.* **2023**, *335*, 111797. [CrossRef] [PubMed]
14. Zeng, R.-F.; Zhou, J.-J.; Liu, S.-R.; Gan, Z.-M.; Zhang, J.-Z.; Hu, C.-G. Genome-Wide Identification and Characterization of SQUAMOSA—Promoter-Binding Protein (SBP) Genes Involved in the Flowering Development of *Citrus clementina*. *Biomolecules* **2019**, *9*, 66. [CrossRef]
15. Qin, S.-W.; Bao, L.-H.; He, Z.-G.; Li, C.-L.; La, H.-G.; Zhao, L.-F. Identification and regulatory network analysis of SPL family transcription factors in *Populus euphratica Oliv. heteromorphic* leaves. *Sci. Rep.* **2022**, *12*, 2856. [CrossRef]
16. He, A.; Zhou, H.; Ma, C.; Bai, Q.; Yang, H.; Yao, X.; Wu, W.; Xue, G.; Ruan, J. Genome-wide identification and expression analysis of the SPL gene family and its response to abiotic stress in barley (*Hordeum vulgare* L.). *BMC Genom.* **2024**, *25*, 1–18. [CrossRef]
17. Zhu, T.; Liu, Y.; Ma, L.; Wang, X.; Zhang, D.; Han, Y.; Ding, Q.; Ma, L. Genome-wide identification, phylogeny and expression analysis of the SPL gene family in wheat. *BMC Plant. Biol.* **2020**, *20*, 420. [CrossRef]
18. Yang, J.; Guo, Z.; Wang, W.; Cao, X.; Yang, X. Genome-Wide Characterization of SPL Gene Family in *Codonopsis pilosula* Reveals the Functions of CpSPL2 and CpSPL10 in Promoting the Accumulation of Secondary Metabolites and Growth of *C. pilosula* Hairy Root. *Genes* **2021**, *12*, 1588. [CrossRef] [PubMed]
19. Zhou, L.; Yarra, R. Genome-Wide Analysis of SPL/miR156 Module and Its Expression Analysis in Vegetative and Reproductive Organs of Oil Palm (*Elaeis guineensis*). *Int. J. Mol. Sci.* **2023**, *24*, 13658. [CrossRef] [PubMed]
20. Shaheen, T.; Rehman, A.; Abeed, A.H.A.; Waqas, M.; Aslam, A.; Azeem, F.; Qasim, M.; Afzal, M.; Azhar, M.F.; Attia, K.A.; et al. Identification and expression analysis of SBP-Box-like (SPL) gene family disclose their contribution to abiotic stress and flower budding in pigeon pea (*Cajanus cajan*). *Funct. Plant Biol.* **2024**, *51*, FP23237. [CrossRef]
21. Cui, L.; Zheng, F.; Wang, J.; Zhang, C.; Xiao, F.; Ye, J.; Li, C.; Ye, Z.; Zhang, J. miR156a-targeted SBP-Box transcription factor SlSPL13 regulates inflorescence morphogenesis by directly activating SFT in tomato. *Plant Biotechnol. J.* **2020**, *18*, 1670–1682. [CrossRef] [PubMed]
22. Li, Z.; Yang, Y.; Chen, B.; Xia, B.; Li, H.; Zhou, Y.; He, M. Genome-wide identification and expression analysis of *SBP-box* gene family reveal their involvement in hormone response and abiotic stresses in *Chrysanthemum nankingense*. *PeerJ* **2022**, *10*, e14241. [CrossRef]
23. Dong, H.; Yan, S.; Jing, Y.; Yang, R.; Zhang, Y.; Zhou, Y.; Zhu, Y.; Sun, J. MIR156-Targeted SPL9 Is Phosphorylated by SnRK2s and Interacts With ABI5 to Enhance ABA Responses in Arabidopsis. *Front. Plant Sci.* **2021**, *12*, 708573. [CrossRef]
24. Chao, L.M.; Liu, Y.Q.; Chen, D.Y.; Xue, X.Y.; Mao, Y.B.; Chen, X.Y. Arabidopsis Transcription Factors SPL1 and SPL12 Confer Plant Thermotolerance at Reproductive Stage. *Mol. Plant* **2017**, *10*, 735–748. [CrossRef] [PubMed]
25. Li, Y.; Han, S.; Sun, X.; Khan, N.U.; Zhong, Q.; Zhang, Z.; Zhang, H.; Ming, F.; Li, Z.; Li, J. Variations in OsSPL10 confer drought tolerance by directly regulating OsNAC2 expression and ROS production in rice. *J. Integr. Plant. Biol.* **2023**, *65*, 918–933. [CrossRef] [PubMed]
26. Lian, T.; Huang, Y.; Xie, X.; Huo, X.; Shahid, M.Q.; Tian, L.; Lan, T.; Jin, J. Rice SST Variation Shapes the Rhizosphere Bacterial Community, Conferring Tolerance to Salt Stress through Regulating Soil Metabolites. *mSystems* **2020**, *5*, e00721-20. [CrossRef] [PubMed]
27. Sun, X.; Lin, L.; Sui, N. Regulation mechanism of microRNA in plant response to abiotic stress and breeding. *Mol. Biol. Rep.* **2019**, *46*, 1447–1457. [CrossRef] [PubMed]
28. Wang, J.; Ye, Y.; Xu, M.; Feng, L.; Xu, L.-A. Roles of the SPL gene family and miR156 in the salt stress responses of tamarisk (*Tamarix chinensis*). *BMC Plant Biol.* **2019**, *19*, 19. [CrossRef]
29. Ma, Y.; Xue, H.; Zhang, F.; Jiang, Q.; Yang, S.; Yue, P.; Wang, F.; Zhang, Y.; Li, L.; He, P.; et al. The miR156/SPL module regulates apple salt stress tolerance by activating MdWRKY100 expression. *Plant Biotechnol. J.* **2021**, *19*, 311–323. [CrossRef]
30. Feng, S.; Liu, Z.; Cheng, J.; Li, Z.; Tian, L.; Liu, M.; Yang, T.; Liu, Y.; Liu, Y.; Dai, H.; et al. Zanthoxylum-specific whole genome duplication and recent activity of transposable elements in the highly repetitive paleotetraploid *Z. bungeanum* genome. *Hortic. Res.* **2021**, *8*, 205. [CrossRef]
31. Xue, G.; Wu, W.; Fan, Y.; Ma, C.; Xiong, R.; Bai, Q.; Yao, X.; Weng, W.; Cheng, J.; Ruan, J. Genome-wide identification, evolution, and role of SPL gene family in beet (*Beta vulgaris* L.) under cold stress. *BMC Genom.* **2024**, *25*, 101. [CrossRef]
32. He, B.; Gao, S.; Lu, H.; Yan, J.; Li, C.; Ma, M.; Wang, X.; Chen, X.; Zhan, Y.; Zeng, F. Genome-wide analysis and molecular dissection of the SPL gene family in *Fraxinus mandshurica*. *BMC Plant Biol.* **2022**, *22*, 451. [CrossRef]
33. Feng, X.; Zhou, B.; Wu, X.; Wu, H.; Zhang, S.; Jiang, Y.; Wang, Y.; Zhang, Y.; Cao, M.; Guo, B.; et al. Molecular characterization of SPL gene family during flower morphogenesis and regulation in blueberry. *BMC Plant Biol.* **2023**, *23*, 40. [CrossRef]
34. Li, L.; Xu, J.B.; Zhu, Z.W.; Ma, R.; Wu, X.Z.; Geng, Y.K. Genome-wide identification and expression analysis of the SPL transcription factor family and its response to abiotic stress in *Pisum sativum* L. *BMC Genom.* **2024**, *25*, 539. [CrossRef]
35. Wang, Y.; Ruan, Q.; Zhu, X.; Wang, B.; Wei, B.; Wei, X. Identification of Alfalfa SPL gene family and expression analysis under biotic and abiotic stresses. *Sci. Rep.* **2023**, *13*, 84. [CrossRef] [PubMed]

36. Cai, C.; Guo, W.; Zhang, B. Genome-wide identification and characterization of SPL transcription factor family and their evolution and expression profiling analysis in cotton. *Sci. Rep.* **2018**, *8*, 762. [CrossRef] [PubMed]
37. Demuth, J.P.; Hahn, M.W. The life and death of gene families. *BioEssays* **2009**, *31*, 29–39. [CrossRef]
38. Wang, M.; Mo, Z.; Lin, R.; Zhu, C. Characterization and expression analysis of the SPL gene family during floral development and abiotic stress in pecan (*Carya illinoinensis*). *PeerJ* **2021**, *9*, e12490. [CrossRef] [PubMed]
39. Singh, S.; Praveen, A.; Bhadrecha, P. Genome-wide identification and analysis of SPL gene family in chickpea (*Cicer arietinum* L.). *Protoplasma* **2024**, *261*, 799–818. [CrossRef]
40. Yao, W.; Li, C.; Fu, H.; Yang, M.; Wu, H.; Ding, Y.; Li, L.; Lin, S. Genome-Wide Analysis of SQUAMOSA-Promoter-Binding Protein-like Family in Flowering *Pleioblastus pygmaeus*. *Int. J. Mol. Sci.* **2022**, *23*, 14035. [CrossRef] [PubMed]
41. Roy, S.W.; Gilbert, W. Complex early genes. *Proc. Natl. Acad. Sci. USA* **2005**, *102*, 1986–1991. [CrossRef] [PubMed]
42. Roy, S.W.; Gilbert, W. Rates of intron loss and gain: Implications for early eukaryotic evolution. *Proc. Natl. Acad. Sci. USA* **2005**, *102*, 5773–5778. [CrossRef]
43. Roy, S.W. Intron-rich ancestors. *Trends Genet.* **2006**, *22*, 468–471. [CrossRef]
44. Roy, S.W.; Penny, D. Patterns of intron loss and gain in plants: Intron loss-dominated evolution and genome-wide comparison of *O. sativa* and *A. thaliana*. *Mol. Biol. Evol.* **2007**, *24*, 171–181. [CrossRef]
45. Volokita, M.; Rosilio-Brami, T.; Rivkin, N.; Zik, M. Combining comparative sequence and genomic data to ascertain phylogenetic relationships and explore the evolution of the large GDSL-lipase family in land plants. *Mol. Biol. Evol.* **2011**, *28*, 551–565. [CrossRef]
46. Kumar, A.; Balbach, J. Folding and Stability of Ankyrin Repeats Control Biological Protein Function. *Biomolecules* **2021**, *11*, 840. [CrossRef]
47. Corchete, L.A.; Rojas, E.A.; Alonso-López, D.; Rivas, J.D.L.; Gutiérrez, N.C.; Burguillo, F.J. Systematic comparison and assessment of RNA-seq procedures for gene expression quantitative analysis. *Sci. Rep.* **2020**, *10*, 19737. [CrossRef]
48. Yi, S.; Lu, H.; Tian, C.; Xu, T.; Song, C.; Wang, W.; Wei, P.; Gu, F.; Liu, D.; Cai, Y.; et al. Selection of Suitable Reference Genes for Gene Expression Normalization Studies in *Dendrobium huoshanense*. *Genes* **2022**, *13*, 1486. [CrossRef]
49. Gour, P.; Kansal, S.; Agarwal, P.; Mishra, B.S.; Sharma, D.; Mathur, S.; Raghuvanshi, S. Variety-specific transcript accumulation during reproductive stage in drought-stressed rice. *Physiol. Plant.* **2021**, *174*, e13585. [CrossRef] [PubMed]
50. Costa, V.; Angelini, C.; De Feis, I.; Ciccodicola, A. Uncovering the Complexity of Transcriptomes with RNA-Seq. *J. Biomed. Biotechnol.* **2010**, *2010*, 1–19. [CrossRef]
51. Berry, H.M.; Argueso, C.T. More than growth: Phytohormone-regulated transcription factors controlling plant immunity, plant development and plant architecture. *Curr. Opin. Plant Biol.* **2022**, *70*, 102309. [CrossRef]
52. Zhang, T.; Wu, A.; Yue, Y.; Zhao, Y. uORFs: Important Cis-Regulatory Elements in Plants. *Int. J. Mol. Sci.* **2020**, *21*, 6238. [CrossRef]
53. Jeyakumar, J.M.J.; Ali, A.; Wang, W.-M.; Thiruvengadam, M. Characterizing the Role of the miR156-SPL Network in Plant Development and Stress Response. *Plants* **2020**, *9*, 1206. [CrossRef] [PubMed]
54. Yuan, J.; Wang, X.; Qu, S.; Shen, T.; Li, M.; Zhu, L. The roles of miR156 in abiotic and biotic stresses in plants. *Plant Physiol. Biochem.* **2023**, *204*, 108150. [CrossRef]
55. Zhao, J.; Shi, M.; Yu, J.; Guo, C. SPL9 mediates freezing tolerance by directly regulating the expression of CBF2 in *Arabidopsis thaliana*. *BMC Plant Biol.* **2022**, *22*, 59. [CrossRef]
56. Arshad, M.; Feyissa, B.A.; Amyot, L.; Aung, B.; Hannoufa, A. MicroRNA156 improves drought stress tolerance in alfalfa (*Medicago sativa*) by silencing SPL13. *Plant Sci.* **2017**, *258*, 122–136. [CrossRef]
57. Zhang, H.; Jia, S.; Zhang, M.; Wang, K.; Teng, F.; Liu, Y.; Zhang, W. Deciphering the regulatory network of miR156 in plant architecture and abiotic stress resistance of alfalfa (*Medicago sativa*) by transcriptome sequencing. *Ind. Crops Prod.* **2022**, *189*, 115828. [CrossRef]
58. Chen, C.; Chen, H.; Zhang, Y.; Thomas, H.R.; Frank, M.H.; He, Y.; Xia, R. TBtools: An Integrative Toolkit Developed for Interactive Analyses of Big Biological Data. *Mol. Plant.* **2020**, *13*, 1194–1202. [CrossRef]
59. Kumar, S.; Stecher, G.; Tamura, K. MEGA7: Molecular Evolutionary Genetics Analysis Version 7.0 for Bigger Datasets. *Mol. Biol. Evol.* **2016**, *33*, 1870–1874. [CrossRef] [PubMed]
60. Mengarelli, D.A.; Zanor, M.I. Genome-wide characterization and analysis of the CCT motif family genes in soybean (*Glycine max*). *Planta* **2021**, *253*, 15. [CrossRef]
61. Goldberg, D.H.; Victor, J.D.; Gardner, E.P.; Gardner, D. Spike train analysis toolkit: Enabling wider application of information-theoretic techniques to neurophysiology. *Neuroinformatics* **2009**, *7*, 165–178. [CrossRef] [PubMed]
62. Kroll, K.W.; Mokaram, N.E.; Pelletier, A.R.; Frankhouser, D.E.; Westphal, M.S.; Stump, P.A.; Stump, C.L.; Bundschuh, R.; Blachly, J.S.; Yan, P. Quality Control for RNA-Seq (QuaCRS): An Integrated Quality Control Pipeline. *Cancer Inform.* **2014**, *13*, 7–14. [CrossRef]
63. Bolger, A.M.; Lohse, M.; Usadel, B. Trimmomatic: A flexible trimmer for Illumina sequence data. *Bioinformatics* **2014**, *30*, 2114–2120. [CrossRef] [PubMed]

64. Kim, D.; Langmead, B.; Salzberg, S.L. HISAT: A fast spliced aligner with low memory requirements. *Nat. Methods* **2015**, *12*, 357–360. [CrossRef]
65. Pertea, M.; Pertea, G.M.; Antonescu, C.M.; Chang, T.C.; Mendell, J.T.; Salzberg, S.L. StringTie enables improved reconstruction of a transcriptome from RNA-seq reads. *Nat. Biotechnol.* **2015**, *33*, 290–295. [CrossRef]
66. Gao, W.; Nie, J.; Yao, J.; Wang, J.; Wang, S.; Zhang, X.; Liu, Y.; Liu, Y. Genomic survey and expression analysis of cellulose synthase superfamily and COBRA-like gene family in *Zanthoxylum bungeanum* stipule thorns. *Physiol. Mol. Biol. Plants* **2024**, *30*, 369–382. [CrossRef]
67. Livak, K.J.; Schmittgen, T.D. Analysis of relative gene expression data using real-time quantitative PCR and the $2^{-\Delta\Delta CT}$ Method. *Methods* **2001**, *25*, 402–408. [CrossRef]

plants

MDPI

Article

Long-Term Salinity-Responsive Transcriptome in Advanced Breeding Lines of Tomato

Monther T. Sadder [1,*], Ahmad Abdelrahim Mohamed Ali [2,3], Abdullah A. Alsadon [2] and Mahmoud A. Wahb-Allah [4]

[1] Department of Horticulture and Crop Science, School of Agriculture, University of Jordan, Amman 11942, Jordan
[2] Department of Plant Production, College of Food and Agricultural Sciences, King Saud University, P.O. Box 2460, Riyadh 11451, Saudi Arabia; abdelrahima@estidamah.gov.sa (A.A.M.A.); alsadon@ksu.edu.sa (A.A.A.)
[3] The National Research and Development Center for Sustainable Agriculture, Riyadh Technology Valley, King Saud University, P.O. Box 2460, Riyadh 11451, Saudi Arabia
[4] Vegetable Crops Department, Faculty of Agriculture, Alexandria University, Alexandria 21545, Egypt; abady625@hotmail.com
* Correspondence: sadderm@ju.edu.jo; Tel.: +962-6-535-5000

Abstract: Soil salinity and the scarcity of freshwater resources are two of the most common environmental constraints that negatively affect plant growth and productivity worldwide. The tomato (*Solanum lycopersicum* Mill.) plant is moderately sensitive to salinity. The identification of salinity-responsive genes in tomato that control long-term salt tolerance could provide important guidelines for its breeding programs and genetic engineering. In this study, a holistic approach of RNA sequencing combined with measurements of physiological and agronomic traits were applied in two advanced tomato breeding lines (susceptible L46 and tolerant L56) under long-term salinity stress (9.6 dS m^{-1}). Genotype L56 showed the up-regulation of known and novel differentially expressed genes (DEGs) that aid in the salinity tolerance, which was supported by a high salt tolerance index (81%). Genotype L46 showed both similar and different gene families of DEGs. For example, 22 paralogs of *CBL-interacting kinase* genes were more up-regulated in L56 than in L45. In addition, L56 deployed more *SALT OVERLY SENSITIVE* paralogs than L45. However, both genotypes showed the up-regulation of ROS-detoxifying enzymes and ROS-scavenging proteins under salinity stress. Therefore, L56 was more effective in conveying the stress message downstream along all available regulatory pathways. The salt-tolerant genotype L56 is genetically robust, as it shows an enhanced expression of a complete network of salt-responsive genes in response to saline conditions. In contrast, the salt-susceptible genotype L46 shows some potential genetic background. Both genotypes have great potential in future breeding programs.

Keywords: *Solanum lycopersicum* L.; salinity stress; RNA sequencing; gene expression

1. Introduction

The most recent assessment report covering salinity was issued by the FAO [1]. Around 1.4 billion hectares (10.7%) of total global land area are affected by salinity, with an additional 1 billion hectares at risk due to the climate change and human mismanagement [1]. Salinity limits crop development and production [2]. One of the major affected crops is tomato (*Solanum lycopersicum* L.), which is a member of the Solanaceae family and is an annual horticultural crop with a wide distribution and high nutritional and economical

value [3–5]. As cultivated tomato is moderately sensitive to salinity, all developmental stages are negatively affected [6–8].

Rapid fluctuation (up- and down-regulation) in stress-responsive genes is well established for several plant species including tomatoes [9]. The products of these genes cause signal transductions that lead to biochemical, physiological, and morphological changes involved in the final adaptation [9–11]. The transcriptome profiling of important regulatory genes is emerging as an important tool to improve plant response to abiotic stresses [12]. These genes include transcription factors, stress sensors or protein kinases that regulate the expression of several target genes for osmolyte biosynthesis enzymes, antioxidant enzymes, and stress proteins such as late embryogenesis abundant (LEA) proteins [13,14]. For the identification of differentially expressed genes, many advanced molecular biology techniques have been used to measure gene expression levels and discover new genes that are responsible for plant responses to different environmental stresses, such as quantitative real-time PCR (qPCR) [7,9] and transcriptome profiling using RNA sequencing [15].

Under abiotic stress, the signal perception of osmotic stress starts earlier than ionic stress, and the plant activates the signal transduction pathways by the generation of secondary messengers such as hormones, inositol, reactive oxygen species (ROS) and early responsive to dehydration (ERD) genes [2,16]. These molecules can stimulate signaling pathways such as the Ca^{2+}-dependent salt overly sensitive (SOS) pathway and osmotic/oxidative stress signaling [6,8,15]. Under stress conditions, plant respiratory metabolism increases. Cytochrome c oxidase appears to play an active role in the electron transfer pathway during respiration within the mitochondria to produce a large amount of free energy (ATP) [17].

Recent studies have reported that calcium-dependent protein kinase (CDPK) is a part of the physiological plant defense mechanisms against biotic or abiotic attacks [18]. One of the most important transcription factors for abiotic stress responses in plant are ethylene-responsive factors (ERFs) [19]. The ERF gene family is part of the AP2/ERF superfamily. The AP2/ERF domain plays a major role in the gene expression regulation of other stress-responsive genes because it is highly conserved and binds to the GCC box present in the promoter region of stress-responsive genes [20]. Myloblastosis (MYB) [9] and (WRKY) [14] transcription factors are major factors in regulating plant metabolism and responses to abiotic stresses. The NAC domain (NAM, ATAF1 and 2, and CUC2) proteins are plant-specific transcription factors that have crucial roles in plant development and abiotic stress responses [9,21]. The plant cellular genome is adversely affected by oxidative, salt, and drought stresses and plants require the activation of the DNA repairing system.

The aim of the current study was to compare contrasting advanced breeding lines of tomato under long-term salinity stress (55 days), which has not been studied in previous articles. It is proposed that novel differentially expressed genes would be resolved between the two genotypes, which would generate applicable resources for future plant breeding.

2. Results

2.1. Agronomic Traits

A total of 19 important agronomically traits in tomato were assessed for two genotypes, L46 (salt-susceptible) and L56 (salt-tolerant). They cover vegetative growth traits (5), yield component traits (3), chemical traits (4), physiological traits (2) and fruit quality traits (4). The obtained data are hierarchically clustered and are illustrated as a heat map (Figure 1). Five major clusters of agronomic traits were visible. The first one clustered plant health, stem diameter, leaf area, leaf fresh and dry weights, indicating their tight correlation. The values of these traits gradually declined with an increasing salinity stress level in the susceptible genotype L46. On the contrary, the tolerant genotype L56 barely showed any

decline with increasing salinity stress levels. The second group clustered leaf K^+ and fruit ascorbic acid levels, where L56 showed a slight decline in the leaf K^+ level at the highest salinity stress level (9.6 dS m^{-1}), while L46 showed a decline in leaf dry weight with increasing salinity stress levels. Moreover, ascorbic acid levels showed a decline with increasing salinity levels in both genotypes. The third cluster included fruit fresh weight, average fruit weight, total yield and WUE, all of which were negatively affected with increasing salinity stress levels; however, this effect was more dramatic in the L46 genotype than in the L56 genotype. The reduction in total yield was a consequence of reduced fruit weight. Cluster IV had four traits, fruit number per plant, fruit pH, fruit TSS and leaf Ca^{2+}, which were the least affected by salinity stress treatments. Cluster V included leaf proline, Na^+ and Cl^- levels. Both Na^+ and Cl^- levels were the most influenced by increasing salinity stress levels, showing a directly proportional relationship with increasing salinity stress levels and for both genotypes. On the other hand, leaf proline content was slightly decreased in the L56 genotype, while it was elevated in the L46 genotype. The K^+/Na^+ ratio did not cluster with any other trait and was the most negatively affected with increasing salinity stress levels, showing an inversely proportional relationship in both genotypes.

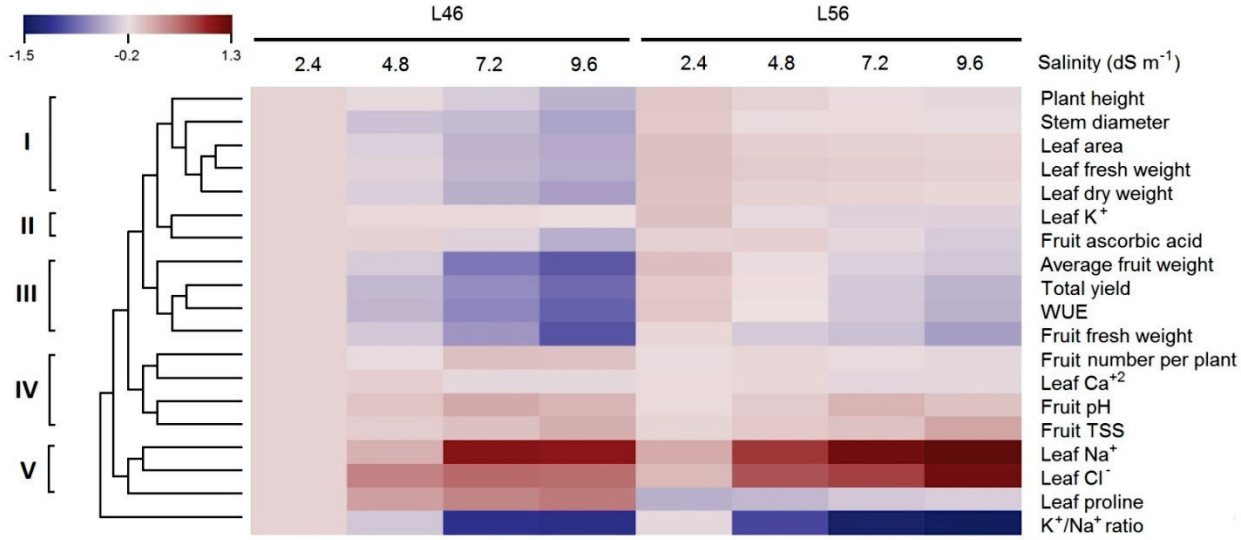

Figure 1. Hierarchical clustering and heat map of measured traits in susceptible (L46) and tolerant (L56) genotypes under four salinity stress levels (2.4, 4.8, 7.2 and 9.6 dS m^{-1}). Each row represents a trait and each column represents a genotype under different stress levels. Five major clusters are evident (each with distinctive traits that differentiate them from other clusters).

As a major index for plant response to salt stress, the salt tolerance trait index (STTI) was calculated for a group of nine major agronomic traits (Figure 2). At the 2.4 dS m^{-1} salinity stress level (the lowest level), both genotypes L46 and L56 were barely affected, showing relatively high STTI values (93–100%). At the second stress level (4.8 dS m^{-1}), the L46 genotype showed a drastic drop in the STTI for the investigated traits (74–86%), while the L56 genotype was still showing high STTI levels (82–95%). At the third salinity stress level (7.2 dS m^{-1}), severe plant damage was visible in the L46 genotype, with low STTI levels (56–80%). On the other hand, the L56 genotype showed two trends in STTI values, where plant growth parameters (plant height, stem diameter, leaf area, leaf fresh and dry weights) were marginally affected, with relatively high STTI levels (90–95%), while yield traits (fruit flesh thickness, average fruit weight and total yield) besides WUE were more negatively affected, with moderate STTI levels (79–82%). At the highest stress level (9.6 dS m^{-1}), agronomic traits in L56 genotype showed two trends that were similar to the trends it showed at a lower stress level (7.2 dS m^{-1}), with plant growth parameters

showing higher STTI levels (85–93%) than yield traits and WUE (70–76%). Likewise, two major trends were clear for the L46 genotype at the highest salinity stress level (9.6 dS m^{-1}), where plant growth parameters were strongly affected, with around 70–73% STTI levels, while yield traits and WUE were more strongly affected, with down to 50–54% STTI levels. The combined salt tolerance index (STI) revealed a huge significant difference between the L46 and L56 genotypes, with 61% and 82% STI values, respectively.

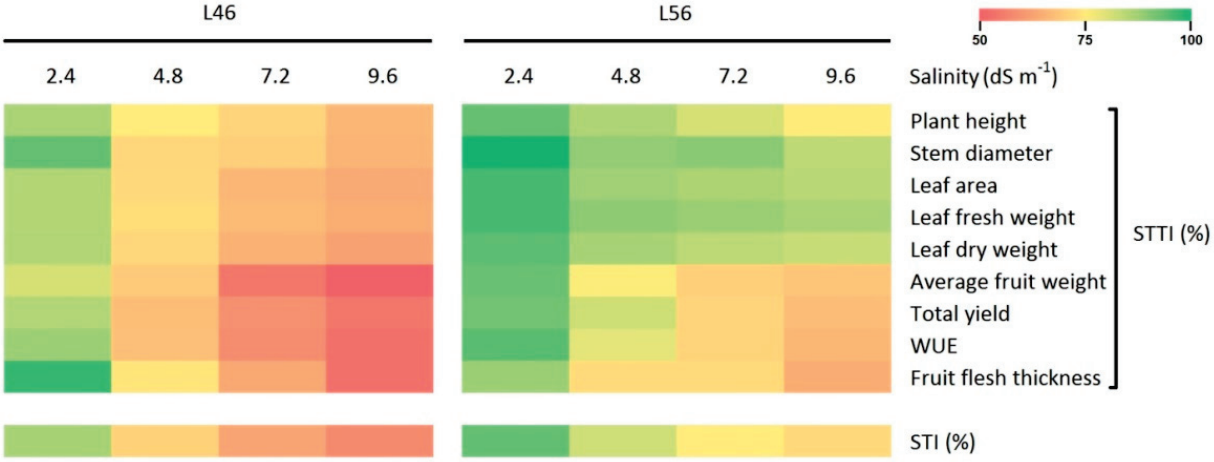

Figure 2. Heat map of salt tolerance trait index (STTI) for major agronomic traits in susceptible (L46) and tolerant (L56) genotypes under four salinity stress levels (2.4, 4.8, 7.2 and 9.6 dS m^{-1}). The combined salt tolerance index (STI) for all traits is presented at the bottom of the figure. See Section 4.2 for STTI and STI calculations.

2.2. RNA Sequencing and Transcriptome Data Analysis

The aim of this part of the study was to investigate transcriptome changes in two tomato genotypes, L46 (salt-susceptible) and L56 (salt-tolerant), in response to salt stress. The cDNA libraries were synthesized for both tomato genotypes under the control (_c)/non-saline (0.5 dS m^{-1}) condition and under the stress (_s)/salinity (9.6 dS m^{-1}) condition. The delivered average data (three replicates) were around 4, 1.6, 2.3 and 5.4 million reads for L46_c, L46_s, L56_c and L56_s, respectively. Illumina reads passed quality filtering, with around 5% of the total reads trimmed at the 92 bp read length; the percentage of ambiguous nucleotides was less than 1%, which confirmed the accuracy of the sequencing. The PCA of all four samples revealed adequate proximity for all biological replicates in each sample (Supplementary Figure S1).

The analysis of differentially expressed genes (DEGs) is an invaluable method to identify genes that may be responsible for salinity tolerance in the tomato L56 genotype. Therefore, DEGs were identified from the transcriptome data, with a p value ≤ 0.05 (Figure 3).

In the case of the L46_s vs. L46_c pair comparison, a total of 5732 DEGs were identified; 5228 with up-regulated expression and 504 with down-regulated expression (Figure 3A). However, with a threshold of Log2FC ≥ 2, only 1995 DEGs were resolved; 1781 with up-regulated expression and 214 with down-regulated expression (Figure 3B). On the other hand, in the L56_s vs. L56_c pair comparison, a total of 6186 DEGs were identified; 5544 with up-regulated expression and 642 with down-regulated expression (Figure 3C), while with a threshold of Log2FC ≥ 2, only 2475 transcripts showed significant changes (2255 up-regulated and 220 with down-regulated genes) (Figure 3D).

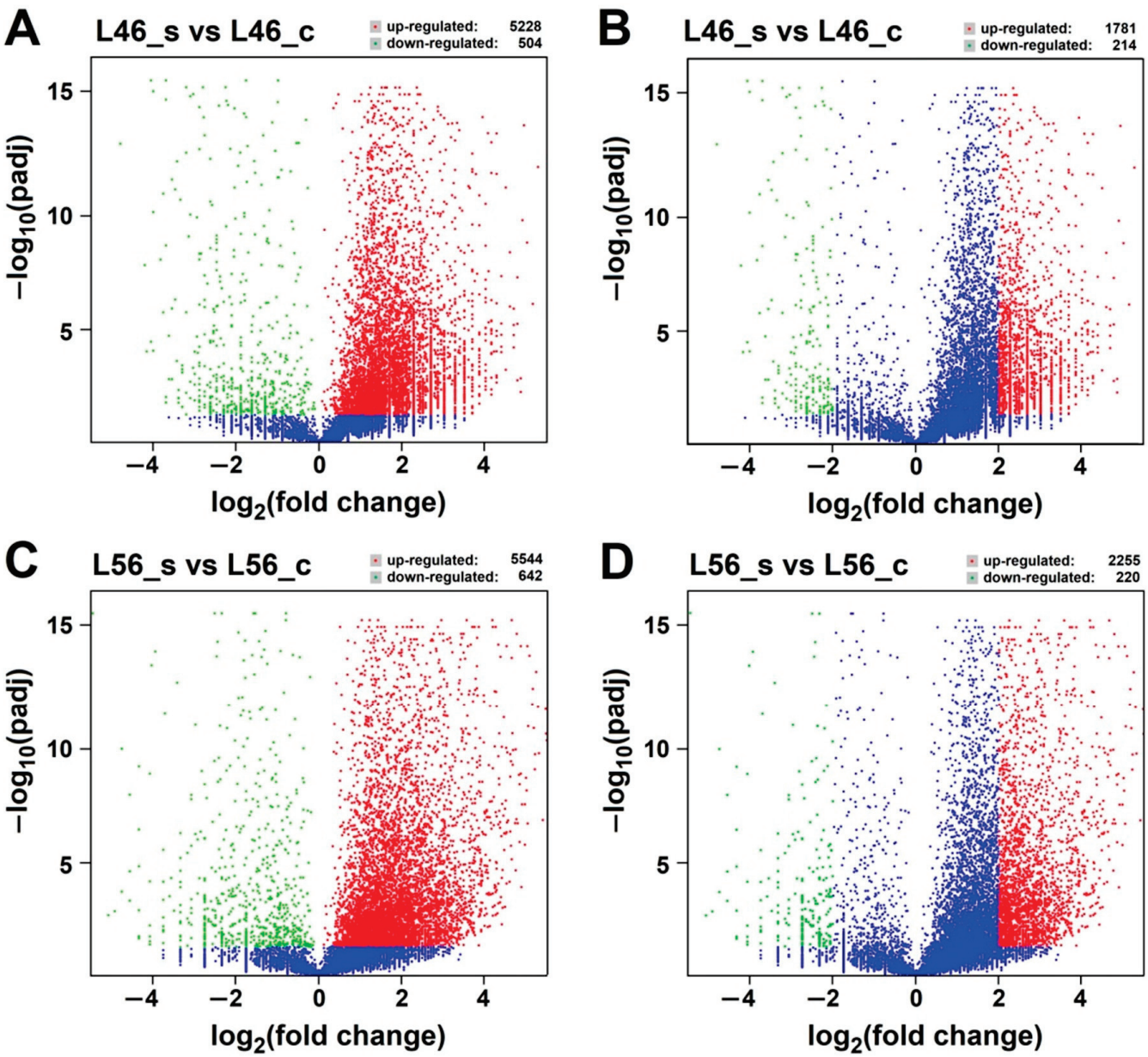

Figure 3. Global analysis of differentially expressed genes (DEGs). (**A**) Volcano plot of all DEGs for L46_s (stress) and L46_c (control) in transcriptome. (**B**) Volcano plot of DEGs (fold change $\geq$ 2) for L46_s (stress) and L46_c (control). (**C**) Volcano plot of all DEGs for L56_s (stress) and L56_c (control) in transcriptome. (**D**) Volcano plot of DEGs (fold change $\geq$ 2) for L56_s (stress) and L56_c (control). The abscissa shows the fold change difference in the expression of genes in different comparison groups, and the vertical coordinates indicate the adjusted *p*-values for the differences in expression. Genes without significant differences (*p* value $\leq$ 0.05) are indicated by blue dots below the threshold value (1.3). The up-regulated genes are represented by red dots, and the down-regulated genes are represented by green dots.

A comprehensive group of Venn diagrams were compiled for all possible combinations of the L56 and L45 genotypes and at a cutoff of fold changes $\geq$ 2, 4, 6, 8 and 10 for up-regulated DEGs (Supplementary Figure S2). When L46_c was used as the baseline, L46_s showed an up-regulation of 1129, 465, 270, 91 and 52 unique DEGs with fold changes $\geq$ 2, 4, 6, 8 and 10, respectively. With the same baseline (L46_c), unique DEGs were also evident for L56_c at all fold levels. On the other hand, when L46_s was used as the baseline, L56_s showed an up-regulation of 3006, 972, 474, 278 and 181 unique DEGs with fold

changes $\geq$ 2, 4, 6, 8 and 10, respectively. Because L56 is more tolerant to salinity compared with L46, the salt-responsive genes of L56 that are also differentially expressed in the L56_s vs. L46_s comparison (Figure S1) are more likely to play roles in the salinity tolerance of L56. Finally, when L56_c was used as the baseline, L56_s showed an up-regulation of 2790, 1690, 1080, 735 and 459 unique DEGs with fold changes $\geq$ 2, 4, 6, 8, and 10, respectively. When using any control genotype (L46_c or L56_c) as a baseline, a large number of DEGs were found to be up-regulated in the overlap between the investigated combination; 1797 and 1196 overlapped genes when L46_c and L56_c were used as the baseline, respectively (Supplementary Figure S2).

Several thousand DEGs during salinity stress showed significant up-regulation or down-regulation (p-value < 0.01, fold change > 2 or <0.5). On the basis of similar kinetic patterns of expression, all DEGs were classified into a total of fifteen unique gene expression patterns (clusters) (Figure 4). Differentially expressed genes (DEGs) of the susceptible (L46) and tolerant (L56) genotypes under both control (_c) and stress (_s) conditions were used to reveal these 15 clusters. Each cluster was built from a large number of DEGs, ranging from 250 up to 1201 genes.

The gene expression patterns of cluster 1 (1192 DEGs), cluster 7 (488 DEGs), cluster 8 (566 DEGs) exhibit similar changes, where DEGs are up-regulated in L56 compared to L46 (under both control and salinity stress). The major difference between them is the fold change, which is minimal in cluster 1, moderate in cluster 7 and prominent in cluster 8 (Figure 4). On the contrary, cluster 5 (954 DEGs) shows the opposite pattern, where DEGs are up-regulated in L46 compared to L56 (under both control and salinity stress). Moreover, the gene expression patterns of cluster 2 (915 DEGs) and cluster 14 (533 DEGs) exhibit similar changes, where DEGs are up-regulated under salinity stress but with higher levels in the L56 genotype. Clustering DEGs in a similar pattern revealed major salinity-responsive genes, with a unique expression pattern in the tolerant genotype compared to the susceptible genotype. This was evident in cluster 3 (464 DEGs), cluster 11 (1201 DEGs), cluster 12 (317 DEGs) and cluster 15 (420 DEGs). Although the gene expression patterns exhibited diverse changes in these clusters, DEGs were largely up-regulated in the L56 genotype under salinity stress (Figure 4). On the contrary, both cluster 9 (394 DEGs) and cluster 13 (250 DEGs) showed the most down-regulated genes in the L56 genotype under salinity stress. On the other hand, cluster 6 (714 DEGs) showed highly expressed genes (up-regulated) with similar levels between both tolerant and susceptible genotypes.

A total of 22 *CBL-interacting kinase* genes were detected in the RNA-seq data. Their expression (FRKM calibration) were subjected to hierarchal clustering for L46_c, L56_c, L46_s and L46_s, and their expression levels are presented as a heat map (Figure 5). A major group of *CBL-interacting kinase* genes was up-regulated under salinity stress in both lines, with higher levels for some genes in the tolerant line (L56).

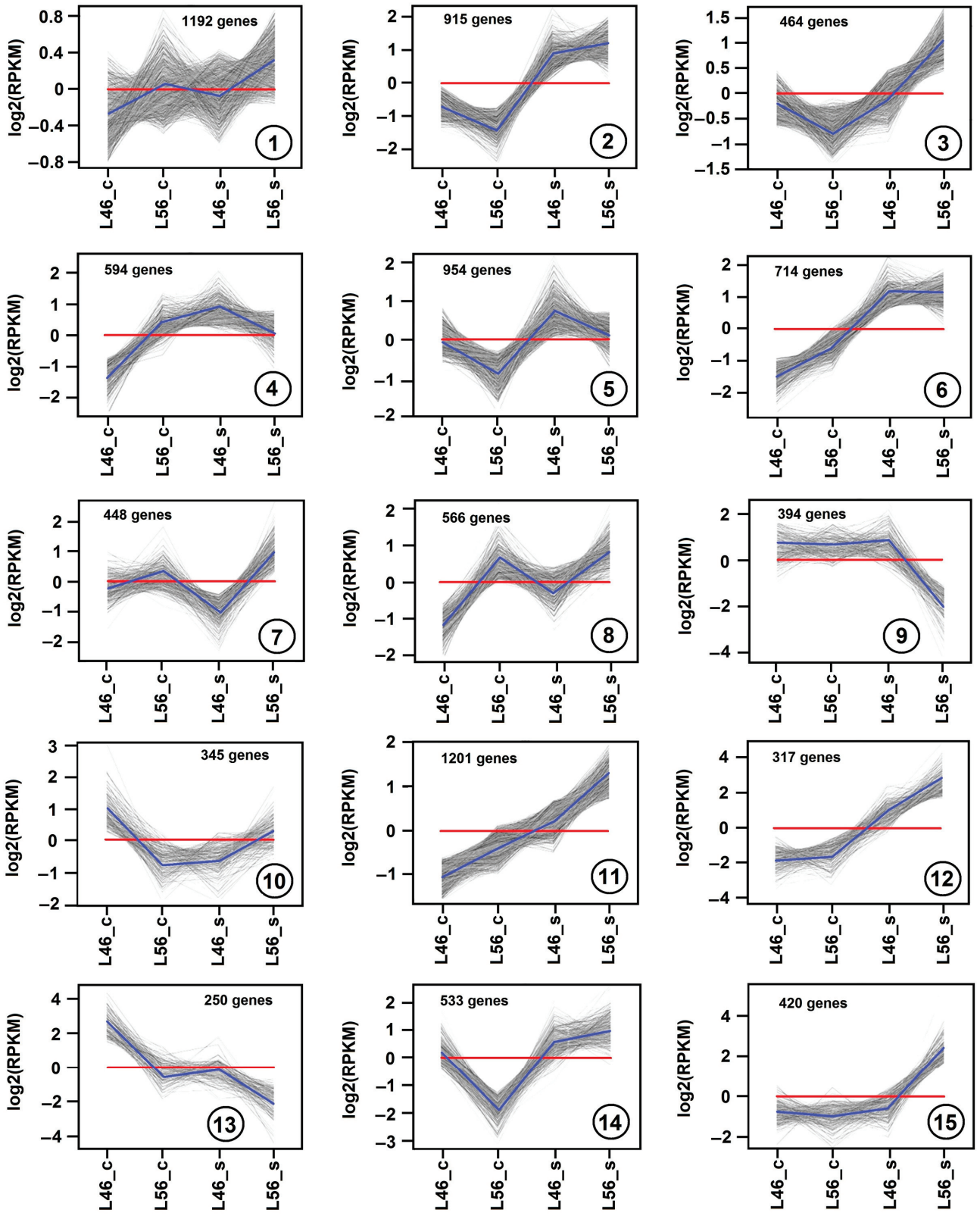

Figure 4. Gene expression patterns obtained by hierarchical clustering. Differentially expressed genes (DEGs) in tomato were categorized into 15 clusters (cluster number is depicted within a circle inside each panel). Gray lines show the relative expression levels of DEGs in the cluster in susceptible (L46) and tolerant (L56) genotypes under both control (_c) and stress (_s) conditions. Blue lines show the average values for each relative expression cluster. Red lines represent the baseline. Levels of gene expression were represented along the y axis as log2(RPKM), and genotypes were represented along the x axis.

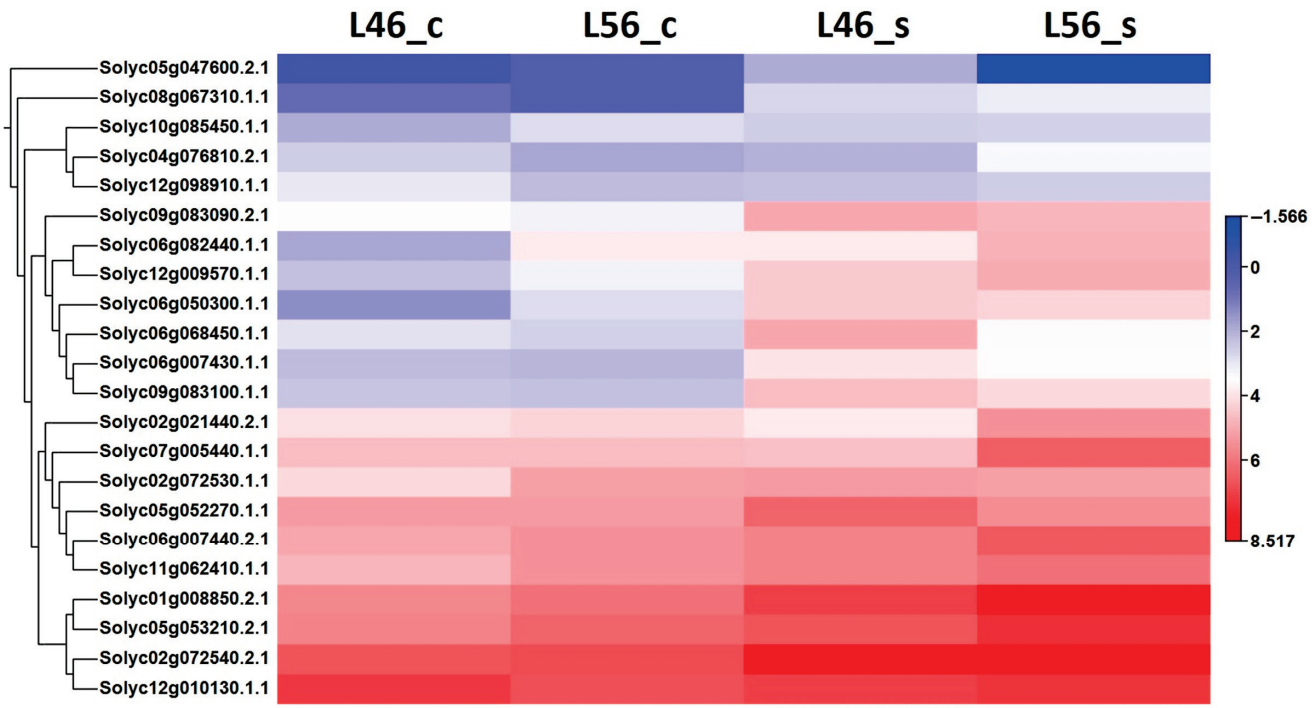

Figure 5. Hierarchical clustering of differentially expressed paralogs of *CBL-interacting kinases* of susceptible (L46) and tolerant (L56) genotypes under both control (_c) and stress (_s) conditions for all available stress-related genes in transcriptome.

3. Discussion

3.1. Agronomic Traits in Response to Salinity Stress

It is very important to point out the most responsive group of traits (cluster V) in response to elevated long-term salinity stress in tomatoes (Figure 1). Cluster V included leaf proline, Na^+ and Cl^- levels, which reflect major critical differences differentiating susceptible tomatoes from tolerant tomatoes. Nonetheless, the STTI was a very helpful index for plant response to salt stress (Figure 2), where you need to verify the tolerance with more clear phenotypic traits.

Most commercially available tomato cultivars are considered moderately sensitive to salinity stress. This was evident from norms of reaction for genotype L46 (susceptible compared to the tolerant genotype L56), placing it in the "moderately sensitive" division (Figure 6A,B). Tomato is classified as a glycophyte concerning response to salinity stress [7,9,22], which is mainly translated into osmolytes synthesis, e.g., proline [22] and sorbitol [23].

On the other hand, the L56 genotype (tolerant compared to the susceptible genotype L56) was placed in the "moderately tolerant" division (Figure 6A,C). This was true for both relative average fruit weight (Figure 6A) and total yield (Figure 6C), which reflects real reduction in crop production along elevated salinity levels. Salinity stress has a presumably less dramatic effect on relative leaf dry weight, which is an indirect contributor to crop production trait (Figure 6B).

Irrespective of classifications into glycophytes [5,23] or halophytes, relative crop production is the key feature to categorize any crop plant into a specific division in response to salinity stress [23,24]. Nonetheless, there are several agronomic traits that can be measured as a salinity stress index, which can be either directly (total yield) or indirectly (leaf dry weight) related to crop production.

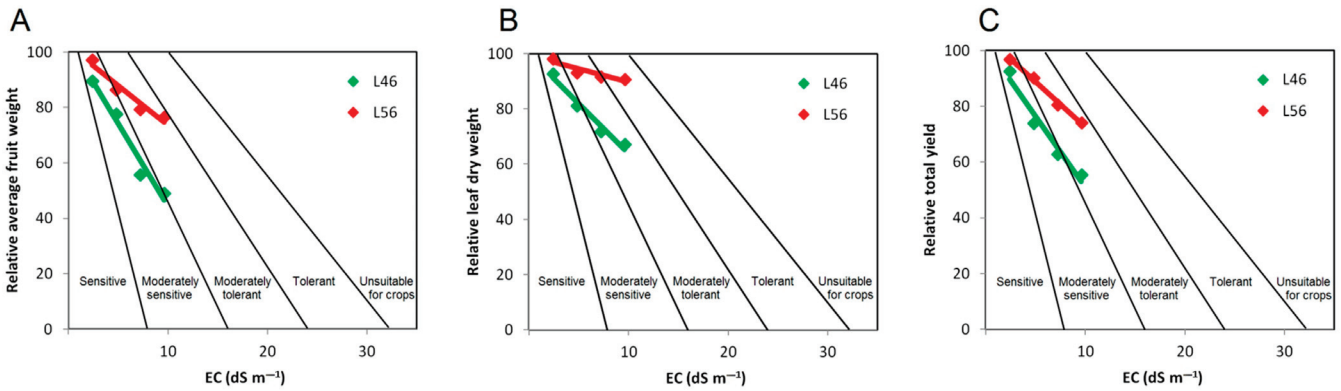

Figure 6. Norms of reaction for two tomato genotypes (L46 and L56) to different EC levels. Divisions represent plant salinity tolerance classes based on relative average fruit weight (**A**), leaf dry weight (**B**) and total yield (**C**) in comparison to control plants (modified from relative yield graph developed by [24]).

3.2. Differential Gene Expression

Recent research in understanding salinity tolerance in different tomato genotypes at the molecular level have focused on identifying key genes and regulatory pathways that boost plant resilience. Above threshold levels, salinity induces oxidative stress in tomatoes, leading to ion imbalance and causing tremendous damage at the biochemical level [25,26].

Several reports have highlighted the role of antioxidants in mitigatoxidative damage, e.g., superoxide dismutase (SOD), catalase (CAT), and ascorbate peroxidase (APX) [27–29]. However, such studies were carried out on short-term exposure to salinity stress compared to the presented long-term study. Interestingly, ascorbic acid levels that should increase under stress conditions declined with increasing salinity levels in both tolerant and susceptible tomato lines in this investigations (Figure 1). These findings agree with similar studies carried out on tomatoes under salinity stress [30–32]. Nonetheless, ROS-mitigating genes were found to be up-regulated under long-term salinity stress compared to the control (Figure 7), which present a couple of each of the major ROS-detoxifying enzymes and ROS-scavenging proteins (superoxide dismutases, catalases, ascorbate peroxidases, glutathione peroxidases, peroxiredoxins, thioredoxins and glutaredoxins).

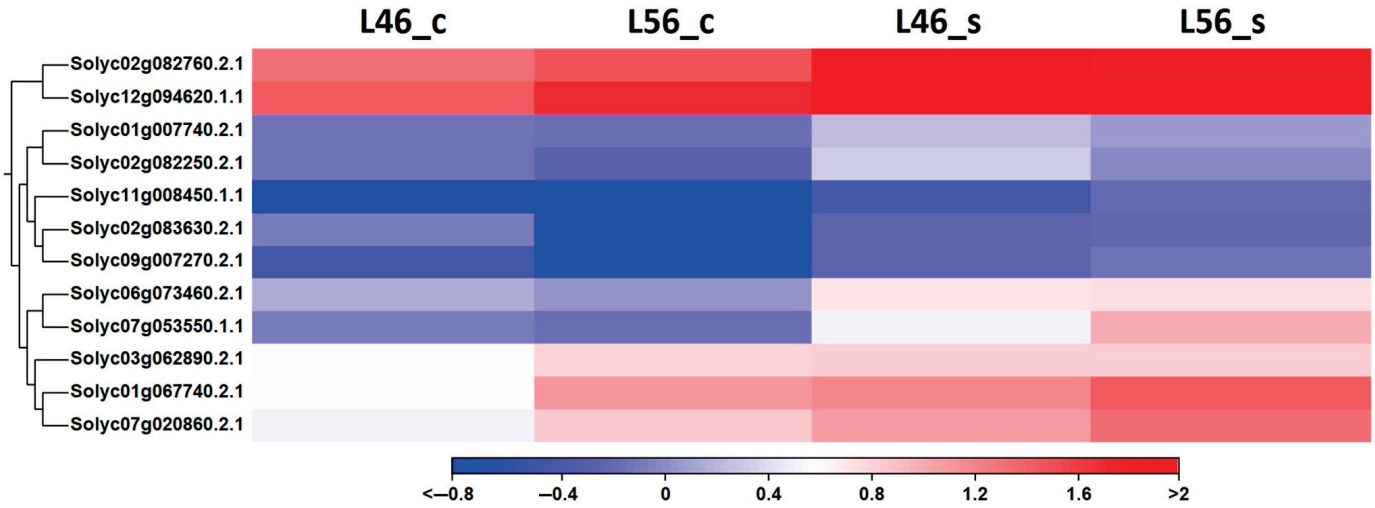

Figure 7. Hierarchical clustering of differentially expressed tomato ROS-detoxifying enzymes and ROS-scavenging proteins of susceptible (L46) and tolerant (L56) genotypes under both control (_c) and stress (_s) conditions for all available stress-related genes in transcriptome.

Moreover, neither the expression of transcription factors (e.g., *NAC* and *WRKY*) [9,33] nor ion homeostasis genes (e.g., *SOS*, *HKT1* and *NHX1*) [29] are enough to confer salinity tolerance for long-term stress exposure; even signaling pathways, e.g., cysteine-rich receptor-like protein kinases [34] or *CBL-interacting kinases* (this study), cannot, but rather, an array of collective genes and interactions from all levels are required as is shown in the comparative transcriptome analysis in this study. In fact, the top DEGs in the tolerant genotype L56 under salinity stress (Supplementary Table S2) reveal both compiled and compelled array of gene families known to mitigate salinity stress in tomatoes including transcription factors (*WRKY*, *MYB*, and *NAC*) and stress signaling pathways (*calmodulin*, *RLK*, and *S/T kinases*) [3–9].

This was clear in the presented long-term salinity study when salinity-related signaling pathways were investigated (Figure 5), where, for example, the *CBL-interacting kinase* genes were found to be up-regulated in L46 (susceptible genotype) as much as in L56 (tolerant genotype) or even more, e.g., Solyc06g068450.1.1 and Solyc05g052270.1.1. However, they were presumably not as effective as the downstream steps were missing a major link in the regulatory pathway.

Likewise, *SALT OVERLY SENSITIVE* (*SOS*) genes showed astonishing profiles comparing the two genotypes under both conditions (control vs. salinity) (Figure 8). None of the tomato *SOS* genes (for a full description, see Supplementary Table S1) were able to offer any decent variation between the two contrasting genotypes. This in turn supports the plausible variation between downstream processes resulting in a reduced damaging effect of salinity-imposed ions (comparing susceptible vs. tolerant genotypes). The tomato locus Solyc01g005020 encodes a Na^+/H^+ antiporter (*SlNHX* or *SOS1*), which is important in maintaining electrostatic balance via controlling ions (particularly Na^+) inside the cell (Figure 8). It can sequester excess sodium into vacuoles under salinity stress (Figure 1). Therefore, it keeps the cellular component undamaged and fully functional [35].

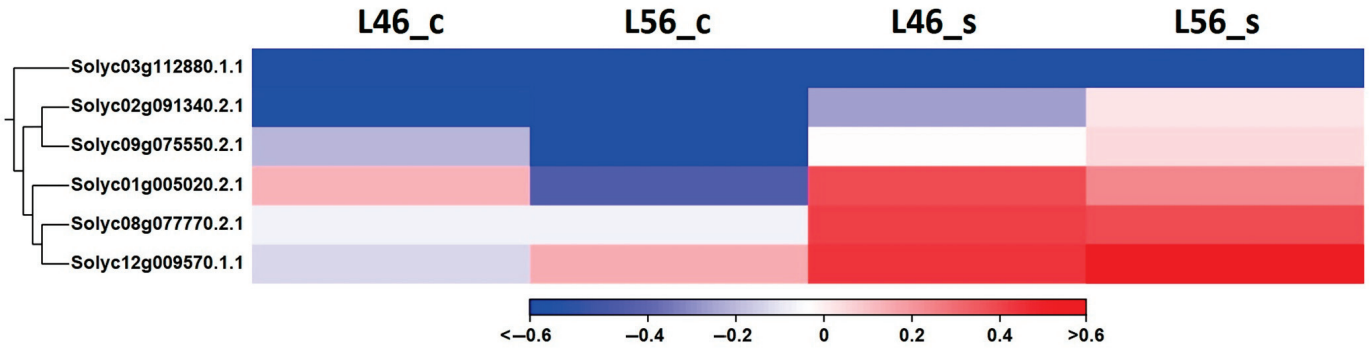

Figure 8. Hierarchical clustering of differentially expressed tomato paralogs for *SOS1-6* genes in susceptible (L46) and tolerant (L56) genotypes under both control (_c) and stress (_s) conditions for all available stress-related genes in transcriptome.

Transcriptome analysis, by RNA-Seq and gene expression estimation using qPCR techniques, has been successfully used to study transcriptome profiling in a wide range of plant species [8,9,11,12,36]. Expression patterns of salinity-responsive genes were investigated with qPCR for a group of tomato genes (Supplementary Figure S3). The fold increase in the expression level was compared to that revealed by the tomato RNA-Seq, which showed comparable trends in expression.

In general, gene expression patterns are not easy to detect in a particular transcriptome analysis. You can detect a few precise trends in Arabidopsis across seasons [37], but they are not well defined under salinity, e.g., in crayfish [38] or maize seedling roots [36]. However, we could distinguish an array of 15 different gene expression patterns from our

transcriptome data (Figure 4). This reveals the power of this analysis to detect major genes in a particular trend in the tolerant genotype.

4. Materials and Methods

4.1. Plant Material, Growth Conditions, and Salt Stress Treatment

Two tomato advanced breeding lines (salt-susceptible (L46) and salt-tolerant (L56)) were used in this study. These lines were produced through the tomato breeding program at the Vegetable Improvement Unit, the College of Food and Agricultural Sciences, King Saud University [4]. This study was conducted under greenhouse conditions at the Agricultural Research and Experiment Station in Dirab. The seeds of both genotypes were sown in JV7 Pellets (Jiffy Products International Bv, Zwijndrecht, Norway) under growth chamber conditions, with diurnal temperatures of 27 ± 1 °C (day) and 19 ± 1 °C (night). One-month-old seedlings were transplanted into soil in a fiberglass greenhouse. The soil used was non-saline (EC 2.0–2.8 dS m^{-1}), calcareous ($CaCO_3$ 25–30%), and sandy in texture, with pH 7.3–7.8. The air temperature in the greenhouse was set to approximately 26 ± 1 °C during the day and 20 ± 1 °C at night, and the relative humidity was maintained at 75 ± 2% for the entire growing season. Fertilization and other cultural practices were applied as recommended for commercial tomato production [39].

Salinity treatment comprised five water salinity levels of NaCl (0.5, 2.4, 4.8, 7.2 and 9.6 dS m^{-1}) applied through a drip irrigation system, where the control (0.5 dS m^{-1}) was irrigated with irrigation water without any addition of NaCl. These salinity levels were selected based on a previous study [3]. Salinity treatments were started 5 days after transplanting using water containers (1 m^3 each) connected to a surface drip irrigation network. Each container was filled with water at one of the salinity levels. The desired salinity level in irrigation water was developed by mixing appropriate amounts of NaCl according to the electric conductivity of the water source and the level of salt stress treatment [3].

The experiment was performed as a split plot in a completely randomized block design with three replications. Irrigation treatments were randomly allocated to the main plots, whereas genotypes were arranged in the sub-plots. The planting distance was 40 cm and 100 cm between plants and lines, respectively.

4.2. Agronomic Traits

Two months after transplanting (55 days of continuous stress treatment) (Supplementary Figure S4), random samples of three plants from each sub-plot (with three blocks, we had a total of 9 plants) were chosen to measure plant height, stem diameter and leaf area. Leaf samples were collected, washed in distilled water and dried at 70 °C in a forced-air oven until the weight became constant (48–72 h), and the dry matter contents were calculated.

Fruits were picked by hand at 2–4-day intervals. Total yield, average fruit weight (the total weight of all harvested fruits per plot divided by their number), fruit number per plant and fruit flesh thickness were recorded.

The dried leaf samples were ground and used to determine the leaf content of Na^+, Ca^{2+}, K^+, and Cl^-. An analysis for sodium (Na^+) and potassium (K^+) was carried out by flame atomic absorption using sulfuric acid/hydrogen peroxide-digested plant material [40]. Calcium (Ca^{2+}) analysis was carried out by atomic absorption spectroscopy (AAS) at 422.7 nm. A simple developed method for the effective extraction of Cl^- from plant tissue was used based on hot water extraction [41].

Water use efficiency (WUE) was calculated according to the following formula: WUE (kg m^{-3}) = Total fruit yield (kg ha^{-1})/applied water (m^3 ha^{-1}). Free proline was determined using the method of [42].

At harvest, fruit samples from both genotypes were collected, juiced, and filtered for measuring the fruit content of total soluble solid (TSS), ascorbic acid or vitamin C, and acidity [43]. The salt tolerance trait index (STTI) was calculated by dividing the value of traits under the stress condition by the value of traits under the controlled condition [44]. In addition, the salt tolerance index (STI) was calculated as the mean of STTIs.

4.3. RNA Isolation and cDNA Preparation

Two months after transplanting, plant leaf tissues from two genotypes (L46 and L56) at two levels were used; the control (c) with 0.5 dS m^{-1} and the highest salt stress treatment (s) with 9.6 dS m^{-1}. Three biological replicates were taken for each sample. Total RNA from tomato leaves was isolated using the RNeasy Plant Midi Kit (Qiagen, Hilden, Germany) according to the manufacturer's protocol. All materials were treated with RNase Away (RNase Away, Molecular Bio Products, San Diego, CA, USA) to avoid the degradation of RNA by RNase. The RNA (5 µg) was used for the subsequent preparation of cDNA for each sample using the SMARTer cDNA Synthesis kit (Clontech, San Jose, CA, USA). The reaction was performed in 0.2 mL nuclease-free PCR tubes (Axgen, Stanford, CA, USA) according to the manufacturer's instructions. The tubes were placed in a thermal cycler (Veriti 96-well; Applied Biosystems, Singapore) according to the manufacturer's protocol.

4.4. RNA Sequencing and Data Analysis of Transcriptome

The RNA sequencing was performed at Virginia Tech (Blacksburg, VA, USA). All samples were bar-coded using dedicated primer adapters (Illumina, San Diego, CA, USA). The amplified and coded libraries were run as single reads with 101 cycles in GAIIx (Illumina, San Diego, CA, USA). The RNA sequencing was analyzed using CLC Genomics Workbench v. 9.1. The RNA-seq analysis was performed in several steps: First, all reads of RNA sequencing and the reference cDNA with their annotation were imported into the program. The 92 bp reads were mapped with the reference tomato cDS with the mapping set as described; up to three mismatches were allowed. The minimum length of the fraction was 0.9, the minimum similarity fraction was 0.8, and the maximum number of hits for a read was 10. The expression levels based on the number of mapped reads for the L46 transcriptome under saline and control conditions (L46 S/C) were compared with each other as were those of the L56 transcriptome under saline and control conditions (L56 S/C). In addition, the expression levels of L56 and L46 transcriptomes under the saline condition were also compared (L56 S/L46 S). The majority of reads could be mapped uniquely to one location within the tomato reference (cDNA) sequence. To normalize for sequencing depth and gene length, reads per kilobase of exon model per million mapped reads (RPKM) were calculated. DEGs with a p-value ≤ 0.05 were selected. CLC Genomics Workbench (Version 9.5) uses Student's t-test as a statistical model to calculate the p-values for each DEG for two or more conditions. In addition, the software automatically adjusts the p-values using the Benjamani–Hochberg method to control the false discovery rate (FDR).

4.5. Primers Design

Genes that were highly expressed according to the transcriptome analysis were selected for confirmation using qPCR (Supplementary Table S3). The primer pairs for these genes were designed using Vector NTI 10 (Invitrogen, Carlsbad, CA, USA) and the Sol Genomics Network "https://solgenomics.net/organism/Solanum_lycopersicum/genome/" (accessed on 10 June 2024). The features were set into the program for primers designed as follows: primer length, 22–28 bp; Tm (°C), 58–60; GC %, 60; amplicon product length, 150–200 bp; and 3′ ends, CG.

4.6. Estimation of Gene Expression Level Using qPCR

To verify the expression level of the potential tomato salt-tolerant genes, qPCR was used. All RNA samples of both stressed and control plants were diluted to 10 ng ML^{-1} in nuclease-free water and subjected to first-strand cDNA synthesis using the GoScript Reverse transcription system (Promega, Madison, WI, USA). The cDNA was synthesized in repeat reactions to obtain a sufficient volume for qPCR. The reaction was performed in 0.2 mL nuclease-free PCR tubes (Axgen, Stanford, CA, USA) according to the manufacturer's instructions. The qPCR assays were performed in 96-well PCR plates (Applied Biosystem, Singapore) using the quantitative PCR master mix (Quantifast SYBR Green PCR Kit; Qiagen, Germany). All qPCR assays were performed in triplicate. The reaction conditions were as recommended by the manufacturer. Quantification was performed using the $2^{-\Delta\Delta CT}$ method [7], and the data were normalized for the quantity of actin transcripts.

5. Conclusions

The presented findings are critical for breeding novel long-term salinity-tolerant tomato varieties by deploying both traditional and molecular techniques. Continued explorations into detailed gene expression and downstream regulatory pathways are crucial for capturing the entirety of any tolerance regulatory network, either in tomato or any other crop. Such an approach could hold promise for mitigating the pronounced impact of salinity on global tomato crop production as climate change is striking each and every growing season around the world.

Supplementary Materials: The following supporting information can be downloaded at: https://www.mdpi.com/article/10.3390/plants14010100/s1, Table S1: SOS genes in tomato and orthologs in Arabidopsis. Table S2: Gene description and fold change for top 30 DEGs in L56 under salinity compared to control. Table S3: Sequence of primers for selected salt stress-responsive genes in tomato. Figure S1: PCA for the biological replicates of RNA-seq data in tomato susceptible (L46) and tolerant (L56) genotypes under control (_c) or under salinity stress (_s) conditions. Figure S2: Venn diagrams showing number of overlapping up-regulated genes expressed in tomato susceptible (L46) and tolerant (L56) genotypes under control (_c) or under salinity stress (_s) conditions. Figure S3: RNA-seq validation by quantitative real-time PCR (qRT-PCR). Figure S4: Water irrigation system and containers which were assigned to salinity levels.

Author Contributions: Conceptualization, M.T.S. and M.A.W.-A.; methodology, A.A.M.A.; software, M.T.S.; validation, A.A.A. and M.A.W.-A.; formal analysis, A.A.A.; investigation, M.A.W.-A.; resources, A.A.A.; data curation, M.T.S.; writing—original draft preparation, A.A.M.A. and M.A.W.-A.; writing—review and editing, M.T.S.; visualization, M.T.S.; supervision, A.A.A.; project administration, A.A.A.; funding acquisition, M.T.S. and A.A.A. All authors have read and agreed to the published version of the manuscript.

Funding: This research was funded by the National Plan for Science and Technology (Project number 10-BIO970-02), Saudi Arabia.

Data Availability Statement: RNA-seq data are available upon request. MTS AA AAA MAWA.

Acknowledgments: The authors are grateful to the University of Jordan and King Saud University for supporting this study.

Conflicts of Interest: The authors declare no conflicts of interest. The funders had no role in the design of the study; in the collection, analyses, or interpretation of data; in the writing of the manuscript; or in the decision to publish the results.

References

1. FAO. *Global Status of Salt-Affected Soils—Main Report*; FAO: Rome, Italy, 2024. [CrossRef]
2. Safdar, H.; Amin, A.; Shafiq, Y.; Ali, A.; Yasin, R.; Shoukat, A.; Hussan, M.U.I.; Sarwar, M.I. Impact of salinity on plant growth. *Nat. Sci.* **2019**, *17*, 34–40.
3. Alsadon, A.A.; Wahb-Allah, M.A.; Khalil, S.O. Evaluation of salinity tolerance of tomato cultivars, breeding lines and their hybrid combinations under greenhouse conditions. *Acta Hortic.* **2009**, *807*, 207–214. [CrossRef]
4. Liang, G.; Liu, J.; Zhang, J.; Guo, J. Effects of drought stress on photosynthetic and physiological parameters of tomato. *Am. Soc. Hortic. Sci.* **2020**, *145*, 12–17. [CrossRef]
5. Brake, M.; Al-Qadumii, L.; Hamasha, H.; Migdadi, H.; Awad, A.; Haddad, N.; Sadder, M.T. Development of SSR markers linked to stress responsive genes along tomato chromosome 3 (*Solanum lycopersicum* L.). *BioTech* **2022**, *11*, 34. [CrossRef] [PubMed]
6. Raja, S.; Shokat, S.; Azhar, F.M.; Azhar, M.T.; Khan, A.A. Screening of tomato (*Solanum lycopersicum* L.) genotypes at different salinity levels. *J. Plant Breed. Crop Sci.* **2012**, *4*, 94–100.
7. Alsadon, A.A.; Ibrahim, A.A.; Wahb-Allah, M.A.; Ali, A.A.M.; Sadder, M.T. Tomato under salinity stress: Correlation between growth and yield components and responsive genes. *Acta Hortic.* **2015**, *1081*, 111–119. [CrossRef]
8. Krishna, R.; Karkute, S.G.; Ansari, W.A.; Jaiswal, D.K.; Verma, J.P.; Singh, M. Transgenic tomatoes for abiotic stress tolerance: Status and way ahead. *3 Biotech* **2018**, *9*, 143. [CrossRef] [PubMed]
9. Sadder, M.T.; Alsadon, A.A.; Wahb-Allah, M.A. Transcriptomic analysis of tomato lines reveals putative stress-specific biomarkers. *Turk. J. Agric. For.* **2014**, *38*, 700–715. [CrossRef]
10. Roșca, M.; Mihalache, G.; Stoleru, V. Tomato responses to salinity stress: From morphological traits to genetic changes. *Front. Plant Sci.* **2023**, *14*, 1118383. [CrossRef] [PubMed]
11. Li, X.; Li, M.; Zhou, B.; Yang, Y.; Wei, Q.; Zhang, J. Transcriptome analysis provides insights into the stress response crosstalk in apple (*Malus* × *domestica*) subjected to drought, cold and high salinity. *Sci. Rep.* **2019**, *9*, 9071. [CrossRef]
12. Nagalakshmi, U.; Waern, K.; Snyder, M. RNA-Seq: A method for comprehensive transcriptome analysis. *Curr. Protoc. Mol. Biol.* **2010**, *89*, 4–11. [CrossRef]
13. Cao, J.; Li, X. Identification and phylogenetic analysis of late embryogenesis abundant proteins family in tomato (*Solanum lycopersicum*). *Planta* **2015**, *241*, 757–772. [CrossRef] [PubMed]
14. Evans, K.V.; Ransom, E.; Nayakoti, S.; Wilding, B.; Mohd Salleh, F.; Gržina, I.; Erber, L.; Tse, C.; Hill, C.; Polanski, K.; et al. Expression of the Arabidopsis redox-related LEA protein, SAG21 is regulated by ERF, NAC and WRKY transcription factors. *Sci. Rep.* **2024**, *14*, 7756. [CrossRef] [PubMed]
15. Bai, Y.; Kissoudis, C.; Yan, Z.; Visser, R.G.; van der Linden, G. Plant behaviour under combined stress: Tomato responses to combined salinity and pathogen stress. *Plant J.* **2018**, *93*, 781–793. [CrossRef] [PubMed]
16. Wu, G.; Tian, N.; She, F.; Cao, A.; Wu, W.; Zheng, S.; Yang, N. Characteristics analysis of Early Responsive to Dehydration genes in Arabidopsis thaliana (AtERD). *Plant Signal. Behav.* **2023**, *18*, 2105021. [CrossRef] [PubMed]
17. Zsigmond, L.; Rigó, G.; Szarka, A.; Székely, G.; Ötvös, K.; Darula, Z.; Szabados, L. *Arabidopsis* PPR40 connects abiotic stress responses to mitochondrial electron transport. *Plant Physiol.* **2008**, *146*, 1721–1737. [CrossRef] [PubMed]
18. Hu, Z.; Lv, X.; Xia, X.; Zhou, J.; Shi, K.; Yu, J.; Zhou, Y. Genome-wide identification and expression analysis of calcium-dependent protein kinase in tomato. *Front. Plant Sci.* **2016**, *7*, 469. [CrossRef]
19. Klay, I.; Gouia, S.; Liu, M.; Mila, I.; Khoudi, H.; Bernadac, A.; Bouzayen, M.; Pirrello, J. Ethylene response factors (ERF) are differentially regulated by different abiotic stress types in tomato plants. *Plant Sci.* **2018**, *274*, 137–145. [CrossRef]
20. Xie, Z.; Nolan, T.M.; Jiang, H.; Yin, Y. AP2/ERF transcription factor regulatory networks in hormone and abiotic stress responses in Arabidopsis. *Front Plant Sci.* **2019**, *10*, 228. [CrossRef] [PubMed]
21. Wang, L.; Hu, Z.; Zhu, M.; Zhu, Z.; Hu, J.; Qanmber, G.; Chen, G. The abiotic stress-responsive NAC transcription factor SlNAC11 is involved in drought and salt response in tomato (*Solanum lycopersicum* L.). *Plant Cell Tissue Organ. Cult.* **2017**, *129*, 161–174. [CrossRef]
22. Chen, N.; Shao, Q.; Lu, Q.; Li, X.; Gao, Y.; Xiao, Q. Research progress on function of NAC transcription factors in tomato (*Solanum lycopersicum* L.). *Euphytica* **2023**, *219*, 22. [CrossRef]
23. Sadder, M.T.; Alshomali, I.; Ateyyeh, H.; Musallam, A. Physiological and molecular responses of common fig (*Ficus carica* L.) to long term salinity stress. *Physiol. Mol. Biol. Plants* **2021**, *27*, 107–1173. [CrossRef] [PubMed]
24. Maas, E.V.; Hoffman, G.J. Crop salt tolerance–current assessment. *J. Irrig. Drain. Div.* **1977**, *103*, 115–134. [CrossRef]
25. Hasanuzzaman, M.; Raihan, M.R.H.; Masud, A.A.C.; Rahman, K.; Nowroz, F.; Rahman, M.; Nahar, K.; Fujita, M. Regulation of reactive oxygen species and antioxidant defense in plants under salinity. *Int. J. Mol. Sci.* **2021**, *22*(17), 9326. [CrossRef]
26. Choudhury, S.; Ali, S.; Sarker, M.R.; Islam, N. Salinity tolerance in tomato genotypes at an early plant growth stage: Morphological and physiological responses. *Trends Hortic.* **2023**, *6*, 3490. [CrossRef]

27. Xu, J.; Kang, Z.; Zhu, K.; Zhao, D.; Yuan, Y.; Yang, S.; Zhen, W.; Hu, X. RBOH1-dependent H_2O_2 mediates spermine-induced antioxidant enzyme system to enhance tomato seedling tolerance to salinity–alkalinity stress. *Plant Physiol. Biochem.* **2021**, *164*, 237–246. [CrossRef] [PubMed]
28. Alzahib, R.H.; Migdadi, H.M.; Al Ghamdi, A.A.; Alwahibi, M.S.; Ibrahim, A.A.; Al-Selwey, W.A. Assessment of morpho-physiological, biochemical and antioxidant responses of tomato landraces to salinity stress. *Plants* **2021**, *10*, 696. [CrossRef]
29. Sivakumar, J.; Sridhar Reddy, M.; Sergeant, K.; Hausman, J.F.; ShaValli Khan, P.S.; Osman Basha, P. Principal component analysis-assisted screening and selection of salt-tolerant tomato genotypes. *Plant Physiol. Rep.* **2023**, *28*, 272–288. [CrossRef]
30. Serio, F.; Gara, L.D.; Caretto, S.; Leo, L.; Santamaria, P. Influence of an increased NaCl concentration on yield and quality of cherry tomato grown in posidonia (*Posidonia oceanica* (L) Delile). *J. Sci. Food Agric.* **2004**, *84*, 1885–1890. [CrossRef]
31. Dorais, M.; Turcotte, G.; Papadopoulos, A.P.; Hao, X.; Gosselin, A. Control of tomato fruit quality and flavor by EC and water management. In *Agriculture and Agri-Food Canada Report*; Agriculture and Agri-Food Canada: Ottawa, ON, Cananda, 2000; pp. 18–21.
32. Abdelgawad, K.F.; El-Mogy, M.M.; Mohamed, M.I.A.; Garchery, C.; Stevens, R.G. Increasing ascorbic acid content and salinity tolerance of cherry tomato plants by suppressed expression of the ascorbate oxidase gene. *Agronomy* **2019**, *9*, 51. [CrossRef]
33. Ali, A.A.M.; Romdhane, W.B.; Tarroum, M.; Al-Dakhil, M.; Al-Doss, A.; Alsadon, A.A.; Hassairi, A. Analysis of salinity tolerance in tomato introgression lines based on morpho-physiological and molecular traits. *Plants* **2021**, *10*, 2594. [CrossRef] [PubMed]
34. Wang, Y.; Cao, X.; Zhang, D.; Li, Y.; Wang, Q.; Ma, F.; Xu, X.; Zhan, X.; Hu, T. SlGATA17, A tomato GATA protein, interacts with SlHY5 to modulate salinity tolerance and germination. *Environ. Exp. Bot.* **2023**, *206*, 105191. [CrossRef]
35. Liu, Y.; Feng, Z.; Zhu, W.; Liu, J.; Zhang, Y. Genome-wide identification and characterization of cysteine-rich receptor-like protein kinase genes in tomato and their expression profile in response to heat stress. *Diversity* **2021**, *13*, 258. [CrossRef]
36. Zhang, X.; Liu, P.; Qing, C.; Yang, C.; Shen, Y.; Ma, L. Comparative transcriptome analyses of maize seedling root responses to salt stress. *PeerJ* **2021**, *9*, e10765. [CrossRef]
37. Footitt, S.; Walley, P.G.; Lynn, J.R.; Hambidge, A.J.; Penfield, S.; Finch-Savage, W.E. Trait analysis reveals DOG1 determines initial depth of seed dormancy, but not changes during dormancy cycling that result in seedling emergence timing. *New Phytol.* **2020**, *225*, 2035–2047. [CrossRef] [PubMed]
38. Luo, L.; Yang, L.S.; Huang, J.H.; Jiang, S.G.; Zhou, F.L.; Li, Y.D.; Jiang, S.; Yang, Q.B. Effects of Different Salinity Stress on the Transcriptomic Responses of Freshwater Crayfish (*Procambarus clarkii*, Girard, 1852). *Biology* **2024**, *13*, 530. [CrossRef]
39. Maynard, D.N.; Hochmuth, G.J. *Knott's Handbook for Vegetable Growers*, 5th ed.; Gohn Wiley & Sons Inc.: Hoboken, NJ, USA, 2007.
40. Westerman, R.L.; Baird, J.V.; Christensen, N.W.; Fixen, P.E.; Whitney, D.A. *Soil Testing and Plant Analysis*, 3rd ed.; Soil Science Society of America: Madison, WA, USA, 1990.
41. Wheal, M.S.; Palmer, L.T. Chloride analysis of botanical samples by ICP-OES. *J. Anal. At. Spectrom.* **2010**, *25*, 1946–1952. [CrossRef]
42. Bates, L.S.; Waldren, R.P.; Teare, I.D. Rapid determination of free proline for water-stress studies. *Plant Soil* **1973**, *39*, 205–207. [CrossRef]
43. A.O.A.C. *Official Methods of Analysis*, 15th ed.; Association of Official Agricultural Chemists: Washington, DC, USA, 1992.
44. Ali, Z.; Salam, A.; Azhar, F.M.; Khan, I.A. Genotypic variation in salinity tolerance among spring and winter wheat (*Triticum aestivum* L.) accessions. *S. Afr. J. Bot.* **2007**, *73*, 70–75. [CrossRef]

plants

MDPI

Article

Identification of *ZmSNAC06*, a Maize NAC Family Transcription Factor with Multiple Transcripts Conferring Drought Tolerance in *Arabidopsis*

Fei Wang [1,†], Yong Chen [2,†], Ruisi Yang [1], Ping Luo [1], Houwen Wang [1], Runze Zhang [1], Wenzhe Li [1], Ke Yang [1], Xinlong Xu [1], Zhuanfang Hao [1,*] and Xinhai Li [1,*]

[1] State Key Laboratory of Crop Gene Resources and Breeding, Institute of Crop Sciences, Chinese Academy of Agricultural Sciences, Beijing 100081, China; wangfei19990908@163.com (F.W.); yangruisixj@163.com (R.Y.); luoping987@126.com (P.L.); whw15797929108@163.com (H.W.); zrz04222022@163.com (R.Z.); liwz16603632000@163.com (W.L.); yk864078904@163.com (K.Y.); xuxinlong0112@163.com (X.X.)

[2] College of Life Science, South China Agricultural University, Guangzhou 510642, China; chenyong9576@126.com

* Correspondence: haozhuanfang@163.com (Z.H.); lixinhai@caas.cn (X.L.)

† These authors contributed equally to this work.

Abstract: Drought is one of the most serious environmental stresses affecting crop production. NAC transcription factors play a crucial role in responding to various abiotic stresses in plants. Here, we identified a maize NAC transcription factor, *ZmSNAC06*, between drought-tolerant and drought-sensitive inbred lines through RNA-seq analysis and characterized its function in *Arabidopsis*. *ZmSNAC06* had five transcripts, of which *ZmSNAC06*-T02 had a typical NAC domain, while ZmSNAC06-P02 was localized in the nucleus of maize protoplasts and had transactivation activity in yeasts. The expression of *ZmSNAC06* in maize was induced by drought. The overexpression of *ZmSNAC06*-T02 in *Arabidopsis* resulted in hypersensitivity to abscisic acid (ABA) at the germination stage, and overexpression lines exhibited higher survival rates and higher antioxidant enzyme activities compared with the wild-type under drought stress. These results suggest that *ZmSNAC06* acts as a positive regulator in drought tolerance and may be used to improve drought tolerance in crops.

Keywords: maize (*Zea mays* L.); *ZmSNAC06*; transcription factor; drought tolerance

1. Introduction

Global climate change has caused a lot of uncertainty in crop growth; permanent or sudden drought often occurs in the main production areas of grain crops, which seriously decreases the agricultural output worldwide [1]. In response to drought stress, plants have developed a variety of adaptive strategies, including drought escape, drought avoidance and drought tolerance [2]. Drought tolerance is a complex trait that involves different tissues and metabolic pathways. In the regulatory network of the plant response to stress, transcription factors (TFs) activate or inhibit the expression of stress-related genes by binding to cis-acting promoter elements [3].

NAC (*NAM*, *ATAF1/2* and *CUC2*) is a plant-specific transcription factor (TF) family. Members of the NAC family have a highly conserved N-terminal NAC binding domain, which contains approximately 160 amino acids [4,5]. The NAC binding domain can be divided into five subdomains (A-E) [6]. Subdomain C belongs to DNA-binding regions [7], subdomain D belongs to the nuclear localization signal region and subdomain A belongs

to the oligomerization site region [8]. Subdomains B and E are relatively variable and may contribute to the function diversity of the NAC protein [9]. The highly variable C-terminal of the NAC protein is a transcriptional activation/repression region [10]. NAC TFs are involved in the regulation of plant growth and stress responses, and they are widely distributed in various plant genomes. Up to now, a large number of NAC genes have been identified in *Arabidopsis*, rice, tobacco, soybean, wheat and maize genomes [11–16].

Some members of the NAC family respond to drought stress based on different molecular mechanisms and have been identified and studied in *Arabidopsis*, rice, soybeans, wheat and maize. As a model plant, *Arabidopsis* has been extensively studied. *NAC016* was negatively involved in the drought stress response, and it inhibited ABA response element binding protein 1 (AREB1) to regulate the drought response in plants [17]. The overexpression of *SNAC3*, *OsNAC5* and *ONAC066* in rice improved drought tolerance and up-regulated the expression of stress-related genes [18–20]. *OsNAC2* was identified as combining the promoters of *OsLEA3* (encoding a group 3 late embryogenesis abundant protein) and *OsNCED3* (encoding rate-limiting enzymes in ABA biosynthesis) and positively regulated drought tolerance through an ABA-dependent signaling pathway in rice [21]. *OsNAC016* was phosphorylated by GSK3/SHAGGY-LIKE KINASE2 (GSK2) and OSMOTIC STRESS/ABA-ACTIVATED PROTEIN KINASE8 (SAPK8) to negatively regulate ABA-mediated drought tolerance pathways [22]. *SNAC1* activated the antioxidant system in rice and improved drought tolerance [23]. Compared with the wild-type soybean, the *GmNAC12* overexpression lines showed enhanced tolerance to drought, while *GmNAC12* knockout lines were sensitive to drought [24]. In wheat, *TaSNAC8-6A* with an ABRE motif (TACGTG) in the promoter could interact with TaABFs to enhance drought tolerance [25]; *TaNAC071-A* significantly enhanced drought tolerance by increasing the water use efficiency [26]. There are a large number of NAC genes in the maize genome, but there are few reports on the mechanism of drought tolerance. *ZmNAC55*, *ZmNAC33* and *ZmSNAC13* were identified to improve drought tolerance in transgenic *Arabidopsis* [27–29]; *ZmNAC49* inhibited the expression of *ZmMUTE* (a bHLH transcription factor) to reduce the stomatal density and improved drought tolerance in maize [30]. The insertion of miniature inverted repeat transposable elements (MITEs) in the promoter region of *ZmNAC111* was associated with drought tolerance in maize. The overexpression of *ZmNAC111* enhanced drought tolerance in transgenic *Arabidopsis* and maize seedlings [31]. *ZmNAC20* enhanced the drought tolerance of maize by promoting stomatal closure and activating the expression of stress-related genes [32].

The total production of maize in 2020 reached 1.163 billion tons, and it has become the crop with the highest production in the world [33]. Maize production requires sufficient water, especially in the flowering stage, but the availability of fresh water is predicted to decline by 50% in 2050 [34,35]. Thus, there is an urgent demand for improving maize drought tolerance. In this study, a transcription factor, *ZmSNAC06*, was identified through RNA-seq analysis between drought-tolerant (Tie7922 and X178) and drought-sensitive (Ji81162 and CA339) inbred lines. *ZmSNAC06*-T02 played an important regulatory role in the drought stress response, which provided information for the further study of its molecular mechanism.

2. Results

2.1. Transcriptome Analysis and Identification of ZmSNAC06 in Maize

In this study, the drought-tolerant inbred lines Tie7922 (heterotic group: BSSS group) and X178 (PB group) and drought-sensitive inbred lines CA339 (LRC group) and Ji81162 (BSSS group) were subjected to RNA-seq analysis [36]. We compared the transcriptome data of four inbred lines under well-watered and drought-stressed conditions. It was

found that under drought stress, 538 genes were identified as up-regulated and 1044 genes were down-regulated in Tie7922, and there were 2245 genes up-regulated and 1545 genes down-regulated in X178, while there were 1062 genes up-regulated and 280 genes down-regulated in CA339 and 1693 up-regulated genes and 1568 down-regulated genes in Ji81162 (Figure 1a).

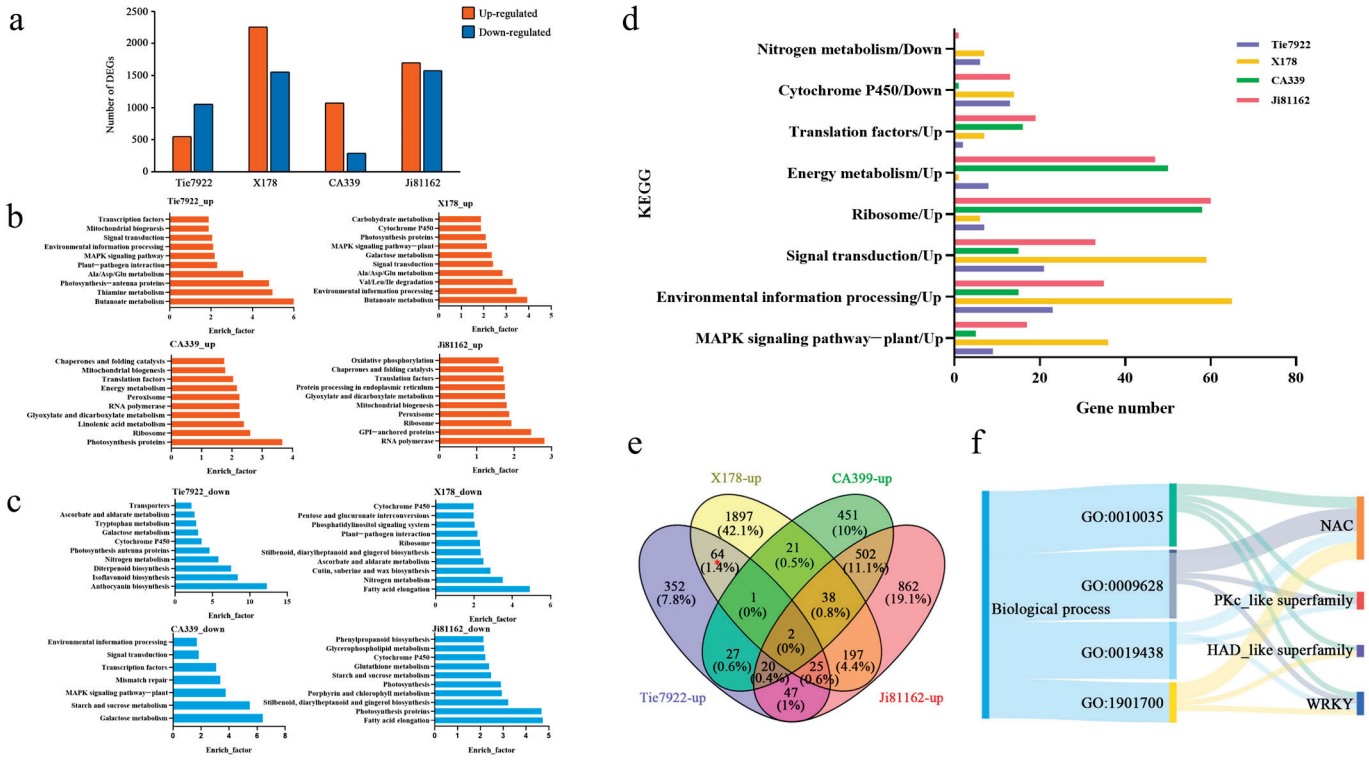

Figure 1. Transcriptome analysis of four inbred maize lines. (**a**) The number of up-regulated or down-regulated genes in four inbred lines under drought stress. (**b**) KEGG map of the up-regulated genes among four inbred lines under drought stress. (**c**) KEGG map of the down-regulated genes among four inbred lines under drought stress. (**d**) The gene expression number of the drought response pathway in four inbred lines. (**e**) Venn diagram of up-regulated genes of four inbred lines under drought stress. "*" means that these 64 genes are upregulated in both Tie7922 and X178. (**f**) GO annotation and family analysis based on the 64 up-regulated genes in Tie7922 and X178.

We analyzed the pathways for the co-enrichment of drought-tolerant or drought-sensitive materials and found that the number of genes expressed differed based on the drought response pathways in the four inbred lines (Figure 1d). KEGG enrichment analysis showed that up-regulated genes in drought-tolerant materials were mainly enriched in signal transduction and stress metabolite anabolic pathways, while in drought-sensitive materials, up-regulated genes were mainly enriched in translation and photosynthetic/respiratory energy metabolic pathways (Figure 1b). The down-regulated genes of the four materials were also analyzed under drought stress. It was found that some secondary metabolite pathways were prevalent in the four materials, such as the MAPK signaling pathway, environmental information processing and signal transduction, but the drought-tolerant materials Tie7922 and X178 were enriched in nitrogen metabolism pathways, which play an important role in the transition from vegetative growth to reproductive growth (Figure 1c).

Sixty-four genes were identified as up-regulated in both the drought-tolerant materials Tie7922 and X178. Among them, four genes belonged to the NAC family, three genes belonged to the kinase family, two genes belonged to the phosphatase family and one gene

belonged to the WRKY family (Figure 1e,f). In the four NAC genes, three of them, including GRMZM2G347043 (*ZmSNAC02*, *ZmSNAC1*, *ZmNAC49*), GRMZM2G014653 (*ZmSNAC04*, *ZmNAC33*, *NAC109*) and GRMZM2G068973 (*ZmSNAC13*, *ZmNAC080308*), have been reported to improve drought tolerance in transgenic *Arabidopsis* or maize [28,29,37–39]. Therefore, another NAC gene, which had not yet been characterized, was named as *ZmSNAC06* (GRMZM2G123667) to be studied in this paper.

2.2. Bioinformatics and Sequence Characterization of *ZmSNAC06*

Five transcripts were found in *ZmSNAC06* from the Zm-B73-REFERENCE-NAM-5.0 version of the sequence annotation. Differences in the five transcripts resulted in two subtypes of proteins, ZmSNAC06-P01 and ZmSNAC06-P02 (Figure 2a,b). The ZmSNAC06-P02 subtype protein was translated from the *ZmSNAC06*-T02 transcript, which had an open reading frame length of 1080 bp with 359 amino acids, and it had a typical NAC domain, while the ZmSNAC06-P01 subtype protein was translated from four transcripts of *ZmSNAC06*-T01/3/4/5 with an open reading frame length of 750 bp, with 250 amino acids. The ZmSNAC06-P01 subtype protein had only the E subdomain of the NAC domain. Subsequently, *ZmSNAC06*-T02 sequences were cloned from the maize inbred lines Tie7922 and Ji81162. A lot of variations were then identified in the *ZmSNAC06*-T02 gene region between the two lines, including insertion, deletion and single nucleotide polymorphisms. Three amino acid differences were identified in the coding region. Compared with Tie 7922, the 173rd amino acid changed from an aspartic acid into an asparagine, and there were the deletions of the 292nd and 293rd alanines, 317th valine and 318th aspartic acid in Ji81162 (Figure S1). The promoter sequence (~2000 bp upstream of the transcription start site) of the *ZmSNAC06*-T02 transcript between Tie7922 and Ji81162 was completely consistent.

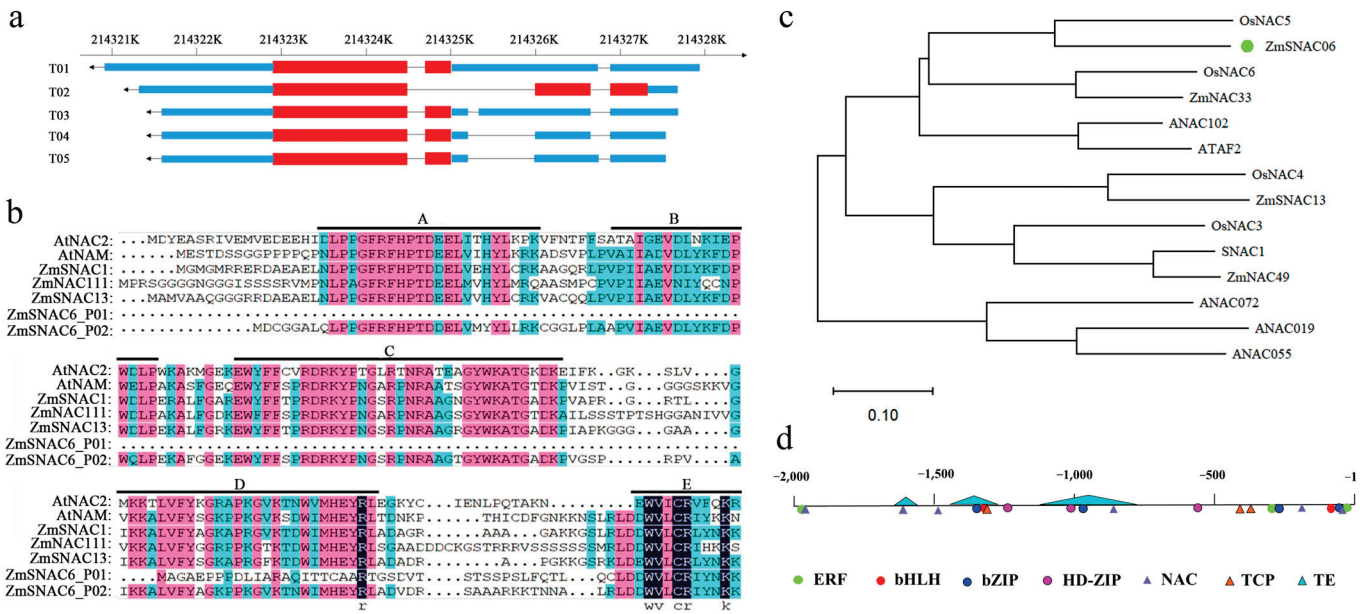

Figure 2. Gene structure, NAC domain sequence alignment, phylogeny and promoter region analysis in *ZmSNAC06*. (**a**) Structure of the *ZmSNAC06* gene transcripts; the blue part represents 5′UTR and 3′UTR, the red part represents the exon of the gene and the black line represents the intron of the gene. (**b**) NAC domain sequence alignment of *ZmSNAC06* and NAC members from other plant species. Identical amino acids are shaded in dark blue, and similar amino acids are shaded in pink or light blue. The locations of the five highly conserved amino acid motifs (A–E) are indicated by black lines. (**c**) Phylogenetic relationships between *ZmSNAC06* and typical stress-responsive NAC proteins. The multiple sequence alignment was performed using ClustalW, and the phylogenetic tree was constructed with MEGA11.0 using the neighbor-joining method. (**d**) Distribution of the transposable elements and binding sites of transcription factors related to stress in the promoter region (~2.0 kb).

Phylogenetic analysis revealed that *ZmSNAC06*-T02 was more closely related to *OsNAC5*, a known drought tolerance gene (Figure 2c). As a member of the NAC transcription factor family, the promoter sequence in *ZmSNAC06*-T02 displayed three transposable elements and a large number of binding sites of transcription factors related to stress responses and plant growth (Figure 2d). We found that there were six NAC transcription factor recognition motifs in the promoter region, and many recognition motifs of other transcription factors, including bZIP, bHLH and HD-ZIP, were also identified in transposable elements. These elements were perhaps related to the functional regulation of *ZmSNAC06* in maize.

2.3. ZmSNAC06 Expression Was Induced by Drought Stress

Tie7922 and Ji81162, which have a close relationship but are significantly different in terms of drought tolerance, were selected as drought-tolerant and drought-sensitive lines to investigate the stress response of *ZmSNAC06*. qRT-PCR results showed that *ZmSNAC06* was differently expressed in the response pattern of tolerant/sensitive materials. In Tie7922, the expression levels of *ZmSNAC06*-T01/3/4/5 peaked at 1 h and 6 h in the roots and leaves, respectively, and peaks appeared at 1 h and 3 h in the roots and leaves, respectively, in Ji81162. The expression of *ZmSNAC06*-T02 in Tie7922 achieved a maximum level at 12 h and 6 h in the roots and leaves, and it peaked at 6 h and 3 h in the roots and leaves in Ji81162, respectively. The different transcripts of *ZmSNAC06* were up-regulated after PEG treatment at 1 h, 3 h and 12 h in the roots and at 1 h, 6 h and 12 h in the leaves, but the expression in Ji81162 was far less obvious than that in Tie7922 (Figure 3).

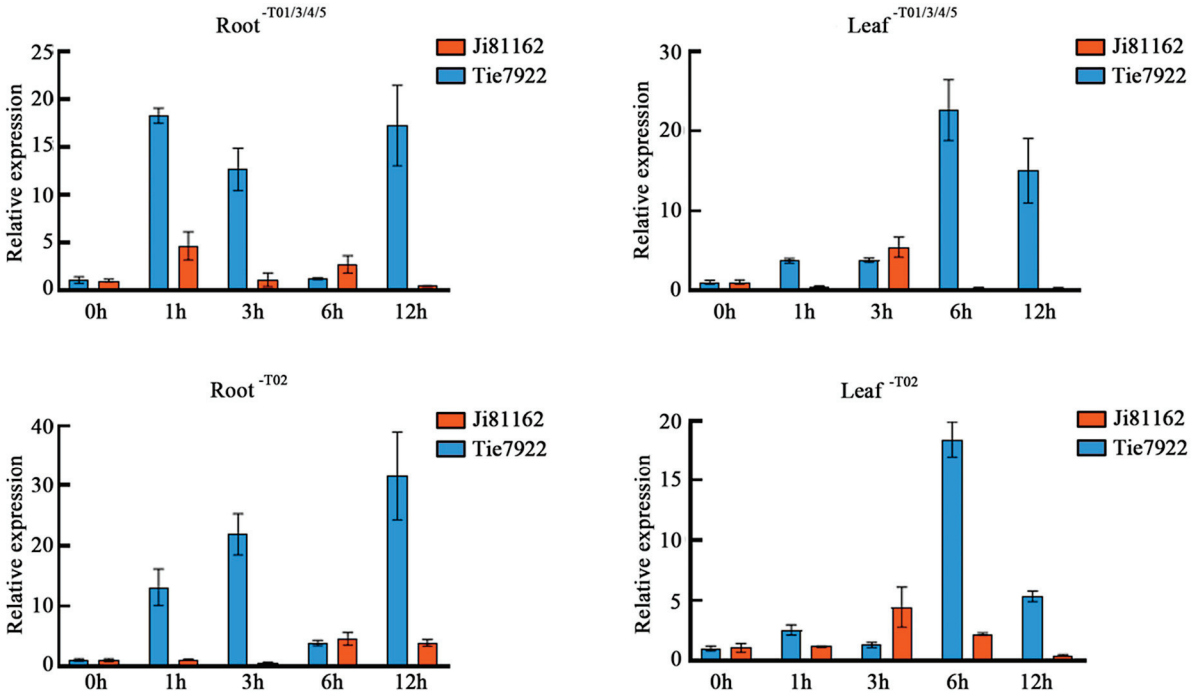

Figure 3. Drought response of *ZmSNAC06* with multiple transcripts in different inbred lines.

2.4. ZmSNAC06 Was Localized in the Nucleus and Had Transactivation Activity

Transcription factors are usually located in the nucleus, where they perform DNA-binding and transcriptional activation functions. To determine the subcellular localization of different transcripts in ZmSNAC06, PAN580-GFP and ZmSNAC06-P01/P02-GFP were transformed into maize protoplasts, and it was found that ZmSNAC06-P01 was localized in the cell membrane, nucleus and cytoplasm, whereas, ZmSNAC06-P02 was localized only

in the nucleus, indicating that the NAC domain of the ZmSNAC06 protein might affect the subcellular localization (Figure 4a).

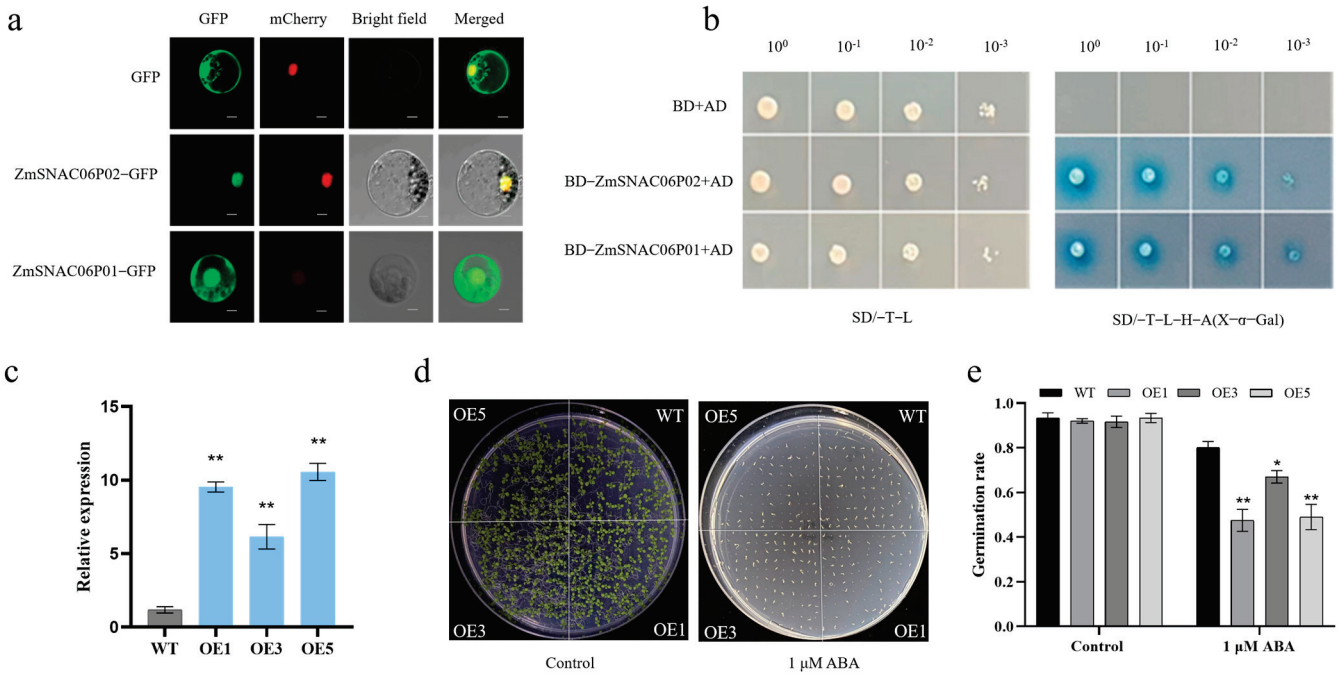

Figure 4. Analysis of the subcellular localization and transactivation activity of ZmSNAC06 and its expression level and germination rate in transgenic *Arabidopsis*. (**a**) Subcellular localization of ZmSNAC06 in maize protoplasts. GFP: Green fluorescent protein; mCherry: nuclear markers; scale bar = 10 μm. (**b**) Transactivation activity of ZmSNAC06 in yeasts. (**c**) qRT-PCR analysis of *ZmSNAC06*-T02 transcript levels in three independent lines. (**d**) Germination phenotype of *Arabidopsis* under normal conditions and ABA treatment. (**e**) Germination rate statistics of *Arabidopsis* under normal conditions and ABA treatment. Significant differences were determined by *t*-test. * $p < 0.05$, ** $p < 0.01$.

Moreover, to study whether the ZmSNAC06-P01/P02 protein had transactivation activity, ZmSNAC06-P01/P02 was fused to the GAL4 DNA-binding domain in the pGBKT7 vector and co-transferred to yeasts with the pGADT7-T vector. The transformants grew normally and turned blue on an SD medium (SD/-Trp-Leu-His-Ade) with X-α-Gal. Both ZmSNAC06-P01/P02 proteins had transactivation activity, indicating that different NAC domains in different transcripts did not affect the transactivation activity of ZmSNAC06 (Figure 4b). The C-terminal of NAC proteins with transcriptional regulatory domains might function to bind to other proteins and thus have transactivation activity.

2.5. Germination Sensitivity of Transgenic Arabidopsis to ABA

Since multiple transcripts of *ZmSNAC06* encode two subtypes of P01 or P02 proteins with an identical C-terminal and the difference in the N-terminal is the presence or absence of NAC domains, the structure of the P02 subtype protein basically contains P01. We selected the major model T02 transcript of *ZmSNAC06* for transformation in *Arabidopsis*. Three independent overexpression lines (OE1, OE3 and OE5) were selected based on expression levels for further study (Figure 4c).

To investigate the sensitivity of transgenic plants to ABA, the germination rate was calculated. Under normal conditions, no significant difference in the germination rate was observed between the wild-type (WT) and overexpression lines (Figure 4d). Under a 1 μM ABA treatment, the germination rates of overexpression lines ranged from 48% to 67%, while the germination rate of the WT was 78% (Figure 4e). The overexpression of *ZmSNAC06*-T02 led to the hypersensitivity of transgenic *Arabidopsis* to ABA.

2.6. ZmSNAC06-T02 Confers Drought Tolerance in Transgenic Arabidopsis

To assess the drought tolerance of transgenic *Arabidopsis*, the survival rates of the WT and the three overexpression lines after drought stress were calculated. Overexpressed plants showed stronger growth recovery (Figure 5a). We found that 56% to 77% of transgenic *Arabidopsis* plants recovered from drought stress after rewatering, which was significantly higher than that of the WT, with a survival rate of 34% (Figure 5b). These results suggest that *ZmSNAC06*-T02 might regulate the plant adaptation to drought stress in maize.

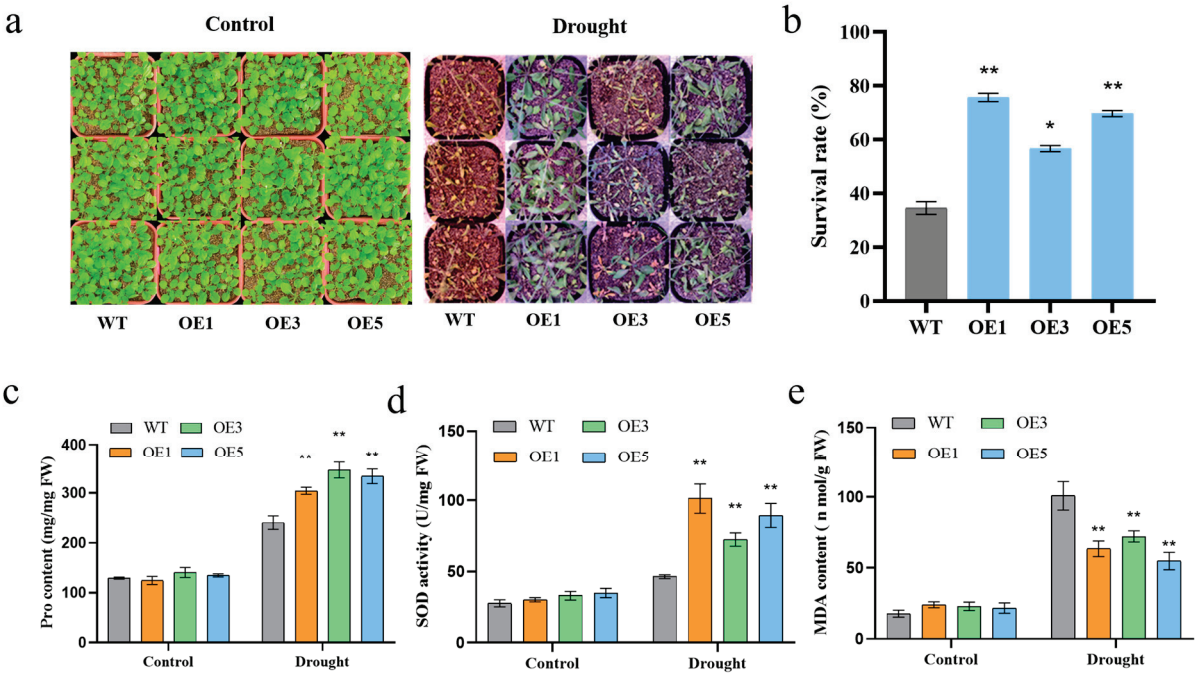

Figure 5. Drought tolerance and physiological indices of transgenic *Arabidopsis* (Pro, SOD, MDA). (**a**) Phenotypes of *ZmSNAC06* overexpression lines and WT. (**b**) Survival rates of *Arabidopsis* after drought treatment. (**c**–**e**) Pro content, SOD activity and MDA content in WT and three overexpression lines were measured before and after 10 days of drought treatment. Significant differences were determined by *t*-test. * $p < 0.05$, ** $p < 0.01$.

Under drought stress, reactive oxygen species (ROS) are accumulated that could damage plant cells. Antioxidant enzymes are involved in the ROS scavenging system and protect plants from damage. Therefore, the three physiological indexes of the proline (Pro) content, superoxide dismutase (SOD) activity and malondialdehyde (MDA) content were measured in the WT and transgenic *Arabidopsis* before and after 10 days of drought treatment (Figure 5c–e). After drought treatment, the content of Pro in the three overexpression lines reached 304.29 mg/mg, 346.41 mg/mg and 333.67 mg/mg, respectively, all of which were significantly higher than the 240.50 mg/mg measured in the WT. Similarly, under drought stress, the SOD activity of transgenic *Arabidopsis* was higher than that of the WT. Then, we found that compared with the WT, the MDA content in transgenic *Arabidopsis* was significantly lower.

3. Discussion

3.1. Multitranscript Characteristics in ZmSNAC06

Multiple transcripts from a gene are usually the result of alternative splicing, which is widely involved in a variety of metabolic pathways within the plant genome [40]. Sequence analysis showed that *ZmSNAC06* has a special structure characterized by five transcripts,

which may be the result of the coexistence of two splicing mechanisms, the intron and exon definition models. When long exons are separated by short (<250 bp) introns, such as in the *ZmSNAC06*-T01 transcript, pairing between splice sites takes place across an intron, and this process is called the intron definition model. On the other hand, in the *ZmSNAC06*-T02 transcript, with a long second intron of up to 604 bp, the splicing machinery is more likely to form across an exon than across an intron [41].

It was speculated that the multiple transcripts of *ZmSNAC06* were not caused by alternative splicing, but by alternative translation initiation. The mature mRNA of eukaryotes enters the cytoplasm for translation after being transcribed in the nucleus, so alternative translation initiation is the result of two splicing mechanisms acting on the same pre-mRNA. The qRT-PCR results showed that multiple transcripts of *ZmSNAC06* showed a synergistic response to drought stress in drought-tolerant and -sensitive materials, but their responses varied among different materials.

There are reports that multiple transcripts of genes perform different functions driven by different factors. For example, *FLM* (*Flowering Locus M*) has two subtypes of transcripts. Under high-temperature conditions, the expression of FLM-β decreased while the expression of FLM-α increased, thus affecting plant flowering [42]. It is worth noting that different transcripts of *ZmSNAC06* can be driven by drought and play drought-tolerant functions. It is speculated that the original transcript of *ZmSNAC06* prior to gene differentiation might have had a strong drought-tolerant function, leading to the preservation of a conserved drought-tolerant function in multiple differentiated transcripts.

3.2. ZmSNAC06-T02 Is an NAC Transcription Factor That Regulates Drought Tolerance

The structure of a transcription factor usually consists of four functional regions: a DNA-binding region, a transcriptional regulatory region, a nuclear localization signaling region and an oligomerization site region for the interaction of a transcription factor with other transcription factors or proteins [43]. *ZmSNAC06*-T02 contains a typical NAC conserved domain in the N-terminal region, and five subdomains have been identified in this domain. ZmSNAC06-P02 has a complete NAC domain, resulting in its localization in the nucleus. ZmSNAC06-P01 has only subdomain E and lacks a nuclear localization signal region, but a transactivation assay showed that the consistency of the C-terminal region of ZmSNAC06-P01/02 ensured that both had transactivation activity without being affected by different NAC domains.

Some members of the NAC transcription factor family have been reported to be involved in many plant regulation and development processes, including the regulation of drought stress. In maize, the drought tolerance function of *ZmNAC55*, *ZmNAC33*, *ZmNAC111*, *ZmNAC48*, *ZmNAC84*, *ZmNAC4*, *ZmNAC19*, *ZmNAC87*, *ZmJUB1*, *ZmNAP* and *ZmSNAC1* has been verified in transgenic plants [27,28,31,44–47]. Phylogenetic analysis showed that *ZmSNAC06*-T02 was more closely related to the known stress-responsive gene *OsNAC5*. The overexpression of *OsNAC5* increased tolerance to drought in rice at the vegetative stage, and more importantly, the root-specific rather than whole-body expression of *OsNAC5* increased the grain yield under drought conditions [48,49]. The analysis of the *ZmSNAC06*-T02 promoter sequence also showed that there were several binding sites of TFs related to a stress response in the promoter. The overexpression of *ZmSNAC06*-T02 made transgenic *Arabidopsis* more sensitive to ABA than the WT, suggesting that it may be involved in ABA-dependent signaling pathways in response to drought stress. It was also verified in our study that compared with the WT, transgenic *Arabidopsis* showed stronger drought tolerance and higher survival rates.

On the other hand, ROS are essential for plant growth and development. During normal physiological metabolism, the ROS system including production and removal in

plants is in a state of equilibrium. However, drought stress can lead to the accumulation of excess ROS, which results in damage to plant cells [50]. Antioxidant enzymes such as MDA, SOD and Pro are known to play vital roles in ROS scavenging. After drought treatment, we also found that compared with the WT, the content of Pro increased, the activity of SOD increased and the content of MDA decreased in overexpression lines. This indicated that the *ZmSNAC06*-T02 transgenic lines had the ability to scavenge reactive oxygen species and suffered less damage under drought stress. In summary, the bioinformatics analysis, combined with the experimental results, indicates that *ZmSNAC06*-T02 is an NAC transcription factor responding to drought stress.

4. Materials and Methods

4.1. Plant Materials and Stress Treatment

The drought-tolerant inbred maize lines Tie7922 and X178, drought-sensitive inbred lines Ji81162 and CA339 and the evaluation of drought tolerance were provided by the Institute of Crop Sciences, Chinese Academy of Agricultural Sciences [51]. They were subjected to drought-stressed conditions at the V10 stage, early-developing young tassels were taken under well-watered and drought-stressed conditions at the V13 stage and total RNA samples were sequenced at the Beijing Genomics Institute, Shenzhen, China. Libraries were sequenced on the Illumina HiSeq 2000 Platform (Illumina, San Diego, CA, USA) according to the manufacturer's recommendations [52].

Seeds of the Tie7922 and Ji81162 inbred lines, which had been surface-sterilized and germinated, were rolled in filter paper and placed vertically in distilled water in darkness for 3 days and then cultivated with Hoagland solution under a 16 h light/8 h dark cycle at 26 °C. At the three-leaf stage, the seedlings were transferred into Hoagland solution containing 20% (*w*/*v*) PEG-6000 for the drought treatment, and samples were collected after 0, 1, 3, 6 and 12 h of treatment. All samples were immediately frozen in liquid nitrogen and stored at −80 °C for RNA extraction.

4.2. Transcriptome Analysis

Transcriptome data of the Tie7922, X178, Ji81162 and CA339 inbred lines under well-watered and drought-stressed conditions were further analyzed. Digital gene expression counts were normalized through $\log_2$ transformation and compared using the reads per kilobase transcriptome per million mapped reads method (RPKM). A false discovery rate (FDR) ≤ 0.001, an absolute value of the Log_2 Ratio ≥ 1 and $p \leq 0.001$ were used as the thresholds to assess the significance of differences in gene expression. The KEGG (Kyoto Encyclopedia of Genes and Genomes) enrichment analysis was conducted using TBtools to compare the differences in the response pathways of the four materials under drought-stressed conditions (https://bioinfogp.cnb.csic.es/tools/venny/index.html, accessed on 29 October 2024). The GO (Gene Ontology) enrichment and gene family analyses of up-regulated response genes in drought-tolerant materials were performed using TBtools (https://dycharts.com/appv2/#/pages/home/chart-template, accessed on 29 October 2024).

4.3. Bioinformatics Analysis of ZmSNAC06

The sequences of *ZmSNAC06* and the NAC members of maize and other species were downloaded from the database website (https://maizegdb.org/, accessed on 29 October 2024; https://ensembl.gramene.org/Zea_mays/Info/Index, accessed on 29 October 2024). Multiple alignments of amino acid sequences were constructed with MEGA 11.0 software using ClustalW; the phylogenetic tree was constructed with MEGA 11.0 software using the neighbor-joining (NJ) method. Bootstrapping was carried out to obtain 1000 replicates with

the pairwise deletion option. The PlantPAN4.0 website (http://plantpan.itps.ncku.edu.tw/plantpan4/index.html, accessed on 29 October 2024) was used to predict the binding sites of transcription factors within 2000 bp of the sequence upstream from the translation initiation codon (ATG) of *ZmSNAC06*.

4.4. RNA Extraction and Quantitative Real-Time PCR

Total RNA was extracted using the TransZol UP reagent. The total RNA was reverse-transcribed into cDNA with a qualified quality and concentration using the FastQuant RT Kit (Tiangen, Beijing, China). Quantitative real-time PCR (qRT-PCR) was performed using Applied Biosystems 7500 (Waltham, MA, USA), and the specificity of each primer pair was verified through melting curve analysis. TUB4/Actin was selected as an internal control, and gene expression was calculated using the $2^{-\Delta\Delta Ct}$ method with the variation in expression being estimated from three biological replicates. The primer pairs used for qRT-PCR analysis are listed in Supplementary Table S1.

4.5. Subcellular Localization and Transactivation Assay in Yeast Cells

The coding region of different transcripts of *ZmSNAC06* without the stop codon (TGA) was amplified using pairs of primers (Supplementary Table S1) and inserted into PAN580 vectors digested with *BamH*I to generate the ZmSNAC06-GFP fusion protein, respectively. The protoplast extraction and transformation methods were used with reference to the scheme of *Arabidopsis* [53]. The PAN580 vector was used as a negative control. The fluorescence of the GFP was observed through confocal microscopy after 12-16 h of incubation in darkness at room temperature.

The coding region of different transcripts of *ZmSNAC06* was amplified and inserted into pGBKT7 vectors digested with *Eco*RI and *BamH*I, respectively (the primers are listed in Supplementary Table S1). The fusion plasmid and the empty vector pGADT7-T were co-transformed into Y2HGlod yeast cells according to the manufacturer's protocol. The empty vectors pGBKT7 and pGADT7-T were co-transformed as a negative control. The transformants were incubated on an SD/-Trp/-Leu or SD/-Trp/-Leu/-His/-Ade/X-α-Gal medium at 30 °C for 48–96 h.

4.6. Transformation of Arabidopsis and Drought Tolerance in Transgenic Arabidopsis

The coding region of *ZmSNAC06*-T02 was amplified from the inbred maize line Tie7922 through PCR (the primers are listed in Supplementary Table S1). The *Arabidopsis* ecotype Col-0 was transformed using the floral dipping method. For the selection of transformants, T_0 seeds were plated on a 1/2 Murashige and Skoog (MS) medium with 1% sucrose and 50 mg/mL hygromycin B. Homozygous T_3 plants were used for further analysis.

Wild-type (WT) and *ZmNAC06*-overexpressed transgenic seedlings that germinated on 1/2 MS medium for one week were transferred into pots containing a soil mixture (vermiculite/nutrient soil = 3:1). They were grown under normal conditions for 2 weeks in a growth chamber under a 16 h light/8 h dark cycle at 22 °C, then water was withheld from the plants for 2 weeks. Watering was then resumed to allow the plants to recover. Three days later, the number of surviving plants was recorded. At least 16 plants of each line were compared with the WT in each test, and statistical data were based on data obtained from three independent experiments.

4.7. Germination and Determination of Physiological Indexes Under Stress

One hundred seeds of WT and *ZmSNAC06*-overexpressed plants were sown on a 1/2 MS medium with or without 1 μM ABA, respectively. There were three replicated experiments. Plates were chilled at 4 °C for 3 days to synchronize germination and moved

to 22 °C with a 16 h light/8 h dark cycle. Germination was scored on the seventh day after germination.

To detect changes in physiological indices, leaves were collected from plants before and after 10 days of drought treatment. The contents of MDA and Pro and the activity of SOD in the leaves of *Arabidopsis* were measured with the corresponding detection kits (Solarbio, Beijing, China).

4.8. Statistical Analyses

Statistical analysis was performed using Microsoft Excel. All values are the mean (±SD) of three biological replicates. Significant differences were determined by a *t*-test (* $p < 0.05$, ** $p < 0.01$).

5. Conclusions

In this study, we identified the *ZmSNAC06* gene between drought-tolerant (Tie7922 and X178) and drought-sensitive (Ji81162 and CA339) inbred lines through RNA-seq analysis. Bioinformatic analysis revealed that *ZmSNAC06*, which had five transcripts, belonged to the NAC transcription factor family. *ZmSNAC06*-T02 had a typical NAC domain. ZmSNAC06-P02 was localized in the nucleus of maize protoplasts and had transactivation activity in yeasts. The overexpression of *ZmSNAC06*-T02 in *Arabidopsis* resulted in hypersensitivity to ABA during germination, increased antioxidant enzyme activities to keep the balance of ROS and enhanced drought tolerance in transgenic *Arabidopsis*. These findings help us understand the function of *ZmSNAC06* and provide a theoretical basis for cultivating drought-tolerant varieties in the future.

Supplementary Materials: The following supporting information can be downloaded at https://www.mdpi.com/article/10.3390/plants14010012/s1: Supplementary Table S1: Primer sequence; Supplementary Figure S1: Differences in the ZmSNAC06 sequence between the two inbred lines. (a) Differences in sequence in gene region. The red region is the exon region, and the gray area is the intron region. (b) Differences in amino acid sequence.

Author Contributions: Z.H. and X.L.: conceptualization, methodology, project administration, writing—review and editing. F.W. and Y.C.: methodology, software, investigation, writing—original draft. R.Y. and P.L. revised the manuscript and modified the language. H.W., R.Z., W.L., K.Y. and X.X. checked the data and formatting in articles. All authors have read and agreed to the published version of the manuscript.

Funding: This work was supported by the National Natural Science Foundation of China (32261143757, 32272049), the Sustainable Development International Cooperation Program of the Bill & Melinda Gates Foundation (2022YFAG1002) and the Provincial Key Research and Development Program (2024B02008-2). The funding agencies were not involved in the design of the study; the collection, analysis and interpretation of the data; or the preparation of the manuscript.

Data Availability Statement: All of the datasets are included within the article and its additional files.

Conflicts of Interest: The authors declare no conflicts of interest.

References

1. Christian, J.I.; Basara, J.B.; Hunt, E.D.; Otkin, J.A.; Furtado, J.C.; Mishra, V.; Xiao, X.; Randall, R.M. Global distribution, trends, and drivers of flash drought occurrence. *Nat. Commun.* **2021**, *12*, 6330. [CrossRef] [PubMed]
2. Ribaut, J.M.; Betran, J.; Monneveux, P.; Setter, T. Drought tolerance in maize. In *Handbook of Maize: Its Biology*; Bennetzen, J.L., Hake, S.C., Eds.; Springer: New York, NY, USA, 2009; pp. 311–344.
3. Todaka, D.; Nakashima, K.; Shinozaki, K.; Yamaguchi-Shinozaki, K. Toward understanding transcriptional regulatory networks in abiotic stress responses and tolerance in rice. *Rice* **2012**, *5*, 6. [CrossRef] [PubMed]

4. Souer, E.; Vanhouwelingen, A.; Kloos, D.; Mol, J.; Koes, R. The no apical meristem gene of petunia is required for pattern formation in embryos and flowers and is expressed at meristem and primordia boundaries. *Cell* **1996**, *85*, 159–170. [CrossRef]
5. Aida, M.; Ishida, T.; Fukaki, H.; Fujisawa, H.; Tasaka, M. Genes involved in organ separation in *Arabidopsis*: An analysis of the cup-shaped cotyledon mutant. *Plant Cell* **1997**, *9*, 841–857. [CrossRef]
6. Ooka, H.; Satoh, K.; Doi, K.; Nagata, T.; Otomo, Y.; Murakami, K.; Matsubara, K.; Osato, N.; Kawai, J.; Carninci, P.; et al. Comprehensive analysis of NAC family genes in *Oryza sativa* and *Arabidopsis thaliana*. *DNA Res.* **2003**, *10*, 239–247. [CrossRef]
7. Ernst, H.A.; Olsen, A.N.; Skriver, K.; Larsen, S.; Leggio, L.L. Structure of the conserved domain of *ANAC*, a member of the NAC family of transcription factors. *EMBO Rep.* **2004**, *5*, 297–303. [CrossRef]
8. Puranik, S.; Sahu, P.P.; Srivastava, P.S.; Prasad, M. NAC proteins: Regulation and role in stress tolerance. *Trends Plant Sci.* **2012**, *17*, 369–381. [CrossRef]
9. Singh, S.; Koyama, H.; Bhati, K.K.; Alok, A. The biotechnological importance of the plant-specific NAC transcription factor family in crop improvement. *J. Plant Res.* **2021**, *134*, 475–495. [CrossRef]
10. Kjaersgaard, T.; Jensen, M.K.; Christiansen, M.W.; Gregersen, P.; Kragelund, B.B.; Skriver, K. Senescence-associated barley NAC (NAM, ATAF1,2, CUC) transcription factor interacts with radical-induced cell death 1 through a disordered regulatory domain. *J. Biol. Chem.* **2011**, *286*, 35418–35429. [CrossRef]
11. Riechmann, J.L.; Heard, J.; Martin, G.; Reuber, L.; Jiang, C.; Keddie, J.; Adam, L.; Pineda, O.; Ratcliffe, O.J.; Samaha, R.R.; et al. *Arabidopsis* transcription factors: Genome-wide comparative analysis among eukaryotes. *Science* **2000**, *290*, 2105–2110. [CrossRef]
12. Xiong, Y.; Liu, T.; Tian, C.; Sun, S.; Li, J.; Chen, M. Transcription factors in rice: A genome-wide comparative analysis between monocots and eudicots. *Plant Mol. Biol.* **2005**, *59*, 191–203. [CrossRef] [PubMed]
13. Rushton, P.J.; Bokowiec, M.T.; Han, S.; Zhang, H.; Brannock, J.F.; Chen, X.; Laudeman, T.W.; Timko, M.P. Tobacco transcription factors: Novel insights into transcriptional regulation in the Solanaceae. *Plant Physiol.* **2008**, *147*, 280–295. [CrossRef] [PubMed]
14. Le, D.T.; Nishiyama, R.; Watanabe, Y.; Mochida, K.; Yamaguchi-Shinozaki, K.; Shinozaki, K.; Tran, L.S. Genome-wide survey and expression analysis of the plant-specific NAC transcription factor family in soybean during development and dehydration stress. *DNA Res.* **2011**, *18*, 263–276. [CrossRef]
15. Guérin, C.; Roche, J.; Allard, V.; Ravel, C.; Mouzeyar, S.; Bouzidi, M.F. Genome-wide analysis, expansion and expression of the NAC family under drought and heat stresses in bread wheat (*T. aestivum* L.). *PLoS ONE* **2019**, *14*, e0213390. [CrossRef]
16. Shiriga, K.; Sharma, R.; Kumar, K.; Yadav, S.K.; Hossain, F.; Thirunavukkarasu, N. Genome-wide identification and expression pattern of drought-responsive members of the NAC family in maize. *Meta Gene* **2014**, *2*, 407–417. [CrossRef]
17. Sakuraba, Y.; Kim, Y.S.; Han, S.H.; Lee, B.D.; Paek, N.C. The Arabidopsis transcription factor *NAC016* promotes drought stress responses by repressing *AREB1* transcription through a trifurcate feed-forward regulatory loop involving NAP. *Plant Cell* **2015**, *27*, 1771–1787. [CrossRef]
18. Fang, Y.; Liao, K.; Du, H.; Xu, Y.; Song, H.; Li, X.; Xiong, L. A stress-responsive NAC transcription factor *SNAC3* confers heat and drought tolerance through modulation of reactive oxygen species in rice. *J. Exp. Bot.* **2015**, *66*, 6803–6817. [CrossRef]
19. Takasaki, H.; Maruyama, K.; Kidokoro, S.; Ito, Y.; Fujita, Y.; Shinozaki, K.; Yamaguchi-Shinozaki, K.; Nakashima, K. The abiotic stress-responsive NAC-type transcription factor *OsNAC5* regulates stress-inducible genes and stress tolerance in rice. *Mol. Genet. Genom.* **2010**, *284*, 173–183. [CrossRef]
20. Yuan, X.; Wang, H.; Cai, J.; Bi, Y.; Li, D.; Song, F. Rice NAC transcription factor *ONAC066* functions as a positive regulator of drought and oxidative stress response. *BMC Plant Biol.* **2019**, *19*, 278. [CrossRef]
21. Jiang, D.; Zhou, L.; Chen, W.; Ye, N.; Xia, J.; Zhuang, C. Overexpression of a microRNA-targeted NAC transcription factor improves drought and salt tolerance in Rice via ABA-mediated pathways. *Rice* **2019**, *12*, 76. [CrossRef]
22. Wu, Q.; Liu, Y.; Xie, Z.; Yu, B.; Sun, Y.; Huang, J. *OsNAC016* regulates plant architecture and drought tolerance by interacting with the kinases GSK2 and SAPK8. *Plant Physiol.* **2022**, *189*, 1296–1313. [CrossRef] [PubMed]
23. Chen, F.; Zhang, H.; Li, H.; Lian, L.; Wei, Y.; Lin, Y.; Wang, L.; He, W.; Cai, Q.; Xie, H.; et al. IPA1 improves drought tolerance by activating *SNAC1* in rice. *BMC Plant Biol.* **2023**, *23*, 55. [CrossRef] [PubMed]
24. Yang, C.; Huang, Y.; Lv, P.; Antwi-Boasiako, A.; Begum, N.; Zhao, T.; Zhao, J. Transcription Factor *GmNAC12* Improved Drought Stress Tolerance in Soybean. *Int. J. Mol. Sci.* **2022**, *23*, 12029. [CrossRef]
25. Mao, H.; Li, S.; Wang, Z.; Cheng, X.; Li, F.; Mei, F.; Chen, N.; Kang, Z. Regulatory changes in *TaSNAC8-6A* are associated with drought tolerance in wheat seedlings. *Plant Biotechnol. J.* **2019**, *18*, 1078–1092. [CrossRef]
26. Mao, H.; Li, S.; Chen, B.; Jian, C.; Mei, F.; Zhang, Y.; Li, F.; Chen, N.; Li, T.; Du, L.; et al. Variation in cis-regulation of a NAC transcription factor contributes to drought tolerance in wheat. *Mol. Plant* **2022**, *15*, 276–292. [CrossRef]
27. Mao, H.; Yu, L.; Han, R.; Li, Z.; Liu, H. *ZmNAC55*, a maize stress-responsive NAC transcription factor, confers drought resistance in transgenic *Arabidopsis*. *Plant Physiol. Biochem.* **2016**, *105*, 55–66. [CrossRef]
28. Liu, W.; Zhao, B.; Chao, Q.; Wang, B.; Zhang, Q.; Zhang, C.; Li, S.; Jin, F.; Yang, D.; Li, X. Function analysis of *ZmNAC33*, a positive regulator in drought stress response in *Arabidopsis*. *Plant Physiol. Biochem.* **2019**, *145*, 174–183. [CrossRef]

29. Luo, P.; Chen, Y.; Rong, K.; Lu, Y.; Wang, N.; Xu, Z.; Pang, B.; Zhou, D.; Weng, J.; Li, M.; et al. *ZmSNAC13*, a maize NAC transcription factor conferring enhanced resistance to multiple abiotic stresses in transgenic *Arabidopsis*. *Plant Physiol. Biochem.* **2022**, *170*, 160–170. [CrossRef]
30. Xiang, Y.; Sun, X.; Bian, X.; Wei, T.; Han, T.; Yan, J.; Zhang, A. The transcription factor *ZmNAC49* reduces stomatal density and improves drought tolerance in maize. *J. Exp. Bot.* **2021**, *72*, 1399–1410. [CrossRef]
31. Mao, H.; Wang, H.; Liu, S.; Li, Z.; Yang, X.; Yan, J.; Li, J.; Tran, L.S.; Qin, F. A transposable element in a NAC gene is associated with drought tolerance in maize seedlings. *Nat. Commun.* **2015**, *6*, 8326. [CrossRef]
32. Liu, H.; Song, S.; Liu, M.; Mu, Y.; Li, Y.; Xuan, Y.; Niu, L.; Zhang, H.; Wang, W. Transcription Factor *ZmNAC20* Improves Drought Resistance by Promoting Stomatal Closure and Activating Expression of Stress-Responsive Genes in Maize. *Int. J. Mol. Sci.* **2023**, *24*, 4712. [CrossRef] [PubMed]
33. FAO. FAOSTAT, Production Indices. 2020. Available online: https://www.fao.org/faostat/en/#data/QI (accessed on 26 March 2023).
34. Zhuo, L.; Liu, Y.; Yang, H.; Hoekstra, A.Y.; Liu, W.; Cao, X.; Wang, M.; Wu, P. Water for maize for pigs for pork: An analysis of inter-provincial trade in China. *Water Res.* **2019**, *166*, 115074. [CrossRef] [PubMed]
35. Gupta, A.; Rico-Medina, A.; Caño-Delgado, A.I. The physiology of plant responses to drought. *Science* **2020**, *368*, 266–269. [CrossRef] [PubMed]
36. Li, X.; Yuan, L.; Li, X.; Zhang, S.; Li, M.; Li, W. Heterotic Grouping of 70 Maize Inbred Lines by SSR Markers. *Sci. Agric. Sin.* **2003**, *36*, 622–627.
37. Xiang, Y.; Bian, X.; Wei, T.; Yan, J.; Sun, X.; Han, T.; Dong, B.; Zhang, G.; Li, J.; Zhang, A. ZmMPK5 phosphorylates ZmNAC49 to enhance oxidative stress tolerance in maize. *New Phytol.* **2021**, *232*, 2400–2417. [CrossRef]
38. Thatcher, S.R.; Danilevskaya, O.N.; Meng, X.; Beatty, M.; Zastrow-Hayes, G.; Harris, C.; Van Allen, B.; Habben, J.; Li, B. Genome-wide analysis of alternative splicing during development and drought stress in maize. *Plant Physiol.* **2016**, *170*, 586–599. [CrossRef]
39. Wang, N.; Cheng, M.; Chen, Y.; Liu, B.; Wang, X.; Li, G.; Zhou, Y.; Luo, P.; Xi, Z.; Yong, H.; et al. Natural variations in the non-coding region of *ZmNAC080308* contributes maintaining grain yield under drought stress in maize. *BMC Plant Biol.* **2021**, *21*, 305. [CrossRef]
40. Lam, P.Y.; Wang, L.; Lo, C.; Zhu, F. Alternative splicing and its roles in plant metabolism. *Int. J. Mol. Sci.* **2022**, *23*, 7355. [CrossRef]
41. De Conti, L.; Baralle, M.; Buratti, E. Exon and intron definition in pre-mRNA splicing. *Wiley Interdiscip. Rev. RNA* **2013**, *4*, 49–60. [CrossRef]
42. Jin, S.; Kim, S.Y.; Susila, H.; Nasim, Z.; Youn, G.; Ahn, J.H. Flowering Locus M isoforms differentially affect the subcellular localization and stability of short vegetative phase to regulate temperature-responsive flowering in *Arabidopsis*. *Mol. Plant* **2022**, *15*, 1696–1709. [CrossRef]
43. Mitsuda, N.; Ohme-Takagi, M. Functional analysis of transcription factors in *Arabidopsis*. *Plant Cell Physiol.* **2009**, *50*, 1232–1248. [CrossRef] [PubMed]
44. Mao, Y.; Xu, J.; Wang, Q.; Li, G.; Tang, X.; Liu, T.; Feng, X.; Wu, F.; Li, M.; Xie, W.; et al. A natural antisense transcript acts as a negative regulator for the maize drought stress response gene *ZmNAC48*. *J. Exp. Bot.* **2021**, *72*, 2790–2806. [CrossRef] [PubMed]
45. Han, T.; Yan, J.; Xiang, Y.; Zhang, A. Phosphorylation of ZmNAC84 at Ser-113 enhances the drought tolerance by directly modulating *ZmSOD2* expression in maize. *Biochem. Biophys. Res. Commun.* **2021**, *567*, 86–91. [CrossRef] [PubMed]
46. Ding, N.; Zhao, Y.; Wang, W.; Liu, X.; Shi, W.; Zhang, D.; Chen, J.; Ma, S.; Sun, Q.; Wang, T.; et al. Transcriptome analysis in contrasting maize inbred lines and functional analysis of five maize NAC genes under drought stress treatment. *Front. Plant Sci.* **2023**, *13*, 1097719. [CrossRef] [PubMed]
47. Lu, M.; Ying, S.; Zhang, D.; Shi, Y.; Song, Y.; Wang, T.; Li, Y. A maize stress-responsive NAC transcription factor, *ZmSNAC1*, confers enhanced tolerance to dehydration in transgenic *Arabidopsis*. *Plant Cell Rep.* **2012**, *31*, 1701–1711. [CrossRef]
48. Song, S.; Chen, Y.; Chen, J.; Dai, X.; Zhang, W. Physiological mechanisms underlying OsNAC5-dependent tolerance of rice plants to abiotic stress. *Planta* **2011**, *234*, 331–345. [CrossRef]
49. Jeong, J.S.; Kim, Y.S.; Redillas, M.C.; Jang, G.; Jung, H.; Bang, S.W.; Choi, Y.D.; Ha, S.; Reuzeau, C.; Kim, J. *OsNAC5* overexpression enlarges root diameter in rice plants leading to enhanced drought tolerance and increased grain yield in the field. *Plant Biotechnol. J.* **2013**, *11*, 101–114. [CrossRef]
50. Huang, H.; Ullah, F.; Zhou, D.; Yi, M.; Zhao, Y. Mechanisms of ROS Regulation of Plant Development and Stress Responses. *Front. Plant Sci.* **2019**, *10*, 800. [CrossRef]
51. Hao, Z.; Li, X.; Su, Z.; Xie, C.; Li, M.; Liang, X.; Weng, J.; Zhang, D.; Li, L.; Zhang, S. A proposed selection criterion for drought resistance across multiple environments in maize. *Breed. Sci.* **2011**, *61*, 101–108. [CrossRef]

52. Wang, N.; Li, L.; Gao, W.; Wu, Y.; Yong, H.; Weng, J.; Li, M.; Zhang, D.; Hao, Z.; Li, X. Transcriptomes of early developing tassels under drought stress reveal differential expression of genes related to drought tolerance in maize. *J. Integr. Agric.* **2018**, *17*, 1276–1288. [CrossRef]
53. Yoo, S.D.; Cho, Y.H.; Sheen, J. *Arabidopsis* mesophyll protoplasts: A versatile cell system for transient gene expression analysis. *Nat. Protoc.* **2007**, *2*, 1565–1572. [CrossRef]

plants

MDPI

Article

GmTRAB1, a Basic Leucine Zipper Transcription Factor, Positively Regulates Drought Tolerance in Soybean (*Glycine max*. L)

Hui Li †, Qiu-Yu Zhang †, Ping Xu, Xiao-Hua Wang, Sheng-Jie Dai, Zhen-Ning Liu, Meng Xu, Xue Cao and Xiao-Yu Cui *

College of Agriculture and Forestry Sciences, Linyi University, Linyi 276000, China; lihuiqau@163.com (H.L.); zhangqiuyu1025@163.com (Q.-Y.Z.); xuping3792@lyu.edu.cn (P.X.); wangxiaohua@lyu.edu.cn (X.-H.W.); daishengjie@lyu.edu.cn (S.-J.D.); liuzhenning@lyu.edu.cn (Z.-N.L.); xumeng@lyu.edu.cn (M.X.); caoxue@lyu.edu.cn (X.C.)

* Correspondence: cuixiaoyu@lyu.edu.cn

† These authors contributed equally to this work.

Abstract: The basic leucine zipper (bZIP) transcription factors play crucial roles in plant resistance to environmental challenges, but the biological functions of soybean bZIP members are still unclear. In this study, a drought-related soybean bZIP gene, *GmTRAB*1, was analyzed. The transcript of *GmTRAB1* was upregulated under drought, ABA, and oxidative stresses. Overexpression of *GmTRAB1* improved the osmotic stress tolerance of transgenic *Arabidopsis* and soybean hairy roots associated with increased proline content and activity of antioxidant enzymes and reduced accumulations of malonaldehyde and reactive oxide species. However, RNA interference silencing of *GmTRAB1* in the soybean hairy roots improved drought sensitivity. Furthermore, GmTRAB1 increased the sensitivity of transgenic plants to ABA and participated in modulating ABA-regulated stomatal closure upon drought stress. In addition, GmTRAB1 stimulated the transcript accumulation of drought-, ABA-, and antioxidant-related genes to respond to drought. Collectively, this research will contribute to understanding the molecular mechanisms of bZIP transcription factors in soybean's resistance to drought.

Keywords: soybean; drought; ABA response; ROS homeostasis; bZIP transcription factor

1. Introduction

Plants usually encounter multiple adverse environments, including extreme temperatures, drought, and salt, and these stresses can greatly affect their growth and development and ultimately destroy their productivity [1]. To survive, plants have evolved a variety of strategies to cope with these environmental challenges. These adaptive responses are highly intricate processes mediated by sophisticated signaling networks [2]. Transcription factors, including those from families including dehydration-responsive element-binding (DREB), myeloblastosis (MYB), NAM, ATAF, and CUC (NAC), WRKY, ethylene-responsive factor (ERF), and basic leucine zipper (bZIP), play critical roles in the signal transduction networks, and they function essentially in transmitting the perceived stress signal to the stress-responsive genes, ultimately leading to physiological and metabolic changes [3–5].

The bZIP transcription factors comprise a large and diverse transcription factor family in plants [6]. Members of bZIP proteins have a conserved bZIP domain, which consists of a leucine zipper motif and a conserved base region [7]. The N-X7-R/K motif is composed of approximately 18 amino acids within the bZIP domain and performs critical functions in DNA binding and nuclear localization [8]. The bZIPs usually interact with the promoter fragments harboring an ACGT core *cis*-element, including C-box (GACGTC), ABRE (CCACGTGG), A-box (TACGTA), and G-box (CACGTG), to influence the expression of downstream targets [9]. The leucine zipper region comprises one or more repeating regions or other hydrophobic amino acids, which is correlated to bZIP recognition and

dimerization [10]. The bZIP proteins were first characterized in *Arabidopsis*, and 75 bZIPs were identified [7]. Subsequent genomics research also found 89 bZIPs in rice [10], 89 bZIPs in barley [11], 55 bZIPs in tomato [12], 247 bZIPs in rapeseed [13], 92 bZIPs in sorghum [14], and 125 bZIPs in maize [15].

The bZIP proteins perform crucial functions in plants' responses to adverse conditions. For example, in *Arabidopsis*, AtbZIP1 increased the expression of *COR15A*, *RD17*, and *RD29A* to enhance *Arabidopsis'* ability to tolerate salt and osmotic stresses [16]. AtABF3 regulated ABRE-dependent gene expression to influence ABA-mediated drought response [17]. In rice, OsbZIP23, OsbZIP42, and OsbZIP72 were upregulated by ABA and drought stresses and act as key regulators in rendering rice ABA-regulated osmotic stress tolerance [18–20]. ZmbZIP4 has been reported to increase ABA synthesis to improve maize adaptation to drought and salt stresses [6]. Under cold conditions, ZmbZIP68 restricts the expression of DREB family proteins to reduce cold tolerance of maize [2]. TabZIP60 is associated with TaCDPK30 to influence the synthesis of ABA and increase the salt tolerance of wheat [5]. *TabZIP15* was shown to respond to salt stress, and *TabZIP15* overexpression conferred the resistance of transgenic wheat to salt [21]. Overexpression of *CsbZIP18* impaired the cold tolerance of transgenic plants through suppressing cold- and ABA-related genes' expression [22]. Furthermore, in pepper, salt promoted *CabZIP25* expression, and *CabZIP25*-overexpressing (OE) plants displayed salt-tolerant phenotypes [23].

Soybean is a critical cereal and oil crop worldwide [24,25]. Drought acts as the main adverse stimulus to destroy the production of soybean [26]. Studying the mechanism in drought response is an effective way to enhance the adaptability of soybean to drought. Previous studies have reported that there are 160 bZIP genes in the soybean genome [27]. Until now, only a very limited number of bZIP members have been functionally analyzed in soybean. In the present research, we characterized a bZIP family transcription factor, GmTRAB1, and show that its expression is significantly upregulated upon drought, ABA, and oxidative stresses. Further physiology and molecular studies displayed that GmTRAB1 influences the ABA response and antioxidant defense system to enhance soybean tolerance to drought.

2. Results

2.1. Identification and Sequence Analysis of GmTRAB1

Results of bioinformatics analysis have shown that 160 bZIP transcription factors were identified in soybean [27]. GmTRAB1 (Glyma.04G039300) encoded a protein with a conserved bZIP domain and highly shared the sequence with GsABL5 from *Glycine soja* (99.52%), GmbZIP50 (89.35%), MpABL5 from *Mucuna pruriens* (87.97%), and VuABL5 from *Vigna unguiculata* (86.35%) (https://blast.ncbi.nlm.nih.gov/Blast.cgi?CMD=Get&RID=JEV01RW2016, accessed on 31 October 2024; Figure 1A). Subsequent phylogenetic analysis demonstrated that GmTRAB1 and its homologous proteins were classified into subgroup A (Figure S1). In the subcellular localization analyses, GmTRAB1-GFP proteins were detected in the nucleus and overlapped with the nuclear marker (OsEHD4-mCherry) [28] (Figure 1B).

2.2. GmTRAB1 Is Induced by Multiple Abiotic Stresses

To assess the function of bZIPs in the modulation of soybean response to environmental challenges, we investigated the expression patterns of *GmTRAB1* under drought, ABA, and oxidative stresses using a qRT-PCR system. Drought stimulated the accumulation of the *GmTRAB1* transcript, reaching a peak at 6 h (Figure 2A). Moreover, *GmTRAB1* transcripts increased under ABA stress and reached their highest level at 24 h (Figure 2B). In addition, oxidative stress also resulted in increased *GmTRAB1* expression (Figure 2C).

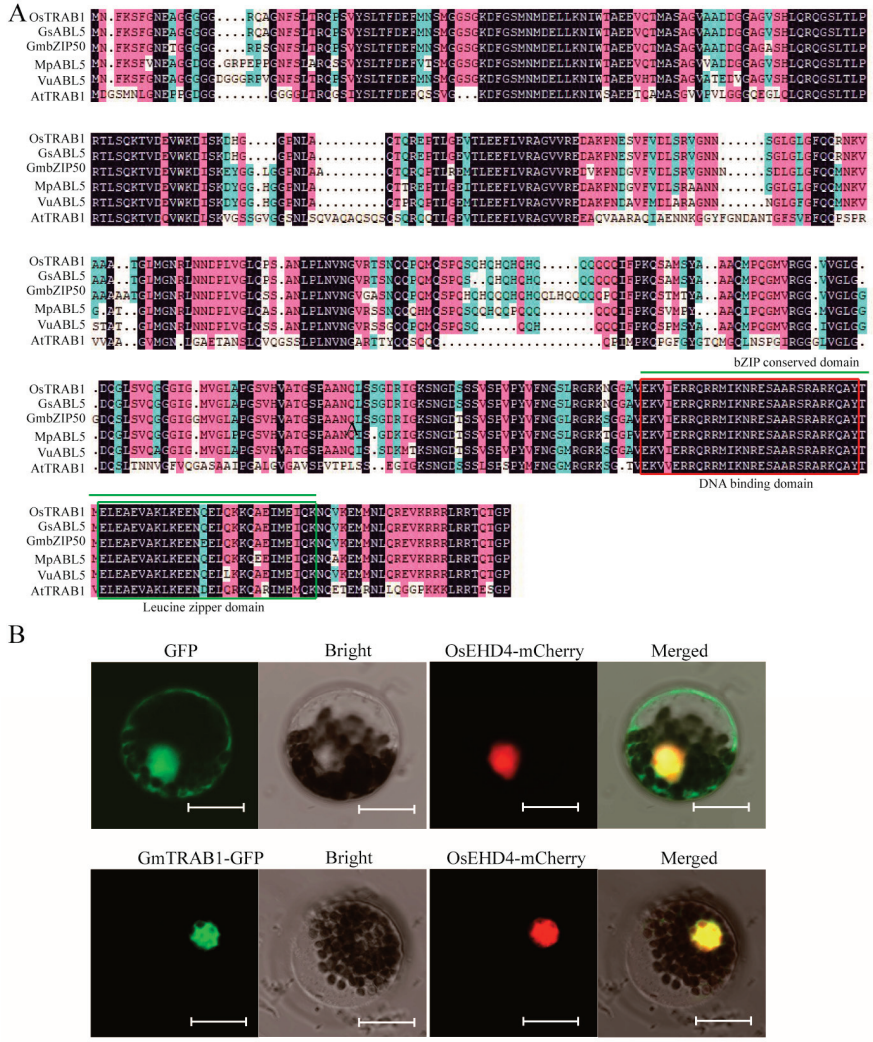

Figure 1. Sequence and localization assay of GmTRAB1. (**A**) Structure analysis of GmTRAB1, GsABL5, GmbZIP50, MpABL5, VuABL5, and AtTRAB1. The bZIP conserved domain is noted with dark lines. The DNA binding domain and leucine zipper domains are marked with red and green rectangles, respectively. (**B**) The subcelluar localization of GmTRAB1. OsEHD4-mCherry is referred to as a nuclear marker. Bar = 12 μm.

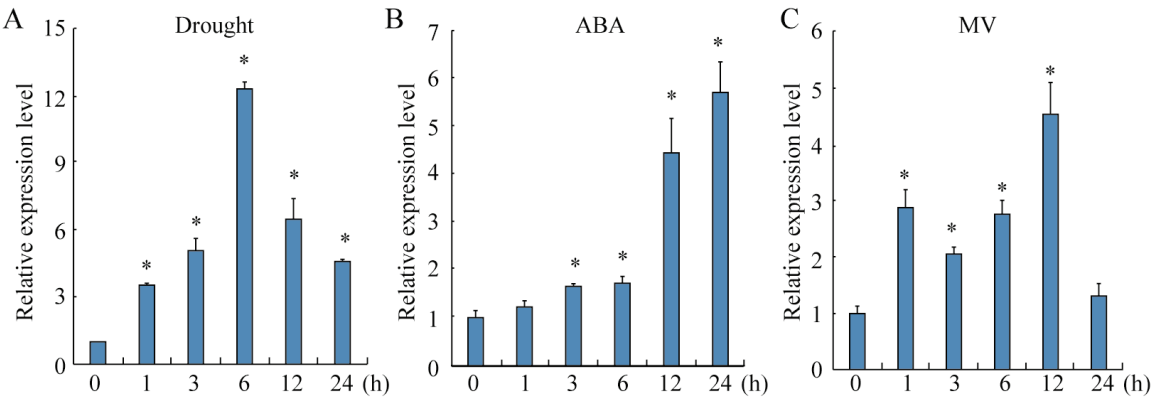

Figure 2. GmTRAB1 was involved in multiple stresses. The expression patterns of *GmTRAB1* under (**A**) drought, (**B**) ABA, and (**C**) MV stresses were detected by qRT-PCR. *GmTubulin* was applied as an internal control. The * suggests significant differences (* $p < 0.05$).

2.3. Overexpression of GmTRAB1 Enhances Arabidopsis Resistance to Drought

To characterize the role of *GmTRAB1* in plants' resistance to drought, we constructed *GmTRAB1*-OE *Arabidopsis* using an *Agrobacterium*-mediated transformation system. The transcript levels of *GmTRAB1* in transgenic plants were detected by semi-qRT-PCR. Three independent homozygous *GmTRAB1*-OE lines (OE1, OE7, and OE12) with relatively high accumulation of *GmTRAB1* transcripts were used for the subsequent functional analysis (Figure 3C,D). *Arabidopsis* plants with similar growth characteristics were applied for osmotic stress tolerance experiments. There was no remarkable difference in plant morphology and physiological metabolism between *GmTRAB1*-OE lines and WT plants under sufficient water conditions. Severe drought stress seriously affected plant growth and physiological metabolism, and obvious differences were detected. Upon drought stress, *GmTRAB1*-OE plants displayed slighter leaf rolling and larger survival rates than the WT plants (Figure 3A,B). Drought usually causes damage to the membranes of plants, restricting their normal growth. The concentration of malonaldehyde (MDA) acted as an indicator to reflect the degree of cell membrane damage. The MDA concentration is proportional to the degree of membrane damage [1]. Proline was an osmoprotectant that functioned crucially in maintaining the stability of the cell membrane and cellular turgor pressure [29,30]. The drought-treated *GmTRAB1*-OE seedlings showed lower MDA levels and larger proline contents as compared with the WT plants (Figure 3E,F).

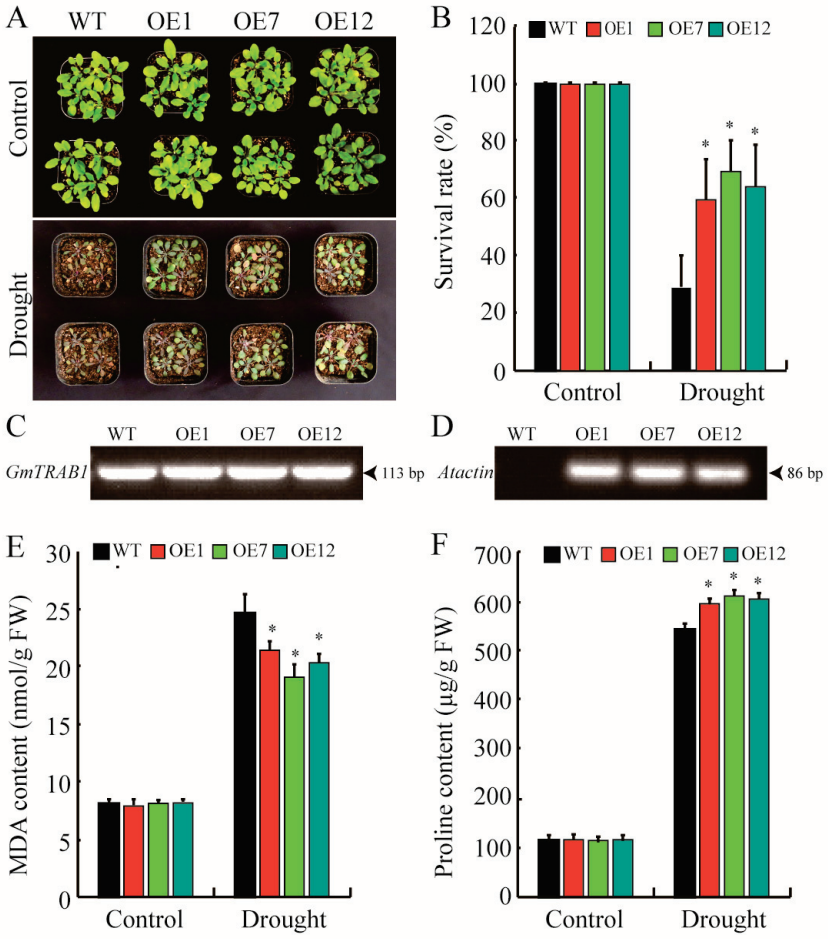

Figure 3. Overexpression of *GmTRAB1* leads to enhanced osmotic stress tolerance in *Arabidopsis*. (**A**) Osmotic stress tolerance assay in *GmTRAB1*-OE and WT plants. (**B**) Survival rates. (**C**,**D**) *GmTRAB1* transcripts were detected by semi-RT-qPCR. *Atactin* was applied as an internal control. (**E**) MDA content and (**F**) proline content in *GmTRAB1*-OE and control plants in response to drought. The data represent the value (±SE) of 3 independent replicates. The * suggests significant differences (* $p < 0.05$).

2.4. GmTRAB1 Overexpression Leads to Increased ABA Sensitivity in Transgenic Plants

Considering that ABA promotes the increase in *GmTRAB1* transcripts, we conducted a seed germination assay to investigate the role of *GmTRAB1* in ABA response. The *GmTRAB1*-OE and WT seeds showed similar germination rates in the absence of ABA (Figure 4A). However, exogenous ABA application inhibited seed germination, but the *GmTRAB1*-OE seeds presented significantly lower germination rates than those of the control with exposure to ABA treatments (Figure 4B,C).

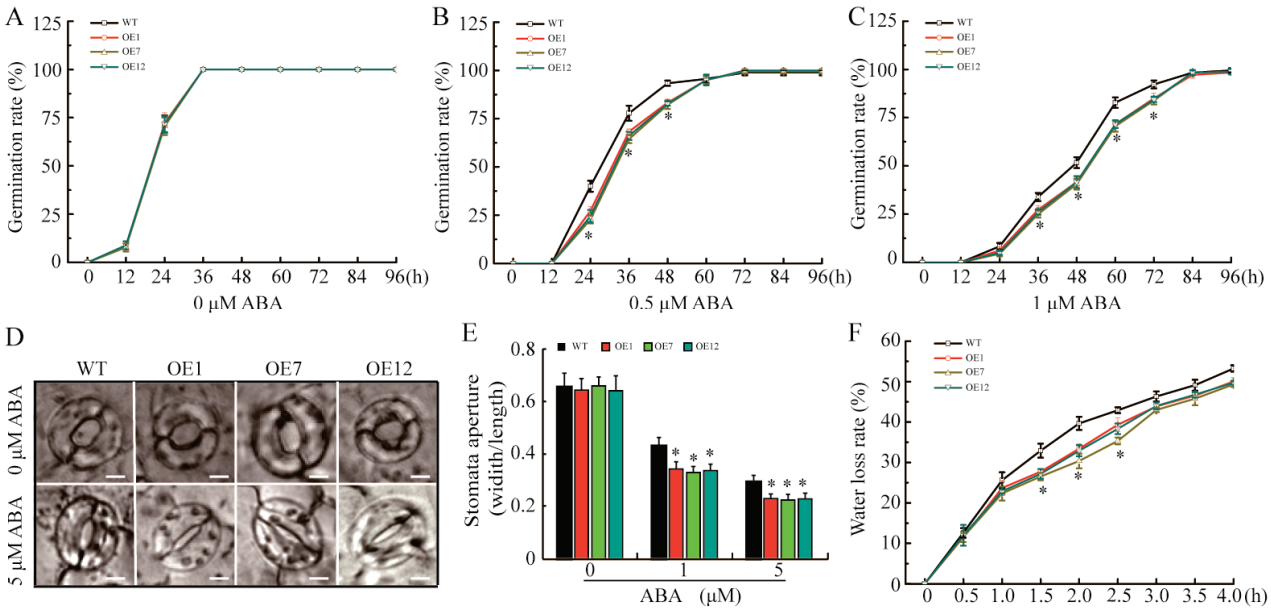

Figure 4. *GmTRAB1* overexpression improved ABA sensitivity in transgenic plants. (**A**–**C**) The germination rates of *GmTRAB1*-OE and WT seeds under 0, 0.5, and 1 μM ABA treatments were analyzed at 0, 12, 24, 36, 48, 60, 72, 84, and 96 h. (**D**) Phenotypes of *GmTRAB1*-OE and WT stomata upon ABA stress, Scale bars = 5 μm. (**E**) Stomatal closure of *GmTRAB1*-OE and WT upon ABA stress. The stomatal width/length ratio was utilized as the stomatal closure index. (**F**) Water loss rate. The detached leaves of *GmTRAB1*-OE and WT plants were calculated at 0, 30, 60, 90, 120, 150, 180, 210, and 240 min. The data represent the value (±SE) of 3 independent replicates. The * suggests significant differences (* $p < 0.05$).

ABA has been demonstrated to influence stomatal movements. In view of *GmTRAB1* overexpression improving ABA sensitivity in transgenic plants, the function of *GmTRAB1* in ABA-regulated stomatal movement was investigated. The stomatal closure index was reflected by the stomatal width/length ratio. Without ABA application, the mean of stomatal apertures between *GmTRAB1*-OE and WT plants is comparable (Figure 4D,E). Nevertheless, with the ABA application, the *GmTRAB1*-OE plants have a significantly lower mean of stomatal apertures as compared to the control plants (Figure 4D,E). Stomatal movement plays a central role in water loss and is closely related to plant adaptation to drought. Therefore, the water loss rates were also analyzed, and *GmTRAB1*-OE exhibited lower water loss rates than WT plants (Figure 4F).

2.5. GmTRAB1 Overexpression Confers Osmotic Stress Tolerance in Transgenic Hairy Roots of Soybean

To verify the role of *GmTRAB1* in soybean resistance to drought, we generated transgenic hairy roots of soybean with *GmTRAB1*-RNA interference (RNAi) silencing or overexpressing by *Agrobacterium rhizogenes*-mediated transformation. The *GmTRAB1* expression was detected through qRT-PCR (Figure 5C). There were no significant differences in the growth and physiological characteristics of *GmTRAB1* transgenic (RNAi and OE) and empty vector (*EV*) control soybean seedlings under suitable conditions. However, drought

treatment caused remarkable morphological and physiological differences among different genotypes. Upon drought stress, the *GmTRAB1*-OE seedlings presented a higher survival rate and a lighter leaf-wilting phenotype than the *EV* seedlings. In contrast, the *GmTRAB1*-RNAi plants displayed a lower survival rate and a heavier leaf-wilting phenotype (Figure 5A,D). The fresh weights of *GmTRAB1*-OE hairy roots were larger than the control roots under drought treatment, but the *GmTRAB1*-RNAi hairy roots displayed lower biomass accumulations (Figure 5B,E). Moreover, the MDA levels in *GmTRAB1*-OE hairy roots were smaller than in the control roots under drought stress, whereas the *GmTRAB1*-RNAi hairy roots presented higher MDA accumulations (Figure 5F). In addition, the *GmTRAB1*-OE hairy roots presented a higher accumulation of proline than the control roots. However, under drought stress, the *GmTRAB1*-RNAi soybean roots had lower levels of proline (Figure 5G).

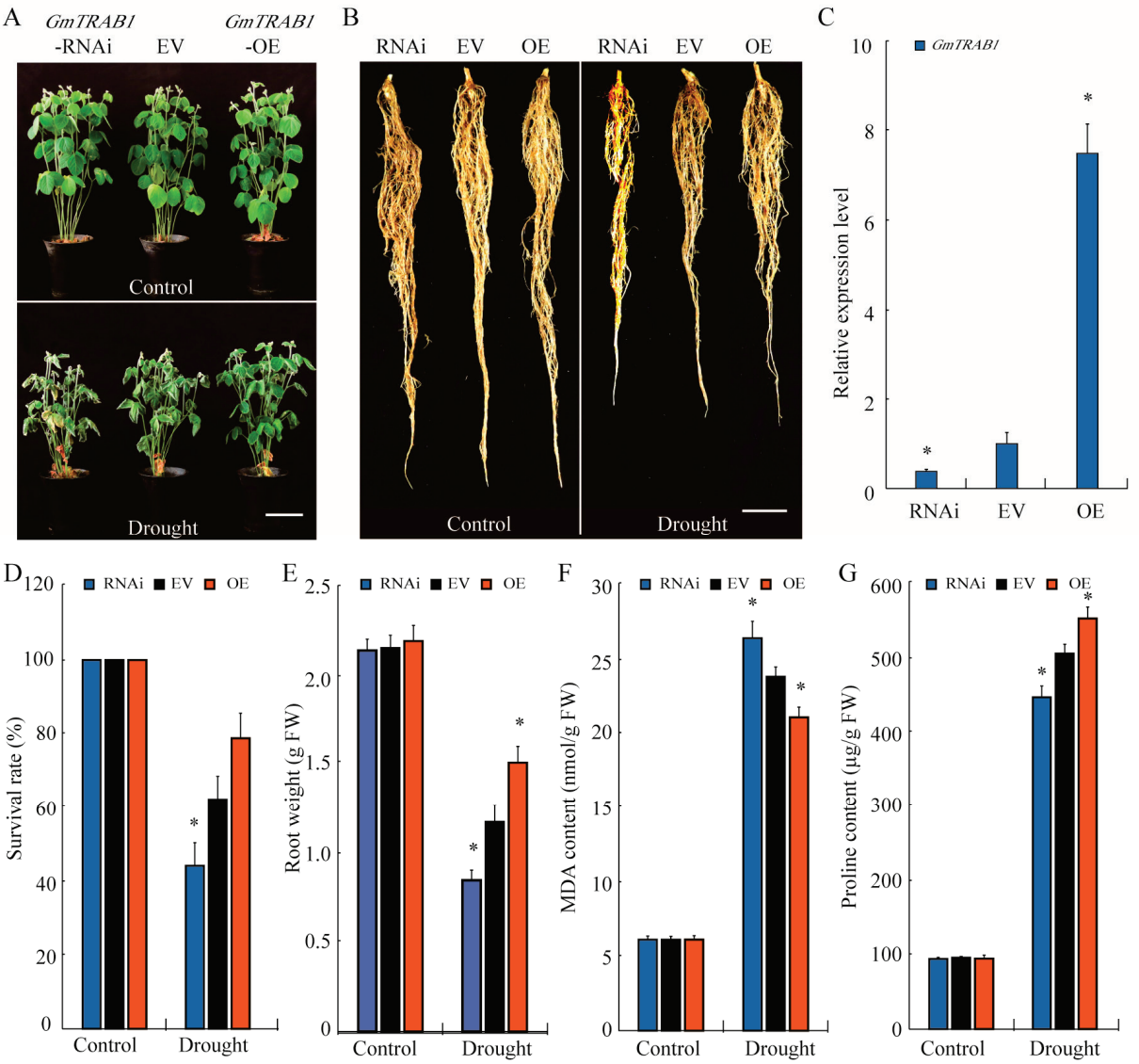

Figure 5. Overexpression of *GmTRAB1* results in improved osmotic stress tolerance in soybean. (**A**,**B**) Phenotypes of *GmTRAB1*-OE, *EV*, and *GmTRAB1*-RNAi soybean plants and hairy roots in response to drought. Scale bars = 3 cm. (**C**) GmTRAB1 transcripts were detected by qRT-PCR. *Gmtubulin* was applied as an internal control. (**D**) Survival rate, (**E**) fresh weight, (**F**) MDA content, and (**G**) proline content in *GmTRAB1*-OE, *EV*, and *GmTRAB1*-RNAi plants in response to drought. The data represent the value (±SE) of 3 independent replicates. The * suggests significant differences (* $p < 0.05$).

2.6. GmTRAB1 Stimulates ROS Scavenging in Response to Drought

Drought caused the excessive production of reactive oxygen species (ROS) that seriously restricted the growth and development of plants. The results of DAB staining and quantitative measurement illustrated that hydrogen peroxide (H_2O_2) accumulation in *GmTRAB1* transgenic hairy roots was comparable to that of the *EV* control roots. With exposure to drought, the H_2O_2 accumulations in *GmTRAB1*-RNAi, *EV*, and *GmTRAB1*-OE hairy roots are increased. Interestingly, significant differences were observed among *GmTRAB1*-RNAi, *EV*, and *GmTRAB1*-OE hairy roots. *GmTRAB1*-RNAi seedlings accumulated a larger H_2O_2 content in comparison with the *EV* control roots, but the *GmTRAB1*-OE hairy roots exhibited a smaller accumulation of H_2O_2 (Figure 6A,B). Antioxidant enzymes play a critical role in eliminating drought-induced ROS. The activity of antioxidant enzymes was measured. After drought treatment, compared with the control, the *GmTRAB1*-OE roots displayed greater enzyme activity of catalase (CAT) and peroxidase (POD). Nevertheless, the *GmTRAB1*-RNAi roots had lower activities of CAT and POD enzymes (Figure 6C,D).

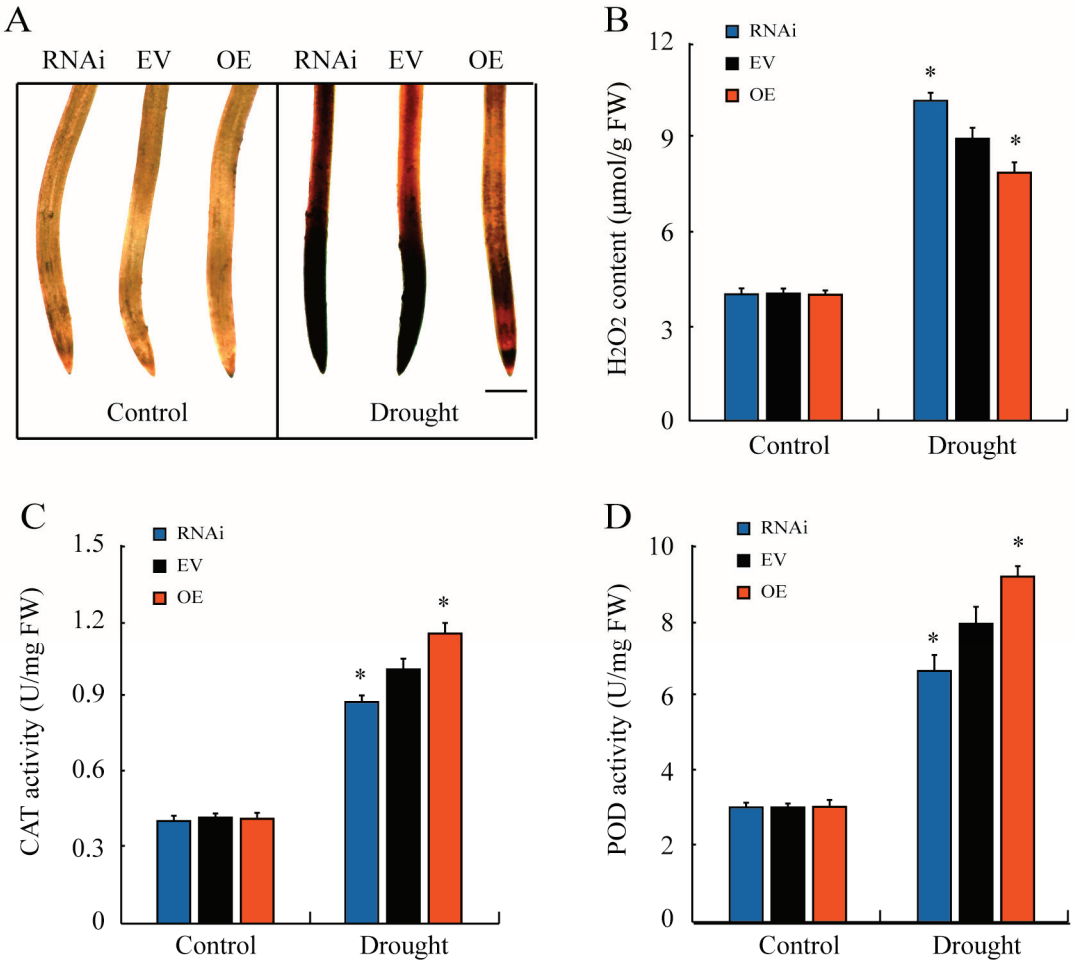

Figure 6. *GmTRAB1* increased ROS scavenging under drought stress. (**A**) DAB staining, scale bars = 0.1 cm; (**B**) H_2O_2 content; (**C**) CAT activity; and (**D**) POD activity of *GmTRAB1* transgenic (RNAi and OE) and *EV* roots under drought treatment. The data represent the value (±SE) of 3 independent replicates. The * suggests significant differences (* $p < 0.05$).

2.7. GmTRAB1 Increases Drought-, ABA-, and Antioxidant-Related Gene Expression in Response to Drought

To gain sight into the GmTRAB1-mediated adaptative mechanism in response to drought, the transcripts of drought-, ABA-, and antioxidant-related genes in *GmTRAB1*-RNAi, *EV*, and *GmTRAB1*-OE hairy roots upon drought stress were detected through qRT-

PCR. No noticeable difference among *GmTRAB1*-RNAi, *EV*, and *GmTRAB1*-OE hairy roots was detected prior to drought treatment. Drought altered the expression of stress-related genes, and the expression of drought-induced genes (*GmDRAB1A*, *GmWRKY27*, and *GmCIPK6*), ABA-responsive genes (*GmP5CS*, *GmLEA5*, and *GmNAC6*), and antioxidant-related genes (*GmPOD3*, *GmPOD5*, and *GmCAT4*) in drought-treated hairy roots of *GmTRAB1*-OE were much greater than those of *EV* hairy roots. In contrast, lower transcript accumulation of the above genes was detected in the *GmTRAB1*-RNAi hairy roots under drought stress (Figure 7).

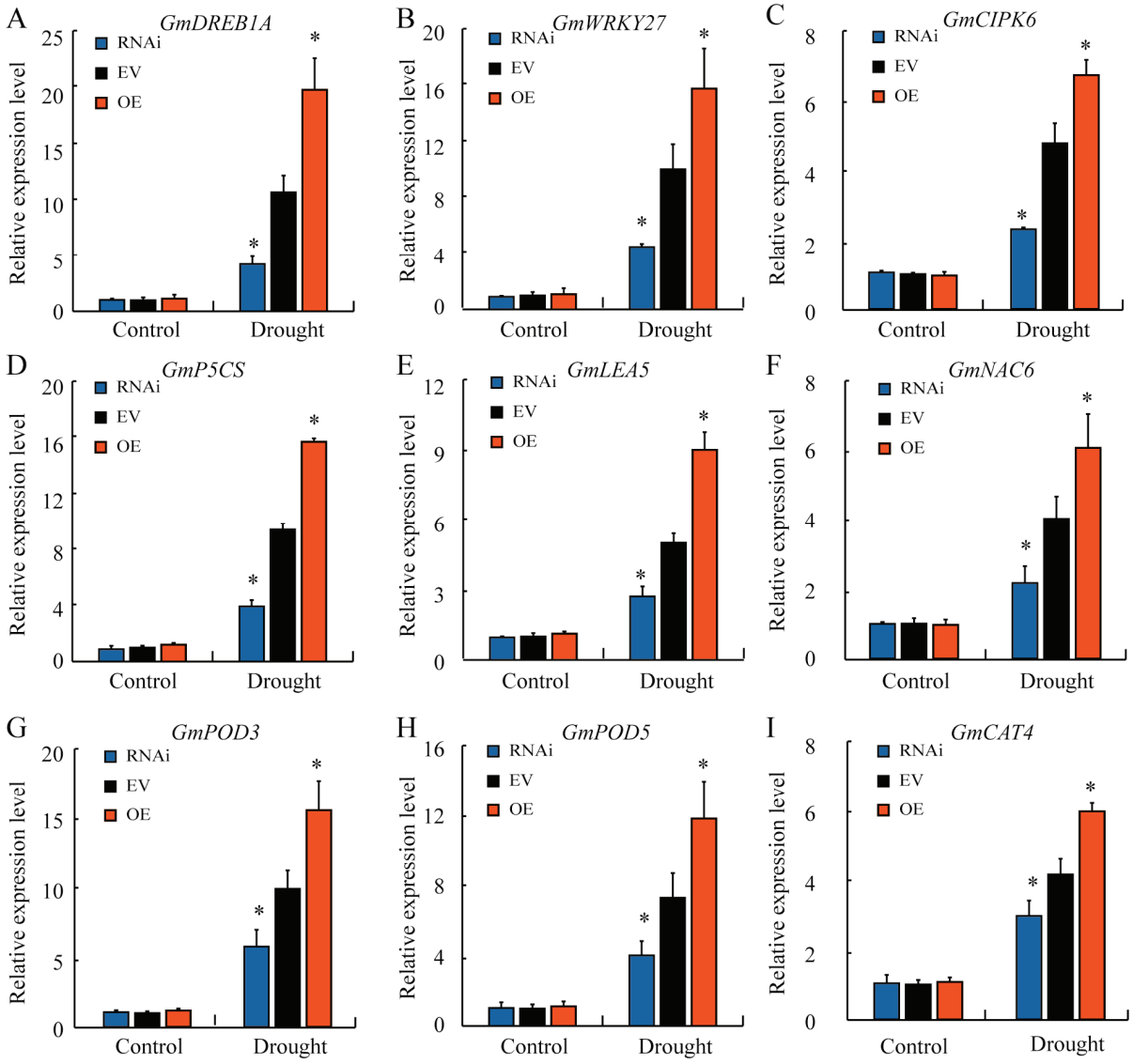

Figure 7. GmTRAB1 activates stress-responsive gene expression. Transcript level of (**A**) *GmDRAB1A*, (**B**) *GmWRKY27*, (**C**) *GmCIPK6*, (**D**) *GmP5CS*, (**E**) *GmLEA5*, (**F**) *GmNAC6*, (**G**) *GmPOD3*, (**H**) *GmPOD5*, and (**I**) GmCAT4 in *GmTRAB1*-RNAi, *EV*, and *GmTRAB1*-OE hairy roots under drought stress. The data represent the value (±SE) of 3 independent replicates. The * suggests significant differences (* $p < 0.05$).

3. Discussion

Drought is usually considered the main environmental constraint that restricts crop quality and production [25]. Members of the bZIP transcription factor have been demonstrated to participate in modulating plant adaptation to drought. Nonetheless, the biological roles of bZIP proteins in enhancing soybean drought tolerance are still unclear. In this

study, drought led to increased expression of the bZIP gene *GmTRAB1* (Figure 2A). Further functional analysis verified that *GmTRAB1*-OE *Arabidopsis* seedlings and soybean hairy roots displayed drought-resistant phenotypes. On the contrary, the *GmTRAB1*-RNAi soybean hairy roots were much more sensitive to drought (Figures 3 and 5). These results indicated that GmTRAB1 positively regulates the osmotic stress tolerance of soybean.

The phytohormone ABA serves as a kind of pivotal signaling molecule that has critical roles in modulating plant response to drought [31]. Drought results in an increase in endogenous ABA, and the increased ABA subsequently alters the transcript accumulation of stress-related genes and stomatal movement in response to drought [32]. It has been shown that members of bZIPs are implicated in ABA-regulated adaptation to drought. For example, OsbZIP42 and OsbZIP71 have been demonstrated to modulate drought adaptation via an ABA-dependent manner [20,33]. In this assay, exogenous ABA induced the accumulation of the *GmTRAB1* transcript (Figure 2B). Moreover, with exposure to ABA treatment, the *GmTRAB1*-OE plants exhibited lower seed germination rate and smaller stomatal aperture as compared with the control plants (Figure 4B–E). Interestingly, GmTRAB1 has a role in reducing the water loss rate (Figure 4F). Additionally, upon drought stress, GmTRAB1 promoted the transcript accumulation of ABA-responsive genes, including *GmP5CS*, *GmLEA5*, and *GmNAC6* (Figure 7D–F). These results imply that GmTRAB1 is associated with modulating ABA-regulated stomatal closure and stress-responsive gene expression to regulate soybean adaptability to drought.

Drought usually stimulates the generation of ROS, including H_2O_2 and O_2^- [34]. The overproduced ROS results in a series of cell toxicity effects, such as membrane damage, nucleic acid and protein degradation, and disruption of enzyme activity [35]. The MDA level is usually used as an important parameter to reflect the degree of cell membrane damage under stress conditions, which is negatively implicated with osmotic stress tolerance in plants [1]. The bZIP proteins have been demonstrated to influence the scavenging of ROS under adverse conditions. For example, HvbZIP21 was implicated in the scavenging of ROS to improve the osmotic stress tolerance in barley [36]. In the assay, oxidative stress induced the expression of *GmTRAB1* (Figure 2C). Subsequent quantitative measurements showed that under drought stress, compared to the control, the hairy roots of *GmTRAB1*-OE accumulated a lower content of MDA and H_2O_2, whereas the MDA and H_2O_2 levels in *GmTRAB1*-RNAi hairy roots were larger (Figures 3E, 5F and 6A,B). Proline is a pivotal osmolyte that functions critically in maintaining ROS homeostasis and stabilizing cell membranes under adverse conditions [29,30]. The proline content of *GmTRAB1*-OE hairy roots under drought stress was larger. Nevertheless, the drought-treated *GmTRAB1*-RNAi hairy roots demonstrated a lower proline level. Moreover, GmTRAB1 activated the expression of *GmP5CS* (Figure 7D). Therefore, GmTRAB1 was associated with promoting the generation of proline to reduce drought-induced oxidative damage in soybean.

To mitigate oxidative damage, plants have built complicated antioxidant defense systems to remove the excessive ROS [37]. Antioxidant enzymes, including CAT, POD, and SOD, are essential parts of the antioxidant defense system [34]. The bZIPs have been reported to influence antioxidant enzyme activity to eliminate ROS under adverse conditions. For example, VvbZIP45 participated in increasing the enzyme activity of POD, SOD, and CAT to eliminate ROS under drought stress [38]. IbbZIP1 has been shown to enhance SOD activity to eliminate H_2O_2 under drought and salt stresses [39]. In this research, GmTRAB1 was found to increase the transcript of antioxidant enzyme genes *GmPOD3*, *GmPOD5*, and *GmCAT4* (Figure 7G–I). Furthermore, compared with the control, the enzyme activity of CAT and POD in *GmTRAB1*-OE hairy roots under drought stress was larger. Nevertheless, the *GmTRAB1*-RNAi hairy roots exhibited minor CAT activity and POD activity in response to drought (Figure 6C,D). Collectively, GmTRAB1 has a role in promoting the antioxidant defense system to eliminate ROS and alleviate drought stress in soybean.

The bZIP transcription factors have been shown to alter drought-related gene expression in response to drought. TabZIP156 was found to increase *TaDREB1A* expression in

wheat in response to drought [40]. It has been demonstrated that VlbZIP30 promotes the expression of *NAC17*, *ABF2*, *PUB19*, and *PP2C9* to enhance grapevine drought tolerance [41]. In this study, GmTRAB1 functioned in improving the transcript accumulations of *GmDREB1A*, *GmCIPK6*, and *GmWRKY27* in response to drought (Figure 7A–C). DREB and WRKY transcription factors play crucial functions in increasing plant adaptability to extreme conditions [42,43]. CIPKs have been shown to participate in regulating hormone signaling, ROS scavenging, and the biosynthesis of antioxidants in response to drought [44]. The above results indicated that GmTRAB1 is implicated in stimulating the expression of drought-related genes, thereby promoting the resistance of soybean to drought.

4. Materials and Methods

4.1. Plant Materials and Growth Conditions

Arabidopsis Columbia-0 and soybean cultivar Williams 82 were used for plant transformation and molecular analysis. The soybean seedlings were cultured in a growth chamber at 70% relative humidity, 25 °C, and a 16 h light/8 h dark photoperiod. To analyze the expression profiles of *GmTRAB1* under drought and oxidative stress treatments, the roots of soybean seedlings (2-week-old) were immersed in 15% PEG6000 and 20 μM methyl viologen (MV) solution, respectively. The leaves of seedlings sprayed with 100 μM ABA were used to investigate *GmTRAB1* expression profiles upon ABA treatment. The leaves were collected at 0, 1, 3, 6, 12, and 24 h, respectively. *Arabidopsis* seedlings were growing in an illumination incubator at 70% relative humidity, 25 °C, and a 16 h light/8 h dark photoperiod.

4.2. Construction of Phylogenetic Tree

GmTRAB1 homologous proteins were retrieved from the non-redundant protein sequence database (https://blast.ncbi.nlm.nih.gov/Blast.cgi?CMD=Get&RID=JEV01RW2016, accessed on 31 October 2024). The amino acid sequence of the *Arabidopsis* bZIP proteins was downloaded from TAIR (https://www.arabidopsis.org/results?mainType=general&searchTex, accessed on 31 October 2024). The ClustalX program in MEGA7.0 software was used to perform multiple sequence alignment. The bootstrap neighbor-joining phylogenetic tree was generated by MEGA7.0 software with 500 bootstrap replicates. Ten different subgroups of AtbZIPs were used as references to classify GmTRAB1 and its homologous proteins. The accession numbers of GmTRAB1 homologous proteins and *Arabidopsis* bZIPs were listed in Table S2.

4.3. Quantative Real Time-PCR

The total RNA from plants was isolated with Trizol reagent, and then the genome DNA was eliminated by RNase-free DNaseI (TransGen, Beijing, China). The cDNA synthesis was performed by the TransScript One-Step RT-PCR SuperMix Kit (TransGen, Beijing, China). The qRT-PCR reactions were then conducted with a TransStart Top Green qPCR SuperMix kit using an ABI 7500 machine. The specific primers used in qRT-PCR were presented in Table S1. *Atactin* (At3g18780) and *GmTubulin* (Glyma.08G014200) were referred to as quantitative controls for *Arabidopsis* and soybean, respectively. The $2^{-\Delta\Delta CT}$ method was applied for quantitative analysis. The reaction of qRT-PCR was conducted by the procedure of 95 °C (180 s), then 42 cycles of 95 °C (10 s), 57 °C (15 s), and 72 °C (45 s).

4.4. Subcellular Localization Analyses

To analyze the subcellular localization, we produced *GmTRAB1*-GFP constructs. *GmTRAB1*-GFP and *OsEHD4*-mCherry plasmids were introduced into the same protoplasts from *Arabidopsis*, and then the protoplasts were cultured in the dark (23 °C) for 12 h. OsEHD4-mCherry was applied as a nuclear marker [28]. The florescence signals of GFP and mCherry were detected with a confocal laser-scanning microscope.

4.5. Construction of Transgenic Arabidopsis and Soybean Plants

To construct *GmTRAB1*-OE *Arabidopsis* plants, the pCAMBIA1302-*GmTRAB1* plasmids were generated and then introduced into *Arabidopsis* via the *Agrobacterium*-mediated floral-dip method [31].

The transgenic soybean plants were generated using the *Agrobacterium rhizogene*-mediated soybean hairy roots transformation system, as described previously [31,42]. To generate the *GmTRAB1*-RNAi vector, a 120-bp-specific DNA fragment of *GmTRAB1* was cloned, and then these fragments were collected and connected to both sense and antisense orientations to flank the intron 6 of the rice zinc finger type family protein gene. The *GmTRAB1*-RNAi fragment was then inserted into the pCAMBIA3301 transformation vector driven by the *CaMV* 35S promoter. The full-length open reading frame of *GmTRAB1* was introduced into pCAMBIA3301 to generate the *GmTRAB1*-OE vector. The *GmTRAB1*-RNAi and *GmTRAB1*-OE vectors were transformed into K599 *Agrobacterium rhizogenes* strains, which were then applied for infecting hypocotyls of soybean to gain transgenic soybean hairy roots.

4.6. Osmotic Stress Tolerance Assay

For *Arabidopsis*, homozygous T3 seedlings of the *GmTRAB1*-OE and WT seedlings (1-week-old) were used for drought treatment. After normal culturing in the illumination incubator for 21 d, the *GmTRAB1*-OE and WT seedlings were subject to drought stress without irrigation for another 17 d until remarkable leaf-wilting differences were identified.

For soybean, 2-week-old *GmTRAB1*-OE, *EV*, and *GmTRAB1*-RNAi soybean seedlings were grown normally in a mixed soil (1:1 vermiculite:humus) for 7 d. These seedlings were then exposed to drought stress with 15% PEG6000 irrigation for another 10 d until remarkable differences in leaf wilting were identified.

4.7. Measurements of Physiological Characteristics

Arabidopsis seedlings (4-week-old) and soybean seedlings (3-week-old) were exposed to drought treatment with irrigating 15% PEG6000 solution for 10 d. The *Arabidopsis* leaves and soybean hairy roots were collected for measuring physiological parameters. The MDA content, proline content, hydrogen peroxide H_2O_2 content, peroxidase POD activity, and CAT activity were detected by their corresponding detection kits.

4.8. Analysis of Seed Germination, Stomatal Closure, and Water Loss Rate

For measurement of germination rate, homozygous T3 seeds of *GmTRAB1*-OE and WT were sterilized and sown on 1/2-strength Murashige and Skoog media containing 0, 0.5, and 1 μM ABA. After vernalization in the dark for 3 days, the germination rates in terms of the seed radicle emergence were counted at 0, 12, 24, 36, 48, 60, 72, 84, and 96 h, respectively.

For the water loss rate analysis, the detached rosette leaves of 4-week-old *GmTRAB1*-OE and WT Arabidopsis were measured at 0, 30, 60, 120, 180, 21, and 240 using a 1/10,000 analytical balance, respectively. The water loss rate was computed as reported previously.

For the stomatal closure analysis, the detached rosette leaves of *GmTRAB1*-OE and WT *Arabidopsis* (4-week-old) were treated with stomata opening solution (7.5 mM iminodiacetic acid, pH = 6.15, 10 mM KCl, and 10 mM MES-Tris) and exposed to bright light. Until the stomata were fully opened, the leaves were exchanged into solutions supplemented with 0, 1, and 5 μM ABA and incubated for another 2.5 h.

4.9. Statistical Analyses

Each experiment was independently conducted three times. Data are presented as the mean ± SE of the three independent replicates. Statistical analysis was performed with the SPSS 27.0 software. The one-way analysis of variance (ANOVA) method was applied to verify significant differences, marked as *, $p < 0.05$.

5. Conclusions

In this study, GmTRAB1 played a positive regulatory role in improving the osmotic stress tolerance of soybean. GmTRAB1 participated in ABA-regulated stomatal closure and stress-related gene expression to regulate the drought stress response. Furthermore, GmTRAB1 was involved in activating the antioxidant defense system to promote the scavenging of ROS under drought stress. Additionally, GmTRAB1 has a role in activating drought-related genes in drought stress response. In summary, these results will provide the theoretical basis for elucidating the molecular mechanism of bZIP transcription factors-mediated drought response in soybean.

Supplementary Materials: The following supporting information can be downloaded at: https://www.mdpi.com/article/10.3390/plants13213104/s1, Figure S1: Phylogenetic analysis of GmTRAB1, GsABL5, GmbZIP50, MpABL5, VuABL5, and *Arabidopsis* bZIP transcription factors. GmTRAB1 and its homologous proteins were divided into the subgroup A; Table S1: Primers used in qRT-PCR assays; Table S2: Accession numbers of bZIPs used for phylogenetic analysis.

Author Contributions: X.-Y.C. designed the experiments, coordinated the project, and finalized the paper; H.L. and Q.-Y.Z. performed experiments, analyzed data, and wrote the paper; P.X. and X.-H.W. performed experiments and conducted the bioinformatic work; Z.-N.L., S.-J.D., M.X. and X.C. performed experiments. All authors have read and agreed to the published version of the manuscript.

Funding: This research was financially supported by the Natural Science Foundation of Shandong Province (No. ZR2020QC123) and the National Natural Science Foundation of China (No. 32001459).

Data Availability Statement: Data is contained within the article or Supplementary Material.

Conflicts of Interest: The authors declare no conflicts of interests.

References

1. Yu, T.F.; Liu, Y.; Fu, J.D.; Ma, J.; Fang, Z.W.; Chen, J.; Zheng, L.; Lu, Z.W.; Zhou, Y.B.; Chen, M.; et al. The NF-Y-PYR module integrates the abscisic acid signal pathway to regulate plant stress tolerance. *Plant Biotechnol. J.* **2021**, *19*, 2589–2605. [CrossRef] [PubMed]
2. Li, Z.; Fu, D.; Wang, X.; Zeng, R.; Zhang, X.; Tian, J.; Zhang, S.; Yang, X.; Tian, F.; Lai, J.; et al. The transcription factor bZIP68 negatively regulates cold tolerance in maize. *Plant Cell* **2022**, *34*, 2833–2851. [CrossRef] [PubMed]
3. Kidokoro, S.; Watanabe, K.; Ohori, T.; Moriwaki, T.; Maruyama, K.; Mizoi, J.; Myint Phyu Sin Htwe, N.; Fujita, Y.; Sekita, S.; Shinozaki, K.; et al. Soybean DREB1/CBF-type transcription factors function in heat and drought as well as cold stress-responsive gene expression. *Plant J.* **2015**, *81*, 505–518. [CrossRef] [PubMed]
4. Wei, W.; Liang, D.W.; Bian, X.H.; Shen, M.; Xiao, J.H.; Zhang, W.K.; Ma, B.; Lin, Q.; Lv, J.; Chen, X.; et al. GmWRKY54 improves drought tolerance through activating genes in abscisic acid and Ca^{2+} signaling pathways in transgenic soybean. *Plant J.* **2019**, *100*, 384–398. [CrossRef]
5. Zhang, L.; Zhao, L.; Wang, L.; Liu, X.; Yu, Z.; Liu, J.; Wu, W.; Ding, L.; Xia, C.; Zhang, L.; et al. TabZIP60 is involved in the regulation of ABA synthesis-mediated salt tolerance through interacting with TaCDPK30 in wheat (*Triticum aestivum* L.). *Planta* **2023**, *257*, 107. [CrossRef]
6. Ma, H.; Liu, C.; Li, Z.; Ran, Q.; Xie, G.; Wang, B.; Fang, S.; Chu, J.; Zhang, J. ZmbZIP4 contributes to stress resistance in maize by regulating ABA synthesis and root development. *Plant Physiol.* **2018**, *178*, 753–770. [CrossRef] [PubMed]
7. Jakoby, M.; Weisshaar, B.; Droge-Laser, W.; Vicente-Carbajosa, J.; Tiedemann, J.; Kroj, T.; Parcy, F. bZIP transcription factors in *Arabidopsis*. *Trends Plant Sci.* **2002**, *7*, 106–111. [CrossRef]
8. Landschulz, W.H.; Johnson, P.F.; McKnight, S.L. The leucine zipper: A hypothetical structure common to a new class of DNA binding proteins. *Science* **1988**, *240*, 1759–1764. [CrossRef]
9. Izawa, T.; Foster, R.; Chua, N.H. Plant bZIP protein DNA binding specificity. *J. Mol. Biol.* **1993**, *230*, 1131–1144. [CrossRef]
10. Nijhawan, A.; Jain, M.; Tyagi, A.K.; Khurana, J.P. Genomic survey and gene expression analysis of the basic leucine zipper transcription factor family in rice. *Plant Physiol.* **2007**, *146*, 333–350. [CrossRef]
11. Pourabed, E.; Ghane Golmohamadi, F.; Soleymani Monfared, P.; Razavi, S.M.; Shobbar, Z.S. Basic leucine zipper family in barley: Genome-wide characterization of members and expression analysis. *Mol. Biotechnol.* **2015**, *57*, 12–26. [CrossRef] [PubMed]
12. Li, D.; Fu, F.; Zhang, H.; Song, F. Genome-wide systematic characterization of the bZIP transcriptional factor family in tomato (*Solanum lycopersicum* L.). *BMC Genom.* **2015**, *16*, 771. [CrossRef] [PubMed]
13. Zhou, Y.; Xu, D.; Jia, L.; Huang, X.; Ma, G.; Wang, S.; Zhu, M.; Zhang, A.; Guan, M.; Lu, K.; et al. Genome-wide identification and structural analysis of bZIP transcription factor genes in *Brassica napus*. *Genes* **2017**, *8*, 288. [CrossRef] [PubMed]

14. Wang, J.; Zhou, J.; Zhang, B.; Vanitha, J.; Ramachandran, S.; Jiang, S.Y. Genome-wide expansion and expression divergence of the basic leucine zipper transcription factors in higher plants with an emphasis on Sorghum. *J. Integr. Plant Biol.* **2011**, *53*, 212–231. [CrossRef] [PubMed]
15. Wei, K.; Chen, J.; Wang, Y.; Chen, Y.; Chen, S.; Lin, Y.; Pan, S.; Zhong, X.; Xie, D. Genome-wide analysis of bZIP-encoding genes in maize. *DNA Res.* **2012**, *19*, 463–476. [CrossRef]
16. Sun, X.L.; Li, Y.; Cai, H.; Bai, X.; Ji, W.; Ding, X.D.; Zhu, Y.M. The *Arabidopsis* AtbZIP1 transcription factor is a positive regulator of plant tolerance to salt, osmotic and drought stresses. *J. Plant Res.* **2012**, *125*, 429–438. [CrossRef]
17. Yoshida, T.; Fujita, Y.; Sayama, H.; Kidokoro, S.; Maruyama, K.; Mizoi, J.; Shinozaki, K.; Yamaguchi-Shinozaki, K. AREB1, AREB2, and ABF3 are master transcription factors that cooperatively regulate ABRE-dependent ABA signaling involved in drought stress tolerance and require ABA for full activation. *Plant J.* **2010**, *61*, 672–685. [CrossRef]
18. Xiang, Y.; Tang, N.; Du, H.; Ye, H.Y.; Xiong, L.Z. Characterization of OsbZIP23 as a key player of the basic leucine zipper transcription factor family for conferring abscisic acid sensitivity and salinity and drought tolerance in rice. *Plant Physiol.* **2008**, *148*, 1938–1952. [CrossRef]
19. Lu, G.; Gao, C.; Zheng, X.; Han, B. Identification of OsbZIP72 as a positive regulator of ABA response and drought tolerance in rice. *Planta* **2009**, *229*, 605–615. [CrossRef]
20. Joo, J.; Lee, Y.H.; Song, S.I. OsbZIP42 is a positive regulator of ABA signaling and confers drought tolerance to rice. *Planta* **2019**, *249*, 1521–1533. [CrossRef]
21. Bi, C.; Yu, Y.; Dong, C.; Yang, Y.; Zhai, Y.; Du, F.; Xia, C.; Ni, Z.; Kong, X.; Zhang, L. The bZIP transcription factor TabZIP15 improves salt stress tolerance in wheat. *Plant Biotechnol. J.* **2021**, *19*, 209–211. [CrossRef] [PubMed]
22. Yao, L.; Hao, X.Y.; Cao, H.L.; Ding, C.Q.; Yang, Y.J.; Wang, L.; Wang, X.C. ABA-dependent bZIP transcription factor, CsbZIP18, from *Camellia sinensis* negatively regulates freezing tolerance in *Arabidopsis*. *Plant Cell Rep.* **2020**, *39*, 553–565. [CrossRef]
23. Gai, W.X.; Ma, X.; Qiao, Y.M.; Shi, B.H.; Ul Haq, S.; Li, Q.H.; Wei, A.M.; Liu, K.K.; Gong, Z.H. Characterization of the bZIP transcription factor family in pepper (*Capsicum annuum* L.): CabZIP25 positively modulates the salt tolerance. *Front. Plant Sci.* **2020**, *11*, 139. [CrossRef] [PubMed]
24. Wei, W.; Lu, L.; Bian, X.H.; Li, Q.T.; Han, J.Q.; Tao, J.J.; Yin, C.C.; Lai, Y.C.; Li, W.; Bi, Y.D.; et al. Zinc-finger protein GmZF351 improves both salt and drought stress tolerance in soybean. *J. Integr. Plant Biol.* **2023**, *65*, 1636–1650. [CrossRef]
25. Yuan, X.B.; Jiang, X.Y.; Zhang, M.Z.; Wang, L.F.; Jiao, W.; Chen, H.T.; Mao, J.R.; Ye, W.X.; Song, Q.X. Integrative omics analysis elucidates the genetic basis underlying seed weight and oil content in soybean. *Plant Cell* **2024**, *36*, 2160–2175. [CrossRef]
26. Zhang, Z.; Ma, J.; Yang, X.; Liu, Z.; Liu, Y.; Liu, X.; Liang, S.; Duan, Z.; Wang, Z.; Yang, X.; et al. Natural allelic diversities of GmPrx16 confer drought tolerance in soybean. *Plant Biotechnol. J.* **2024**, *22*, 535–537. [CrossRef]
27. Zhang, M.; Liu, Y.; Shi, H.; Guo, M.; Chai, M.; He, Q.; Yan, M.; Cao, D.; Zhao, L.; Cai, H.; et al. Evolutionary and expression analyses of soybean basic Leucine zipper transcription factor family. *BMC Genom.* **2018**, *19*, 159. [CrossRef]
28. Gao, H.; Zheng, X.M.; Fei, G.; Chen, J.; Jin, M.; Ren, Y.; Wu, W.; Zhou, K.; Sheng, P.; Zhou, F.; et al. Ehd4 encodes a novel and oryza-genus-specific regulator of photoperiodic flowering in rice. *PLoS Genet.* **2013**, *9*, e1003281. [CrossRef] [PubMed]
29. Gou, C.; Huang, Q.; Rady, M.M.; Wang, L.; Ihtisham, M.; El-Awady, H.H.; Seif, M.; Alazizi, E.M.Y.; Eid, R.S.M.; Yan, K.; et al. Integrative application of silicon and/or proline improves Sweet corn (*Zea mays* L. saccharata) production and antioxidant defense system under salt stress condition. *Sci. Rep.* **2023**, *13*, 18315. [CrossRef]
30. Hayat, S.; Hayat, Q.; Alyemeni, M.N.; Wani, A.S.; Pichtel, J.; Ahmad, A. Role of proline under changing environments: A review. *Plant Signal. Behav.* **2012**, *7*, 1456–1466. [CrossRef]
31. Xu, M.; Li, H.; Liu, Z.N.; Wang, X.H.; Xu, P.; Dai, S.J.; Cao, X.; Cui, X.Y. The soybean CBL-interacting protein kinase, GmCIPK2, positively regulates drought tolerance and ABA signaling. *Plant Physiol. Biochem.* **2021**, *167*, 980–989. [CrossRef] [PubMed]
32. Liu, Y.; Yu, T.F.; Li, Y.T.; Zheng, L.; Lu, Z.W.; Zhou, Y.B.; Chen, J.; Chen, M.; Zhang, J.P.; Sun, G.Z.; et al. Mitogen-activated protein kinase TaMPK3 suppresses ABA response by destabilising TaPYL4 receptor in wheat. *New Phytol.* **2022**, *236*, 114–131. [CrossRef] [PubMed]
33. Liu, C.; Mao, B.; Ou, S.; Wang, W.; Liu, L.; Wu, Y.; Chu, C.; Wang, X. OsbZIP71, a bZIP transcription factor, confers salinity and drought tolerance in rice. *Plant Mol. Biol.* **2014**, *84*, 19–36. [CrossRef] [PubMed]
34. Xiang, Y.; Bian, X.; Wei, T.; Yan, J.; Sun, X.; Han, T.; Dong, B.; Zhang, G.; Li, J.; Zhang, A. ZmMPK5 phosphorylates ZmNAC49 to enhance oxidative stress tolerance in maize. *New Phytol.* **2021**, *232*, 2400–2417. [CrossRef]
35. Qi, J.; Song, C.P.; Wang, B.; Zhou, J.; Kangasjärvi, J.; Zhu, J.K.; Gong, Z. Reactive oxygen species signaling and stomatal movement in plant responses to drought stress and pathogen attack. *J. Integr. Plant Biol.* **2018**, *60*, 805–826. [CrossRef]
36. Pan, R.; Buitrago, S.; Feng, Z.; Abou-Elwafa, S.F.; Xu, L.; Li, C.; Zhang, W. HvbZIP21, a novel transcription factor from wild barley confers drought tolerance by modulating ROS scavenging. *Front. Plant Sci.* **2022**, *13*, 878459. [CrossRef]
37. Cui, X.Y.; Gao, Y.; Guo, J.; Yu, T.F.; Zheng, W.J.; Liu, Y.W.; Chen, J.; Xu, Z.S.; Ma, Y.Z. BES/BZR transcription factor TaBZR2 positively regulates drought responses by activation of TaGST. *Plant Physiol.* **2019**, *180*, 605–620. [CrossRef]
38. Niu, S.; Gu, X.; Zhang, Q.; Tian, X.; Chen, Z.; Liu, J.; Wei, X.; Yan, C.; Liu, Z.; Wang, X.; et al. Grapevine bZIP transcription factor bZIP45 regulates VvANN1 and confers drought tolerance in *Arabidopsis*. *Front. Plant Sci.* **2023**, *14*, 1128002. [CrossRef]
39. Kang, C.; Zhai, H.; He, S.; Zhao, N.; Liu, Q. A novel sweetpotato bZIP transcription factor gene, IbbZIP1, is involved in salt and drought tolerance in transgenic *Arabidopsis*. *Plant Cell Rep.* **2019**, *38*, 1373–1382. [CrossRef]

40. Bu, Y.; Yu, Y.; Song, T.; Zhang, D.; Shi, C.; Zhang, S.; Zhang, W.; Chen, D.; Xiang, J.; Zhang, X. The transcription factor TabZIP156 acts as a positive regulator in response to drought tolerance in *Arabidopsis* and wheat *(Triticum aestivum* L.). *Plant Physiol. Biochem.* **2024**, *216*, 109086. [CrossRef]
41. Tu, M.; Wang, X.; Zhu, Y.; Wang, D.; Zhang, X.; Cui, Y.; Li, Y.; Gao, M.; Li, Z.; Wang, Y.; et al. VlbZIP30 of grapevine functions in dehydration tolerance via the abscisic acid core signaling pathway. *Hortic. Res.* **2018**, *5*, 49. [CrossRef] [PubMed]
42. Wang, F.; Chen, H.W.; Li, Q.T.; Wei, W.; Li, W.; Zhang, W.K.; Ma, B.; Bi, Y.D.; Lai, Y.C.; Liu, X.L.; et al. GmWRKY27 interacts with GmMYB174 to reduce expression of GmNAC29 for stress tolerance in soybean plants. *Plant J.* **2015**, *83*, 224–236. [CrossRef] [PubMed]
43. Zhou, Y.; Chen, M.; Guo, J.; Wang, Y.; Min, D.; Jiang, Q.; Ji, H.; Huang, C.; Wei, W.; Xu, H.; et al. Overexpression of soybean *DREB1* enhances drought stress tolerance of transgenic wheat in the field. *J. Exp. Bot.* **2020**, *71*, 1842–1857. [CrossRef] [PubMed]
44. Deng, J.; Yang, X.; Sun, W.; Miao, Y.; He, L.; Zhang, X. The calcium sensor CBL2 and its interacting kinase CIPK6 are involved in plant sugar homeostasis via interacting with tonoplast sugar transporter TST2. *Plant Physiol.* **2020**, *183*, 236–249. [CrossRef]

plants

MDPI

Article

Genome-Wide Identification of PR10 Family Members in Durum Wheat: Expression Profile and In Vitro Analyses of TdPR10.1 in Response to Various Stress Conditions

Emna Khanfir [1], Ikram Zribi [1], Hanen Dhouib [2], Mouna Ghorbel [3], Karama Hamdi [1], Olfa Jrad [1], Inès Yacoubi [1] and Faiçal Brini [1,*]

[1] Biotechnology and Plant Improvement Laboratory, Centre of Biotechnology of Sfax, University of Sfax, P.O. Box 1177, Sfax 3018, Tunisia; emna.khanfir@cbs.rnrt.tn (E.K.); ikram.zribi@cbs.rnrt.tn (I.Z.); karama.hamdi@cbs.rnrt.tn (K.H.); olfa.jrad@cbs.rnrt.tn (O.J.); ines.bouchrityaccoubi@cbs.rnrt.tn (I.Y.)
[2] Biopesticides Laboratory, Centre of Biotechnology of Sfax, University of Sfax, P.O. Box 1177, Sfax 3018, Tunisia; hanen.dhouib@cbs.rnrt.tn
[3] Department of Biology, College of Sciences, University of Hail, P.O. Box 2440, Ha'il City 81451, Saudi Arabia; m.ghorbel@uoh.edu.sa
* Correspondence: faical.brini@cbs.rnrt.tn

Abstract: The functional characterization of PR10 proteins has been extensively studied in many plant species. However, little is known about the role of TdPR10 in the response of durum wheat (*Triticum durum* Desf.) to stress. In this study, we identified members of the *T. durum* PR10 family, which are divided into three major subfamilies based on phylogenetic analyses. The analysis revealed that tandem duplication was the primary driver of the expansion of the *T. durum PR10* gene family. Additionally, gene structure and motif analyses showed that *PR10* family genes were relatively conserved during evolution. We also identified several cis-regulatory elements in the *TdPR10* promoter regions related not only to abiotic and biotic stress but also to phytohormonal responses. In response to abiotic stresses and phytohormones, several *TdPR10* genes were highly expressed in the leaves and roots of durum wheat. Moreover, TdPR10.1 family members improve RNase activity, increase LDH protective activity under abiotic stress conditions, and ensure resistance to fungi in vitro. Collectively, these findings provide a basis for further functional studies of *TdPR10* genes, which could be leveraged to enhance stress tolerance in durum wheat.

Keywords: abiotic and biotic stress; antifungal activity; durum wheat; genome-wide analysis; LDH activity; PR10 family; phytohormones; RNase activity

1. Introduction

Due to climatic and environmental variations, plants face challenges such as salinity, cold, drought, heavy metals, and phytopathogen attacks. To overcome these harsh conditions, plants activate complex molecular mechanisms that lead to the production of protective proteins [1]. One of the most important groups of proteins involved in responding to these threats is the pathogenesis-related (PR) proteins [1,2]. PR proteins are sub-divided into 19 groups based on their structural and functional characteristics. PR proteins have crucial roles in regulating plant growth and development under different stressors. Among them, PR10 is one of the most studied groups [3]. PR10 proteins are small, acidic proteins with molecular weights ranging from 16 to 19 kDa. They possess unique three-dimensional β-sheet topologies, enclosed by a compact bipartite framework held together by hydrophobic interactions [4]. PR10 proteins are well known for their role in stress resistance, acting as defense proteins under harmful conditions [5]. These proteins are part of a multigene family, as seen in *Solanum lycopersicon* (45 genes, [6]) and *Hevea brasiliensis* (rubber tree, 132 genes) [7]. Based on phylogenetic studies, PR10 proteins are

classified into different subfamilies such as the PR10/Bet v1-like proteins, major latex-like (MLP) proteins, phytohormones binding proteins (PBP), proteins with the enzymatic function that are the (S)-norcoclaurine synthase (NCS) protein, polyketide cyclase-like protein and even monocot PR10 and dicot PR10 [8].

PR10 proteins are related to the major pollen allergen Bet v 1 of white birch (*Betula verrucosa*) [8]. Homologs of Bet v 1 have been identified in many plants, such as cherry (Pru a 1) [9], apple (*Malus domestica*) [10], and carrot (Dau c1) [11]. A highly conserved glycine-rich motif (GXGGXGXXK) is found in all PR10 protein sequences, which enables RNA binding with specific affinity [12]. PR10 proteins are also known for their ribonuclease activity, along with at least eight other distinct enzymatic functions [13]. For instance, PR10 proteins act similarly to neopinone isomerase in opium poppy and to beta-1,3-glucanase in MaPR10 [14,15], as well as other secondary metabolic enzyme functions, such as protein phosphatase inhibitor activity [7]. In *Brassica napus*, the ribonuclease PR10.1 has been shown to enhance germination under salinity stress [9]. Despite the tiny size of PR10 proteins, they can bind small molecules in the hydrophobic cavity formed by the Bet v 1-fold [7]. According to a review by [16], three primary classes of chemicals—cytokinins, flavonoids, and sterols—are associated with potential roles of PR10 proteins in plant metabolite biosynthesis, host defense, and plant growth and development [17–20]. Moreover, PR10 proteins can interact with hormones and other molecules, such as flavonoids, fatty acids, steroids, gibberellic acid, and cytokinin, due to their hydrophobic cavity [10]. It is thought that the function of PR10 proteins is not always connected to the protein's contribution to host defense because not all of them have ribonuclease activity [5]. Similarly, the *HcPR10* gene from *Halostachys caspica* was significantly upregulated during development [21]. In addition, *ABR17A* gene exhibits enhancement during germination and in the early seedling growth of *Arabidopsis thaliana* plants [22]. Moreover, PR10 proteins present antimicrobial activities [23]. A *PR10* gene from rice, OsBet v1, exhibits upregulation after infection with the nematode *Meloidogyne graminicola* [24]. In *Escherichia coli*, the production of PmPR10-3.1 from white pine (*Pinus monticola*) inhibited the fungi growth of *Cronartium ribicola* [25]. CaPR-10 isolated from pepper (*Capsicum annuum*) responds against Tobacco Mosaic Virus (TMV) infection with its ribonucleolytic activity [26]. In addition to the biotic stress response, PR10 protein is also involved in abiotic stress tolerance. In rice roots, a *PR10* gene named the *RSOsPR10* gene (root-specific rice PR10) shows both stress resistances, with induction upon blast fungus infection and also after salt and drought stresses [27]. In addition, transgenic *Arabidopsis thaliana* plants overexpress the *PR10* gene from pea (ABR17) and tolerate salinity, heat, and cold stresses [22].

Durum wheat (*Triticum durum* Desf.) is one of the most important cereal crops for human consumption, providing essential bioactive components, proteins, fibers, and carbohydrates [28]. Wheat production and yield are highly dependent on climatic conditions [5]. To date, little is known about the PR10 protein family in durum wheat and its biological function in stress responses.

In this study, we examine the gene and protein features, chromosomal locations, classification, and evolution of PR10 members in durum wheat. We also identify cis-regulatory elements in their promoters and analyze the expression patterns of *TdPR10* genes in response to abiotic stress and hormone treatments. Finally, we explore the role of TdPR10.1 in enhancing LDH protective activity, RNase activity, and antifungal activity in vitro. This study provides a genome-wide analysis of the PR10 family and investigates the expression of *TdPR10* genes under various conditions in durum wheat.

2. Results

2.1. Genome-Wide Identification and Analysis of T. durum PR10 Family Members

Using the isolated PR10.1 protein sequence previously defined by our group as a query, we identified 15 PR10 genes in the durum wheat genome using the EnsemblPlants database. These genes were classified into three major subfamilies (Figure 1A). Two online tools, InterPro and CDD, were employed to confirm the presence of the Bet v 1 conserved domain

within the PR10 protein sequences (Figure 1B,C). A high degree of similarity was observed when comparing the Bet v 1 signature logo generated for TdPR10 proteins (Figure 1B) with the Bet v 1 signature motif from Prosite (ID: PS00451) (Figure 1C).

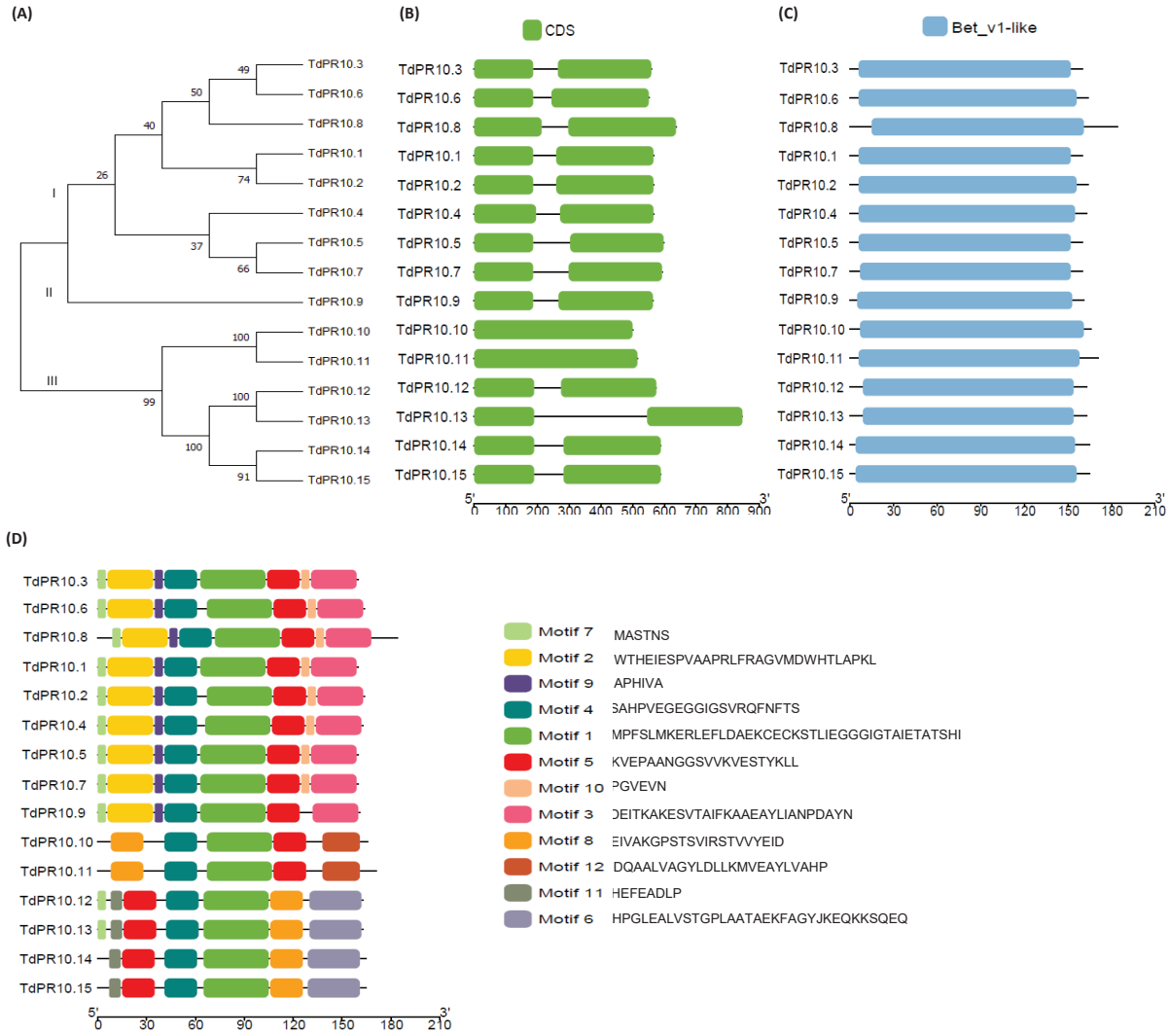

Figure 1. Analysis of *T. durum* PR10 family members. (**A**) Phylogenetic tree of TdPR10 proteins constructed using the maximum likelihood with 1000 bootstraps in MEGA 11 software. (**B**) Structure of *TdPR10* genes. (**C**) Conserved Bet v 1 domains present in PR10 proteins of durum wheat. (**D**) Motifs of TdPR10 proteins visualized using Tbtools II v.070.

A total of 12 novel motifs were predicted from the amino acid sequences of all 15 TdPR10 proteins from durum wheat using TbTools II v.070 software (Figure 1D). Motif 1 and motif 4 were present in all the putative TdPR10 proteins. The fewest motifs were identified in group II proteins, specifically TdPR10.10 and TdPR10.11 (Figure 1A,D). Additionally, a specific motif arrangement was observed for each protein group. While different types and localizations of motifs were found among the TdPR10 sequences, each phylogenetic tree group exhibited a conserved motif pattern and order. This variability in motif types, locations, and numbers may suggest distinct functions for PR10 proteins in durum wheat. Furthermore, all identified sequences contained the conserved Bet v 1 domain and the glycine-rich P-loop motif (Supplemental Figure S1A). The alignment of amino acid sequences showed high similarity across all PR10 proteins (Supplemental Figure S1A).

Table 1 summarizes the basic properties of TdPR10 proteins. Based on the theoretical isoelectric point (pI) values, which range from 4.59 to 5.94, all deduced PR10 proteins were

classified as acidic. The sequence lengths of these proteins vary from 160 to 184 amino acids, while their predicted molecular weights (Mw) range from 16.9 to 19.8 kDa. Among the 15 identified TdPR10 proteins, three exhibited an instability index greater than 40, suggesting that these proteins may be unstable under stress conditions. However, all identified proteins showed a high aliphatic index, indicating that they are likely thermostable. Additionally, the GRAVY (Grand Average of Hydropathicity) index values for the TdPR10 proteins varied, indicating that they could be either hydrophilic or hydrophobic.

Table 1. Physico-chemical properties of TdPR10 proteins using the Protparam online tool.

Gene Name	Transcript ID	Protein Length (aa)	Molecular Weight (Da)	Theoretical pI:	The Instability Index (II)	Aliphatic Index	GRAVY
TdPR10.1	MK570865.1	160	17,113.47	5.19	41.79 unstable	83.62	0.011
TdPR10.2	TRITD4Bv1G117510.2	164	17,469.88	5.07	41.23 unstable	87.50	0.016
TdPR10.3	TRITD7Bv1G026790.1	160	17,078.41	5.19	38.27 stable	86.00	−0.034
TdPR10.4	TRITD2Bv1G226310.3	163	17,372.76	5.94	31.33 stable	81.47	−0.067
TdPR10.5	TRITD2Av1G263640.1	160	16,990.30	5.51	37.65 stable	84.25	−0.027
TdPR10.6	TRITD7Av1G052120.1	164	17,538.95	5.06	37.12 stable	86.34	−0.024
TdPR10.7	TRITD2Av1G263650.1	160	17,080.38	5.57	39.16 stable	83.00	−0.091
TdPR10.8	TRITD5Av1G005340.2	184	19,821.80	5.22	41.08 unstable	91.85	0.081
TdPR10.9	TRITD2Bv1G209060.1	161	17,015.27	5.08	34.43 stable	82.42	0.014
TdPR10.10	TRITD5Av1G049040.1	166	17,127.53	4.62	30.23 stable	94.16	0.213
TdPR10.11	TRITD5Bv1G045600.1	171	17,701.17	4.70	23.12 stable	97.08	0.184
TdPR10.12	TRITD2Bv1G217530.1	163	17,983.73	4.98	27.50 stable	101.78	−0.001
TdPR10.13	TRITD2Av1G253700.1	163	18,047.77	4.91	35.75 stable	100.55	−0.055
TdPR10.14	TRITD2Av1G278210.1	165	17,996.20	4.59	35.79 stable	88.55	−0.255
TdPR10.15	TRITD2Bv1G242310.1	165	18,180.48	4.84	25.76 stable	92.06	−0.251

2.2. Gene Structure and Physical Location of T. durum PR10 Genes

Analyzing the exon and intron distribution patterns provides valuable insights into the structural evolution of the durum wheat *PR10* gene family. The exon–intron organization of the *TdPR10* genes displayed a similar structure, with most genes containing two exons separated by one intron. However, genes from family II (*TdPR10.10* and *TdPR10.11*) were an exception, as they contained only a single exon (Supplemental Figure S1B; Table 1).

To further investigate the distribution of *TdPR10* genes in the durum wheat genome, we found that four genes were localized on chromosomes 2A and 2B, while one gene was located on each of chromosomes 4A, 4B, 5A, 5B, 7A, and 7B (Figure 2). These chromosomes

may play a key role in the *TdPR10* gene family and are promising candidates for improving durum wheat traits related to PR10 functional phenotypes.

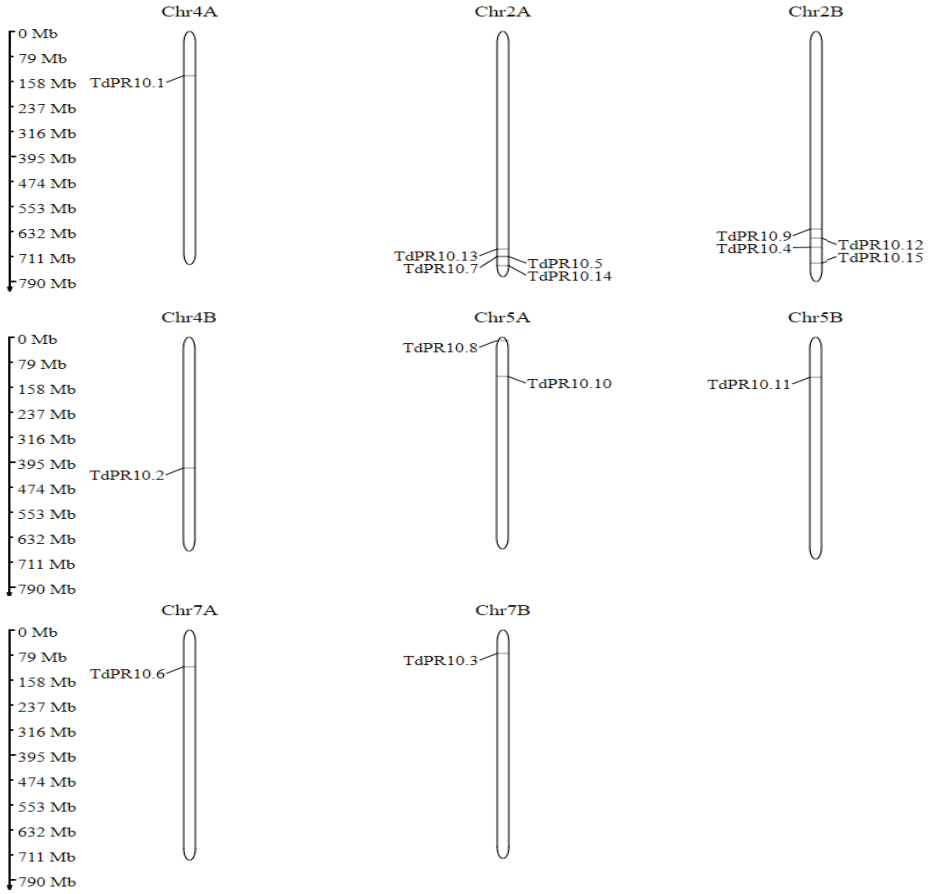

Figure 2. Chromosomal localisation of *TdPR10* genes by using MG2C tool.

2.3. Phylogenetic Analysis of TdPR10 Proteins

To classify the identified TdPR10 proteins, a maximum likelihood tree was constructed using a bootstrap of 1000 replicates. The durum wheat PR10 proteins were grouped into three major subfamilies: the Bet v1-like subfamily (TdPR10.1 to TdPR10.9), the PBP/NCS subfamily (TdPR10.12 to TdPR10.15), and the major latex protein (MLP) subfamily, consisting of TdPR10.10 and TdPR10.11 (Figure 3).

In parallel, identity and similarity analyses were performed to predict the molecular functions of TdPR10 proteins (Supplemental Figure S2). Proteins in the Bet v1 group (TdPR10.1 to TdPR10.9) showed a similarity of 42% to 58% to well-known allergens, including Pru av 1 [29], Mal d 1 [10], Bet v 1 [30], Pyr c 1 [31], Api g 1 [32], Dau c 1 [11], Cor a 1 [33], Ara h 8 [34], and Cas s 1 [33]. Additionally, members of this group exhibited 47% to 55% identity with PmPr10-3.1, an antifungal protein resistant to white pine blister rust [35], and PinmIII, which has a role in cold tolerance [36]. Furthermore, comparison of the tomato PR10 protein sequence (Solyc09g090980) [6] with proteins clustered in the Bet v1 and MLP groups revealed 47% to 54% identity, suggesting that these TdPR10 proteins may be involved in virus resistance. Additionally, TdPR10.10 and TdPR10.11 showed close similarity to the rice PBZ1 protein, with 68% and 66% similarity, respectively. Like PBZ1, which functions as an RNase/DNase enzyme [37], TdPR10.10 and TdPR10.11 may play roles in salt tolerance and fungal resistance [38]. TdPR10.12 and TdPR10.13 exhibited 45% similarity to the PR10 protein of soybean, Gly m 4, which is known for its resistance to *Phytophthora sojae* infection [20]. Meanwhile, TdPR10.14 and TdPR10.15 showed approximately 45% similarity to the allergens Bet v 1, Cor a 1, and Cas s 1.

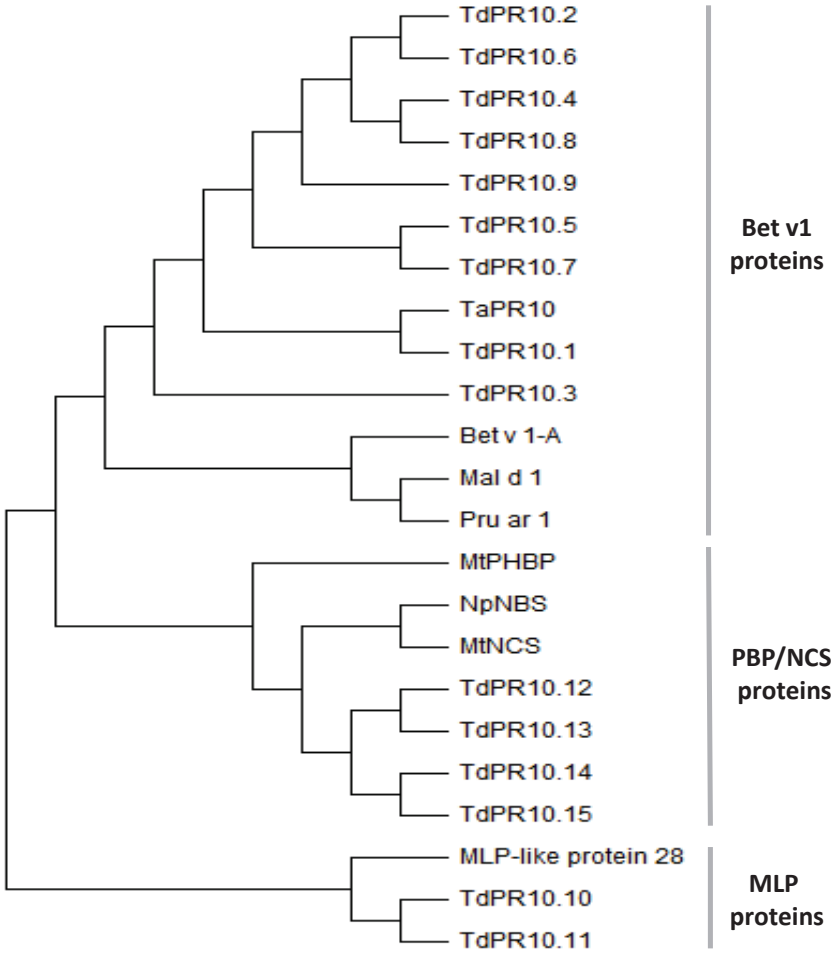

Figure 3. Phylogenetic clustering of TdPR10 proteins alongside well-characterized PR10 proteins: Bet v 1A from birch pollen (*Betula verrucosa*, P15494.2); Mal d 1, the major allergen from *Malus domestica* (NP_001281292.1); NpNBS, norbelladine synthase from *Narcissus pseudonarcissus* (A0A3G5BB24.1); MtNCS, S-norcoclaurine synthase-like protein (KEH30672.1) and MtPHBP, phytohormone-binding protein (G7J032.1) from *Medicago truncatula*; Pru ar 1 from *Prunus armeniaca* (O50001.1); TaPR10, a pathogenesis-related protein 10 from *Triticum aestivum* (ACG68733.1); and MLP-like protein 28 from *Arabidopsis thaliana* (NP_001117579.1). The phylogenetic tree was generated using the maximum likelihood method with 1000 bootstrap replicates in MEGA 11 software.

2.4. In Silico Subcellular Localisation and Gene Ontology Analysis of the T. durum PR10

The in silico subcellular localization prediction showed that the 15 proteins were predominantly localized in the cytoplasm (Figure 4). In addition, TdPR10.6 was also predicted to be associated with the cytoskeleton, and TdPR10.13 was predicted to be present in the nucleus. The other proteins were localized in the mitochondria, peroxisome, chloroplast, extracellular matrix, and plasma membrane. A total of 15 TdPR10 proteins were analyzed for their reported Gene Ontology (GO) terms in the InterPro database (Figure 5). For all TdPR10 proteins, three main molecular functions were identified: protein phosphatase inhibitor activity (GO:0004864), abscisic acid binding activity (GO:0010427), and signaling receptor activity (GO:0038023). Additionally, two biological processes were associated with these proteins: defense response (GO:0006952) and the abscisic acid-activated signaling pathway (GO:0009738).

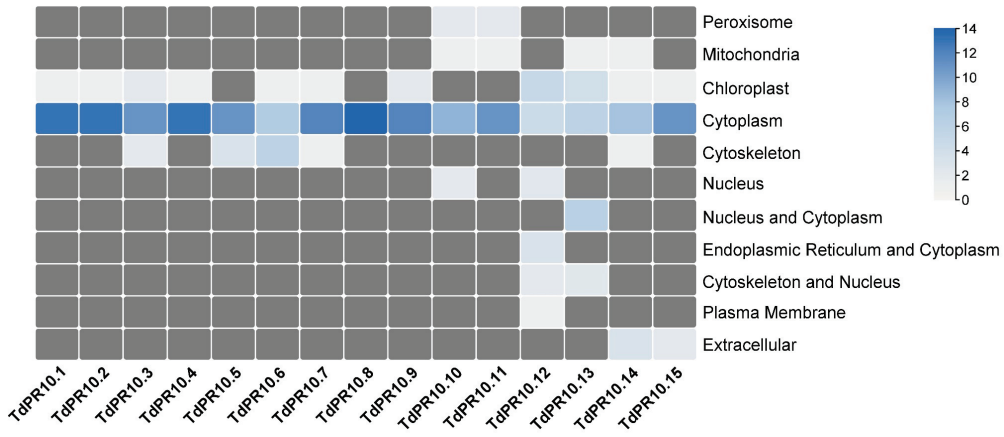

Figure 4. In silico subcellular localisation prediction of TdPR10 proteins using the WoLFPSORT online server.

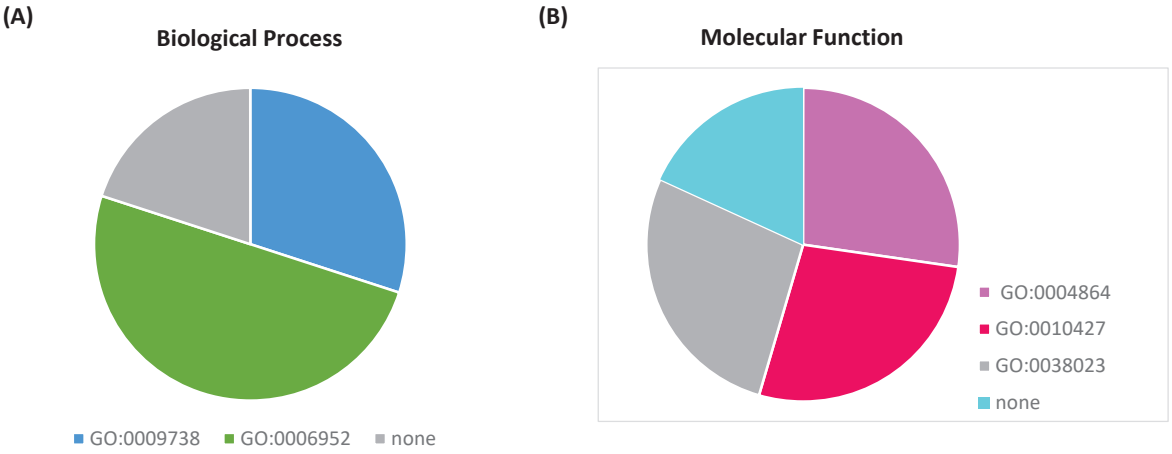

Figure 5. Prediction of biological processes (**A**) and molecular functions (**B**) of PR10 proteins identified in durum wheat based on GO terms in the InterPro database.

2.5. Tertiary Structure of TdPR10 Proteins

The constructed 3D models showed that TdPR10 proteins share a common structure. This structure is organized into a seven-stranded antiparallel β-sheet and three α-helices (Figure 6). Additionally, the models revealed differences in their predicted binding pockets. These findings suggest variability in the substances that may bind to the TdPR10 cavities, indicating different roles for these proteins.

2.6. In Silico Analysis of Cis-Elements

Cis-elements are involved in gene function and regulation. In the current study, we identified them from the 1.5 kb promoter region of *PR10* genes in durum wheat (Figure 7). Cis-regulatory elements related to hormone responses were found in most of the PR10 promoters. Specifically, MeJA-responsive cis-elements were identified in all prTdPR10 promoters except for prTdPR10.13. Two *PR10* genes, *prTdPR10.14* and *prTdPR10.15*, contained three ABRE elements, while *prTdPR10.3*, *prTdPR10.6*, and *prTdPR10.10* had six ABRE elements. These elements are involved in the abscisic acid response. In contrast, only one or two cis-elements related to auxin and gibberellin responses were present in some of the *PR10* promoter regions. Among the cis-elements implicated in growth and development, G-box elements associated with light responses were detected in most *TdPR10* promoter sequences. Regarding stress responses, ARE elements were present in most *prTdPR10* promoters, with frequencies ranging from 1 to 5 elements. The *TdPR10.10* promoter region possessed the highest number of G-box (6), ABRE (7), and ARE (5) elements.

Regulatory cis-elements were found in only a few *PR10* promoters, with a maximum of two elements. Similarly, the MYBHv1 binding site element was present in only 8 out of 15 *TdPR10* promoter regions.

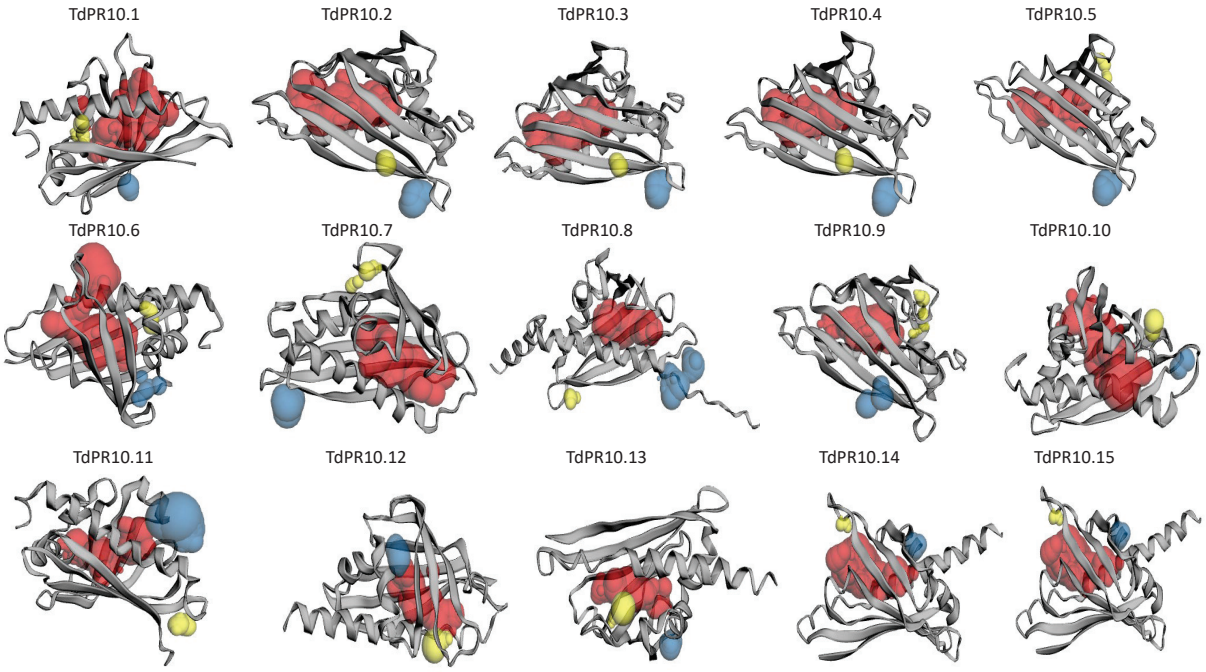

Figure 6. Prediction of TdPR10 3D structure using SWISS-MODEL. Pockets were visualized from largest to smallest using red, blue, and yellow colors, respectively, with the CASTp 3.0 online tool.

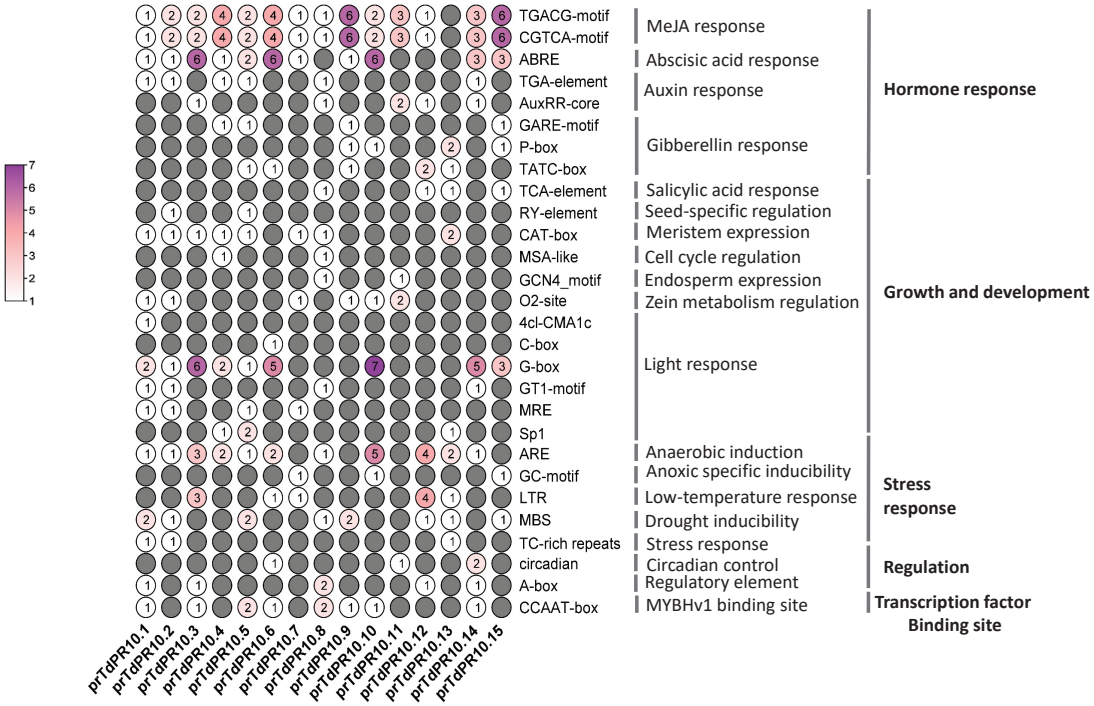

Figure 7. Predicted cis-regulatory elements in the promoter regions (approximately 1500 bp) of *TdPR10* genes were analyzed using the PlantCare and PLACE web tools. The figure was created using TBtools II v.070 software. The putative cis-element numbers are highlighted in different colors, with specific counts marked in each grid.

2.7. Response of TdPR10 Genes to Several Abiotic Stress and Phytohormones

We conducted RT-qPCR studies on the leaves and roots of durum wheat cv. Om Rabiaa, which had been exposed to various abiotic stimuli (salt, cold, and cadmium toxicity) as well as phytohormone treatments (ABA and SA) for 24 and 72 h to investigate the expression profiles of *TdPR10* genes. Our results indicate that the expression of *TdPR10* genes varies depending on the type of stress. Specifically, within 24 h of applying salt stress, the majority of *TdPR10* genes in leaves were upregulated; however, after 72 h, this response diminished or remained unchanged. In contrast, during both salt exposure durations, all *TdPR10* genes were significantly upregulated in roots (Figure 8A). Similarly, under cadmium toxicity, most *TdPR10* genes exhibited positive expression in roots at both time points, although their expression in leaves varied between positive and negative responses (Figure 8B). Notably, during cadmium stress, *TdPR10.1*, *TdPR10.3*, and *TdPR10.14* genes consistently showed upregulation in both leaves and roots. The expression of different *TdPR10* genes varied in response to cold stress (Figure 8C), with some genes consistently upregulated in both leaves and roots during the stress periods. After 24 h of cold stress, *TdPR10.2* exhibited a brief downregulation in leaves, but at 72 h, it increased significantly (by approximately three times). Overall, our results demonstrate that distinct abiotic stresses regulate *TdPR10* genes differently. They also indicate that while responses in leaves varied among *TdPR10* genes, root tissues showed strong induction under all stress conditions.

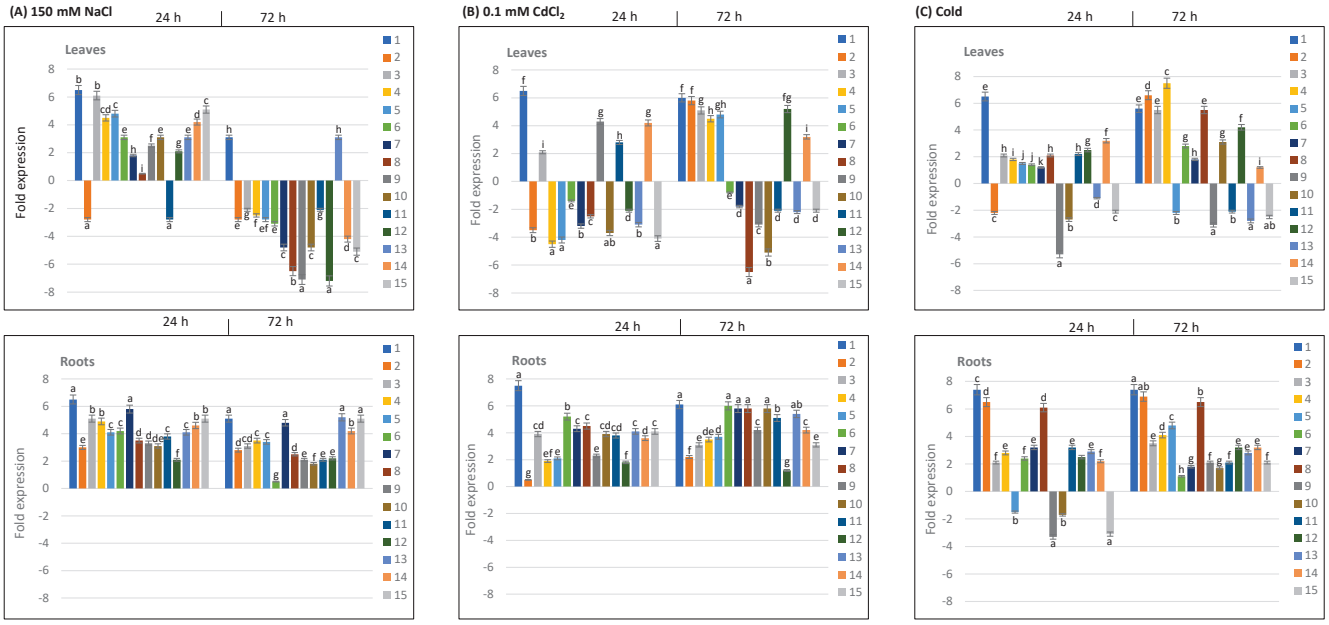

Figure 8. Analysis of the expression profiles of *TdPR10* genes (*TdPR10.1* to *TdPR10.15*) in the leaves and roots of *T. durum* exposed to various abiotic stresses for 24 and 72 h was conducted. Three types of abiotic stress were applied: 150 mM NaCl (**A**), 0.1 mM $CdCl_2$ for cadmium toxicity (**B**), and cold at 4 °C (**C**). The expression value of each *TdPR10* gene in the leaves and roots of non-treated plants (control) was set to 1 to calculate the relative expression. Log_2-transformed values were presented in bar charts. The *TdActin* gene was used as an internal control. Four plants were used per treatment per replicate, and error bars indicate the standard deviation of three biological replicates. In each period of stress application (24 or 72 h), different letters marked on the same bar chart indicate significant differences ($p < 0.05$).

Likewise, *TdPR10* genes were both up- and downregulated in leaves and roots in response to phytohormone treatments (Figure 9). Notably, during the 24 and 72 h of stress, TdPR10.7, TdPR10.8, TdPR10.12, and TdPR10.13 were consistently downregulated in leaves across all phytohormone treatments. In contrast, leaves treated with ABA exhibited significantly higher expression levels of TdPR10.3, TdPR10.6, and TdPR10.10 (Figure 9A).

TdPR10.1 was upregulated in leaves under both ABA and SA treatments, which was particularly evident 72 h after treatment (Figure 9A,B). Furthermore, after receiving hormone treatments for 72 h, the majority of *TdPR10* genes displayed significant expression levels in roots (Figure 9). Among the *TdPR10* genes, *TdPR10.9* and *TdPR10.15* were notably most significantly expressed in leaves treated with JA (Figure 9C). All these results confirm the results of in silico analysis of the cis-elements and highlight the important roles of various *TdPR10* genes in durum wheat's response to abiotic stress and in regulatory pathways involving plant hormones. Further research will be beneficial to clarify their unique roles in stressful conditions.

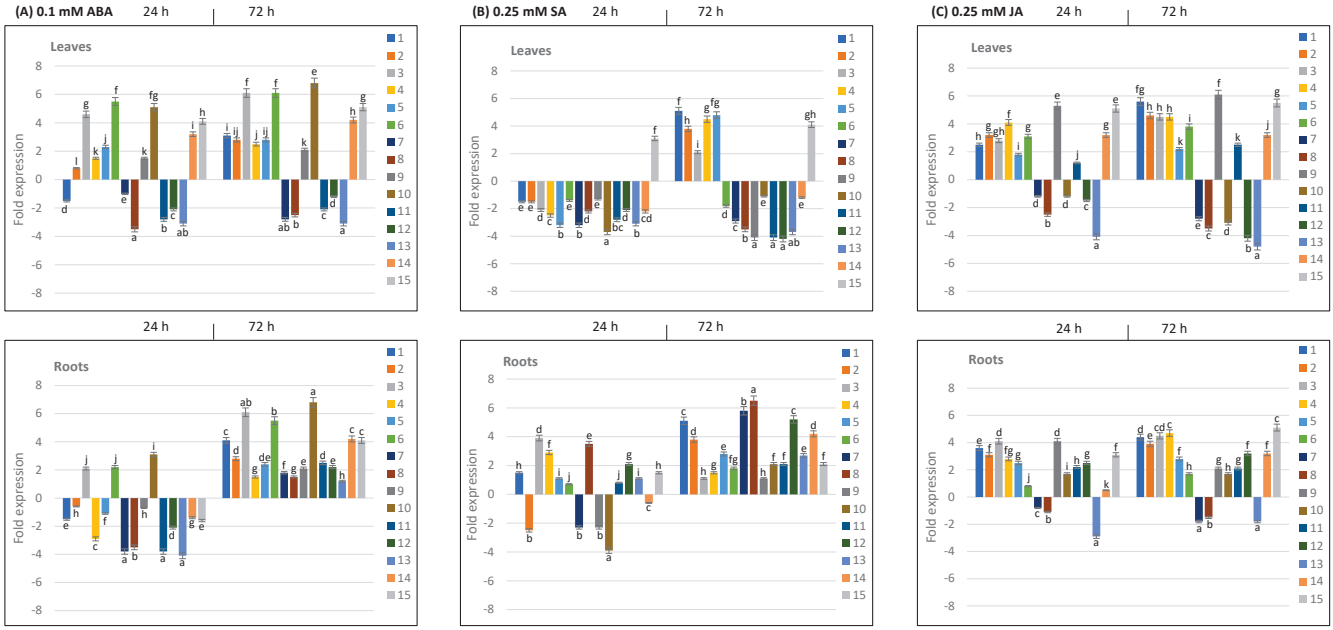

Figure 9. Analysis of the expression profiles of *TdPR10* genes (*TdPR10.1* to *TdPR10.15*) in the leaves and roots of *T. durum* exposed to phytohormones: (**A**) 0.1 mM ABA, (**B**) 0.25 mM SA and (**C**) 0.25 mM JA. The expression value of each *TdPR10* gene in the leaves and roots of non-treated plants (control) was set to 1 to calculate the relative expression. Log_2-transformed values are presented in bar charts. The *TdActin* gene was used as an internal control. Four plants were used per treatment per replicate, and error bars indicate the standard deviation of three biological replicates. In each period of stress application (24 or 72 h), different letters marked on the same bar chart indicate significant differences ($p < 0.05$).

2.8. Expression of TdPR10.1 Protein in E. coli Strain

The TdPR10.1 cDNA was cloned into the *Eco*RI site of the pGEX4T-1 expression vector. The target protein can be expressed by *E. coli* strain BL21 cells as a fusion protein attached to a GST tag that can be cleaved. When thrombin removes the GST tag, a protein with an N-terminal GSPEF amino acid extension, encoded by the vector, is produced. Size-exclusion chromatography (SEC), thrombin cleavage to eliminate the GST tag, and affinity chromatography were used to purify the tagged proteins. TdPR10 migrates in SDS-PAGE with an apparent molecular mass (MM) of 17 kDa (Supplemental Figure S3).

2.9. Functional Characterization of TdPR10.1 In Vitro

2.9.1. TdPR10.1 Protects LDH Activity Under Stress Conditions

We tested the ability of TdPR10.1 to prevent the loss of LDH activity after heating, dehydration, cold, and freezing. We compared the effects of TdPR10.1 with those of BSA as a non-specific protective agent and with LDH treated in buffer without additional protein. We investigated TdPR10.1's impact on LDH enzyme activity under cold and heat stresses. The LDH enzyme was combined with either BSA or a TdPR10.1-free phosphate buffer.

Activity was assessed immediately after aliquots were incubated at 0 °C and 43 °C for various exposure durations, ranging from 0 to 30 min (Figure 10A,B). The LDH activity rapidly drops at 0 °C, reaching just 26.7% of its relative activity after 30 min of incubation. However, LDH inactivation is significantly reduced in the presence of BSA or TdPR10.1. After 30 min of incubation at 0 °C with BSA, its relative activity was approximately 37.38%, while for TdPR10.1, it was around 40.75% (Figure 10A). The same results were obtained under heat stress. In fact, the enzyme's activity rapidly declined at 43 °C, reaching just 22.1% of its relative activity after 30 min of incubation. However, LDH inactivation is greatly reduced in the presence of BSA or TdPR10.1. After 30 min of incubation at 43 °C, the profile of LDH activity in the presence of TdPR10.1 was significantly higher than that of BSA, according to our data. In contrast to the activity in the presence of BSA, which was approximately 30.38%, TdPR10.1 sustained an LDH activity of 60.14% for up to 30 min (Figure 10B). These experimental results demonstrate that TdPR10.1 can shield LDH from heat effects in vitro, indicating a potential protective function during heat stress. Following hydration and dehydration, LDH activity was around 20.8% of the starting value. At all mass ratios, TdPR10.1 provided greater stability to the enzyme, reaching 60%, compared to BSA, which reached 40% (Figure 10C). After two cycles of freezing and thawing, LDH activity decreased to 29.82%, while BSA activity increased to 43.86%. In contrast, TdPR10.1 increased LDH activity to 58.60% (Figure 10D). These results confirm that TdPR10.1 offered a greater degree of protection to LDH than BSA after various stress treatments, indicating that the TdPR10.1 protein has protective activity beyond the non-specific effects of BSA (Figure 10).

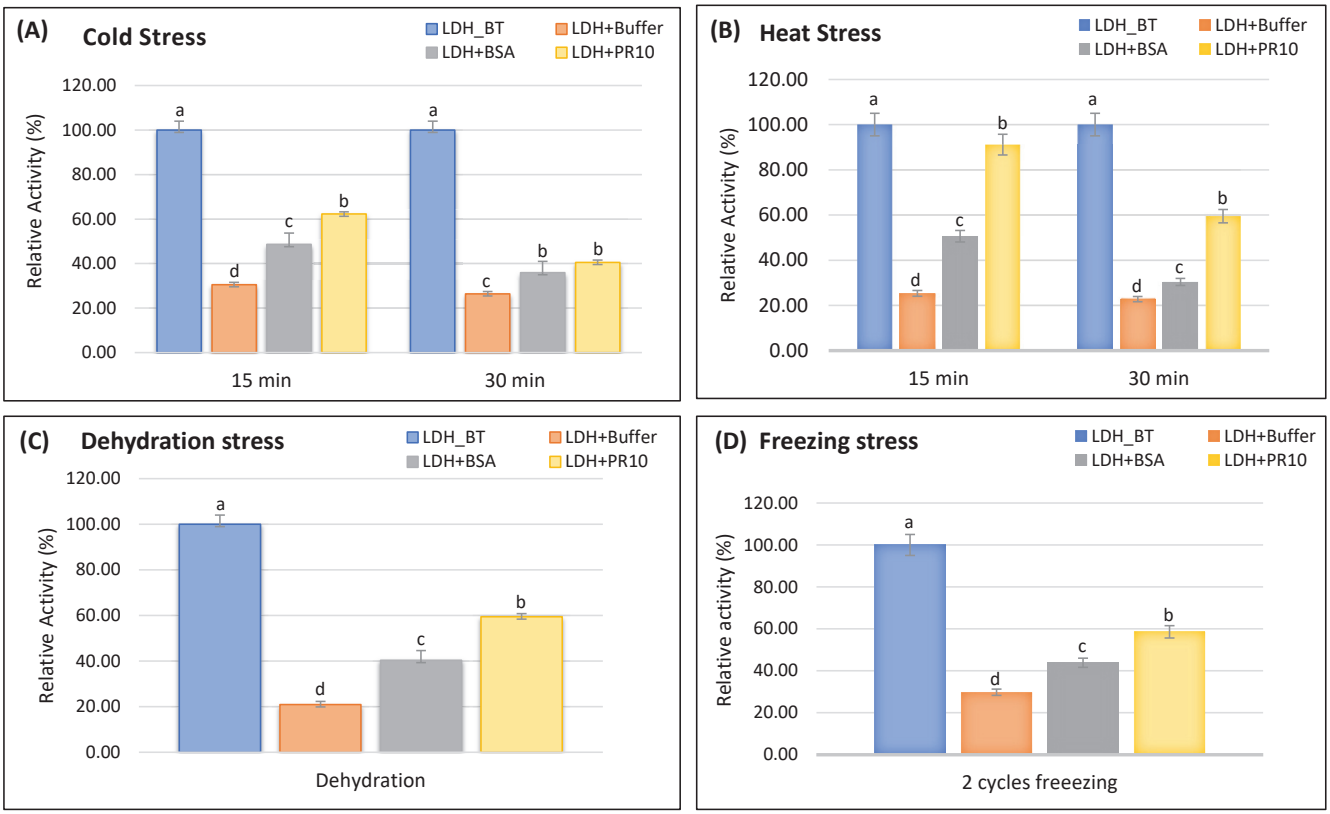

Figure 10. Analysis of the protective role of TdPR10.1 on LDH activity under various stresses in vitro was conducted. LDH activity was measured in solutions mixed with sucrose (buffer), BSA (buffer + BSA), or the purified His-tagged TdPR10.1 protein (buffer + TdPR10.1) under cold (**A**), heat (**B**), dehydration (**C**), and freezing (**D**) conditions. LDH activity before treatment (BT) was taken as 100%. Error bars indicate the standard deviation of four biological replicates. In each period of stress application, different letters marked on the same bar chart indicate significant differences ($p < 0.05$).

2.9.2. TdPR10.1 Improves RNase Activity Under Stress Conditions

We tested the potential role of the TdPR10.1 protein in degrading RNA. As shown in Figure 11, RNA alone in nuclease-free water remained intact, whereas RNA with 10 µg of TdPR10.1 was partially degraded after 1 h and completely degraded after 4 h. The results from the RNase activity assays confirm that the TdPR10.1 protein exhibits ribonuclease activity.

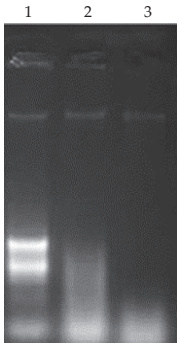

Figure 11. Ribonuclease activity of recombinant TdPR10.1 purified protein was assessed using 30 µg of total RNA extracted from 'Om Rabiaa' durum wheat leaves. Gel electrophoresis was performed to separate the RNAs on a 1.2% agarose gel. (1) RNA from 'Om Rabiaa'; (2) RNA after 1 h of incubation with TdPR10.1; (3) RNA after 4 h of incubation with TdPR10.1.

2.9.3. Antifungal Activity of TdPR10.1 Protein

To evaluate the inhibitory effect of the TdPR10.1 protein against the tested fungi, the minimum inhibitory concentrations (MICs) and minimum fungicidal concentrations (MFCs) were determined and are presented in Table 2. Interestingly, the MIC and MFC values indicate that the protein has a fungicidal effect against *F. graminearum* and *A. niger*, as the MFC/MIC ratio (500/500 = 1) was less than 4. However, for *F. oxysporum*, *F. culmorum*, and *B. cinerea*, the MFC/MIC ratio was greater than 1 (Table 2).

Table 2. Minimum inhibitory concentration (MIC) and minimum fungicidal concentration (MFC) values (µg/mL) of the TdPR10.1 protein determined by the microdilution method.

Phytopathogens	CMI (µg/mL)	CMF (µg/mL)	CMF/CMI
F. oxysporum	>500	500	
F. culmorum	>500	-	
F. graminearum	500	500	1
B. cinerea	>500	500	
A. niger	500	500	1

3. Discussion

Tetraploid wheat (*Triticum turgidum* subsp. *durum* (Desf.)) is one of the most economically important cereal crops worldwide. During its lifecycle, various atmospheric and pathogenic stresses negatively affect its growth. In response, plants employ molecular mechanisms to defend against these circumstances. Pathogenesis-related protein 10 (PR10) is a well-recognized protein known for its contribution to plant defense across several species. In the current study, we performed a genome-wide analysis of PR10 in durum wheat. We identified 15 *TdPR10* genes clustered into three major subfamilies (Figure 3). The Bet v 1 group possesses the highest number of TdPR10 members, while the MLP group contains only two proteins (TdPR10.10 and TdPR10.11). Zhang et al. [39] confirm that MLP proteins have a smaller gene number in monocots compared to dicot plants.

Recently, it has been shown that the genome of *H. brasiliensis* (rubber tree) contains 132 *PR10*-encoding genes clustered into two major groups: the major allergen Pru ar 1-like

proteins and the major latex protein (MLP)-like proteins. Additionally, three minor groups (three phytohormone-binding proteins (PhBPs), two norbelladine synthase proteins, and LP423/uncharacterized proteins) were identified within the two major groups. Most of these genes are located on chromosome 15. The corresponding PR10 proteins are small, acidic proteins with molecular weights ranging from 11 to 41.52 kDa that lack any signal peptide, in contrast to other PR proteins such as PR-1 [40]. Predicted protein functions indicate that HbPR10 may be involved in protein phosphatase inhibitor activity, abscisic acid binding activity, and signaling receptor activity. These proteins are implicated in plant defense and responses to ABA-activated signaling pathways [7]. In grape, identified PR10 proteins were classified into five groups: ABA receptors, MLP-like proteins, major allergen Pru av 1 protein/STH-2 proteins, S-norcoclaurine synthase (NCS)-like proteins, and uncharacterized proteins [39]. Moreover, the putative PR10 proteins identified in durum wheat were closely related to allergens such as Bet v 1 [41], Pru av 1 [29], Mal d 1 [10], and Cas s 1 [33], suggesting their potential functions as allergens. However, a myriad of allergens play crucial roles in plant defense against abiotic and biotic stresses [42]. For instance, the allergen Gly m 4 from *Glycine max* enhances resistance to *Phytophthora sojae* infection [20]. The major allergen from apple (*Malus domestica*), Mal d 1, exhibits tolerance against *Alternaria alternata* infection [43] and also against stressful environmental challenges (chemical exposure, wounding) [44]. These data allow us to formulate further hypotheses regarding the possible roles of TdPR10 proteins. Furthermore, the P-loop motif of the nucleotide binding proteins, which is involved in binding, catalysis, recognition and regulation of activity of the substrate [45], was harbored by all the putative TdPR10 proteins. Thus, motif 1 present in all the TdPR10 sequences (Figure 1D) is associated with the glycine rich P-loop motif (Supplemental Figure S1). This affirmation led us to suggest the role of TdPR10 wheat plants. Bet V 1 signatures were presented by motif 1 (which was harbored in all PR 10 sequences) and motif 5 (group I and II) or motif 8 (group III). These results are explained by the different classifications of TdPR10 proteins (Figure 3). On the other side, a unique motif arrangement was strongly associated with one protein subgroup, based the classification of TdPR10 proteins in the phylogenetic tree (Figure 1A,D).

Based on the predicted coding sequences and their corresponding genomic sequence results, each TdPR10 subfamily shares a common exon-intron distribution, as well as a similar arrangement and localization of conserved motifs. Thus, during their evolution, variations in gene structures may have occurred. In durum wheat, most PR10 genes from different plant species contain two exons and one intron, while a few possess a unique exon [6,46]. In contrast, in *Vitis vinifera*, two *VvMLP* genes have three exons [39].

Analysis of the physicochemical characteristics of PR10 proteins from various species yields similar results. Almost all PR10 proteins have a pI of less than 7. For instance, as observed in durum wheat, all PR10 proteins in cashew nuts are acidic [47], while only 7 out of 45 in tomato [6] and 3 out of 34 in common bean [46] are basic. In this study, in silico analysis shows that the deduced PR10 proteins of wheat are located in the cytoplasm, similar to their orthologues in tomato plants [6]. Moreover, TdPR10.13 is potentially localized in both the cytoplasm and nucleus, akin to PvMLP2 [46] and HcPR10 [48].

Different localizations of PR10 proteins have been reported in previous studies. For instance, VpPR10.2 proteins were dynamically distributed inside or outside of host cells upon the invasion of the oomycete *Plasmopara viticola* [19]. Gly m 4l proteins were found at the cell membrane in *Arabidopsis* protoplast cells [20]. The HcPR10 protein was present in both the nucleus and cytoplasm during plant development [48]. These findings provide insights into the roles of PR10 proteins in plant defense and stress tolerance and will aid our future analyses to advance our understanding of the roles of PR10 proteins in durum wheat plants.

To gain insights into the role of *TdPR10* genes, we analyzed the predicted cis-elements in their promoter regions (Figure 7). The findings indicated that cis-regulatory elements related to hormonal signaling and stress responses are prevalent in most TdPR10 promoters. Among these, the prTdPR10.1 promoter contains the highest number of cis-elements

associated with hormone signaling, growth and development, and stress responses. Previous studies have similarly highlighted the involvement of *PR10* genes in both biotic and abiotic stress responses, as well as in phytohormone signaling [39,46]. Therefore, we suggest that the expression of *PR10* genes is induced in response to various environmental conditions. Furthermore, the diversity of these cis-regulatory mechanisms may contribute to the evolution of gene expression [49].

Stressors such as salt, cold, and metal toxicity induce complex physiological, biochemical, and molecular responses in plants [7,44]. Our RT-qPCR data (Figures 8 and 9) demonstrate that *TdPR10* genes exhibit distinct expression patterns in response to abiotic stress and phytohormone treatments. Notably, after 24 h of exposure to these abiotic stresses, the *TdPR10.1*, *TdPR10.3*, and *TdPR10.14* genes were significantly activated in leaves (Figure 8), indicating their critical role in durum wheat's adaptation to various environmental conditions. Similar findings regarding the induction of PR10 expression by hormones and abiotic stressors have been reported in different plant species. For instance, roots being subjected to salt, dehydration, and fungal infections induces RsOsPR10 [30]. Additionally, salicylic acid (SA) and copper stress activate SsPR10 in *Solanum surattense* and ZmPR10 in maize [46,47]. In common bean roots, PvPR1 and PvPR2 proteins are induced by copper stress [48], while jasmonate (JA) signaling activates many *PR10* genes [19,30].

Quantitative real-time PCR (RT-qPCR) analyses showed that 10 *PR10* genes are involved in roots under cold and NaCl stresses during 72 h of stress application, with the exception of PR10.2, PR10.9, and PR10.10. In leaves, PR10.1 was downregulated during the 72 h following NaCl stress application, whereas other genes were upregulated after 24 h of stress and subsequently downregulated at 72 h. Interestingly, the majority of PR10 genes were downregulated in leaves after hormonal application (SA, ABA) [46]. Moreover, *PvPR10* genes in leaves are upregulated by exogenous JA and ethylene precursor (ETP) application, suggesting their involvement in JA/ET signaling pathways [37]. Recent investigations have demonstrated that PR10/Bet v1 proteins play critical roles during the biotrophic phase of common bean infection cycles through their interactions with the ethylene (ET), SA, and JA pathways [49].

In our study, we observed that exogenous treatments with ABA, SA, or JA significantly increased TdPR10.15 expression in leaves, while many *TdPR10* genes exhibited strong expression in roots (Figure 9). Recently, 24 *SsPR10* family genes were identified in the *Saccharum spontaneum* genome, subdivided into two subfamilies: IPR10 (SsIPR10-1–14) and NCS (SsNCS-1–10). Bioinformatics analyses indicated that six and two sets of SsPR10 underwent tandem and fragmental duplication events, respectively. Foliar application of exogenous SA in two sugarcane cultivars (LCP85-384 and ROC20) resulted in significant differences in the expression profiles of several *PR10* genes. For instance, SsPR10-1, -2, -4, -7, -11, and -12 were upregulated in LCP85-384 at 12 h post-treatment (hpt) but downregulated by 81.3% in ROC20 at 24 hpt compared to the control [50].

To date, cryoprotective activity has been tested in various cold-induced proteins, such as COR15 in *Arabidopsis* [51] and CAP85 in spinach [52], using lactate dehydrogenase (LDH) as a freeze-labile model enzyme. However, these proteins belong to the late embryogenesis abundant (LEA) protein family [53]. To our knowledge, AHCSP33, a PR5 protein from groundnut, is the only example within the PR protein family that has demonstrated in vitro cryoprotective activity against LDH [54]. Additionally, WAP18, a member of the PR-10/Bet v 1 protein family in mulberry, has also exhibited cryoprotective activity against the freeze-labile enzyme LDH [55]. These findings suggest that WAP18 may play a crucial role in enhancing freezing tolerance in mulberry trees during winter [55]. In our study, TdPR10.1 demonstrated protective effects against heat, cold, freezing, and dehydration, showing more significant activity than BSA, a well-known protective protein [56]. Our data confirm that TdPR10.1 effectively preserves LDH activity against enzymatic inactivation caused by these stress treatments.

In addition to their involvement in the signaling pathways of defense genes, PR10 proteins are known for their ribonucleolytic activity, which allows them to cleave the

RNA of invading pathogens [4]. During pathogen infection, the RNase activity of PR10 proteins can exert a cytotoxic effect on cells and inhibit pathogen growth by degrading pathogen RNA [6,57–59]. This inhibition primarily occurs through the penetration of ribonucleases into the pathogen, followed by the phosphorylation of PR10 proteins, leading to the degradation of pathogenic cell RNAs [60]. A novel PR10 protein, SaPR10.1, was isolated from *Saccharum arundinaceum*. SaPR10.1 is a small, hydrophilic, acidic protein that lacks the P-loop motif typically associated with RNase activity in other PR10 proteins. Its complex 2D structure suggests that SaPR10.1 may bind to multiple molecules of trans-zeatin, which differs from other orthologs. The authors propose that SaPR10.1 could play a role in the more efficient depletion of free trans-zeatin [61]. In rice, the RNase activity of JIOsPR10 was found to be abolished following treatment with DTT in a native in-gel assay. Additionally, the substitution of specific serine residues (C81S, C83S, C81/83S) significantly decreased the RNase activity of the C83S mutant, highlighting the critical role of disulfide bonds between cysteine residues in PR-10 proteins. These bonds may be important for the constitutive self-defense mechanisms in plants against both biotic and abiotic stresses [37]. While several PR10 proteins exhibit RNase activity, it is not considered a universal characteristic [62]. RNase activity is particularly relevant under biotic and abiotic stress conditions, as these proteins participate in plant hypersensitive response (HR) signaling, programmed cell death, and apoptosis processes [18,63].

Additionally, PR10 proteins can interact with plant hormones such as ABA, JA, IAA, ET, and SA, which are involved in hormone-mediated signaling pathways that mitigate damage caused by biotic and abiotic stress [4,64]. For example, in plants infected with *Verticillium dahliae*, *PR10* genes were found to be upregulated following an expression profile investigation in the leaves, roots, and stems of strawberry plants [65]. The induction of several phytohormones, including ABA, SA, JA, and GA, was observed during the early stages of plant–pathogen interactions. In contrast, only two hormones, IAA and JA, were induced in the roots, and this occurred during the later stages of infection [65].

There is substantial evidence supporting the general efficacy of PR10 proteins against a range of phytopathogens, including fungi, bacteria, and viruses [4,16]. Furthermore, one study highlighted the protease inhibitory activity of PR10 proteins against the root-knot nematode *Meloidogyne incognita* [66]. Regarding the activity of PR10 proteins against pathogens, although the mechanisms are not fully elucidated, these enzymes are believed to be associated with endogenous cytokinin (CK) concentrations and may participate in negative feedback regulation. CK plays a crucial role in modulating plant immunity, directly influencing the plant's defense response to various pathogens [4,67,68].

In our study, we found that the TdPR10.1 protein exhibits antifungal activity against *Fusarium graminearum* and *Botrytis cinerea*, with both minimum inhibitory concentration (MIC) and minimum fungicidal concentration (MFC) values around 500 μg/mL. Since the MFC/MIC ratio equals 1 for these fungi, TdPR10.1 is classified as a fungicidal agent. Furthermore, the same ratio of 1 was observed for *Aspergillus niger* and *Fusarium graminearum*, indicating that the minimum concentration required to inhibit fungal growth is the same as that needed to kill the fungi completely. This suggests that TdPR10.1 is an effective fungicidal agent.

4. Materials and Methods

4.1. Identification of PR10 Family Members of T. durum

Members of the PR10 family in the *Triticum durum* (Svevo.v1) genome were identified using a BLAST search, with our previously identified TdPR10.1 serving as the query. This search utilized the Ensembl Plants database (https://plants.ensembl.org/index.html (accessed on 20 February 2024)). The presence of the conserved domain characteristic of PR proteins, specifically the Bet v 1 domain (PF00407), was verified in the retrieved sequences through InterPro (https://www.ebi.ac.uk/interpro/ (accessed on 20 February 2024)) and CD-search (https://www.ncbi.nlm.nih.gov/Structure/cdd/wrpsb.cgi (accessed

on 22 February 2024)) [69]. Any redundant sequences were manually removed from the dataset.

4.2. Characterization of T. durum PR10 Family Members

The conserved motifs and the Bet v 1 domain (PF00407) of the *Triticum durum* PR10 family members were identified using TBtools-II v 2.070 software [70]. Gene structures were visualized with the same program after obtaining GFF3 files for the *TdPR10* genes from the Ensembl Plants website (https://plants.ensembl.org/index.html (accessed on 22 February 2024)). Chromosomal gene mapping of the *T. durum* PR10 family was conducted using the MG2C v2.1 online tool (http://mg2c.iask.in/mg2c_v2.1/ (accessed on 24 February 2024)). Physicochemical parameters, including molecular weight, theoretical pI, and instability index for the members of the *T. durum* PR10 family, were determined using the ProtParam tool (https://web.expasy.org/protparam/ (accessed on 25 February 2024)). Additionally, the in silico subcellular localization of these proteins was predicted using the WolfPsort subcellular localization predictor (https://wolfpsort.hgc.jp/ (accessed on 25 February 2024)) [71]. Biological processes and molecular functions of the TdPR10 proteins were retrieved from the InterPro database (https://www.ebi.ac.uk/interpro/ (accessed on 26 February 2024)).

4.3. Phylogenetic Relationships Analysis of TdPR10

A multiple sequence alignment of TdPR10 proteins was performed using the MUSCLE algorithm in MEGA 11 software [72] and visualized with GeneDoc v2.7 [73]. The PR10 protein family in *Triticum durum* was clustered into a phylogenetic tree alongside known PR10 proteins from various plant species using the maximum likelihood method with 1000 replicates in MEGA 11 [72]. Furthermore, to determine the percentage of identity between proteins, we utilized TBtools-II v 2.070 software [70].

4.4. Prediction of Tridimensional Structure of TdPR10 Proteins

The 3D structures of TdPR10 proteins were predicted using the SWISS-MODEL server [74]. To visualize the molecular pockets of these proteins, we employed the CASTp 3.0 online server (http://sts.bioe.uic.edu/castp/calculation.html (accessed on 27 February 2024)).

4.5. Analysis of Cis-Acting Regulatory Elements in the TdPR10 Promoter Regions

TdPR10 promoter sequences extending 1.5 Kb upstream of the start codons were retrieved from the EnsemblPlants database (https://plants.ensembl.org/index.html (accessed on 2 March 2024)). Each sequence was then analyzed using the PlantCare web tool (https://bioinformatics.psb.ugent.be/webtools/plantcare/html/ (accessed on 2 March 2024)) [75].

4.6. Plant Material and Stress Treatments

Seeds of durum wheat, cv. Om Rabiaa, were used as plant material and surface-sterilized with 95% alcohol followed by treatment with 0.2% mercuric chloride [76]. The seeds were then germinated in a mixture of peat and perlite (2:1 ratio) in a glasshouse maintained at day and night temperatures of 24 °C and 18 °C, respectively, with relative humidity ranging from 60% to 70%. Two-week-old seedlings were subjected to salt stress by irrigation with a 150 mM NaCl solution [77] or cadmium chloride ($CdCl_2$) at a concentration of 0.1 mM [78]. Cold stress was induced by transferring the seedlings to 4 °C. Phytohormones, including jasmonate (JA; 0.25 mM) and salicylic acid (SA; 0.25 mM), were applied via foliar spraying as described by [79]. Additionally, the seedlings were treated with abscisic acid (ABA; 0.1 mM) [80]. Control seedlings were maintained under normal conditions without stress. After 24 and 72 h of stress application, leaf and root tissues were collected from both treated and control plants, immediately frozen in liquid nitrogen,

and stored at −80 °C for total RNA extraction. Three separate biological replicates were performed, with four plants used per replicate.

4.7. RNA Isolation and Real-Time Quantitative PCR

Total RNA was isolated from plant tissues using TRIzol reagent (Thermo Fisher Scientific, Waltham, MA, USA) with the modifications to the method described by [62]. The extracted RNA was treated with 1 U of RNase-free DNase (Thermo Fisher Scientific, Waltham, MA, USA) for 10 min at 37 °C to degrade any residual genomic DNA. Subsequently, the RNA was used for the synthesis of first strand cDNA using M-MLV reverse transcriptase (Invitrogen) and Oligo-dT(18 mer). For RT-qPCR experiments, 3 µL of synthetic cDNA (equivalent to 40 ng) was mixed with 5 µL of Maxima SYBR Green qPCR Master Mix (2×) (Thermo Fisher Scientific, Waltham, MA, USA), 0.5 µL of each primer (10 µM), resulting in a total mixture volume of 10 µL. PCR reactions were performed using the CFX96 real-time PCR detection system (Bio-Rad, Hercules, CA, USA) as described by [81]. The quantitative RT-qPCR reactions began with initial denaturation at 94 °C for 10 min, followed by 45 cycles at 94 °C for 10 s, 60 °C for 10 s, and 72 °C for 15 s. The reference gene TdActin was used to normalize gene expression levels. Primer sequences for RT-qPCR were designed for gene specificity using Primer3 web v4.1.0 (https://primer3.ut.ee/ (accessed on 15 July 2024)) (see Table S1). Relative expression levels were calculated using the $2-\Delta\Delta CT$ method [82]. Each sample was analyzed in triplicate (technical replication), and each experimental condition was performed in triplicate (biological replication).

4.8. Production and Purification of TdPR10.1 Protein

To construct the expression vector pGEX-TdPR10.1, specific primers with restriction enzyme sites (*Eco*RI) were designed to ensure in-frame cloning: PR10_EcoI_Fw (5′-GAATTCATGGCATCTTCCAAGAGT-3′) and PR10_NotI_Rev (5′-GAATTCGGCTTCG GCGTCAAG-3′). The amplified products were cloned into the pGEX vector at the *Eco*RI site to express the pGEX-TdPR10.1 fusion protein. The E. coli strain BL21 was used for recombinant protein expression. Cultures were grown overnight in LB medium supplemented with 100 µg/mL ampicillin. An aliquot of the overnight culture was diluted 1:50 with 1 L of LB medium and grown at 28 °C. When the optical density at 600 nm (OD) reached 1, isopropyl β-D-thiogalactopyranoside (IPTG) was added to a final concentration of 1 mM. The induced cells were harvested, washed, and collected by centrifugation at 6000 rpm for 20 min at 4 °C. The resulting pellets were frozen at −20 °C. Each bacterial pellet was resuspended in an equal volume of active aluminum oxide and ground on ice. Subsequently, 35 mL of lysis buffer (20 mM Tris-HCl, pH 8; 100 mM NaCl; 1 mM PMSF; 0.5% NP-40) was added and mixed well. The lysates were clarified by centrifugation at 6000 rpm for 20 min at 4 °C. The clarified supernatant was then incubated overnight with 1 mL of glutathione Sepharose 4B resin (GE Healthcare, Chicago, IL, USA), which had been previously equilibrated with 1X PBS, for 1 h with gentle shaking at 4 °C. The resin was washed three times with 1X PBS. To remove the GST-tag, 1 mL of Phosphate Buffered Saline (PBS, pH 7.3) containing 5 U of bovine thrombin (Calbiochem, Darmstadt, Germany) was added to the resin. After a 16-h incubation at 22 °C, the non-retained fraction was recovered by pelleting the resin. To ensure optimal recovery of the protein of interest, the resin was washed with 1 mL of PBS, yielding a final volume of 2 mL. The presence of the protein was confirmed by SDS-PAGE, and protein concentrations were determined using a spectrophotometer at 595 nm with the Bradford protein assay.

4.9. In Vitro Analysis of TdPR10 Protein

4.9.1. LDH Protective Assay

A solution of freeze-labile lactate dehydrogenase (LDH) enzyme (EC 1.1.1.27, rabbit muscle LDH) from Sigma (Tokyo, Japan) was prepared at a concentration of 20 µg/mL in 10 mM sodium phosphate, pH 7.4. This LDH solution was mixed with an equal volume of buffer containing either 20 µg/mL of bovine serum albumin (BSA) or TdPR10-1.

The samples were then subjected to heat stress, cold stress, freezing stress, and dehydration stress treatments. To determine LDH activity, 20 µL of the LDH mixture was diluted to 1 mL with assay buffer (10 mM sodium phosphate, pH 7.4, 2 mM NADH, and 10 mM pyruvic acid). The oxidation of NADH was monitored by measuring the absorbance at 340 nm (A340) over 3 min, during which the reaction rate remained linear. The rate of absorbance change was used to calculate the activity using the formula ΔDO/min × 8095 = U/L\Delta DO/min\times 8095 = U/LΔDO/min × 8095 = U/L (Biomaghreb kit). All samples were assayed in triplicate.

4.9.2. Ribonuclease Activity

The RNase activity of the purified recombinant TdPR10.1 protein was assessed by incubating the reaction mixtures at 37 °C for 1 to 4 h, following the method described in [83]. To evaluate the RNA degradation activity, 20 µL of reaction mixture was prepared, containing 10 µg of total RNA extracted from durum wheat 'cv. Om Rabiaa' and 30 µg of TdPR10.1 protein. The reaction mixture was then extracted with phenol-chloroform (1:1), and the aqueous layer was analyzed on a 1.2% agarose gel. RNA was visualized under UV light.

4.9.3. Antifungal Activity Tests/Evaluation of Minimal Inhibitory Concentration (MIC) and Minimal Fungicidal Concentration (MFC)

The minimum inhibitory concentration (MIC) of the TdPR10.1 protein was determined against various phytopathogenic fungi, namely *Fusarium oxysporum*, *Fusarium culmorum*, *Fusarium graminearum*, *Aspergillus niger*, and *Botrytis cinerea*, using the broth microdilution method in 96-well microplates, as described in [84]. A twofold serial dilution of the protein was prepared in the microplate wells, ranging from 1.95 to 500 µg/mL. Subsequently, 10 µL of a fungal spore solution (10^5 spores/mL) was added to each well, and the plates were incubated at 25 °C for 72 h. Wells containing fungal spores without TdPR10.1 served as positive controls. The MIC was defined as the lowest concentration of the protein that exhibited no visible growth of the tested microorganisms after incubation.

For the minimum fungicidal concentration (MFC) evaluation, 10 µL was taken from each well showing fungal proliferation, plated on PDA agar, and incubated at 25 °C for 72 h. The lowest concentration that yielded no growth on the agar was considered the MFC, indicating that >99.9% of the original inoculum was killed. The experiments were repeated three times to ensure reliability.

4.10. Statistical Analysis

Statistical analysis of the results was conducted using SPSS version 20, employing the ANOVA method. Means were compared using Tukey's HSD test, with different letters indicating significant differences ($p < 0.05$).

5. Conclusions

In the current study, we identified 15 genes belonging to the PR10 family in the durum wheat genome. Using phylogenetic analysis, we grouped these genes into three major subfamilies. We further investigated their evolution by examining their structure, relationships, chromosomal arrangement, synteny, and repeat patterns. Our results revealed a significant increase in the activity of several *TdPR10* genes in the leaves and roots under stress, indicating their involvement in various metabolic pathways in durum wheat. Moreover, TdPR10.1 demonstrated protective effects on lactate dehydrogenase (LDH) and exhibited RNase activity in vitro, confirming its role as a pathogenesis-related enzyme. Finally, the TdPR10.1 protein displayed fungicidal effects against *A. niger* and *F. graminearum*, while serving as a growth inhibitor for *F. oxysporum* and *B. cinerea*. However, further research is needed to elucidate the functions of these *TdPR10* genes and their potential contributions to enhancing crop stress tolerance.

Supplementary Materials: The following supporting information can be downloaded at: https://www.mdpi.com/article/10.3390/plants13223128/s1, Figure S1: (A) Alignment of the durum wheat PR10 proteins by using the muscle algorithm of MEGA 11 and visualized by genedoc software. (B) A specific Bet v 1 signature of TdPR10 created with the WebLogo tool. Figure S2. Identity analysis of TdPR10 proteins and other PR10 proteins from different species known by their functions: Pru av 1 from *Prunus avium* (sweet cherry) (O24248.1); Pyrc1 from *Pyrus communis* (AAC13315.1); Api g 1(P49372.1) from *Apium graveolens*; Dau c 1 (O04298.1); Cor a 1 (Q08407.3) from *Corylus avellana*; Ara h 8 from *Arachis hypogaea* (AAQ91847.1); Cas s 1 (ACJ23861.1) from *Castanea sativa*; *PmPr10-3.1* (AAL50006.1) from *Pinus monticola*; HbPR10 (XP_021658365.1) from *Hevea brasiliensis*; NbMLP28: MLP-like protein 28 from *Nicotiana benthamiana* (QEH62705.1); PBZ1: (BAA24277.1) from *Oryza sativa* Japonica; *Gly m 4l* (HQ913577.1) from *Glycine max*; Intracellular pathogenesis-related protein PinmIII from *Pinus monticola* (AAC33531.1) and Solyc09g090980 from *Solanum lycopersicum.* Figure S3: Production and purification of TdPR10-1 protein from *E. coli* strain. Coomassie blue staining of SDS PAGE gel. (MW), molecular weight markers; (Ex), Extract of TdPR10-1 protein after induction; (Pr), The final purified product of TdPR10-1 as obtained after thrombin cleavage. Table S1: List of primers used in QRT-PCR analysis.

Author Contributions: Conceptualization, I.Y. and F.B.; methodology, E.K., M.G., H.D. and O.J.; software, I.Z.; validation, E.K., I.Z. and F.B.; formal analysis, I.Z. and F.B.; investigation, E.K., H.D., K.H. and M.G.; resources, F.B.; data curation, I.Y. and F.B.; writing—original draft preparation, E.K. and I.Z.; writing—review and editing, I.Y. and F.B.; visualization, I.Y. and F.B.; supervision, F.B.; project administration, F.B.; funding acquisition, F.B. All authors have read and agreed to the published version of the manuscript.

Funding: This research was funded by the Ministry of Higher Education and Scientific Research, grant number: CP2019-2022.

Data Availability Statement: No datasets were generated or analyzed during the current study.

Acknowledgments: The authors are grateful to the Ministry of Higher Education and Scientific Research of Tunisia. Our heartfelt thanks go to Riyadh Koubaa, a teaching assistant at the University of California, Santa Barbara, for his thorough proofreading and constructive feedback on the manuscript.

Conflicts of Interest: The authors declare no conflicts of interest.

References

1. Nykiel, M.; Gietler, M.; Fidler, J.; Prabucka, B.; Rybarczyk-Płońska, A.; Graska, J.; Boguszewska-Mańkowska, D.; Muszyńska, E.; Morkunas, I.; Labudda, M. Signal transduction in cereal plants struggling with environmental stresses: From perception to response. *Plants* **2022**, *11*, 1009. [CrossRef]
2. Agarwal, P.; Agarwal, P.K. Pathogenesis related-10 proteins are small, structurally similar but with diverse role in stress signaling. *Mol. Biol. Rep.* **2014**, *41*, 599–611. [CrossRef] [PubMed]
3. Zribi, I.; Ghorbel, M.; Brini, F. Pathogenesis related proteins (PRs): From cellular mechanisms to plant defense. *Curr. Protein Pep. Sci.* **2021**, *22*, 396–412. [CrossRef]
4. Sinha, R.K.; Verma, S.S.; Rastogi, A. Role of Pathogen-Related Protein 10 (PR 10) under abiotic and biotic stresses in plants. *Phyton* **2020**, *89*, 167. [CrossRef]
5. Liu, X.; Huang, B.; Lin, J.; Fei, J.; Chen, Z.; Pang, Y.; Sun, X.; Tang, K. A novel pathogenesis-related protein (SsPR10) from *Solanum surattense* with ribonucleolytic and antimicrobial activity is stress-and pathogen-inducible. *J. Plant Physiol.* **2006**, *163*, 546–556. [CrossRef] [PubMed]
6. Islam, M.M.; Qi, S.; Zhang, S.; Amin, B.; Yadav, V.; El-Sappah, A.H.; Zhang, F.; Liang, Y. Genome-wide identification and functions against tomato spotted wilt tospovirus of PR-10 in *Solanum lycopersicum*. *Int. J. Mol. Sci.* **2022**, *23*, 1502. [CrossRef] [PubMed]
7. Longsaward, R.; Viboonjun, U. Genome-wide identification of rubber tree pathogenesis-related 10 (PR-10) proteins with biological relevance to plant defense. *Sci. Rep.* **2024**, *14*, 1072. [CrossRef]
8. Breiteneder, H.; Pettenburger, K.; Bito, A.; Valenta, R.; Kraft, D.; Rumpold, H.; Scheiner, O.; Breitenbach, M. The gene coding for the major birch pollen allergen Betv1, is highly homologous to a pea disease resistance response gene. *EMBO J.* **1989**, *8*, 1935–1938. [CrossRef]
9. Scheurer, S.; Son, D.Y.; Boehm, M.; Karamloo, F.; Franke, S.; Hoffmann, A.; Haustein, D.; Vieths, S. Cross-reactivity and epitope analysis of Pru a 1, the major cherry allergen. *Mol. Immunol.* **1999**, *36*, 155–167. [CrossRef]
10. Vanekkrebitz, M.; Hoffmannsommergruber, K.; Machado, M.; Susani, M.; Ebner, C.; Kraft, D.; Scheiner, O.; Breiteneder, H. Cloning and sequencing of Mal d 1, the major allergen from apple (*Malus domestica*), and its immunological relationship to Bet v 1, the major birch pollen allergen. *Biochem. Biophys. Res. Commun.* **1995**, *214*, 538–551. [CrossRef]

11. Marković-Housley, Z.; Basle, A.; Padavattan, S.; Maderegger, B.; Schirmer, T.; Hoffmann-Sommergruber, K. Structure of the major carrot allergen Dau c 1. *Acta Crystallogr. Sect. D Biol. Crystallogr.* **2009**, *65*, 1206–1212. [CrossRef]
12. Balmeh, N.; Mahmoudi, S.; Pourhoseyni, H.; Fard, N.A. An in-silico approach of allergenicity reduction in PR10 and profilin families of pan allergens using allergen-IgE docking analysis. *Rev. Fr. Allergol.* **2022**, *62*, 521–528. [CrossRef]
13. Morris, J.S.; Caldo, K.M.P.; Liang, S.; Facchini, P.J. PR10/Bet v1-like proteins as novel contributors to plant biochemical diversity. *ChemBioChem* **2021**, *22*, 264–287. [CrossRef] [PubMed]
14. Rajendram, A.; Mostaffa, N.H.; Dumin, W.; Oke, M.A.; Simarani, K.; Somasundram, C.; Razali, Z.; Rejab, N.A.; Al-Idrus, A. Dual activity of *Meloidogyne incognita*-regulated *Musa acuminata* Pathogenesis-related-10 (MaPR-10) gene. *Gene* **2022**, *809*, 146041. [CrossRef] [PubMed]
15. Dastmalchi, M.; Chen, X.; Hagel, J.M.; Chang, L.; Chen, R.; Ramasamy, S.; Yeaman, S.; Facchini, P.J. Neopinone isomerase is involved in codeine and morphine biosynthesis in opium poppy. *Nat. Chem. Biol.* **2019**, *15*, 384–390. [CrossRef]
16. Aglas, L.; Soh, W.T.; Kraiem, A.; Wenger, M.; Brandstetter, H.; Ferreira, F. Ligand binding of PR-10 proteins with a particular focus on the Bet v 1 allergen family. *Curr. Allergy Asthma Rep.* **2020**, *20*, 25. [CrossRef]
17. Pungartnik, C.; Da Silva, A.C.; de Melo, S.A.; Gramacho, K.P.; de Mattos Cascardo, J.C.; Brendel, M.; Micheli, F.; da Silva Gesteira, A. High-affinity copper transport and Snq2 export permease of *Saccharomyces cerevisiae* modulate cytotoxicity of PR-10 from *Theobroma cacao*. *Mol. Plant-Microbe Interact.* **2009**, *22*, 39–51. [CrossRef]
18. Choi, D.S.; Hwang, I.S.; Hwang, B.K. Requirement of the cytosolic interaction between pathogenesis-related protein10 and leucine-rich repeat protein1 for cell death and defense signaling in pepper. *Plant Cell Rep.* **2012**, *24*, 1675–1690. [CrossRef]
19. He, M.; Xu, Y.; Cao, J.; Zhu, Z.; Jiao, Y.; Wang, Y.; Guan, X.; Yang, Y.; Xu, W.; Fu, Z. Subcellular localization and functional analyses of a PR10 protein gene from *Vitis pseudoreticulata* in response to *Plasmopara viticola* infection. *Protoplasma* **2013**, *250*, 129–140. [CrossRef]
20. Fan, S.; Jiang, L.; Wu, J.; Dong, L.; Cheng, Q.; Xu, P.; Zhang, S. A novel pathogenesis-related class 10 protein Gly m 4l, increases resistance upon *Phytophthora sojae* infection in soybean (*Glycine max* [L.] Merr.). *PLoS ONE* **2015**, *10*, e0140364. [CrossRef]
21. Fernandes, H.; Michalska, K.; Sikorski, M.; Jaskolski, M. Structural and functional aspects of PR-10 proteins. *FEBS J.* **2013**, *280*, 1169–1199. [CrossRef] [PubMed]
22. Saraste, M.; Sibbald, P.R.; Wittinghofer, A. The P-loop—A common motif in ATP-and GTP-binding proteins. *Trends Biochem. Sci.* **1990**, *15*, 430–434. [CrossRef] [PubMed]
23. Michalska, K.; Fernandes, H.; Sikorski, M.; Jaskolski, M. Crystal structure of Hyp-1, a St. John's wort protein implicated in the biosynthesis of hypericin. *J. Struct. Biol.* **2010**, *169*, 161–171. [CrossRef]
24. Osmark, P.; Boyle, B.; Brisson, N. Sequential and structural homology between intracellular pathogenesis-related proteins and a group of latex proteins. *Plant Mol. Biol.* **1998**, *38*, 1243–1246. [CrossRef] [PubMed]
25. Ruszkowski, M.; Sliwiak, J.; Ciesielska, A.; Barciszewski, J.; Sikorski, M.; Jaskolski, M. Specific binding of gibberellic acid by cytokinin-specific binding proteins: A new aspect of plant hormone-binding proteins with the PR-10 fold. *Acta Crystallogr. Sect. D Biol. Crystallogr.* **2014**, *70*, 2032–2041. [CrossRef]
26. Samanani, N.; Liscombe, D.K.; Facchini, P.J. Molecular cloning and characterization of norcoclaurine synthase, an enzyme catalyzing the first committed step in benzylisoquinoline alkaloid biosynthesis. *Plant J.* **2004**, *40*, 302–313. [CrossRef]
27. Chen, J.-Y.; Dai, X.-F. Cloning and characterization of the *Gossypium hirsutum* major latex protein gene and functional analysis in *Arabidopsis thaliana*. *Planta* **2010**, *231*, 861–873. [CrossRef]
28. Holmquist, L.; Dölfors, F.; Fogelqvist, J.; Cohn, J.; Kraft, T.; Dixelius, C. Major latex protein-like encoding genes contribute to *Rhizoctonia solani* defense responses in sugar beet. *Mol. Genet. Genom.* **2021**, *296*, 155–164. [CrossRef]
29. Scheurer, S.; Metzner, K.; Haustein, D.; Vieths, S. Molecular cloning, expression and characterization of Pru a 1, the major cherry allergen. *Mol. Immunol.* **1997**, *34*, 619–629. [CrossRef]
30. Jarolim, E.; Tejkl, M.; Rohac, M.; Schlerka, G.; Scheiner, O.; Kraft, D.; Breitenbach, M.; Rumpold, H. Monoclonal antibodies against birch pollen allergens: Characterization by immunoblotting and use for single-step affinity purification of the major allergen Bet v I. *Int. Arch. Allergy Immunol.* **1989**, *90*, 54–60. [CrossRef]
31. Karamloo, F.; Scheurer, S.; Wangorsch, A.; May, S.; Haustein, D.; Vieths, S. Pyr c 1, the major allergen from pear (*Pyrus communis*), is a new member of the Bet v 1 allergen family. *J. Chromatogr. B Biomed. Appl.* **2001**, *756*, 281–293. [CrossRef]
32. Breiteneder, H.; Hoffmann-Sommergruber, K.; O'Riordain, G.; Susani, M.; Ahorn, H.; Ebner, C.; Kraft, D.; Scheiner, O. Molecular Characterization of Api g 1, the Major Allergen of Celery (*Apium graveolens*), and Its Immumological and Structural Relationships to a Group of 17-kDa Tree Pollen Allergens. *Eur. J. Biochem.* **1995**, *233*, 484–489. [CrossRef] [PubMed]
33. Hirschwehr, R.; Valenta, R.; Ebner, C.; Ferreira, F.; Sperr, W.R.; Valent, P.; Rohac, M.; Rumpold, H.; Scheiner, O.; Kraft, D. Identification of common allergenic structures in hazel pollen and hazelnuts: A possible explanation for sensitivity to hazelnuts in patients allergic to tree pollen. *J. Allergy Clin. Immunol.* **1992**, *90*, 927–936. [CrossRef]
34. Riecken, S.; Lindner, B.; Petersen, A.; Jappe, U.; Becker, W.-M. Purification and characterization of natural Ara h 8, the Bet v 1 homologous allergen from peanut, provides a novel isoform. *Biol. Chem.* **2008**, *389*, 415–423. [CrossRef] [PubMed]
35. Liu, J.-J.; Fernandes, H.; Zamany, A.; Sikorski, M.; Jaskolski, M.; Sniezko, R.A. In-vitro anti-fungal assay and association analysis reveal a role for the *Pinus monticola* PR10 gene (PmPR10-3.1) in quantitative disease resistance to white pine blister rust. *Genome* **2021**, *64*, 693–704. [CrossRef]

36. Liu, J.-J.; Ekramoddoullah, A.K.; Hawkins, B.; Shah, S. Overexpression of a western white pine PR10 protein enhances cold tolerance in transgenic Arabidopsis. *Plant Cell Tissue Organ Cult. (PCTOC)* **2013**, *114*, 217–223. [CrossRef]
37. Kim, S.G.; Kim, S.T.; Wang, Y.; Yu, S.; Choi, I.S.; Kim, Y.C.; Kim, W.T.; Agrawal, G.K.; Rakwal, R.; Kang, K.Y. The RNase activity of rice probenazole-induced protein1 (PBZ1) plays a key role in cell death in plants. *Mol. Cell.* **2011**, *31*, 25–31. [CrossRef] [PubMed]
38. Hashimoto, M.; Kisseleva, L.; Sawa, S.; Furukawa, T.; Komatsu, S.; Koshiba, T. A novel rice PR10 protein, RSOsPR10, specifically induced in roots by biotic and abiotic stresses, possibly via the jasmonic acid signaling pathway. *Plant Cell Physiol.* **2004**, *45*, 550–559. [CrossRef]
39. Zhang, N.; Li, R.; Shen, W.; Jiao, S.; Zhang, J.; Xu, W. Genome-wide evolutionary characterization and expression analyses of major latex protein (MLP) family genes in *Vitis vinifera*. *Mol. Genet. Genom.* **2018**, *293*, 1061–1075. [CrossRef]
40. Zribi, I.; Ghorbel, M.; Haddaji, N.; Besbes, M.; Brini, F. Genome-wide identification and expression profiling of pathogenesis-related protein 1 (PR-1) genes in durum wheat (*Triticum durum* desf.). *Plants* **2023**, *12*, 1998. [CrossRef]
41. Swoboda, I.; Hoffmann-Sommergruber, K.; O'Ríordáin, G.; Scheiner, O.; Heberle-Bors, E.; Vicente, O. Bet v 1 proteins, the major birch pollen allergens and members of a family of conserved pathogenesis-related proteins, show ribonuclease activity in vitro. *Physiol. Plant.* **1996**, *96*, 433–438. [CrossRef]
42. Sinha, M.; Singh, R.P.; Kushwaha, G.S.; Iqbal, N.; Singh, A.; Kaushik, S.; Kaur, P.; Sharma, S.; Singh, T.P. Current overview of allergens of plant pathogenesis related protein families. *Sci. World* **2014**, *2014*, 543195. [CrossRef]
43. Zhang, C.-x.; Tian, Y.; Cong, P.-h. Proteome analysis of pathogen-responsive proteins from apple leaves induced by the alternaria blotch *Alternaria alternata*. *PLoS ONE* **2015**, *10*, e0122233. [CrossRef]
44. Puehringer, H.M.; Zinoecker, I.; Marzban, G.; Katinger, H.; Laimer, M. MdAP, a novel protein in apple, is associated with the major allergen Mal d 1. *Gene* **2003**, *321*, 173–183. [CrossRef]
45. Prasad, G. Glycine rich P-loop motif in deoxyuridine pyrophosphatase. *Curr. Protein Pept. Sci.* **2001**, *2*, 301–311. [CrossRef]
46. Feki, K.; Tounsi, S.; Jemli, S.; Boubakri, H.; Saidi, M.N.; Mrabet, M.; Brini, F.; Mhadhbi, H. Genome-wide identification of PR10 family members and expression profile analysis of PvPR10 in common bean (*Phaseolus vulgaris* L.) in response to hormones and several abiotic stress conditions. *Plant Growth Regul.* **2024**, *102*, 279–295. [CrossRef]
47. Bastiaan-Net, S.; Pina-Pérez, M.C.; Dekkers, B.J.; Westphal, A.H.; America, A.H.; Ariëns, R.M.; de Jong, N.W.; Wichers, H.J.; Mes, J.J. Identification and in silico bioinformatics analysis of PR10 proteins in cashew nut. *Protein Sci.* **2020**, *29*, 1581–1595. [CrossRef]
48. Feng, Y.; Ren, Y.; Zhang, H.; Heng, Y.; Wang, Z.; Wang, Y. *Halostachys caspica* pathogenesis-related protein 10 acts as a cytokinin reservoir to regulate plant growth and development. *Front. Plant Sci.* **2023**, *14*, 1116985. [CrossRef] [PubMed]
49. Baudouin-Gonzalez, L.; Santos, M.A.; Tempesta, C.; Sucena, É.; Roch, F.; Tanaka, K. Diverse cis-regulatory mechanisms contribute to expression evolution of tandem gene duplicates. *Mol. Biol. Evol.* **2017**, *34*, 3132–3147. [CrossRef]
50. Xu, L.-N.; Jiang, X.-R.; Lin, J.-X.; Li, J.; Javed, T.; Zhao, J.-Y.; Gao, S.-J. Pathogenesis-Related Protein 10 Family Genes Involved in Sugarcane Responses to Biotic Stressors and Salicylic Acid. *J. Plant Growth Regul.* **2024**, *43*, 3907–3919. [CrossRef]
51. Lin, C.; Thomashow, M.F. A cold-regulated Arabidopsis gene encodes a polypeptide having potent cryoprotective activity. *Biochem. Biophys. Res. Commun.* **1992**, *183*, 1103–1108. [CrossRef]
52. Kazuoka, T.; Oeda, K. Purification and characterization of COR85-oligomeric complex from cold-acclimated spinach. *Plant Cell Physiol.* **1994**, *35*, 601–611. [CrossRef]
53. Thomashow, M.F. Plant cold acclimation: Freezing tolerance genes and regulatory mechanisms. *Annu. Rev. Plant Biol.* **1999**, *50*, 571–599. [CrossRef]
54. Dave, R.S.; Mitra, R.K. A low temperature induced apoplastic protein isolated from *Arachis hypogaea*. *Phytochem.* **1998**, *49*, 2207–2213. [CrossRef]
55. Ukaji, N.; Kuwabara, C.; Takezawa, D.; Arakawa, K.; Fujikawa, S. Accumulation of pathogenesis-related (PR) 10/Bet v 1 protein homologues in mulberry (*Morus bombycis* Koidz.) tree during winter. *Plant Cell Environ.* **2004**, *27*, 1112–1121. [CrossRef]
56. Tamiya, T.; Okahashi, N.; Sakuma, R.; Aoyama, T.; Akahane, T.; Matsumoto, J.J. Freeze denaturation of enzymes and its prevention with additives. *Cryobiology* **1985**, *22*, 446–456. [CrossRef]
57. Jain, D.; Khurana, J.P. Role of pathogenesis-related (PR) proteins in plant defense mechanism. In *Molecular Aspects of Plant-Pathogen Interaction*; Springer: Cham, Switzerland, 2018; pp. 265–281.
58. Besbes, F.; Franz-Oberdorf, K.; Schwab, W. Phosphorylation-dependent ribonuclease activity of Fra a 1 proteins. *J. Plant Physiol.* **2019**, *233*, 1–11. [CrossRef]
59. Wieczorek, P.; Wrzesińska, B.; Frąckowiak, P.; Przybylska, A.; Obrępalska-Stęplowska, A. Contribution of Tomato torrado virus Vp26 coat protein subunit to systemic necrosis induction and virus infectivity in *Solanum lycopersicum*. *Virol. J.* **2019**, *16*, 9. [CrossRef]
60. Kaur, A.; Kaur, S.; Kaur, A.; Sarao, N.K.; Sharma, D. *Pathogenesis-Related Proteins and Their Transgenic Expression for Developing Disease-Resistant Crops: Strategies Progress and Challenges*; IntechOpen: London, UK, 2022.
61. Mohan, C.; Santos Júnior, C.D.; Chandra, S. In silico characterisation and homology modelling of a pathogenesis-related protein from Saccharum arundinaceum. *Arch. Phytopathol. Plant Protect.* **2020**, *53*, 199–216. [CrossRef]
62. McBride, J.K.; Cheng, H.; Maleki, S.J.; Hurlburt, B.K. Purification and characterization of pathogenesis related class 10 panallergens. *Foods* **2019**, *8*, 609. [CrossRef]
63. Lee, O.R.; Pulla, R.K.; Kim, Y.-J.; Balusamy, S.R.D.; Yang, D.-C. Expression and stress tolerance of PR10 genes from Panax ginseng CA Meyer. *Mol. Biol. Rep.* **2012**, *39*, 2365–2374. [CrossRef]

64. Gao, L. Structure Analysis of a Pathogenesis-Related 10 Protein from *Gardenia jasminoides*. In *IOP Conference Series: Earth and Environmental Science*; IOP Publishing: Bristol, UK, 2019; p. 042005.
65. Besbes, F.; Habegger, R.; Schwab, W. Induction of PR-10 genes and metabolites in strawberry plants in response to *Verticillium dahliae* infection. *BMC Plant Biol.* **2019**, *19*, 128. [CrossRef]
66. Andrade, L.B.d.S.; Oliveira, A.S.; Ribeiro, J.K.; Kiyota, S.; Vasconcelos, I.M.; de Oliveira, J.T.A.; de Sales, M.P. Effects of a novel pathogenesis-related class 10 (PR-10) protein from *Crotalaria pallida* roots with papain inhibitory activity against root-knot nematode *Meloidogyne incognita*. *J. Agric. Food. Chem.* **2010**, *58*, 4145–4152. [CrossRef]
67. Li, B.; Wang, R.; Wang, S.; Zhang, J.; Chang, L. Diversified regulation of cytokinin levels and signaling during *Botrytis cinerea* infection in Arabidopsis. *Front. Plant Sci.* **2021**, *12*, 584042. [CrossRef]
68. Kanwar, M.K.; Yu, J.; Zhou, J. Phytomelatonin: Recent advances and future prospects. *J. Pineal Res.* **2018**, *65*, e12526. [CrossRef]
69. Wang, J.; Chitsaz, F.; Derbyshire, M.K.; Gonzales, N.R.; Gwadz, M.; Lu, S.; Marchler, G.H.; Song, J.S.; Thanki, N.; Yamashita, R.A. The conserved domain database in 2023. *Nucleic Acids Res.* **2023**, *51*, D384–D388. [CrossRef]
70. Chen, C.; Wu, Y.; Li, J.; Wang, X.; Zeng, Z.; Xu, J.; Liu, Y.; Feng, J.; Chen, H.; He, Y. TBtools-II: A "one for all, all for one" bioinformatics platform for biological big-data mining. *Mol. Plant.* **2023**, *16*, 1733–1742. [CrossRef]
71. Horton, P.; Park, K.-J.; Obayashi, T.; Fujita, N.; Harada, H.; Adams-Collier, C.; Nakai, K. WoLF PSORT: Protein localization predictor. *Nucleic Acids Res.* **2007**, *35*, W585–W587. [CrossRef]
72. Tamura, K.; Stecher, G.; Kumar, S. MEGA11: Molecular evolutionary genetics analysis version 11. *Mol. Biol. Evol.* **2021**, *38*, 3022–3027. [CrossRef]
73. Nicholas, K.; Nicholas, B. Genedoc: A Tool for Editing and Annoting Multiple Sequence Alignments. 1997. Available online: http://www.pscedu/biomed/genedoc (accessed on 22 February 2024).
74. Waterhouse, A.; Bertoni, M.; Bienert, S.; Studer, G.; Tauriello, G.; Gumienny, R.; Heer, F.T.; de Beer, T.A.P.; Rempfer, C.; Bordoli, L. SWISS-MODEL: Homology modelling of protein structures and complexes. *Nucleic Acids Res.* **2018**, *46*, W296–W303. [CrossRef]
75. Lescot, M.; Déhais, P.; Thijs, G.; Marchal, K.; Moreau, Y.; Van de Peer, Y.; Rouzé, P.; Rombauts, S. PlantCARE, a database of plant cis-acting regulatory elements and a portal to tools for in silico analysis of promoter sequences. *Nucleic Acids Res.* **2002**, *30*, 325–327. [CrossRef] [PubMed]
76. Mhamdi, R.; Jebara, M.; Aouani, M.; Ghrir, R.; Mars, M. Genotypic diversity and symbiotic effectiveness of rhizobia isolated from root nodules of *Phaseolus vulgaris* L. grown in Tunisian soils. *Biol. Fertil. Soils* **1999**, *28*, 313–320. [CrossRef]
77. Al Hassan, M.; Morosan, M.; López-Gresa, M.d.P.; Prohens, J.; Vicente, O.; Boscaiu, M. Salinity-induced variation in biochemical markers provides insight into the mechanisms of salt tolerance in common (*Phaseolus vulgaris*) and runner (*P. coccineus*) beans. *Int. J. Mol. Sci.* **2016**, *17*, 1582. [CrossRef] [PubMed]
78. Wael, M.S.; Mostafa, M.R.; Taia, A.A.E.-M.; Saad, M.H.; Magdi, T.A. Alleviation of cadmium toxicity in common bean (*Phaseolus vulgaris* L.) plants by the exogenous application of salicylic acid. *J Horti. Sci. Biotechnol.* **2015**, *90*, 83–91. [CrossRef]
79. Ghorbel, M.; Zribi, I.; Chihaoui, M.; Alghamidi, A.; Mseddi, K.; Brini, F. Genome-Wide Investigation and Expression Analysis of the Catalase Gene Family in Oat Plants (*Avena sativa* L.). *Plants* **2023**, *12*, 3694. [CrossRef]
80. Pospíšilová, J. Interaction of cytokinins and abscisic acid during regulation of stomatal opening in bean leaves. *Photosynthetica* **2003**, *41*, 49–56. [CrossRef]
81. Tounsi, S.; Kamoun, Y.; Feki, K.; Jemli, S.; Saïdi, M.N.; Ziadi, H.; Alcon, C.; Brini, F. Localization and expression analysis of a novel catalase from *Triticum monococcum* TmCAT1 involved in response to different environmental stresses. *Plant Physiol. Biochem.* **2019**, *139*, 366–378. [CrossRef]
82. Livak, K.J.; Schmittgen, T.D. Analysis of relative gene expression data using real-time quantitative PCR and the $2-\Delta\Delta CT$ method. *Methods* **2001**, *25*, 402–408. [CrossRef]
83. Bantignies, B.; Séguin, J.; Muzac, I.; Dédaldéchamp, F.; Gulick, P.; Ibrahim, R. Direct evidence for ribonucleolytic activity of a PR-10-like protein from white lupin roots. *Plant Mol. Biol.* **2000**, *42*, 871–881. [CrossRef]
84. Eloff, J.N. A sensitive and quick microplate method to determine the minimal inhibitory concentration of plant extracts for bacteria. *Planta Med.* **1998**, *64*, 711–713. [CrossRef]

plants

MDPI

Article

Genome-Wide Identification of the GPAT Family in *Medicago sativa* L. and Expression Profiling Under Abiotic Stress

Jianzhi Ma [1,2,†], Mingyang Du [1,†], Huiyan Xiong [3] and Ruijun Duan [1,2,*]

[1] College of Eco-Environmental Engineering, Qinghai University, Xining 810016, China; 18194578185@163.com (J.M.); d2501457943@outlook.com (M.D.)
[2] Academy of Agriculture and Forestry Sciences, Qinghai University, Xining 810016, China
[3] College of Agriculture and Animal Husbandry, Qinghai University, Xining 810016, China; huiyanxqh@163.com
* Correspondence: ruijunduan@163.com; Tel.: +86-158-9708-1509
† These authors contributed equally to this work.

Abstract: Glycerol-3-phosphate acyltransferase (GPAT), as a rate-limiting enzyme engaged in lipid synthesis pathways, exerts an important role in plant growth and development as well as environmental adaptation throughout diverse growth stages. Alfalfa (*Medicago sativa* L.) is one of the most significant leguminous forages globally; however, its growth process is frequently exposed to environmental stress, giving rise to issues such as impeded growth and decreased yield. At present, the comprehension of the *GPAT* genes in alfalfa and their reactions to abiotic stresses is conspicuously deficient. This study identified 15 GPATs from the genome of "Zhongmu No. 1" alfalfa, which were phylogenetically categorized into three major groups (Groups I ~ III). Furthermore, Group III is further subdivided into three distinct subgroups. MsGPATs belonging to the same subfamily exhibited similar protein conserved motifs and gene structural characteristics, in which groups with simple conserved motifs had more complex gene structures. A multitude of regulatory *cis*-elements pertinent to hormones and responses to environmental stress were detected in their promoter regions. In addition, a spatial–temporal expression analysis showed that *MsGPATs* have significant tissue specificity. Furthermore, the transcriptomic analysis of ABA treatment and the qRT-PCR results under drought, salt, and cold stress demonstrated that the majority of *MsGPATs* respond to abiotic stress with pronounced timely characteristics. It was also ascertained that these *GPAT* genes might assume a crucial role in salt and drought stress. This research can further constitute a fundamental basis for the exploration of the alfalfa GPAT family, the screening of key GPATs, and the investigation of their functionalities.

Keywords: *Medicago sativa* L.; glycerol-3-phosphate acyltransferase (GPAT); gene family; abiotic stress; expression analysis

1. Introduction

Plant lipids constitute a diverse array of organic compounds that exert critical functions in the structure and operation of plant cells. They mainly encompass triglycerides, phospholipids, glycolipids, and sterols. These compounds are essential components of cell membranes, storage structures, extracellular protective layers, and signaling molecules [1]. Cuticular waxes and cutin play crucial roles as essential lipids that form a protective barrier for plants against biotic and abiotic stress, while also regulating the transportation of water and solutes [2]. Glycerol-3-phosphate acyltransferases (GPATs) are crucial enzymes facilitate glycerol lipid biosynthesis by transferring acyl groups from acyl-CoA(coenzyme A) or acyl-ACP (Acyl carrier protein) to the sn-1 position of G3P (3-phosphoglycerol), resulting in the formation of LPA (lysophosphatidic acid), a key intermediate in the synthesis of extracellular lipid polyesters, as well as storage and membrane lipids; these GPATs belong to the sn-1 type [3]. In contrast, other GPATs exhibit phosphatase activity that facilitates the

formation of 2-MAG (monoacylglycerol), which does not yield LPA as a primary product; these GPATs are classified as sn-2 type [4,5]. The sn-2 type GPAT specifically promotes the acylation of G3P at the sn-2 site, manifesting a propensity for oxidized lipid acyls. This enzyme assumes a pivotal role in safeguarding the stability of plant membrane lipids and is implicated in the biosynthesis of diverse lipids, encompassing cuticular waxes and cutin, thereby engaging in the signal transduction pathways associated with abiotic stress responses.

Currently, the GPAT family is well studied in *Arabidopsis thaliana*, with 10 *AtGPAT*s characterized, including AtGPAT1-AtGPAT9 and ATS1 [6]. ATS1 and AtGPAT9 are of the sn-1 type. In a previous study, these GPATs were classified into three distinct clades: Group I (ATS1), Group II (AtGPAT9), and Group III (AtGPAT1-AtGPAT8). Group III can also be divided into three sub-branches (AtGPAT1-*3*, AtGPAT5/AtGPAT7, and AtGPAT4/AtGPAT6/AtGPAT8) [7]. Studies have reported that GPAT proteins belonging to different branches have different biological functions. For instance, the up-regulation of *ATS1* enhances the accumulation of unsaturated lipids in the plasma membrane and mitigates the degree of phase transition of the plasma membrane under low-temperature circumstances, thereby augmenting the plant's tolerance to cold stress [8]. *AtGPAT9* is critical for the biosynthesis of TAG (triacylglycerols) in Arabidopsis, and its expression level is reduced; there is a notable decrease in the accumulation of TAGs within developing seeds, which results in severe phenotypic consequences related to gametophyte development [9]. AtGPAT1-8 are a group of acyltransferases that exhibit characteristics typical of the sn-2 type, which is significant in lipid metabolism. These enzymes play a crucial role in the synthesis of cutin and suberin, two important biopolymers found in plant tissues [10,11]. AtGPAT1, AtGPAT2, and AtGPAT3 are implicated in the development of plant pollen and anthers and are predominantly expressed in flowers and siliques to contribute to the structural and functional integrity of pollen grains [12]. In the *Atgpat1* mutant, the fibrous material and vacuoles in anther compartments are reduced, and pollen grains collapse [13]. AtGPAT4, AtGPAT6, and AtGPAT8 are biofunctional acyltransferase/phosphatase enzymes that play significant roles in various metabolic pathways within plants, with AtGPAT4 and AtGPAT6 related to cutin synthesis and pollen development. The mutant of *AtGPAT6* has abnormal flower organ morphology, and seed setting rate and cutin content were decreased in flowers [14]. AtGPAT4 is functionally redundant with AtGPAT8, and the *Atgpat4*/*Atgpat8* double mutant has a severe blockage of cutin synthesis, increased cuticle permeability, and accelerated water loss [11,15]. Additionally, AtGPAT5 and AtGPAT7 are involved in root and seed suberin synthesis. In the *Atgpat5* mutant, the content of root suberin, ω-OH fatty acid, and DCA (dicarboxylic acid) decreased by 50% and 80% compared with the wild type, with a significant increase in salt permeability and reduced salt tolerance [16].

Simultaneously, numerous GPAT studies related to abiotic stresses have been conducted in non-model plants. The overexpression of the tomato *LeGPAT* in *Arabidopsis thaliana* elevates the level of PG (Phosphatidylglycerol), and the plants exhibit a superior ability to adapt to cold circumstances [17]. Overexpression of *Suaeda salsa SsGPAT* in Arabidopsis led to increased plant salt tolerance through the accumulation of unsaturated fatty acid in PGs [18]. The overexpression of the *AmGPAT* derived from *Ammopiptanthus mongolicus* in Arabidopsis can markedly augment the content of unsaturated fatty acids within plant tissues, thereby facilitating the plant to maintain the fluidity and stability of its membranes under low-temperature stress [19]. Under low-temperature stress, *Paeonia lactiflora PlGPAT* was highly expressed and increased the saturated lipid content of leaf vesicle membranes, thereby enhancing tolerance [20]. At low temperatures, the expression level of *AhGPAT9* in peanuts is significantly increased, which helps to improve the plant's cold resistance [21]. These studies demonstrate a significant correlation between *GPAT* and plant fertility, seed oil content, and abiotic stress.

Alfalfa (*Medicago sativa* L.), a perennial flowering plant belonging to the legume family, is extensively distributed worldwide. Renowned for its high yield, superior grass

quality, and richness in crude protein and other nutrients, it exhibits a wide range of growth adaptability and strong resistance to adverse conditions, earning it the title "king of grass" [22]. Additionally, alfalfa possesses robust nitrogen-fixing capacity and a well-developed root system, which contribute to the prevention of sandstorms and the protection of the ecological environment [23]. At present, the research on alfalfa variety primarily focus on the characteristics of plants at various growth stages under salt stress and the proteomic analysis of salt stress response proteins [24,25]. With the publication of the genome of the alfalfa varieties "Zhongmu No. 1" and "Xinjiang Daye", it is beneficial to the subsequent exploration of functional genes [26,27]. Consequently, it is essential to further investigate the function of stress-related genes in modulating the growth, development, and responses of alfalfa to abiotic stresses. GPAT participates in various lipid biosynthesis pathways and is vital for plant growth and resistance to stress. It has been reported that 73 members of the GPAT family were identified based on the tetraploid genome data of "Xinjiang Daye" Alfalfa, which can be classified into three subgroups, with diversity in gene structures, protein conserved motifs, and the expression patterns of *MsGPATs* under saline–alkali stress were analyzed with "Zhongmu No. 1" and salt-sensitive variety "WL323" [28]. Nonetheless, knowledge regarding the GPAT family in the "Zhongmu No. 1" genome and its expression patterns in different tissues and in response to abiotic stresses, including cold, drought, and salinity, remains insufficient. This study involved a comprehensive investigation of the GPAT family, encompassing physicochemical properties, phylogenetic relationships, gene structure, promoter *cis*-elements, and duplication event analysis using the alfalfa genome. Moreover, the *GPAT* expression profile in different tissues of alfalfa and under various abiotic stresses were also analyzed. The results of this research are of great significance in revealing the factors affecting the growth of alfalfa, guiding agricultural production and breeding, as well as laying a foundation for future investigations into the biological functions of alfalfa *GPAT* in response to abiotic stress.

2. Results

2.1. Identification and Chromosomal Localization of MsGPATs in the M. sativa Genome

A total of 27 GPAT members were identified by Blastp (Protein Sequence Alignment) in the *M. sativa* genome using the 10 AtGPAT proteins from *A. thaliana* as a query sequence. Additionally, 21 GPAT members were retrieved by HMM (hidden Markov model) search to query the alfalfa genome database using the GPAT domain (PF01553). After structural domain validation with NCBI-CDD (https://www.ncbi.nlm.nih.gov/cdd/ (accessed on 6 August 2023)) and SMART (http://smart.embl-heidelberg.de/ (accessed on 6 August 2023)), 15 *GPAT*s were confirmed and distributed across six alfalfa chromosomes. Based on their chromosomal positions, these genes were named *MsGPAT1* to *MsGPAT15*. Chromosomal visualization (Figure 1) showed that the *MsGPAT*s are evenly distributed on six of the eight chromosomes, excluding chromosomes 3 and 6. Chromosomes with two genes: chromosome 2 (*MsGPAT4* and *MsGPAT5*), chromosome 4 (*MsGPAT6* and *MsGPAT7*), and chromosome 8 (*MsGPAT14* and *MsGPAT15*); chromosomes with three genes: chromosome 1 (*MsGPAT1*, *MsGPAT2*, and *MsGPAT3*), chromosome 5 (*MsGPAT8*, *MsGPAT9*, and *MsGPAT10*), and chromosome 7 (*MsGPAT11*, *MsGPAT12*, and *MsGPAT13*); with a pair of tandemly duplicated genes identified on chromosome 1.

For the 15 MsGPAT proteins, their molecular weight (MW), protein size (aa, amino acids), isoelectric point (pI), and grand average of hydropathicity (GRAVY) were determined via the Expasy online service (https://web.expasy.org/protparam/ (accessed on 7 August 2023)) (Table 1). The amino acid lengths of MsGPAT proteins ranged from 247 aa (MsGPAT4) to 1329 aa (MsGPAT14), with an average length of approximately 500 aa, corresponding to molecular weights ranging from 28.93 kDa to 150.73 kDa. The pI values of MsGPAT proteins spanned from 7.85 (MsGPAT2) to 9.80 (MsGPAT8), indicating alkaline proteins. Hydrophilicity analysis showed that 9 of 15 are hydrophobic except MsGPAT4, 5, 8, 13, 14, and 15, which are hydrophilic proteins. Subcellular location predictions revealed that MsGPAT9 and MsGPAT14 were localized in the cell membrane, while the remainder

were detected in the endoplasmic reticulum, chloroplast, and mitochondria, suggesting that MsGPAT proteins primarily accumulate and function within organelles.

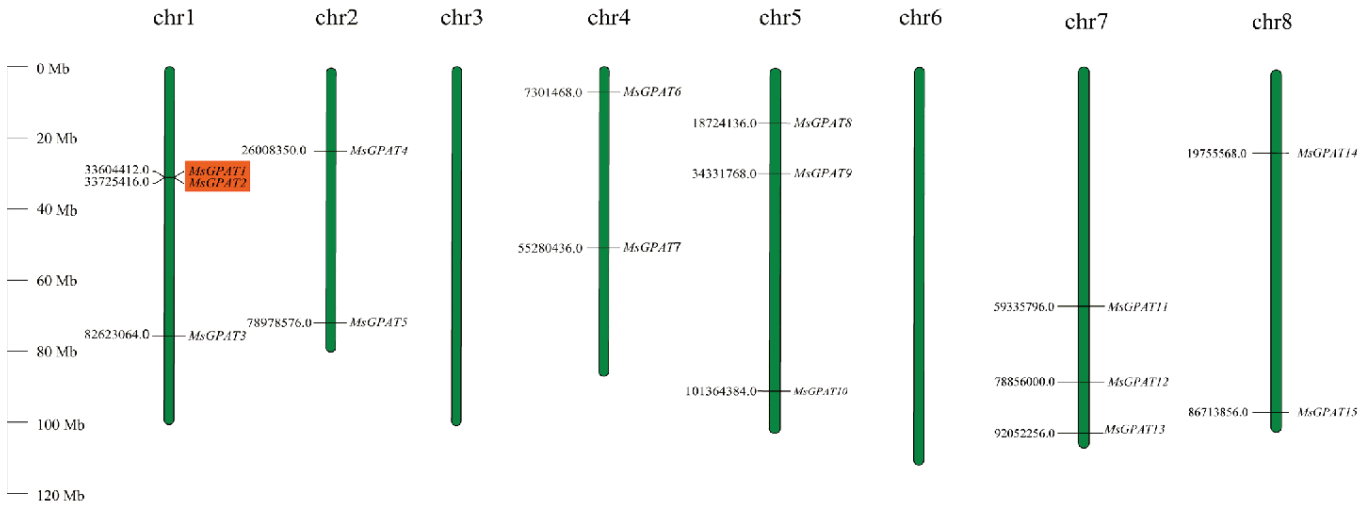

Figure 1. Chromosomal localization of *MsGPAT*s on alfalfa chromosomes. Chromosome numbers are indicated at the top of each respective chromosome. Positional data are displayed on the left side, and the corresponding *MsGP*AT's name is connected by a short line on the right side. The rectangle marked in orange represent one pair of tandemly duplicated genes. The scale (Mb) represents the length of the chromosome.

Table 1. Physical and biochemical properties of the *MsGPAT*s.

Gene Name	Gene ID	Chromosome Location	Length of Amino Acid (aa)	Molecular Weight (KDa)	pI	GRAVY	Localization
MsGPAT1	MsG0180002144.01.T01	Ch1r	504	55.04199	9.25	0.242	Mitochondrion
MsGPAT2	MsG0180002147.01.T01	Ch1r	460	49.86203	7.85	0.119	Endoplasmic reticulum
MsGPAT3	MsG0180004776.01.T01	Ch1r	542	61.57195	9.33	0.065	Mitochondrion
MsGPAT4	MsG0280008145.01.T02	Ch2r	247	28.93137	9.31	−0.119	Mitochondrion
MsGPAT5	MsG0280011060.01.T01	Ch2r	405	47.09177	9.72	−0.201	Mitochondrion
MsGPAT6	MsG0480018607.01.T01	Ch4r	495	55.08081	9.34	0.166	Endoplasmic reticulum, mitochondrion
MsGPAT7	MsG0480021218.01.T01	Ch4r	380	44.02557	9.28	0.262	Endoplasmic reticulum
MsGPAT8	MsG0580025445.01.T01	Ch5r	426	46.53116	8.86	−0.329	Chloroplast
MsGPAT9	MsG0580026299.01.T01	Ch5r	281	32.30629	9.8	0.08	Endoplasmic reticulum
MsGPAT10	MsG0580029736.01.T01	Ch5r	539	60.86481	9.26	0.17	Mitochondrion
MsGPAT11	MsG0780039186.01.T01	Ch7r	498	55.54921	9.27	0.108	Endoplasmic reticulum, mitochondrion
MsGPAT12	MsG0780040534.01.T02	Ch7r	415	46.78413	9.43	0.213	Cytomembrane
MsGPAT13	MsG0780041529.01.T01	Ch7r	463	52.96296	9.51	−0.425	Chloroplast
MsGPAT14	MsG0880043148.01.T01	Ch8r	1329	150.73197	8.6	−0.037	Cytomembrane
MsGPAT15	MsG0880047464.01.T01	Ch8r	376	43.25495	9.26	−0.128	Endoplasmic reticulum

2.2. Phylogenetic and Synteny Analysis of MsGPATs

For the purpose of conducting the classification, a phylogenetic tree was constructed by means of the neighbor-joining (NJ) methodology via MEGA 11.0 software using the sequences of 10 *A. thaliana*, 15 *M. sativa*, and 24 *M. truncatula* GPAT proteins (Figure 2). The MsGPATs were clustered into three groups (Groups I ~ III), similar to their counterparts in *M. truncatula* and *A. thaliana*. MsGPAT8, MsGPAT13, and MsGPAT9 belong to Group I and are closely related to ATS1; members of Group II, including MsGPAT15, MsGPAT4, MsG-

PAT7, MsGPAT5, and MsGPAT12, exhibit close relationships with AtGPAT9; the remaining seven MsGPATs are categorized within Group III and show strong similarities to AtGPAT1 through AtGPAT8. Group III can be further divided into three sub-branches, in which Group IIIA comprises three MsGPATs (MsGPAT3,10) and three AtGPATs (AtGPAT1,2,3), Group IIIB contains two MsGPATs (MsGPAT1,2) and two AtGPATs (AtGPAT5,7), and Group III C includes three MsGPATs (MsGPAT6,11,14) and three AtGPATs (AtGPAT4,6,8).

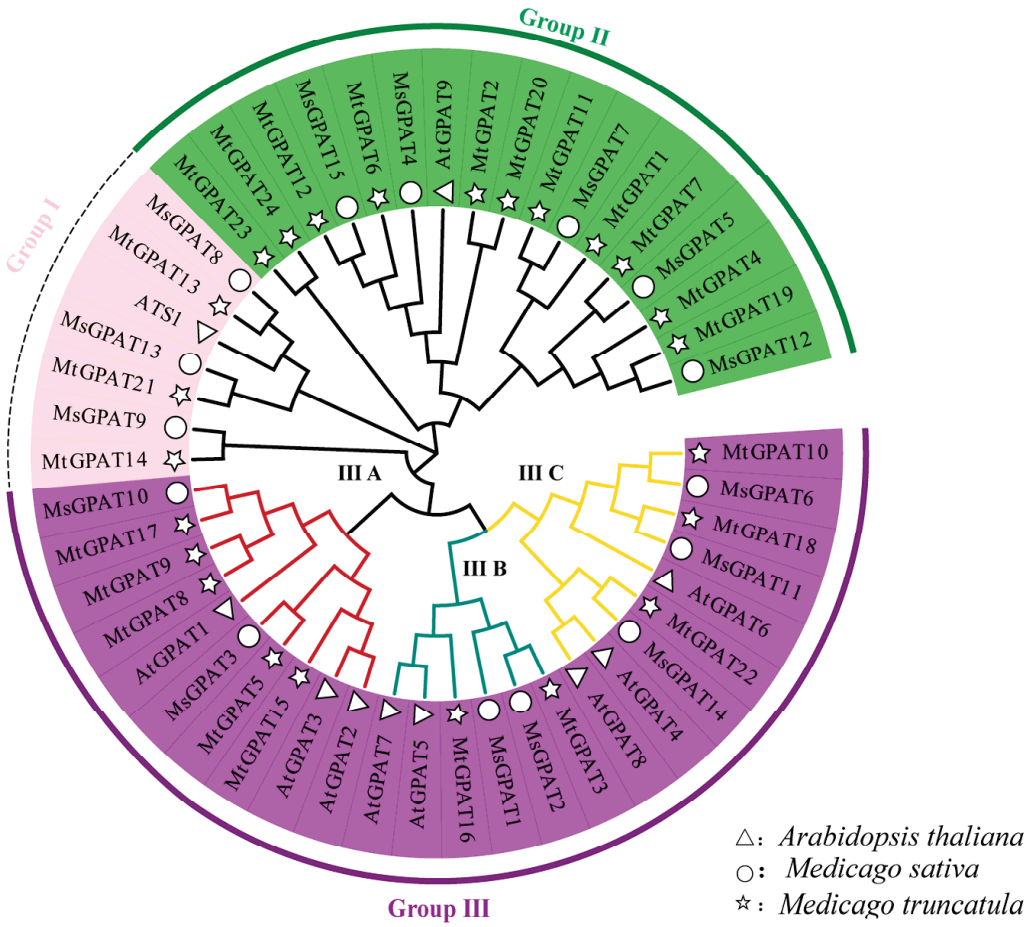

Figure 2. Phylogenetic analysis of the MsGPAT proteins. The GPAT proteins from *M. sativa*, *M. truncatula*, and *A. thaliana* are marked with the circle, pentagram, and triangle, respectively. The 15 MsGPAT proteins can be categorized into three clades (Group I, Group II, and Group III are marked in pink, green, and purple, respectively), and the third cluster can be further divided into three subclades (Group III A, Group III B, and Group III C).

To investigate the evolutionary relationships of MsGPATs, synteny analysis of GPATs was conducted across three dicots (Figure 3). A total of 9 out of 15 MsGPAT proteins exhibited collinear relationships with *Arabidopsis thaliana*, 14 with *Medicago truncatula*, and 11 with *Glycine max*. Among these gene pairs, there were 11 pairs in *Arabidopsis thaliana*, 19 pairs in *Medicago truncatula*, and 31 pairs in *Glycine max*. The quantity of orthologous pairs between alfalfa and *Glycine max* as well as *Medicago truncatula* was higher than that between *Medicago sativa* and *Arabidopsis thaliana*, suggesting a greater homology among the GPAT family members of alfalfa compared to those from *Medicago truncatula* and *Glycine max*.

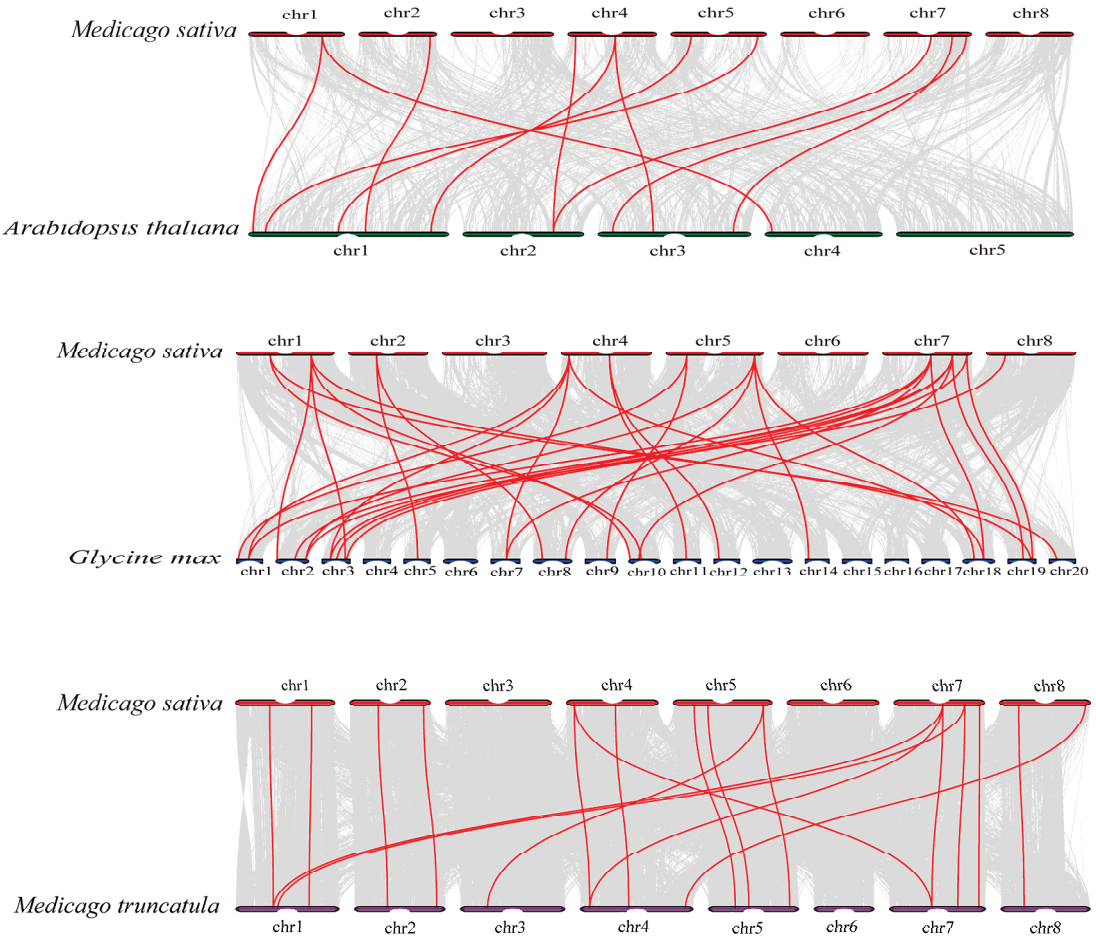

Figure 3. Synteny analysis of *Medicago sativa* GPAT proteins between *Arabidopsis thaliana*, *Medicago truncatula*, and *Glycine max*. Gray lines in the background represent alignment blocks between paired genomes, and red lines indicate syntenic GPAT pairs.

2.3. Conserved Motifs and Gene Structures of MsGPATs

A unique clustering of alfalfa GPAT proteins is depicted in Figure 4a. The results showed that the cluster tree was consistent with the phylogenetic tree constructed from the GPAT protein sequences of the three plant species shown in Figure 2. The conserved motifs of the MsGPAT proteins were detected using MEME (Figure 4b). Genes belonging to the same subfamily demonstrate resemblance in protein conserved motifs and gene structure. The motifs of Group I and Group II are relatively straightforward, encompassing one to three motifs, while those of Group III are rather intricate, spanning from 7 to 14 motifs. Among them, conserved Motifs 1, 5, and 12 constitute the typical structural domains of acyltransferases (PlsC). The shared conserved motif of the structural domain within Group III is Motif 1; for MsGPAT4 and MsGPAT15 in Group II, it is Motif 5; and for MsGPAT5, MsGPAT7, and MsGPAT12 in the same group, it is Motif 12. It is noteworthy that proteins in Group I display a low quantity of conserved motifs that remain unclear—likely attributable to their shorter protein sequences.

The gene structure of *MsGPATs* revealed variability of introns and exons across each gene (Figure 4c). Notably, the gene structures of Group I and Group II are relatively straightforward, whereas those in Group III exhibit greater complexity. These observations, coupled with the results regarding conserved motifs, suggest that MsGPATs within the same subfamily share similar structural characteristics. Furthermore, there is an inverse relationship between the composition of conserved motifs and gene structures; specifically, simpler conserved motifs correspond to more complex gene architectures, while more intricate conserved motifs are associated with simpler gene structures.

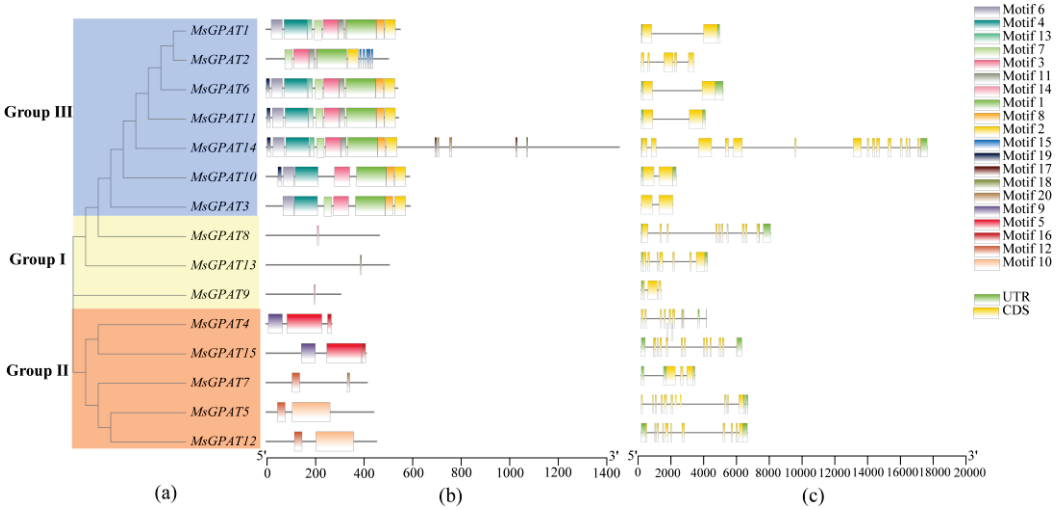

Figure 4. Gene structure of *MsGPAT*s and the conserved motifs in MsGPAT proteins. (**a**) Phylogenetic tree based on the conserved domain of MsGPAT proteins. (**b**) Analysis of conserved motifs in MsGPAT proteins. Colored boxes represent distinct conserved motifs that vary in sequence and size. (**c**) Exon–intron structure of the *MsGPAT*s. The yellow and green rectangles represent coding sequence (CDS) and untranslated region (UTR), respectively, while the black lines denote introns.

2.4. Cis-Acting Elements in the Promoter Regions of MsGPATs

To acquire profound comprehension regarding the transcriptional regulation and potential functions of *MsGPAT* genes, *cis*-regulatory elements within the 1500 bp upstream region of these genes were displayed using PlantCARE (http://bioinformatics.psb.ugent.be/webtools/plantcare/html/ (accessed on 23 August 2023)). A constellation of elements associated with light response, hormonal signaling, and stress response were ascertained to be relatively copious (Figure 5). Light response elements, particularly GT1 motifs, were prevalent in 90% of the *MsGPAT* upstream regions. Stress-related elements (MBS, ARE, and LTR) were also abundant, with AREs (anaerobic response elements) present in nearly 80% of upstream regions, indicating a potential association with abiotic stress responses. Furthermore, hormone-related *cis*-elements such as ABRE (abscisic acid), P-box (gibberellin), TGACG-motif (MeJA), and AuxRE (auxin) were also identified, suggesting regulation by multiple phytohormones.

2.5. Expression of MsGPATs in Different Tissues and Under ABA Treatment

To ascertain the expression status of *MsGPATs* in diverse tissues and under ABA treatment, an expression profile was constructed by employing the publicly accessible RNA-seq data acquired from NCBI (https://www.ncbi.nlm.nih.gov/ (accessed on 17 August 2023)) (Figure 6). Due to the incompleteness of RNA-seq data, *MsGPAT14* and *MsGPAT15* were not identified, resulting in a total of 13 genes available for analysis. Spatial expression profiles revealed significant tissue specificity (Figure 6a, Table S2), with five genes (*MsGPAT1*, *MsGPAT2*, *MsGPAT6*, *MsGPAT11*, and *MsGPAT12*) exhibiting high expression levels in flowers; in elongating stems, higher expression was observed for *MsGPAT5*, *MsGPAT7*, *MsGPAT10*, and *MsGPAT13*; both *MsGPAT8* and *MsGPAT9* demonstrated elevated expression in leaves; the expression of *MsGPAT4*, *MsGPAT5*, and *MsGPAT13* were relatively high in roots; however, gene expression was not significantly detected in nodules.

Furthermore, the expression levels of *MsGPATs* under ABA treatment exhibited significant timely (Figure 6b, Table S3). The results indicated that three genes (*MsGPAT5*, *MsGPAT7*, and *MsGPAT9*) demonstrated markedly elevated expression levels at 1 h and 3 h; *MsGPAT1* and *MsGPAT2* displayed high expression levels at 12 h; while *MsGPAT3*, *MsGPAT4*, and *MsGPAT12* showed increased expression at 1 h and 3 h. Additionally, *MsGPAT6*, *MsGPAT8*, *MsGPAT10*, *MsGPAT11*, and *MsGPAT13* exhibited significantly high expression levels at 3 h and 12 h.

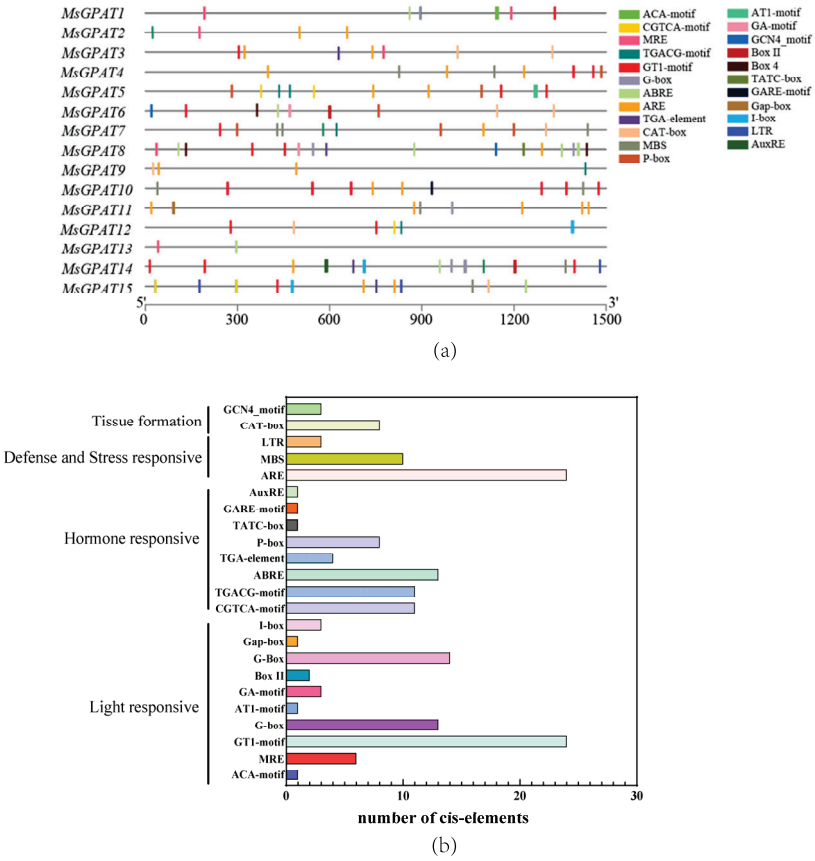

Figure 5. Display of *cis*-acting elements within putative promoters of *MsGPATs*. (**a**) A multitude of *cis*-acting elements were identified within the regulatory regions of each *MsGPAT*, with varying colors and shapes denoting elements. (**b**) The number of *cis*-acting elements.

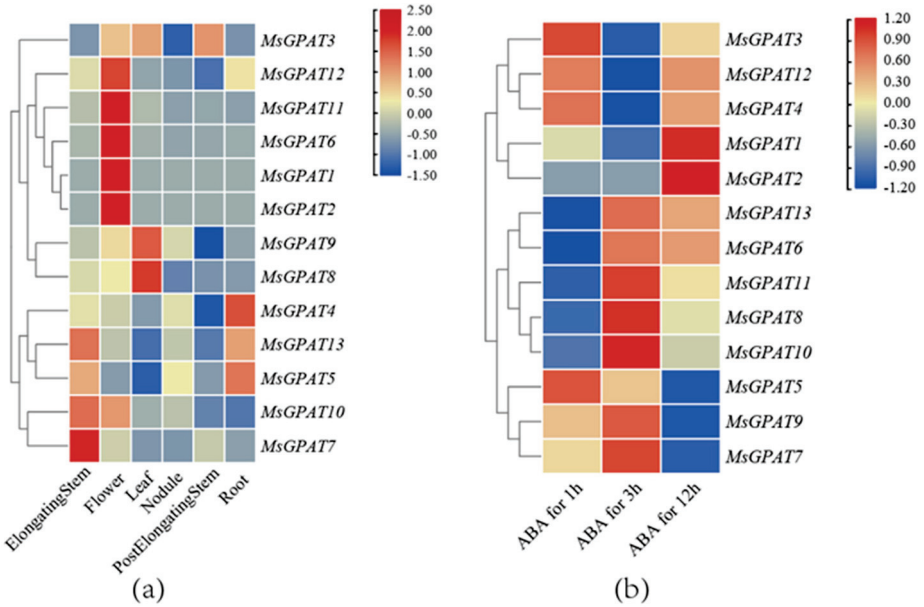

Figure 6. A heat map representation of *MsGPAT* expression between different tissues (**a**) and under ABA treatment (**b**). Red or blue colors represent the difference in expression levels in each sample, according to the color code shown on the right of the heat maps.

2.6. Gene Expression Pattern of MsGPATs Under Abiotic Stresses

To elucidate the expression patterns of *MsGPAT*s under abiotic stress more deeply, nine genes from three subfamilies were randomly selected to assess their expression levels under cold, drought, and salt treatments using qRT-PCR (Figure 7). The expression level of *MsGPATs* was also analyzed under abiotic stresses. Under cold stress, *MsGPAT15* was significantly up-regulated at 9 h, whereas seven genes (*MsGPAT5*, *MsGPAT6*, *MsGPAT8*, MsGPAT9, *MsGPAT10*, *MsGPAT11*, and *MsGPAT13*) were consistently down-regulated compared to the control across all treatment durations, indicating a response to cold stress (Figure 7a, Table S4). In contrast, under drought stress (Figure 7b, Table S5), the expression level of *MsGPAT5* decreased at 6 h, whereas *MsGPAT10* was up-regulated at all different treatment times, reaching approximately 30-fold the expression of the control group at 9 h. Both *MsGPAT3* and *MsGPAT15* were both up-regulated at 24 h; additionally, *MsGPAT6*, *MsGPAT8*, *MsGPAT9*, *MsGPAT11*, and *MsGPAT13* were up-regulated at 24 h. Furthermore, these genes displayed fluctuating expression patterns with increased treatment time. Under salt stress (Figure 7c, Table S6), *MsGPAT3* was significantly expressed at 3 h; meanwhile, *MsGPAT5*, *MsGPAT6*, *MsGPAT8*, *MsGPAT9*, *MsGPAT10*, *MsGPAT11*, *MsGPAT13*, and *MsGPAT15* reached peak expression levels at 9 h. The results indicated that the response of *MsGPAT*s to salt stress was primarily observed at 9 h, suggesting that these genes respond positively to salt stress.

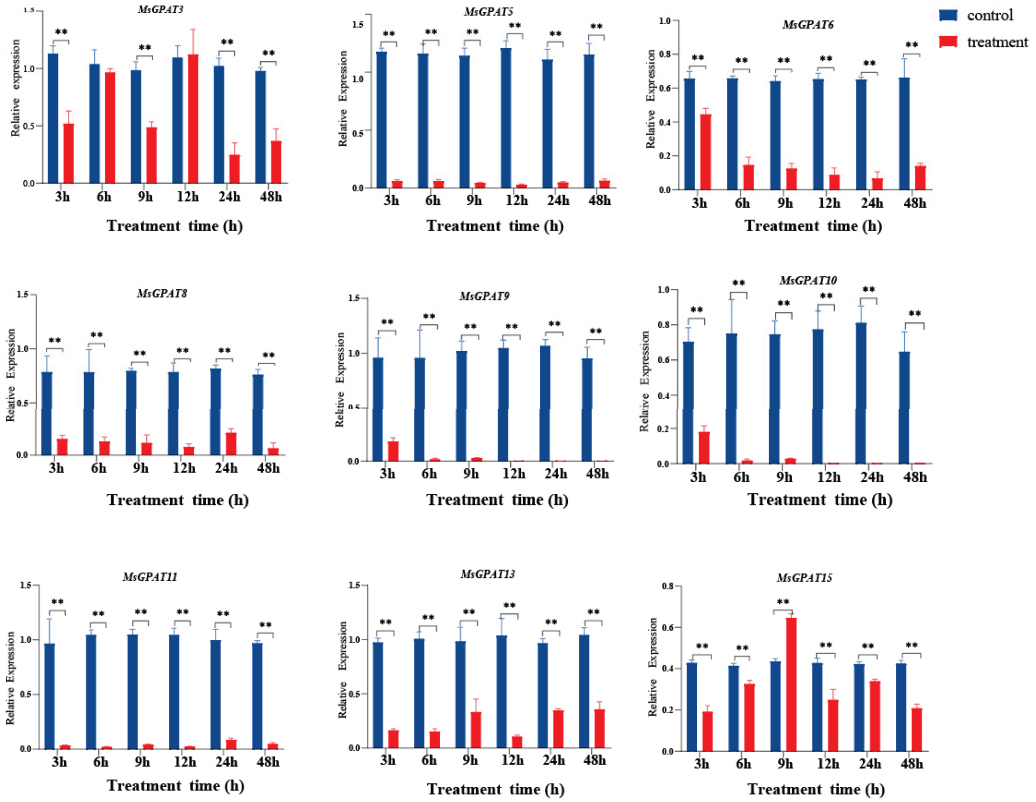

(a)

Figure 7. *Cont.*

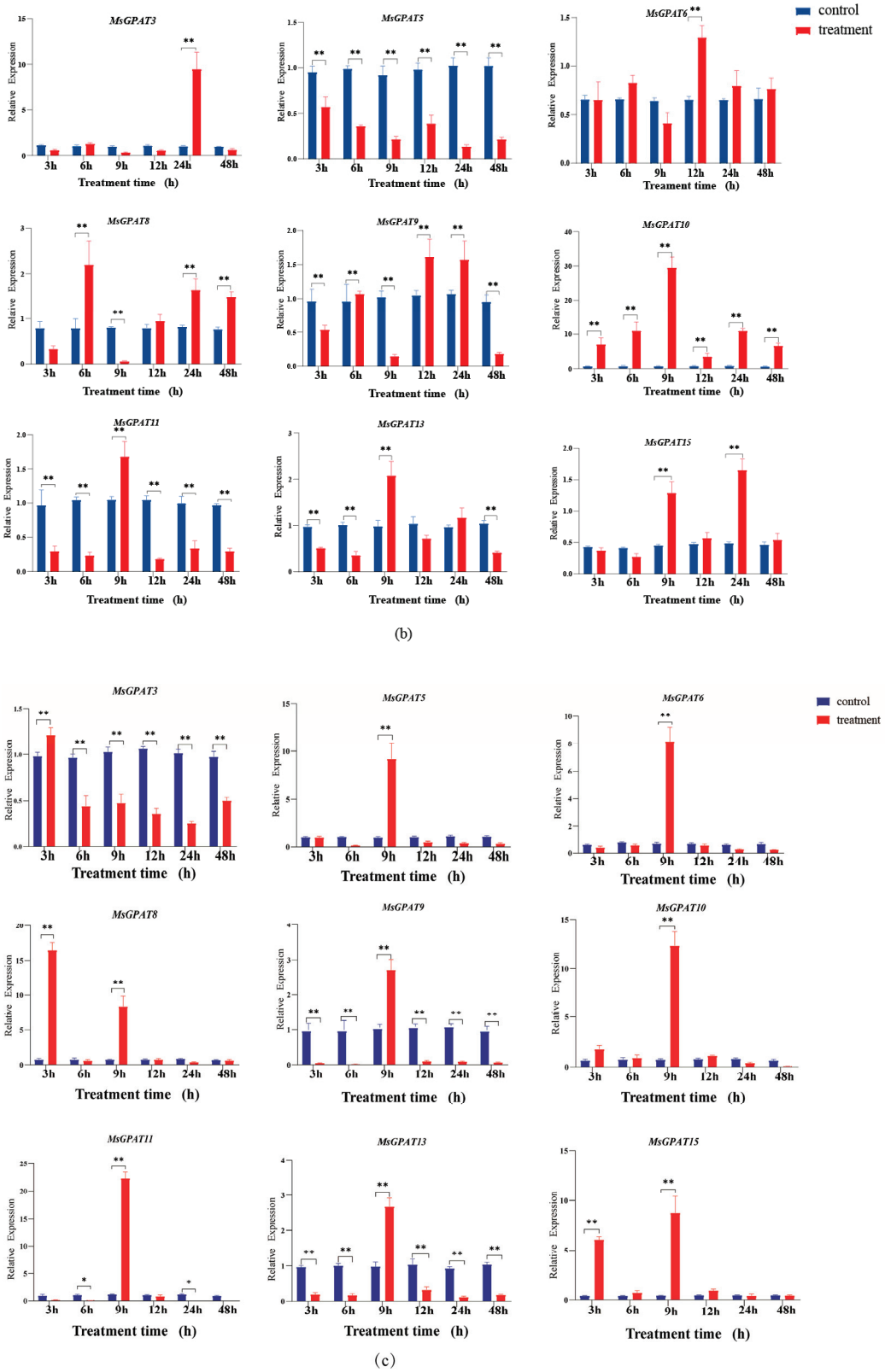

Figure 7. Expression analysis of *MsGPAT*s under abiotic stresses of cold (**a**), drought (**b**), and salt (**c**). X-axis represents the hours of stress treatment. Y-axis represents the expression level of each *MsGPAT*. Data represent the mean ± SE of three replicates. Asterisks represent significant difference at $p \leq 0.05$ (*) and $p \leq 0.01$ (**).

3. Discussion

Plant lipid synthesis-associated GPATs are widely present in eukaryotic organisms and have an impact on plant growth and adaptation to the environment [29]. Identifying and analyzing the plant GPAT family can provide a deeper understanding of their potential functions. Currently, the GPAT family has been identified in various plants, including 10 genes in Arabidopsis [6], 24 genes in *Medicago truncatula* based on the results of our previous studies, 32 in *Brassica rapa* [30], 20 in maize [31], and 85 in *Gossypium* spp. [32], respectively. In this study, we identified 15 GPAT family members evenly distributed on six chromosomes (Table 1, Figure 1). This represents a reduced number of GPAT family members compared to the above species and the identification of alfalfa 73 GPAT members based on the "Xinjiang Daye" genome [28], because we used the haploid genome of "Zhongmu No. 1", a heterozygous autotetraploid, which reported a higher-quality chromosome-level genome assembly wherein genes exhibited a low degree of repetition based one set of chromosome [26]. To some extent, this haploid genome avoids the differences between homologous chromosomes and the presence of chimeric sequences of the parental genome, which may enable a more distinct and lucid analysis of the classification and other characteristics of this family, which is more conducive to the subsequent mining and verification of GPATs. Furthermore, significant variations exist in the physicochemical characteristics of these members, such as isoelectric point and acidity/basicity, highlighting the diversity within the gene family.

This study demonstrates that alfalfa exhibits distinct GPAT family collinear relationships with two other leguminous plants. Specifically, among the MsGPATs, 31 pairs of orthologous genes were identified with *Glycine max*, 19 pairs with *Medicago truncatula*, and 11 pairs with *Arabidopsis thaliana*. Alfalfa GPAT is more closely related to *Glycine max* and *Medicago truncatula*, which possess a greater number of orthologous GPAT pairs due to their classification within the legume family. This suggests that GPATs are more conserved among closely related species throughout evolution [33]. Phylogenetic analysis demonstrates that the 15 MsGPATs are classified in accordance with the classification of Arabidopsis GPATs into three subfamilies (Figure 2). It is presumed that closely related proteins share similar biological functions. For instance, MsGPAT8, MsGPAT13, MsGPAT9, and ATS1 are members of Group I. In the *ATS1* mutant, compared with the wild type, the amount of fatty acid accumulation was significantly reduced and phospholipid content decreased by 25%, resulting in slower plant growth and a reduced seed setting rate [34]. This phenotype is correlated with the integrated regulation of lipid metabolism and plant development. Therefore, it is speculated that these two genes could be pertinent in the oil synthesis of seeds in plants. Five proteins (MsGPAT4, MsGPAT5, MsGPAT7, MsGPAT12, and MsGPAT15) along with AtGPAT9 are classified into Group II. AtGPAT9 is crucial for TAG biosynthesis; down-regulation of its expression leads to a reduction in seed oil content and manifests lethal phenotypes in both male and female gametophytes [35]. It is conjectured that these five genes could be associated to the generation of seed TAG. The remaining MsGPATs are classified into Group III, while AtGPAT1-8 are primarily involved in cutin synthesis [36]. Among them, MsGPAT11 and MsGPAT6, which belong to Group IIIA, were manifested a conspicuous up-regulation at 9h in the context of drought and salt stress. It is hypothesized that MsGPAT11 and MsGPAT6 may be involved in cutin synthesis as a response to abiotic stresses. Additionally, most of the MsGPATs are localized in chloroplast, mitochondria, and the endoplasmic reticulum, while a few are found in the cell membrane (Table 1), which aligns with the localization results observed for Gossypium GPAT [32]. Among them, MsGPAT8 and MsGPAT13 are localized in plastids, which is consistent with ATS1 (Group I), while most MsGPATs belonging to the same group are also found in the endoplasmic reticulum. MsGPAT3/MsGPAT10 in Group IIIA are consistently localized to mitochondria alongside AtGPAT1, AtGPAT2, and AtGPAT3. These results indicate that subcellular localization of genes within the same clade is similarly conserved. Based on the phylogenetic tree, conserved motifs, and gene structure analyses of alfalfa MsGPAT proteins (Figure 4), MsGPATs within the same group manifested similar

motif types and numbers, while their gene structures displayed analogous characteristics, including comparable exon/intron arrangements, positions, and intron counts. This observation is consistent with findings in the GPAT family of *Medicago truncatula* and *Brassica rapa* [30]. Furthermore, the conserved motifs of MsGPATs belonging to the same subfamily are relatively similar, suggesting that similar subfamilies may perform analogous functions, which could lead to redundancy in gene functions. In contrast, the conserved motifs across different subfamilies exhibit significant differences, indicating that distinct subfamilies may fulfill divergent roles. This finding aligns with evolutionary analyses and suggests that diverse structural features imply varied functions of GPATs. Additionally, we observed an inverse relationship between the composition of conserved motifs and gene structures in MsGPATs; specifically, simpler conserved motifs correspond to more complex gene structures, while more complex conserved motifs are associated with simpler gene structures. This observation is particularly intriguing and may hold special significance for GPAT evolution.

The promoter region of the *MsGPATs* in alfalfa encompasses multiple *cis*-acting elements that are associated with light, hormone response, and stress response. (Figure 5). This indicates that the *MsGPATs* might be implicated in the growth, development, and metabolic processes of plants, and concurrently participates in the biological processes that modulate the responses of plants to various abiotic stresses. Each *MsGPAT* contains multiple light-sensitive elements similar to those found in *Avena sativa* [37]. It has been demonstrated by previous research that light has an impact on the expression of genes associated with lipid synthesis [38], and microalgae accumulate TAG under illuminated conditions [39]. Integrating these findings with promoter analysis leads to the hypothesis that *GPAT* might be implicated in the pathway of light-induced lipid synthesis in plants. Furthermore, spatial–temporal expression analysis of *MsGPATs* revealed that *MsGPAT1*, *MsGPAT2*, *MsGPAT6*, and *MsGPAT11* exhibit particularly high expression levels in flowers (Figure 6a), implying their potential involvement in floral development.

Abscisic acid (ABA) serves as a key regulatory factor for plants in response to environmental and organismal alterations, exerting an extremely vital role in modulating responses to diverse stress conditions [40,41]. ABA also governs the expression of *GPAT*. For instance, it can inhibit the expression of *BnGPAT9* in response to external stimuli [30]. Additionally, *LlaGPAT* is significantly induced by ABA, resulting in up-regulation of its expression [42]. In this study, alfalfa *MsGPAT*s exhibited temporal characteristics in response to ABA treatment. For instance, *MsGPAT1* and *MsGPAT2* demonstrated significant up-regulation, while the expression levels of *MsGPAT7*, *MsGPAT5*, and *MsGPAT9* were markedly down-regulated. Other *MsGPAT*s showed fluctuating expression changes under ABA treatment, i.e., *MsGPAT*s might be involved in ABA-mediated drought stress response. Numerous studies have verified that *GPAT*s are down-regulated under abiotic stress, as observed in sunflower *GPAT* [43], *Ammopiptanthus mongolicus AmGPAT* [19], and *Lepidium latifolium LlaGPAT* [42]. *MsGPAT*s also exhibited timely specificity in response to abiotic stresses. The *MsGPATs* were consistently down-regulated throughout all treatment durations under cold stress, suggesting that these genes might exert a negative regulatory effect in such circumstances. Conversely, the expression levels of *GPAT* from different species increased under other abiotic stresses; for instance, rice *OsGPAT5*, *14*, *18*, *19*, and *24* were significantly up-regulated under both salt and drought stress [44]. In our previous research, barley *HvGPAT5*, *8*, *14*, *17*, *18*, and *HtGPAT14* were up-regulated in the context of salt and drought stress. In the present study, the majority of *MsGPAT*s manifested up-regulation, peaking after 9 h of salt stress treatment. Under drought stress, the expression of *MsGPAT*s fluctuated with each treatment time; except for *MsGPAT5*, which was down-regulated under drought, other *MsGPAT*s were significantly up-regulated at certain times. Notably, *MsGPAT10* was persistently up-regulated throughout all treatment times under drought stress, suggesting its potential pivotal functionality in the response to such conditions.

4. Materials and Methods

4.1. Identification of GPAT Gene Family

The genome-wide data for alfalfa were procured from (https://figshare.com (accessed on 2 August 2023)). To discern all members of the GPAT gene family in alfalfa, we accessed the sequence and annotation particulars of the Arabidopsis GPAT gene family from the TAIR database (https://www.arabidopsis.org/ (accessed on 2 August 2023)). BLASTp searches (E-value = 0.00001) were performed to identify candidate GPAT proteins based on reference sequences from the Arabidopsis GPAT gene family. Additionally, hidden Markov model (HMM) profiles corresponding to the GPAT domain (PF01553) were downloaded from the Pfam database (http://pfam.xfam.org (accessed on 2 August 2023)) and genes containing these domains were searched for. The potential *M. sativa* GPAT members identified through these two approaches were compiled into a comprehensive dataset. Furthermore, WebCDD-search (https://www.ncbi.nlm.nih.gov/cdd (accessed on 6 August 2023)) and SMART (http://smart.embl.de/ (accessed on 6 August 2023)) were utilized to analyze the domains of candidate GPAT proteins, thereby confirming which genes would be selected for subsequent analysis.

4.2. Basic Physicochemical Properties and Chromosomal Location of MsGPATs

We employed the online website ExPASY (https://web.expasy.org/protparam/ (accessed on 7 August 2023)) to analyze the molecular weight (MW), isoelectric point (pI), amino acid count, and average hydrophilicity (GRAVY) of MsGPATs, thereby comprehending their physicochemical properties. The Plant-PLoc server (Plant-PLoc server: sjtu.edu.cn) was utilized to predict the localization of these proteins. Based on the annotation data from the alfalfa genome database, the distribution of the GPATs across chromosomes was analyzed.

4.3. Phylogenetic and Synteny Analysis of MsGPAT Proteins

The entire genomic information of *A. thaliana* and *M. truncatula* was retrieved from the NCBI database (https://www.ncbi.nlm.nih.gov/ (accessed on 7 August 2023)). By employing ClustalW technology, the protein sequences of 15 MsGPAT, 10 AtGPAT, and 24 MtGPAT were subjected to multiple sequence alignment. The alignment parameters were set in the multiple comparison mode (with other parameters remaining in the default configuration), and the resultant alignments were utilized to construct a neighbor-joining (NJ) phylogenetic tree, which was generated in MEGA 11.0 through 1000 bootstrap replications. Furthermore, the synteny analysis between MsGPAT proteins and those of *A. thaliana*, *G. max*, and *M. truncatula* GPAT proteins was carried out using JCVI (https://github.com/tanghaibao/jcvi (accessed on 8 August 2023)).

4.4. Gene Structure and Conserved Motif Analysis

Employing the GFF (General Feature Format) annotation file of the alfalfa genome, we availed ourselves of the online Gene Structure Display Server (GSDS) (http://gsds.cbi.pku.edu.cn/ (accessed on 8 August 2023)) to engender a visual manifestation of exon–intron structures. The conserved motifs encompassed within MsGPATs were scrutinized using the Multiple Expectation Maximization for Motif Elicitation (MEME) Suite (http://meme-suite.org/ (accessed on 9 August 2023)), with the motif quantity configured to 20.

4.5. Analysis of Cis-Acting Elements of MsGPATs

The 1500 bp promoter region located upstream of the transcriptional start site for MsGPAT genes was obtained from the M. sativa genome and analyzed using PlantCARE (https://bioinformatics.psb.ugent.be/webtools/plantcare/html/ (accessed on 23 August 2023)). The results of this analysis were visualized with GSDS online website (http://gsds.gao-lab.org/ (accessed on 23 August 2023)).

4.6. Expression Profiling of the MsGPATs in Different Tissues and ABA Treatment

RNA-Seq data for different tissues (elongating stems, post-elongating stems, flowers, leaves, nodules, and roots) and ABA treatments at different times (1 h, 3 h, and 12 h) were downloaded at project numbers PRJNA276155 and PRJNA450305 from the NCBI public database, respectively. The expression levels of *MsGPAT*s in various tissues and under ABA treatments were quantified as fragments per kilobase per million mapped reads (FPKM values). A heatmap representing the expression profile of *MsGPAT*s was generated using R software (version R-4.3.1).

4.7. Plant Growth and Abiotic Treatments

The seeds of alfalfa "Zhongmu No. 1" were sterilized and planted in nutrient soil, grown under a light/dark regime of 12 h/12 h, with diurnal/nocturnal temperatures of 30 °C/25 °C and a relative humidity of 65%. The seedlings were then transferred to Hoagland's nutrient solution for further incubation after one week. Four-week-old alfalfa seedlings were subjected to drought, salt, and cold stress treatments with 15% PEG6000, 250 mM NaCl, and 4 °C, respectively, with seedlings under normal conditions used as controls. Leaf samples were collected after 3 h, 6 h, 9 h, 12 h, 24 h, and 48 h, and store at −80 °C for subsequent quantitative experiments. Three biological replicates were performed for each sample.

4.8. Quantitative Real-Time RT-PCR (qRT-PCR) of MsGPAT Genes

The total RNA of alfalfa from each sample was extracted using an RNAprep Pure Plant kit (TaKaRa, Dalian, China), and RNA quality and concentration were detected using a Nano-Drop 2000 UV spectrophotometer. First-strand cDNA was generated from RNA through reverse transcription using the PrimerScript 1st Strand cDNA Synthesis Kit (Tiangen, Beijing, China). After measuring the concentration, the cDNA was uniformly diluted to 100 ng for use as a template in qRT-PCR reactions. Primers for *MsGPATs* were designed using Primer Premier 5.0 software and are detailed in Table S1, with β-Actin serving as an internal control. qRT-PCR was conducted with SYBR Green (Tiangen, Beijing, China) on a Roche real-time Detection System (Applied Biosystems, Foster City, CA, USA). The thermal cycling conditions included an initial step at 95 °C for 15 min, followed by 40 cycles of denaturation at 95 °C for 10 s, annealing at 60 °C for 20 s, and extension at 72 °C for 32 s. Three biological replicates were performed to calculate the relative gene expression using the $2^{-\Delta\Delta Ct}$ method.

5. Conclusions

A total of 15 *MsGPATs* were identified and uniformly distributed across six chromosomes based on the genomic information of alfalfa. This family can be categorized into three clades in accordance with evolutionary relationships. Subcellular localization, conserved motifs, and gene structures display considerable resemblance within each subgroup, but manifested significant disparities between subgroups. The promoter regions of the *MsGPAT*s encompass *cis*-regulatory elements pertinent to stress responses, hormonal modulation, plant tissue morphogenesis, and light perception. Spatial and temporal expression analysis indicated that the *MsGPAT*s showed significant specificity in different tissues. Additionally, qRT-PCR analysis unveiled varying degrees of responsiveness to abiotic stress among the *MsGPAT*s. The majority of *MsGPAT*s were conspicuously up-regulated under drought and salt stress, suggesting their involvement and crucial role in salt and drought stress. Overall, the findings of this research will constitute a significant basis for future studies on the functions of *GPAT* and the molecular mechanisms underlying stress regulation in alfalfa.

Supplementary Materials: The following supporting information can be downloaded at: https://www.mdpi.com/article/10.3390/plants13233392/s1.

Author Contributions: Conceptualization, H.X. and R.D.; methodology, J.M., M.D. and R.D.; software, J.M. and M.D.; writing—original draft preparation, J.M. and R.D.; writing—review and editing, J.M., M.D., H.X. and R.D. All authors have read and agreed to the published version of the manuscript.

Funding: This research was supported by the Key R&D and Transformation Project of Qinghai Province (2022-NK-135) and the Fundamental Project for "Kunlun Talent—Top Innovation and Entrepreneurship Talents" in Qinghai Province.

Data Availability Statement: The transcriptome sequencing data of different tissues and ABA treatment are available in the NCBI database (project ID PRJNA276155, PRJNA450305). All methods were carried out in accordance with relevant guidelines and regulations. All experimental studies on plants were complied with relevant institutional, national, and international guidelines and legislation. Further inquiries can be directed to the corresponding authors.

Conflicts of Interest: The funders had no role in the design of this study; in the collection, analyses, or interpretation of data; in the writing of the manuscript; or in the decision to publish the results.

References

1. Nakamura, Y. Plant Phospholipid Diversity: Emerging Functions in Metabolism and Protein-Lipid Interactions. *Trends Plant Sci.* **2017**, *22*, 1027–1040. [CrossRef] [PubMed]
2. Fernández, V.; Bahamonde, H.A.; Javier Peguero-Pina, J.; Gil-Pelegrín, E.; Sancho-Knapik, D.; Gil, L.; Goldbach, H.E.; Eichert, T. Physico-chemical properties of plant cuticles and their functional and ecological significance. *J. Exp. Bot.* **2017**, *68*, 5293–5306. [CrossRef] [PubMed]
3. Chen, X.; Snyder, C.L.; Truksa, M.; Shah, S.; Weselake, R.J. sn-Glycerol-3-phosphate acyltransferases in plants. *Plant Signal. Behav.* **2011**, *6*, 1695–1699. [CrossRef]
4. Beisson, F.; Li-Beisson, Y.; Pollard, M. Solving the puzzles of cutin and suberin polymer biosynthesis. *Curr. Opin. Plant Biol.* **2012**, *15*, 329–337. [CrossRef]
5. Yang, W.; Simpson, J.P.; Li-Beisson, Y.; Beisson, F.; Pollard, M.; Ohlrogge, J.B. A land-plant-specific glycerol-3-phosphate acyltransferase family in Arabidopsis: Substrate specificity, sn-2 preference, and evolution. *Plant Physiol.* **2012**, *160*, 638–652. [CrossRef]
6. Murata, N.; Tasaka, Y. Glycerol-3-phosphate acyltransferase in plants. *Biochim. Biophys. Acta* **1997**, *1348*, 10–16. [CrossRef]
7. Ohba, Y.; Sakuragi, T.; Kage-Nakadai, E.; Tomioka, N.H.; Kono, N.; Imae, R.; Inoue, A.; Aoki, J.; Ishihara, N.; Inoue, T.; et al. Mitochondria-type GPAT is required for mitochondrial fusion. *EMBO J.* **2013**, *32*, 1265–1279. [CrossRef]
8. Xu, C.; Yu, B.; Cornish, A.J.; Froehlich, J.E.; Benning, C. Phosphatidylglycerol biosynthesis in chloroplasts of Arabidopsis mutants deficient in acyl-ACP glycerol-3- phosphate acyltransferase. *Plant J.* **2006**, *47*, 296–309. [CrossRef]
9. Shockey, J.; Regmi, A.; Cotton, K.; Adhikari, N.; Browse, J.; Bates, P.D. Identification of Arabidopsis GPAT9 (At5g60620) as an Essential Gene Involved in Triacylglycerol Biosynthesis. *Plant Physiol.* **2016**, *170*, 163–179. [CrossRef]
10. Yang, Y.; Benning, C. Functions of triacylglycerols during plant development and stress. *Curr. Opin. Biotechnol.* **2018**, *49*, 191–198. [CrossRef]
11. Li, Y.; Beisson, F.; Koo, A.J.; Molina, I.; Pollard, M.; Ohlrogge, J. Identification of acyltransferases required for cutin biosynthesis and production of cutin with suberin-like monomers. *Proc. Natl. Acad. Sci. USA* **2007**, *104*, 18339–18344. [CrossRef] [PubMed]
12. Zheng, Z.; Xia, Q.; Dauk, M.; Shen, W.; Selvaraj, G.; Zou, J. Arabidopsis AtGPAT1, a member of the membrane-bound glycerol-3-phosphate acyltransferase gene family, is essential for tapetum differentiation and male fertility. *Plant Cell* **2003**, *15*, 1872–1887. [CrossRef] [PubMed]
13. Lei, J.; Miao, Y.; Lan, Y.; Han, X.; Liu, H.; Gan, Y.; Niu, L.; Wang, Y.; Zheng, Z. A Novel Complementation Assay for Quick and Specific Screen of Genes Encoding Glycerol-3-Phosphate Acyltransferases. *Front. Plant Sci.* **2018**, *9*, 353. [CrossRef] [PubMed]
14. Mazurek, S.; Garroum, I.; Daraspe, J.; De Bellis, D.; Olsson, V.; Mucciolo, A.; Butenko, M.A.; Humbel, B.M.; Nawrath, C. Connecting the Molecular Structure of Cutin to Ultrastructure and Physical Properties of the Cuticle in Petals of Arabidopsis. *Plant Physiol.* **2017**, *173*, 1146–1163. [CrossRef]
15. Chen, X.; Truksa, M.; Snyder, C.L.; El-Mezawy, A.; Shah, S.; Weselake, R.J. Three homologous genes encoding sn-glycerol-3-phosphate acyltransferase 4 exhibit different expression patterns and functional divergence in Brassica napus. *Plant Physiol.* **2011**, *155*, 851–865. [CrossRef]
16. Beisson, F.; Li, Y.; Bonaventure, G.; Pollard, M.; Ohlrogge, J.B. The acyltransferase GPAT5 is required for the synthesis of suberin in seed coat and root of Arabidopsis. *Plant Cell* **2007**, *19*, 351–368. [CrossRef]
17. Sui, N.; Li, M.; Zhao, S.J.; Li, F.; Liang, H.; Meng, Q.W. Overexpression of glycerol-3-phosphate acyltransferase gene improves chilling tolerance in tomato. *Planta* **2007**, *226*, 1097–1108. [CrossRef]
18. Sui, N.; Tian, S.; Wang, W.; Wang, M.; Fan, H. Overexpression of Glycerol-3-Phosphate Acyltransferase from *Suaeda salsa* Improves Salt Tolerance in Arabidopsis. *Front. Plant Sci.* **2017**, *8*, 1337. [CrossRef]

19. Xue, M.; Guo, T.; Ren, M.; Wang, Z.; Tang, K.; Zhang, W.; Wang, M. Constitutive expression of chloroplast glycerol-3-phosphate acyltransferase from *Ammopiptanthus mongolicus* enhances unsaturation of chloroplast lipids and tolerance to chilling, freezing and oxidative stress in transgenic Arabidopsis. *Plant Physiol. Biochem.* **2019**, *143*, 375–387. [CrossRef]
20. Li, X.; Liu, P.; Yang, P.; Fan, C.; Sun, X. Characterization of the glycerol-3-phosphate acyltransferase gene and its real-time expression under cold stress in *Paeonia lactiflora* Pall. *PLoS ONE* **2018**, *13*, e0202168. [CrossRef]
21. Shen, Y.; Shen, Y.; Liu, Y.; Bai, Y.; Liang, M.; Zhang, X.; Chen, Z. Characterization and functional analysis of AhGPAT9 gene involved in lipid synthesis in peanut (*Arachis hypogaea* L.). *Front. Plant Sci.* **2023**, *14*, 1144306. [CrossRef] [PubMed]
22. Dai, H.P.; Shan, C.J.; Zhao, H.; Li, J.C.; Jia, G.L.; Jiang, H.; Wu, S.Q.; Wang, Q. The difference in antioxidant capacity of four alfalfa cultivars in response to Zn. *Ecotoxicol. Environ. Saf.* **2015**, *114*, 312–317. [CrossRef] [PubMed]
23. Song, X.; Fang, C.; Yuan, Z.Q.; Li, F.M.; Sardans, J.; Penuelas, J. Long-term alfalfa (*Medicago sativa* L.) establishment could alleviate phosphorus limitation induced by nitrogen deposition in the carbonate soil. *J. Environ. Manag.* **2022**, *324*, 116346. [CrossRef] [PubMed]
24. Yin, Y.; Fan, S.; Li, S.; Amombo, E.; Fu, J. Involvement of cell cycle and ion transferring in the salt stress responses of alfalfa varieties at different development stages. *BMC Plant Biol.* **2023**, *23*, 343. [CrossRef]
25. Xiong, J.; Sun, Y.; Yang, Q.; Tian, H.; Zhang, H.; Liu, Y.; Chen, M. Proteomic analysis of early salt stress responsive proteins in alfalfa roots and shoots. *Proteome Sci.* **2017**, *15*, 19. [CrossRef]
26. Shen, C.; Du, H.; Chen, Z.; Lu, H.; Zhu, F.; Chen, H.; Meng, X.; Liu, Q.; Liu, P.; Zheng, L.; et al. The Chromosome-Level Genome Sequence of the Autotetraploid Alfalfa and Resequencing of Core Germplasms Provide Genomic Resources for Alfalfa Research. *Mol. Plant* **2020**, *13*, 1250–1261. [CrossRef]
27. Chen, H.; Zeng, Y.; Yang, Y.; Huang, L.; Tang, B.; Zhang, H.; Hao, F.; Liu, W.; Li, Y.; Liu, Y.; et al. Allele-aware chromosome-level genome assembly and efficient transgene-free genome editing for the autotetraploid cultivated alfalfa. *Nat. Commun.* **2020**, *11*, 2494. [CrossRef]
28. Tang, F.; Mei, T.; Gao, J.H.; Wang, J.N.; Shi, F.L.; Gao, C.P. Identification and expression analysis of the GPAT gene Family in *Medicago sativa* under Saline Alkali Stress. *Acta Agrestia Sin.* **2023**, *31*, 2608–2620. [CrossRef]
29. Lyublinskaya, O.G.; Pugovkina, N.A.; Borisov, Y.G.; Zenin, V.V.; Nikolsky, N.N. How to Assess Reactive Oxygen Species (ROS) Concentration Instead of ROS Level in the Cell and Why the Quantitative Redox Biology Approach Is Useful for the Analysis of ROS Homeostasis in Embryonic Stem Cells: Overcoming Misconceptions. *Free Radic. Biol. Med.* **2015**, *87*, S16. [CrossRef]
30. Wang, J.; Singh, S.K.; Geng, S.; Zhang, S.; Yuan, L. Genome-wide analysis of glycerol-3-phosphate O-acyltransferase gene family and functional characterization of two cutin group GPATs in Brassica napus. *Planta* **2020**, *251*, 93. [CrossRef]
31. Zhu, T.; Wu, S.; Zhang, D.; Li, Z.; Xie, K.; An, X.; Ma, B.; Hou, Q.; Dong, Z.; Tian, Y.; et al. Genome-wide analysis of maize GPAT gene family and cytological characterization and breeding application of ZmMs33/ZmGPAT6 gene. *Theor. Appl. Genet.* **2019**, *132*, 2137–2154. [CrossRef] [PubMed]
32. Cui, Y.; Ma, J.; Liu, G.; Wang, N.; Pei, W.; Wu, M.; Li, X.; Zhang, J.; Yu, J. Genome-Wide Identification, Sequence Variation, and Expression of the Glycerol-3-Phosphate Acyltransferase (GPAT) Gene Family in Gossypium. *Front. Genet.* **2019**, *10*, 116. [CrossRef] [PubMed]
33. Zhang, H.; Liu, X.; Wang, X.; Sun, M.; Song, R.; Mao, P.; Jia, S. Genome-Wide Identification of GRAS Gene Family and Their Responses to Abiotic Stress in *Medicago sativa*. *Int. J. Mol. Sci.* **2021**, *22*, 7729. [CrossRef] [PubMed]
34. Jayawardhane, K.N.; Singer, S.D.; Weselake, R.J.; Chen, G. Plant sn-Glycerol-3-Phosphate Acyltransferases: Biocatalysts Involved in the Biosynthesis of Intracellular and Extracellular Lipids. *Lipids* **2018**, *53*, 469–480. [CrossRef] [PubMed]
35. Singer, S.D.; Chen, G.; Mietkiewska, E.; Tomasi, P.; Jayawardhane, K.; Dyer, J.M.; Weselake, R.J. Arabidopsis GPAT9 contributes to synthesis of intracellular glycerolipids but not surface lipids. *J. Exp. Bot.* **2016**, *67*, 4627–4638. [CrossRef]
36. Waschburger, E.; Kulcheski, F.R.; Veto, N.M.; Margis, R.; Margis-Pinheiro, M.; Turchetto-Zolet, A.C. Genome-wide analysis of the Glycerol-3-Phosphate Acyltransferase (GPAT) gene family reveals the evolution and diversification of plant GPATs. *Genet. Mol. Biol.* **2018**, *41*, 355–370. [CrossRef]
37. Ling, L.; Li, M.; Chen, N.; Xie, X.; Han, Z.; Ren, G.; Yin, Y.; Jiang, H. Genome-Wide Identification of NAC Gene Family and Expression Analysis under Abiotic Stresses in *Avena sativa*. *Genes* **2023**, *14*, 1186. [CrossRef]
38. Gaytán-Luna, D.E.; Ochoa-Alfaro, A.E.; Rocha-Uribe, A.; Pérez-Martínez, A.S.; Alpuche-Solís, Á.G.; Soria-Guerra, R.E. Effect of green and red light in lipid accumulation and transcriptional profile of genes implicated in lipid biosynthesis in *Chlamydomonas reinhardtii*. *Biotechnol. Prog.* **2016**, *32*, 1404–1411. [CrossRef]
39. Lima, S.; Lokesh, J.; Schulze, P.S.C.; Wijffels, R.H.; Kiron, V.; Scargiali, F.; Petters, S.; Bernstein, H.C.; Morales-Sánchez, D. Flashing lights affect the photophysiology and expression of carotenoid and lipid synthesis genes in *Nannochloropsis gaditana*. *J. Biotechnol.* **2022**, *360*, 171–181. [CrossRef]
40. Boominathan, P.; Shukla, R.; Kumar, A.; Manna, D.; Negi, D.; Verma, P.K.; Chattopadhyay, D. Long term transcript accumulation during the development of dehydration adaptation in *Cicer arietinum*. *Plant Physiol.* **2004**, *135*, 1608–1620. [CrossRef]
41. Nakashima, K.; Yamaguchi-Shinozaki, K. ABA signaling in stress-response and seed development. *Plant Cell Rep.* **2013**, *32*, 959–970. [CrossRef] [PubMed]
42. Gupta, S.M.; Pandey, P.; Grover, A.; Patade, V.Y.; Singh, S.; Ahmed, Z. Cloning and characterization of GPAT gene from *Lepidium latifolium* L.: A step towards translational research in agri-genomics for food and fuel. *Mol. Biol. Rep.* **2013**, *40*, 4235–4240. [CrossRef] [PubMed]

43. Payá-Milans, M.; Venegas-Calerón, M.; Salas, J.J.; Garcés, R.; Martínez-Force, E. Cloning, heterologous expression and biochemical characterization of plastidial sn-glycerol-3-phosphate acyltransferase from *Helianthus annuus*. *Phytochemistry* **2015**, *111*, 27–36. [CrossRef] [PubMed]
44. Safder, I.; Gaoneng, S.; Sheng, Z.; Hu, P.; Tang, S. Identification and analysis of the structure, expression and nucleotide polymorphism of the GPAT gene family in rice. *Plant Gene* **2021**, *26*, 100290. [CrossRef]

plants

MDPI

Article

Enhancing Coleoptile Length of Rice Seeds under Submergence through *NAL11* Knockout

Zhe Zhao [1,†], Yuelan Xie [2,†], Mengqing Tian [1], Jinzhao Liu [1], Chun Chen [1], Jiyong Zhou [3], Tao Guo [1,*] and Wuming Xiao [1,*]

[1] National Engineering Research Center of Plant Space Breeding, South China Agricultural University, Guangzhou 510642, China; zhezhao3016@163.com (Z.Z.); 18110520310@163.com (M.T.); ljz666666@stu.scau.edu.cn (J.L.); chchun@scau.edu.cn (C.C.)
[2] Yangjiang Institute of Agricultural Sciences, Yangjiang 529500, China; m13751844286@163.com
[3] Guangdong Agricultural Technology Extension Center, Guangzhou 510520, China; nytzjy@126.com
* Correspondence: guoguot@scau.edu.cn (T.G.); heredity24@126.com (W.X.)
† These authors contributed equally to this work.

Abstract: Submergence stress challenges direct seeding in rice cultivation. In this study, we identified a heat shock protein, *NAL11*, with a DnaJ domain, which can regulate the length of rice coleoptiles under flooded conditions. Through bioinformatics analyses, we identified *cis*-regulatory elements in its promoter, making it responsive to abiotic stresses, such as hypoxia or anoxia. Expression of *NAL11* was higher in the basal regions of shoots and coleoptiles during flooding. *NAL11* knockout triggered the rapid accumulation of abscisic acid (ABA) and reduction of Gibberellin (GA), stimulating rice coleoptile elongation and contributes to flooding stress management. In addition, *NAL11* mutants were found to be more sensitive to ABA treatments. Such knockout lines exhibited enhanced cell elongation for coleoptile extension. Quantitative RT-PCR analysis revealed that *NAL11* mediated the gluconeogenic pathway, essential for the energy needed in cell expansion. Furthermore, *NAL11* mutants reduced the accumulation of reactive oxygen species (ROS) and malondialdehyde under submerged stress, attributed to an improved antioxidant enzyme system compared to the wild-type. In conclusion, our findings underscore the pivotal role of *NAL11* knockout in enhancing the tolerance of rice to submergence stress by elucidating its mechanisms. This insight offers a new strategy for improving resilience against flooding in rice cultivation.

Keywords: rice seed germination; coleoptile elongation; submergence; *NAL11*; stress tolerance

1. Introduction

Rice (*Oryza sativa* L.) stands as one of the most pivotal crops cultivated globally, with over half of the world's population relying on it as a primary staple food [1]. The practice of direct seeding plays a crucial role in rice cultivation and is widely employed in both rainfed and irrigated fields due to its substantial benefits, including reductions in labor, energy consumption, water usage, production costs, and mechanization [2,3]. However, rice's vulnerability to prolonged flooding poses a significant challenge, leading to oxygen starvation and energy depletion in submerged plants [4]. Enhanced seedling vigor, characterized by the elongation of mesocotyls, coleoptiles, and shoots, is crucial for improving seedling emergence under such conditions [5,6]. Rice employs an escape strategy to reduce submergence stress during seed germination [7], increasing coleoptile and/or mesocotyl length to improve survival under submerged conditions [8,9].

Several genetic factors affect rice shoot growth, such as expansin genes, anaerobic metabolic pathways including glycolysis and fermentation, ROS scavenging and phytohormone signaling. Overexpression of the expansin gene *OsEXP4* has been shown to promote mesocotyl and coleoptile elongation by cell wall stress relaxation and volumetric extension, a process that is repressed in *OsEXP4-antisense* plants [10]. In addition, up-regulation

of *EXPA7* and *EXPB12* promotes the elongation of rice coleoptile under hypoxic conditions [11]. In rice, sugar availability has been considered one of the critical factors for tolerance to submergence [12]. Rice seeds can germinate and produce α-amylase enzymes required for starch degradation even without oxygen [13]. Under flooded conditions, anaerobic metabolic pathways, including glycolysis and fermentation, play a crucial role in coleoptile elongation [14]. Under sugar starvation, the transcription factor *MYBS1* activates the *Ramy3D* gene, facilitating starch degradation to provide the necessary energy for subsequent leaf and root development [15]. During germination under submergence, rice gene *CIPK15* (calcineurin B-like-interacting protein kinase 15) regulates coleoptile length through a sugar signaling pathway [16]. Alcohol dehydrogenase (ADH) activity in rice coleoptiles is correlated with a deceleration in coleoptile elongation under submergence conditions [17].

Abiotic stresses, like drought, salt, and temperature variations, enhance the production of ROS in plants [18]. However, excessive ROS can lead to oxidative damage to lipids, DNA, and proteins [19]. To mitigate ROS-induced damage, plants have developed an antioxidant system consisting of enzymes, such as catalase (CAT), ascorbate peroxidase (APX), glutathione peroxidase (GPX), glutathione reductase (GR), and glutathione sulfotransferase (GST) [20]. Abscisic acid (ABA) is a pivotal stress hormone that accumulates in response to stress and concurrently associated with a reduction in growth in stressed plants [21]. However, a growing body of evidence suggests that ABA plays a dual role in plant stress responses; while high concentrations inhibit growth, low concentrations can promote it [22,23]. This balance is crucial in stressed plants, where ABA concentrations are finely tuned through a balance between ABA biosynthesis and catabolism processes [24]. Recent studies have shown that the crosstalk between ABA and ROS in the phytohormone network play important roles in many aspects of plant growth and development, including the response to adversity stresses [25,26]. For example, it has been reported that alterations in ROS levels can affect ABA biosynthesis and signaling, as well as change ABA sensitivity [27], and ABA can also regulate the expression of ROS producing and scavenging genes [25]. For instance, overexpression of the rice ABA receptor 6 (*OsPYL6*) can improve drought tolerance by increasing ABA content and improving ROS detoxification, thereby stabilizing membrane [28]. Studies had suggested that ABA could improve oxidase activity and induce stomatal closure to reduce CO2 fixation, thereby inhibit the accumulation of ROS [29]. In addition to ABA, other phytohormones play crucial roles in regulating growth and developmental process and signaling networks involved in plant responses to environmental stresses, including flooding [30]. Gibberellin (GA) is considered essential in regulating the expression of α-amylase genes, which catalyse hydrolytic starch degradation during cereal seed germination in the air. However, under anoxic conditions, starch degradation through the gibberellin-induced α-amylase pathway fails to function properly because oxygen is also required for gibberellin biosynthesis, and rice become gibberellin insensitive under anoxic or hypoxic conditions [12]. Auxin is well known for promoting coleoptile elongation and rapid seedling growth during germination [31], but little is known about its role in rice germination and seedling establishment under submergence. A recent study has shown that auxin biosynthesis and the auxin influx carrier AUX1 regulated the final length of rice coleoptile under submergence [32].

Heat-shock proteins are proteins with molecular chaperone activity, responsible for protein folding, assembly, translocation and degradation in many normal cellular processes, stabilize proteins and membranes [33]. And HSPs may be newly synthesized or otherwise increase in abundance in vivo when plants are subjected to stress. Heat-shock proteins have been reported to play critical roles in stress resistance. For example, transgenic rice plants overexpressing *sHSP17.7* showed increased survival under high-temperature conditions [34]. The overexpression of *Hsp70* genes positively correlates with the acquisition of thermotolerance [27] and results in enhanced tolerance to salt, water and high-temperature stress in plants. *HSP70s* reduce heat tolerance, but under high-salt conditions, these proteins enhance seed germination and regulate the developmental transition from seed to

seedling by repressing seed-specific gene expression [35]. The expression of *Hsp90* in Arabidopsis is developmentally regulated and responds to heat, cold, salt stress, heavy metals, phytohormones, and light/dark transitions [36]. A correlation between HSPs and anaerobiosis has been observed in the hearts of turtles and mammals, where constitutive expression of certain HSP genes is associated with increased tolerance to anoxia [37].

Coleoptile and mesocotyl elongation are critical for rice survival under submerged conditions, and these processes are closely linked to hormonal regulation (ABA, GA, auxin) [3,32]. Our previous studies demonstrated that *NAL11*, which encodes a heat shock protein containing the DnaJ structural domain, regulates rice plant architecture and is involved in GA metabolism [38], showing the influence of *NAL11* on hormone regulation. This prompted us to investigate whether the regulatory function of *NAL11* in growth would intersect with stress response pathways, particularly under environmental stresses such as flooding, which can challenge plant survival. Therefore, this study aims to investigate the effect of *NAL11* on the elongation of rice coleoptile under flooded conditions. To further explore the interactions between *NAL11* and gibberellins, auxins and abscisic acid under submergence stress. Our findings unveil a novel mechanism by which HSPs contribute to flood tolerance in rice, which lays a foundation for further investigations into flooding tolerance in rice.

2. Results

2.1. Bioinformatics Characteristics

All amino acid and nucleotide sequences were retrieved and downloaded from the NCBI website. Using the NCBI blast online comparison, 28 homologous proteins were screened in *Oryza sativa Japonica*, *Brachypodium distachyon*, *Sorghun bicolor*, *Zea mays*, *Glycine max*, *Nymphaea colorata*, *Arabidopsis*, and wild rice (*Oryza brachyantha*, *Oryza glaberrima*). To comprehensively characterize *NAL11* and its homologous proteins, a phylogenetic tree was constructed for the 28 homologous proteins and the NAL11 protein using MEGA software (v11.0). The constructed evolutionary tree was then merged with the phylogenetic tree of the conserved structural domain elements of the proteins using the TBtools software (v1.120). Remarkably, in our phylogenetic analysis showed that NAL11 (XP_015645205.1) and XP_040381942.1 clustered together on the same branch (Figure 1). NP_001412649.1 was found to be orthologous to *NAL11* in rice, suggesting that *NAL11* has undergone a gene duplication event during evolution. Using the online software MEME (v5.5.7) was used to analyze the 28 homologous proteins, Motif 1 was identified in all 28 members, with conserved motifs 1, 2, and 3 in 22 encoding proteins (Figure 1). All homologues of *NAL11*, except for NP_001146964.1, contained the DnaJ structural domain (Figure S1). In addition to its conserved nature, NAL11 exhibited high homology with homologues in wild rice. These findings highlight *NAL11* as a highly conserved gene throughout evolution. To further investigate potential regulatory mechanisms, we analyzed the 2.0-kb nucleotide sequences upstream of the start codon using Plant CARE. This revealed multiple cis-elements associated with stress response (Figure S2), including the ABRE-motif (ABA response element), the TGACG-motif (MeJA-responsiveness), the GGTCCAT-motif (Auxin-responsiveness), the TCTGTTG-motif (Gibberellin-responsiveness), and other elements critical for endosperm expression, anaerobic induction, anoxic specific regulation, and meristem expression. These results suggest that the *NAL11* gene may respond to hypoxia or anoxia during rice growth and development.

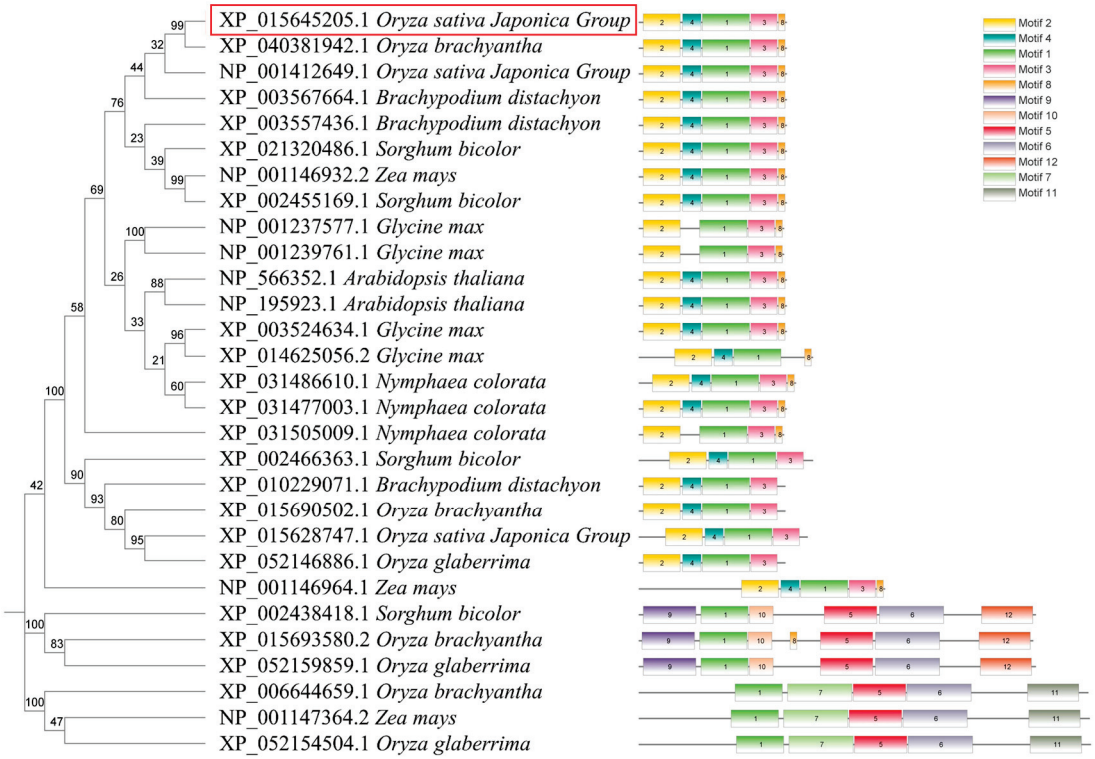

Figure 1. Evolutionary tree of NAL11 homologs with Oryza sativa Japonica, Brachypodium distachyon, Sorghun bicolor, Zea mays, Glycine max, Nymphaea colorata, Arabidopsis, and wild rice (Oryza brachyantha, Oryza glaberrima). XP_015645205.1 is the accession number of NAL11 in NCBI, which is highlighted in the red box.

2.2. The Expression of NAL11 Was Induced during Seed Germination under Submerged Conditions

Under aerobic conditions, *NAL11* exhibited a consistently low level of expression, with a discernible decline at both 12 h and 72 h compared to the baseline at 0 h (Figure 2A). In contrast, during submergence, the gene was induced to express at high levels at 12 h, 24 h, 48 h, and 60 h, compared to the corresponding expression levels under submerged conditions. This finding highlights a substantial upregulation in the expression of *NAL11* under submergence conditions compared to that under aerobic conditions. Peak expression occurred at 60 h under submergence, representing an approximately 3-fold increase compared to the expression levels under aerobic conditions. Despite a subsequent decrease in the expression at 72 h under submergence, the level remained significantly elevated compared to the expression level observed under aerobic conditions.

The expression pattern was assessed in transgenic plants carrying the *pNAL11::GUS* construct (GUS reporter gene driven by the promoter of the *NAL11* gene) in the ZH11 background under both submerged and aerobic conditions (Figure 2C). The analysis revealed that *NAL11* was predominantly expressed in the parenchyma tissues of the protruding embryo at 24 h and 48 h under aerobic conditions. Whereas at 72 h after seed germination, however, its expression was mainly observed in the growing bud, with minimal presence in the developing radicle. Conversely, under submergence conditions, *NAL11* exhibited distinct expression patterns. At 24 h, expression was concentrated in the protruding embryo, and extended to both the embryo and the growing bud at 48 h. Under submerged conditions, the expression in the parenchyma tissues of the embryo was prominent. Due to the limited observation of radicles during seed germination under submergence, *NAL11* expression was mainly observed in the elongating coleoptile, with a more pronounced signal closer to the base.

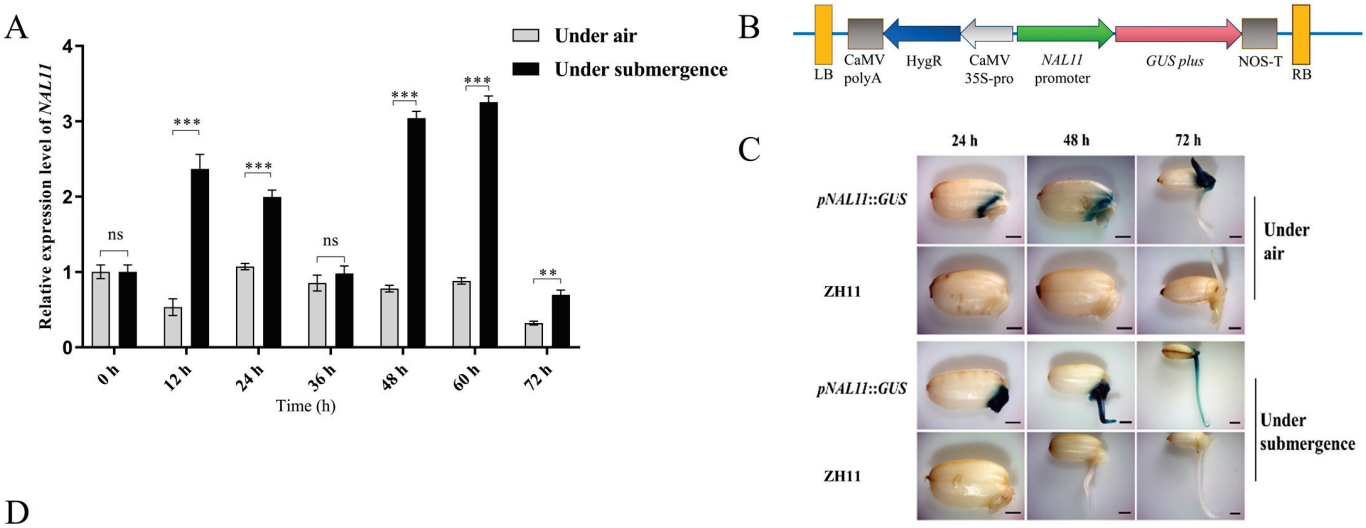

GCATGCATAAAGAGGGTAGGAAGTTGTGCATACTCTATCATGTCATCCTGTAAGATTGATTAGTACGCCATGAGGAAAATATTCTATTTGAGCCCTCAGAATGGCAGTTTGTGCAAAATCCATCATGTGAACATTTT
TTTCCCCAGTAAATTGAATTAAGGAACATATTCCCTCTGTTCCAAAAGTAACATTTCGGATATAGTATGGCCTACAACATGCTACACAGACCACTTTTTACAGGTATACACTTCTTATAGAAATAAGTTCTATGATAA
ATTAACTAGTAACAATTTCATACAAAAACTTTAATAGATTTATTGTTATTAGCAGGCAAAAATAACTACTCCAATGTTATATGCTTTATAAAATACCAAAATGTGCAAGAGAAGGAAGTATATCCATTTGTGTAATT
GTGCTATAAGATGATAAAAGTAAAATCATACCTAATATATCAACCCTCTAAACTCTTAATTCTAGTGACATACATTGCAACAAGAGCCGACATAGTAACGGTACACACCGCACAAGGAATCTTCCAAATAAGTTCA
CCTTGGATGCGCGGGAGAGGGAGATGGGCATAGCCGCGGCAGCGCTTCGAGGGCTTCCATCTGCATGGCGGCCGCGCTCCTGAGGTCCACAATGCAGTACAACGCCTCAGTGGCAGGGGCTGGGGACGCTGCTGC
GTTCAGGAGAGTGGAGATGGTGTGTGGCCTGGCGAGTGCGAGCGGGGCTAGACGCCTAGACGCCTTGGACTTTGGCCCAGCCGCAGGCGGCGTGGACACGAGGAGCCAGGGGAGGAGAGGACGCTGATGCCAGC
AGTGGGGGAGACCTGTGACAATGGGGTGGAGCTGATGCCGGCGCGGTGGGGGAGAGGAATGAGGGCTTAGGATTAGGGCTCACTACCTCGCCTGAACCTGGTGGAGAGGGAGAGGGAGTAGGTGGCGCGCGCGC
GCGGTGGGGGATTTTGGCGGCGGCACCGGCGGCGGAGGGGAGGAGGACTGAGGCGGCGGCGGCGGGGGAAGGGAGGCGCCGTGGAGGTGACGCGCTGAGCAGATGGAGGCGGTGGCGATGGCCGCGGGACCAC
CGTAGCGGACCTAACAAGCAGTGACCTGTCCTCAAGAACTAAGTGCATACGTATAATCCCATAAACCTGCATTCGCTGTTGGCTATCCAAAAGCGCATAGGTCTCAACGGAGTACCCAATAGACCCGTGCTCTCGA
CACACAGGGACAACAAACCCATAAACCTGTGTGTCTGTAAGGGCATCGGCAACATTTACTATCCACATCGGTATTAGCGTAGGCCCAAATGACAGGCGGTAATAGAGGGAGACGTGCTCCACATTGCTTATTTCTG
TGAGTTGGCAGTAAGGTAGGGTCCATGGGGTAAAAAAAATCGTAGCAAGGACAGAGCATGCATGCAACGCTGGGGAGAAGCAATTCTTTTGCTGTAAGAAAACACTATGTACATGCATATACTATTCCTTGCTTCC
AGAAGTAGTGGTATGACCCGGTTGTAGTTATGTACTAGCCCCACAATGCTTAATACCTCGTAGTAAAGATGTATTTATTGCTTACGACCGATTTGTGAGCACGTTGCTGATGCCCTAACATCGGAAACACTCACTCA
GGGACCTGATTGTAAAATACGCAACAATTACAACAGGGACCCGATTGCAAAATGTTTGGGCCCCTAACACTGCTGCCGATCCCAATTAGGGACTGGATTGCAAAACAGCCCAACGAAATGGGCCGCATCACTAGCT
CTCCAGAAGACCCAACTCCGAAGCAGCACAAGCCCAAGTAGGGTTTCCTCGCTCCCACCTTCACCCACGAGGTCTCCGCCGCCGCCGCGGCCGACGACGACTACCTCCGGCGACCGCCGGGGCGGCCTTA
GCGCCGGGTACCCTGCCGCCTCCGCGTAGCCGAGCCCTATCGCGTACCCGTCCCTCTCGCGCCTAGTGCGCCGGGCTGGCCGGTGGCGGAGTACCGGAA

Figure 2. Spatiotemporal expression analysis of *NAL11*. (**A**) Transcription levels of *NAL11* in germinating seeds of ZH11 under aerobic and submerged conditions using quantitative reverse transcription polymerase chain reaction (RT-PCR). Gene expression was normalized to that of *OsActin*, with relative expression levels represented as fold change relative to the expression level of *NAL11* at 0 h. (**B**) Schematic structure of the expression vector for pro$_{NAL11}$:GUS. (**C**) β-glucuronidase (GUS) staining of seeds after 24 h, 48 h, and 72 h of submergence stress. Scale Bar, 0.5 cm. (Data are presented as mean ± SD, $n = 5$; significant differences were determined by two-tailed Student's *t*-tests. ** $p < 0.01$, *** $p < 0.001$, ns, no significance). (**D**) 2000 bp promoter sequence of *NAL11*.

2.3. Knockout Lines Exhibited Longer Coleoptiles during Seed Germination under Submerged Conditions

We used two independent homozygous hygromycin-free transgenic lines with different editing effects (*osnal11-1* with 1 bp deletion and *osnal11-2* with 1 bp insertion) on the target gene (Figure S3B). The *NAL11* knockout lines had significantly lower transcript levels than the wild type (Figure S3C). Mature dry seeds of the WT (ZH11) and two knockout lines were subjected to germination under both air (aerobic) and waterlogged (anoxic) conditions. The coleoptile length of dry seeds on day 4 under submergence exhibited significant differences between the WT and the two knockout lines (Figure S4B). The average coleoptile length of the two knockout lines reached 4.64 cm and 4.55 cm, respectively, which was significantly greater than the 3.82 cm observed in the WT (Figure S4C). Moreover, the surface area of the coleoptile in the knockout lines was significantly greater than that observed in the WT (Figure S4D). However, no evident differences in coleoptile diameter were observed between the WT and knockout lines (Figure S4E). Remarkably, by day 4, both the WT and knockout lines achieved an impressive germination rate of approximately 100% on day 4 (Figure S4A). Additionally, when germinated under aerobic conditions on day 4, no evident differences in bud and root lengths were observed between the WT and knockout lines (Figure S4B). In conclusion, knockout of *NAL11* significantly improved rice seed coleoptile growth under submerged conditions.

It has previously demonstrated that coleoptile elongation under anoxic conditions is attributed to cell expansion, and that expansins are likely to be key players in this physiological process [10,39]. To further understand the role of expansins in this context,

we compared the expression patterns of some expansin genes in ZH11 and knockout lines after 48 h of flooding. Interestingly, only *OsEXP7* showed downregulation in the coleoptiles of the knockout lines at 48 h. In contrast, the mRNA levels of *OsEXP2*, *OsEXP4*, *OsEXP8*, *OsEXPB11*, *OsEXPB12*, and *OsEXPB15* were significantly higher in the coleoptiles of the knockout lines after submerged germination compared to those of the WT at the same time point (Figure 3), with *OsEXP4* showing an impressive approximately 4-fold increase (Figure 3). The notable upregulation of the expression of these expansin genes in the knockout lines may provide a molecular basis for the accelerated growth of rice coleoptiles under submerged conditions compared to that in the WT. This suggests that expansins are likely to contribute to the elongation of coleoptiles in rice when exposed to anoxic conditions.

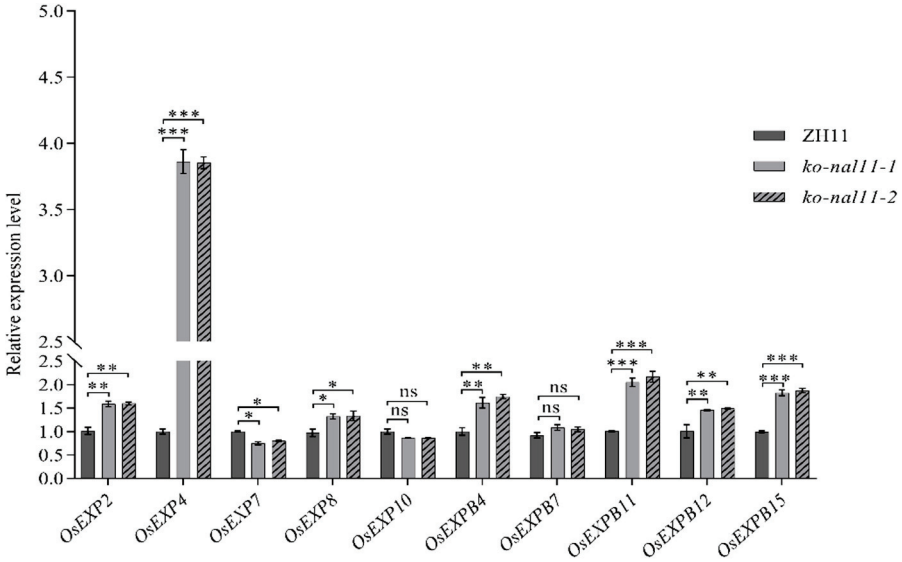

Figure 3. Relative expression level of expansin genes in ZH11 and knockout lines at 48 h after submergence. (Data are presented as mean ± SD, $n = 5$; significant differences were determined by two-tailed Student's *t*-tests. * $p < 0.05$, ** $p < 0.01$, *** $p < 0.001$, ns, no significance).

2.4. Knockout of NAL11 Affected Sugar and Energy Pathways under Submerged Conditions

As a crucial enzyme responsible for catalyzing the degradation of starch in cereal seeds, α-AMS plays a pivotal role in various key agronomic traits, including the germination rate [40] and resistance to hypoxia stress [41]. In our study, we aimed to identify the specific α-AMS family member directly involved in the response to endosperm starch degradation under submergence stress. To achieve this, we investigated the expression of rice *α-AMS* genes in seeds (containing coleoptiles) of ZH11 and knockout lines at 48 h after submergence treatment (Figure 4A). Our findings revealed that the expression levels of *RAmy1A* and *RAmy2A* in the knockout lines were significantly lower than those in ZH11. Conversely, the transcript levels of *Ramy3A*, *RamyC*, and *RAmy3D* were significantly higher in the knockout lines than ZH11 and that of *RAmy3A* in the knockout lines was approximately 5-fold higher in the knockout lines than in ZH11. Interestingly, no evident differences were observed in the expression levels of *RAmy3C* and *RAmy3E* between ZH11 and the knockout lines. Furthermore, the α-AMS activity in both knockout lines and WT showed a consistently significant increase from 12 h to 96 h during submerged germination. Compared to the WT, the knockout lines consistently showed higher α-AMS activity at different stages (Figure 4B).

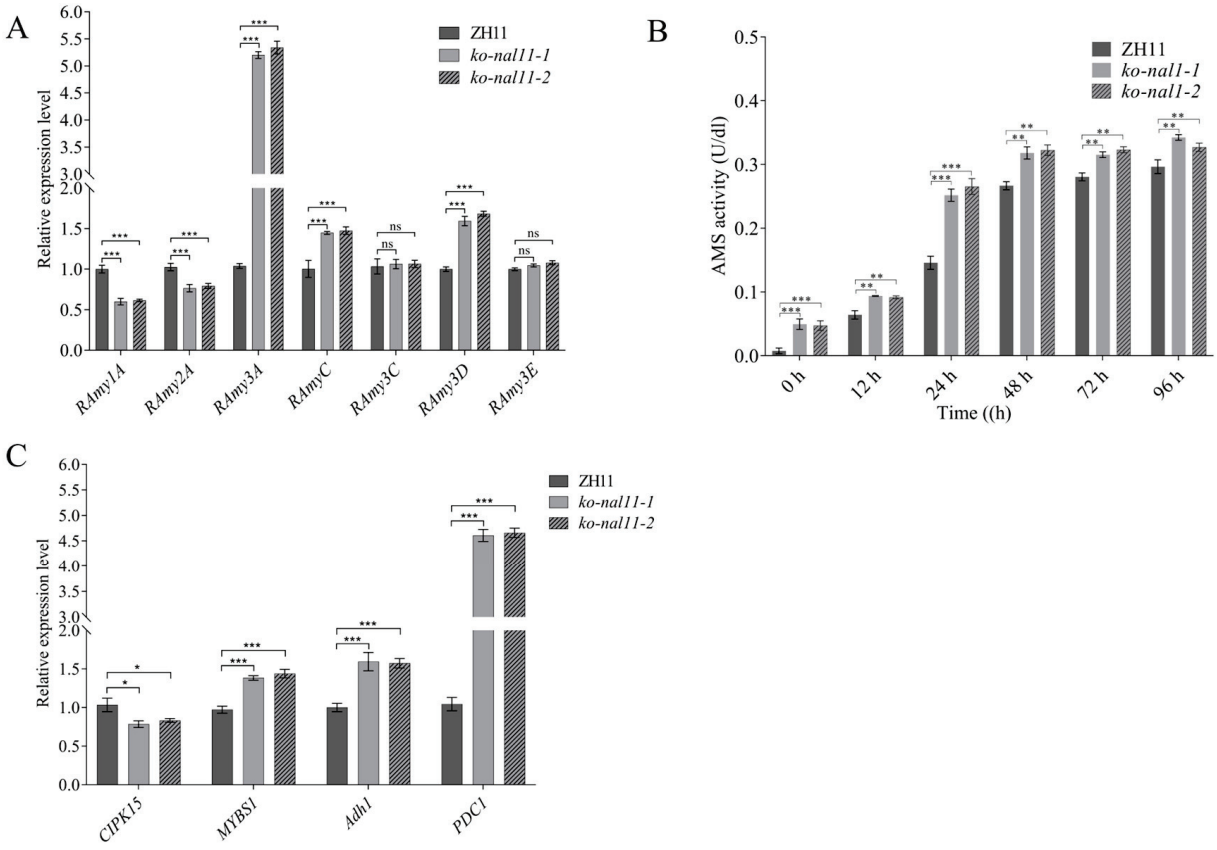

Figure 4. *NAL11* is involved in the sugar and energy pathway. (**A**) Quantitative RT-PCR analysis of nine α-amylase family genes in seeds of ZH11 and knockout lines at 48 h after submergence treatment. (**B**) α-AMS activity at different stages. (**C**) RT-qPCR analysis of sugar and energy metabolism genes at 48 h after submergence treatment, respectively. (Data are presented as mean ± SD, $n = 5$; significant differences were determined by two-tailed Student's *t*-ests. * $p < 0.05$, ** $p < 0.01$, *** $p < 0.001$, ns, no significance).

Long-term submergence can lead to substantial carbohydrate consumption, resulting in energy deficiency [42]. Therefore, we investigated the expression patterns of glycolytic pathway genes in rice seeds (containing coleoptiles) under submerged conditions (Figure 4C). *CDPK15*, *MYBS1*, *Adh1*, and *PDC1* exhibited distinct submergence-dependent expression. The expression of *CDPK15* decreased in the knockout lines, while other key genes associated with energy pathways, including *MYBS1*, *Adh1*, and *PDC1*, showed a significant upregulation in the knockout lines at 48 h after submergence treatment. Concurrently, the enzyme activity of α-AMS exhibited a similar increasing trend mirroring the transcript levels of the energy-synthesizing genes. The observed expression patterns of these genes suggest that the knockout of *NAL11* may have a substantial impact on the regulation of *α-AMS* genes and energy-synthesizing genes, potentially affecting the plant's ability to cope with submergence stress.

2.5. Knockout of NAL11 Affects ROS Levels and the Expression of Some Stress-Related Genes under Submerged Conditions

Given the anaerobic stress experienced by both the knockout lines and the WT during submergence, it is imperative to investigate into the potential physiological changes at different stages, aiming to elucidate he differences in coleoptile length. ROS are important signals that regulate the stress tolerance. Here, we compare the accumulation of hydrogen peroxide (H_2O_2) and MDA between seeds of the WT and knockout lines after submergence treatment. It shows that the seeds of the knockout lines accumulated more MDA and H_2O_2 than the WT (Figure 5A,B). Considering that *OsRbohA* and *OsRbohE* belong to the NOX

family [43], which is key to the production of ROS. We determined the transcription level of these two genes. We found that both were reduced in the knockout lines compared to WT (Figure 5C,D), which was consistent with ROS levels.

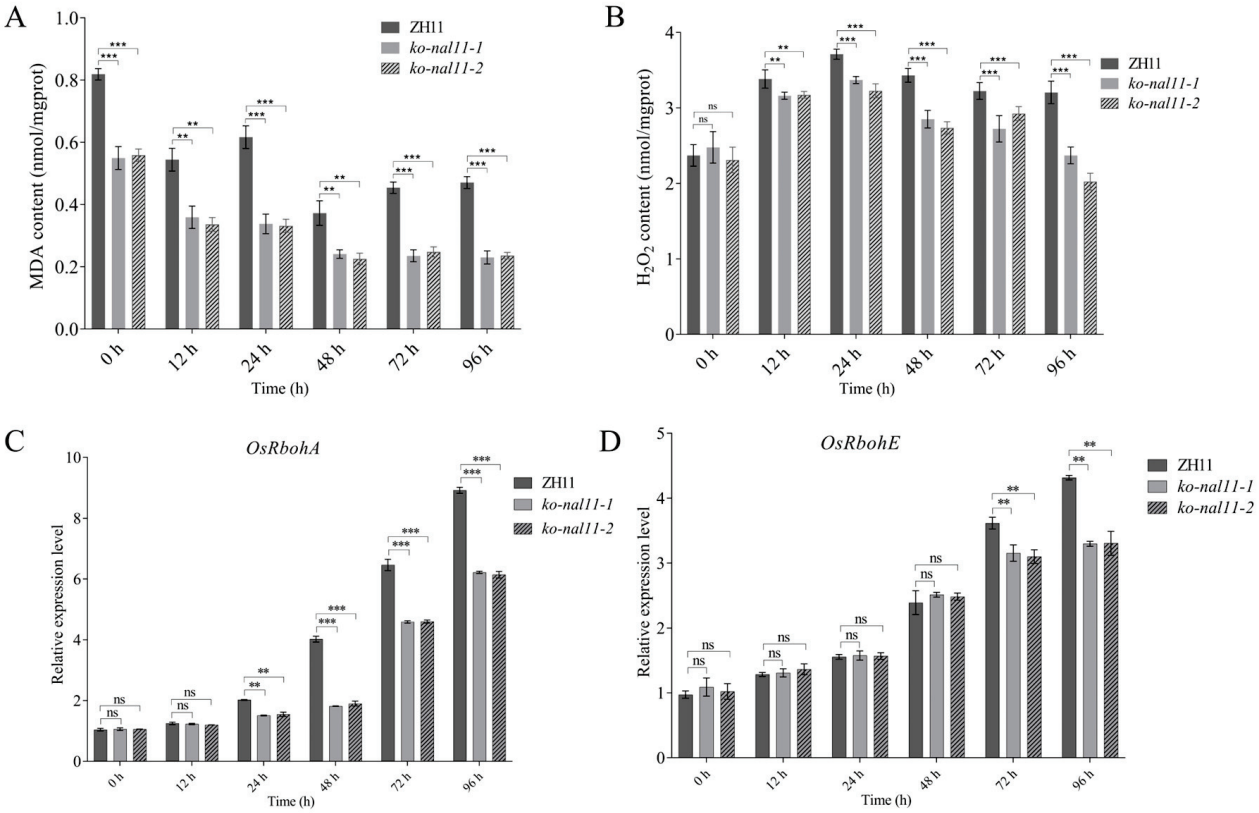

Figure 5. Analysis of MDA and H_2O_2 content, transcript levels of ROS-production gene, *OsRbohA* and *OsRbohE* of WT and transgenic plants under normal and submerged conditions. (**A**) MDA content. (**B**) H_2O_2 content. (**C**) *OsRbohA*. (**D**) *OsRbohE*. (Data are presented as mean ± SD, $n = 5$; significant differences were determined by two-tailed Student's *t*-tests. ** $p < 0.01$, *** $p < 0.001$, ns, no significance).

In addition, we also determined the activities of ROS-scavenging enzymes (SOD, POD, CAT). The results showed that there was no significant difference between WT and knockout lines in the control group. CAT activity in the knockout lines was evidently lower than that in the WT at the beginning (0 h). Surprisingly, the knockout lines exhibited significantly higher CAT activity than the WT at 12 h, 72 h, and 96 h of seed germination under submergence, with no apparent differences at 24 h and 48 h (Figure S5A). Moreover, the knockout lines showed significantly increased SOD activity from 0 h to 96 h under submerged conditions compared to the WT (Figure S5B). However, no evident difference was observed at 48 h. In contrast, POD activity was increased in both knockout lines and WT after submergence compared to that at the baseline (0 h). From 12 h to 96 h under submergence, no evident differences in POD activity were observed between the knockout lines and WT (Figure S5C). The above results indicated that knockout of *NAL11* can enhance rice tolerance to submergence stress by improving ROS scavenging ability.

To further investigate the possible molecular mechanisms of *NAL11* in regulating submergence tolerance in plants, we also determined the transcript levels of some well-known stress-responsive genes. These included *OsSUB1A* and *OsNAC9*, encoding typical stress-related NAC-type transcription factors (TFs); *OsSnRK1A* and *OsTPP7*, encoding trehalose-6-phosphate(T6P) phosphatasegene (*OsTPP7*) proteins. After submergence treatment for 48 h, compared to WT, the mRNA levels of the above genes were both increased in knockout lines (Figure S6).

2.6. NAL11 Is Involved in the Phytohormone-Mediated Regulatory Pathway

Previous studies have revealed that plant hormones are signaling compounds that regulate crucial aspects of growth, development and environmental stress responses [43]. The contents of several endogenous phytohormones, including ABA, IAA and GA, were measured in the WT and knockout lines to determine the regulatory pathway in which *NAL11* is involved. There were no significant differences in endogenous ABA, GA and IAA concentrations between the WT and knockout lines at 24 h after the initiation of submergence treatment. However, as the submergence time increased, a significant increase in ABA and IAA concentrations was observed in the knockout lines, whereas no significant change was observed in the WT (Figure 6A). The knockout lines showed a significantly higher ABA and IAA levels than the WT at 48 h and 72 h after submergence treatment, while the opposite was true for GA (Figure 6B).

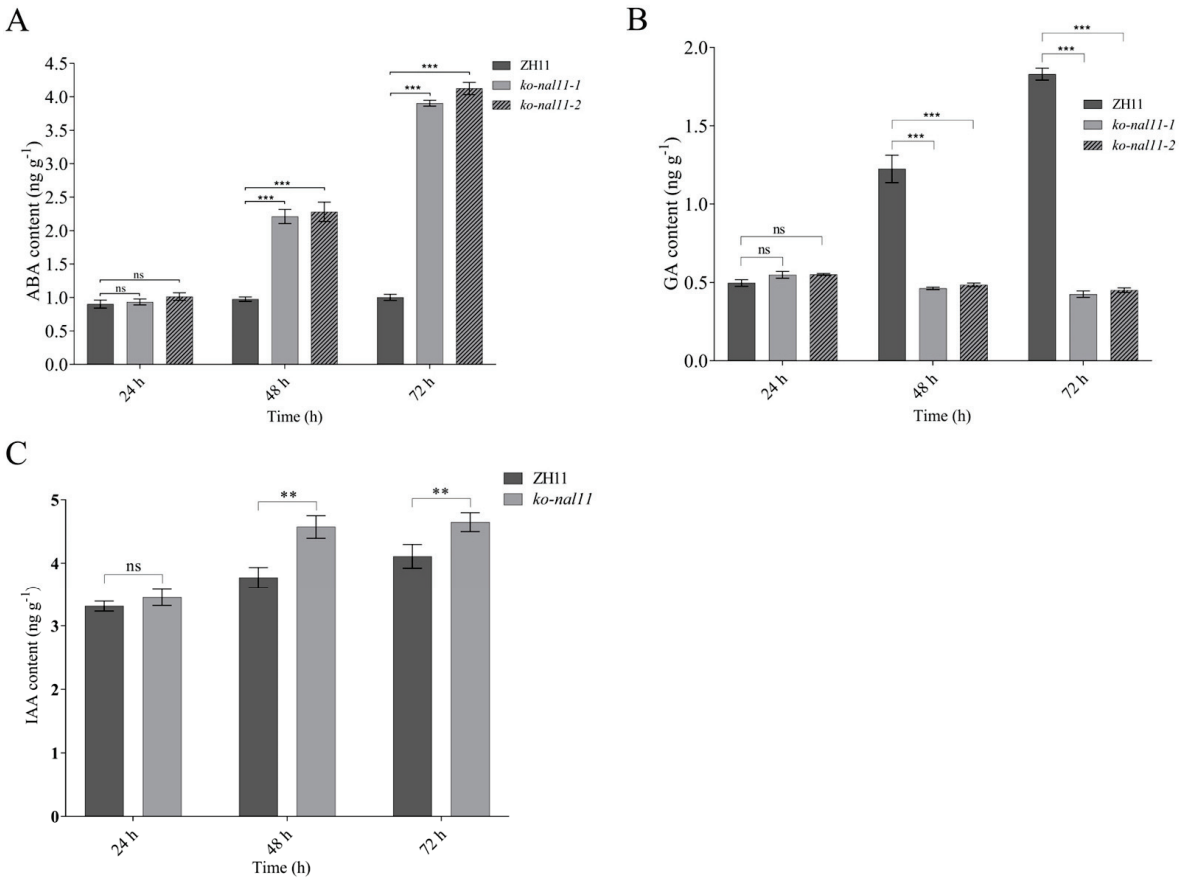

Figure 6. Knockout of *NAL11* affects the levels of ABA, GA and IAA. (**A**–**C**) Content of endogenous ABA, GA and IAA at 24 h, 48 h, and 72 h after submergence. (Data are presented as mean ± SD, $n = 5$; significant differences were determined by two-tailed Student's *t*-tests. ** $p < 0.01$, *** $p < 0.001$, ns, no significance).

Therefore, we further analyzed the expression of genes related to ABA, GA and IAA synthesis and metabolism in the WT and knockout lines at 24 h, 48 h and 72 h after submergence. Consistent with the increase in the ABA and IAA levels, most of the genes related to ABA and IAA synthesis in the knockout lines were upregulated (Figures S7A–C and S9). Moreover, most of the genes related to ABA metabolism, including several genes of the *ABAox* family genes, were downregulated simultaneously (Figure S7D–F). To further elucidate the effects of *NAL11* knockout on the ABA signaling pathway, we examined the expression levels of key genes involved in ABA regulation and signaling. Since *OsDET1*, *OsbZIP46*, and *OsbZIP72* have been identified as positive regulators of ABA signaling [44], our study specifically focused on analyzing the expression levels of *OsDET1*,

two *bZIP* genes (*OsbZIP46* and *OsbZIP72*) involved in ABA regulation, and several ABA receptor genes in both the WT and knockout lines under anaerobic conditions. At 48 h after submergence, the knockout lines exhibited a significant increase in the expression of *OsbZIP72*, whereas no significant differences were observed in the expression levels of *OsDET1* and *OsbZIP46* between the WT and knockout lines (Figure S7G). Moreover, *OsPYL1*, *OsPYL2*, *OsPYL3*, *OsPYL8*, and *OsPYL10* were significantly upregulated compared to the WT, whereas *OsPYL5* and *OsPYL9* were downregulated in the knockout lines. In contrast, no significant changes were observed in the transcript levels of *OsPYL4* and *OsPYL7* in the WT and knockout lines (Figure S7H). At 72 h after submergence, most of the genes related to ABA signaling were upregulated (Figure S7I). This suggests that knockout of *NAL11* has a significant effect on the expression of genes related to ABA biosynthesis, catabolism and signal transduction processes. Interestingly, the expression of most GA-related genes in the *NAL11* knockout lines showed the opposite trend compared to ABA (Figure S8), indicating reduced GA activity. We therefore speculate that the longer coleoptiles of the *NAL11* knockout lines under submergence could be attributed to the upregulated expression of ABA- and IAA-related genes and down-regulated expression of GA-related genes. Furthermore, we also analyzed the expression of genes related to auxin biosynthesis in one of the knockout lines. The expression of *YUCCA2*, *YUCCA3* and *YUCCA6*, which are involved in auxin biosynthesis, was significantly increased in the knockout line compared to the WT under submerged conditions (Figure S9A–C). Besides, the expression pattern of *TAA1*, another phytoalexin biosynthesis gene, was also similar to that of these genes (Figure S9D). As a result, the endogenous IAA levels were significantly increased (Figure 6C). It suggests that under submerged conditions, *NAL11* knockout may prolong the coleoptile by increasing the accumulation of auxin in rice seeds. Taken together, *NAL11* is involved in the ABA, GA and auxin pathways to improve tolerance to submergence stress tolerance in rice. This intricate regulatory network contributes to the improved tolerance of the knockout lines to submergence stress during the germination stage of rice seeds.

2.7. Knockout Lines Are Sensitive to ABA

Crosstalk between ABA and ROS in the phytohormone network has been shown to be involved in the regulation of plant stress tolerance [29], and exogenous ABA treatment will decrease the level of ROS in rice seed germination embryos [45]. Based on these studies, we conducted the following experiment to assess the sensitivity of *NAL11* to ABA. We conducted a statistical analysis of the growth status of the WT and knockout lines on day 4 after treatment with different concentrations of exogenous ABA (0 μM, 0.001 μM, 0.01 μM, 0.1 μM, 1 μM, and 10 μM). Under submerged conditions, the knockout lines exhibited longer coleoptiles compared to the WT in the absence of ABA treatment. However, the coleoptile length of the knockout lines was significantly reduced compared to that of the WT when treated with higher concentrations (10 μM, 1 μM, or 0.1 μM) of exogenous ABA (Figure 7A,B). Remarkably, at an ABA concentration of 0.01 μM, no significant difference in coleoptile length was observed between the WT and knockout lines. Interestingly, when treated with a lower concentration of 0.001 μM ABA, the coleoptile length of the knockout lines was significantly greater than that of the WT. These results suggest that high concentrations of exogenous ABA inhibit coleoptile elongation in the knockout lines, while low concentrations of exogenous ABA promote coleoptile elongation in the knockout lines. This suggests that the knockout of *NAL11* may enhance sensitivity to ABA.

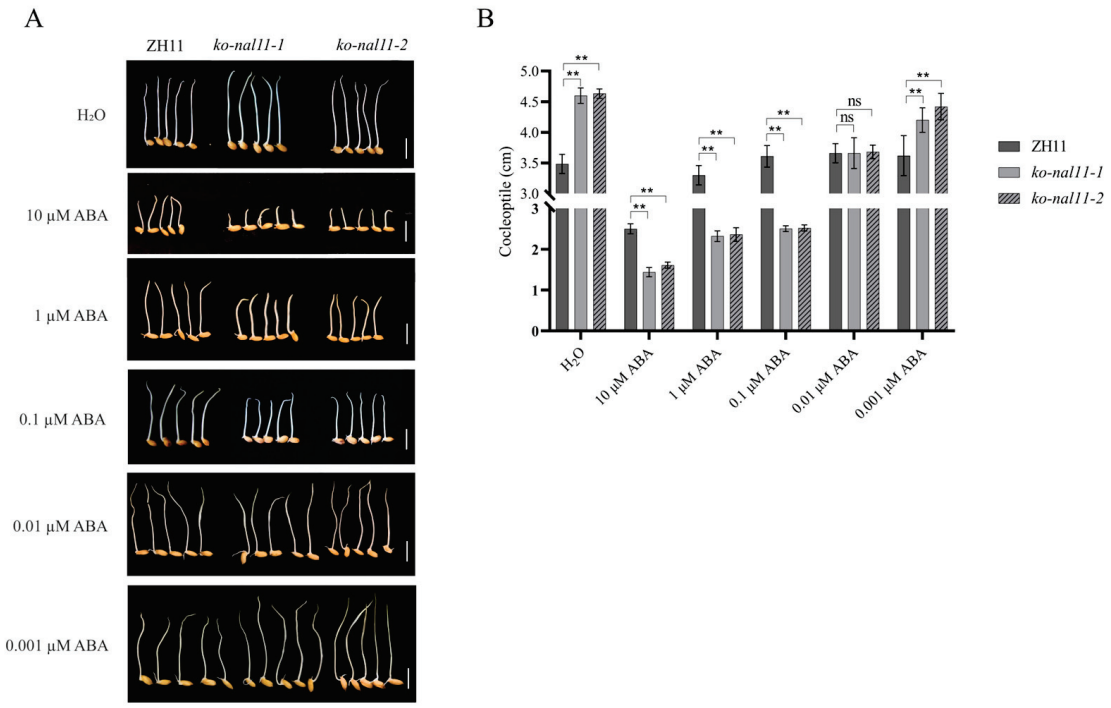

Figure 7. Knockout of *NAL11* shows sensitivity to ABA. (**A**) Representative images of coleoptile length in response to different concentrations of ABA (0 μM, 0.001 μM, 0.01 μM, 0.1 μM, 1 μM, and 10 μM, respectively) after 4 d of submergence for both WT and knockout lines. Scale bars: 1 cm. (**B**) Comparison of coleoptile lengths in WT and knockout lines in response to control (H_2O) and ABA treatments after 4 d of submergence. (Data are presented as mean ± SD, $n = 5$ biologically independent samples; significant differences were determined by two-tailed Student's *t*-tests. ** $p < 0.01$, ns, no significance).

3. Discussion

The length and elongation rate of the coleoptile and/or mesocotyl are the crucial developmental traits that determines deterring the success of direct seeding in many cereal crops. In the case of rice submerged seed germination, the long and rapidly elongating coleoptiles may promote submergence tolerance by providing oxygen when they reach to the water surface [10]. Interestingly, the high expression of some HSPs in response to hypoxia is also a prominent phenomenon. This observation suggests a potential close relationship between *NAL11* and hypoxia stress responses. Supporting this hypothesis, our study suggests the involvement of at least four biological processes in *NAL11*-regulation of hypoxia response, encompassing substance metabolism, abiotic stress responses, redox reactions, and crosstalk with other hormones. While this highlights the involvement of *NAL11* in hypoxia response, we acknowledge that it may not serve as a key integrator of these pathways. Rather, *NAL11* may contribute to stress responses through its regulatory role within these processes. By identifying hypoxia-responsive genes and pathways, our research contributes to the understanding of the escape strategy of submergence tolerance in rice, which may be helpful in improving submergence tolerance in other cereal crops.

Expansin genes, known for their role in promoting cell wall relaxation and expansion, were significantly upregulated in the *NAL11* knockout lines. Previous research has demonstrated that overexpression of expansin genes, such as *OsEXP4*, enhances coleoptile and mesocotyl elongation in rice [10]. Consistent with these findings, we observed significant upregulation of expansin genes in the knockout lines, which suggests that *NAL11* may negatively regulate coleoptile elongation by controlling expansin activity. This regulatory effect on cell elongation is likely a key mechanism by which *NAL11* influences submergence tolerance during the germination stage. Additionally, our analysis revealed the presence of various response-related cis-elements in the promoter of the *NAL11* gene (Figure S2),

including ABA, GA, and auxin response elements, further supporting its involvement in hormonal regulation (Figures 6 and S6–S8). In this study, we were the first to investigate the role of *NAL11*, a DnaJ domain-containing HSP gene, in regulating coleoptile elongation through expansin expression and hormone crosstalk. Reactive oxygen species (ROS) function as crucial signaling molecules, but excessive ROS accumulation can cause irreversible cell damage [46]. Plants adapt to abiotic stress by regulating ROS metabolism [47,48]., and our results showed enhanced activities of antioxidant enzymes (CAT and SOD) in *NAL11* knockout lines under submergence stress, although POD activity was not significantly affected (Figure S5). This increase in antioxidant enzyme activity likely contributes to the enhanced submergence tolerance observed in the knockout lines [49–51]. Furthermore, the knockout lines exhibited reduced levels of MDA, a marker for ROS-induced lipid peroxidation [52], indicating that *NAL11* knockout may enhance antioxidant capacity to mitigate oxidative stress.

Energy supply is crucial for rice seed germination under anoxic conditions, where starch is degraded into fermentable carbohydrates to sustain embryo growth [53]. Our results showed that amylase activity was significantly higher in NAL11 knockout lines during submergence, which is consistent with longer coleoptiles observed in these lines (Figure S4C,D). This increased amylase activity likely facilitates more efficient starch hydrolysis, contributing to submergence tolerance. Notably, expression levels of key amylase genes, including RAmy3A, RAmyC, and RAmy3D, were upregulated in the knockout lines under submergence, suggesting an accelerated starch metabolism (Figure 4B). These findings align with previous studies showing that the upregulation of amylase genes supports seed germination and early seedling establishment under submerged conditions [42,54]. Although the expression of *RAmy1A* and *RAmy2A* was reduced after submergence (Figure 4A), this did not affect the rate of band starch hydrolysis, as the isozymes they encode are not dominant during hypoxic sprouting [11,55]. α-AMS 3 emerges as a major player, its mRNA accounting for approximately 60% of the total mRNA of amylase genes in glucose-starved rice cells [56]. In this study, high expression of α-AMS 3 accelerated the hydrolysis of starch (Figure 4A), thereby providing the energy required for the germination process and sustaining the subsequent alcoholic fermentation process. Previous studies have shown that submergence triggers sugar starvation and induces mRNA accumulation of calcineurin B-like (CBL) protein-interacting protein kinase 15 (*CIPK15*), thereby enhancing the accumulation of SnRK1A proteins. These two proteins interact and induce the *MYBS1* transcription factor, subsequently activating the expression of starvation-induced α-amylase gene, *αAmy3/RAmy3D* [16]. As expected, the expression of *CIPK15* and *MYBS1* was significantly higher in the knockout lines compared to WT (Figure 4C). Alcoholic fermentation plays a crucial role in providing ATP under hypoxic conditions [57,58], and our results showed that *NAL11* knockout plants exhibited higher expression of pyruvate decarbox-ylase (PDC) and ADH after 48 h of submergence (Figure 4C), which supports glycolysis and ATP synthesis [59]. This observation suggests that *NAL11* knockout enhances rice's ability to cope with submergence through more efficient anaerobic metabolism. But it remains unclear whether sugar could affect the accumulation of endogenous free phytohormones to influence submergence tolerance and seedling establishment in rice.

Many transcription factors play critical roles in regulating the stress response in plants, including *SUB1A* and *OsNAC9*, which improve submergence tolerance when overexpressed [60,61]. Under sugar starvation conditions, SnRK1A is an important mediator in the sugar signaling cascade response, acts upstream of *MYBS1* and *αAmy3* SRC interactions, and plays a key regulatory role in rice seed germination and seedling growth [62]. In our result, both were up-regulated in transcription level in the knockout lines compared to WT. Meanwhile, it has been shown that *OsTPP7* is involved in T6P metabolism and catalyzes the conversion of T6P to trehalose, thereby allowing increased starch mobilization in the form of easily fermentable sugar, which ultimately enhances coleoptile elongation and embryo germination [2]. Similarly, in our research, better developed coleoptiles and higher levels of *OsTPP7* expression were observed in the knockout lines (Figure S6). This suggests,

therefore, that knockout of *NAL11* could improve submergence tolerance in rice by affecting the transcript levels of these stress-responsive genes.

The phytohormone auxin has long been known to be important in stimulating coleoptile elongation and rapid seedling growth in the air [31], but little is known about its role in influencing the rice coleoptile elongation under water. To understand the role of plant hormones in rice under air and hypoxic conditions, we carried out some analyses on ABA, GA and auxin and related genes under submerged conditions. ABA is a well-documented stress hormone that accumulates in response to stress [21]. Consequently, ABA levels in the *NAL11* knockout lines gradually increased after 48 h of submergence treatment. We also found that ABA and GA levels were reversed at 48 h and 72 h after submergence treatment regardless of in both knockout lines and WT (Figure 6). It has previously been shown that the vivipary phenotype in maize kernels due to ABA deficiency can be reversed through inhibition of GA synthesis, demonstrating the role of GA in antagonizing the action of ABA. In this study, this phenomenon was well explained by the expression of genes related to the biosynthesis and metabolism of ABA and GA (Figures S7 and S8). These results suggest that *NAL11* negatively regulates the antagonistic effects of ABA and GA by mediating the activities of a number of enzymes involved in ABA- and GA-related biosynthesis. Thus, we can reasonably infer that the antagonistic regulation of GA and ABA metabolism mainly occurs by activating and repressing the opposing metabolic genes (*NCED/GA2ox or ABA8ox/GA3ox* family) to maintain a hormonal balance during plant growth and development and to respond to environmental cues. Auxin is well known for promoting coleoptile elongation and rapid seedling growth during germination [62], but little is known about its role in rice germination and seedling establishment under submergence. A recent report has also demonstrated that auxin is required for rice seed germination under submergence. The results indicate that auxin availability and transport play a critical role in determining the final coleoptile length in Japonica rice [32]. In submerged seeds, the knockout lines had higher levels of endogenous auxin than WT, which is consistent with the fact that the expression of four auxin biosynthesis genes, *YUCCA2*, *YUCCA3*, *YUCCA6* and *TAA1*, was significantly increased in seedlings of hypoxic knockout lines in comparison to WT (Figure S9), consistent with the observed phenotype (Figure S4) and the previous studies. This suggests that *NAL11* may regulate auxin biosynthesis, enhancing coleoptile elongation under submergence. Whether or not the auxin transport or distribution in hypoxic rice seedlings would be influenced by excessive accumulation of endogenous free IAA and affect the submergence tolerance remains to be investigated.

Finally, ABA plays a dual role in growth regulation, promoting growth at low concentrations and inhibiting it at high concentrations [25,63]. In our study, *NAL11* knockout lines exhibited enhanced ABA sensitivity (Figure 7A,B). This phenomenon was further confirmed by experiments using low concentrations (0.001 μM) of exogenous ABA treatment, which stimulated coleoptile growth. However, when exposed to higher concentrations of exogenous ABA, coleoptile growth was inhibited. When the optimal concentration for plant growth was exceeded, the addition of exogenous ABA led to the inhibition of coleoptile growth in both the knockout lines and the WT when treated with 0.1 μM and 1.0 μM ABA (Figure 7A), in agreement with which is consistent with the previous studies [64]. The increased sensitivity of the knockout lines to exogenous ABA (Figure 7A,B) implies an enhanced responsiveness of these lines to ABA. This enhanced sensitivity was supported by increased expression of ABA signaling genes, including *OsPYL* [1] and *OsbZIP72* [65,66] (Figure S7G–I). These results indicate that *NAL11* may balance ABA signaling and GA biosynthesis to modulate coleoptile elongation and stress responses under submergence.

4. Materials and Methods

4.1. Bioinformatics Analysis of NAL11

The information and sequences of NAL11 homologues were retrieved from the NCBI database (http://www.ncbi.nlm.nih.gov), accessed on 3 November 2023. Utilizing ClustalW with default parameters, multiple sequence alignments were performed on

protein sequences, followed by manual adjustments. Subsequently, a phylogenetic tree was constructed with aligned protein sequences using MEGA (v11.0) software, employing the neighbor-joining (NJ) method. Bootstrap values, derived from 1000 iterations, were calculated to assess the robustness of the tree [67]. For the identification of conserved motifs within protein sequences, online MEME (v5.5.7) (http://meme-suite.org/) was utilized with default parameters. Putative *cis*-acting elements were identified by analyzing the 2000-bp promoter region sequences of these paralogous genes, obtained from the NCBI database, using PlantCARE (http://bioinformatics.psb.ugent.be/webtools/plantcare/html/). TBtools software (v1.120) facilitated the visualization of the phylogenetic tree, conserved motifs, gene structure, domains, and *cis*-acting elements in promoters [68].

4.2. Plant Materials and Growth Conditions

Zhonghua 11 (ZH11) is a japonica rice (*Oryza sativa* L.) variety used as the WT plant and the recipient for genetic transformation in this study. The T_1 and T_2 generation knockout lines were consecutively assayed for the target gene and the hygromycin resistance gene. Two stable T_3-generation knockout lines *(ko-nal11-1* and *ko-nal11-2*) without hygromycin were selected for follow-up studies. All plants were cultivated under natural conditions in the experimental field at South China Agricultural University (Guangzhou, Guangdong, China, 23.13° N, 113.27° E). The WT and knockout lines without hygromycin were planted in a randomized block design. Each plot consisted of six rows with six plants per row at a planting interval of 20 cm × 20 cm. Field management was in accordance with normal agricultural practices.

4.3. Construction of Transgenic Plants

To achieve the knockout lines of *NAL11*, target sites were designed through the online tool Clustered Regularly Interspaced Short Palindromic Repeats (CRISPR)-GE/targetDesign (http://skl.scau.edu.cn/) [69]. Genome-targeting constructs were then prepared using the pRGEB32 vector [70]. The structure of the *NAL11* CRISPR/Cas9 knockout vector is shown in Figure S3A. Pre-cultured Zhonghua 11 (ZH11) seeds were immersed in the Agrobacterium suspension by gently inverting the tube for 1.5 min, then blotted dry with a sterilized filter paper to remove excess bacteria. These seeds were transferred onto a sterilized filter paper (9-cm diameter) that had been moistened with 0.5 mL of AAM medium placed on 2N6-AS medium solidified with 0.4% Gelrite. After 3 days of co-cultivation at 25 °C in the dark, seeds were washed five times in sterile water and then washed once in sterile water containing 500 mg L^{-1} carbenicillin (Wako Pure Chemicals, Osaka, Japan) to remove Agrobacterium. The seeds were rapidly blotted dry on a sterilized filter paper and cultured on N6D medium containing 50 mg L^{-1} hygromycin and 400 mg L^{-1} carbenicillin under continuous light at 32 °C for 2 weeks. Proliferating calli emerging from the scutellum were transferred to RE-III medium. Plantlets emerging from the calli were transferred to HF medium to induce roots. For validation, the target sites of T_1 and T_2 generation plants were sequenced and analyzed using CRISPR-GE/DSDecodeM [71].

To obtain the expression profile of *NAL11*, the 2000 bp promoter sequence was identified from Ensemble Plants (*LOC_Os07g09450*) and amplified from rice genomic DNA. The *pCAMBIA1305* vector was double digested with *SacI* and *BglII* endonucleases, followed by recombination to generate the *pNAL11::GUS* vector. The *pNAL11::GUS* vector was introduced into Agrobacterium tumefaciens strain EHA105, and the transformation procedure described above was used to generate transgenic rice lines. Transgenic plants carrying the *pNAL11::GUS* construct were screened and confirmed by PCR. All primers used in the construction process are detailed in Supplementary Table S1.

4.4. Evaluation of Germination Rate and Coleoptile Length

Seeds of each line were grown in the field, and their seeds were harvested 45 days after heading, air dried, and stored at 42 °C for 7 days to break dormancy. Three independent biological replicates of 30 seeds per replicate were then sterilized with 1.5% (*v*/*v*) sodium

hypochlorite and subsequently incubated in a 9-cm diameter Petri dish. Seeds were considered germinated when the white embryo protrusion was visible, at which point the germination percentage was then calculated. For the anoxic experiments, five seeds were placed in a test tube (diameter: 2.7 cm; height: 11.7 cm) filled with distilled water to simulate anaerobic conditions [72]. All germination experiments were performed in a controlled environment at 28 °C under a 12 h/12 h light/dark cycle. After 4 days, a WinRHIZO root image analysis system (Regent Instruments Inc., Québec, QC, Canada) was used to measure the coleoptile length (CL), coleoptile surface area (CSA), and coleoptile diameter (CD). Three biological replicates were tested.

4.5. Germination Test by Exogenous Application of ABA

A total of 15 seeds of the WT and knockout line (*nal11*) were anaerobically incubated at 28 °C with a gradient concentration of ABA solution as treatment and with pure water as control, respectively. The concentration of the ABA solution was adjusted to 0.001, 0.01, 0.1, 0, 1, and 10 μM, respectively. Photographs were taken and coleoptile lengths were measured after 4 d of incubation.

4.6. Measurement of Endogenous ABA, GA and IAA Levels

To measure the endogenous levels of ABA, GA and IAA, the seeds were prepared at 24, 48 and 72 HAI (hours after imbibition) under anaerobic stress. Liquid nitrogen-frozen germinated seeds (50 mg fresh weight) were ground to powder and extracted with the traction method (methanol/water/formic acid = 15:4:1, *V/V/V*). The extracts were vortexed and centrifuged at 4694× *g* at 4 °C for 10 min. The supernatants were dried by evaporation under the flow of nitrogen gas at room temperature, then dissolved in 200 μL of methanol. The sample extracts were analyzed using an LC-ESI-MS/MS system (HPLC, Shim-pack UFLC SHIMADZU CBM30A system; MS, Applied Biosystems 6500 Triple), and the data were analyzed by Zoonbio Biotechnology Co., Ltd., Nanjing, China. Three replicates of each assay were performed [73].

4.7. Analysis of Physiological Parameters Related to Submergence Stress

Ten seeds each from the WT and knockout lines were anaerobically incubated at 28 °C, respectively. The treatment time was set at 0 h, 12 h, 24 h, 48 h, 72 h and 96 h, respectively, and the analysis of catalase (CAT), superoxide dismutase (SOD), peroxidase (POD) activity and content of malondialdehyde (MDA) and H_2O_2 content was performed as previous described [74] and adjusted. For all assays, the data for each time point represent the average of at least three biological replicates. Calculations were carried out according to the equations recommended by the manufacturer (Nanjing Jiancheng Bioengineering Institute, Nanjing, China).

4.8. RNA Extraction and Analysis of Gene Expression

Total RNA from germinated seeds was extracted using TRIzol reagent (R401-01, Vazyme, Nanjing, China). The first-strand cDNA was synthesized from 600 ng total RNA using a reverse transcription kit (R133-01, Vazyme). The qRT-PCR reaction was performed using ChamQ Universal SYBR qPCR Master Mix (Q711-03, Vazyme) on an ABI Step One Plus Real-Time PCR System (Applied Biosystems, Foster City, CA, USA) [75]. Normalized transcript levels were calculated using the comparative $2^{-\Delta\Delta CT}$ method [76], with the *OsActin* serving as an internal control. Five biological replicates were performed. All primers used for qRT-PCR are listed in Table S1.

The developing seeds of *pNAL11::GUS* transgenic plants were collected and detected according to the previous method [77]. The developing seeds of *pNAL11::GUS* transgenic plants were collected and incubated in GUS staining buffer (750 μg·mL-1 X-gluc, 10 mM EDTA, 3 mM K3Fe(CN)6, 100 mM $NaPO_4$ pH 7, and 0.1% Nonidet-P40) at 37 °C for 6 h. The samples were then transferred to 70% ethanol to remove chlorophyll. Finally, photographs were taken using a ZEISS stereomicroscope.

4.9. Statistical Analysis

Statistical analysis of the data was performed using the Prism 8.3.0 software package. Student's *t*-tests were employed, with statistical significance set at $p < 0.05$. Significant differences between means are indicated by asterisks (* $p < 0.05$, ** $p < 0.01$, *** $p < 0.001$). All data are presented as mean ± standard deviation (SD), with "n" representing the sample size.

5. Conclusions

Bioinformatic analysis reveals that the *NAL11* gene belongs to the family of HSPs containing the DnaJ structural domain. Knockout of *NAL11*, which regulates the expression of genes involved in ABA, GA and auxin biosynthesis, catabolism and signaling pathways, increases the activities of many antioxidant defence enzymes to maintain ROS balance and improve tolerance to submergence stress in rice. Additionally, knockout of *NAL11* significantly increased sugar metabolism and the expression of expansin genes in rice seeds, which promoted the elongation of rice coleoptiles. Taken together, these molecular and physiological changes resulted in improved tolerance to submergence stress in rice. These findings not only deepen our understanding of the function of *NAL11*, but also provide a solid foundation for future research aimed at improving crop tolerance to flooding, potentially leading to more resilient agricultural practices in flood-prone areas.

Supplementary Materials: The following supporting information can be downloaded at: https://www.mdpi.com/article/10.3390/plants13182593/s1, Supplementary Table S1. The primer pairs used in this study. Supplementary Figure S1. Protein domain and gene structure analysis of *NAL11* and 28 homologous genes. Schematic diagram of *NAL11* proteins and 28 homologous proteins functional domai; Structural analysis of *NAL11* and 28 homologous genes based on their own genome annotation file GFF3; Exon–intron structure of the 28 homologous genes, with introns indicated by black lines, exons by yellow wedges, and upstream (5′)/downstream (3′) untranslated regions (UTRs) by green rectangles. Supplementary Figure S2. Promoter prediction analysis of *NAL11* and 28 homologous genes, with introns indicated by black lines, exons by yellow wedges, and upstream (5′)/downstream (3′) untranslated regions (UTRs) by green rectangles. D, Distribution of various cis-elements in the promoters of 28 homologous genes. E, Color-coded patterns corresponding to each motif box. Supplementary Figure S3. (**A**), Schematic of the CRISPR/Cas9 knockout vector cloning of *NAL11*. (**B**), Gene structure diagram of *NAL11*. The UTRs and CDS are indicated by black and orange rectangles, respectively; the black arrows indicate the start (ATG) and stop codon (TGA). The red box indicates the location of the target. The green background fonts indicate the mutation site of *NAL11* in the three mutants. Sequence length is shown below. (**C**), Expression levels of *NAL11* in transgenic lines and wild type. (Data are presented as mean ± SD, n = 3; significant differences were determined by two-tailed Student's *t*-tests. * $p < 0.05$, ** $p < 0.01$, ns, no significance). Supplementary Figure S4. *NAL11* regulates rice seedling emergence under submergence. (**A**), Germination percentage after 4 d under normal conditions. (**B**), Representative images of coleoptile length for both WT and knockout lines after 4 d under aerobic conditions and 4 d under submergence conditions. Scale bars, 1 cm. (**C**–**E**), Average coleoptile length, coleoptile surface, and diameter of WT and knockout lines after 4 d under submergence, respectively. (Data are presented as mean ± SD, $n = 5$; significant differences were determined by two-tailed Student's *t*-tests. * $p < 0.05$, ** $p < 0.01$, *** $p < 0.001$, ns, no significance). Supplementary Figure S5. Analysis of CAT, SOD and POD activity of WT and transgenic plants under normal and submergence conditions. (**A**). CAT activity. (**B**). SOD activity. (**C**). POD activity. (Data are presented as mean ± SD, $n = 5$; significant differences were determined by two-tailed Student's *t*-tests. ** $p < 0.01$, *** $p < 0.001$, ns, no significance). Supplementary Figure S6. Transcript accumulation of stress-related genes in seeds after 48 h of submergence treatment. (**A**). *OsSnRK1A*. (**B**). *OsSUB1A*. (**C**). *OsTPP7*. (**D**). *OsNAC9*. (Data are presented as mean ± SD, $n = 3$; Asterisks indicate significant differences between transgenic lines and WT using *t*-test. *** $p < 0.001$). Supplementary Figure S7. *NAL11* is involved in the ABA signaling pathway. (**A**–**C**) qRT-RCR of ABA biosynthesis-related genes in the WT and knockout lines at 24 h, 48 h, and 72 h after submergence. (**D**–**F**) qRT-RCR of ABA catabolism-related genes in the WT and knockout lines at 24 h, 48 h, and 72 h after submergence. G-I qRT-RCR of ABA signal transduction-related genes in the WT and knockout lines at 24 h, 48 h, and 72 h after submergence. (Data are presented as mean ± SD, $n = 5$; significant

differences were determined by two-tailed Student's *t*-tests. * $p < 0.05$, ** $p < 0.01$, *** $p < 0.001$, ns, no significance). Supplementary Figure S8. *NAL11* is involved in the GA signaling pathway. (**A**–**E**) qRT-RCR of GA biosynthesis-related genes in the WT and knockout lines at 24 h, 48 h, and 72 h after submergence. (**F**–**H**) qRT-RCR of GA catabolism-related genes in the WT and knockout lines at 24 h, 48 h, and 72 h after submergence. (Data are presented as mean ± SD, $n = 5$; significant differences were determined by two-tailed Student's *t*-tests. * $p < 0.05$, ** $p < 0.01$, *** $p < 0.001$, ns, no significance). Supplementary Figure S9. *NAL11* is involved in the auxin signaling pathway. (**A**–**E**) qRT-RCR of auxin biosynthesis-related genes in the WT and knockout lines at 24 h, 48 h, and 72 h after submergence. (Data are presented as mean ± SD, $n = 5$; significant differences were determined by two-tailed Student's *t*-tests. * $p < 0.05$, ** $p < 0.01$, *** $p < 0.001$, ns, no significance).

Author Contributions: W.X. and T.G. raised the project conception and designed the research. Z.Z. and Y.X. carried out most of the experiments and analyzed data. Z.Z. and Y.X. wrote, the manuscript. W.X. and T.G. provided laboratory support. Z.Z., M.T., C.C., J.Z. and J.L. analyzed the data. All authors have read and agreed to the published version of the manuscript.

Funding: This work was supported by the Natural Science Foundation of China (Grant no. 31872885), the Guangdong Basic and Applied Basic Research Foundation (Grant no. 2021A1515010410), and the Seed Industry Revitalization Project of Guangdong Provincial Rural Revitalization Strategy Special Fund (2022-NPY-00-016).

Data Availability Statement: All of the datasets are included within the article and its additional files.

Conflicts of Interest: The authors declare no conflicts of interest.

References

1. Long, L.; Qiu, S.; Man, J.; Ren, D.; Xu, N.; Luo, R. *OsAAI1* increases rice yield and drought tolerance dependent on ABA-mediated regulatory and ROS scavenging pathway. *Rice* **2023**, *16*, 35. [CrossRef] [PubMed]
2. Kretzschmar, T.; Pelayo, M.A.F.; Trijatmiko, K.R.; Gabunada, L.; Alam, R.; Jimenez, R.; Mendioro, M.S.; Slamet-Loedin, I.H.; Sreenivasulu, N.; Bailey-Serres, J.; et al. A trehalose-6-phosphate phosphatase enhances anaerobic germination tolerance in rice. *Nat. Plants* **2015**, *1*, 1–5. [CrossRef] [PubMed]
3. Sun, J.; Zhang, G.; Cui, Z.; Kong, X.; Yu, X.; Gui, R.; Han, Y.; Li, Z.; Lang, H.; Hua, Y.; et al. Regain flood adaptation in rice through a 14-3-3 protein OsGF14h. *Nat. Commun.* **2022**, *13*, 5664. [CrossRef] [PubMed]
4. Perata, P.; Alpi, A. Plant responses to anaerobiosis. *Plant. Sci.* **1993**, *93*, 1–17. [CrossRef]
5. Bailey-Serres, J.; Voesenek, L. Flooding Stress: Acclimations and genetic diversity. *Annu. Rev. Plant Biol.* **2008**, *59*, 313–339. [CrossRef]
6. Yang, J.; Guo, Z.; Luo, L.; Gao, Q.; Xiao, W.; Wang, J.; Wang, H.; Chen, Z.; Guo, T. Identification of QTL and candidate genes involved in early seedling growth in rice via high-density genetic mapping and RNA-seq. *Crop J.* **2021**, *9*, 360–371. [CrossRef]
7. Bailey-Serres, J.; Lee, S.C.; Brinton, E. Waterproofing crops: Effective flooding survival strategies. *Plant Physiol.* **2012**, *160*, 1698–1709. [CrossRef]
8. Pucciariello, C. Molecular mechanisms supporting rice germination and coleoptile elongation under low oxygen. *Plants* **2020**, *9*, 1037. [CrossRef]
9. Zhan, J.; Lu, X.; Liu, H.; Zhao, Q.; Ye, G. Mesocotyl elongation, an essential trait for dry-seeded rice (*Oryza sativa L.*): A review of physiological and genetic basis. *Planta* **2019**, *251*, 27. [CrossRef]
10. Choi, D.; Lee, Y.; Cho, H.; Kende, H. Regulation of expansin gene expression affects growth and development in transgenic rice plants. *Plant Cell* **2003**, *15*, 1386–1398. [CrossRef]
11. Lasanthi-Kudahettige, R.; Magneschi, L.; Loreti, E.; Gonzali, S.; Licausi, F.; Novi, G.; Beretta, O.; Vitulli, F.; Alpi, A.; Perata, P. Transcript profiling of the anoxic rice coleoptile. *Plant Physiol.* **2007**, *144*, 218–231. [CrossRef] [PubMed]
12. Loreti, E.; Yamaguchi, J.; Alpi, A.; Perata, P. Sugar modulation of α-amylase genes under anoxia. *Ann. Bot.* **2003**, *91*, 143–148. [CrossRef] [PubMed]
13. Perata, P.; Geshi, N.; Yamaguchi, J.; Akazawa, T. Effet of anoxia on the induction of α-amylase in cereal seeds. *Planta* **1993**, *191*, 402–408. [CrossRef]
14. Kato-Noguchi, H.; Kugimiya, T. Preferential induction of alcohol dehydrogenase in coleoptiles of rice seedlings germinated in submergence condition. *Biol. Plant.* **2003**, *46*, 153–155. [CrossRef]
15. Li, X.; Chen, L.; Forde, B.G.; Davies, W.J. The biphasic root growth response to abscisic acid in Arabidopsis involves interaction with ethylene and auxin signaling pathways. *Front. Plant. Sci.* **2017**, *8*, 1493.
16. Lee, K.; Chen, P.; Lu, C.; Chen, S.; Ho, T.D.; Yu, S. Coordinated responses to oxygen and sugar deficiency allow rice seedlings to tolerate flooding. *Sci. Signal.* **2009**, *2*, ra61. [CrossRef]

17. Takahashi, H.; Saika, H.; Matsumura, H.; Nagamura, Y.; Tsutsumi, N.; Nishizawa, N.K.; Nakazono, M. Cell division and cell elongation in the coleoptile of rice alcohol dehydrogenase 1-deficient mutant are reduced under complete submergence. *Ann. Bot.* **2011**, *108*, 253–261. [CrossRef]
18. Mittler, R.; Vanderauwera, S.; Gollery, M.; Van Breusegem, F. Reactive oxygen gene network of plants. *Trends Plant Sci.* **2004**, *9*, 490–498. [CrossRef]
19. Apel, K.; Hirt, H. Reactive oxygen species: Metabolism, oxidative stress, and signal transduction. *Annu. Rev. Plant Biol.* **2004**, *55*, 373–399. [CrossRef]
20. Xu, N.; Chu, Y.; Chen, H.; Li, X.; Wu, Q.; Jin, L.; Wang, G.; Huang, J. Rice transcription factor *OsMADS25* modulates root growth and confers salinity tolerance via the ABA-mediated regulatory pathway and ROS scavenging. *PLoS. Genet.* **2018**, *14*, e1007662. [CrossRef]
21. Brookbank, B.P.; Patel, J.; Gazzarrini, S.; Nambara, E. Role of basal ABA in plant growth and development. *Genes* **2021**, *12*, 1936. [CrossRef] [PubMed]
22. Zhang, S.; Cai, Z.; Wang, X. The primary signaling outputs of brassinosteroids are regulated by abscisic acid signaling. *Proc. Natl. Acad. Sci. USA* **2009**, *106*, 4543–4548. [CrossRef] [PubMed]
23. Gao, Q.; Liu, J.; Weng, H.; Yuan, X.; Xiao, W.; Wang, H. A long noncoding RNA derived from lncRNA-mRNA networks modulates eeed vigor. *Int. J. Mol. Sci.* **2022**, *23*, 9472. [CrossRef]
24. Li, W.; Zhu, Z.; Chern, M.; Yin, J.; Yang, C.; Ran, L.; Cheng, M.; He, M.; Wang, K.; Wang, J.; et al. A natural allele of a transcription factor in rice confers broad-spectrum blast resistance. *Cell* **2017**, *170*, 114–126. [CrossRef] [PubMed]
25. Chen, Q.; Wang, W.; Zhang, Y.; Zhan, Q.; Liu, K.; Botella, J.; Bai, L.; Song, C. Abscisic acid-induced cytoplasmic translocation of constitutive photomorphogenic 1 enhances reactive oxygen species accumulation through the HY5-ABI5 pathway to modulate seed germination. *Plant Cell Environ.* **2022**, *45*, 1474–1489. [CrossRef] [PubMed]
26. Chen, Y.; Li, Z.; Sun, T.; Wang, D.; Wang, Z.; Zhang, C.; Que, Y.; Guo, J.; Xu, L.; Su, Y. Sugarcane *ScDREB2B-1* l Nicotiana benthamiana by regulating the ABA signal, ROS level and stress-related gene expression. *Int. J. Mol. Sci.* **2022**, *23*, 9557. [CrossRef]
27. Postiglione, A.; Muday, G. The Role of ROS Homeostasis in ABA-Induced Guard Cell Signaling. *Front Plant Sci.* **2020**, *11*, 968. [CrossRef] [PubMed]
28. Santosh, K.V.; Yadav, S.K.; Verma, R.K.; Shrivastava, S.; Ghimire, O.; Pushkar, S.; Rao, M.V.; Senthil, K.T.; Chinnusamy, V. The abscisic acid receptor OsPYL6 confers drought tolerance to indica rice through dehydration avoidance and tolerance mechanisms. *J. Exp. Bot.* **2021**, *72*, 1411–1431. [CrossRef]
29. Kurup, S.; Jones, H.D.; Holdsworth, M.J. Interactions of the developmental regulator ABI3 with proteins identied from developing arabidopsis seeds. *Plant J.* **2000**, *21*, 143–155. [CrossRef]
30. Khan, N.A.; Nazar, R.; Iqbal, N.; Anjum, N.A. *Phytohormones and Abiotic Stress Tolerance in Plants*; Anjum, N.A., Ed.; Springer Science & Business Media: Berlin/Heidelberg, Germany, 2012.
31. Gallei, M.; Luschnig, C.; Friml, J. Auxin signaling in growth: Schrödinger's cat out of the bag. *Curr. Opin. Plant Biol.* **2020**, *53*, 43–49. [CrossRef]
32. Nghi, K.; Tagliani, A.; Mariotti, L.; Weits, D.; Perata, P.; Pucciariello, C. Auxin is required for the long coleoptile trait in japonica rice under submergence. *New Phytol.* **2021**, *229*, 85–93. [CrossRef] [PubMed]
33. Wang, W.; Vinocur, B.; Shoseyov, O.; Altman, A. Role of plant heat-shock proteins and molecular chaperones in the abiotic stress response. *Trends Plant Sci.* **2004**, *9*, 244–252. [CrossRef] [PubMed]
34. Murakami, T.; Matsuba, S.; Funatsuki, H.; Kawaguchi, K.; Saruyama, H.; Tanida, M.; Sato, Y. Over-expression of a small heat shock protein, sHSP17.7, confers both heat tolerance and UV-B resistance to rice plants. *Mol. Breed.* **2004**, *13*, 165–175. [CrossRef]
35. Zhao, H.; Jan, A.; Ohama, N.; Kidokoro, S.; Soma, F.; Koizumi, S.; Mogami, J.; Todaka, D.; Mizoi, J.; Shinozaki, K. Cytosolic *HSC70s* repress heat stress tolerance and enhance seed germination under salt stress conditions. *Plant Cell Environ.* **2021**, *44*, 1788–1801. [CrossRef] [PubMed]
36. Krishna, P.; Gloor, G. The Hsp90 family of proteins in Arabidopsis thaliana. *Cell Stress Chaperones* **2001**, *6*, 238–246. [CrossRef]
37. Chang, J.; Knowlton, A.A.; Wasser, J.S. Expression of heat shock proteins in turtle and mammal hearts: Relationship to anoxia tolerance. *Am. J. Physiol.-Regul. Integr. Comp. Physiol.* **2000**, *278*, R209–R214. [CrossRef]
38. Luo, L.; Xie, Y.; Yu, S.; Yang, J.; Chen, S.; Yuan, X.; Guo, T.; Wang, H.; Liu, Y.; Chen, C.; et al. The DnaJ domain-containing heat-shock protein NAL11 determines plant architecture by mediating gibberellin homeostasis in rice (*Oryza sativa*). *New Phytol.* **2023**, *237*, 2163–2179. [CrossRef]
39. Magneschi, L.; Kudahettige, R.L.; Alpi, A.; Perata, P. Expansin gene expression and anoxic coleoptile elongation in rice cultivars. *J. Plant Physiol.* **2009**, *166*, 1576–1580. [CrossRef]
40. Asatsuma, S.; Sawada, C.; Itoh, K.; Okito, M.; Kitajima, A.; Mitsui, T. Involvement of α-Amylase I-1 in starch degradation in rice chloroplasts. *Plant Cell Physiol.* **2005**, *46*, 858–869. [CrossRef]
41. Hwang, Y.; Thomas, B.; Rodriguez, R. Differential expression of rice α-amylase genes during seedling development under anoxia. *Plant Mol. Biol.* **1999**, *40*, 911–920. [CrossRef]
42. Jackson, M.B.; Ram, P.C. Physiological and molecular basis of susceptibility and tolerance of rice plants to complete submergence. *Ann. Bot.* **2003**, *91*, 227–241. [CrossRef] [PubMed]
43. Hu, C.; Wang, P.; Zhang, P.; Nie, X.; Li, B.; Tai, L.; Liu, W.; Li, W.; Chen, M. NADPH oxidases: The vital performers and center hubs during plant growth and signaling. *Cells* **2020**, *9*, 437. [CrossRef] [PubMed]

44. Hewage, K.A.; Yang, J.; Wang, D.; Hao, G.; Yang, G.; Zhu, J. Chemical manipulation of abscisic acid signaling: A new approach to abiotic and biotic stress management in agriculture. *Adv. Sci.* **2020**, *7*, 2001265. [CrossRef] [PubMed]
45. Ye, N.; Zhu, G.; Liu, Y.; Zhang, A.; Li, Y.; Liu, R.; Shi, L.; Jia, L.; Zhang, J. Ascorbic acid and reactive oxygen species are involved in the inhibition of seed germination by abscisic acid in rice seeds. *J. Exp. Bot.* **2012**, *63*, 1809–1822. [CrossRef] [PubMed]
46. Mittler, R.; Vanderauwera, S.; Suzuki, N.; Miller, G.; Tognetti, V.B.; Vandepoele, K.; Gollery, M.; Shulaev, V.; Van Breusegem, F. ROS signaling: The new wave? *Trends Plant Sci.* **2011**, *16*, 300–309. [CrossRef] [PubMed]
47. Fang, Y.; Liao, K.; Du, H.; Xu, Y.; Song, H.; Li, X.; Xiong, L. A stress-responsive NAC transcription factor *SNAC3* confers heat and drought tolerance through modulation of reactive oxygen species in rice. *J. Exp. Bot.* **2015**, *66*, 6803–6817. [CrossRef] [PubMed]
48. Ning, J.; Li, X.; Hicks, L.M.; Xiong, L. A Raf-like MAPKKK gene DSM1 mediates drought resistance through reactive oxygen species scavenging in rice. *Plant Physiol.* **2010**, *152*, 876–890. [CrossRef] [PubMed]
49. Panda, D.; Mishra, S.; Behera, P.K. Drought tolerance in rice: Focus on recent mechanisms and approaches. *Rice Sci.* **2021**, *28*, 119–132. [CrossRef]
50. Aleem, M.; Aleem, S.; Sharif, I.; Wu, Z.; Aleem, M.; Tahir, A.; Atif, R.M.; Cheema, H.M.; Shakeel, A.; Lei, S.; et al. Characterization of *SOD* and *GPX* gene families in the Soybeans in response to drought and salinity stresses. *Antioxidants* **2022**, *11*, 460. [CrossRef]
51. Gill, S.; Tuteja, N. Reactive oxygen species and antioxidant machinery in abiotic stress tolerance in crop plants. *Plant Physiol. Biochem.* **2010**, *8*, 909–930. [CrossRef]
52. Hnilickova, H.; Kraus, K.; Vachova, P.; Hnilicka, F. Salinity stress affects photosynthesis, malondialdehyde formation, and proline content in *Portulaca oleracea* L. *Plants* **2021**, *10*, 845. [CrossRef] [PubMed]
53. Miro, B.; Ismail, A. Tolerance of anaerobic conditions caused by flooding during germination and early growth in rice (*Oryza sativa* L.). *Front. Plant Sci.* **2013**, *4*, 269. [CrossRef]
54. Perata, P.; Guglielminetti, L.; Alpi, A. Mobilization of endosperm reserves in cereal seeds under anoxia. *Ann. Bot.* **1997**, *79*, 49–56. [CrossRef]
55. Banti, V.; Loreti, E.; Novi, G.; Santaniello, A.; Alpi, A.; Perata, P. Heat acclimation and cross-tolerance against anoxia in Arabidopsis. *Plant Cell Environ.* **2008**, *31*, 1029–1037. [CrossRef] [PubMed]
56. Lu, C.; Lim, E.; Yu, S. Sugar response sequence in the promoter of a rice α-amylase gene serves as a transcriptional enhancer. *J. Biol. Chem.* **1998**, *273*, 10120–10131. [CrossRef] [PubMed]
57. Ismail, A.M.; Ella, E.S.; Vergara, G.V.; Mackill, D.J. Mechanisms associated with tolerance to flooding during germination and early seedling growth in rice (*Oryza sativa* L.). *Ann. Bot.* **2008**, *103*, 197–209. [CrossRef]
58. Gibbs, J.; Morrell, S.; Valdez, A.; Setter, T.; Greenway, H. Regulation of alcoholic fermentation in coleoptiles of two rice cultivars differing in tolerance to anoxia. *J. Exp. Bot.* **2000**, *51*, 785–796. [CrossRef]
59. Quimio, C.A.; Torrizo, L.B.; Setter, T.L.; Ellis, M.; Grover, A.; Abrigo, E.M.; Oliva, N.P.; Ella, E.S.; Carpena, A.L.; Ito, O.; et al. Enhancement of submergence tolerance in transgenic rice overproducing Pyruvate decarboxylase. *J. Plant. Physiol.* **2000**, *156*, 516–521. [CrossRef]
60. Singh, P.; Sinha, A.K. A positive feedback loop governed by SUB1A1 interaction with MITOGEN-ACTIVATED PROTEIN KINASE3 imparts submergence tolerance in rice. *Plant Cell.* **2016**, *28*, 1127–1143. [CrossRef]
61. Liu, G.; Li, X.; Jin, S.; Liu, X.; Zhu, L.; Nie, Y.; Zhang, X. Overexpression of rice NAC gene *SNAC1* improves drought and salt tolerance by enhancing root development and reducing transpiration rate in transgenic cotton. *PLoS ONE* **2014**, *9*, e86895. [CrossRef]
62. Lee, K.; Chen, J.; Wu, C.; Chang, H.; Chen, H.; Kuo, H.; Lee, Y.; Chang, Y.; Chang, H.; Shiue, S.; et al. Auxin plays a role in the adaptation of rice to anaerobic germination and seedling establishment. *Plant Cell Environ.* **2023**, *46*, 1157–1175. [CrossRef] [PubMed]
63. Miao, R.; Yuan, W.; Wang, Y.; Garcia-Maquilon, I.; Dang, X.; Li, Y.; Zhang, J.; Zhu, Y.; Rodriguez, P.L.; Xu, W. Low ABA concentration promotes root growth and hydrotropism through relief of ABA INSENSITIVE 1-mediated inhibition of plasma membrane H^+-ATPase 2. *Sci. Adv.* **2021**, *7*, eabd4113. [CrossRef] [PubMed]
64. Jiang, D.; Zhou, L.; Chen, W.; Ye, N.; Xia, J.; Zhuang, C. Overexpression of a microRNA-targeted NAC transcription factor improves drought and salt tolerance in Rice via ABA-mediated pathways. *Rice* **2019**, *12*, 76. [CrossRef] [PubMed]
65. Wang, Y.; Hou, Y.; Qiu, J.; Wang, H.; Wang, S.; Tang, L.; Tong, X.; Zhang, J. Abscisic acid promotes jasmonic acid biosynthesis via a 'SAPK10-bZIP72-AOC' pathway to synergistically inhibit seed germination in rice (*Oryza sativa*). *New. Phytol.* **2020**, *228*, 1336–1353. [CrossRef] [PubMed]
66. Wang, S.; Liu, W.; He, Y.; Adegoke, T.; Ying, J.; Tong, X.; Li, Z.; Tang, L.; Wang, H.; Zhang, J.; et al. *bZIP72* promotes submerged rice seed germination and coleoptile elongation by activating *ADH1*. *Plant Physiol. Biochem.* **2021**, *169*, 112–118. [CrossRef] [PubMed]
67. Tamura, K.; Stecher, G.; Kumar, S. MEGA11: Molecular evolutionary genetics analysis version 11. *Mol. Biol. Evol.* **2021**, *38*, 3022–3027. [CrossRef]
68. Chen, C.; Wu, Y.; Li, J.; Wang, X.; Zeng, Z.; Xu, J.; Liu, Y.; Feng, J.; Chen, H.; He, Y.; et al. TBtools-II: A "one for all, all for one" bioinformatics platform for biological big-data mining. *Mol. Plant.* **2023**, *16*, 1733–1742. [CrossRef]
69. Xie, X.; Ma, X.; Zhu, Q.; Zeng, D.; Li, G.; Liu, Y. CRISPR-GE: A convenient software toolkit for CRISPR-based genome editing. *Mol. Plant* **2017**, *10*, 1246–1249. [CrossRef] [PubMed]

70. Zhao, Z.; Yin, X.; Li, S.; Peng, Y.; Yan, X.; Chen, C.; Hassan, B.; Zhou, S.; Pu, M.; Zhao, J.; et al. miR167d-ARFs module regulates flower opening and stigma size in rice. *Rice* **2022**, *15*, 40. [CrossRef]
71. Liu, W.; Xie, X.; Ma, X.; Li, J.; Chen, J.; Liu, Y. DSDecode: A web-based tool for decoding of sequencing chromatograms for genotyping of targeted mutations. *Mol. Plant* **2015**, *8*, 1431–1433. [CrossRef]
72. Su, L.; Yang, J.; Li, D.; Peng, Z.; Yang, M.; Luo, L.; Huang, C.; Wang, J.; Wang, H.; Chen, Z.; et al. Dynamic genome-wide association analysis and identification of candidate genes involved in anaerobic germination tolerance in rice. *Rice* **2021**, *14*, 1. [CrossRef] [PubMed]
73. Ma, X.; Ma, J.; Zhai, H.; Xin, P.; Chu, J.; Qiao, Y.; Han, L. CHR729 is a CHD3 protein that controls seedling development in rice. *PLoS ONE* **2015**, *10*, e0138934. [CrossRef]
74. Peng, X.; Luo, L.; Cui, H.; Wang, H.; Guo, T.; Liu, Y.; Wang, J.; Huang, M.; Yang, G.; Chen, Z.; et al. Characterization and fine mapping of a leaf wilt mutant, m3, induced by heavy ion irradiation of rice. *Crop Sci.* **2019**, *59*, 2679–2688. [CrossRef]
75. Chen, T.; Luo, L.; Zhao, Z.; Wang, H.; Chen, C.; Liu, Y.; Li, X.; Guo, T.; Xiao, W. Fine mapping and candidate gene analysis of *qGL10* affecting rice grain length. *Crop J.* **2023**, *11*, 540–548. [CrossRef]
76. Schmittgen, T.D.; Livak, K.J. Analyzing real-time PCR data by the comparative CT method. *Nat. Protoc.* **2008**, *3*, 1101–1108. [CrossRef] [PubMed]
77. Huang, L.; Hua, K.; Xu, R.; Zeng, D.; Wang, R.; Dong, G.; Zhang, G.; Lu, X.; Fang, N.; Wang, D.; et al. The LARGE2-APO1/APO2 regulatory module controls panicle size and grain number in rice. *Plant Cell* **2021**, *33*, 1212–1228. [CrossRef]

plants

MDPI

Article

The Physiological and Molecular Mechanisms of Exogenous Melatonin Promote the Seed Germination of Maize (*Zea mays* L.) under Salt Stress

Jiajie Wang [1,†], Di Yan [1,†], Rui Liu [1], Ting Wang [1], Yijia Lian [1], Zhenzong Lu [1], Yue Hong [1], Ye Wang [1,2] and Runzhi Li [1,2,*]

[1] College of Plant Science and Technology, Beijing University of Agriculture, Beijing 102206, China; jiajie.wang@bua.edu.cn (J.W.); di.yan@bua.edu.cn (D.Y.); rui.liu@bua.edu.cn (R.L.); ting.wang@bua.edu.cn (T.W.); yijia.lian@bua.edu.cn (Y.L.); zhenzong.lu@bua.edu.cn (Z.L.); yue.hong@bua.edu.cn (Y.H.); ye.wang@bua.edu.cn (Y.W.)

[2] Beijing Key Laboratory for Agricultural Application and New Technique, Beijing 102206, China

* Correspondence: lirunzhi7639@163.com

† These authors contributed equally to this work.

Abstract: Salt stress caused by high concentrations of Na^+ and Cl^- in soil is one of the most important abiotic stresses in agricultural production, which seriously affects grain yield. The alleviation of salt stress through the application of exogenous substances is important for grain production. Melatonin (MT, N-acetyl-5-methoxytryptamine) is an indole-like small molecule that can effectively alleviate the damage caused by adversity stress on crops. Current studies have mainly focused on the effects of MT on the physiology and biochemistry of crops at the seedling stage, with fewer studies on the gene regulatory mechanisms of crops at the germination stage. The aim of this study was to explain the mechanism of MT-induced salt tolerance at physiological, biochemical, and molecular levels and to provide a theoretical basis for the resolution of MT-mediated regulatory mechanisms of plant adaptation to salt stress. In this study, we investigated the germination, physiology, and transcript levels of maize seeds, analyzed the relevant differentially expressed genes (DEGs), and examined salt tolerance-related pathways. The results showed that MT could increase the seed germination rate by 14.28–19.04%, improve seed antioxidant enzyme activities (average increase of 11.61%), and reduce reactive oxygen species accumulation and membrane oxidative damage. In addition, MT was involved in regulating the changes of endogenous hormones during the germination of maize seeds under salt stress. Transcriptome results showed that MT affected the activity of antioxidant enzymes, response to stress, and seed germination-related genes in maize seeds under salt stress and regulated the expression of genes related to starch and sucrose metabolism and phytohormone signal transduction pathways. Taken together, the results indicate that exogenous MT can affect the expression of stress response-related genes in salt-stressed maize seeds, enhance the antioxidant capacity of the seeds, reduce the damage induced by salt stress, and thus promote the germination of maize seeds under salt stress. The results provide a theoretical basis for the MT-mediated regulatory mechanism of plant adaptation to salt stress and screen potential candidate genes for molecular breeding of salt-tolerant maize.

Keywords: maize; melatonin; salt stress; seed germination; transcriptome analysis

1. Introduction

With the continuous deterioration of the global ecological environment and the emergence of extreme climate, countries around the world are facing an increasingly severe food security crisis [1]. Rising global temperatures and increased evaporation rates of water from the surface layer of arable land lead to salt accumulation, aggravating salinization of arable land, which inhibits seed germination and leads to crop growth inhibition, and

reduced survival and yield [2–4]. In addition, salt stress induces other secondary stresses in crops, such as ionic toxicity, osmotic stress, and oxidative stress, disrupting intracellular environmental homeostasis and even leading to cell death [5–10].

To adapt to high-salt environments, plants need to maintain their ion homeostasis. Ion transporter proteins (e.g., Na^+ and K^+ transporter proteins), which control the input and output of ions, are the first line of defense in the cytoplasmic membrane. The Salt Overly Sensitive (SOS) pathway, discovered and characterized by Zhu's team, is an important component of the stress signaling pathway that regulates ion homeostasis and salt tolerance in plants [11,12]. Meanwhile, plants have evolved many mechanisms to sense and adapt to osmotic stress, including perception and transduction of osmotic stress signals, phytohormone-related regulation and response, intracellular synthesis, and metabolism of osmotic substances [13–19]. When oxidative stress induces the production of large amounts of reactive oxygen species (ROS), plants increase the activity of their antioxidant enzymes (such as superoxide dismutase, catalase and peroxidase) to effectively improve the ability to scavenge ROS, reduce plasma membrane damage, and improve tolerance to abiotic stress, including drought, high temperature, salinity, and cold [1,20,21]. Pesticides, as plant protectants, can cause pesticide toxicity when used in excess or inappropriately, and the antioxidant enzyme system is effective in scavenging the accumulation of ROS caused by pesticide toxicity [22].

The use of exogenous hormones to improve plant stress resistance under abiotic stress is one of the most used tools today. MT is an indole-like small molecule that is considered a novel phytohormone. Although this view is still controversial, MT has been found to have many biological functions and plays an important role in plant growth and development and stress response processes [23–29]. The ability of MT to alleviate growth retardation caused by salt stress and to promote seed germination and plant root development was confirmed by applying MT to soybean, wheat, maize, and rice crops [30–33]. MT can directly and effectively scavenge ROS and reactive nitrogen species (RNS), as well as other free radicals and harmful oxidative molecules, and act as a signaling molecule to enhance the activity of antioxidant enzymes, including superoxide dismutase (SOD), catalase (CAT), and peroxidase (POD) [2,34–37]. In addition, MT regulates the expression of the *Arabidopsis* K^+ transporter protein gene (*AKT1*) and Na^+/H^+ reverse transporter protein gene (*NHX1*) to maintain ion homeostasis and mitigate plant damage from salt stress [38,39]. MT is involved in multiple signaling pathways and interacts with several phytohormones to regulate plant growth and improve stress tolerance. MT has been reported to interact with abscisic acid (ABA) and gibberellin (GA) to affect the biosynthesis and catabolism of ABA and GA, disrupt ABA/GAs, and promote seed germination under salt stress [30,36,40]. MT activates the MAPK cascade and enhances tolerance to salt stress and immunity to pathogens in *Arabidopsis* [41], tobacco [42], Bermuda grass, and other plants [43]. Exogenous MT upregulates the expression of key genes in the GA synthesis pathway, such as $GA_{20}ox$ and GA_3ox, leading to an increase in GA content, and regulates the crop response to GA by modulating DALLE proteins in the GA signaling pathway under salt stress [30,36]. However, most of the current studies on MT are at the physiological level, and the molecular mechanism of its action is still not clearly resolved.

Maize (*Zea mays* L.) is one of the most important and widely grown crops in the world. In addition to being a grain, maize is an important source of feed and industrial raw materials with high economic value [44]. At the same time, maize cultivation is being threatened by a variety of environmental problems, such as high and low temperatures, drought, salinity, and flooding. Therefore, how to improve the stress tolerance of maize seeds has become a research priority. Despite several studies on MT in crop stress tolerance, the molecular mechanisms during maize seed germination after MT application under salt stress are still unclear. In this study, we investigated the germination indexes, physiological indexes, endogenous hormone contents, and transcript levels of maize seeds at different germination stages under salt stress to gain insights into the exogenous MT-mediated

physiological mechanisms and gene regulatory networks of maize seed germination stages in response to salt stress.

2. Results

2.1. Effect of Exogenous MT on Emergence Traits of Maize under Salt Stress

As shown in Figure 1A, the seed germination rate was significantly decreased under NaCl stress of 150 mM compared with the control, and 150 mM NaCl was selected as the salt stress concentration for this experiment, in combination with the sampling needs of the subsequent experiments. Pretreatment with MT significantly increased the germination rate of maize seeds by 7.07–33.33% under NaCl stress conditions, with SM50 treatment having the most significant effect (Figure 1C). In addition, the radicle protrusion rate was promoted by 44.98–59.97% under MT treatment compared to salt stress (Figure 1B). Combined with its radicle protrusion rate, the results showed that MT was able to significantly increase the seed germination rate and alleviate the growth and developmental retardation induced by salt stress (Figure 1B,C). Both radicle length and germination length are important indicators of seed germination. Salt stress inhibits the development of seed radicle and germination (decreased by 60.29% and 89.86%, respectively), but the application of MT alleviated this developmental retardation caused by salt stress (29.24–46.84% and 119.58–155.19% increases, respectively, compared to S treatment) (Figure 1D,E). Notably, MT promoted the development of the secondary radicle of maize seeds under salt stress. The percentage of germinated seeds that developed secondary radicles increased by an average of 38.73% after MT treatment compared to group S (Figure 1F). These results are consistent with observations on seed phenotypes (Figure S1), suggesting that MT is effective in promoting growth and development during seed germination.

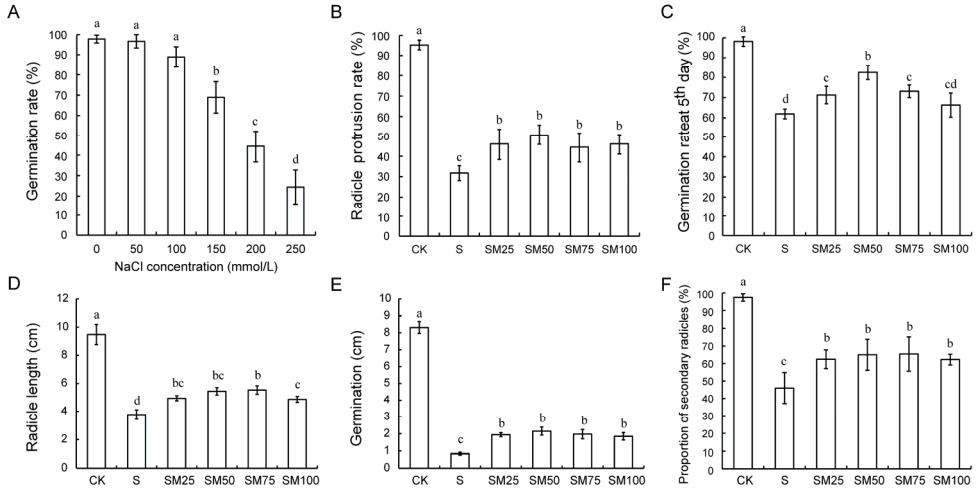

Figure 1. The germination effect of 150 mM NaCl on maize seeds. (**A**) Germination rate of maize seeds at different NaCl concentrations; (**B**) rate of radicle breakthrough of seed coat at the 36th hour; (**C**) germination rate at 5th day; (**D**) radicle length; (**E**) germination length; (**F**) proportion of secondary radicle occurrence. Different letters indicate statistically significant differences (ANOVA with LSD Fisher's multiple comparison test, $p < 0.05$).

2.2. Effect of MT on Oxidative Damage and Osmoregulation in Seeds

Under salt stress induction, ROS content and MDA, a product of oxidative damage to membrane plasma, were significantly higher in maize seeds compared with CK. In contrast, O_2^-, H_2O_2, and MDA contents were significantly reduced after pretreatment with MT (Figure 2A–C).

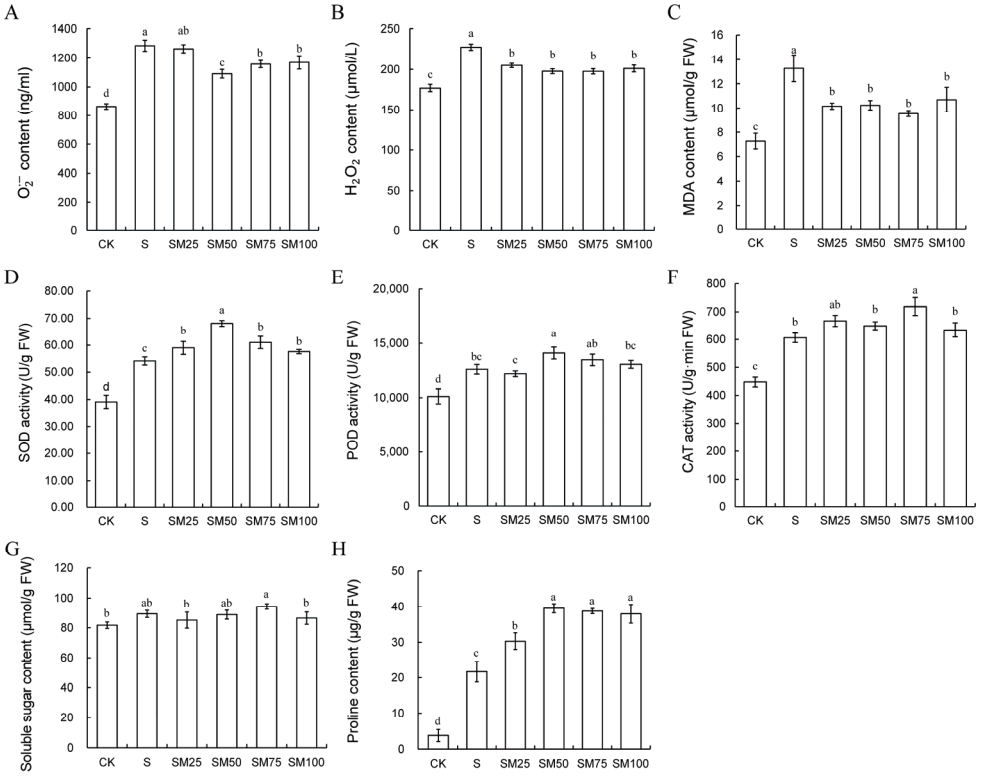

Figure 2. Effect of MT on physiological traits during germination of maize seeds. (**A**) O_2^- content; (**B**) H_2O_2 content; (**C**) MDA content; (**D**) SOD activity; (**E**) POD activity; (**F**) CAT activity; (**G**) soluble sugar content; and (**H**) proline content. Different letters indicate statistically significant differences (ANOVA with LSD Fisher's multiple comparison test, $p < 0.05$).

ROS stimulated the plants to increase antioxidant enzyme activities, in which SOD activity was elevated by 38.52%, POD and CAT activities by 24.48% and 35.47%, respectively, in the S group compared to the CK group (Figure 2D–F). However, the antioxidant enzyme activities of maize seeds were significantly higher under SM treatment than S treatment. The SOD and POD activities of maize seeds reached their maximum at SM50 treatment, which increased by 25.9% and 11.88%, respectively, compared with S group (Figure 2D,E). And among all SM groups, only the SM75 group significantly increased CAT activity by 18.56% relative to S group (Figure 2F).

The content of soluble sugars showed that salt stress, as well as MT treatment, had little effect on the content of soluble sugars in maize seeds (Figure 2G). This may be caused by the fact that at this time the seeds were in the period of germination and the nutrients in the endosperm were being converted into soluble sugars. However, the determination of proline content showed that salt stress caused a large accumulation of proline in maize seeds (473.26% increase compared with the CK group), and MT pretreatment further significantly increased the proline content under salt stress, where SM50 increased by 82.44% (Figure 2H).

Considering the results of seed germination, ROS content, and the activities of various antioxidant enzymes, the MT concentration of 50 μM was finally selected as the optimal concentration for subsequent experimental analyses.

2.3. Effect of MT on Endogenous Hormone Levels

To investigate the mechanism of the MT-induced germination of maize seeds under salt stress, we measured the contents of several phytohormones at three stages: seed imbibition (19 h), radicle protrusion (36 h), and germination (60 h). Under normal conditions, the contents of all four phytohormones, GA_3, ABA, IAA, and JA, increased during seed germination (Figure 3). Compared with CK, under salt stress conditions, the contents of

JA and ABA were significantly increased at all three germination stages, with increases of 15.75–20.15% and 34.39–73.82%, respectively (Figure 3A,C). The contents of GA_3 and IAA increased by 26.07% at 19 h and 29.73% at 36 h and decreased by 20.42% and 1.76% at 60 h, respectively (Figure 3B,D). In the MT pre-treated samples, the content of JA was significantly reduced (7.24–16.78%) at all three germination stages compared to untreated ones, whereas the opposite was true for IAA (increased by 4.38–28.37%) (Figure 3A,B). The content of ABA and GA_3 increased by 20.06% and 39.14% at 60 h and decreased by 37.94% and 13.05% at 19 h, respectively. But, at 36 h ABA decreased by 32.44%, while GA_3 increased by 13.52% (Figure 3C,D).

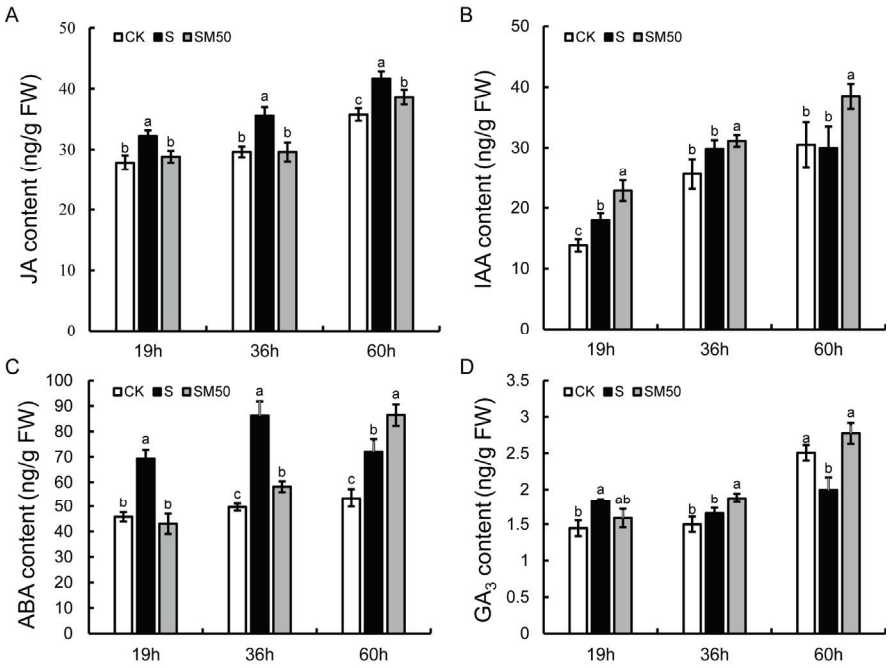

Figure 3. Hormone contents under different germination stages of different treatments. (**A**) JA content; (**B**) IAA content; (**C**) ABA content; (**D**) GA_3 content. Different letters indicate statistically significant differences (ANOVA with LSD Fisher's multiple comparison test, $p < 0.05$).

2.4. Transcriptome Data Quality Assessment and Analysis of DEGs

To reveal the transcriptional mechanism by which MT promotes maize seed germination under salt stress, transcriptome sequencing was performed for S-vs-SM50 at three different stages (19 h, 36 h, and 60 h) during seed germination. The quality assessment of the sequencing data of all samples was shown in Table S2, and a total of 851,402,640 Clean Reads were obtained from the transcriptome sequencing. The average Q20 and Q30 of all samples were 97.03% and 92.45%, respectively, while the average GC content was 55.12%. The expression patterns of the four genes used for qRT-PCR analysis followed the same trend as that of the transcriptome data (Table S1, Figure S2), indicating that the sequencing results were good for subsequent analysis. The results of sample correlation analysis showed that the three biological replicates of each treatment were well clustered together, indicating good reproducibility of the samples within the group and better reflecting the fact that the MT pretreatment has a regulatory effect on gene transcription in maize seeds at the germination stage (Figure 4B). Interestingly, samples from the S and SM50 groups clustered together at 19 h and 60 h but were clearly distinguished at 36 h, which was during the radicle protrusion stage, suggesting that MT affects gene transcription in maize seeds mainly at that stage (Figure 4B).

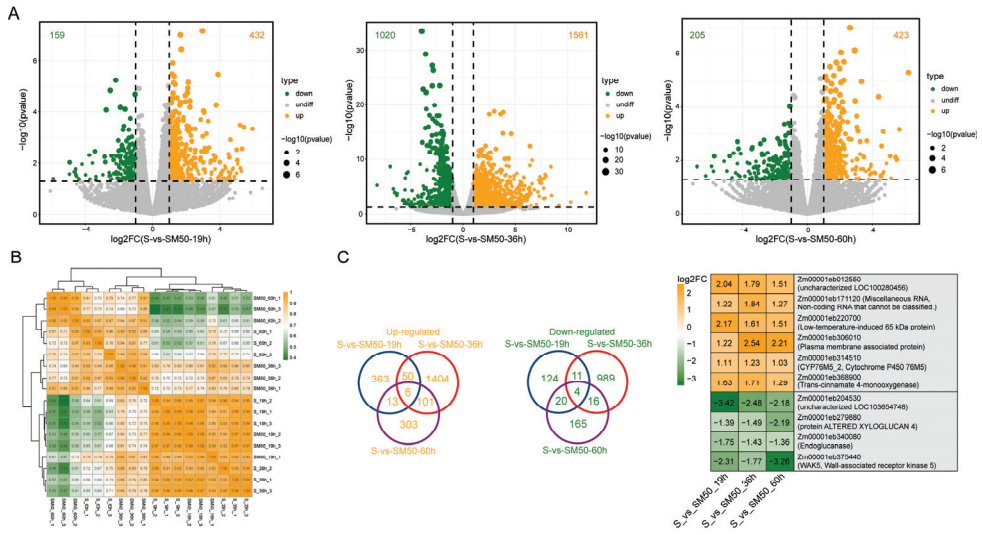

Figure 4. Effect of MT on gene expression of maize seeds at different germination stages under salt stress. (**A**) Volcano plot of differential genes; (**B**) correlation analysis of all samples and sample clustering; (**C**) Venn plot of up- and down-regulated differential genes and heat map of differential expression fold change of overlapping genes.

A total of 3509 DEGs were identified in the comparison of S-vs-SM50 at the three stages of germination, and 432 up-regulated genes and 159 down-regulated genes at 19 h and 423 up-regulated genes and 205 down-regulated genes at 60 h were observed. The highest number of DEGs was identified at 36 h, with 1561 up-regulated and 1020 down-regulated genes (Figure 4A). This result likewise indicates that MT has a greater effect on gene transcript expression during the radicle protrusion stage. To further understand the effect of MT on DEGs at different germination stages in S-vs-SM50, a Venn diagram analysis was performed on the up-regulated DEGs and down-regulated DEGs at the three germination stages, respectively (Figure 4C). The results showed that a total of six of the up-regulated DEGs were affected by MT and continued to be up-regulated throughout the germination phase, whereas a total of four of the down-regulated DEGs were affected by MT and continued to be down-regulated throughout the germination phase (Figure 4C).

2.5. GO and KEGG Enrichment Analysis of DEGs

To identify the major pathways regulated by MT to promote seed germination, all DEGs were analyzed for GO and KEGG enrichment, and 11 significantly enriched entries and pathways were each selected from the enrichment results for bubble mapping. GO enrichment analysis showed that these DEGs were mainly enriched in the xyloglucan metabolic process, response to stress, response to reactive oxygen species, response to hormones, response to abscisic acid, positive regulation of secondary cell wall biogenesis, oxidoreductase activity, DNA unwinding involved in DNA replication, cellular response to nitric oxide, the carbohydrate metabolic process, and antioxidant activity (Figure 5A). Unsurprisingly, MT further affects seed germination under stress mainly by regulating the expression of genes involved in stress response, hormone response, antioxidant capacity, and energy substance metabolism-related genes. KEGG enrichment analysis showed that MT-affected DGEs were mainly enriched in phenylpropane-related synthetic pathways such as phenylpropanoid biosynthesis and flavonoid biosynthesis. DEGs were similarly enriched in lipid-related pathways such as linoleic acid metabolism and fatty-acid elongation and glycan-related pathways such as glycolysis/gluconeogenesis and starch and sucrose metabolism (Figure 5B). In addition, the pathways of plant hormone signal transduction and benzoxazinoid biosynthesis were also enriched by DEGs (Figure 5B).

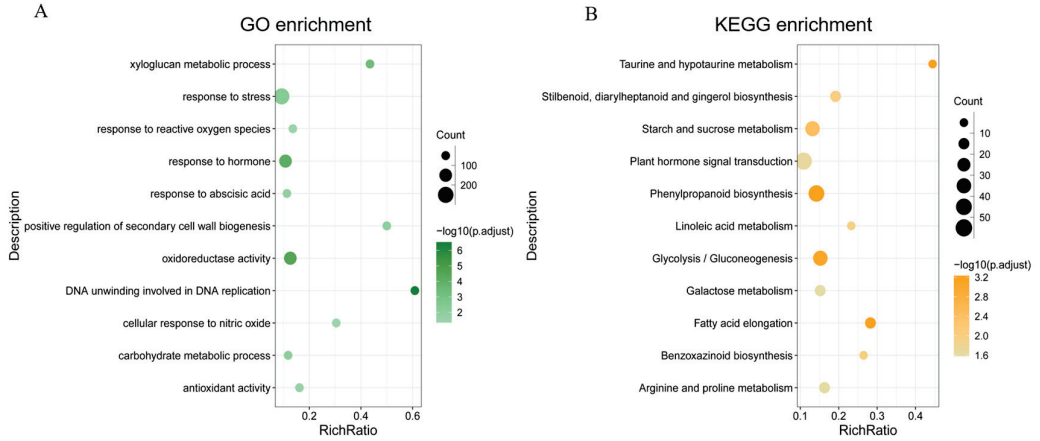

Figure 5. Differentially expressed gene enrichment analysis. (**A**) GO enrichment analysis; (**B**) KEGG enrichment analysis. The vertical axis represents the pathway name, the horizontal axis represents the Rich Ratio, the size of dots in the pathway represents the count of DEGs, and −log10 (p.adjust) is the significance of the enrichment reflected by the color of dots.

2.6. Time Series Analysis of Expression Patterns of DEGs

To investigate the expression and function of DEGs at different germination stages, time series analysis of all DEGs was performed to further analyze their expression patterns. As shown, all DEGs were clustered into eight clusters according to their expression patterns (Figure 6). Based on the expression patterns of the genes in these eight clusters, as well as the expression heat map, C5, C8, C6, and C3, which were more in line with expectations, were selected for further analysis. These gene clusters clustered 323, 429, 500, and 530 DEGs, respectively. The genes clustered in C5 were similarly expressed at 19 h and 60 h, but the expression of MT-pretreated DEGs was significantly higher than that of the S group at 36 h, whereas the expression pattern of DEGs in C8 and C3 was the opposite of that of C5 (Figure 6). Expression pattern plots of C6 showed that the expression of such DEGs in the S and SM50 groups was similar in the early stage (19 h), but the expression of these genes gradually increased as the germination process progressed, and MT pretreatment further increased their expression (Figure 6).

GO enrichment analyses of DEGs in each of these gene clusters showed that DEGs in C5 were mainly involved in epigenetic regulation of gene expression and trehalose biosynthetic process. This suggests that MT may protect normal gene expression from salt stress by suppressing the epigenetic regulation of gene expression and increase energy supply and promote seed radicle development by inhibiting the conversion of glucose to trehalose (Figure 6). DEGs in C6 are mainly associated with the amine biosynthetic process, cellular metal ion homeostasis, and the flavonoid metabolic process (Figure 6). This suggests that MT has a positive effect on ion homeostasis in cells. The expression patterns of DEGs in C8 and C3 were similar and GO enrichment analysis showed that they were involved in the cellular response to auxin stimulus, positive regulation of cell wall organization or biogenesis, antioxidant activity, and cellular response to oxidative stress, respectively. This further suggests that MT has a greater impact on seeds during the radicle protrusion stage, increasing their ability to scavenge reactive oxygen species and their response to phytohormones, which in turn has the effect of promoting seed germination (Figure 6).

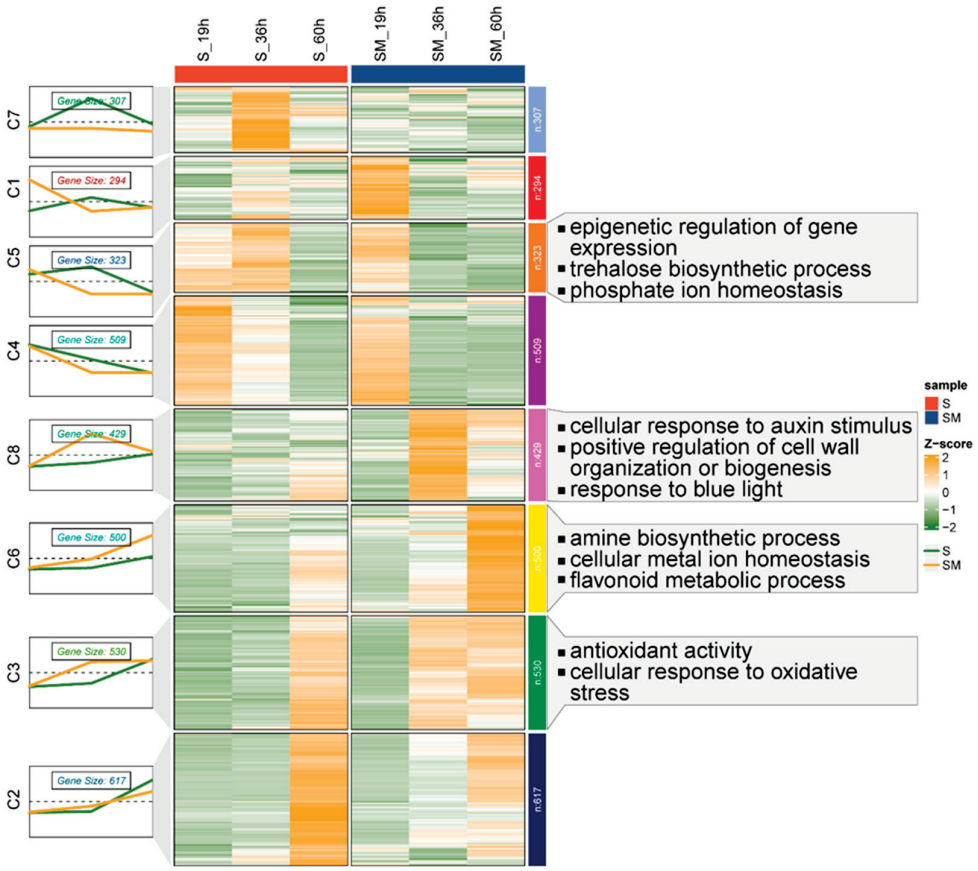

Figure 6. Time series analysis of differentially expressed genes. Heat map of expression pattern clustering and GO enrichment analysis of DEGs in SM vs. S comparison. The folded line graph represented the Mfuzz clustered expression pattern of DEGs.

2.7. Gene Set Enrichment Analysis of S-vs-SM50 in Different Germination Stages

In order to reveal the unique roles played by MT in the three key stages of germination, GO and KEGG gene set enrichment analyses were performed for all genes in the three germination stages.

GO gene set enrichment analysis (Figure 7A) showed that genes related to the xyloglucan metabolic process were down-regulated in maize seeds and genes related to cellular response to abscisic acid stimulus, response to salt, and post-embryonic plant morphogenesis were up-regulated in maize seeds at the time of seed imbibition stage (19 h). This suggests that MT at this time enhances seed response to ABA and salt in response to salt stress and inhibits xyloglucan metabolism to promote seed embryo development. When the seeds were in the radicle protrusion stage (36 h), the genes related to xyloglucan metabolic process and epigenetic regulation of gene expression were down-regulated, and the genes related to antioxidant activity and the cell wall macromolecule catabolic process were up-regulated. This is consistent with the results obtained from the time series analysis. When the seeds were in the germination stage (60 h), the GO entries showed that MT mainly up-regulated positive regulation of seed germination, positive regulation of post-embryonic development, photosynthesis, and regulation of the seed dormancy process. This demonstrated that MT promoted maize seed germination under salt stress by up-regulating seed germination-related genes.

The results of the KEGG gene set enrichment analysis (Figure 7B) showed in the MT affected genome set an overall down-regulation of ribosome-related genes, and an overall up-regulation of genes related to benzoxazinoid biosynthesis, brassinosteroid biosynthesis, and phenylalanine metabolism in the seed imbibition stage (19 h). Among the gene sets at the seed radicle protrusion stage (36 h), there was an overall down-regulation

of genes related to zeatin biosynthesis, and an overall up-regulation of genes related to phenylpropanoid biosynthesis, oxidative phosphorylation, and benzoxazinoid biosynthesis. It is noteworthy that the biosynthetic pathways of benzoxazoles were up-regulated by MT, both in the DEG enrichment analysis and in the gene set enrichment analysis, implying that MT has a positive impact on insect resistance and the antimicrobial and chemosensory effects of crops, in addition to the enhancement of crop resistance and the promotion of seed germination. The genes related to photosynthesis were up-regulated, while the genes related to zeatin biosynthesis, alpha-linolenic acid metabolism, and glutathione metabolism were down-regulated at the seed germination stage (60 h). At this time, MT inhibited the expression of genes related to glutathione metabolism and increased its accumulation, which helped the seeds to improve salt tolerance.

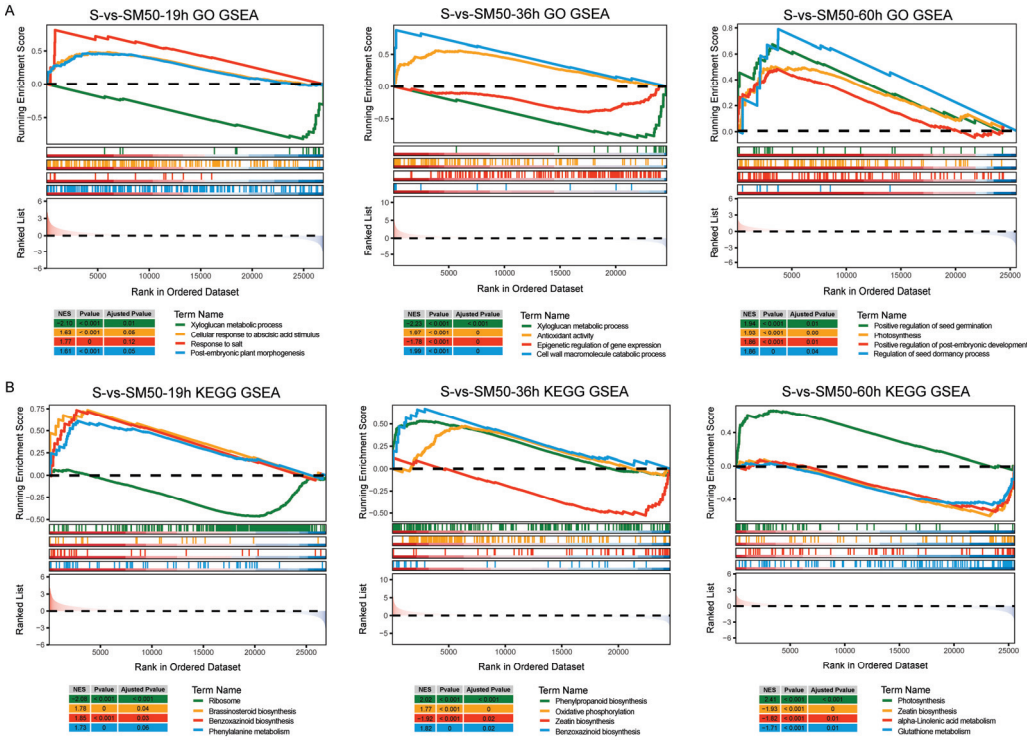

Figure 7. Gene set enrichment analysis of S-vs-SM50 in different germination stages. (**A**) GO gene set enrichment analysis; (**B**) KEGG gene set enrichment analysis.

2.8. Effect of MT on Phytohormone Signal Transduction Pathways during Seed Germination under Salt Stress

Based on the KEGG enrichment analysis of DEGs and the results of the determination of endogenous plant hormone contents, this study speculates that MT largely influences the germination process of seeds under adversity by interacting with other plant hormones. Throughout the three key stages of the germination process, a total of 57 DEGs belonged to genes related to the phytohormone signal transduction pathway, of which the IAA pathway had the highest number of DEGs with 25, followed by the ABA pathway with 11 DEGs (Figure 8). Both the SA pathway and the ETH pathway had five DEGs, CTK, BR, and JA had three DEGs each, and GA had only two DEGs (Figure 8). Based on the differential gene expression and pathway maps, it can be seen that although the expression of the negative regulator *ZmPP2C* in the ABA pathway was up-regulated, the expression of its downstream genes, *ZmSnRK2* and the ABA response element binding factor *ZmABF*, were similarly up-regulated (Figure 8). In the IAA pathway, partial up-regulation and partial down-regulation of *ZmAUX/IAA* promoted *ZmSUAR* expression overall, whereas *ZmCH3* expression was up-regulated at both 19 h and 60 h and was significantly down-regulated only at 36 h (Figure 8). Among the remaining hormone pathways, the ETH, CTK, SA, and GA pathways were overall positively regulated by MT, whereas the BR and JA

pathways were negatively regulated by MT (Figure 8). This suggests that MT is involved in regulating the signal transduction of multiple phytohormones, thus affecting a variety of biological processes and that MT further regulates seed salt tolerance and germination processes mainly by regulating the expression of genes related to the IAA and ABA signal transduction pathways.

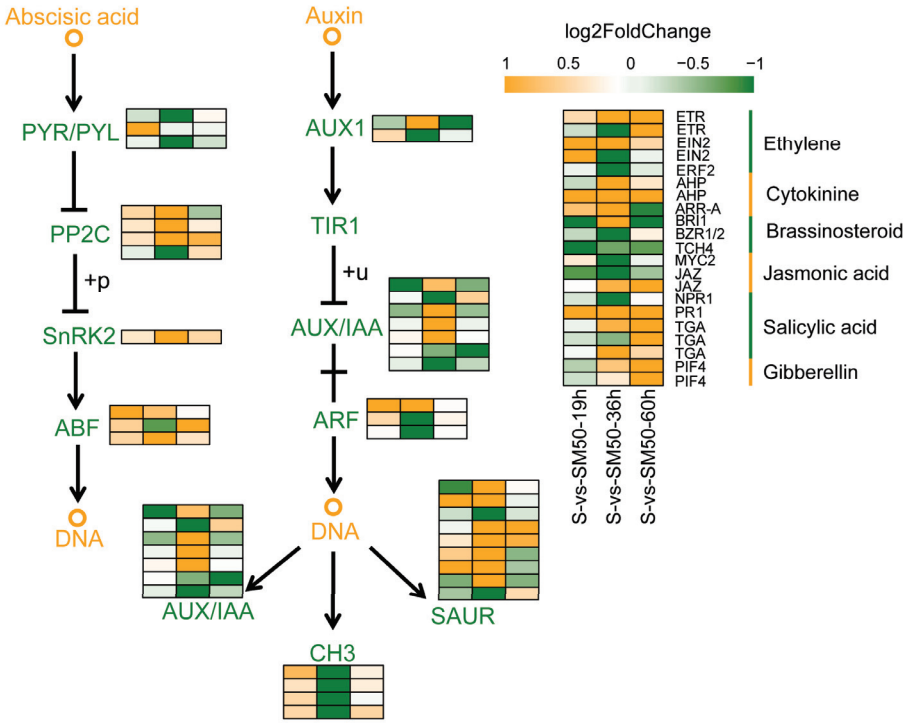

Figure 8. Effect of MT during germination on phytohormone signaling pathways in maize seeds under salt stress.

2.9. Effect of MT on Starch and Sucrose Metabolic Pathways during Seed Germination under Salt Stress

MT regulated a total of 39 DEGs in the starch and sucrose metabolic pathway. Analysis of the starch and sucrose metabolic pathway showed that MT up-regulated starch and sucrose catabolic genes, such as *ZmINV*, encoding β-fructofuranosidase, and *ZmSUS*, encoding sucrose synthetase, which are associated with the catabolism of sucrose, and *ZmBAM* and *ZmAMY*, encoding α-amylase, which are associated with the catabolism of starch (Figure 9). In addition, MT up-regulated genes related to the synthesis of D-glucose, such as *ZmE3.2.1.21*, encoding β-glucosidase, and repressed genes related to the catabolism of D-glucose, such as *ZmHK*, encoding hexokinase (Figure 9). Meanwhile, MT treatment reduced the expression of genes related to the synthesis of trehalose, such as *ZmTPS*, encoding trehalose-6-phosphate synthase, and *ZmTPP*, encoding trehalose-6-phosphate phosphatase, compared with that of group S (Figure 9). In conclusion, MT pretreatment promoted the decomposition of starch and sucrose and the synthesis of glucose in maize seeds under salt stress, providing sufficient energy for seed germination.

2.10. Effect of MT on Transcription Factors during Seed Germination under Salt Stress

In the plant hormone response and signal transduction pathways, there are many DEGs of transcription factors involved in the response to salt stress, MT, and the regulation of seed germination, such as ABF in the ABA pathway, ARF in the IAA pathway, PIF in the GA pathway, and JAZ and MYC2 in the JA pathway, among others. In addition to their involvement in hormone signaling, some transcription factors are also associated with plant stress tolerance. In this study, 19 transcription factor family members were identified in all DEGs. Regardless of the germination stage, these transcription factor genes were

mainly classified into the AP2/ERF, bHLH, MYB, NAC, and WRKY families (Figure 10A). The heatmap shows the expression differences of TFs in the comparison of S-vs-SM50, which are mainly regulated by MT at 36 h (Figure 10B). In addition, MT-regulated genes of the NAC, MYB, and WRKY families were associated with salt tolerance in plants, which may be one of the ways in which MT improves salt tolerance in maize seeds and promotes seed germination.

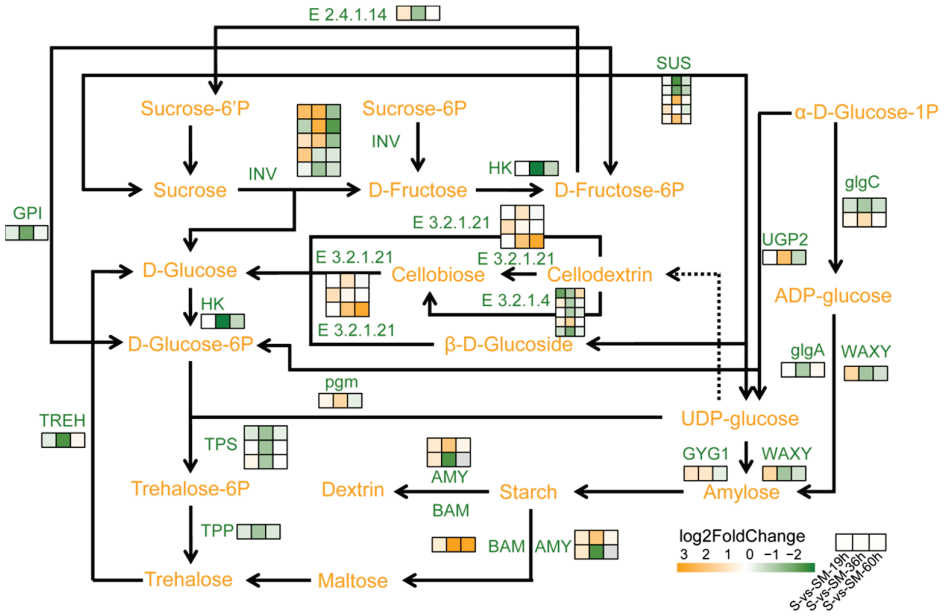

Figure 9. Effect of MT during germination on starch and sucrose metabolism in maize seeds under salt stress.

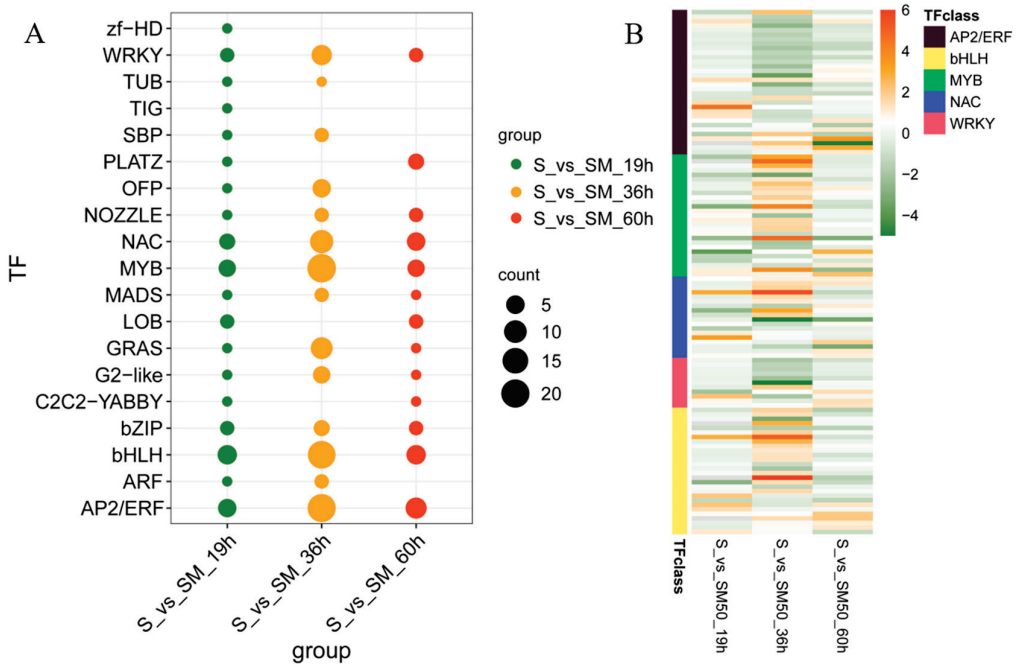

Figure 10. Effect of MT during germination on gene expression of transduction factors in maize seeds under salt stress. (**A**) Classifications and counts of TFs in the S-vs-SM comparisons at different times. (**B**) Heatmaps of the top 5 TFs families in the S-vs-SM comparisons at different times.

3. Discussion

3.1. MT Alleviates Salt Stress-Induced Oxidative Damage by Enhancing the Ability to Scavenge, R.O.S.

Excessive accumulation of salt in the soil inhibits seed germination. In practical agricultural production, plant hormones and growth regulators, such as GA, JA, SA, IAA, CTK, ABA, and their functional analogues, are commonly used to promote seed germination, reduce insect pests and diseases, and mitigate damage caused by environmental stresses [31,32,45–51]. MT is a new indole hormone, which is also widely used to alleviate developmental retardation and oxidative damage caused by salt stress and to improve plant stress tolerance [46]. The results of this study showed that salt stress inhibited maize seed germination, but exogenous MT pretreatment effectively alleviated salt stress-induced developmental retardation, promoted seed germination, and significantly promoted lateral rooting (Figure 1). Changes in MDA content represented the degree of oxidative damage to the plant plasma membrane caused by salt stress. In this study, salt stress led to an increase in MDA content in maize seeds, but MDA content was significantly lower in MT treatment compared with no MT treatment. This indicated that MT mitigated the salt stress oxidative damage to maize seeds (Figure 2C).

O_2^- and H_2O_2 in ROS can act as signaling molecules to activate plant responses to unfavorable environmental conditions. However, high-salinity-induced over-accumulation of O_2^- and H_2O_2 can seriously threaten the membrane structure of plant cells [52]. MT, an antioxidant, is capable of scavenging excessive accumulation of ROS directly through a cascade reaction [53]. According to the results of this study, O_2^- and H_2O_2 were maintained at low levels in MT-treated maize seeds under salt stress (Figure 2A,B). In addition, MT has been reported to be able to regulate ROS homeostasis by increasing the activity of antioxidant enzymes [46,54]. The results of this study showed that MT increased the activities of SOD, CAT, and POD in maize seeds under salt stress (Figure 4). The same results were obtained when exogenous MT was applied to wheat, rice, soybean, and tomato under salt stress [55–58]. Based on these results, the present study suggests that MT promotes seed germination by directly or indirectly participating in the regulation of ROS homeostasis in plants under stress to avoid overreaction to stress.

3.2. MT Improves Seed Germination under Salt Stress by Regulating Phytohormone Levels and Phytohormone Signal Transduction Pathways

Endogenous hormones play a crucial role in seed germination [59]. In addition to enhancing the antioxidant capacity of plants under salt stress, MT is also involved as a signaling molecule in regulating hormone signal transduction and activating the stress response of plants, thereby improving stress tolerance [35]. As shown in previous studies, phytohormones (e.g., ABA, IAA, BR, CTK, JA, SA, and ETH) enable plants to regulate their growth and development in response to the growing environment and help them adapt to unfavorable conditions [60]. For example, ABA plays a role in all adversity stresses and enhances stress tolerance in wheat [61], maize [62], and soybean [63] through exogenous ABA. IAA and JA play crucial roles as endogenous signaling molecules in both plant growth and response to adversity [64,65].

In the ABA signal transduction pathway, PYR/PYL/RCAR, as ABA receptors, phosphorylate the ABA response element binding factor ABF by activating SnRK2 and initiate the expression of genes downstream of the ABA response pathway by inhibiting the activity of the ABA negative regulator PP2C [66]. In this study, MT significantly reduced ABA levels in seeds and suppressed the response to ABA signaling. The transcriptome results showed that *ZmPP2C* was significantly up-regulated in SM50 treatment, but *ZmPYR/PYL* was significantly down-regulated (Figures 3 and 8). Interestingly, *ZmSnRK2* and *ZmABF*, which should have been repressed due to the up-regulation of *ZmPP2C*, were both up-regulated in the SM50 treatment (Figure 8). In view of these results, this study speculated that MT promotes seed germination under salt stress by reducing ABA signaling to avoid inhibition of seed germination due to accumulation of ABA and over-responsiveness to

ABA, while activating stress-responsive genes through other pathways to achieve a balance between plant growth and stress tolerance. Previous studies have shown similar results; e.g., MT alleviated salt stress damage to wheat and cucumber seeds and promoted seed germination by reducing ABA biosynthesis and signaling pathways [30,36]. In this study, MT increased IAA levels at three different stages of seed germination (Figure 3). Whereas in the IAA signaling pathway some *ZmAUX/IAA* was partially up-regulated and partially down-regulated and in general promoted the expression of *ZmSUAR*, *ZmCH3* was up-regulated at both 19 and 60 h and was significantly down-regulated only at 36 h (Figure 8). In the IAA pathway, IAA is sensed by TIR1 in the E3 ubiquitin–protein ligase SCF complex, and the complex then ubiquitinates AUX/IAA and degrades it via the 26 S proteasome, releasing ARF to activate downstream response genes [60]. The results of the present study were similar to those of MT applied to *Arabidopsis* and cucumber, suggesting that MT may improve germination of maize seeds under salt stress by activating IAA downstream response genes [67,68].

3.3. MT Promotes Seed Germination under Salt Stress by Regulating Starch and Sucrose Metabolic Pathways during Seed Germination

Sugars function as structural materials for seed development and energy supply during germination to maintain osmotic pressure in plants to resist salt stress [69]. For example, carbohydrate metabolites (e.g., sucrose, D-glucose, and D-fructose) are up-regulated during the later stages of salt stress in watermelon to improve salt tolerance [70]. Starch is the end product of plant photosynthesis and is one of the sources of energy for plants. When subjected to extreme environmental stimuli, plants often increase sugar accumulation by regulating starch catabolic pathways to improve their salt tolerance [71–73]. In this study, MT upregulated *ZmAMY*, a gene encoding α-amylase, and *ZmBAM*, a gene encoding β-amylase, to promote starch catabolism (Figure 9). Both sucrose and trehalose are key metabolites in starch and sucrose metabolism. Among them, sucrose can be further degraded to UPD glucose, a precursor for the synthesis of trehalose 6-phosphate, and both trehalose and sucrose have been found to improve salt tolerance in plants [74–76]. However, transcriptome analysis in this study showed that the transcript levels of trehalose-6-phosphatase (TPP), responsible for the synthesis of trehalose, and trehalose-6-synthase (TPS), responsible for the synthesis of trehalose 6-phosphate, were lower in the SM50 treatment than in the S treatment, while the expression of genes coding for enzymes responsible for the degradation of sucrose (e.g., β-fructofuranosidase, INV, and sucrose synthetase, SUS) was up-regulated, which suggests that the MT promoted the breakdown of sugar in maize seeds under salt stress and inhibited the synthesis of trehalose, which promoted the accumulation of D-glucose (Figure 9). This result seems to be in conflict with previous results [77], and in this study, we speculate that MT promotes sucrose and starch catabolism and increases D-glucose content in order to increase energy supply and promote seed germination while improving the salt tolerance of seeds through other pathways such as increasing antioxidant capacity and up-regulation of stress-responsive genes.

3.4. MT Regulates the Expression of Different Functional Genes at Different Seed Germination Stages to Promote Seed Germination under Salt Stress

Seed germination is a complex and unique physiological process that initiates crop growth and development [78]. How to improve the seedling establishment rate of crops under stress has been the focus of attention, but most of the research has stayed on physiology and phenotype and has not carried out in-depth studies on seed germination at the molecular level [79]. Seed imbibition, radicle protrusion, and emergence are three important stages in the seed germination process, but the effects of MT on these three germination stages have not been reported yet. The results of this study showed that MT affects the expression of genes with different functions at different stages of seed germination, thus improving salt tolerance and promoting seed germination throughout the germination period. For example, at the seed imbibition stage (19 h), MT mainly regulated the formation of cell

walls and the response of ABA and salt stress during embryo development, which was the same function as in the wheat seed [30].

Just like our previous research on the wheat seed [30], at the radicle protrusion stage (36 h), MT mainly affected the expression of epigenetic regulation of gene expression, antioxidant enzymes, and cell wall formation. At the seed germination stage (60 h), MT affected genes related to the positive regulation of seed germination, photosynthesis, and zeatin biosynthesis (Figure 7). This study demonstrated that MT, as a multifunctional indole hormone, plays an important role in promoting seed germination through a complex regulatory network throughout the germination process under salt stress. However, since the signal transduction pathway of MT is still not well resolved, the question of how MT functions during seed germination needs to be further explored.

4. Materials and Methods

4.1. Materials and Treatments

The material used in this experiment was the maize inbred line B73, provided by the Seed Science Laboratory, College of Plant Science and Technology, Beijing University of Agriculture. Full, uniformly sized B73 maize seeds with undamaged surfaces were selected and sterilized with a 1% NaClO solution for 10 min and then rinsed three times with deionized water before use.

4.2. Salt Stress Concentration Screening

The salt solution concentration gradient was set at 0, 50, 100, 150, 200, 250 mM NaCl. Seeds were soaked in deionized water for 12 h, neatly arranged in germination boxes and placed in a smart light incubator for seven days for seed germination experiments (temperature: 20–25 °C, light: dark incubation for the first three days, and 12 h each of light and darkness for the last four days). Three biological replicates were set up for each treatment, and 30 seeds were placed in each replicate.

4.3. Optimal MT Concentration Screening

The treatment of MT-dipped seeds was adopted for the concentration screening experiment. Six treatment groups were set up: control (CK), 150 mM NaCl + 0 μM MT (S), 150 mM NaCl + 25 μM MT (SM25), 150 mM NaCl + 50 μM MT (SM50), 150 mM NaCl + 75 μM MT (SM75), 150 mM NaCl + 100 μM MT (SM100). Four biological replicates were set up for each treatment and 40 seeds were placed in each replicate. Sampling was performed when incubated under salt stress conditions until the seventh day. The samples were snap-frozen with liquid nitrogen and stored in an ultra-low-temperature refrigerator at −80 °C, and three biological replicates were taken for each treatment.

4.4. Endogenous Hormone Content and Transcriptome Sequencing

Three treatments were set up: control (CK), salt treatment (S), and salt + MT treatment (SM50). Three biological replicates were set up for each treatment, and each replicate was used with 40 seeds placed in the incubator for germination experiments. The germinated seeds at 19 h, 36 h, and 60 h were sampled for the determination of endogenous plant hormone content and transcriptome sequencing, respectively.

4.5. Measurement of Germination and Morphological Indicators

The number of seeds dewed and sprouted and the lateral radicle occurrence were counted regularly every day, and radicle length and germ length were measured at the 7th day. Lateral radicle, i.e., in addition to the main radicle, is the radicle that grows from the upper side of the shield stem at the base of the mesocotyl.

4.6. Measurement of Antioxidant Enzyme Activities

The frozen samples were quickly ground to powder in a pre-cooled mortar with liquid nitrogen, and 0.2 g of powder was added to a 2 mL centrifuge tube, and then 1.6 mL

of phosphate buffer (pH = 7.8, 0.05 M) was added for extraction and then put into a centrifuge to be centrifuged (4 °C, 10,000 rpm, 20 min). The supernatant was used for the determination of antioxidant enzyme activity and stored in the refrigerator at 4 °C.

The SOD activity was measured by the nitrogen blue tetrazolium (NBT) method [80]. Briefly, 100 μL of crude extract was added to 3.9 mL of the reaction mixture and placed under 4000 Lx intense light for 30 min, then protected from light. The control group was an equal amount of reaction solution. The SOD activity was determined and calculated at 560 nm.

POD activity was measured by guaiacol method [81]. Briefly, 40 μL of crude extract was taken and added to 3 mL of reaction solution at 470 nm to determine the change in absorbance for 1 min. The control was the inactivated enzyme solution after boiling. POD activity was calculated as one unit of enzyme activity per minute increase in absorbance value of 0.01.

The CAT activity was measured by UV spectrophotometric method [81]. Briefly, 50 μL of enzyme solution was added to 3 mL of buffer (PH = 7.8, 0.05 M), and 200 μL of 0.3% H_2O_2 was added, shaken quickly, and then the change in absorbance was measured at 240 nm for 1 min. The inactivated enzyme solution after boiling was used as a control to calculate CAT activity.

4.7. Measurement of MDA and Soluble Sugar Content

The MDA content was determined by the thiobarbituric acid method 30 by mixing 0.2 g of sample powder with 8 mL of 10% trichloroacetic acid (TCA) and centrifuging (4 °C, 4000 rpm, 10 min). Then, 2 mL of supernatant (water as control) was taken, and 2 mL of 0.6% thiobarbituric acid (TBA) solution was added and mixed well, and the mixture was put in boiling water for 15 min, cooled quickly, and centrifuged. The absorbance values of the supernatant were measured at 450 nm, 532 nm, and 600 nm, and the MDA and soluble sugar contents were calculated.

4.8. Reactive Oxygen Content Measurement

The H_2O_2 and O_2^- content were determined with reference to the method of Lu et al. [81].

H_2O_2 content measurement: 0.2 g of the sample was taken in 4 mL of 0.1% (*w*/*v*) TCA and ground to homogenization and centrifuged at 10,000 rpm for 10 min. The precipitates were then thoroughly mixed to 1 mL with 0.2 mL of ammonia and 0.1 mL of 95% (*v*/*v*) hydrochloric acid solution containing 20% (*v*/*v*) $TiC1_4$ and centrifuged (4 °C, 4000 rpm, 10 min). After removing the supernatant, the precipitate was washed successively with pre-cooled acetone (−20 °C) and dissolved in 3 mL of 1 mM sulfuric acid. The resulting solution was measured for absorbance at 410 nm.

O_2^- Content measurement: In 4 mL of 65 mM phosphate buffer solution (PBS, pH = 7.8), 0.2 g of sample was added and grinded well and then centrifuged (4 °C, 10,000 rpm, 15 min). Then, 0.5 mL of the supernatant was taken and mixed with 1 mL of hydroxylamine hydrochloride and 0.5 mL of 65 mM phosphate buffer and left for 1 h. One mL of p-aminobenzenesulfonamide (17 mM) and one mL of α-naphthylamine (7 mM) were added to the above mixture and incubated at 25 °C for 20 min. An equal volume of ether was added and centrifuged (4500 rpm, 3 min), the supernatant was taken, and the absorbance value was measured at 530 nm.

4.9. Measurement of Proline Content

Proline was determined using the ninhydrin colorimetric method [82]. Into 0.5 g of sample, 2.5 mL of glacial acetic acid was added and centrifuged (10,000 rpm for 2 min) after 10 min in a boiling water bath. One mL of the supernatant was reacted with two mL of acidic ninhydrin solution for 30 min in a boiling water bath and then centrifuged (10,000 rpm for 2 min) and finally extracted by adding toluene. The absorbance at 520 nm was measured by UV spectrophotometer and calculated.

4.10. Measurement of Endogenous Hormone Content

Maize seeds of CK, S, and SM50 were taken at 19 h, 36 h, and 60 h of germination, respectively, and endogenous hormone contents were determined. The milled samples were mixed with methanol/water/formic acid (15:4:1, $v/v/v$). The mixture was shaken for 10 min and then centrifuged (4 °C, 12,000 rpm, 5 min). The supernatant was evaporated and dissolved in 80% methanol (v/v), then filtered through a membrane filter and further detected using high-performance liquid chromatography/mass spectrometry (HPLC-MS, column: Waters ACQUITY UPLC HSS T3 C18, 1.8 μm, 2.1 mm × 100 mm; solvent system: water with 0.04% acetic acid: acetonitrile with 0.04% acetic acid; gradient program: 90:10 v/v at 0 min, 40:60 v/v at 5.0 min, 40:60 v/v at 7.0 min, 90:10 v/v at 7 min and 90:10 v/v at 10 min; injection volume: 2 μL). The contents of IAA, GA_3, JA, and ABA in the seeds were determined by Wuhan Metware Biotechnology Co. (Wuhan, China). Each treatment contained three biological replicates.

4.11. Transcriptome Sequencing and Analysis

Total RNA was isolated from maize seeds at 19 h, 36 h, and 60 h from the S and SM50 treatment groups using RNA isolater Total RNA Extraction Reagent produced by Nanjing Novozymes Biotechnology Co., Ltd. (Nanjing, China) according to the instruction manual. Each treatment contained three biological replicates. Transcriptome sequencing was entrusted to Beijing Novozymes Technology Co. (Beijing, China) using the Illumina sequencing platform. Company-delivered Clean Data were aligned to the maize B73 reference genome (Zm-B73-REFERENCE-NAM-5.0) using Hisat2 (v2.2.1), followed by quantification of gene expression using featureCounts (v2.0.0). DEGs were screened between SM50 treatment and S treatment using DESeq2 (v1.38.3). GO enrichment analysis and KEGG enrichment analysis of DEGs and gene set enrichment analysis (GSEA) of all genes in each treatment separately were performed using clusterProfiler (v4.6.1). Time series analysis of DEGs was based on soft clustering-based Mfuzz in CluserGVis (v0.0.4).

4.12. Quantitative Real-Time PCR Assays

Quantitative real-time PCR (qRT-PCR) assays were performed using the same RNA samples as used for transcriptome analysis, with each sample containing three biological replicates. The gene-specific primers used for qRT-PCR assays are listed in Table S1. qRT-PCR was performed with SYBR Green Premix Pro Taq HS Kit II (Accurate Biotechnology, Changsha, China) on a LightCycler® 96 Instrument fluorescent quantitative PCR instrument. Relative expression was calculated by the $2^{-\Delta\Delta CT}$ method [83].

4.13. Data Processing and Analysis

One-way ANOVA was used to assess the significance of differences and the final results were expressed as mean ± standard deviation. Data were statistically and analyzed using SPSS 22.0, and $p < 0.05$ was considered a statistically significant difference. Downstream analysis of transcriptome data and graphical plotting were performed in R (v4.2.2).

5. Conclusions

In conclusion, salt stress inhibited seed germination, but MT pretreatment promoted maize seed germination. Melatonin pretreatment alleviated the inhibitory effect of salt stress on maize seed germination by increasing the antioxidant ability of maize seeds under salt stress and reducing the accumulation of ROS, as well as the content of MDA. Meanwhile, melatonin was involved in regulating the content changes of endogenous hormones during the germination of maize seeds under salt stress, which reduced the content of ABA and JA, increased the content of IAA and GA_3, and broke the balance between GA_3 and ABA to promote the germination. Melatonin also regulated the expression of genes related to starch and sucrose metabolism pathways and phytohormone signal transduction pathways by affecting the expression of antioxidant enzymes, response to stress, and seed germination-

related genes in maize seeds under salt stress and affected the expression of different functional genes at different germination stages, thus achieving the enhancement of seed salt tolerance throughout the germination stage.

Supplementary Materials: The following supporting information can be downloaded at: https://www.mdpi.com/article/10.3390/plants13152142/s1, Table S1: Primers designed by qRT-PCR; Table S2: Transcriptome sequencing quality assessment; Figure S1: The phenotypic differences in seed morphology at 5th day. Genes: Zm00001eb283530, Zm00001eb003440, Zm00001eb148130 and Zm00001eb327450. SM: germination of seeds treated with 50 μM melatonin under 150 mM NaCl solution; S: germination of seeds treated with 150 mM NaCl. Figure S2: Effects of melatonin on gene expression under salt stress in maize seed by qRT-PCR.

Author Contributions: Conceptualization, R.L. (Runzhi Li); Data curation, J.W. and D.Y.; Investigation, J.W., D.Y., R.L. (Rui Liu), T.W., Y.L., Z.L. and Y.H.; Methodology, J.W., D.Y. and R.L. (Runzhi Li); Resources, Y.W.; Supervision, R.L. (Runzhi Li); Writing—original draft, J.W. and D.Y.; Writing—review and editing, R.L. (Runzhi Li). All authors have read and agreed to the published version of the manuscript.

Funding: This research was funded by the Science and Technology Innovation Support program of Beijing University of Agriculture (China), grant numbers BUA-HHXD2024003.

Data Availability Statement: The RNA-seq dataset in this study has been uploaded to SRA database in NCBI (BioProject ID: PRJNA1120961).

Conflicts of Interest: The authors declare no conflicts of interest. The funders had no role in the design of the study; in the collection, analyses, or interpretation of data; in the writing of the manuscript; or in the decision to publish the results.

References

1. Mahajan, S.; Tuteja, N. Cold, salinity and drought stresses: An overview. *Arch. Biochem. Biophys.* **2005**, *444*, 139–158. [CrossRef] [PubMed]
2. Zhang, Z.; Liu, L.; Li, H.; Zhang, S.; Fu, X.; Zhai, X.; Li, D. Exogenous melatonin promotes the salt tolerance by removing active oxygen and maintaining ion balance in wheat (*Triticum aestivum* L.). *Front. Plant Sci.* **2022**, *12*, 787062. [CrossRef] [PubMed]
3. Kolář, J.; Johnson, C.H.; Macháčková, I. Exogenously applied melatonin (N-acetyl-5-methoxytryptamine) affects flowering of the short-day plant *Chenopodium rubrum*. *Physiol. Plant* **2003**, *118*, 605–612. [CrossRef]
4. Hernández-Ruiz, J.; Cano, A.; Arnao, M.B. Melatonin acts as a growth-stimulating compound in some monocot species. *J. Pineal Res.* **2005**, *39*, 137–142. [CrossRef] [PubMed]
5. Munns, R.; Tester, M. Mechanisms of salinity tolerance. *Annu. Rev. Plant Biol.* **2008**, *59*, 651–681. [CrossRef] [PubMed]
6. Yang, Y.; Guo, Y. Unraveling salt stress signaling in plants. *J. Integr. Plant Biol.* **2018**, *60*, 796–804. [CrossRef] [PubMed]
7. Li, S.; Wang, Y.; Gao, X.; Lan, J.; Fu, B. Comparative physiological and transcriptome analysis reveal the molecular mechanism of melatonin in regulating salt tolerance in alfalfa (*Medicago sativa* L.). *Front. Plant Sci.* **2002**, *13*, 919177. [CrossRef] [PubMed]
8. Park, H.S.; Kazerooni, E.A.; Kang, S.M.; Al-Sadi, A.M.; Lee, I.J. Melatonin enhances the tolerance and recovery mechanisms in *Brassica juncea* (L.) Czern. Under saline conditions. *Front. Plant Sci.* **2021**, *12*, 593717. [CrossRef] [PubMed]
9. Ismail, A.M.; Horie, T. Genomics, physiology, and molecular breeding approaches for improving salt tolerance. *Annu. Rev. Plant Biol.* **2017**, *68*, 405–434. [CrossRef]
10. Chen, M.; Yang, Z.; Liu, J.; Zhu, T.; Wei, X.; Fan, H.; Wang, B. Adaptation mechanism of salt excluders under saline conditions and its applications. *Int. J. Mol. Sci.* **2018**, *19*, 3668. [CrossRef]
11. Zhu, J.K. Genetic analysis of plant salt tolerance using Arabidopsis. *Plant Physiol.* **2000**, *124*, 941–948. [CrossRef] [PubMed]
12. Zhu, J.K. Plant salt tolerance. *Trends Plant Sci.* **2001**, *6*, 66–71. [CrossRef] [PubMed]
13. Zhao, S.; Zhang, Q.; Liu, M.; Zhou, H.; Ma, C.; Wang, P. Regulation of plant responses to salt stress. *Int. J. Mol. Sci.* **2021**, *22*, 4609. [CrossRef] [PubMed]
14. Ahmad, P.; Jaleel, C.A.; Salem, M.A.; Nabi, G.; Sharma, S. Roles of enzymatic and nonenzymatic antioxidants in plants during abiotic stress. *Crit. Rev. Biotechnol.* **2010**, *30*, 161–175. [CrossRef] [PubMed]
15. Bressan, R.A.; Hasegawa, P.M.; Pardo, J.M. Plants use calcium to resolve salt stress. *Trends Plant Sci.* **1998**, *3*, 411–412. [CrossRef]
16. Singh, P.; Choudhary, K.K.; Chaudhary, N.; Gupta, S.; Sahu, M.; Tejaswini, B.; Sarkar, S. Salt stress resilience in plants mediated through osmolyte accumulation and its crosstalk mechanism with phytohormones. *Front. Plant Sci.* **2022**, *13*, 1006617. [CrossRef] [PubMed]
17. Ashraf, M.; Foolad, M.R. Roles of glycine betaine and proline in improving plant abiotic stress resistance. *Environ. Exp. Bot.* **2007**, *59*, 206–216. [CrossRef]

18. Wong, C.E.; Li, Y.; Labbe, A.; Guevara, D.; Nuin, P.; Whitty, B.; Moffatt, B.A. Transcriptional profiling implicates novel interactions between abiotic stress and hormonal responses in Thellungiella, a close relative of Arabidopsis. *Plant Physiol.* **2006**, *140*, 1437–1450. [CrossRef] [PubMed]
19. Alvarez, M.E.; Savouré, A.; Szabados, L. Proline metabolism as regulatory hub. *Trends Plant Sci.* **2022**, *27*, 39–55. [CrossRef]
20. Alnusairi, G.S.; Mazrou, Y.S.; Qari, S.H.; Elkelish, A.A.; Soliman, M.H.; Eweis, M.; ElNahhas, N. Exogenous nitric oxide reinforces photosynthetic efficiency, osmolyte, mineral uptake, antioxidant, expression of stress-responsive genes and ameliorates the effects of salinity stress in wheat. *Plants* **2021**, *10*, 1693. [CrossRef]
21. Ke, Q.; Ye, J.; Wang, B.; Ren, J.; Yin, L.; Deng, X.; Wang, S. Melatonin mitigates salt stress in wheat seedlings by modulating polyamine metabolism. *Front. Plant Sci.* **2018**, *9*, 914. [CrossRef] [PubMed]
22. Iwaniuk, P.; Kaczyński, P.; Pietkun, M.; Łozowicka, B. Evaluation of titanium and silicon role in mitigation of fungicides toxicity in wheat expressed at the level of biochemical and antioxidant profile. *Chemosphere* **2022**, *308*, 136284. [CrossRef] [PubMed]
23. Santosh, K.B.; Prianka, H. Melatonin plays multifunctional role in horticultural crops against environmental stresses: A review. *Environ. Exp. Bot.* **2020**, *176*, 104063. [CrossRef]
24. Hattori, A.; Migitaka, H.; Iigo, M.; Itoh, M.; Yamamoto, K.; Ohtani-Kaneko, R.; Reiter, R.J. Identification of melatonin in plants and its effects on plasma melatonin levels and binding to melatonin receptors in vertebrates. *Biochem. Mol. Biol. Int.* **1995**, *35*, 627–634. [PubMed]
25. Xu, T.; Chen, Y.; Kang, H. Melatonin is a potential target for improving post-harvest preservation of fruits and vegetables. *Front. Plant Sci.* **2019**, *10*, 488368. [CrossRef] [PubMed]
26. Wei, W.; Li, Q.T.; Chu, Y.N.; Reiter, R.J.; Yu, X.M.; Zhu, D.H.; Chen, S.Y. Melatonin enhances plant growth and abiotic stress tolerance in soybean plants. *J. Exp. Bot.* **2015**, *66*, 695–707. [CrossRef] [PubMed]
27. Li, J.; Xie, J.; Yu, J.; Lv, J.; Zhang, J.; Ding, D.; Gao, F. Melatonin enhanced low-temperature combined with low-light tolerance of pepper (*Capsicum annuum* L.) seedlings by regulating root growth, antioxidant defense system, and osmotic adjustment. *Front. Plant Sci.* **2022**, *13*, 998293. [CrossRef] [PubMed]
28. Kurt-Celebi, A.; Colak, N.; Torun, H.; Dosedělová, V.; Tarkowski, P.; Ayaz, F.A. Exogenous melatonin ameliorates ionizing radiation-induced damage by modulating growth, osmotic adjustment and photosynthetic capacity in wheat seedlings. *Plant Physiol. Biochem.* **2022**, *187*, 67–76. [CrossRef] [PubMed]
29. Lou, J.; Wu, C.; Wang, H.; Cao, S.; Wei, Y.; Chen, Y.; Xu, F. Melatonin treatment delays postharvest senescence of broccoli with regulation of carotenoid metabolism. *Food Chem.* **2023**, *408*, 135185. [CrossRef]
30. Wang, J.; Lv, P.; Yan, D.; Zhang, Z.; Xu, X.; Wang, T.; Li, R. Exogenous melatonin improves seed germination of wheat (*Triticum aestivum* L.) under salt stress. *Int. J. Mol. Sci.* **2022**, *23*, 8436. [CrossRef]
31. Hamayun, M.; Khan, S.A.; Khan, A.L.; Shin, J.H.; Ahmad, B.; Shin, D.H.; Lee, I.J. Exogenous gibberellic acid reprograms soybean to higher growth and salt stress tolerance. *J. Agric. Food Chem.* **2010**, *58*, 7226–7232. [CrossRef] [PubMed]
32. Ahmad, S.; Cui, W.; Kamran, M.; Ahmad, I.; Meng, X.; Wu, X.; Han, Q. Exogenous application of melatonin induces tolerance to salt stress by improving the photosynthetic efficiency and antioxidant defense system of maize seedling. *J. Plant Growth Regul.* **2021**, *40*, 1270–1283. [CrossRef]
33. Wei, L.; Zhao, H.; Wang, B.; Wu, X.; Lan, R.; Huang, X.; Zheng, Q. Exogenous melatonin improves the growth of rice seedlings by regulating redox balance and ion homeostasis under salt stress. *J. Plant Growth Regul.* **2022**, *41*, 2108–2121. [CrossRef]
34. Reiter, R.J.; Mayo, J.C.; Tan, D.X.; Sainz, R.M.; Alatorre-Jimenez, M.L.; Qin, L. Melatonin as an antioxidant: Under promises but over delivers. *J. Pineal Res.* **2016**, *61*, 253–278. [CrossRef]
35. Arnao, M.B.; Hernández-Ruiz, J. Melatonin: A new plant hormone and/or a plant master regulator? *Trends Plant Sci.* **2019**, *24*, 38–48. [CrossRef] [PubMed]
36. Zhang, H.J.; Zhang, N.A.; Yang, R.C.; Wang, L.; Sun, Q.Q.; Li, D.B.; Guo, Y.D. Melatonin promotes seed germination under high salinity by regulating antioxidant systems, ABA and GA4 interaction in cucumber (*Cucumis sativus* L.). *J. Pineal Res.* **2014**, *57*, 269–279. [CrossRef] [PubMed]
37. Zhang, Y.; Fan, Y.; Rui, C.; Zhang, H.; Xu, N.; Dai, M.; Ye, W. Melatonin improves cotton salt tolerance by regulating ROS scavenging system and Ca^{2+} signal transduction. *Front. Plant Sci.* **2021**, *12*, 693690. [CrossRef]
38. Li, Y.; Zhang, Y.; Feng, F.; Liang, D.; Cheng, L.; Ma, F.; Shi, S. Overexpression of a *Malus* vacuolar Na^+/H^+ antiporter gene (MdNHX1) in apple rootstock M. 26 and its influence on salt tolerance. *Plant Cell Tissue Organ Cult.* **2010**, *102*, 337–345. [CrossRef]
39. Shao, Q.; Han, N.; Ding, T.; Zhou, F.; Wang, B. SsHKT1; 1 is a potassium transporter of the C3 halophyte Suaeda salsa that is involved in salt tolerance. *Funct. Plant Biol.* **2014**, *41*, 790–802. [CrossRef]
40. Chen, L.; Lu, B.; Liu, L.; Duan, W.; Jiang, D.; Li, J.; Bai, Z. Melatonin promotes seed germination under salt stress by regulating ABA and GA3 in cotton (*Gossypium hirsutum* L.). *Plant Physiol. Biochem.* **2021**, *162*, 506–516. [CrossRef]
41. Lee, H.Y.; Byeon, Y.; Back, K. Melatonin as a signal molecule triggering defense responses against pathogen attack in Arabidopsis and tobacco. *J. Pineal Res.* **2014**, *57*, 262–268. [CrossRef] [PubMed]
42. Lee, H.Y.; Byeon, Y.; Tan, D.X.; Reiter, R.J.; Back, K. Arabidopsis serotonin N-acetyltransferase knockout mutant plants exhibit decreased melatonin and salicylic acid levels resulting in susceptibility to an avirulent pathogen. *J. Pineal Res.* **2015**, *58*, 291–299. [CrossRef]

43. Shi, H.; Jiang, C.; Ye, T.; Tan, D.X.; Reiter, R.J.; Zhang, H.; Chan, Z. Comparative physiological, metabolomic, and transcriptomic analyses reveal mechanisms of improved abiotic stress resistance in bermudagrass (*Cynodon dactylon* L. Pers.) by exogenous melatonin. *J. Exp. Bot.* **2015**, *66*, 681–694. [CrossRef] [PubMed]
44. Cao, Y.; Zhou, X.; Song, H.; Zhang, M.; Jiang, C. Advances in deciphering salt tolerance mechanism in maize. *Crop J.* **2023**, *11*, 1001–1010. [CrossRef]
45. Zhang, N.; Zhang, H.J.; Sun, Q.Q.; Cao, Y.Y.; Li, X.; Zhao, B.; Guo, Y.D. Proteomic analysis reveals a role of melatonin in promoting cucumber seed germination under high salinity by regulating energy production. *Sci. Rep.* **2017**, *7*, 503. [CrossRef] [PubMed]
46. Li, J.; Liu, J.; Zhu, T.; Zhao, C.; Li, L.; Chen, M. The role of melatonin in salt stress responses. *Int. J. Mol. Sci.* **2019**, *20*, 1735. [CrossRef] [PubMed]
47. Jain, M.; Khurana, J.P. Transcript profiling reveals diverse roles of auxin-responsive genes during reproductive development and abiotic stress in rice. *FEBS J.* **2009**, *276*, 3148–3162. [CrossRef] [PubMed]
48. Wei, T.; Sun, Y.; Li, H.; Hua, L.; Ren, X.; Jia, H.; Guo, J. Methyl jasmonate triggers cadmium detoxification in tomato plants via depressing Cd^{2+} influx, altering the subcellular distribution, and chemical forms of cadmium. *Water Air Soil Pollut.* **2022**, *233*, 460. [CrossRef]
49. Zhao, Y. Essential roles of local auxin biosynthesis in plant development and in adaptation to environmental changes. *Annu. Rev. Plant Biol.* **2018**, *69*, 417–435. [CrossRef]
50. Zhang, L.; Gao, M.; Hu, J.; Zhang, X.; Wang, K.; Ashraf, M. Modulation role of abscisic acid (ABA) on growth, water relations and glycinebetaine metabolism in two maize (*Zea mays* L.) cultivars under drought stress. *Int. J. Mol. Sci.* **2012**, *13*, 3189–3202. [CrossRef]
51. Yang, J.; Duan, G.; Li, C.; Liu, L.; Han, G.; Zhang, Y.; Wang, C. The crosstalks between jasmonic acid and other plant hormone signaling highlight the involvement of jasmonic acid as a core component in plant response to biotic and abiotic stresses. *Front. Plant Sci.* **2019**, *10*, 1349. [CrossRef] [PubMed]
52. Zhang, H.; Zhu, J.; Gong, Z.; Zhu, J.K. Abiotic stress responses in plants. *Nat. Rev. Genet.* **2022**, *23*, 104–119. [CrossRef] [PubMed]
53. Yang, X.; Zhang, Y.; Liu, T.; Shi, J.; Qi, M.; Liu, Y.; Li, T. Integrated physiological, transcriptomic, and proteomic analyses reveal the regulatory role of melatonin in tomato plants' response to low night temperature. *Antioxidants* **2022**, *11*, 2060. [CrossRef] [PubMed]
54. Yan, D.; Wang, J.; Lu, Z.; Liu, R.; Hong, Y.; Su, B.; Li, R. Melatonin-Mediated Enhancement of Photosynthetic Capacity and Photoprotection Improves Salt Tolerance in Wheat. *Plants* **2023**, *12*, 3984. [CrossRef] [PubMed]
55. Talaat, N.B.; Todorova, D. Antioxidant machinery and glyoxalase system regulation confers salt stress tolerance to wheat (*Triticum aestivum* L.) plants treated with melatonin and salicylic Acid. *J. Soil Sci. Plant Nutr.* **2022**, *22*, 3527–3540. [CrossRef]
56. Liang, C.; Zheng, G.; Li, W.; Wang, Y.; Hu, B.; Wang, H.; Chu, C. Melatonin delays leaf senescence and enhances salt stress tolerance in rice. *J. Pineal Res.* **2015**, *59*, 91–101. [CrossRef]
57. Alharbi, B.M.; Elhakem, A.H.; Alnusairi, G.S.; Soliman, M.H.; Hakeem, K.R.; Hasan, M.M.; Abdelhamid, M.T. Exogenous application of melatonin alleviates salt stress-induced decline in growth and photosynthesis in *Glycine max* (L.) seedlings by improving mineral uptake, antioxidant and glyoxalase system. *Plant Soil Environ.* **2021**, *67*, 208–220. [CrossRef]
58. Altaf, M.A.; Shahid, R.; Ren, M.X.; Altaf, M.M.; Khan, L.U.; Shahid, S.; Jahan, M.S. Melatonin alleviates salt damage in tomato seedling: A root architecture system, photosynthetic capacity, ion homeostasis, and antioxidant enzymes analysis. *Sci. Hortic.* **2021**, *285*, 110145. [CrossRef]
59. Miransari, M.; Smith, D.L. Plant hormones and seed germination. *Environ. Exp. Bot.* **2014**, *99*, 110–121. [CrossRef]
60. Waadt, R. Phytohormone signaling mechanisms and genetic methods for their modulation and detection. *Curr. Opin. Plant Biol.* **2020**, *57*, 31–40. [CrossRef]
61. Luo, Y.; Li, W.; Huang, C.; Yang, J.; Jin, M.; Chen, J.; Wang, Z. Exogenous abscisic acid coordinating leaf senescence and transport of assimilates into wheat grains under drought stress by regulating hormones homeostasis. *Crop J.* **2021**, *9*, 901–914. [CrossRef]
62. Jiang, Z.; Zhu, H.; Zhu, H.; Tao, Y.; Liu, C.; Liu, J.; Li, M. Exogenous ABA enhances the antioxidant defense system of maize by regulating the AsA-GSH cycle under drought stress. *Sustainability* **2022**, *14*, 3071. [CrossRef]
63. He, J.; Jin, Y.; Palta, J.A.; Liu, H.Y.; Chen, Z.; Li, F.M. Exogenous ABA induces osmotic adjustment, improves leaf water relations and water use efficiency, but not yield in soybean under water stress. *Agronomy* **2019**, *9*, 395. [CrossRef]
64. Zhang, Y.; Li, Y.; Hassan, M.J.; Li, Z.; Peng, Y. Indole-3-acetic acid improves drought tolerance of white clover via activating auxin, abscisic acid and jasmonic acid related genes and inhibiting senescence genes. *BMC Plant Biol.* **2020**, *20*, 150. [CrossRef] [PubMed]
65. Zhao, Y.; Song, C.; Qi, S.; Lin, Q.; Duan, Y. Jasmonic acid and salicylic acid induce the accumulation of sucrose and increase resistance to chilling injury in peach fruit. *J. Sci. Food Agric.* **2021**, *101*, 4250–4255. [CrossRef] [PubMed]
66. Wang, Y.; Shi, J.; Ren, Z.; Fan, X.; Li, R.; Yu, C.; Duan, L. Physiological and transcriptomic analyses of the effects of coronatine on drought tolerance in *Carex leucochlora*. *Environ. Exp. Bot.* **2023**, *206*, 105184. [CrossRef]
67. Jing, T.; Liu, K.; Wang, Y.; Ai, X.; Bi, H. Melatonin positively regulates both dark-and age-induced leaf senescence by reducing ROS accumulation and modulating abscisic acid and auxin biosynthesis in cucumber plants. *Int. J. Mol. Sci.* **2022**, *23*, 3576. [CrossRef] [PubMed]
68. Shi, H.; Reiter, R.J.; Tan, D.X.; Chan, Z. INDOLE-3-ACETIC ACID INDUCIBLE 17 positively modulates natural leaf senescence through melatonin-mediated pathway in Arabidopsis. *J. Pineal Res.* **2015**, *58*, 26–33. [CrossRef] [PubMed]

69. Keunen, E.L.S.; Peshev, D.; Vangronsveld, J.; Van Den Ende, W.I.M.; Cuypers, A.N.N. Plant sugars are crucial players in the oxidative challenge during abiotic stress: Extending the traditional concept. *Plant Cell Environ.* **2013**, *36*, 1242–1255. [CrossRef]
70. Liu, Y.; Zhang, W.; Elango, D.; Liu, H.; Jin, D.; Wang, X.; Wu, Y. Metabolome and transcriptome analysis reveals molecular mechanisms of watermelon under salt stress. *Environ. Exp. Bot.* **2023**, *206*, 105200. [CrossRef]
71. Thalmann, M.; Santelia, D. Starch as a determinant of plant fitness under abiotic stress. *New Phytol.* **2017**, *214*, 943–951. [CrossRef] [PubMed]
72. Mahmoud, L.M.; Stanton, D.; Amin, B.H.; Grosser, J.W.; Dutt, M. Overexpression of the Arabidopsis NPR1 gene confers enhanced salt tolerance by regulating antioxidant and starch accumulation in citrus. *Plant Cell Tissue Organ Cult.* **2022**, *150*, 695–707. [CrossRef]
73. Punia, H.; Tokas, J.; Mor, V.S.; Bhuker, A.; Malik, A.; Singh, N.; Hefft, D.I. Deciphering reserve mobilization, antioxidant potential, and expression analysis of starch synthesis in sorghum seedlings under salt stress. *Plants* **2021**, *10*, 2463. [CrossRef]
74. Li, X.; Wang, C.; Cheng, J.; Zhang, J.; da Silva, J.A.T.; Liu, X.; Sun, H. Transcriptome analysis of carbohydrate metabolism during bulblet formation and development in *Lilium davidii* var. unicolor. *BMC Plant Biol.* **2014**, *14*, 358. [CrossRef] [PubMed]
75. Abdallah, M.S.; Abdelgawad, Z.A.; El-Bassiouny, H.M.S. Alleviation of the adverse effects of salinity stress using trehalose in two rice varieties. *S. Afr. J. Bot.* **2016**, *103*, 275–282. [CrossRef]
76. Wang, Y.; Zhao, H.; Xu, L.; Zhang, H.; Xing, H.; Fu, Y.; Zhu, L. PUB30-mediated downregulation of the HB24-SWEET11 module is involved in root growth inhibition under salt stress by attenuating sucrose supply in Arabidopsis. *New Phytol.* **2023**, *237*, 1667–1683. [CrossRef] [PubMed]
77. Zhou, Z.; Liu, J.; Meng, W.; Sun, Z.; Tan, Y.; Liu, Y.; Tan, M.; Wang, B.; Yang, J. Integrated Analysis of Transcriptome and Metabolome Reveals Molecular Mechanisms of Rice with Different Salinity Tolerances. *Plants* **2023**, *12*, 3359. [CrossRef] [PubMed]
78. He, D.; Yang, P. Proteomics of rice seed germination. *Front. Plant Sci.* **2013**, *4*, 246. [CrossRef]
79. Rajora, N.; Vats, S.; Raturi, G.; Thakral, V.; Kaur, S.; Rachappanavar, V.; Kumar, M.; Kesarwani, A.K.; Sonah, H.; Sharma, T.R.; et al. Seed priming with melatonin: A promising approach to combat abiotic stress in plants. *Plant Stress* **2022**, *4*, 100071. [CrossRef]
80. Giannopolitis, C.N.; Ries, S.K. Superoxide dismutases, I. Occurrence in higher plants. *Plant Physiol.* **1977**, *59*, 309–314. [CrossRef]
81. Lu, X.; Min, W.; Shi, Y.; Tian, L.; Li, P.; Ma, T.; Luo, C. Exogenous melatonin alleviates alkaline stress by removing reactive oxygen species and promoting antioxidant defence in rice seedlings. *Front. Plant Sci.* **2022**, *13*, 849553. [CrossRef] [PubMed]
82. Zhao, C.; Guo, H.; Wang, J.; Wang, Y.; Zhang, R. Melatonin enhances drought tolerance by regulating leaf stomatal behavior, carbon and nitrogen metabolism, and related gene expression in maize plants. *Front. Plant Sci.* **2021**, *12*, 779382. [CrossRef] [PubMed]
83. Livak, K.J.; Schmittgen, T.D. Analysis of relative gene expression data using real-time quantitative PCR and the $2^{-\Delta\Delta CT}$ method. *Methods* **2001**, *25*, 402–408. [CrossRef] [PubMed]

MDPI AG
Grosspeteranlage 5
4052 Basel
Switzerland
Tel.: +41 61 683 77 34

Plants Editorial Office
E-mail: plants@mdpi.com
www.mdpi.com/journal/plants

Academic Open
Access Publishing

mdpi.com

ISBN 978-3-7258-6869-8